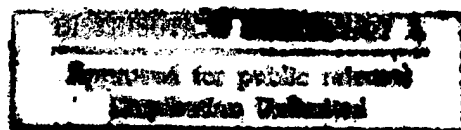


Conference Proceedings

1998 International Conference on

Mathematical Methods in Electromagnetic Theory

MMET 98



19981013 069

June 2-5, 1998

AQF99-01-0044

REPORT DOCUMENTATION PAGE

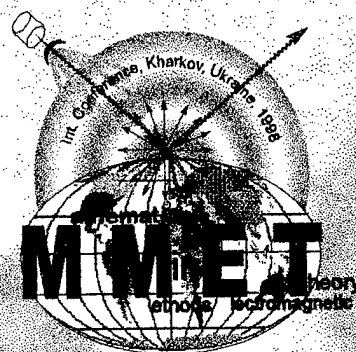
Form Approved OMB No. 0704-0188

Public reporting burden for this collection of information is estimated to average 1 hour per response, including the time for reviewing instructions, searching existing data sources, gathering and maintaining the data needed, and completing and reviewing the collection of information. Send comments regarding this burden estimate or any other aspect of this collection of information, including suggestions for reducing this burden to Washington Headquarters Services, Directorate for Information Operations and Reports, 1215 Jefferson Davis Highway, Suite 1204, Arlington, VA 22202-4302, and to the Office of Management and Budget, Paperwork Reduction Project (0704-0188), Washington, DC 20503.

1. AGENCY USE ONLY (Leave blank)		2. REPORT DATE 26 June 1998	3. REPORT TYPE AND DATES COVERED Conference Proceedings	
4. TITLE AND SUBTITLE Mathematical Methods in Electromagnetic Theory			5. FUNDING NUMBERS F6170898W0024	
6. AUTHOR(S) Conference Committee			8. PERFORMING ORGANIZATION REPORT NUMBER N/A	
7. PERFORMING ORGANIZATION NAME(S) AND ADDRESS(ES) Department of Computational Electromagnetics, Institute of Radiophysics and Electronics National Academy of Sciences, Ulitza Akademika Proskury, 12 Kharkov 310085 Ukraine				
9. SPONSORING/MONITORING AGENCY NAME(S) AND ADDRESS(ES) EOARD PSC 802 BOX 14 FPO 09499-0200			10. SPONSORING/MONITORING AGENCY REPORT NUMBER CSP 98-1010	
11. SUPPLEMENTARY NOTES Two volumes				
12a. DISTRIBUTION/AVAILABILITY STATEMENT Approved for public release; distribution is unlimited.			12b. DISTRIBUTION CODE A	
13. ABSTRACT (Maximum 200 words) The Final Proceedings for Mathematical Methods in Electromagnetic Theory, 2 June 1998 - 5 June 1998 This is an interdisciplinary conference. Topics include antenna theory, asymptotic methods, beam electronics, complex media, computational techniques, electromagnetic theory, fiber optics, function theoretic methods, gratings inverse problems, radar cross section, radomes, scattering and diffraction, time-domain methods, waveguide circuits, and others.				
14. SUBJECT TERMS Computational Electromagnetics, Antennas			15. NUMBER OF PAGES 935	
			16. PRICE CODE N/A	
17. SECURITY CLASSIFICATION OF REPORT UNCLASSIFIED	18. SECURITY CLASSIFICATION OF THIS PAGE UNCLASSIFIED	19. SECURITY CLASSIFICATION OF ABSTRACT UNCLASSIFIED	20. LIMITATION OF ABSTRACT UL	

NSN 7540-01-280-5500

Standard Form 298 (Rev. 2-89)
Prescribed by ANSI Std. Z39-18
298-102



Conference Proceedings

1998 International Conference on

Mathematical Methods in Electromagnetic Theory

MMET

98

Volume 1

Kharkov, Ukraine

June 2-5, 1998

Organized and sponsored by

IEEE AP/MTT/ED/AES Societies East Ukraine Joint Chapter

in cooperation with

Ukrainian URSI Commission "B"

Institute of Radiophysics & Electronics
of the National Academy of Sciences of Ukraine

Institute of Radio Astronomy
of the National Academy of Sciences of Ukraine

Kharkov State University

technically co-sponsored by

IEEE AP, MTT & ED Societies
URSI - International Union of Radio Science

*We wish to thank the following co-sponsors for their contribution
to the success of this Conference:*

International Association of Geomagnetism and Aeronomy

IEEE MTT & ED Societies

US Air Force European Office of Aerospace R&D

US Office of Naval Research European Office

INTAS – International Association

1998 International Conference on Mathematical Methods in Electromagnetic Theory

IEEE Catalog Number: 98EX114

ISBN: 0-7803-4360-3

0-7803-4361-1

Library of Congress: 97-80498

Softbound Edition

Microfiche Edition

This work relates to Department of the Navy Grant N 00014-98-1-1015 issued by the Office of Naval Research European Office. The United States has a royalty-free license throughout the world in all copyrightable material contained herein.

Copyright and Reprint Permission: Abstracting is permitted with credit to the source. Libraries are permitted to photocopy beyond the limit of U.S. copyright law for private use of patrons those articles in this volume that carry a code at the bottom of the first page, provided the per-copy fee indicated in the code is paid through Copyright Clearance Center, 222 Rosewood Drive, Danvers, MA 01923. For other copying, reprint or republication permission, write to IEEE Copyrights Manager, IEEE Service Center, 445, Hoes Lane, P.O. Box 1331, Piscataway, NJ 08855-1331. All rights reserved. Copyright © 1998 by the IEEE, Inc.

MMET*98 Organizing Committee

Dr. V. F. Apeltcin, Moscow State University, Russia
Special Representative in Moscow

Mrs. S. V. Boriskina, Kharkov State University
Secretary and editor

Prof. L. N. Litvinenko, Director, IRA NAS, Kharkov

Prof. V. I. Naidenko, NTU- Kiev Politechnical Institute
Special representative in Kiev

Prof. A. G. Nerukh, Kharkov Technical University of Radio Electronics

Dr. S. Shulga, Kharkov State University

Prof. V. A. Svich, Rector, Kharkov State University

Prof. O. F. Tyrnov, Vice-Rector, Kharkov State University

Mr. A. D. Ustimenko, IRE NAS, Kharkov

Prof. D. M. Vavriv, IRA NAS, Kharkov

Dr. I. Y. Vorgul, Kharkov State University
Web site and arts designer

Prof. V. M. Yakovenko, Director, IRE NAS, Kharkov

MMET*98 Chairman

Prof. E. I. Veliev, IRE NAS Kharkov, Ukraine

MMET*98 Technical Program Committee

Co-chairmen:

Prof. W. Ross Stone, IEEE AP-S & URSI, La Jolla, USA

Prof. A. I. Nosich, IRE NAS, Kharkov, Ukraine

Members:

Prof. I. D. Abrahams, Keele University, UK

Prof. J. Bartolic, Zagreb University, Croatia

Prof. van den Berg, Technical University of Delft, the Netherlands

Prof. V. S. Buldyrev, St. Petersburg State University, Russia

Prof. R. Dowden, University of Otago, Dunedin, New Zealand

Prof. F. Gadiol, Ecole Polytechnique Federale, Lausanne, Switzerland

Prof. M. Hashimoto, Electro-Communication University, Osaka, Japan

Prof. E. Jull, University of B. Columbia, Vancouver, USA

Prof. N. A. Khizhnyak, Nat. Center- KIPT, Kharkov, Ukraine

Prof. A. A. Kirilenko, IRE NAS, Kharkov, Ukraine

Prof. K. Kobayashi, Chuo University, Tokyo, Japan

Prof. M. Lenoir, ENSTA, Palaiseau, France

Prof. E. Michielssen, University of Illinois, Urbana-Champaign, USA

Prof. Z.T. Nazarchuk, PMI NAS, Lviv, Ukraine

Prof. A. A. Nikolaenko, IRE NAS, Kharkov, Ukraine

Prof. D. Nyquist, University of Michigan, East Lansing, USA

Prof. Y. Okuno, Kumamoto University, Japan

Prof. S. L. Prosvirnin, IRE NAS, Kharkov, Ukraine

Prof. Y. S. Shifrin, Kharkov Technical University of Radio Electronics, Ukraine

Prof. P. D. Smith, University of Dundee, Scotland, UK

Prof. S. Ström, Royal Institute of Technology, Stockholm, Sweden

Prof. I. A. Sukhoivanov, Kharkov Technical University of Radio Electronics, Ukraine

Prof. M. Tateiba, Kyushu University, Fukuoka, Japan

Prof. O. A. Tretyakov, Kharkov State University, Ukraine

Prof. G. I. Zaginailov, Kharkov State University, Ukraine

TABLE OF MMET*98 GEOGRAPHY

Entity	Papers
KHARKOV	105
RUSSIA	68
UKRAINE non-Kharkov	38
USA	6
BELARUS	4
INDIA	4
POLAND	4
UKRAINE+JAPAN	4
BULGARIA	3
FRANCE	3
TURKEY	3
UKRAINE+TURKEY	4
GEORGIA	2
IRAN	2
JAPAN	2
LITHUANIA	2
UKRAINE+RUSSIA	2
UKRAINE+UK	1
UKRAINE+FINLAND	1
RUSSIA+TURKEY	1
BELARUS+USA+GERMANY	1
BRAZIL	1
CHINA	1
CROATIA	1
GEORGIA+USA+GERMANY	1
GERMANY	1
GREECE	1
LATVIA	1
NEW ZEALAND+JAPAN	1
SWITZERLAND	1
UK	1
UK+NEW ZEALAND	1
UK+USA+NEW ZEALAND	1
TOTAL	272

Dear colleagues:

MMET*98 is, no doubt, a development of all the previous meetings of this series. By now it has established itself as a truly unique professional forum on the whole space between the Baltic Sea and Pacific, and between the North Pole and the Caucasus. However, this time it is also a very different meeting. For the first time it has reached, in the number of papers in the program (272), and in the scale of international organizations involvement and support, the level of major world conferences in electromagnetics. In the technical quality of the program, we believe that it is even higher, due to a reasonable mixture of applied mathematics and microwave engineering. As all of you perfectly know, the more mathematics we manage to put in the electromagnetic problem solution, the better algorithms we obtain.

There is a tremendous variety of problems, both canonical and new ones, that meet a researcher in the hilly terrain of computational electromagnetics; there is a reciprocally great variety of solution methods. Rope-way of MoM and industrial rock-climbing with FDTD electric hammers is a necessary technology here; but a winter solo climb at the Everest of analytical regularization is still a fascinating achievement. We are grateful to all the authors who submitted their papers to MMET*98 and have come to participate and share their devotion to the exciting world of solutions of Maxwell's equations. It was a pleasure to work with the members of Organizing Committee and Technical Committee; all of us should be especially thankful to the small team of the editors of these Proceedings.

We wish you to enjoy the conference and hope to be able to gather you again at the future MMET's in the next millenium.

Eldar I. Veliev and Alexander I. Nosich

The MMET*98 conference program looks truly wonderful. I really, really wish I could be there. It is an honor that my name has been associated with it. I am sure that it will be a great experience. Best wishes for the meeting.

W. Ross Stone, *IEEE Antennas and Propagation Society*

It is an impressive program that MMET*98 organizers have managed to put together. I wish everybody all possible success with the conference. I will have to look into the future for a new possibility to go to Ukraine.

Staffan Strom, *URSI Commission "B"*

IAGA is honored to co-sponsor the international conference MMET*98. Besides fostering advances in electromagnetic theory, IAGA notes that benefits of this meeting will include in-depth scientific discussions, opportunities for student and young scientist participation, and leadership development. We wish every success for the meeting.

Jo Ann Joselyn, *International Association of Geomagnetism and Aeronomy*

TABLE OF CONTENTS

PLENARY SESSIONS

<i>K.P. Gaikovich</i> , Ill-posed Inverse Problems Based on Volterra-type Equations	23
<i>R. Dowden, J.B. Brundell, M. Hayakawa</i> , Remote Sensing by VLF Using «Absolute Omnipal»: Investigation of Short Path Propagation for Possible Earthquake Precursor Detection	29
<i>M. Lenoir</i> , Regularization of Maxwell Equations, Corner Singularities and Numerical Approximation	35
<i>L.N. Litvinenko, Y.M. Yampolski</i> , Ukrainian Radio Physical System for Seismo-Ionospheric Monitoring	42
<i>N. Engheta</i> , Fractional Calculus and Fractional Paradigm in Electromagnetic Theory	43
<i>N.P. Yashina</i> , Time-Domain Electromagnetics of Waveguide-Type Open Resonators	50
<i>D. P. Nyquist</i> , Asymptotic Radiation Field of Asymmetric Planar Dielectric Waveguide ..	55
<i>T. Jablonski</i> , An Efficient Iterative Scheme for Solving Eigenproblems in the Theory of Electromagnetic Waves	61
<i>K. Shifrin</i> , A Simple Method Inverting Light-Scattering Data of a Diffusive System into the Particle Size Distribution Function	69
<i>P.D. Smith</i> , Time-Domain Solvers versus Analytical Regularization in Integral-Equation Analysis of Canonical Scatterers	73
<i>A. Chakrabarti</i> , Galerkin Methods in Solving Integral Equations with Applications to Scattering Problems	79
<i>S. E. Lyshevsky</i> , Analytic Solutions to Maxwell Equations: Sinusoidal Steady-State and Transient Space-Time Problems in Transverse Magnetic and Transverse Electric Field Analysis	88
<i>E. Michielssen, W. Chew, A. Ergin, V. Jandhyala, B. Shanker, J. Song</i> , Recent Developments in Fast-Multipole Based Frequency and Time Domain Solvers	92
<i>S.V. Sukhinin</i> , Waveguiding and Anomalous Properties of a Knife-Type Periodic Strip Grating	98
<i>A.I. Nosich</i> , The Cost of Pleasure: about some Catastrophes in Time-Harmonic Wave Scattering	104
<i>M. Marciniak</i> , Beam Propagation Method Modeling the Light Propagation in Optical Waveguides	106
<i>Inverse and Synthesis Problems</i>	
<i>V.A. Mikhnev, A.A. Palto</i> , Microwave Method for the Step-Like Reconstruction of Lossless Multilayered Dielectrics	115
<i>Yu. V. Yukhanov</i> , Analysis and Synthesis of Impedance Plane	118
<i>B. Podlevskyi, P. Savenko, M. Tkach</i> , Synthesis of the Adapted Hybrid Reflector Antennas	121
<i>R. Zaridze, G. Bit-Babik, K. Tavzarashvili</i> , The Method of Auxiliary Sources for Investigation of Scattered Fields Singularities and its Application for Inverse Problems	124
<i>M.I. Andriychuk</i> , Investigation of the Solutions of the Non-linear Antenna Synthesis Problems	127

<i>Yu. V. Yukhanov, S. N. Sorokin</i> , Synthesis of Impedance Reflectors with Given Scattering Characteristics	130
<i>N.N. Voitovich, O.M. Gis, O.O. Reshnyak, Yu.P. Topolyuk</i> , New Rigorous Solution of Some Antenna Synthesis Problems According to Prescribed Amplitude Radiation Pattern	133
<i>V.A. Obukhovets</i> , Arbitrary Geometry Phased Array Pattern Synthesis Procedure	136
<i>P. Savenko</i> , On the Structure of the Solutions of the Antenna Synthesis Problems According to the Prescribed Amplitude Directivity Pattern Using the Regularization Functionals	139
<i>G.V. Alekseev, D.V. Panov, V.G. Sinko, A.S. Panasyuk</i> , Nonlinear Inverse Problems of Time-harmonic Wave Suppression in Regular Waveguides	142
<i>N.E. Nikolaev, V.V. Shevchenko</i> , Permittivity Profile Synthesis of Planar Buried Waveguides	145
<i>I.Yu. Vorgul, A.G. Nerukh</i> , Inhomogeneous Transient Conductive Half-Space: Reconstruction of Conductivity Time-Dependence by Scattered Field	148
<i>M.B. Tchernyava, K.P. Gaikovich</i> , Limb-Viewing Refraction Inverse Problem in the Duct Case	151
<i>L.F. Chernogor, K.P. Garmash, V.T. Rozumenko</i> , Regularization Algorithms for Inverse Problems in the Radio Wave Probing of the Ionospheric Plasma	154
<i>V.A. Kaloshin, A.S. Venetsky</i> , Numerical Technique of Solving Inverse Problems of Geometrical Optics of Inhomogeneous Media	157
<i>V. Anokhin, P. Savenko</i> , On Grounding One Class of Nonlinear Inverse Problems of Mathematical Physics	160
<i>C. Kechribaris, K.S. Nikita, N.K. Uzunoglu</i> , Improved Algorithm Based on Rytov Approx- imation for Three-Dimensional Structure Determination of Biological Objects	163
<i>A.A. Vertiy, S.P. Gavrilov, I.V. Voinivskiy, V.N. Stepanyuk</i> , Quasi-optical Diffraction Tomography	164
<i>V.Ya. Epp, T.G. Mitrofanova</i> , Solution of Inverse Problem for a Charge Combined with a Point-Like Dipole	167

Gratings and FSS

<i>Z. Sipus, R. Zentner, J. Bartolic</i> , Validity of Approximate Boundary Conditions for Periodic Strips on Cylindrical Substrates	171
<i>E. K. Lipachev</i> , Diffraction of Electromagnetic Waves by Gratings with Piecewise Smooth Boundaries	174
<i>L.G. Velichko</i> , Model Synthesis of Efficiently Absorbing Structures with Diffraction Gratings	177
<i>S. N. Vorobiov, D.L. Litvinenko</i> , Electromagnetic Wave Scattering by Semi-Infinite Grating Consisting of Metal Strips Placed in Magnetic-Dielectric Half-Space	180
<i>A.A. Shirnen</i> , Waveguiding and Anomalous Properties of Periodic Slanted Strip Grating .	183
<i>S. Prosvirnin, T. Vasilyeva</i> , Moment-Method Analysis of Electromagnetic Wave Scattering by Plane Array of Chiral Strip Elements	186
<i>A.S. Ilinski, T.N. Galishnikova</i> , Electromagnetic Wave Scattering on Transparent Wavy Interfaces	189

<i>N.V. Ryazantseva, V.V. Yachin</i> , Electromagnetic Wave Scattering by Rectangular-Cell Double-Periodic Magneto-Dielectric Gratings	192
<i>Z. Nazarchuk, O. Ovsyannikov, T. Senyk</i> , Plane Wave Scattering by a Cascaded Diffraction Grating (H-case)	195
<i>J. Ziemelis, P. Chertov</i> , Analysis of Scattered Field from the Grating of Thin Resistive Dipoles	198
<i>S.Y. Sadov</i> , Examples of «Faked Unitarity» in the Diffraction Grating Computations	201
<i>Yu. Terent'ev</i> , Classification of Wave Instabilities Produced by Interaction of Grating Modes	204
<i>K.Yu. Kramarenko, N.A. Khizhnyak</i> , Diffraction of Plane Wave on a Dielectric Groove ...	206
<i>V.V. Podlozny</i> , Scattering and Absorption of a Videopulse by a Set of Alternated Layers with Resistive Films	209
<i>V.A. Obukhovets, A.O. Kasyanov, S.V. Piven</i> , Simulation of Controllable Solid-State Structures	212
<i>I.L. Verbitskii</i> , Low-Frequency Asymptotics in the Diffraction of Waves by Echelette	214
Electromagnetic Theory	
<i>V. Onufrienko</i> , New Description of Spatial Harmonics of Surface Waves	219
<i>S.A. Gayvoronskaja, V. I. Sergeev</i> , Analytical Expression Transformation for the Engineering Calculation of Parametric Absorption Effect	222
<i>I.O. Girka, N.B. Marushchenko, I.V. Pavlenko</i> , Numerical Calculation of the Electron Distribution Function with the Goal of Simulating a Current Drive	225
<i>V.F. Kravchenko</i> , Electrodynamics of Superconducting Structures	228
<i>A.M. Zabolotskiy, S. I. Tarapov</i> , Evolution of a Magnetic Resonance Line under Microwave Field of High Intensity	231
<i>B. Nevzlin, Yu. Dyachenko</i> , Analysis of Methods of Calculation of Electric Field in Granular Materials	234
<i>N.G. Kokodiy</i> , Forces of Interaction between Macroscopic Objects in the Field of Electromagnetic Wave	237
<i>Yu.A. Branspiz, A.A. Kovalevsky</i> , Analysis of the Oersted Experiments	240
<i>V. I. Selin</i> , Method of Asymptotic Perturbation of Fundamental Solution and Its Application for Problems of Wave Field Investigation	243
<i>P.L. Tokarsky, V.V. Dolzhikov</i> , Simple Approximate Formulas for Evaluating Sommerfeld Type Integrals	246
<i>V. Chursin, E. Odarenko, A. Shmat'ko</i> , Nonlinear Theory of Relativistic Microwave Electron Devices	249
<i>V. Ivaska, V. Jonkus, V. Palenskis</i> , Magnetic Field Distribution for Superconductors with Rotational Symmetry	252
<i>A.N. Reznik, K.P. Gaikovich</i> , Technique for Determination of RF-Magnetic Field Dependence of the NTSC Surface Impedance by Microwave Resonators	255
<i>M.V. Zagirnyak, Yu.A. Branspiz</i> , Modern Methods for Calculation of Magnetic Field Force Acting on Magnetics	258
<i>L. Pankratov</i> , Homogenization Theory and Impure Superconductors	260

<i>V.A. Shcherbina, G.I. Zaginaylov, S.A. Zhuchenko</i> , Numerical Theory of Excitation of Axisymmetric Open-Ended Finite Length Slow Wave Structure on the Basis of Boundary Singular Integral Equation Method	265
<i>V.V. Gushchin</i> , Hamiltonian Approach to the Problem of Wave Collapse	266

Ionospheric Electromagnetics

<i>A.M. Gokov, S.I. Martynenko, V.T. Rozumenko, A.M. Tsymbal, O.F. Tyrnov</i> , A Method for Derivation of Electric Fields in the Lower Ionosphere from Measurements with a Partial Reflection Facility	271
<i>N.A. Kazakova, A.G. Kolesnik, B.M. Shinkevich</i> , About Possible Harbingers of Earthquakes in Characteristics of VLF Signals of Electromagnetic Background	274
<i>M. Hayakawa, O.A. Molchanov, A.V. Shvets, N. Yamamoto</i> , Multi-Signal Studying of Seismo-Ionospheric Interconnections Using VLF OmniPAL Receiver	277
<i>A.S. Mazmanishvili, E.V. Rogozhkin, A.S. Suriadnyi</i> , Statistical Analysis of a Displacement of Autocorrelated Functions Processing Procedures by Incoherent Scattering in Ionosphere	279
<i>C. J. Rodger, J. R. Wait, N. R. Thomson</i> , VLF Scattering from Red Sprites: Vertical Columns of Ionisation in the Earth-Ionosphere Waveguide	282
<i>V.V. Vinogradov, G.V. Litvinenko</i> , Wavelet Analysis of the ELF Signatures of Global Thunderstorm Activity	285
<i>Y.M. Yampolski, V.S. Beley, S.B. Kascheev, B.V. Lazebny, V.E. Paznukhov, A.G. Rokhman</i> , Cross-Mode Modulation of Schumann Resonances	288
<i>V.A. Donchenko, V.T. Kalaida, E.V. Ovcharenko</i> , Calculation of Atmospheric Electricity Day Trend	292
<i>A.P. Nickolaenko, L.M. Rabinowicz</i> , Seasonal Drift of the Global Thunderstorms and Schumann Resonance Frequencies	294
<i>I.G. Kudintseva, S.V. Myand, A.P. Nickolaenko, L.M. Rabinowicz</i> , Time Domain Solution for the Natural Sub-Ionospheric ELF Pulse	295
<i>A.P. Nickolaenko, M. Hayakawa, Y. Hobara</i> , Schumann Resonance and Global Lighting Activity	296
<i>S.I. Martynenko, R.S. Shubova</i> , Impact of Variations in the Radioactive Background above the Earth on the Ionization Balance in the Lower Ionosphere	298
<i>S. Prosvirnin</i> , Magnetic Field Polarimetry of Seismic Sources	301
<i>M.A. Korol, A.P. Nickolaenko, A.V. Shvets</i> , Wave Impedance Technique to Derive Distance from Nearby Lightning Discharges	303
<i>R. Dowden, J. B. Brundell, C. J. Rodger</i> , Remote sensing by VLF Using «Absolute Omnipal»: Investigation of the Decay of Sprite Plasma	304

Time Domain Electromagnetics

<i>I. Scherbatko, A. Nerukh</i> , Time-Domain Numerical Simulation of EM Pulse Propagation Through a Time-Varying Slab	309
<i>Yu. I. Buyanov, V.I. Koshelev, V.V. Plisko</i> , Radiation of a Long Conductor Excited by a Short Pulse	312

<i>O.I. Sukharevsky, S.A. Gorelyshev, A.V. Muzychenko</i> , Pulse Signal Scattering by Object Located near the Earth Interface	315
<i>V.V. Borisov</i> , Construction of Bessel-type Beamlike Solutions to the Maxwell Equations	318
<i>A.O. Perov</i> , Evolutionary Basis and Operators of Transformation of Nonstationary Waves in Periodic Structures	321
<i>A. Cheldavi</i> , Transient Analysis of Transmission Lines with Time-Dependent Boundary Terminations and General Input	324
<i>P. Shubitidze, R. Jobava, R. Zaridze, R. Beria, D. Pommerenke, S. Frei</i> , FDTD Method in the Problems of Penetration of the Transient Fields of Electrostatic Discharge into a Cavity	327
<i>A.M. Dumin, O.A. Tretyakov</i> , Arbitrary Signal Radiation of Coaxial Waveguide	330
<i>I.Yu. Vorgul</i> , Some Exact Solutions for Electromagnetic Field in Media with Different Types of Transient Conductivity	333
<i>O. Rybin, A. Nerukh</i> , Transient Electromagnetic Field in a Dissipative Medium with Rectangular Pulse Modulated Parameters	336
<i>A. Cheldavi</i> , Optimum Design of Radar Pulses for Stealth Targets (Time — Domain Approach)	339
<i>M.I. Bakunov, S.N. Zhukov</i> , Trapping of an Electromagnetic Wave by the Boundary of a Suddenly Created Plasma Half-space	340
<i>V.I. Koshelev, V.T. Sarychev, S.E. Shipilov</i> , Time and Frequency Domain Algorithms of Impulse Responses Evaluation	343
<i>N.N. Kolchigin, S.N. Pivnenko</i> , Numerical Modeling of Measurements of Dielectric Material Characteristics Using Non-Sinusoidal Signals	346
<i>K.P. Garmash</i> , Modeling Studies of Nonlinear Interaction of Non-Stationary High-Power Electromagnetic Waves with the Ionospheric Plasma	349
<i>V.V. Borisov</i> , Transient Waves Produced by a Moving Source on a Circle	352
<i>S.V. Chumachenko, O.A. Tretyakov</i> , Rotational Mode Oscillations in a Cavity with a Time-Varying Medium	355
<i>S.A. Masalov, A.O. Puzanov</i> , Modeling of Time-Dependent Wave Scattering from Subsurface Ground Medium	358

Waveguide Circuits

<i>H. Rahman</i> , A Novel Approach to the Computation of Fields inside Waveguides and Cavities by Fourier Series	363
<i>D.V. Semenikhina</i> , Microwave Cavity with Nonlinear Load	366
<i>I. Petrusenko</i> , The Method of Analysis of the Diffraction on Step Discontinuities	369
<i>O. V. Gavril'yako</i> , Diffraction by a Thick Inhomogeneous Diaphragm in Parallel-Plate Waveguide	372
<i>A. Trubin</i> , Architecture of Dielectric Bandpass Filters with Symmetrical Characteristics	375
<i>S. A. Ivanov, P. I. Dankov</i> , Numerical Simulation of Some Planar Microwave Gyrotropic Structures	378

<i>Y.M. Penkin</i> , Solution of the Problem of Excitation of Rectangular Waveguide Section with Longitudinally-Inhomogeneous Medium	381
<i>A.K. Poddar, J.K. Bansal, K.N. Padney</i> , Millimeter Wave Evanescent Mode Power Combiner — Gunn Oscillator in Suspended Stripline Configuration	384
<i>A.A. Kirilenko</i> , Numerical Algorithm for the Design of Plane Junction of Two Waveguides with Arbitrary Stepped Boundaries of Cross-sections	387
<i>L.P. Mos'pan, A.A. Kirilenko, V.I. Tkachenko</i> , Numerical Investigation of Multiple Rectangular Aperture Irises in Rectangular Waveguide	390
<i>L.P. Yatsuk</i> , Magnetic Field Finding in the Source Region of Longitudinal Slot in a Waveguide Filled with Layered Dielectric	393
<i>V.B. Kazanskiy, V.V. Podlozny, V.V. Khardikov</i> , Waveguide Section of Sequentially Included Identical Elements	396
<i>T. Vasilyeva, A. Kirilenko, L. Rud', V. Tkachenko</i> , Calculation of Full-wave S-matrices of Monoaxially Uniform (2-D) Elements in Rectangular Waveguides	399
<i>V.A. Karlov</i> , Electromagnetic Analysis of the E-Plane Waveguide Step	402
<i>V.I. Tkachenko</i> , Object-oriented Approach to the Development of Specialized and General Software for Microwave CAE&D	405
<i>G.I. Zaginailov, V. D. Dushkin, V. Kovostyshevski, P.V. Turbin</i> , Modelling the Beam Excitation of Planar Waveguide with Rectangular Irregularities	409
<i>F. M. Repa</i> , Some Ferrite Control Components in a Section of Cutoff Waveguide	411
<i>V.I. Naidenko, S.P. Kapustyanskii, A.P. Prokopenko</i> , Method of Measuring Electromagnetic Characteristics of Materials	412
<i>O.V. Bondarenko, V.B. Kazanskiy</i> , Resonant System of Selection and Absorption of Waveguide Modes	415

Electromagnetic Signal Processing

<i>G.A. Kouzaev, A.S. Tcherkasov</i> , Circuit Modeling for Super-High Speed Processing Spatially Modulated Field Signals	421
<i>V.I. Slyusar, V.L. Buryachok</i> , Model of Signals for Digital Antenna Array with Mutual Coupling on the Basis of Face-Splitting Matrices Product	424
<i>K. Egiazarian, D. Gevorkian, S. Atourian, J. Astola, T. Saramaki, V. Lukin</i> , Unified Structure and Approach for Performing Fast Transformations and Nonlinear Operations	426
<i>A.A. Galuza, A.S. Mazmanishvili</i> , Analysis of the Ishimaru Parabolic Equation: the Laguerre Invariance of the Output Time Impulses Shape	429
<i>M.V. Andreev, V.F. Borulko, O.O. Drobakhin</i> , Successive Approach and Non-Traditional Regularization to Spectral Parameter Estimation by Least Square Method	432
<i>K.E. Yushtin, S.N. Savenkov</i> , Analysis of the Mueller Matrix Elements Measurement Error Influence on Its Physical Realisability	435
<i>D. Biela-Wiraszka</i> , Two-Stage Approach to Image Compression Using Wavelet and Piecewise-Linear Transforms	438
<i>O.O. Drobakhin</i> , Regularization of Data Processing in Six-Port Reflectometry	442
<i>S.N. Savenkov, K.E. Yushtin, B.M. Kolisnychenko, Yu.A. Skoblya</i> , On the One-to-One Corre- spondence of Mueller and Jones Matrix Formalisms under Natural Conditions	444

<i>V. Trigubovich</i> , On Some Characteristics of Electromagnetic Environment	447
<i>V.O. Kovalenko</i> , On Subsurface Radar Data Processing	450
<i>O.O. Drobakhin</i> , Principle of Fourier Holographic Processing in Multifrequency Microwave Measurements	453
<i>S.G. Leus, S.N. Pokhil'ko</i> , Estimating the Parameters of Spectra in Problems of Remote Radio Sounding of Near-Earth Plasmas	456
<i>L.F. Chernogor, O.V. Lazorenko</i> , The Radar Equation for Remote Radio Sounding of Distributed Targets with Ultra-Wideband Radio Signals	457
<i>V.A. Kovalchuk</i> , Results of the Dynamic Radar Target Characteristics Calculations in the Decametric Wave Band	459
<i>V.G. Galushko</i> , Detecting Quadratic Nonlinearities in Random Processes in the Presence of Additive Noise	462
<i>S.N. Savenkov, R.I. Gorelko</i> , General-Purpose Computer-Controlled Polarization State Transformer for Modern Automatic Mueller-Polarimeter	465
Authors Index	468

Scattering and RCS

<i>V.F. Apelt'cin</i> , Generalized Sommerfeld Approach for the Coated Metallic Bodies Excitation	495
<i>N.Z. Kolev</i> , An Application of the Method of Moments for Computation of RCS of PEC Wire-grid Models of Complicated Objects	499
<i>A.B. Hashimov</i> , Minimization of the Obstacle Scattering Fields	502
<i>A.Yu. Afinogenov</i> , On Radar Images Modelling of Structures with Complex Microgeometry	505
<i>O.I. Sukharevsky, G.S. Zalevsky</i> , Scattering by Resonant Objects Buried in Dielectric Half-Space	508
<i>Ye.V. Shepilko</i> , Electromagnetic Scattering by a Dielectric Cylinder Half-Immersed in the Perfectly Conducting Half-Space	511
<i>V.P. Chumachenko, E. Karacuha, M. Dumanli</i> , TE-Wave Scattering by a Multiangular Trough in a Conducting Plane	514
<i>T. Ikiz, M.A. Lyalinov, A.H. Serbest</i> , Diffraction of Plane Waves by a Two-Impedance Wedge in Cold Plasma	517
<i>A. Bakumenko, A.N. Khizhnyak</i> , Description of the Gaussian Beam Excited Surface Wave	520
<i>I. A. Borzenkov</i> , Integral Equations in the Problem of Diffraction by Several Parallel Impedance Strips	523
<i>A.V. Boriskin</i> , Two-dimensional Beam Excitation of a Circular Dielectric Shell	525
<i>P.-M. Cutzach</i> , Numerical Solution of Maxwell Equations in a Two-Layered Medium	528
<i>I. Donets, A.M. Lerer, S. Tsvetkovskaya</i> , Analysis of Diffraction by a Shielded Sphere	531
<i>A.M. Osharin</i> , Plane Electromagnetic Wave Scattering by a Spherical Inclusion Embedded in a Lossy Film	534

<i>I.V. Sukharevsky, S.E. Vashinsky</i> , About the Stationary Phase Points and Caustics Influence on Radiation of Antenna System with Radome	537
<i>K.P. Yatzuk, R.R. Shvelidze</i> , H_{11} -Wave Radiation from a Circular Waveguide with Spiral in Waveguide Aperture	540
<i>N.A. Popenko</i> , Scattering of Electromagnetic Waves in Millimeter Range from Canonic Scatterers	543
<i>F. Bogdanov, D. Karkashadze, D. Metskhvarishvili, P. Shubitidze</i> , Control of Electromagnetic Radiation and Scattering by Usage of Smart Coatings	544

Antennas and Arrays

<i>F.F. Dubrovka, V.M. Tereshchenko</i> , Full Surface Wave Analysis of Radiation Characteristics of Tapered Slot Antennas on Dielectric Substrates	547
<i>A.K. Poddar, J.K. Bansal, K.N. Padney</i> , Broad Band Tunable Planar Active Radiating Elements with Evanescent Mode Resonator Using Notch Antenna	550
<i>V.V. Artemiev, Yu.Yu. Radtsig, S.I. Eminov</i> , Electrodynamics Analysis of Dipole Arrays ...	553
<i>A.A. Bulgakov, N.N. Gorobets, V.A. Lyaschenko</i> , Matching and Radiation Patterns of Waveguide and Sectorial Horn Radiators	556
<i>P.H.F. Silva, A.D.D. Neto, W. Damata</i> , Electromagnetic Field of an Asymmetrically Driven Dipole Antenna for Heating Dissipative Media	559
<i>N. Galchenko, S. Vartanyan</i> , Development of Electromagnetic Methods of Printed Dipole Antennas Design	562
<i>R. Aleksiejunas, V. Ivaska</i> , Geometric Phase for the Far Zone Field Emitted by an Open Rectangular Waveguide	565
<i>N.N. Gorobets, N.P. Yeliseyeva</i> , Influence of Diffraction Effects on Radiation Characteristics of a Wire Antenna with Finite-Size Plane and Corner Reflector of Arbitrary Apex Angle	568
<i>S. N. Sorokin, V.V. Saveljev</i> , Mathematical Modeling of Radiation of Antenna Arrays	571
<i>N. Jatsenko, Y. Jatsenko, N.A. Khizhnyak</i> , Radiation of a System of Wire Antennas in Anisotropic Medium	574
<i>V.I. Selin</i> , Mathematical Model of Strip Dipole Antenna on Stratified Substrate	577
<i>H.H. Balik</i> , Interpolation for Fast Efficient Excitation Modeling Technique of Open Planar Circuits and Antennas in SDM	580
<i>N.P. Egorova</i> , Mathematical Modeling of an Antenna with Corner Reflector	583
<i>L.P. Yatsuk, N.K. Blinova, A.V. Zhironkina</i> , Influence of Reflecting Loading on the Polarization Properties of Cross-Like Slots in a Waveguide	586
<i>V.I. Markov, A.B. Filonenko, Chernigov, V.A. Usin, O.D. Anohina, A.V. Nechesa</i> , Computer Simulation in Antenna Design and Measurements	589
<i>V.A. Usin, O.D. Anohina, A.V. Nechesa, V.I. Markov, A.B. Filonenko</i> , The Automatic Diagnostics and Alignment in a Phased Array Antennas	591

Computational Techniques

<i>S.A. Komarov, P.M. Zatcepin</i> , Variational Principle in Three-Dimensional Problem of Diffraction by Impedance Screen	597
-------------------------------------------------------------------------------------------------------------------------------------	-----

<i>S.A. Ivanov, B.V. Sestroretskii</i> , Dispersion of Plane Waves in 3-D Stream-type Grids	600
<i>I.Yu. Chudinovich, A.Yu. Lytova</i> , Boundary Equations in the Problems of Electromagnetic Wave Diffraction on 3-D Unclosed Surfaces	603
<i>H.H. Balik</i> , Analysis of Multi Dielectric Layer Structures in SDM by Iterative Green's Function Calculation Technique	606
<i>Y.A. Branspiz, A.V. Pastushenko</i> , Universal Method of Calculation of Optimal Parameters of Bipolar Electromagnets	609
<i>V.I. Naidenko, E.V. Guseva, A.P. Prokopenko</i> , Solution of Direct Problem of Tomography of Applied Potentials	612
<i>Y. Brand, A.K. Skriversvik, Ju.R. Mosig, F.E. Gardiol</i> , New Iterative Integral Equation Technique for Multilayered Printed Array Antennas	615
<i>A.B. Samokhin, U.U. Kapustin</i> , Mathematical Modeling of Electromagnetic Scattering Problems	618
<i>O.V. Lazorenko</i> , Application of the Wavelet Transform to Analysis of Ultra-Wideband Processes	621
<i>A.V. Zhilin, K.P. Gaikovich</i> , Tikhonov's Algorithm for Two-Dimensional Image Retrieval	622
<i>V. Shcherbina</i> , Mathematical Models for Electromagnetic Scattering in R^3	625
<i>S.G. Tanyer, M. Karaman, I. Ozturk</i> , Analysis of Wave Propagation in Inhomogeneous Media Using FDTD Method and Its Applications	629
<i>K.V. Nikitin, S.P. Skobelev</i> , An Algorithm of the Method of Volume Integral Equations for Analysis of Waveguide Antenna Arrays with Protruding Dielectric Elements	632
<i>A. Spivak, I. Shvedchikova</i> , Field Calculation of the Open Magnetic Systems by the Regularization of Cauchy Problem	635
<i>A.G. Tyzhnenko</i> , New Approach to the Wave Diffraction by Arbitrary Dielectric Wedge..	638
<i>R.N. Kochergov</i> , Method of Solution for the Wake Field Excited by Relativistic Electron Bunch in a Dielectric Waveguide	641
<i>W. Yuan, Q. Chu, C. Liang</i> , Equivalence and Optimization of Absorbing Boundary Conditions	644

Complex Media

<i>A.A. Alexandrova, Y.N. Alexandrov, N.A. Khizhnyak</i> , General Problem of MHD Wave Diffraction by MHD Irregularities of Arbitrary Shape	649
<i>I.O. Girka, P.K. Kovtun</i> , The Influence of 3D Nonhomogeneity of External Magnetic Field on Dispersion Properties of Low-Frequency MHD Waves in Stellarator	652
<i>N.A. Azarenkov, I.B. Denisenko, Yu.O. Tishetskiy</i> , Ion Motion Control by the Field of Ion-Acoustic Wave	658
<i>G.G. Goshin, N.E. Lugina</i> , Boundary Problem on Excitation of Spiral Wire System on a Plane Chiral Substrate	664
<i>K. Vytovtov</i> , The Matrix Formalism for Anisotropic and Bianisotropic Layered Medium	667
<i>Ju.E. Filipov, V. G. Papkovich</i> , Electromagnetic Waves on Gyrotropic Rod with Arbitrary Direction of External Magnetic Field	673

<i>V.F. Borulko</i> , Polarization Transformation in Irregular Circular Waveguides with Helical Corrugation and Gyrotropic Filling	676
<i>D.A. Marakasov, V.V. Fisanov</i> , Eigenwaves of a Bigyrotropic Chiral Medium under Transverse Propagation	682
<i>G. N. Georgiev, M. N. Georgieva-Gross</i> , On an Application of Iterative Method to the Circular Ferrite-dielectric Waveguide Analysis	685
<i>E.P. Kontar, V.I. Lapshin, V.N. Mel'nik</i> , Numerical Simulations of Quasilinear Two Electron Beam Interaction in a Plasma	688
<i>N.A. Azarenkov, A.V. Gapon, I.B. Denisenko</i> , Self-Consistent Modeling of High-Frequency Discharges Sustained by Azimuthally Nonsymmetric Surface Waves	691
<i>S.Yu. Puzirkov, V.O. Girka, V.I. Lapshin</i> , Parametric Excitation of the Surface Cyclotron Waves by Nonmonochromatic Electric Field	697
<i>V.F. Borulko, V.E. Ivanilov</i> , Resonance Properties of Bragg Structures with Parameter Distortion	700
<i>N.I. Pyatak, B.N. Mizernik</i> , Resonance Dissipation of Electromagnetic Waves in Plane-Parallel Waveguide with Transversely Magnetized Ferrite Layer	706
<i>I.O. Girka, V.I. Lapshin</i> , Structure of the Local Alfvén Resonance in Cylindrical Plasmas Placed into Rippled Magnetic Field	710
<i>A.V. Malyushkin, S.N. Shulga</i> , Low Frequency Scattering of a Plane Wave by an Anisotropic Ellipsoid in Anisotropic Medium	716
<i>V.A. Pogrebnyak</i> , Electron Standing Wave Resonances in 2D Quantum Well and Fractional Quantum Hall Effect	719
<i>A.A. Rozhkov, M.Yu. Kovalevsky</i> , Hydrodynamic Spectra of Magnetics with Spontaneously Broken Spin Symmetry and B-Phase of Fermi-Superfluid	722

Analytical Regularizations

<i>E.I. Veliev, K. Kobayashi, M. Ogata, S. Koshikawa</i> , Diffraction by a Strip with Different Surface Impedances: The Case of H-Polarization	727
<i>S.I. Eminov</i> , Integro-Differential Equations of Dipole Antennas. Theory and Methods of Computation	730
<i>Y.A. Tuchkin, E. Karacuha, A. Turk</i> , Analytical Regularization Method for E-Polarized Electromagnetic Wave Diffraction by Arbitrary Shaped Cylindrical Obstacles	733
<i>S.A. Komarov, A.I. Mashutin, P.M. Zatcepin</i> , Diffraction Effects in the Problems of Impedance Slit Structure Emissivity	736
<i>N.Y. Bliznyuk, A.I. Nosich</i> , Approximate versus Exact Methods in Modeling a Coaxially Excited Circular Patch Antenna	739
<i>A.N. Khizhnyak, S.S. Vinogradov</i> , Accurate Numerical Solution of Some Diffraction Problems for Axisymmetric Thin Screens	742
<i>Y.A. Tuchkin, E. Karacuha, F. Dikmen</i> , Scalar Wave Diffraction from Infinitely Thin Perfectly Conducting Circular Ring	745
<i>L.J. Voinova, S.I. Eminov</i> , Theory of Biconical and Disk-Conical Dipole Antennas	748
<i>T. L. Zinenko, A. Matsushima, Y. Okuno</i> , Plane Wave Scattering from Multilayered Resistive-Strip Grating Embedded in a Dielectric Slab	751

<i>V.A. Doroshenko</i> , Nonstationary Excitation Problem Solution for a Biconical Structure Consisting of an Unclosed Cone and Isotropic One	754
<i>M. Davidovich</i> , New Technique for Kernel Regularization of Surface Integral Equations in Electromagnetics	757
<i>E.D. Vinogradova, P.D. Smith</i> , Impact of a Hollow Spheroidal Cylinder on Electric Dipole Radiation Features	760
<i>D. Kuryliak, K. Kobayashi, Z. Nazarchuk, S. Koshikawa</i> , Wiener-Hopf Analysis of Axial Symmetric Diffraction Problems for Open-Ended Cylindrical Waveguide Cavities	763
<i>V.P. Chumachenko, V.P. Piankov, L.I. Zinenko</i> , Mathematical Method for Electromagnetic Analysis of Two-Dimensional Waveguide Junctions and Radiators of Complicated Shape	766
<i>V.V. Radchenko</i> , Modeling a Spherical Patch Antenna Axisymmetrically Excited by a Radial Probe	769
<i>V.V. Khoroshun</i> , On the Modification of the Method of the Riemann-Hilbert Problem	772
<i>A.V. Brovenko A. Y. Poyedinchuk</i> , Regularization Method for a Class of Dual Series Equations in Diffraction Theory	775

Open Waveguides

<i>I.E. Pleshchinskaya, N.B. Pleshchinskii</i> , On Classification of Eigen Waves of Planar Cylindrical and Spherical Dielectric Waveguides	781
<i>E. Glushkov, N. Glushkova</i> , Energy Fluxes and Resonances in Waveguides with Obstacles	784
<i>E.M. Karchevskii</i> , Study of Spectrum of Guided Waves of Dielectric Fibers	787
<i>G.Ya. Slepyan, A.S. Maksimenko</i> , Analysis of Electromagnetic Wave Propagation in Sculptured Thin Films with Zigzag Morphology	789
<i>A.-S. Bonnet-BenDhia, K. Ramdani</i> , Mathematical Analysis of Conductive and Superconductive Transmission Lines	792
<i>A.Ye. Svezhentsev</i> , Analysis of Coupled Cylindrical Slot and Strip Lines Based on the Riemann-Hilbert Problem Method	795
<i>V.P. Chumachenko, A.V. Krapyvny, V.G. Zasovenko</i> , Electrodynamical Analysis of the Eigenmode System of Open Bilateral Slot Line	798
<i>N.B. Pleshchinskii, D.N. Tumakov</i> , On Solving Diffraction Problems for the Junctions of Open Waveguides in the Classes of Distributions	801
<i>Z. Nazarchuk, O. Ovsyannikov, R. Drogobitsky</i> , Electromagnetic Wave Diffraction on Screens in Dielectric-Metallic Waveguide (H-Case)	804
<i>K. Tanaka, M. Tanaka, K. Ichikawa, K. Katayama</i> , Guided-Mode Extracted Integral Equations for Accurate CAD of Dielectric Branching Waveguide Circuits	807
<i>S.V. Boriskina, A.I. Nosich</i> , Numerical Simulation of Whispering-Gallery-Mode Coupler in Dielectric Slab Waveguide	810
<i>I.S. Chikichev</i> , Waveguiding and Anomalous Properties of Circular Disk Periodic Chain Embedded in 3D Space	813

Eigenvalue Problems

<i>S.D. Prijmenko, G.A. Brjuzgalov, N.A. Khizhnyak</i> , Resonance Frequency of the H-type Accelerator Structure	819
<i>A. Lakhtakia, G.Ya. Slepian, S.A. Maksimenko, O.M. Yevtushenko, A.V. Gusakov</i> , Eigen-value Electrodynamical Problems for IR Carbon Nanowaveguides	822
<i>A.E. Serebryannikov</i> , Generalized Method of Natural Oscillations Applied to Azimuthally-Corrugated Coaxial Cavity	825
<i>N.A. Syvozalizov, V.V. Khoroshun</i> , Analysis of Dispersion Characteristics of Shielded Microstrip Line	828
<i>A.M. Lerer, Ya.A. Reizenkind, V.A. Sledkov</i> , Arbitrary Shape Planar Resonator Analysis by Galerkin Method with Edge-Accounting Basis Functions.....	829
<i>B.Y. Kapilevich, S. Ogourtsov</i> , Numerical Evaluation of Complex Natural Frequencies for Symmetrical Modes of Cylindrical Resonator with Lossy Sample	832
<i>S. V. Sukhinin, D.A. Kondratenko</i> , Wave Propagation in Strongly Non-homogeneous Waveguide	835
<i>I.B. Yumov</i> , On the Scattering Vibrations in Waveguides	838
<i>E.R. Bartuli</i> , Eigenoscillations Near the System of Strips in a Channel	841
<i>A.S. Bugaev, V.V. Pogrebnyak</i> , Interference of Acoustic Waves in Solid Layer with Periodically Irregular Boundary	844
<i>A.Yu. Panchenko</i> , Effect of Mutual Excitation of Electromagnetic and Acoustic Waves in Cavity Resonator	847
<i>A.I. Makarov</i> , Eigenoscillations Near the Arrow-Type Strip in a Channel, 3D Effects	850
<i>E.A. Gevorkyan</i> , Electromagnetic Waves in a Waveguide with a Space-Time Multiperiodic Dielectric Filling	853

Random Media and Rough Surfaces

<i>S.A. Zhevakin</i> , The Probability Distribution of Electromagnetic Wave Intensity Formed by Its Passage Through Rain Fractal Model	857
<i>L.G. Grechko, A.Y. Blank, V.V. Motrich, L.V. Garanina</i> , Effective Dielectric Permittivity of a Random Collection of Fine Metallic Particles with an Account of Multipole Interaction	860
<i>A.I. Timchenko</i> , Influence of Angular Correlations on the Intensity of Scattering from Icebergs	863
<i>V.G. Spitsyn</i> , Stochastic Model of Interaction of Electromagnetic Waves with Active Random Media	866
<i>M. Gilman</i> , Averaged Rough Surface Backscattering vs. Bispectral Characteristics of Surface Shape	869
<i>N.M. Makarov, A.V. Moroz</i> , Is There a Physical Coherence between the Problems of Wave Scattering from Absolutely Soft and Impedance Rough Surfaces?	872
<i>K.P. Gaikovich</i> , Damping of Thermal Emission Interference in Oil-Water Emulsions.....	874
<i>M.A. Guzev, G.V. Popov</i> , Joint Influence of Regular and Random Nonhomogeneities of the Statistical Characteristics of Waves in Layered Medium	877

<i>A.V. Poljarus, A.A. Koval, V.V. Fatafutdinov</i> , Mathematical Method of the Analysis of «Radar-Tropospheric Waveguide-Low Flying Target over Sea Surface» Radar Channel	880
<i>M.V. Tinin, N.T. Afanasyev, A.V. Kulizhsky</i> , Signal Structure in the Vicinity of the Background Simple Caustic of Randomly-Inhomogeneous Medium	883
<i>O.V. Bagatskaya, S.N. Shulga</i> , Plane Wave Scattering Coefficients for a Random Surface of Arbitrary Layered Anisotropic Dielectric	886
<i>A.N. Churyumov, Y.A. Kravtsov, K.C. Litovchenko, M.I. Mityagina</i> , Non-Resonant Mechanism of Electromagnetic Backscattering from the Sea Surface Disturbed by Internal Waves	889
<i>N.M. Makarov, Yu.V. Tarasov</i> , The Resonance Expansion Method in Surface Scattering Problems: Transmittance of Narrow Rough-Boundary 2D Strips	891
<i>N. Singh, A. Mohan</i> , Determination of Size and Number Density of Water Droplets in the Measurement of Intensity of Scattered Light	894

Lasers and Optical Fibers

<i>I.A. Sukhoivanov</i> , Large Signal Analysis of the Modulation Response of High Speed Quantum Well Lasers	899
<i>M. Samokhvalov</i> , Beam Propagation Method for Simulation of Performances of Vertical Cavity Surface Emitting Lasers	902
<i>A.A. Khrutchinsky, D.Y. Churmakov</i> , Numerical Simulation of Interaction of Shortwave High Laser Pulses with Substance	905
<i>R. Kravetz, Yu. Gaidai, W. Zaets</i> , Nonreciprocal Effect in Transverse-Magnetized Ferromagnetic-Metal-on-Amplifier Magneto-optical Waveguides	908
<i>A. Ehrhardt, C. Caspar, H.-M. Foisel, B. Strebel</i> , 4000 km 2.5 Gbit/s Single Channel Laboratory and 245 km 4x2.5 Gbit/s Field Transmission Experiment of Chirped WDM Signals over Dispersion Compensated Standard Single-Mode Fibre Trunks ..	911
<i>V.V. Lysak</i> , Nonlinear Effects of Optical Gain in the Quantum-Well Laser Diodes	914
<i>K.A. Milstein, E.A. Pogoryelov</i> , Frequency Characteristics of Optical Traveling-Wave Modulator Built on Tapered Coupler	917
<i>E.V. Kuzmichova</i> , Method of Investigation of Linear Polarization of Intensive Laser Radiation	920
<i>W. Szczesny, M. Marciniak</i> , Results of Numerical Simulation of Wavelength Multiplexed Transmission in Non-Linear Optical Fiber Telecommunication System	923
<i>I.V. Meglinsky, V.V. Tuchin, S.E. Skipetrov, S.S. Chesnokov</i> , Diffuse Photon Probes of Dynamic Nonhomogeneities in Random High Scattering Media	927
<i>K.N. Gura, F.M. Repa</i> , Current Suppression by External Electromagnetic Self-Detecting Structure in Galvanomagnetic Converters of Electromagnetic Field	930
<i>Authors Index</i>	931

Plenary Sessions

Ill-posed Inverse Problems Based on Volterra-Type Equations¹ (invited)

K.P. Gaikovich

*Radiophysical Research Institute, B. Pecherskaya st., 25,
Nizhny Novgorod, Russia, 603600,
Phone: 8312 367294, Fax: 8312 369902, E-mail: gai@nirfi.nnov.su*

Abstract - As it is well known, inverse problems based on Volterra equations are, as a rule, well-posed. But in the case when a function should be retrieved in the range which is wider than the range where the right side of the equation is given, the solution appears an ill-posed inverse problem. A number of physical examples is given, and it is shown that such inverse problems could be successfully solved on the basis of Tikhonov's method of general discrepancy.

Introduction

Let us consider the Volterra-type equations of the 1-st and 2-nd kind:

$$\int_a^t K(t,s)\varphi(s)ds = f(t), \quad (1)$$

$$\varphi(t) + \lambda \int_a^t K(t,s)\varphi(s)ds = f(t). \quad (2)$$

These equations are practically well-posed in $[a,b]$, when the right side of (1) or (2) is given in the same range $a \leq t \leq b$. More exactly, the equation (2) has a continuous and unique solution, if the kernel and the right side of (1) are continuous in $[a,b]$. The equation (1) has the continuous solution, if there are continuous derivatives $\frac{df}{dt}$ and $\frac{\partial K}{\partial t}$, $f(a) = 0$, and $K(t,t) \neq 0$ in $[a,b]$.

There is the possibility of the new formulation of the problem for the Volterra-type equations. It appears, when the right side of equations (1) and (2) is given in the $[a,c]$, where $c < b$, i.e., when the retrieval range is wider than the range, in which the right side $f(t)$ is given. In that case (1) and (2) can be rewritten as

$$\int_a^c K(t,s)\varphi(s)ds = f(t) - \int_c^t K(t,s)\varphi(s)ds = F(t), \quad (3)$$

$$\lambda \int_a^c K(t,s)\varphi(s)ds = f(t) - \varphi(t) - \int_c^t K(t,s)\varphi(s)ds = F'(t). \quad (4)$$

¹ This work was supported by RFBR under grant 96-02-16514 and by grant of Russian Education Ministry.

One can see that if we suppose that not only $f(t)$ is known in $[a, c]$ but also the function $\varphi(s)$, we have the effective right sides $F(t)$ and $F'(t)$, and equations (3) and (4) are Fredholm integral equations of the 1-st kind relative the solution in $[c, b]$. Such equations are typical ill-posed problems. It is clear, that the solution of (1) and (2) in the whole range $[a, b]$ by $f(t)$ given in $[a, c]$ is still more complicated problem. In this case these integral equations are the ill-posed, type of which has yet no special name.

The most effective approach to solution of ill-posed integral equations is the Tikhonov's theory based on generalized discrepancy principle and the solution method of the same name [1]. The main preference of Tikhonov's method consist in the uniform convergence of the retrieval error to zero at mean square convergence of right side errors. As it is in all ill-posed problems, its accuracy could be determined only on the basis of numerical simulation.

Physical problems based on ill-posed Volterra-type equations

Physical problems related with integral equations are, as a rule, inverse problems. Some of them consist in the solution of Volterra equations, and could be considered in the described above formulation as ill-posed problems. Some examples are presented here.

1. Refraction inverse problem in a spherical symmetry medium [2,3].

a. Limb-viewing geometry [2].

For limb-viewing measurements the refraction inverse problem can be expressed as the Volterra-type integral equation of the 1-st kind (the dependence of refraction ε on radial distance of ray perigee):

$$10^{-6} \int_{p_0}^{p_{\max}} \frac{dN}{dp}(p) \frac{-2p}{\sqrt{p^2 - p_0^2}} dp = \varepsilon(p_0), \quad p_1 \leq p_0 \leq p_{\max}, \quad (1)$$

where $p = nr$, $n_0 = n(r_0)$, $p_0 = n_0 r_0$, r, r_0 are radial distances, $N = 10^6(n-1)$ is refraction index, n is refractive index.

b. Immersion geometry [3].

The dependence of refraction on radial position (distance) of the source or receiver in the medium can be expressed as Volterra integral equation of the 2-nd kind:

$$N(p_0) - \int_{p_0}^{p_{\max}} N(p) \frac{pp_0 \cos \theta(p_0)}{[p^2 - [p_0 \cos \theta(p_0)]^2]^{3/2}} dp = 10^6 \operatorname{tg} \theta \varepsilon(p_0), \quad p_1 \leq p_0 \leq p_{\max}, \quad (2)$$

where θ is the elevation angle of the ray at the source position.

If one considers the equations (1) or (2) in the case, when their right side is given in the region $p_1 \leq p_0 \leq p_2$, $p_2 < p_{\max}$, the solution for the region $p_1 \leq p \leq p_{\max}$ becomes an ill-posed problem. Similar equations describe the radiometry inverse problems of limb-viewing and immersion remote sensing of planet atmospheres [4].

2. Diagnostics of the superconductive films in a strong electromagnetic field [5-6].

The measured dependence of averaged over the conductor surface resistance on magnetic field amplitude in the case of one-dimensional distribution of magnetic field H in a rectangular cavity resonator is related with the true resistance dependence $R_s(H)$ as

$$\langle R_s(H_m) \rangle = \frac{4}{\pi H_m} \int_0^{H_m} \frac{(H/H_m)^2}{\sqrt{1-(H/H_m)^2}} R_s(H) dH, \quad 0 \leq H_m \leq H_{\max}, \quad (3)$$

The inverse problem of $R_s(H)$ retrieval in the range $0 \leq H_m \leq H_{\max}$ becomes ill-posed in real conditions, when the measurements region is limited at low magnetic field values, and there are measurements only in the range $H_2 \leq H_m \leq H_{\max}$.

3. Thermal history inverse problems.

a. Thermal conductivity equation for half-space.

Let us consider the homogeneous half-space $z \leq 0$ with the constant parameters: thermal diffusivity coefficient α^2 . If we have boundary condition for temperature $T(0,t) = T_0(t)$, then the dynamics of the temperature distribution inside the half-space can be determined from thermal conductivity equation as a function of depth and time as follows:

$$T(z,t) = \int_{-\infty}^t T_0(\tau) \frac{-z}{\sqrt{4\pi\alpha^2(t-\tau)^3}} \exp\left(-\frac{z^2}{4\alpha^2(t-\tau)}\right) d\tau. \quad (4)$$

The inverse problem consist of retrieval of the boundary condition $T_0(t)$ by measurements $T(z,t)$. There are two possibilities: the first of them (Tikhonov's [1]) is based on measurements of depth profile $T(z)$ at time t_0 , and the second (considered here as ill-posed Volterra-type equation) is based on measurements $T(t)$ at some arbitrary depth z_0 in the range $a \leq t \leq b$. The retrieval in this, second, case should be found in the region $[c,b]$, where $c < a$. For the solution the necessary condition is $T_0(t) \equiv 0$ at $t < c$ (otherwise, it will be unaccounted source of error).

b. Thermal conductivity equation for space with the spherically symmetric source.

If we have the homogeneous space $r \geq 0$ with the boundary condition $T(R,t) = T_0(t)$ on the sphere $r = R$, the temperature evolution in the region $r > R$ is determined by

$$T(r,t) = \int_{-\infty}^t T_0(\tau) \frac{R(r-R)}{r\sqrt{4\pi\alpha^2(t-\tau)^3}} \exp\left(-\frac{(r-R)^2}{4\alpha^2(t-\tau)}\right) d\tau \quad (5)$$

The ill-posed Volterra-type equation for (5) is the same as for (4) - to retrieve the $T_0(R,t)$ in the range $a \leq t \leq b$ by $T(r_0,t)$ at some arbitrary radial distance r_0 in the region $[c,b]$, $c < a$.

c. Retrieval of temperature evolution of media by thermal emission dynamics.

More sophisticated inverse problems are based on simultaneous solution of thermal conductivity and thermal emission transfer equations [7]. The brightness temperature of upward thermal radio emission of half-space $z \leq 0$ at wavelength λ is determined from emission transfer equation, assuming that the reflection on half-space interface is absent :

$$T_b(\lambda) = \int_{-\infty}^0 T(z)\gamma(\lambda)\exp(\gamma z)dz, \quad (6)$$

where $\gamma(\lambda)$ is the absorption coefficient.

The substitution of (4) into (6) gives [7]:

$$T_b(t) = \int_{-\infty}^t T_0(\tau) \left[\frac{\gamma a}{\sqrt{\pi(t-\tau)}} - (\gamma a)^2 \operatorname{erfc}(\gamma a \sqrt{t-\tau}) e^{(\gamma a)^2(t-\tau)} \right] d\tau \quad (7)$$

If the function $T_b(t)$ is known in the whole region $(-\infty, b]$, the equation (7) has the exact solution [7]:

$$T_0(t) = T_b(t) + \frac{1}{\gamma a} \int_{-\infty}^t (T_b(t) - T_b(\tau)) \frac{d\tau}{\sqrt{\pi(t-\tau)^3}} \quad (8)$$

Otherwise, if $T_b(t)$ is known in some limited region $[a, b]$, the problem of retrieval of $T_0(t)$ in the region $[c, b]$, where $c < a$, is also the Volterra-type ill-posed problem.

For the sphere case (see item b), there are different possibilities to choose the beam geometry, which determines the form of emission transfer integral. The most simple equation corresponds to the case of radial directed (from sphere) measurements:

$$T_b(t) = \int_{-\infty}^t T_0(\tau) \left[\int_R^{\infty} \frac{\gamma}{\sqrt{4\pi a^2}} \frac{R(r-R)}{r} e^{-\frac{(r-R)^2}{4a^2(t-\tau)} - \gamma(r-R)} dr \right] \frac{d\tau}{\sqrt{(t-\tau)^3}} \quad (9)$$

More common case, when a ray perigee radial distance $r_0 \neq 0$ ($r_0 > R$), the radiobrightness can be expressed as

$$T_b(t) = \int_{-\infty}^t T_0(\tau) \left[\int_{r_0}^{R_0} \frac{\gamma}{\sqrt{4\pi a^2}} \frac{R(r-R)}{\sqrt{r^2 - r_0^2}} e^{-\frac{(r-R)^2}{4a^2(t-\tau)} - \gamma(\sqrt{R_0^2 - r_0^2} - \sqrt{r^2 - r_0^2})} dr + \right. \\ \left. + \int_{r_0}^{\infty} \frac{\gamma}{\sqrt{4\pi a^2}} \frac{R(r-R)}{\sqrt{r^2 - r_0^2}} e^{-\frac{(r-R)^2}{4a^2(t-\tau)} - \gamma(\sqrt{R_0^2 - r_0^2} + \sqrt{r^2 - r_0^2})} dr \right] \frac{d\tau}{\sqrt{(t-\tau)^3}} \quad (10)$$

where R_0 is the radial distance of the receiver. The ill-posed Volterra-type equations for (9) and (10) are the same as for (7). For the equation (10) there is also the possibility to formulate the limb-viewing inverse problems, similar with refraction inverse problems (see equations (1) and (2)), using the dependence $T_b(r_0)$.

Let us consider the solution of equation (7) in detail as a typical example of ill-posed Volterra-type equations. If to introduce the time parameter $\Gamma = 1/(\gamma a)^2$, which is a typical time of the heating of the medium at the skin-depth $z_s = 1/\gamma$, it is possible to rewrite (7) in simpler, dimensionless form, using dimensionless parameters $r = t/\Gamma$, $\rho = \tau/\Gamma$:

$$T_b(r) = \int_{-\infty}^r T_0(\rho) \left[\frac{1}{\sqrt{\pi(r-\rho)}} - \operatorname{erfc}(\sqrt{r-\rho}) e^{(r-\rho)} \right] d\rho \quad (11)$$

To solve such a problem it is necessary to use additional (*a priori*) information about the exact solution. This information determines a regularization method. There are various approaches, but in the present paper Tikhonov's method of generalized discrepancy is applied, which uses the common information about the exact solution as a function []. It is supposed in this method that the exact solution belongs to the set of square-integrable functions with square-integrable derivatives. The results of numerical simulation give us the retrieval accuracy at various levels of the radiobrightness error. It appears possible to retrieve the function $T_0(\rho)$ in the range $[c/\Gamma, b/\Gamma]$ by measurements $T_b(r)$ in the range $[a/\Gamma, b/\Gamma]$, $c < a$, up to values $a - c \approx 2 \div 5 \Gamma$ at measurement accuracy about 1%. The main preference of Tikhonov's method consist of the uniform convergence of the retrieval error to zero at mean square convergence of measurement errors. As in all ill-posed problems, this convergence is slower than it is in well-posed problems.

The numerical algorithm of the Tikhonov's method (the same as in [6]) was applied to the retrieval of diurnal temperature dynamics of soil by its thermal radio emission evolution measurements [8]. The measurements have been carried out using radiometers at wavelengths 0.8; 3; 9, and 13 cm under metallic screen (to eliminate the influence of reflection on interface air-soil). In the Fig.1 is shown an example of retrieval of the surface temperature in time interval from 15^h ($r = 0$) to 12^h20^m ($r = 8.25$) next day by measurements of radiobrightness at wavelength 3 cm in time interval from 3^h10^m (after midnight) to 12^h20^m. The parameters values were: $\alpha^2 = 0.001 \text{ cm}^2/\text{s}$, $\gamma = 0.33 \text{ cm}^{-1}$, $\Gamma = 2.55 \text{ h}$. So, $a = 15^{\text{h}}$, $b = 12^{\text{h}}20^{\text{m}}$, $c = 3^{\text{h}}10^{\text{m}}$.

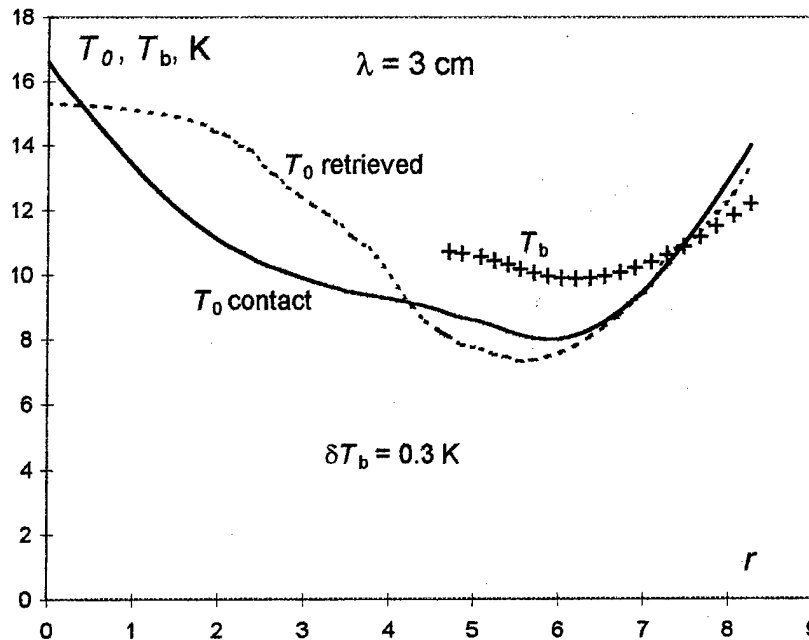


Fig.1.

It is possible to see that the retrieval in the time interval $t > a$, where there are measurements $T_b(t)$, is very close to contact measured dynamics $T_0(t)$. At $c \leq t \leq a$ the

accuracy of the surface temperature history retrieval reduces, but it appeared possible to retrieve the process of night surface cooling. It is clear that the problem is more difficult for retrieval of the thermal history than for retrieval of simultaneous surface temperature dynamics.

The retrieval of the surface temperature dynamics permit then to retrieve the temperature profile dynamics in the medium from the equation (4), and to calculate the thermal flux evolution [7].

Conclusions

The results of the solution of various physical problems based on Volterra-type integral equation in considered here ill-posed formulation show that the domain of definition of the solution consist of two very different sub-ranges. The first sub-region (which could be called «inner») coincides with the domain of definition of equations right side. The second (outer) sub-range is located outside the domain of definition of equations right side. The approximate solution in the outer region (as, for example, for the considered here in detail thermal history inverse problem) diverges to the exact one much more slowly than in the inner sub-region. In the inner sub-region the requirements to data accuracy could be very different in different physical problems, but always they are less than for outer sub-region. Moreover, in the outer sub-region the retrieval accuracy reduces with the distance to the boundary of inner sub-region. Considered here new formulation solves the problem of influence of unknown non-zero initial conditions on the solution of Volterra equations. No doubt, there are many possible applications of this approach, which remain unmentioned in this communication.

References

1. Tikhonov A.N., Goncharsky A.V., Stepanov V.V., Yagola A.G. Regularization algorithms and *a priori* information. Moscow, Nauka, 1983.
2. Gaikovich K.P., Tchernyaeva M.B. Limb-viewing refraction inverse problem in duct case. The present issue.
3. Gaikovich K.P., Khacheva G.Yu. Interrelation of refraction and atmosphere refractive index in partial immersion geometry. Conf. Proc. of 7-th Int. Crimean Conf. «Microwave and Telecommunication Technology» (Crimea, Ukraine, Sevastopol, Sept.15-18, 1997), 1997, Sevastopol: Weber Co., pp.681-683.
4. Gaikovich K.P., Tchernyaeva M.B. The problem of limb-viewing microwave remote sensing in ill-posed formulation. Conf. Proc. of 7-th Int. Crimean Conf. «Microwave and Telecommunication Technology» (Crimea, Ukraine, Sevastopol, Sept.15-18, 1997), 1997, Sevastopol: Weber Co., pp.681-683.
5. Gaikovich K.P., Reznik A.N. A.N. Inverse problems of nonlinear electrodynamics of HTSC. X German - Russian - Ukrainian Seminar on High Temperature Superconductivity (N.Novgorod, Russia, 11-15 Sept.1997), 1997, N.Novgorod: IPM RAS, p.149.
6. Gaikovich K.P., Reznik A.N. Technique for determination of RF-magnetic field dependence of the HTS surface impedance by microwave resonators. The present issue.
7. Gaikovich K.P. Simultaneous solution of emission transfer and thermal conductivity equations in the problems of atmosphere and subsurface radiothermometry. IEEE Trans. Geosci. Remote Sens., vol.32, pp.885-889, 1994.
8. Gaikovich K.P., Reznik A.N., and Troitskii R.V. Microwave subsurface profile thermometry. Digest of IGARSS'91, 1991, Univ. Technol., Espoo, Finland, vol.3, pp.1195-1198.

REMOTE SENSING BY VLF USING "ABSOLUTE OMNIPAL": 1. INVESTIGATION OF SHORT PATH PROPAGATION FOR POSSIBLE EARTHQUAKE PRECURSOR DETECTION

R. L. Dowden, J. B. Brundell, University of Otago, Dunedin, New Zealand
M. Hayakawa, University of Electro-Communications, Chofu, Tokyo, Japan

Abstract. The latest version of the OmniPAL receiver uses GPS to allow drift free logging of the phase and amplitude of phase stable transmissions. Any drift in phase or amplitude can then be attributed to temporal variation of the lower ionosphere. In this paper, the first six weeks of data logged of JG2AS phase and amplitude at three sites in Japan is examined for perturbations. Two sources are identified: solar flares during daytime and hiss-induced electron precipitation during nighttime. Both of these sources have durations of the order of an hour and, in principle, could be detected by other means and the LF effects allowed for. However, if earthquake precursors have much longer periods (days), the effects of solar flares and electron precipitation can be ignored.

VLF/LF Receivers

OmniPAL. The OmniPAL VLF/LF receiver consists of a special DSP card, software which is the heart of the receiver, and various ancillaries which may be user supplied. "Omni" means that "all" modulations can be decoded. Currently these are MSK (Minimum Shift Keyed), CW (Carrier Wave only) and ICW (Interrupted Carrier Wave or On/Off modulation including 10 dB modulation). Others (e.g. FSK) are not used by any phase stable VLF (< 50 kHz) transmitters and so are not supported. The OmniPAL VLF receiver can log up to six transmitters at a time, logging phase and amplitude (PAL) with time resolutions ranging from 50 ms to 60 s. Special techniques (see Section 2. "Validation Procedures" in Dowden, *et al.*, 1994) make OmniPAL almost insensitive to sferics. Measurement of the phase and amplitude perturbations (Trimpis) enables calculation of the phase and amplitude of the diffracted wave [Dowden and Adams, 1988]. If this is done at two sites simultaneously, the direction of arrival of the scattered wave can be found [Dowden and Adams, 1990]. Measurement of the phase and amplitude perturbations at all time points from onset to ultimate decay, and the transformation of these to scatter phase and amplitude, can be used to identify the plasma formed by a "Red Sprite" which exhibits scatter amplitude decay with the logarithm of time [Dowden *et al.*, 1997; Dowden and Rodger, 1997]. The scatter phase variation (Doppler shift) during decay may be due to high altitude (60 - 80 km) winds [Dowden, 1996].

For MSK transmissions, phase and amplitude at both MSK frequencies, 50 or 100 Hz apart, are logged separately. Measurements of all four perturbations enable calculation of the arrival delay of the scattered wave relative to the direct wave from the transmitter [Adams and Dowden, 1990]. In principal this allows location of the source of the VLF perturbation [Dowden and Adams, 1993].

In its basic form, OmniPAL requires a stable frequency standard (5 MHz). For Trimpis studies this would need to be stable to at least 1 part in 10^8 . This would keep the phase drift of a 20 kHz signal to within 5 degrees per minute — more drift than this would seriously degrade phase measurement of Trimpis. Such stability can be provided by a well-aged, temperature controlled quartz standard. To measure departures in phase of a few degrees over days, months, or even years, requires a frequency stability of a million times better than this (1 part in 10^{14}) which is beyond the ability of even Cesium standards and certainly beyond the financial reach of researchers requiring a network of receivers.

AbsPAL. The AbsPAL VLF receiver, an extension of the OmniPAL receiver, gets around this difficulty with an all-up cost of about US\$5000. The AbsPAL still has all of the good features of OmniPAL for Trimpi studies as described above, as well as logging the phase of VLF and LF signals as a time independent absolute. This means that if the received phase of a perfectly stable transmission is (say) 121 degrees now, the received phase will still be 121 degrees in a year's time, even if the AbsPAL receiver is turned off many times for extended periods, intentionally or by accident.

Clearly this requires that both the VLF/LF transmitters and the AbsPAL receivers be locked to the same world time standard as is now disseminated by GPS.

AbsPAL achieves this in the following way. A "Service Unit" contains a quartz oscillator inside a small box having a thermal time constant of about 30 minutes. The 10 MHz output synthesises 30 kHz and 30.1 kHz. The GPS 1pps pulse, which arrives within 1 μ s of true time, resets (zeros) all the dividers and so the phase of the 30 kHz and 30.1 kHz signals every second. These frequencies need to be accurate to only 1 in 10^6 .

The AbsPAL software can synthesise several frequencies at once which are multiples of 1 Hz. On startup it reads the batch file to find which frequencies are required by the user (which must include 30 kHz), then waits for the GPS 1pps to set the phase of all these frequencies to zero at the GPS pulse. Although the latter can be up to 1 μ s early or late with respect to true Universal Time (UT), implying a phase error of up to 15 degrees at 40 kHz (JG2AS), any such error is removed as follows. A software phase locked loop (PLL) locks AbsPAL to the phase of the 30 kHz from the Service Unit. This PLL has a bandwidth of initially 1 Hz or reciprocal bandwidth (RBW) of 1 s. At every later second the RBW is increased by 1 s so that after 1000 s, the PLL bandwidth is only 1 mHz. Eventually, the RBW reaches the value set by the user in the batch file (such as 30 minutes or 1800 s) and remains at that value. Averaged over this period the GPS time error, and so the 30 kHz phase error is very small, and in any case is absolutely drift free. All the frequencies synthesised by AbsPAL are "gear wheeled" (like clockwork) to this 30 kHz.

Generation and logging of the 30.1 kHz might seem to have no purpose since both its phase and that of 30 kHz "must" be near to zero. However, if the GPS signal is removed from the Service Unit, the phase locking stops. If returned many minutes or hours later, and if AbsPAL is not then restarted, the 30.1 kHz will probably not have the same phase as 30 kHz. Should this happen, a correction calculated from the phase difference can be applied to the data at analysis time.

Investigation of Short Path Propagation of the JG2AS Transmission

The first AbsPAL VLF receivers were designed and built under contract to NASDA (the Japanese National Space Development Agency) for research into possible VLF precursors to earthquakes. Three of the five provided were installed in September, 1997, at the sites shown on the map in Figure 2. The first six weeks of data from these three are discussed here. These data used the Japanese time and frequency transmitter, JG2AS (40 kHz, 1kW radiated power) whose location is also shown on that map. The distances to each of the AbsPAL receivers from JG2AS are 800 km (Sapporo), 170 km (Shimizu) and 600 km (Kochi). The JG2AS signal/noise ratio was best at Sapporo and worst at Shimizu. This was due to the high noise environment at the Shimizu site which was only some 200 m from a large 4 x 3-phase EHT power transmission line.

Figure 1 shows the diurnal variation of the phase (lower set) and amplitude (upper set) of JG2AS observed at Sapporo. This consists of 38 superimposed traces. The strange appearance of the amplitude trace is due to many random transmission gaps by JG2AS usually lasting a few minutes and occurring a few times per day. This is not the regular On-Off Keying (OOK) for time code transmission which AbsPAL is designed to cope with. The data have

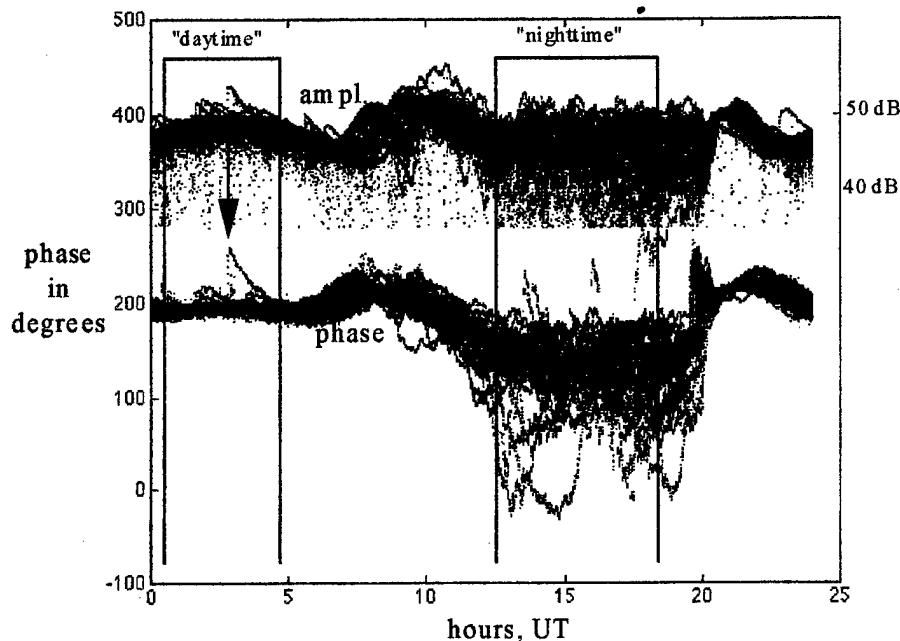


Figure 1. Superposition of 38 days of phase (lower set) and amplitude (upper) variation of the JG2AS signal received at Sapporo. The arrow at 02:47 marks the largest of many solar flare effects during the 38-day period. Local noon in Japan is at about 0300 UT. The inverted U-shaped windows mark the periods used to calculate the daytime and nighttime means shown in Figure 2.

been filtered by MATLAB to remove all rows (20 s apart) for which the amplitude dropped below 35 dB (rendering the phase meaningless), hence the cutoff in Figure 1.

Similar traces, but noisier, were obtained at Kochi. At Shimizu the noise was generally (it varied from day to day) too great for meaningful measurements.

A large solar flare occurred on the UT day 267 (24 September, 1997). This began at 02:47 UT, only about 10 minutes before local noon in Japan, increased to maximum within four minutes and then decayed to zero in about one hour. Further details on this flare can be obtained on the WWW at <ftp://uleth.ca/pub/solar/1997/>. The perturbation in phase and amplitude of the JG2AS signal is clearly seen at Sapporo (see double headed arrow in Figure 1) where the phase perturbation was 65 degrees and the amplitude perturbation was 4.2 dB. At Kochi, the perturbations are less obvious but measurable as 33 degrees in phase and 6.4 dB in amplitude (the ordinate scale in Figure 1 is in degrees for phase and in dB/8 for amplitude). At Shimizu, the perturbations are lost in the noise.

One would expect the effect of the flare on the lower ionosphere to be uniform over Japan. If we express all perturbations in terms of ratios (phase in radians, amplitude normalised to the unperturbed amplitude) the magnitude of the total perturbation is approximately given by the square root of the sum of the squares. Thus the magnitude of the flare-induced perturbation measured at Sapporo is within about 10% of that at Kochi and so essentially the same within the approximations and errors involved, though the Kochi amplitude perturbation is nearly four times the Kochi phase perturbation in these ratio units, while the amplitude and phase amplitudes are about equal at Sapporo. This is due to modal interference — the phase difference between the dominant modes may be decreased by the solar flare modification of the ionosphere (lowering the effective LF reflection altitude) thus increasing the received amplitude. In any case, whatever the reason for this, an earthquake precursor may effect the ionosphere the same way so both phase and amplitude perturbations should be measured to calculate the total perturbation.

Careful inspection of the traces in Figure 1 during the times around local noon (23 UT to 07 UT) show many smaller perturbations having the characteristic shape of solar flare-induced perturbations ("flare trimpis"? — fast up, slow down. The periods indicated in Figure 1 by the inverted U shapes are those used for finding the "daytime" and "nighttime" average for each day to be discussed later. Note that the relatively frequent solar flares will have a significant effect on the day to day variation of the daytime averages. If we assume that solar flares affect the daylit ionosphere uniformly, it might be possible to remove the flare effects from the phase and amplitude data later.

On the other hand, the nighttime means cannot be directly affected by solar flares, though maybe indirectly via electron precipitation with a delay of a few days. The Sun's steady XUV is by far the dominant source of ionisation of the lower ionosphere, and so of the LF reflection altitude, during the day. Thus one would expect that the nighttime JG2AS phase and amplitude means would be a sensitive measure of the much weaker causes of ionospheric modification such as cosmic rays, electron precipitation and earthquake precursors. Of these, the slowly varying (months) cosmic ray flux would effect the lower ionosphere uniformly over vast areas. Electron precipitation and (presumably) earthquake precursors effect the lower ionosphere over small areas having lateral dimensions of 100 km or so. As seen in Figure 1, the day to day nighttime means are likely dominated by large perturbations having a duration of a few hours. Earthquake precursors are supposed to develop over a few days. Mid latitude hiss bursts, which are thought to result in electron precipitation, have similar durations to those observed in Figure 1 [Dowden, 1962]. With continuous recording of hiss at two or three sites (for location), it might be possible to remove electron precipitation effects from the nighttime phase and amplitude data later.

Figure 2 shows the phase and amplitude means during daytime and (except for Shimizu) nighttime. No attempt has been made to "correct" the data for solar flare or electron precipitation effects. In fact, the effect of the solar flare on Day 267 is clearly seen in the Sapporo data and, less clearly, in the Kochi data. Trends such as the slow increase in the JG2AS phase means at Shimizu and (less clearly due to gap) at Kochi may be an earthquake precursor (no earthquake data was available at the time of writing). If this slow change over many days is typical of earthquake precursors, we can probably ignore the effects of solar flares and electron precipitation which vary randomly from day to day.

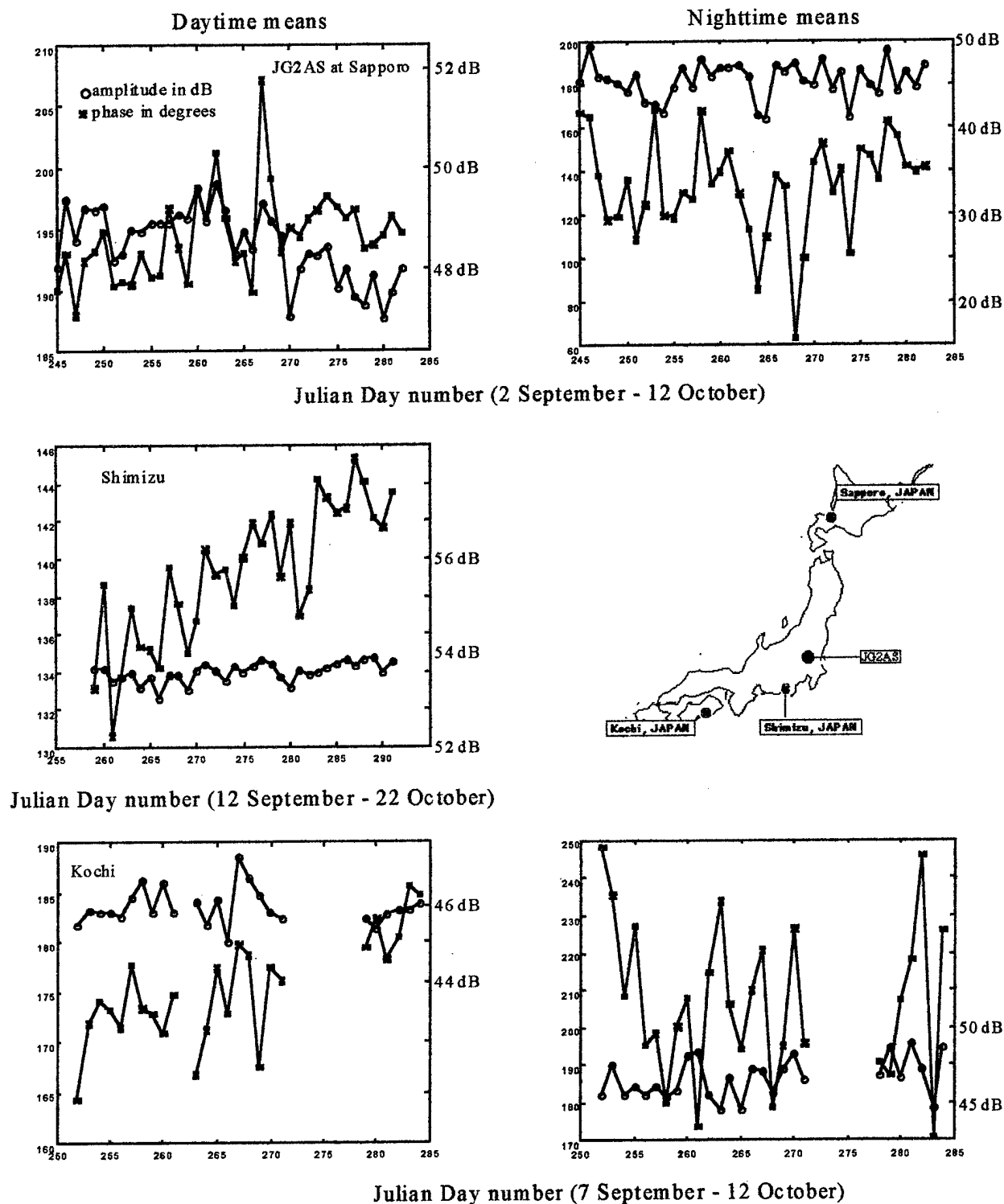


Figure 2. Phase and amplitude means during daytime and (except for Shimizu) nighttime. The panels show the means for Sapporo (top), Shimizu (middle) and Kochi (bottom) in the same order, north to south, as the site positions shown on the map. The phase means (in degrees on left hand scales) are shown as asterisks (*) and the amplitudes (right hand scales) as circles (o). Gaps in the panels for Kochi show data lost when the GPS signal was accidentally removed.

References

- [1]. Adams, C.D.D. and Dowden, R.L., VLF group delay of LEP echoes from measurement of phase and amplitude perturbations at two frequencies, *J. Geophysical Research*, **95**:2457 (1990).
- [2]. Dowden, R. L., Wide band bursts of VLF radio noise ('hiss') at Hobart, *Australian J. Physics*, **15**:114-119 (1962).
- [3]. Dowden, R.L., Distortion of Trimpis shapes by high altitude winds, *J. Geophysical Research*, **101**:315-321 (1996).
- [4]. Dowden, R.L., and Adams, C.D.D., Phase and amplitude perturbations on subionospheric signals explained in terms of echoes from lightning-induced electron precipitation ionization patches, *J. Geophysical Research*, **93**:11,543, 1988.
- [5]. Dowden, R.L., and Adams, C.D.D., Location of LEP from measurement of phase and amplitude perturbations on spaced antennas and on two frequencies, *J. Geophysical Research*, **95**:4135-4145, 1990.
- [6]. Dowden, R.L., Adams, C.D.D., Brundell, J. and Dowden, P.E., Rapid onset, rapid decay (RORD), phase and amplitude perturbations of VLF subionospheric transmissions, *J. Atmospheric and Terrestrial Physics*, **56**:1513-1527 (1994).
- [7]. Dowden, R.L., and Adams, C.D.D., Size and location of lightning-induced ionisation enhancements from measurement of VLF phase and amplitude perturbations on multiple antennas, *J. Atmospheric and Terrestrial Physics*, **55**:1335-1359 (1993).
- [8]. Dowden, R. L., and Rodger, C. J., Decay of a vertical plasma column: A model to explain VLF sprites, *Geophysical Research Letters*, **24**:2765-2768 (1997).
- [9]. Dowden, R.L., Brundell, J. B., and Rodger, C. J., Temporal evolution of very strong Trimpis observed at Darwin, Australia, *Geophysical Research Letters*, **24**:2419-2423 (1997).

Regularization of Maxwell Equations, Corner Singularities and Approximation

Marc Lenoir

LSM ENSTA-CNRS, Palaiseau, France, e-mail: lenoir@ensta.fr

The aim of this paper is to describe different formulations for the time-harmonic scattering of electromagnetic waves, with special emphasis about the consequences of the choice of the formulation on the finite elements discretization. Despite the fact that any solution of the problem is divergence-free, one must take account explicitly of this condition, for the associated operator is not strongly elliptic. Roughly speaking, one may handle this constraint either by duality or by penalty. Actually, the special form of Maxwell's equations makes the Lagrange multiplier a priori known, and the solution independent of the penalization coefficient. An other particular feature of the problem comes from the low regularity of the electromagnetic field in the vicinity of edges and conical points, from which follows that special care must be taken of the choice of the function space for the penalty method.

1 The classical problem

We address the problem of the scattering by a perfect conductor, possibly surrounded by a bounded inhomogeneous region. For the sake of definiteness, we only consider the non dissipative case. By U we denote the electric or the magnetic field, and by ζ and ξ the dielectric permittivity and the magnetic permeability (assumed real positive), the choice depending on the signification of U . In the vicinity of infinity, the medium is assumed homogeneous and the values of the coefficients is denoted by ζ_0 and ξ_0 . In this region, Maxwell's equations write as

$$\operatorname{curl} \operatorname{curl} U - k_s^2 U = 0 \text{ with } k_s^2 = \omega^2 \zeta_0 \xi_0 \quad (1)$$

where ω is the pulsation of the incoming wave U_I , and $U - U_I$ is subject to the Silver-Müller radiation condition:

$$\lim_{R \rightarrow \infty} \int_{\partial B_R} \|\operatorname{curl}(U - U_I) \wedge n - ik_s(U - U_I)\|^2 d\gamma = 0. \quad (2)$$

In the whole exterior domain Ω , and especially in the vicinity of the conductor we have

$$\operatorname{curl} (\zeta^{-1} \operatorname{curl} U) - \omega^2 \xi U = 0, \quad (3)$$

with one of the following boundary conditions,

$$U \wedge n = 0 \text{ (electric field), or } \operatorname{curl} U \wedge n = 0 \text{ (magnetic field).} \quad (4)$$

1.1 Weak formulation

At least locally, the more natural variational formulation would be

$$\begin{aligned} &\text{Find } U \in \mathcal{F}^{E/H}, \text{ such that } \forall V \in \mathcal{F}^{E/H}, \text{ compactly supported,} \\ &\int_{\Omega} \zeta^{-1} (\operatorname{curl} U | \operatorname{curl} V) - \omega^2 \int_{\Omega} \xi (U | V) = 0, \text{ with} \end{aligned} \quad (5)$$

$$\mathcal{F}^E = \{V \in H_{\text{loc}}(\text{curl}; \Omega) \mid V \wedge n|_{\Gamma} = 0\} \text{ and } \mathcal{F}^H = H_{\text{loc}}(\text{curl}; \Omega) \quad (6)$$

It turns out that the natural injection $\mathcal{F}^{E/H} \rightarrow L^2(\Omega)$ is not locally compact, which leads to the choice of smaller spaces, namely

$$\mathcal{F}_{\infty}^E = \{V \in \mathcal{F}^E \mid \text{div } \xi V = 0\} \text{ and } \mathcal{F}_{\infty}^H = \left\{V \in \mathcal{F}^H \mid (H|n)|_{\Gamma} = 0, \text{div } \xi V = 0\right\}, \quad (7)$$

the constraints being actually easy consequences of the equations itself. If we denote by Σ a boundary surrounding the inhomogeneous region and by Ω' the bounded domain limited by Γ and Σ , a new formulation can be written as

$$\text{Find } U \in \mathcal{F}_{\infty}^{E/H}, \text{ verifying (2), such that } \forall V \in \mathcal{F}_{\infty}^{E/H}, \quad \int_{\Omega'} \zeta^{-1} (\text{curl } U | \text{curl } V) - \omega^2 \int_{\Omega'} \xi (U | V) + \zeta_0^{-1} \int_{\Sigma} (\text{curl } U \wedge n | n \wedge (V \wedge n)) d\gamma = 0 \quad (8)$$

Due to the constraints, recovering the strong equations from the weak ones is more difficult and makes use of the de Rham field decomposition, in a similar way as for Stokes equations.

1.2 Uniqueness

It is a consequence of the conservation of the incoming energy flux:

$$F_{\partial D}(U) = \frac{1}{2\omega} \text{Im} \int_{\partial D} \zeta^{-1} (\text{curl } U | U \wedge n) d\gamma \quad (9)$$

and of the radiation condition. Assume $U_I = 0$, as U satisfies (3) in the vicinity of infinity, then $\Delta U + k_s^2 U = 0$. Moreover from $F_{\partial \Omega}(U) = 0$, and the radiation condition it follows that $\lim_{R \rightarrow \infty} \int_{\partial B_R} \|U\|^2 d\gamma = 0$, and from Rellich's [5] theorem, that $U = 0$ in the vicinity of infinity. Now, U vanishes in the whole domain Ω as a consequence of the unique continuation theorem of [6].

1.3 Reduction to a bounded domain

A complete formulation must take properly into account the radiation condition, which can be imposed as a condition on the fictitious boundary Σ via the integral representation formula

$$U = U_I + \mathcal{R}_F^{\infty}[U] \quad (10)$$

with

$$\mathcal{R}_F^{\infty}[U](x) = \int_F (\mathbb{G}_{\infty}(x-y) \text{curl } U(y) \wedge n_y - \text{curl}_y \mathbb{G}_{\infty}(x-y) U(y) \wedge n_y) d\gamma_y \quad (11)$$

where the boundary F surrounds the inhomogeneous region and lies inside Σ , and \mathbb{G}_{∞} is the outgoing Green matrix given by

$$\mathbb{G}_{\infty} = g_{k_s} \mathbb{I} + k_s^{-2} \text{Hess } g_{k_s}, \text{ with } g_k = -\frac{e^{-ik\|x\|}}{4\pi \|x\|}$$

Indeed, let

$$T_{\lambda} U = \text{curl } U \wedge n + \lambda n \wedge (U \wedge n)|_{\Sigma} \quad (12)$$

then, one can prove that for $\text{Im}(\lambda k_s^{-2}) < 0$, the following problem, set in the bounded domain Ω' limited by Γ and Σ :

$$\text{Find } U' \in \mathcal{H}_{\infty}^{E/H}, \text{ such that } \forall V' \in \mathcal{H}_{\infty}^{E/H}, a_{\infty}(U', V') = \ell_{\infty}(V'), \quad (13)$$

with

$$\begin{aligned} \mathcal{H}_{\infty}^E &= \{V \in H(\text{curl}; \Omega') \mid \text{div } \xi V \in L^2(\Omega'), V \wedge n|_{\Gamma} = 0, V \wedge n|_{\Sigma} \in L^2(\Sigma)\} \\ \mathcal{H}_{\infty}^H &= \{V \in H(\text{curl}; \Omega') \mid \text{div } \xi V \in L^2(\Omega'), (V|n)|_{\Gamma} = 0, V \wedge n|_{\Sigma} \in L^2(\Sigma)\} \end{aligned} \quad (14)$$

and

$$\begin{aligned} a_{\infty}(U', V') &= \int_{\Omega'} \zeta^{-1} (\text{curl } U' | \text{curl } V') - \omega^2 \int_{\Omega'} \xi (U' | V') \\ &\quad + \zeta_0^{-1} \lambda \int_{\Sigma} (U' \wedge n | V' \wedge n) d\gamma - \zeta_0^{-1} \int_{\Sigma} (T_{\lambda} \mathcal{R}_F^{\infty}[U'] | V') d\gamma, \\ \ell_{\infty}(V') &= \zeta_0^{-1} \int_{\Sigma} (T_{\lambda} U_I | V') d\gamma, \end{aligned} \quad (15)$$

has one and only one solution: $U' = U|_{\Omega'}$, if and only if (8) has.

1.4 Existence

From the equivalence between (8) and (13), uniqueness for the reduced problem follows from uniqueness for (8). As problem (13) is set in a bounded domain, via Fredholm alternative, the existence of U' is an easy consequence of the regularity of the Green function outside zero and the local compactness result of Weber [7]; the existence of U follows.

This result is only interesting from a theoretical point of view, as divergence-free finite elements are rather untractable; it is the reason why other formulations must be sought.

2 The regularized problem

An easy way for making $\mathcal{A} = \text{curl curl } U$ a strongly elliptic operator is to replace it by $\mathcal{A}_t = \mathcal{A} - t^{-1} \text{grad div } U$; actually if we denote by ξ_i the variables in the Fourier space, we obtain $\det \hat{\mathcal{A}}_t = t^{-1} \left(\sum_{i=1}^3 \xi_i^2 \right)^3$. A generalization of this idea to inhomogeneous media leads to replace Maxwell's equations by

$$\text{curl} (\zeta^{-1} \text{curl } U) - \bar{\xi} \text{grad} (\tau^{-1} \text{div } \xi U) - \omega^2 \xi U = 0, \quad (16)$$

where the function τ is an arbitrary positive real datum. In the vicinity of infinity equation (16) takes the simplified form

$$\text{curl curl } U - t^{-1} \text{grad div } U - k_s^2 U = 0 \text{ with } t^{-1} = \tau_0^{-1} \zeta_0 |\xi_0|^2, \quad (17)$$

similar to linear elasticity, which can be written as

$$\mu \text{curl curl } U - (\lambda + 2\mu) \text{grad div } U - \omega^2 \rho U = 0.$$

As a consequence, two sorts of waves, namely s - and p - waves, are carried by (17), and the associated radiation condition takes the following form:

$$\begin{aligned} \lim_{R \rightarrow \infty} \int_{\partial B_R} \|\text{curl } U \wedge n - ik_s n \wedge (U \wedge n)\| d\gamma &= 0 \\ \lim_{R \rightarrow \infty} \int_{\partial B_R} \|\text{div } U - ik_p (U|n)\| d\gamma &= 0 \text{ with } k_p^2 = tk_s^2 \end{aligned} \quad (18)$$

The boundary conditions must be also completed; choosing condition $\operatorname{div} U|_{\Gamma} = 0$, which is natural for the electric field, and is a consequence of $\operatorname{curl} U \wedge n|_{\Gamma} = 0$ and $(U|n)|_{\Gamma} = 0$ for the magnetic field, will actually make p -waves disappear and (16) be equivalent to (3), as we shall see later.

2.1 Weak formulation

For irregular coefficients, the meaning of (16) is dubious, consequently, we only consider the weak form in the non-homogeneous region:

$$\begin{aligned} \text{Find } U \in \mathcal{F}_{\tau}^{E/H}, \text{ verifying (18), such that } \forall V \in \mathcal{F}_{\tau}^{E/H}, \\ \int_{\Omega'} \zeta^{-1} (\operatorname{curl} U | \operatorname{curl} V) + \int_{\Omega'} \tau^{-1} \operatorname{div} \xi U \operatorname{div} \xi \bar{V} - \omega^2 \int_{\Omega'} \xi (U | V) \\ + \zeta_0^{-1} \int_{\Sigma} (\operatorname{curl} U \wedge n | n \wedge (V \wedge n)) d\gamma - t^{-1} \zeta_0^{-1} \int_{\Sigma} \operatorname{div} U (n | V) d\gamma = 0 \end{aligned} \quad (19)$$

where

$$\begin{aligned} \mathcal{F}_{\tau}^E &= \{V \in \mathcal{F}^E \mid \operatorname{div} \xi V \in L_{\operatorname{loc}}^2(\Omega)\} \\ \mathcal{F}_{\tau}^H &= \{V \in \mathcal{F}^H \mid (H|n)|_{\Gamma} = 0, \operatorname{div} \xi V \in L_{\operatorname{loc}}^2(\Omega)\}. \end{aligned} \quad (20)$$

2.2 Uniqueness

The energy flux is now

$$F_{\partial D}(U) = \frac{1}{2\omega} \operatorname{Im} \int_{\partial D} (\zeta^{-1} (\operatorname{curl} U | U \wedge n) - \tau^{-1} \operatorname{div} \xi U (n | \xi U)) d\gamma. \quad (21)$$

We remark that a solution of the homogeneous problem (19) satisfies (17) in the vicinity of infinity, and consequently that $\Delta\varphi + k_s^2\varphi = 0$ for $\varphi = \operatorname{div} U$. As $F_{\partial B_R}(U) = 0$, then $\lim_{R \rightarrow \infty} \int_{\partial B_R} |\operatorname{div} U|^2 d\gamma = 0$, and $\operatorname{div} U = 0$ from Rellich's theorem. The previous proof shows now that $U = 0$ in the vicinity of infinity, and in the whole domain Ω by unique continuation.

2.3 Reduction to a bounded domain

The integral representation formula reads now as

$$U = U_I + \mathcal{R}_F^t[U] \quad (22)$$

with

$$\begin{aligned} \mathcal{R}_F^t[U](x) &= \int_F \mathbb{G}_t(x-y) (\operatorname{curl} U(y) \wedge n_y + t^{-1} n_y \operatorname{div} U(y)) d\gamma_y \\ &\quad - \int_F \operatorname{curl}_y \mathbb{G}_t(x-y) U(y) \wedge n_y d\gamma_y - t^{-1} \int_F (\operatorname{div}_y \mathbb{G}_t(x-y))^T (U(y) | n) d\gamma \end{aligned} \quad (23)$$

where

$$\mathbb{G}_t = g_{k_s} \mathbb{I} + k_s^{-2} \operatorname{Hess} (g_{k_s} - g_{k_p}), \quad (24)$$

whose singularity at the origin is only r^{-1} , whereas it was r^{-3} for the classical problem. Let

$$N_\nu U = \operatorname{div} U + \nu (U|n)|_\Sigma, \quad (25)$$

similarly we can prove that for $\operatorname{Im}(\lambda k_s^{-2})$ and $\operatorname{Im}(\nu k_p^{-2}) < 0$, the reduced problem

$$\text{Find } U' \in \mathcal{H}_\tau^{E/H}, \text{ such that } \forall V' \in \mathcal{H}_\tau^{E/H}, a_\tau(U', V') = \ell_\tau(V') \quad (26)$$

with

$$\begin{aligned} \mathcal{H}_\tau^E &= \{V \in H(\operatorname{curl}; \Omega') \mid \operatorname{div} \xi V \in L^2(\Omega'), V \wedge n_\Gamma = 0, V \wedge n|_\Sigma \in L^2(\Sigma), (V|n)_\Sigma \in L^2(\Sigma)\} \\ \mathcal{H}_\tau^H &= \{V \in H(\operatorname{curl}; \Omega') \mid \operatorname{div} \xi V \in L^2(\Omega'), (V|n)_\Gamma = 0, V \wedge n|_\Sigma \in L^2(\Sigma), (V|n)_\Sigma \in L^2(\Sigma)\} \end{aligned} \quad (27)$$

and

$$\begin{aligned} a_\tau(U', V') &= \int_{\Omega'} \zeta^{-1} (\operatorname{curl} U' | \operatorname{curl} V') + \tau^{-1} \operatorname{div} \xi U' \operatorname{div} \overline{\xi V'} - \omega^2 \int_{\Omega'} \xi (U' | V') \\ &\quad + \zeta_0^{-1} \int_{\Sigma} (\lambda (U' \wedge n | V' \wedge n) + t^{-1} \nu (U' | n) (V' | n)) d\gamma \\ &\quad - \zeta_0^{-1} \int_{\Sigma} ((T_\lambda \mathcal{R}_F^t[U'] | V') + t^{-1} (N_\nu \mathcal{R}_F^t[U'] | V')) d\gamma \\ \ell_\tau(V') &= \zeta_0^{-1} \int_{\Sigma} ((T_\lambda U_I | V') + t^{-1} (N_\nu U_I | V')) d\gamma \end{aligned} \quad (28)$$

is well-posed and equivalent to (19).

2.4 An alternative choice of spaces

When the coefficients ζ , ξ , and τ are regular enough, Costabel [3] has shown that

$$b(U', V') = \int_{\Omega'} \zeta^{-1} (\operatorname{curl} U' | \operatorname{curl} V') + \tau^{-1} \operatorname{div} \xi U' \operatorname{div} \overline{\xi V'}$$

is coercive on $\{V \in H^1(\Omega') \mid V \wedge n|_{\Gamma \cup \Sigma} = 0\}$ and on $\{V \in H^1(\Omega') \mid (V|n)|_{\Gamma \cup \Sigma} = 0\}$, from which we deduce that (28) is well-posed on $\mathcal{E}^{E/H}$, with

$$\begin{aligned} \mathcal{E}^E &= \{V \in H^1(\Omega') \mid V \wedge n_\Gamma = 0\} \\ \mathcal{E}^H &= \{V \in H^1(\Omega') \mid (V|n)_\Gamma = 0\}. \end{aligned} \quad (29)$$

Such a result is meaningful when Ω' is not regular nor convex, as in this case $H^1(\Omega') \not\subseteq H(\operatorname{curl}; \Omega') \cap H(\operatorname{div}; \Omega')$; it proves that the solution of (28) can be approximated by H^1 -conforming elements only when Ω' is regular or convex.

2.5 Classical versus regularized

Consider first the solution U of (19), following [2] choose any $f \in L^2(\Omega')$ and put $V = \operatorname{grad} \varphi$, where φ is the solution of $\operatorname{div}(\xi \operatorname{grad} \varphi) = f$ in Ω' with $\varphi|_{\Gamma \cup \Sigma} = 0$ (electric field) or $\partial \varphi / \partial n|_\Gamma = 0$ and $\varphi|_\Sigma = 0$ (magnetic field). Let ψ a truncation function identical to 1 in the vicinity of Γ , and to 0 in the vicinity of Σ , let $U' = \psi U$ and $U'' = (1 - \psi)U = U - U'$. As $V \in \mathcal{H}^{E/H}$, we deduce from (19) that $\forall f \in L^2(\Omega')$,

$$\int_{\Omega'} \varphi' f = \omega^2 \int_{\Omega'} \xi (U | \operatorname{grad} \varphi) + t^{-1} \zeta_0^{-1} \int_{\Omega'} (\operatorname{grad} \operatorname{div} U'' | \operatorname{grad} \varphi), \quad (30)$$

where $\varphi' = \tau^{-1} \operatorname{div} \xi U'$. Consider now the H^1 - solution $\tilde{\varphi}$ of

$$\int_{\Omega'} \bar{\xi} (\operatorname{grad} \tilde{\varphi} | \operatorname{grad} \varphi'') = -\omega^2 \int_{\Omega'} (\xi U | \operatorname{grad} \varphi'') - t^{-1} \zeta_0^{-1} \int_{\Omega'} (\operatorname{grad} \operatorname{div} U'' | \operatorname{grad} \varphi''), \quad (31)$$

where $\tilde{\varphi}|_{\Gamma \cup \Sigma} = \varphi''|_{\Gamma \cup \Sigma} = 0$ (electric field) or $\tilde{\varphi}|_{\Sigma} = \varphi''|_{\Sigma} = 0$ (magnetic field) and take $\varphi'' = \varphi$, we obtain thus

$$\int_{\Omega'} \tilde{\varphi} \Delta \bar{\varphi} = \omega^2 \int_{\Omega'} \xi (U | \operatorname{grad} \varphi) + t^{-1} \zeta_0^{-1} \int_{\Omega'} (\operatorname{grad} \operatorname{div} U'' | \operatorname{grad} \varphi). \quad (32)$$

From (30) and (32) we deduce that $\varphi' = \tilde{\varphi} \in H^1(\Omega')$, and then from (31) that $\tau^{-1} \operatorname{div} \bar{\xi} \operatorname{grad} \varphi' + \omega^2 \varphi' = 0$ in Ω' and $\varphi'|_{\Gamma} = 0$; as a consequence $\varphi \in H_{\text{loc}}^1(\Omega)$, $\varphi|_{\Gamma} = 0$ and $\operatorname{div} \bar{\xi} \operatorname{grad} \varphi + \omega^2 \tau \varphi = 0$ in the whole domain Ω . By the integral representation formula (22), we show that φ satisfies the outgoing radiation condition, and thus vanishes by Rellich's theorem; the solution of the regularized problem is thus identical to that of the classical one.

Such a proof is not valid for the alternative choice of spaces for the singular case, for $\operatorname{grad} \varphi \notin \mathcal{E}^{E/H} \forall f \in L^2(\Omega')$; consequently $\operatorname{div} \xi U \notin H_{\text{loc}}^1(\Omega)$ and does not necessarily vanish.

2.6 A singular field method

For the sake of simplicity, let us consider the case where the coefficients and the artificial boundary Σ are regular. By \mathcal{S}^E we denote the space of singular functions of the Laplacien, which is of finite dimension, i.e.

$$\mathcal{S}^E = \{ \varphi \in H_0^1(\Omega') \mid \exists f \in \mathcal{N}^E, (\operatorname{grad} \varphi | \operatorname{grad} \psi) + (f | \psi) = 0, \forall \psi \in H_0^1(\Omega') \}, \quad (33)$$

\mathcal{N}^E being any closed supplementary of the range of Δ , considered as an unbounded operator with domain $H_0^1(\Omega') \cap H^2(\Omega')$. Similarly, let

$$\mathcal{S}^H = \{ \varphi \in H_0^1(\Omega') \mid \exists f \in \mathcal{N}^H, (\operatorname{grad} \varphi | \operatorname{grad} \psi) + (f | \psi) = 0, \forall \psi \in H(\Omega') \}, \quad (34)$$

where $H(\Omega') = \{ \varphi \in H^1(\Omega') \mid \varphi|_{\Sigma} = 0 \}$ and \mathcal{N}^H is any closed supplementary of the range of Δ with domain $H(\Omega') \cap H^2(\Omega')$. Bonnet et al. (see also [1] and [4]) have shown that

$$\mathcal{H}_\tau^{E/H} = \mathcal{E}^{E/H} \oplus \operatorname{grad} \mathcal{S}^{E/H} \quad (35)$$

Problem (26) can thus be written as

$$\begin{aligned} & \text{Find } U' = P' + \operatorname{grad} \varphi \in \mathcal{E}^{E/H} \oplus \operatorname{grad} \mathcal{S}^{E/H}, \\ & \text{such that } \forall V' = Q' + \operatorname{grad} \psi \in \mathcal{E}^{E/H} \oplus \operatorname{grad} \mathcal{S}^{E/H}, \\ & a_\tau(U', V') = \ell_\tau(V') \end{aligned} \quad (36)$$

where P' and $Q' \in \mathcal{E}^{E/H}$ can be approximated by standard H^1 - conforming elements even for non-regular Ω' .

References

- [1] F. ASSOUS, P. CIARLET JR., E. SONNENDRÜCKER, *Resolution of the Maxwell equations in a domain with reentrant corners*, M²AN (to appear).

- [2] A-S. BONNET-BEN DHIA, C. HAZARD, S. LOHRENGEL, *A singular field method for the solution of Maxwell's equations in polyhedral domains*, SIAM J. Appl. Math (to appear).
- [3] M. COSTABEL, *A coercive bilinear form for Maxwell's equations*, J. Math. Anal. Appl., 157, 2, pp. 365-368, 1991.
- [4] M. COSTABEL, M. DAUGE, *Singularities of Maxwell's equations on polyhedral domains*, Preprint 96-30 IRMAR, 1996.
- [5] F. RELICH, *Über das asymptotische Verhalten der Lösungen von $\Delta u + \lambda u = 0$ in unendlichen gebieten*, Jber. Deutschen Math. Verein., 53, pp. 57-65, 1943.
- [6] V. VOGELSANG, *On the strong unique continuation principle for inequalities of Maxwell type*, Math. Ann., 2, pp. 12-25, 1991.
- [7] C. WEBER, *A local compactness theorem for Maxwell equations*, Math. Meth. Appl. Sci., 2, pp. 12-25, 1980.

UKRAINIAN RADIO PHYSICAL SYSTEM OF SEISMO-IONOSPHERIC MONITORING

Leonid N. Litvinenko, Yuri M. Yampolskii

Institute of Radio Astronomy, National Academy of Sciences of Ukraine
Ulitsa Krasnoznamennaya 4, Kharkov 310002, Ukraine

The paper reviews basic ideas, goals and structure of the System of Under-Satellite Ionospheric Sensing (SUIS), which is currently under development within the framework of research project "Warning". The team of principal developers of this system is with the IRA NAS in Kharkov.

It is supposed that SUIS will be based on two sub-systems (SS), namely, *Monitoring* and *Calibration*. The output data of both SS will be first transferred to and processed at the Central Terminal of Ground Data Processing (CTGDP), and further transmitted to the Center of Scientific Data Processing.

In the framework of the *Monitoring* SS, four observatories: *West, South, East, and Antarctic*, are planned to be built. They will be equipped with identical radio physical instruments in 4 radio frequency bands and with preliminary processing terminals (PPT). Such a concept of the ground-based system is recognized to be the most economic, reasonably corresponding to the existing research background and experience, and will provide a sensing of the whole ionosphere in the interval of heights from 50 km to 1000 km. After a preliminary processing at the observatories, the data streams will be transferred to CTGDP.

About the research goals of SUIS, the following should be mentioned. The *Monitoring* SS is planned to work in a continuous routine regime. It will be put into operation half a year before placing the satellite into orbit.

The other SS of SUIS, *Calibration* one, will involve all existing active radio systems in Ukraine that are purposed at the ionospheric sensing. It will work only according to a special timetable based on the satellite passing and on the international geophysical calendar. As all the equipment of this SS operates with powerful transmitters, its work requires significant expenses and resources. The data from this SS also are gathered at CTGDP. SS *Calibration* is purposed at the calibration of the satellite sensors and the sensors of the *Monitoring* SS. The diagrams showing the connections of its equipment with the ionospheric and other sensors of satellite will be presented. Integration of the data of this SS with the other data of the whole SUIS will make it possible to model ionospheric phenomena, extract the seismic precursors and carry out the data interpretation. Here, it is supposed to arrange an exchange of data with all major centers of ionospheric sensing. Using the foreign observatories for the under-satellite sensing is possible; the needed agreements have been obtained from many of them. This will naturally require a direct link to Internet from CTGDP.

Now consider a planned strategy of the SUIS output data processing (SIDP). Here, two blocks can be separated: processing the *Monitoring* data, and the *Calibration* one. The system of the data processing should be integrated with all the data streams from the observatories through PPT, calibration equipment, world ionospheric observatories, and global data center. The SUIS data processing is planned to be three-level one: sensor – PPT – CTGDP. A sensor transforms the streams of radio data into radio physical parameters. PPT determines, at every location, the background levels, makes archiving and storage of data, extracts the anomalies, and sends the latter to CTGDP. The Center compares the data of all the PPT and *Calibration* SS, and sends them to CPSD in terms of real-time and modeling representations.

Making up a decision about a seismic warning then is done as follows. At PPT, the "Zero" (Calm) level corresponds to the absence of anomalies detected by sensors; level "One" (Suspicion) implies an anomaly detected by a single sensor; level "Two" (Trouble) means a correlated in frequencies and routes anomalies in several parameters. This information is sent from PPT's to CTGDP. There, the level "Three" (Alarm) is initiated: correlated in time, space and frequency anomalous variations of physical parameters detected by different observatories and SUIS.

Fractional Calculus and Fractional Paradigm in Electromagnetic Theory

Nader Engheta

University of Pennsylvania
Moore School of Electrical Engineering
Philadelphia, Pennsylvania 19104, U.S.A.
Tel: (215) 898-9777, Fax: (215) 573-2068
E-mail: engheta@pender.ee.upenn.edu

Introduction

In recent years, we have been interested in bringing the concept of fractional calculus and the theory of electromagnetism together [1-7], and to develop an area in electromagnetics which we are naming *Fractional Paradigm in Electromagnetism*. The field of fractional calculus addresses mathematical operations involving differentiation and integration to arbitrary non-integer real or complex orders -- operators such as $\frac{d^{\nu}f(x)}{dx^{\nu}}$ where ν can be a non-integer real or complex number [see e.g., 8]. In other words, in this field the operators that are so-called "intermediate" cases between the integer-order differentiation and integration are addressed and studied. The electromagnetic theory, on the other hand, is a classical field in which the usual differential and integral operators are commonly used. So it is interesting to explore what possible applications and physical implications one would find if one brought the fractionalization of operators and electromagnetism together. In our earlier work, we have applied the concept of fractional calculus in certain electromagnetic problems, and have obtained some interesting results demonstrating some salient features and potential applications of these operators [1-7]. Inspired and motivated by our earlier work in application of fractional calculus in electromagnetism, we have also been interested to explore fractionalization of some other operators commonly used in electromagnetic problems and to search for potential applications and physical meanings of such fractionalization of linear operators in electromagnetism. We recently introduced the concept of fractionalization of the cross-product and the curl operators [1,2] and showed that such operators can provide us with fractionalization of duality principle in electromagnetism [1].

In this paper, we provide a brief overview of some of our ideas and recent work in this area and discuss some of the salient features of the results obtained in our analysis. The interested reader is referred to our work reported in [1-7] for more details. Before we give this overview, for the sake of easy reference we first give a brief summary of some of the definitions of fractional integrals and derivatives that have been utilized by mathematicians over years.

What is Fractional Derivative/Integral?

Fractional calculus is a branch of mathematics that deals with generalization of well-known operations of differentiation and integration to arbitrary non-integer orders -- orders that can be non-integer real or complex numbers [see e.g., 8-11]. The mathematical idea of fractional derivatives/integrals, which dates back to the seventeenth century, has been the subject of interest for many mathematicians and has seen much development over the years [see e.g., references given in 8, pp. 3-15]. Fractional derivatives and integrals are shown symbolically by some of the

notations such as ${}_a D_x^\nu f(x)$ [see Davis, 10] or $\frac{d^\nu f(x)}{d(x-a)^\nu}$ [see Oldham and Spanier, 8] where ν is the general order of the operator (not necessarily positive or negative *integer*), and a is the lower limit of the integrals used to define these operators (as shown below).

One of the definitions of fractional integrals is that known as the Riemann-Liouville integral [8, p. 49; 9, p. 33]. It is the generalization of Cauchy's repeated integration formula. Cauchy's formula states that the n th-order (or n -fold) integration of a given function $f(x)$ can be written as

$${}_a D_x^{-n} f(x) \equiv \int_a^x dx_{n-1} \int_a^{x_{n-1}} dx_{n-2} \dots \int_a^{x_1} f(x_0) dx_0 = \frac{1}{(n-1)!} \int_a^x (x-u)^{n-1} f(u) du \quad (1)$$

where ${}_a D_x^{-n}$ denotes the n -fold integration with the lower limit of the integrals being a . It is clear that $(n-1)! = \Gamma(n)$ where $\Gamma(\cdot)$ is the Gamma function. Replacing $-n$ with ν which is a non-integer negative number, the Riemann-Liouville integral for definition of fractional integration is obtained [8, p. 49] as follows

$${}_a D_x^\nu f(x) \equiv \frac{1}{\Gamma(-\nu)} \int_a^x (x-u)^{-\nu-1} f(u) du, \quad \text{for } \nu < 0 \text{ and } x > a \quad (2)$$

For fractional derivatives with $\nu > 0$, this definition can still be used if combined with the following additional step ${}_a D_x^\nu f(x) = \frac{d^m}{dx^m} {}_a D_x^{\nu-m} f(x)$, for $\nu > 0$, where m is chosen such that $(\nu-m)$ becomes negative and thus Eq. (2) can be applied for ${}_a D_x^{\nu-m} f(x)$. Then $\frac{d^m}{dx^m}$ is the ordinary m th-order differential operator [8, p. 50].

Another definition of fractional differentiation/integration was given by Liouville for functions that can be expanded in a series of exponentials. For a function $g(x)$ which can be written as $g(x) = \sum_{i=0}^{\infty} c_i e^{u_i x}$, according to Liouville [12], [8, page 53] the ν th-order fractional differentiation/integration (with lower limit $a = -\infty$) can be given as

$${}_{-\infty} D_x^\nu g(x) \equiv \frac{d^\nu g(x)}{dx^\nu} \equiv \sum_{i=0}^{\infty} c_i u_i^\nu e^{u_i x}. \quad (3)$$

There are several other definitions for fractional derivatives and integrals which can be found in some of the references on fractional calculus [see e.g., 8, ch. 3]. Fractional calculus has had applications in various topics such as differential equations, complex analysis, Mellin transforms, and generalized functions to name a few. For a historical review of the field of fractional calculus, the reader is referred to the excellent bibliography prepared by B. Ross that is reprinted in pp. 3-15 of the monograph by Oldham and Spanier [8], and also the historical outline given in [9].

Our interest in fractional calculus has been particularly focused on finding out what possible mathematical applications and/or physical roles these mathematical operators can have in electromagnetic theory. Needless to say, electromagnetics is a field in which the use of conventional (integer-order) calculus plays a major role, and it is of interest to see how *fractional* calculus may offer useful mathematical tools in this field and how these tools help us to develop the area of fractional paradigm in electromagnetism. We have applied the concept of fractional derivatives/integrals to certain electromagnetic problems, and have obtained interesting results

and ideas showing that these mathematical operators can be interesting and useful mathematical tools in electromagnetic theory ([1]-[7]). Some of these ideas, which are the steps in developing fractional paradigm in electromagnetism, include the novel concept of "fractional" multipoles in electromagnetism [3], electrostatic "fractional" image methods for perfectly conducting wedges and cones [4], "fractional" solutions for the standard scalar Helmholtz equation [6], mathematical link between the electrostatic image methods for the conducting sphere and the dielectric sphere [5], fractionalization of curl operator and its role in fractionalization of duality principle in electromagnetism [1,2]. Below a brief review of some of these problems is given. Due to the space limitation here, only some of these problems are reviewed. The interested reader may refer to our work reported in [1-7] for further details and for our other findings.

What is our Fractional Paradigm in Electromagnetic Theory?

In the mathematical treatment of electromagnetic theory, for any given general problem we often solve canonical cases. For example, if the goal is to solve the standard problem of propagation of electromagnetic wave in a source-free region we usually consider well-known canonical cases of one-dimensional *plane* wave, two-dimensional *cylindrical* wave, and three-dimensional *spherical* wave propagation. Here if we just consider two of these canonical cases, e.g., plane wave and cylindrical wave, we can symbolically show the chart of Fig. 1 where the box entitled "problem" is what describes the general problem of interest (in this example, the wave propagation in free space), and the two boxes "Case 1" and "Case 2" indicate the two canonical situations (in this case plane and cylindrical waves). Now, one can ask the following questions:

Are there any "intermediate" situations between the two well-known cases represented as canonical situations for the "problem"? In other words, as symbolically depicted in Fig. 2 can we have fractional "intermediate" domains between the two cases shown in Fig. 1?

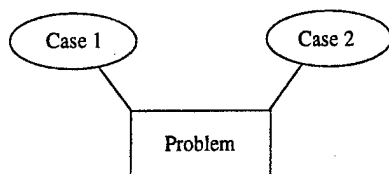


Fig. 1

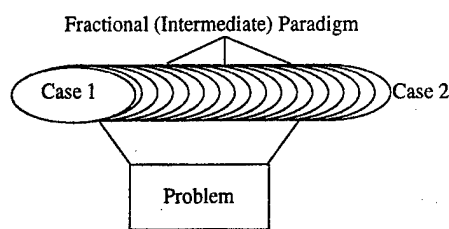


Fig. 2

These questions can be rephrased and interpreted in the following way:

If we consider certain "entity" whose properties (or identifiers) depend on a parameter with integer values, can we still consider (or think of) that entity when that specific parameter takes a non-integer "fractional" value? In other words, can we conceive an "intermediate" case for that entity?

In order to illustrate this idea, let us consider the following example: The concept of multipoles and multipole expansion in electromagnetic theory has been well known and studied extensively. Let us take our "problem" as, for instance, the electrostatic potential distribution, and consider

the canonical "cases" as the "entities" of electric point-monopoles, electric point-dipoles, electric point-quadrupoles, etc. These entities have specific properties. For instance, for the static electric point-monopole, the scalar electric potential has the radial dependence of R^{-1} . The scalar potential of electrostatic point-dipole, however, varies as R^{-2} (and of course it has an angular variation). Comparing the scalar potentials of these two entities, we obviously notice that the R -dependences of these electrostatic multipoles have exponents that are negative integers. Now the above questions that we posed can be rephrased as follows: Can we have an "intermediate" electrostatic multipoles whose R -dependence varies as $R^{-\alpha}$ where α takes a non-integer value between 1 and 2? If yes, how would such a "fractional"-order multipole look like? Of course, such an "intermediate" multipole should not, and cannot, simply be made by a linear combination of one point-multipole and one point-dipole with appropriate coefficients. Because if that were the case, the scalar potential in the distant region of such a combination would be dominated by the potential of the monopole only, since the static dipole's scalar potential drops faster than that of the monopole. Therefore, a specific charge distribution should be sought in order to have a potential with R -dependence of $R^{-\alpha}$. We have studied this issue and have introduced the idea of fractional-order multipoles using the tool of fractional calculus [3] and have shown that such fractional multipoles can be used in describing potential distribution in front of a perfectly conducting cones (for the 3-D case) and perfectly conducting wedges (for the 2-D case) [4]. We have found the volume charge density of a fractional multipole in 3-D case as

$$\rho_{2^\alpha, z}(\mathbf{r}) \equiv q l^\alpha {}_{-\infty}D_z^\alpha \delta(\mathbf{r}) = q l^\alpha \frac{\partial^2}{\partial z^2} \left[\delta(x)\delta(y)U(z) \frac{1}{\Gamma(2-\alpha)} z^{1-\alpha} \right] \quad (4)$$

where α is in general a non-integer number between zero and unity, $U(z)$ is the unit step function, and the multiplicative constant l^α , where l is an arbitrary constant with dimension of *length*, is used here to keep the physical dimension of this charge density as Coulomb/m³. The subscript 2^α in $\rho_{2^\alpha, z}(\mathbf{r})$ describes the multipole fractional order of this new charge distribution. This subscript is chosen such that it provides the right order of multipoles in the limiting cases of $\alpha = 0$ and $\alpha = 1$. For $\alpha = 0$, we get the point-monopole $\rho_1(\mathbf{r})$, and for $\alpha = 1$ we obtain the first z -derivative of $\delta(\mathbf{r})$, thus showing a charge distribution of *dipole* $\rho_2(\mathbf{r})$ along the z -axis. The subscript z in $\rho_{2^\alpha, z}(\mathbf{r})$ indicates the fact that we have this charge distribution along the z axis (resulted from the α th-order z -derivative of the point-monopole). We have analyzed the scalar electrostatic potential function of this fractional 2^α -pole multipole [3]. It can be written explicitly as

$$\Phi_{2^\alpha, z}(x, y, z) = l^\alpha {}_{-\infty}D_z^\alpha \left[\frac{q}{4\pi\epsilon R} \right] = \frac{q l^\alpha \Gamma(\alpha+1)}{4\pi\epsilon R^{1+\alpha}} P_\alpha(-\cos\theta) \quad \text{for } 0 < \alpha < 1 \quad (5)$$

$0 < \theta < \pi$

where $P_\alpha(-\cos\theta)$ is the Legendre function of the first kind and the (non-integer) degree α . A series of contour plots in the x - z plane for this potential for several values of α , $0 \leq \alpha \leq 1$ is shown in Fig. 3. (See the caption for more details). It is interesting to note from Eq. (5) that, as predicted, the scalar potential function of the intermediate "fractional" 2^α -pole drops as $R^{-1-\alpha}$ (with $0 < \alpha < 1$), as R increases. Thus, it is a potential distribution that can be regarded as the "intermediate" case between potentials of the point-monopole and point-dipole. The angular dependence of this potential is $P_\alpha(-\cos\theta)$ with the degree α which is, in general, non-integer.

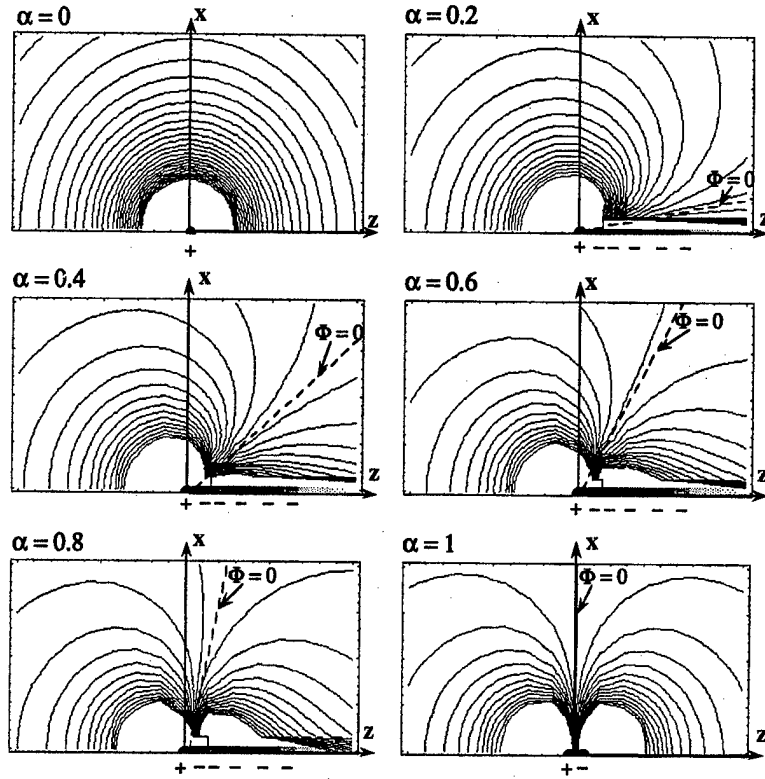


Fig. 3. Contour plots for the electrostatic scalar potential of 2^α -pole charge distribution of Eq. (4) for $0 \leq \alpha \leq 1$. The expression for the potential is given in Eq. (5). Since this scalar potential is azimuthally symmetric, the intersection of equipotential surfaces with the x-z plane is only shown here. The contours are shown for the region $-2 \leq z \leq 2$ and $0 < x \leq 2$, and for six different values of α . For $\alpha = 0$ (top left Panel), the source is a single electric point-monopole (shown as +) located at $x = y = z = 0$, and the contours are independent of θ . For $\alpha = 1$ (bottom right Panel), the source is an electric point-dipole (shown at + -) located at the origin, and the angular dependence of the

potential is $-\cos(\theta)$. For fractional values of α between zero and unity, we can see from the above contour plots that the scalar potential of fractional 2^α -pole are "intermediate" cases between those of the point-monopole and point-dipole, and in a way it "evolves" from one case into the other. The dashed lines, which are added later on top of the contour plots show the approximate location of zero potential (root of $P_\alpha(-\cos\theta) = 0$). In the region of x-z plane shown above, to the left of these dashed line, potential is positive and to the right it is negative. Along the positive z-axis, the charge distribution is also sketched. The plus and minus signs below the z axis indicate the sign of the charge distribution along the z axis. (Originally published in N. Engheta, "On Fractional Calculus and Fractional Multipoles in Electromagnetism," *IEEE Transactions on Antennas and Propagation*, Vol. 44, No. 4, pp. 554-566, April 1996. Copyright© 1996 IEEE.)

We have also addressed the case of fractional "intermediate" situations between the plane wave and the cylindrical wave propagation in free space, have obtained "fractional" solutions to the standard Helmholtz equation, and have found specific sources that generate such intermediate fractional solutions [6]. Our results show that for the time-harmonic two-dimensional electric current distribution described in the Cartesian coordinate system as

$$J(x, y; t) = \hat{z} \frac{I_0 e^{-i\omega t}}{2} \left[-D_y^{-\alpha} \delta(x) \delta(y) + \dots D_{-y}^{-\alpha} \delta(x) \delta(y) \right] = \hat{z} I_0 e^{-i\omega t} \frac{\delta(x) |y|^{\Gamma-1+\alpha}}{2\Gamma(\alpha)} \quad (6)$$

where $0 < \alpha < 1$, the z-component of the radiated electric field in the far zone can be expressed, for θ not being too small, as

$${}_αE_z(x, y; k) \equiv \frac{\omega\mu I_0}{4\pi} \cos\left(\frac{(2-\alpha)\pi}{2}\right) (k \sin|\theta|)^{-\alpha} \sqrt{\frac{2\pi}{kp}} e^{ik\rho - i\pi/4} - \frac{\omega\mu I_0}{4k^\alpha \Gamma(\alpha)} \frac{e^{ik|x|}}{(k|y|)^{1-\alpha}} \quad (7)$$

where $\rho \equiv \sqrt{x^2 + y^2}$, $\theta = \sin^{-1}(y/x)$, and $k \equiv \omega\sqrt{\mu\varepsilon}$. For $\theta = 0$ when the observer is along the x axis, another expression is obtained for E_z [see Ref. 6], which shows that the magnitude of this field along the x axis drops as $|x|^{-\alpha/2}$. It can be shown that the source expressed in Eq. (6) and its far-zone radiation field given in Eq. (7) are the intermediate case between the two cases of the *line* current and the *sheet* current. (Note that the source given in Eq. (6) is not a simple linear combination of a single line current and a single sheet current.) More specifically, we notice that when $\alpha = 0$ in Eqs. (6) and (7), the current source becomes an infinitely long thin line current along the z axis and its far-zone radiation field approaches ${}_0E_z(x, y; k) \equiv \frac{-\omega\mu I_0}{4\pi} \sqrt{\frac{2\pi}{kp}} e^{ik\rho - i\pi/4}$

which is the far-zone cylindrical wave of an infinitely long two-dimensional wire antenna. When $\alpha = 1$, Eq. (6) represents a one-dimensional sheet current with intensity $I_0/2$, and its corresponding far-zone field is ${}_1E_z(x, y; k) \equiv -\frac{\omega\mu I_0}{4k} e^{ik|x|}$ which is, as expected, a plane wave. Therefore, Eq. (7) represents an example of a wave which is an "intermediate" case between a plane and a cylindrical wave.

In some cases, however, the fractional cases may not be directly or obviously related to the known parameters for the so-called "integer" cases. As an illustrative example, let us consider the very well-known concept of duality principle in electromagnetic theory, that is for any given electromagnetic problem there is another problem named *dual problem* that can be obtained by appropriate transformation of fields, sources, and material parameters, namely, $E \rightarrow H'$, $H \rightarrow -E'$, $\mu \rightarrow \varepsilon'$, $\varepsilon \rightarrow \mu'$, $J \rightarrow J'_m$, $J_m \rightarrow -J'$, $\rho \rightarrow \rho'_m$, and $\rho_m \rightarrow -\rho'$. Following the same line of inquiry, we should ask: Can we have "fractional duality" in electromagnetism where the fractional dual problems would be intermediate problems between the original and its dual counterpart? To answer this question, first we needed to seek an "operator" which "connects" the two cases together, i.e., a mapping which takes the original case and brings it into the "dual" case. Symbolically, we can show such an operator (which can be linear) as a mapping between the "Case 1" and "Case 2". We should then "fractionalize" this operator \underline{L} , and the new fractional operator, which we symbolically denote by \underline{L}^α , can be used to obtain the intermediate cases from the original case 1. This fractional operator should have the following properties: (I) For $\alpha = 1$, one gets the original operator \underline{L} and this provides us with Case 2 from Case 1; (II) For $\alpha = 0$, one obtains the identity operator \underline{I} and Case 1 can be attained; and (III) For two numbers α and β , we should have $\underline{L}^\alpha \underline{L}^\beta = \underline{L}^\beta \underline{L}^\alpha = \underline{L}^{\alpha+\beta}$. We have used this technique to fractionalize some of the well known operators such as *cross-product* operator and the *curl* operator [1-2]. The *fractional curl* operator, as we defined, is a new operator shown symbolically as curl^α with parameter α that is in general non-integer. When $\alpha=1$, we get the conventional *curl* operator. When $\alpha=0$, we should obtain the identity operator. For values of α other than zero and unity, one then gets operator curl^α with appropriate mathematical operation [see Ref. 2]. Under certain appropriate mathematical conditions, this operator, when applied repeatedly, is additive and also commutes, i.e., $\text{curl}^\alpha \text{curl}^\beta = \text{curl}^\beta \text{curl}^\alpha = \text{curl}^{\alpha+\beta}$. This operator is an interesting mathematical operation that may offer some possible utility in certain electromagnetic problems. In particular, we have found that using "fractional curl" operator we can fractionalize the duality principle in electromagnetism [1,2].

Our hopes in introducing the fractional paradigm in electromagnetic theory are to explore various fractional intermediate cases in electromagnetic problems which may lead to some interesting possibilities. Many real-world problems in electromagnetism may not always be identified or modeled as one of the standard ideal canonical problems. For example, in some situations it may not be possible to model waves as ideal canonical plane, cylindrical, or spherical waves. Similarly we may not be able to model antennas as having simple canonical shapes. So it is hoped that "intermediate" cases we study will shed light on mathematical treatment of some of the real-world problems in electromagnetic theory.

References

- [1] N. Engheta, "Fractional Curl Operator in Electromagnetics," in *Microwave and Optical Technology Letters*, Vol. 17, No. 2, pp. 86-91, February 5, 1998.
- [2] N. Engheta, "Fractionalization of the Curl Operator and Its Electromagnetic Application," a talk presented in the *1997 IEEE AP-S/URSI North American Radio Science Meeting*, Montreal, Canada, July 13-18, AP Digest, Vol. 2, pp. 1480-1483, 1997.
- [3] N. Engheta, "On Fractional Calculus and Fractional Multipoles in Electromagnetism," *IEEE Transactions on Antennas & Propagation*, Vol. 44, No. 4, pp. 554-566, April 1996.
- [4] N. Engheta, "Electrostatic "Fractional" Image Methods for Perfectly Conducting Wedges and Cones," *IEEE Transactions on Antennas & Propagation*, Vol. 44, No. 12, pp. 1565-1574, December 1996.
- [5] N. Engheta, "A Note on Fractional Calculus and the Image Method for Dielectric Spheres," *Journal of Electromagnetic Waves and Applications*, Vol. 9, No. 9, pp. 1179-1188, September 1995.
- [6] N. Engheta, "Use of Fractional Integration to Propose Some "Fractional" Solutions for the Scalar Helmholtz Equation," a chapter in *Progress in Electromagnetics Research (PIER)* monograph Series Vol. 12, Jin A. Kong (ed.), EMW Pub., Cambridge, MA, pp. 107-132, 1996.
- [7] N. Engheta, "On the Role of Fractional Calculus in Electromagnetic Theory," in *IEEE Antennas and Propagation Magazine*, Vol. 39, No. 4, pp. 35-46, August 1997.
- [8] K. B. Oldham and J. Spanier, *The Fractional Calculus*, Academic Press, New York, 1974.
- [9] S. G. Samko, A. A. Kilbas, and O. I. Marichev, *Fractional Integrals and Derivatives, Theory and Applications*, Gordon and Breach Science Publishers, Langhorne, Pennsylvania, 1993. (Originally published in Russian by Nauka i Tekhnika, Minsk, 1987).
- [10] H. T. Davis, *The Theory of Linear Operators*, The Principia Press, Bloomington, Indiana, 1936. pp. 64-77, and pp. 276-292.
- [11] I. M. Gel'fand and G. E. Shilov, *Generalized Functions*, Academic Press, New York, 5 volumes, 1964-68.
- [12] J. Liouville, "Mémoire: Sur le Calcul des Différentielles à Indices Quelconques," *J. Ecole Polytechn.* Vol. 13, p. 71, 1832.

TIME-DOMAIN ELECTROMAGNETICS OF WAVEGUIDE-TYPE OPEN RESONATORS

Nataliya P. Yashina

*Dept. of Diffraction Theory and Diffraction Electronics
Institute of Radiophysics and Electronics, NAS of the Ukraine
12 Proskura St., Kharkov 310085, Ukraine*

Introduction

New algorithmic schemes for modeling the problems of linear theory of waveguide discontinuities are presented. Numerical experiment is still the main tool for investigation of the resonant wave scattering phenomena, which are characteristic for such structures. The mathematical approaches employed for such purposes have to satisfy relevant demands as for accuracy, efficiency and versatility, and for ability to be focused on particular details of various practically interesting regimes.

The approaches for analyses of transient processes in the waveguide-type open resonators considered herein satisfy all these requirements. They rely on the description of the scattering properties of discontinuities in regular waveguides in terms of transform operators related to "evolutionary basis" of non-stationary signals that are qualitatively the same for all guiding structures [1]. They suppose an application of the analytical regularization technique at key stages of the solving procedure [2]. The approaches developed can be applied to the solution of wide range of electromagnetic and acoustic boundary value and initial value problems. The class of considered model problems comprises resonant type discontinuities in circular and coaxial waveguides excited by an axisymmetric TE_{op} electromagnetic wave. The choice of modeling objects is motivated by scientific interests of the author.

Evolutionary basis of non-stationary wave and transform operators

Investigation of a TE-type axisymmetric wave scattering in circular waveguiding structures, such as coaxial bifurcation or annular iris, is reduced to solving the following initial boundary-value problem:

$$\begin{cases} \left[-\varepsilon(z) \frac{\partial^2}{\partial t^2} U - \sigma(z) \frac{\partial}{\partial t} U + \frac{\partial^2}{\partial z^2} U + \frac{\partial}{\partial \rho} \left(\frac{1}{\rho} \frac{\partial}{\partial \rho} (\rho U) \right) \right] = F(z, \rho, t), \quad t > 0, \{z, \rho\} \in Q; \\ U(z, \rho, 0) = \varphi(z, \rho), \quad \left. \frac{\partial}{\partial t} U(z, \rho, t) \right|_{t=0} = \psi(z, \rho); \\ U(z, \rho, t) \Big|_{g \in S} = 0, \end{cases} \quad (1)$$

where $\varepsilon(z)$ is the relative dielectric permittivity of the material filling the discontinuity,

$\sigma(z) = \left(\frac{\mu_0}{\varepsilon_0} \right)^{1/2} \sigma_0(z)$, ε_0, μ_0 are the free-space permittivity and permeability, $\sigma_0(z)$ is the specific conductivity, $U(z, \rho, t) = E_\varphi$. For the axisymmetric wave, $E_\rho = E_z = H_\varphi = 0$, while

the non-zero components of the magnetic field vector are given by the relationships:

$$\frac{\partial}{\partial t} H_\rho = \left(\frac{\varepsilon_0}{\mu_0} \right)^{1/2} \frac{\partial}{\partial z} E_\varphi; \quad \frac{\partial}{\partial t} H_z = - \left(\frac{\varepsilon_0}{\mu_0} \right)^{1/2} \frac{\partial}{\partial \rho} (\rho E_\varphi).$$

It is supposed that the functions $F(g, t)$, $\varphi(g)$, $\psi(g)$, $\varepsilon(g) - 1$, and $\sigma(g)$ are finite in Q and satisfy the conditions of the theorem about a unique solution of the problem (1) in the energy class (Sobolev's space) $W_2^1(Q^T)$, $Q^T = Q \times (0, T)$, $T < \infty$ [3].

The separation of variables in (1) enables us to represent the solution of the problem (1), at any section of regular waveguide (i.e., where its cross-section is constant along the axis z , and $\varepsilon(g) - 1 = \sigma(g) \equiv 0$), as follows:

$$U(z, \rho, t) = \sum_n v_n(z, t) \Psi_n(\rho) \quad \{z, \rho\} \in Q, \quad t > 0, \quad (2)$$

where the sequence of functions $v(z, t) = \{v_n(z, t)\}$ solve the equation

$$\begin{aligned} \left[-\frac{\partial^2}{\partial t^2} + \frac{\partial^2}{\partial z^2} - \lambda_n^2 \right] v_n(z, t) &= a_n(z, t) - \delta^{(1)}(t) b_n(t) - \delta(t) c_n(t) + \\ &+ \left[(\varepsilon - 1) \frac{\partial^2}{\partial t^2} + \sigma \frac{\partial}{\partial t} \right] v_n(z, t), \quad -\infty < t < \infty, \quad |z| < \infty, \end{aligned} \quad (3)$$

with initial conditions

$$v_n(z, 0) = b_n(z); \quad \left. \frac{\partial}{\partial t} v_n(z, t) \right|_{t=0} = c_n(z); \quad (4)$$

$\{\lambda_n\}$ is the set of eigenvalues relevant to eigenfunctions $\Psi_n(\rho)$, $\delta^{(m)}$ is the generalized derivative of the Dirac delta-function, $a_n(z, t)$, $b_n(z)$, $c_n(z)$ are the Fourier coefficients of the functions $F(g, t)$, $\varphi(g)$, $\psi(g)$ expanded in terms of the series of basis functions.

Suppose now that a wave of the type (2) excites the open waveguide resonator. We consider the field of excitation $U^i(g, t) = \sum_n v_n(z, t) \Psi_n(\rho)$ to be nonzero only in the waveguide A,

which is regular for all $z_1 > 0$ (left bound is placed in the plane $z_1 = 0$). The scattered field that is exited in the regular semi-infinite waveguides A and B and propagates in each waveguide towards the increasing values of z_1 and z_2 can be expressed in the form

$$U_j^s(z, \rho, t) = \sum_n w_{nj}(z_j, t) \Psi_n(\rho); \quad z_j \geq 0, \quad j = 1, 2. \quad (4)$$

Boundary transformation operators R^{AA} and T^{BA} (at the boundaries $z_j = 0$) of the evolutionary basis of nonstationary wave coming from the waveguide A are introduced via expressions

$$\begin{aligned} w_{nj}'(0, t) &\equiv \\ &\equiv \frac{\partial}{\partial z_j} w_{nj}(z_j, t) \Big|_{z_j=0} = \int_0^t \sum_m \left[R_{nm}^{AA}(t-\tau) \delta_j^1 + T_{nm}^{BA}(t-\tau) \delta_j^2 \right] v_m(0, \tau) d\tau, \quad j = 1, 2 \end{aligned} \quad (5)$$

$$w_{nj}(z_j, t) = - \int_0^t \left[\lambda_{nj} \left((t-\tau)^2 - z_j^2 \right)^{1/2} \right] \chi[(t-\tau) - z_j] w'_{nj}(0, \tau) d\tau, \quad (6)$$

The transporting diagonal operators $\mathcal{E}^A(z_1)$ and $\mathcal{E}^B(z_2)$ that characterize the field variation while propagating along a finite distance in a regular waveguide, are defined as follows:

$$\begin{aligned} w'_j(0, t) &= \left\{ w'_{nj}(0, t) \right\} = \left[R^{AA} \delta_j^1 + T^{BA} \delta_j^2 \right] \left[v(0, \tau) \right]; \quad j=1,2. \\ w_j(z_j, t) &= \left\{ w_{nj}(z_j, t) \right\} = \left[\mathcal{E}^A(z_1) \delta_j^1 + \mathcal{E}^B(z_2) \delta_j^2 \right] \left[w'_j(0, \tau) \right]; \end{aligned} \quad (7)$$

It is clear, that all together these operators characterize the scattering features of discontinuity (in the case of A-side excitation) in complete manner. Here $J_q(\dots)$ is the Bessel function, χ is the Heaviside step function.

Elementary discontinuities in circular and coaxial waveguides

In this section we shall outline the principal ideas of the approach, which can be used for the solution of rather wide range of problems of transient scattering theory.

Hereinafter the wave of excitation, $U_j^s(z, \rho, t)$, is supposed as coming to the discontinuity from the left-hand side and chosen to have the form (2) with $v_n(0, t) = \delta_n^p \delta(t - \eta)$. Integer number $p \geq 0$ and the time when the observation started, $\eta > 0$, are fixed.

1. Coaxial bifurcation of a circular waveguide will serve us as the first example. This configuration is characteristic for all the structures of so the called Wiener-Hopf geometry. According to (4)-(6), the scattered field $U(z, \rho, t)$ formed in the regions $z > 0$ and transformed by the bifurcation (regions **A** is coaxial waveguide, **B** is the circular waveguide of radius b ; the region of the regular circular waveguide of radius a is denoted by **E**) can be represented as

$$\begin{aligned} U(E) &= - \sum_n \int_0^t J_0 \left[\lambda_n \left((t-\tau)^2 - z^2 \right)^{1/2} \right] \chi[(t-\tau) - z] R_{np}^{EE}(\tau - \eta) d\tau \cdot \Psi_n(\rho) + U^i; \\ U(B, A) &= - \sum_n \int_0^t J_0 \left[\lambda_{nj} \left((t-\tau)^2 - z^2 \right)^{1/2} \right] \chi[(t-\tau) + z] T_{np}^{(B,A)E}(\tau - \eta) d\tau \cdot \Psi_{nj}(\rho); \quad j=1,2. \end{aligned} \quad (8)$$

The eigenfunctions $\psi_n(\rho)$, $\psi_{nj}(\rho)$ and the eigenvalues λ_n, λ_{nj} are defined as follows

$$\begin{aligned} \psi_n(\rho) &= J_1 \left(v_n \frac{\rho}{a} \right) \left[\pi^{1/2} a J_0(v_n) \right]^{-1}; \\ \psi_{n1}(\rho) &= G_1 \left(\mu_n, \frac{\rho}{a} \right) \left[\pi \left[a^2 G_0^2(\mu_n, 1) - b^2 G_0^2(\mu_n, \theta) \right] \right]^{-1/2}; \\ G_q \left(\mu_n, \frac{\rho}{a} \right) &= J_q \left(\mu_n \frac{\rho}{a} \right) N_1(\mu_n \theta) - N_q \left(\mu_n \frac{\rho}{a} \right) J_1(\mu_n \theta); \\ \psi_{n2}(\rho) &= J_1 \left(v_n \frac{\rho}{a} \right) \left[\pi^{1/2} b J_0(v_n) \right]^{-1}; \end{aligned}$$

$$\lambda_n = \frac{v_n}{a}, \quad \gamma_n = (\kappa^2 - v_n^2)^{1/2}, \quad \lambda_{n1} = \frac{\mu_n}{a}, \quad \gamma_{n1} = (\kappa^2 - \mu_n^2)^{1/2},$$

$$\lambda_{n2} = \frac{v_n}{b} = \frac{v_n}{\theta a}, \quad \theta = b/a, \quad \gamma_{n2} = \left(\kappa^2 - \left(\frac{v_n}{\theta} \right)^2 \right)^{1/2};$$

where $J_q(\dots)$, $N_q(\dots)$ are the Bessel and Neumann functions; $v_n, \mu_n, n=1,2,\dots$ are non-zero positive roots of equations $J_1(v)=0$ and $G_1(\mu,1)=0$. The eigenfunctions $\psi_n(\rho), \psi_{n1}(\rho), \psi_{n2}(\rho)$ form the orthonormal φ -independent bases in the relevant plane domains: two circular and one annular waveguides, respectively.

Satisfying the boundary conditions for the functions u and $\partial u / \partial z$ at $z=0$ (i.e., the conditions of continuity of the total field tangential components) providing the uniqueness of the solution of (2)-(4), we arrive at functional equations. In terms of the Fourier coefficients of matching functions, one of them has the following form:

$$\begin{cases} \sum_n R_n (v_n^2 - \mu_m^2)^{-1} = \omega_{m1} \\ \sum_n R_n (v_n^2 - v_m^2 / \theta^2)^{-1} = \omega_{m2}; \end{cases} \quad m=1,2,\dots \quad (9)$$

where $R_n = 2R_{np}^{EE}(t-\eta) J_1(v_n \theta) / J_0(v_n)$;

$$\omega_{m1} = -f_{m1} [G_0^2(\mu_m, 1) - \theta^2 G_0^2(\mu_m, \theta)]^{1/2} / \theta \mu_m G_0(\mu_m, \theta);$$

$$\omega_{m2} = f_{m2} \theta / v_m;$$

$$F_{nmj} = 2\pi \int_{\delta_j^1 b}^{\delta_j^1 a + \delta_j^2 b} \psi_n(\rho) \psi_{mj}(\rho) \rho d\rho, \quad j=1,2,\dots$$

$$\begin{aligned} f_{mj}(t) = & \frac{1}{2} \left\{ \sum_n F_{nmj} \int_0^t \left\{ \lambda_n J_1[\lambda_n(t-\tau)] + \lambda_{mj} J_1[\lambda_{mj}(t-\tau)] \right\} \chi(t-\tau) R_{np}^{EE}(\tau-\eta) d\tau + \right. \\ & \left. + F_{pmj} \frac{\partial}{\partial t} \left[\delta(t-\eta) - \int_0^t J_0[\lambda_{mj}(t-\tau)] \chi(t-\tau) v_p'(0, \tau) d\tau \right] \right\} \end{aligned}$$

Expression (9) is a dual series operator equation with respect to the set of unknown functions $\{R_{np}^{EE}(t-\eta)\}$. It is well known from the theory of matrix operators of convolution type [4], that (9) provides the solution in explicit form via application of the residue calculus of meromorphic functions over a contour in the complex plane. It is noteworthy that the elements of the vector function $\{R_{np}^{EE}(t-\eta)\}$ in the right-hand side of (9) make invest only by their values at the moments of time τ that are strictly earlier than t . Thus, the initial boundary value problem is reduced to the Volterra integral equation of the second kind. The properties of the matrix kernel enable us to solve this Volterra equation numerically, without inverting the ma-

trix kernel at each step of integration, that considerably increases efficiency of numerical algorithm. It has been thoroughly tested and cross-checked.

2. *Thin axially symmetric irises have been chosen as the second example*, to demonstrate that the mode matching technique in time domain can arrive at a considerably simpler example then described above. The total field in domains A ($z > 0$) and B ($z < 0$) can be presented as:

$$U \begin{pmatrix} A \\ B \end{pmatrix} = - \sum_n \int_0 J_0 \left[\lambda_n \left((t-\tau)^2 - z^2 \right)^{1/2} \right] \chi \left[(t-\tau) \mp z \right] \begin{pmatrix} R_{np}^{AA} \\ T_{np}^{BA} \end{pmatrix} (t-\tau) d\tau \cdot \Psi_n(\rho) + \begin{pmatrix} U^i \\ 0 \end{pmatrix}.$$

After satisfying the boundary and continuity conditions at the plane $z=0$ and carrying out several obvious transformations we obtain that

$$R_{np}^{AA}(t-\tau) = 2\pi \sum_m F_{nmj} \left\{ \lambda_m \int_0 J_1[\lambda_m(t-\tau)] \chi(t-\tau) R_{np}^{AA}(\tau-\eta) d\tau + \delta_m^p \delta^{(1)}(t-\eta) \right\} \quad (10)$$

$$n=1,2,\dots; \quad j=1,2.$$

Here $F_{nmj} = 2\pi \int_{\delta_j^1 b}^{\delta_j^1 a + \delta_j^2 b} \psi_n(\rho) \psi_m(\rho) \rho d\rho$. If $j=1$, formula (10) characterizes the scattering properties of an annular-type iris, and if $j=2$, it corresponds to the one of circular shape. Similar to the bifurcation problem, the elements of unknown vector function $\{R_{np}^{AA}(t-\tau)\}$ that are in the right hand side of (10) influence its value at the moment t only by means of their values at the time moments τ that are earlier than t . Thus, for a fixed t (regular step in time) we can consider (10) as explicit solution of the problem of non-stationary excitation of symmetrical irises in circular waveguides.

Conclusions

The discussed above algorithms have been implemented in numerical codes for computer-aided simulation of several key problems. Characteristic cases studied showed these algorithms to be a powerful and reliable software tool for fundamental and application-oriented investigation of the physical features and peculiarities of time-space field transformations in the resonant structures that are of practical interest in many areas of today microwave engineering and scientific devices design.

REFERENCES

1. E. G. Bessonov, Yu. K. Sirenko, N. P. Yashina, Non stationary model problems of the theory of waveguide open resonators, *Uspekhi Sovremennoi Radioelektroniki* (Moscow), 1997, No 12, pp. 18-33 (in Russian).
2. Yu.K. Sirenko, N. P. Yashina, Operator method in nonstationary theory of waveguide open resonators, *Radiofizika Radioastronomiya*, 1997, v. 2, No 1, pp. 78-84 (in Russian).
3. O. A. Ladizhenskaya, *Boundary Problems of Mathematical Physics*, Moscow: Nauka, 1973 (in Russian).
4. V. P. Shestopalov, A. A. Kirilenko, S. A. Masalov, *Convolution Type Matrix Equations in Diffraction Theory*, Kiev: Naukova Dumka, 1984 (in Russian)

ASYMPTOTIC RADIATION FIELD OF ASYMMETRIC PLANAR DIELECTRIC WAVEGUIDE

Dennis P. Nyquist

Department of Electrical Engineering, Michigan State University
East Lansing, Michigan 48824, U.S.A.

Abstract: In the spectral analysis of practical open integrated waveguiding structures, multiple non-removable branch points occur in the axial Fourier-transform plane. When the inversion integral for the distant radiation field is approximated asymptotically by deforming the real-axis integration contour (C) into a steepest-descents contour (SDC) all of the associated branch cuts are crossed twice. Passage from the top Riemann sheet to lower sheets and back to the top sheet occurs so both ends of the contour lie on the top sheet and C can be directly connected into SDC. If the observation aspect angle is sufficiently large, however, all but one of the cuts are crossed a third time and the two ends of the SDC lie on different sheets. Deformation of C into SDC then requires a fourth crossing of those cuts and integration around them to remain on the top sheet. A continuous spectrum contribution consequently augments the saddle-point term contributed by the SDC approximation. These wave phenomena are studied in detail for the asymmetric planar dielectric waveguide, which is the simplest canonical structure for which multiple non-removable branch points occur.

INTRODUCTION:

Integrated waveguide structures consist of conducting or dielectric guiding regions immersed in a planar-layered background environment. The analysis of such configurations proceeds typically from a spectral formulation for the currents/fields in the axial Fourier-transform domain. Integral representations for the complete electromagnetic field maintained by excitatory electric currents are obtained by subsequent inverse transformation of the spectral-domain fields. Evaluation of the integral representations requires that singularities of the spectral-domain currents/fields be identified. Those singularities consist of simple poles associated with the integrated guiding structure and branch points contributed by the layered background environment. The author has demonstrated previously [1,2] that the latter branch points arise from both the wavenumber parameters and the discrete surface/leaky-wave poles of the layered background. Asymptotic evaluation of the distant fields proceeds through a steepest-descents approximation of the axial inverse-transform integral representations. The latter procedure is complicated by the presence of multiple non-removable branch-point singularities in the spectral-domain fields. For simple canonical waveguides (such as the symmetric planar dielectric slab), the steepest-descents integration contour (SDC) crosses the single branch cut twice so both of its ends lie on the top Riemann sheet; the original real-axis integration contour (C) is consequently directly deformed into the SDC. When applied to spectral fields of integrated guiding structures, a SDC crosses all of the branch cuts twice, but can cross all but one a third time for adequately large observation aspect angles. As a result, those latter cuts must be crossed a fourth time and the integration path deformed around them to return to the top sheet prior to connecting C into the SDC. Additional continuous-spectrum wave contributions consequently arise in distant approximations to the complete field. Since no prior efforts on asymptotic evaluation of integrated waveguide fields is apparent, a simple canonical waveguiding structure which shares the presence of multiple non-removable branch points is investigated to obtain insight into the more practical integrated structures.

CONFIGURATION AND ANALYSIS:

The asymmetric, planar dielectric-slab waveguide is perhaps the simplest canonical waveguiding structure for which multiple non-removable branch points are present in its spectral-domain field. The configuration of such a structure excited by a line source is indicated in Fig. 1. It consists of a dielectric guiding layer with refractive index n_2 and thickness t located between semi-infinite cover and substrate layers having refractive indices n_1 and n_3 , respectively, where $n_1 < n_3 < n_2$. Wavenumbers in the various layers are $k_l = n_l k_0$, $l=1,2,3$, where $k_0 = 2\pi/\lambda_0$ is the free-space wavenumber. An axial Fourier-transform solution for the TE field is constructed by well-known methods [3-5] leading to an integral representation for the region 1 field as

$$E_{1y}(x, z) = -j\omega\mu_0 \int_{-\infty}^{\infty} \frac{e^{-p_1|x-x'|} + R(\zeta)e^{-p_1(x+x')}}{4\pi p_1} e^{-j\zeta(z-z')} d\zeta \quad (1)$$

where reflection coefficient $R(\zeta)$ depends upon the wavenumber parameters $p_1 = \sqrt{\zeta^2 - k_1^2}$.

The spectral-domain field has two types of singularities in the complex axial transform (ζ) plane. The p_1 lead to branch points at $\pm k_1$, although those at $\pm k_2$ are removable, while $R(\zeta)$ leads to simple pole singularities. Those complex ζ -plane singularities are indicated, along with the relevant wavenumber locations, in Fig. 2. Sommerfeld-type branch cuts, also shown in Fig. 2, are selected leading to a 4-sheeted Riemann surface for which the spectral field decays or remains bounded transversely for all points on the top sheet, while it grows transversely on the lower sheets. The pole singularities consist of two distinct types; proper surface-wave poles occur on the top Riemann sheet while improper leaky-wave poles appear on the remaining three. Various representations of the total field are considered below, including asymptotic steepest-descents approximations to the distant (from the line source) field.

ALTERNATIVE FIELD REPRESENTATIONS:

The real-axis integration path C in Fig. 2 can be deformed in various ways to obtain alternative field representations. Of particular interest is the distant radiation field, for which asymptotic techniques, such as the method of steepest descents, are applicable to approximate the inversion integral in Eq. (1).

A polar coordinate representation of the field point is defined by $(x \pm x') = r \cos \theta$, $(z - z') = r \sin \theta$ where θ is the polar angle measured from the x -axis. For asymptotic evaluation of the cover field, the steepest-descents contour SDC is found to depend upon the observation aspect angle as indicated in Fig. 3.

If θ is sufficiently small then the SDC crosses both branch cuts twice and its ends both lie on the top Riemann sheet. There exists a critical angle θ_c , however, beyond which the SDC crosses the k_3 branch cut a third time and the two ends of the SDC lie on different sheets. That angle is found to be given by

$$\theta_c = \frac{\pi}{2} - \cos^{-1}\left(\frac{k_1}{k_3}\right) = \frac{\pi}{2} - \cos^{-1}\left(\frac{n_1}{n_3}\right). \quad (2)$$

Asymptotic evaluation of the integral in Eq. (1) consequently depends upon whether that critical angle is exceeded. The two possibilities are considered below.

case no. 1: $\theta < \theta_c$ (two k_3 branch-cut crossings)

In this case, the two ends of C and SDC lie on the top sheet so they can be connected along C_∞ to form a closed contour as indicated in Fig. 4. Note that a segment of the SDC, between the two pairs of branch cut crossings, lies on the bottom Riemann sheet. The SDC may consequently capture surface-wave poles on the top sheet and leaky-wave poles on the bottom sheet, although this is unlikely at small aspect angles. The SDC must be deformed about such captured poles, and the contour which excludes all such poles is designated as C_p . Cauchy's integral theorem then provides

$$\oint_{-C+SDC+C_p+C_\infty} (\dots) d\zeta = 0 \Rightarrow \int_C (\dots) d\zeta = \int_{SDC} (\dots) d\zeta + \int_{C_p} (\dots) d\zeta \quad (3)$$

but it is well known that

$$\int_{C_p} (\dots) d\zeta \sim e^{-ar} \quad (4)$$

along radial lines as $k_1 r \rightarrow \infty$. The pole residues consequently do not contribute to the distant radiation

field. The SDC can also be deformed into the lower half plane and about branch cuts C_{b1} and C_{b3} , as indicated in Figs. 2 and 4, leading to

$$\oint_{-SDC+C_p+C_\infty+C_{b1}+C_{b3}} (\dots) d\zeta = 0 \Rightarrow \int_{SDC} (\dots) d\zeta = \int_{C_{b1}+C_{b3}} (\dots) d\zeta \quad (5)$$

where the pole contribution is neglected. It is concluded that in this case the SDC contribution includes the entire proper radiation spectrum. Finally the saddle point approximation to the SDC integral provides the well-known result

$$E'_{1y}(r, \theta) = -j\omega\mu_0 \int_{SDC} (\dots) d\zeta \sim -\frac{\omega\mu_0}{4} \sqrt{\frac{2}{\pi}} R(\theta) \frac{e^{-j(k_1 r - \pi/4)}}{\sqrt{k_1 r}} \quad (6)$$

case no. 2: $\theta > \theta_c$ (three k_3 branch cut crossings)

In this case, the left side of the SDC lies on the top sheet (of the k_3 -related Riemann surface) while its right side lies on the bottom sheet as indicated in Fig. 5. The right end of the SDC must consequently be deformed along C_∞ to cross the C_{b3} branch cut a fourth time and pass back to the top sheet; it is subsequently deformed about the C_{b1} cut to remain on the top sheet and connected into the left end of the SDC. By Cauchy's theorem

$$\oint_{-SDC+C_\infty+C_p+C_{b1}} (\dots) d\zeta = 0 \Rightarrow \int_{SDC} (\dots) d\zeta = \int_{C_{b1}} (\dots) d\zeta \quad (7)$$

where pole contributions have been neglected. The SDC integral now represents the **incomplete** radiation field. It **includes** the C_{b1} component but **excludes** the C_{b3} component. This implies that the SDC contribution is discontinuous at $\theta = \theta_c$ unless the C_{b3} contribution vanishes there.

The two ends of C lie on the top sheet, while the left end of the SDC lies on the top sheet and its right end lies on the bottom sheet. C is deformed into the SDC as indicated in Fig. 6. The left ends of C and the SDC are connected directly on the top sheet along C_∞ . The right end of C is deformed along C_∞ and around C_{b3} on the top sheet. Finally C_{b3} is crossed to pass to the bottom sheet and connection with the SDC is made along C_∞ . Cauchy's theorem then requires

$$\oint_{-C+SDC+C_p+C_{b3}+C_\infty} (\dots) d\zeta = 0 \Rightarrow \int_C (\dots) d\zeta = \int_{SDC} (\dots) d\zeta + \int_{C_{b3}} (\dots) d\zeta \quad (8)$$

and the **complete** radiation field is recovered by augmenting the **incomplete** SDC component with the missing C_{b3} component. The additive continuous-spectrum component is a lateral wave discussed briefly in [6-8] in a different context. Replacing the SDC component by the asymptotic saddle-point approximation leads to

$$E'_{1y}(r, \theta) \sim -\frac{\omega\mu_0}{4} \sqrt{\frac{2}{\pi}} R(\theta) \frac{e^{-j(k_1 r - \pi/4)}}{\sqrt{k_1 r}} - j\omega\mu_0 \int_{C_{b3}} (\dots) d\zeta \quad (9)$$

which includes the additive continuous-spectrum component.

The significance of the additive continuous-spectrum component to the reflected field is studied in Figs. 7 and 8, where the saddle-point contribution $(E_{yp})_{sp}$, branch-cut contribution $(E_{yp})_{bc}$ and the total

reflected field $E_{yr} = (E_{yr})_{sp} + (E_{yr})_{bc}$ are displayed. These numerical results are for a dielectric waveguide having $t/\lambda_0 = .5$ and $n_1 = 1.$, $n_2 = 3.2$, $n_3 = 3.0$ which supports only the principal surface-wave mode and leads to a critical angle of $\theta_c = 19.5^\circ$. Fig. 7 displays the radial dependence of the field for $\theta = 88^\circ$; clearly the branch-cut contribution is negligible except for relatively small r/λ_0 . The angular dependence is shown in Fig. 8 for fixed r/λ_0 and again the branch-cut contribution is negligible except for $\theta \rightarrow 90^\circ$.

CONCLUSIONS:

The spectral analysis of open-boundary waveguides leads to multiple non-removable branch points in the axial Fourier-transform plane. The presence of multiple branch points complicates the asymptotic evaluation of the distant radiation field. The SDC crosses all of the associated branch cuts twice but, for sufficiently large observation aspect angles, can cross all but the cut associated with the field region a third time. This results in one end of the SDC residing on the top Riemann sheet while the other end lies on a lower sheet. Connection of the SDC into the original integration path C consequently requires deformation of the SDC to cross the cuts a fourth time to return to the top sheet and then pass around them to remain on the top sheet before connecting with C. The result is a continuous spectrum branch-cut contribution which augments the asymptotic approximation arising from the SDC integration. These lateral waves are found to decrease more rapidly than the asymptotic contribution with distance from the line source. The portion of the SDC which lies on the bottom sheet can capture leaky-wave poles while surface-wave poles can be captured on the top sheet. The pole residue terms decay exponentially with radial distance from the line source and consequently do not contribute to the distant radiation field. Modifications necessary to extend this technique to practical integrated waveguiding structures are will be identified.

REFERENCES:

- [1] Nyquist, D.P. and Infante, D.J., "Discrete Higher-Order Leaky-Wave Modes and the Continuous Spectrum of Stripline," IEICE Trans. on Electronics (Institute of Electronics, Information and Communication Engineers, Japan), Special Issue on Electromagnetics, vol. E78-C, no. 10, Oct. 1995, pp. 1331-1338.
- [2] Nyquist, D.P., Grimm, J.M., Infante, D.J. and Braunisch, H., "Classification of the Proper Propagation-Mode Spectrum and Leaky-Wave Modes on Open Planar Waveguides," Electromagnetics, vol. 17, no. 2, March-April 1997, pp.105-130.
- [3] Tai, C.T., "Effect of a Grounded Slab on Radiation from a Line Source," J. Appl. Phys., vol. 22, April 1951, pp. 405-414.
- [4] Marcuvitz, N., "On Field Representations in Terms of Leaky Modes," IRE Trans., vol. AP-4, July 1956, pp. 192-194.
- [5] Cassedy, E.S. and Cohn, M., "On the Existence of Leaky Waves Due to a Line Source Above a Grounded Dielectric Slab," IRE Trans., vol. MTT-9, May 1961, pp. 243-247.
- [6] Felsen, L. and Marcuvitz, N., *Radiation and Scattering of Waves*, Prentice-Hall, Englewood Cliffs, N.J., 1973, Chapter 5.
- [7] Chew, W.C., *Waves and Fields in Inhomogeneous Media*, Van Nostrand Reinhold, New York, 1990, pp. 101-104.
- [8] Vassallo, C., *Optical Waveguide Concepts*, Elsevier, Amsterdam, pp. 142-159.

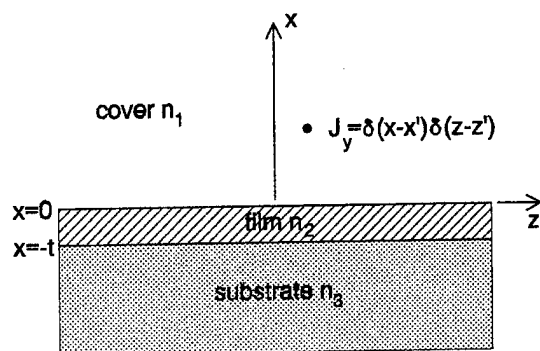


Fig. 1 Configuration of asymmetric planar dielectric waveguide with unit line-source excitation.

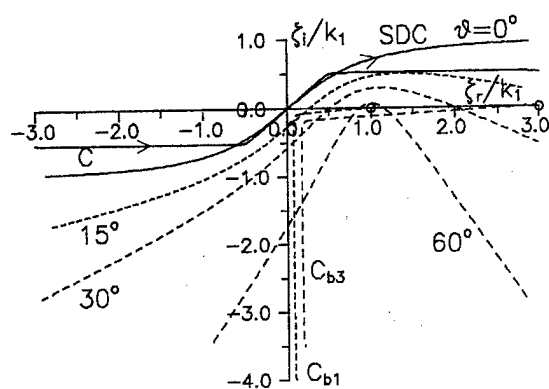


Fig. 3 SDC in ζ -plane for various observation aspect angles; relation to k_3 branch cut.

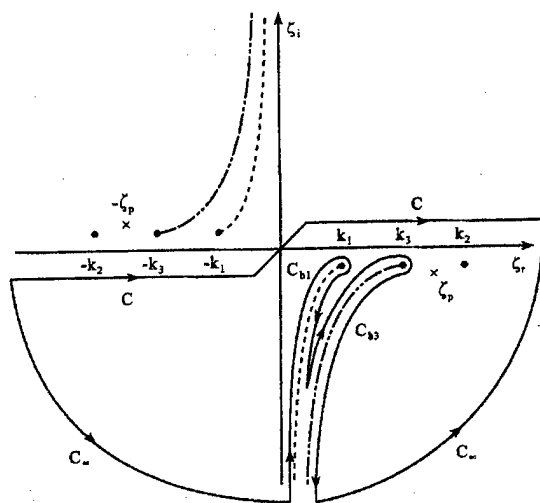


Fig. 2 Integration path and singularity points in complex ζ -plane.

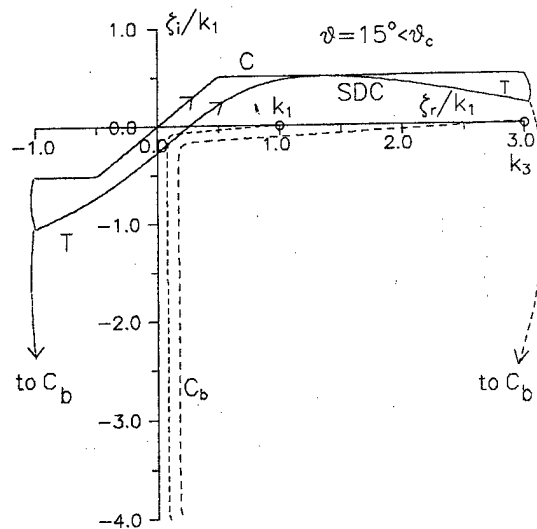


Fig. 4 Appropriate closure of C into SDC when $\theta < \theta_c$.

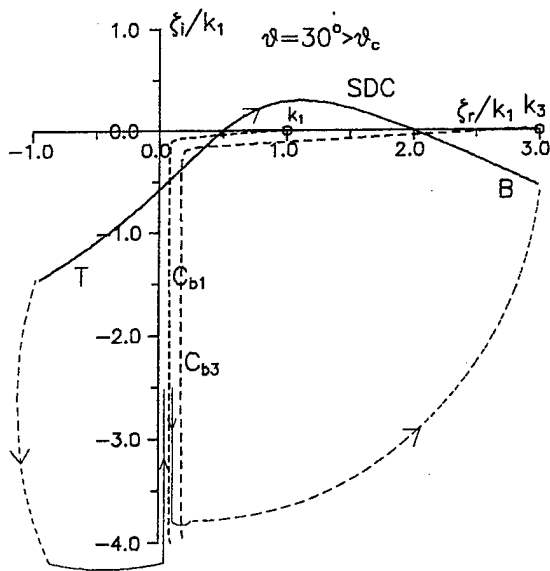


Fig. 5 Appropriate closure of SDC into C_{b1} branch cut when $\theta > \theta_c$.

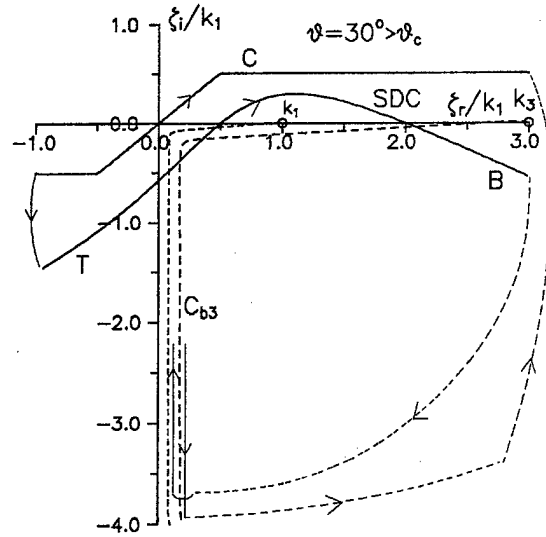


Fig. 6 Appropriate closure of C into SDC and C_{b3} branch cut when $\theta > \theta_c$.

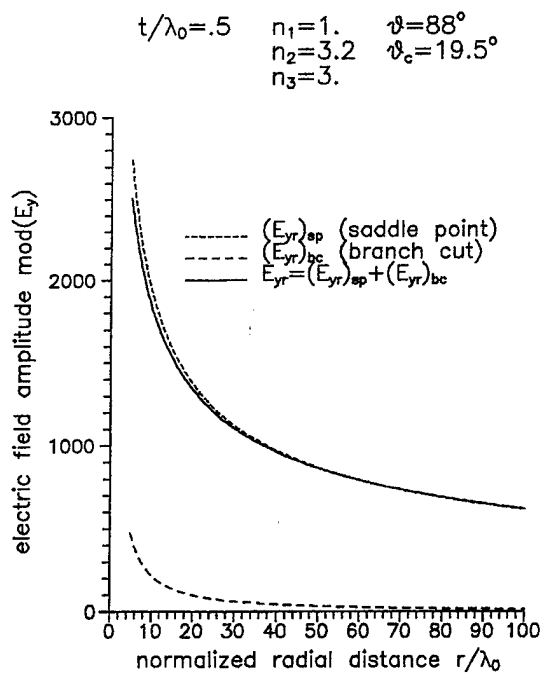


Fig. 7 Radial dependence of saddle-point and branch-cut contributions to the reflected wave component of the distant radiation field in the cover layer of an asymmetric planar dielectric waveguide.

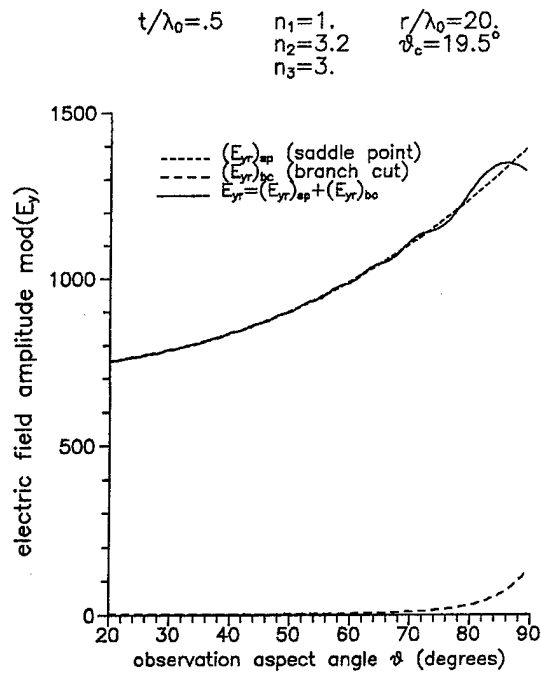


Fig. 8 Angular dependence of saddle-point and branch-cut contributions to the reflected wave component of the distant radiation field in the cover layer of an asymmetric planar dielectric waveguide.

An Efficient Iterative Scheme for Solving Eigenproblems in the Theory of Electromagnetic Waves

Tomasz F. Jabłoński

*Polish Academy of Sciences
Institute of Fundamental Technological Research
Świętokrzyska 21, 00-049 Warsaw, Poland
Internet: tjablon@ippt.gov.pl, fax: +48-22 826 98 15*

Abstract

A universal and efficient iterative scheme for solving eigenproblems is presented. It is based on a functional analysis approach. Several variants of numerical implementation of the method are proposed. The application to the problem of electromagnetic waves propagation in anisotropic waveguides with arbitrary transversal inhomogeneity of the permittivity is briefly specified. Several examples of the computed mode vector fields in various complex dielectric guiding structures are shown.

1 Introduction

The main difficulties of solving eigenproblems of electromagnetic waves propagation are due to the following facts:

- electrodynamical coupling between the magnetic and electric field components of a mode in the region of the permittivity variation,
- energy radiation from an open guiding structure,
- complicated geometry and profile of the transversal inhomogeneity of the permittivity.

The mathematical difficulties corresponding to the above physical facts, when one seeks the solution in the space of square integrable functions, are the following:

- nonselfadjointness of the operators constructed from the vectorial equations describing propagation and possible nonorthogonality of the eigenfunctions (guided modes),
- existence of unbounded or nonvanishing at infinity solutions (corresponding to the continuous part of the spectrum of the constructed operators),
- complexity of the boundary conditions and/or of the (variable) coefficients of the equations.

Because of the above difficulties there exist not many full-wave (vectorial) methods which can provide satisfactory solution especially for complicated structures. There dominate purely numerical methods, mainly the variants of finite difference or of finite element methods [1]–[3] (for more complete reference see [4]). The common feature of all these methods is that the original *differential* problem is reduced to numerically solving an *algebraic* matrix eigenproblem, after making more or less arbitrary choice of the discrete and finite subbasis in the function space the solution is sought for. Often, the correspondence between the original differential problem and the discretized algebraic one is difficult to be maintained or is even violated. Moreover, these methods require a large amount of memory (mainframes) to be effective in more complicated cases.

Here we present the method called Iterative Spectral Decomposition Method (ISDM) [5], [4]. It was derived with a help of functional analysis techniques and after investigating spectral properties of the suitably defined propagation operator resulting from Maxwell's equations [6], [7]. The proposed iterative process is rapidly convergent, has low computer memory requirements and has proved to be an efficient and universal tool for the analysis and numerical simulation of various dielectric guiding structures. Some examples are mentioned in this short paper.

2 Abstract scheme of the ISDM

Let T be an unbounded, densely defined and closed linear operator in the Hilbert space $(\mathcal{H}, (\cdot, \cdot)_{\mathcal{H}})$, with nonempty discrete spectrum $\sigma_{disc}(T) \neq \emptyset$. Suppose that T can be decomposed

$$T = L - F$$

in such a way that L is a selfadjoint operator with known spectral properties and the (unbounded) operator F is L -compact, meaning that $D(F) \supseteq D(L)$ and $\forall \rho \notin \sigma(L)$ the operator $F(L - \rho)^{-1}$ is compact.

Under the above conditions, the eigenproblem

$$(T - \tau)u = 0, \quad u \in D(T)$$

which can be written equivalently as $u = (L - \tau)^{-1}Fu$ if $\tau \notin \sigma(L)$, is solved by the following iterative process

$$\begin{aligned} \tilde{u}_n &= (L - \tau_{n-1})^{-1}Fu_{n-1} \\ u_n &= \tilde{u}_n / \|\tilde{u}_n\|_{\mathcal{H}}, \quad \tau_n = (Tu_n, u_n)_{\mathcal{H}} \end{aligned} \quad (*)$$

This iterative process, called Iterative Spectral Decomposition Method (ISDM), is rapidly convergent, has low computer memory requirements and has proved to be superior to many large-scale mainframe numerical methods.

Several variants of numerical implementation of the process are proposed, relatively to the accessible means of solving inhomogeneous equation (*) in various physical situations.

2.1 Variant I (eigenfunction expansion)

Spectral measure of the operator L is known, e.g. L has compact resolvent and is semibounded; the solution u_n is expanded in the basis of eigenvectors of L (corresponding special functions). This variant is called the Iterative Eigenfunction Expansion Method (IEEM).

The spectrum $\sigma(L) = \sigma_{disc}(L)$ is discrete and the eigenvectors e_m

$$(L - \lambda_m)e_m = 0, \quad \|e_m\|_{\mathcal{H}} = 1, \quad m = 1, 2, 3, \dots$$

form an orthonormal basis in \mathcal{H} . In the iterative process we utilize known eigenpairs $(e_m, \lambda_m)_{m=1}^{\infty}$ of the operator L :

$$\begin{aligned} \tilde{u}_n &= \sum_m C_m^n e_m, \\ C_m^n &= (\lambda_m - \tau_{n-1})^{-1} (Fu_{n-1}, e_m)_{\mathcal{H}}, \end{aligned} \quad (*)$$

$$\begin{aligned} u_n &= \sum_m D_m^n e_m, \quad D_m^n = C_m^n (\sum_m |C_m^n|^2)^{-1/2}, \\ \tau_n &= \sum_m [\lambda_m |D_m^n|^2 - (Fu_n, e_m)_{\mathcal{H}} \overline{D_m^n}] \end{aligned}$$

2.2 Variant II (using Fourier transform)

T is a differential operator in $L^2(\mathbb{R}^n)$; the action of the operator $(L - \tau)^{-1}F$ is simplified by means of the Fourier transform in $L^2(\mathbb{R}^n)$:

$$u^\wedge(\lambda) = (2\pi)^{-n/2} \int_{\mathbb{R}^n} e^{-ix \cdot \lambda} u(x) dx.$$

To this end, for any $z \in L^\infty(\mathbb{R}^n)$, let us define the operator:

$$\begin{aligned} L^2(\mathbb{R}^n) \ni u &\mapsto (zu^\wedge)^\vee \\ z(-i\nabla)u &\equiv (z(\lambda)u^\wedge(\lambda))^\vee \end{aligned}$$

The operator $z(-i\nabla)$ is well defined and bounded in $L^2(\mathbb{R}^n)$. Since F is L -compact, the operator $(L - \tau)^{-1}F$ is compact for $\tau \notin \sigma(L)$. Hence it is bounded and can be expressed in the form:

$$\begin{aligned} (L - \tau)^{-1}Fu &= z_\tau(-i\nabla)u = \\ &= (z_\tau(\lambda)u^\wedge(\lambda))^\vee = fl_\tau(-i\nabla)u \end{aligned}$$

for a function $z_\tau = z_\tau(\lambda) \in L^\infty(\mathbb{R}^n)$ of the form determined by the choice of the spectral decomposition of $T = L - F$. We can now perform the iterative process on the Fourier transforms of u_n :

$$\tilde{u}_n^\wedge = (z_{\tau_{n-1}}(-i\nabla)u_{n-1})^\wedge = z_{\tau_{n-1}}(\lambda)u_{n-1}^\wedge(\lambda) \quad (*)$$

$$u_n^\wedge = \tilde{u}_n^\wedge \|\tilde{u}_n^\wedge\|_2^{-1} = \tilde{u}_n^\wedge \left(\int_{\mathbb{R}^n} |\tilde{u}_n^\wedge(\lambda)|^2 d\lambda \right)^{-1/2}$$

$$\begin{aligned} \tau_n &= (((L - F)u_n)^\wedge, u_n^\wedge)_2 = \\ &= \int_{\mathbb{R}^n} (l_0^{-1}(\lambda) - f(\lambda)) |u_n^\wedge(\lambda)|^2 d\lambda \end{aligned}$$

2.3 Variant III (using Green's function)

T is a differential operator in $L^2(\mathbb{R}^n)$; the Green's function of the operators L or $(L - \tau)^{-1}F$ is used to solve (*).

If $l_\tau \in L^2(\mathbb{R}^n) \cap L^\infty(\mathbb{R}^n)$ or $l_\tau^\vee \in L^1(\mathbb{R}^n)$, then the convolution:

$$(l_\tau u^\wedge)^\vee = (2\pi)^{-n/2} l_\tau^\vee * u$$

exists for $u \in L^2(\mathbb{R}^n)$ and $l_\tau^\vee(x, y)$ is the Green's function of L . Then

$$(L - \tau_n)^{-1}Fu = l_\tau(-i\nabla)Fu = (l_\tau(Fu)^\wedge)^\vee$$

If we choose the spectral decomposition of $T = L - F$ such that $l_\tau^\vee(x, y)$ is known, then the equation (*) can be effectively solved as follows:

$$\tilde{u}_n = (2\pi)^{-n/2} \int_{\mathbb{R}^n} l_{\tau_{n-1}}^\vee(x - y) F u_{n-1}(y) dy \quad (*)$$

Analogously, if the analytical form of z_τ^\vee can be obtained, then

$$\tilde{u}_n = (2\pi)^{-n/2} \int_{\mathbb{R}^n} z_{\tau_{n-1}}^\vee(x - y) u_{n-1}(y) dy \quad (*)$$

3 Application of the ISDM to dielectric waveguides

3.1 Assumptions about the guiding structure

Let us consider a waveguide that is: homogeneous along the direction of propagation x_3 , transversely inhomogeneous, magnetically isotropic with $\mu = \mu_0 = \text{const}$, electrically anisotropic with the principal axis o_3 along x_3 :

$$\mathcal{E}(x) = \begin{bmatrix} \epsilon_{11} & \epsilon_{12} & 0 \\ \epsilon_{21} & \epsilon_{22} & 0 \\ 0 & 0 & \epsilon_{33} \end{bmatrix}, \quad x = (x_1, x_2) \in \mathbb{R}^2,$$

where the dielectric tensor $\mathcal{E}(x)$ is hermitian, positively defined and

$$\begin{aligned}\epsilon_{ij} : \mathbb{R}^2 \ni x = (x_1, x_2) &\longrightarrow \mathbb{C}, \quad i, j = 1, 2, 3 \\ \epsilon_{ij}(x) = \epsilon_{cl} = \text{const} &\quad \text{for } |x| > R_s.\end{aligned}$$

3.2 Formulation of the eigenproblem

Assuming harmonic time dependence $e^{-i\omega t}$, after expressing all the six vector field components of the guided mode by:

$$\begin{aligned}H_{\perp} &= [h_1(x_1, x_2), h_2(x_1, x_2)] e^{i(\beta x_3 - \omega t)} = \\ &= h_{\perp} e^{i(\beta x_3 - \omega t)},\end{aligned}$$

Maxwell's equations for the waveguide can be reduced to the following eigenproblem:

$$\begin{aligned}(T - \beta^2) h_{\perp} &= 0, \\ T h_{\perp} &= (L - F) h_{\perp} = \\ L &\leftrightarrow \boxed{\nabla_{\perp}^2 h_{\perp}} + \\ -F &\leftrightarrow \boxed{\begin{aligned} &k^2 \begin{bmatrix} \epsilon_{22} & -\epsilon_{12} \\ -\epsilon_{21} & \epsilon_{11} \end{bmatrix} h_{\perp} + \\ &\frac{1}{\epsilon_{33}^2} \begin{bmatrix} \epsilon_{22} & -\epsilon_{12} \\ -\epsilon_{21} & \epsilon_{11} \end{bmatrix} \{ \nabla_{\perp} \epsilon_{33} \times (\nabla_{\perp} \times h_{\perp}) \} + \\ &\frac{1}{\epsilon_{33}} \begin{bmatrix} \epsilon_{33} - \epsilon_{22} & \epsilon_{12} \\ \epsilon_{21} & \epsilon_{33} - \epsilon_{11} \end{bmatrix} \{ \nabla_{\perp} \times (\nabla_{\perp} \times h_{\perp}) \} \end{aligned}}$$

where $\nabla_{\perp} = [\frac{\partial}{\partial x_1}, \frac{\partial}{\partial x_2}]$, $k^2 = \omega^2 \mu_0 \epsilon_0$.

3.3 Spectral decomposition of T

Since guided modes are square integrable, we define operator T in the Hilbert space \mathcal{H} of square integrable complex valued vector functions defined on the cross-sectional plane \mathbb{R}^2 of an open waveguide, or on the bounded region Ω denoting the cross-section of a shielded waveguide:

$$\mathcal{H} = L^2(\mathbb{R}^2) \otimes \mathbb{C}^2 \quad \text{or} \quad \mathcal{H} = L^2(\Omega) \otimes \mathbb{C}^2.$$

We introduce in \mathcal{H} the scalar product:

$$(v, w)_{\mathcal{H}} \equiv (v_{x_1}, w_{x_1})_2 + (v_{x_2}, w_{x_2})_2,$$

where for $v = [v_{x_1}, v_{x_2}]$, $w = [w_{x_1}, w_{x_2}] \in \mathcal{H}$

$$(v_{x_j}, w_{x_j})_2 = \int_{\mathcal{O}} v_{x_j} \overline{w_{x_j}} dx, \quad j = 1, 2$$

and $\mathcal{O} = \mathbb{R}^2$, or $\mathcal{O} = \Omega$, respectively.

Decomposing the operator T

$$T = L - F,$$

we pick out as the operator L :

$$L = \nabla_{\perp}^2, \quad D(L) = D(l) \otimes \mathbb{C}^2$$

with the domain $D(\mathbf{l})$ such that Laplacian $\mathbf{l}u = \Delta u$ is selfadjoint. Hence, we choose

$$D(\mathbf{l}) = \{u \in L^2(\mathbb{R}^2) : \Delta u \in L^2(\mathbb{R}^2)\} = H^2(\mathbb{R}^2)$$

for open waveguides, and

$$D(\mathbf{l}) = \{u \in H_0^1(\Omega) : u \in C^2 \text{ down to } \partial\Omega, u|_{\partial\Omega} = 0\} \text{ or}$$

$$D(\mathbf{l}) = \{u \in H_0^1(\Omega) : u \in C^2 \text{ down to } \partial\Omega, \frac{\partial}{\partial n} u|_{\partial\Omega} = 0\}$$

for shielded waveguides with Dirichlet's or Neumann's boundary conditions, respectively. Now we define

$$D(\mathbf{F}) \equiv \{u \in \mathcal{H} : \mathbf{F}u \in \mathcal{H}\}, \quad D(\mathbf{T}) \equiv D(\mathbf{L}).$$

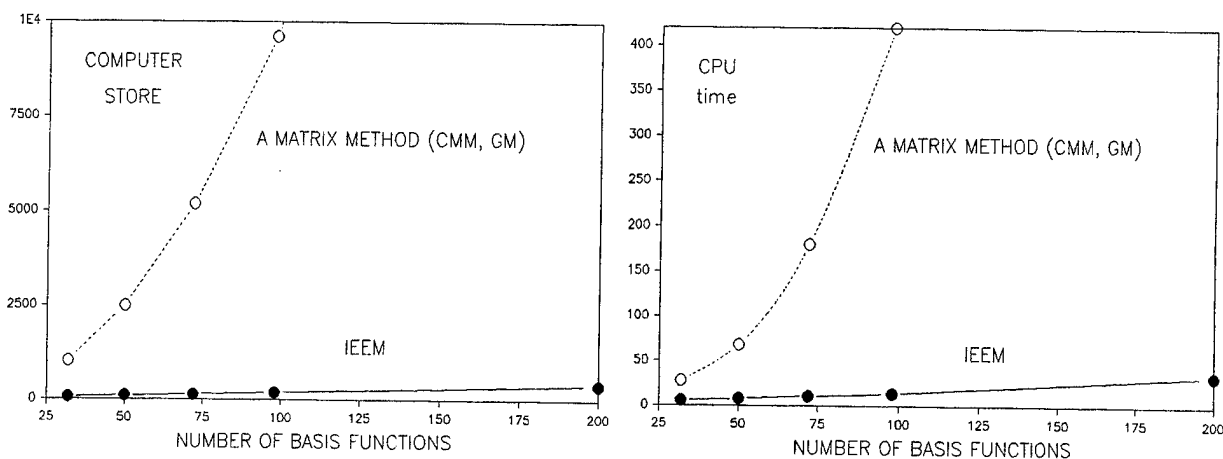
We proved in [6] that \mathbf{T} is a densely defined, closed operator in \mathcal{H} , that $D(\mathbf{F}) \supset D(\mathbf{L})$, and that \mathbf{F} is \mathbf{L} -compact for isotropic structures and \mathbf{L} -bounded for anisotropic ones.

In the numerical implementation of ISDM for open waveguides we discretize the spectrum of Laplacian substituting $D(\mathbf{l}) = H^2(\mathbb{R}^2)$ by the domain of Dirichlet Laplacian defined on bounded, sufficiently large region P such that the guided mode field together with its derivatives is negligible outside P .

3.4 Features of the numerical implementation of the ISDM

- Computes mode propagation constants and vector fields of (multi-core, anisotropic, lossy, shielded or open) dielectric guiding structures with virtually any cross-section and refractive index profile.
- Compact — requires very little computer storage; runs on IBM/PC with 512K RAM and a math-coprocessor.
- Versatile — shape of the structure and its refractive index profile can easily be modified by a user during a computing session.
- Efficient — mode solution accurate to five digits is obtained after literally seconds of computation (5–8 iterations) on an IBM/AT platform.
- Simplicity of the numerical code of the iterative scheme and capability of effective calculation of mode vector fields makes the ISDM a powerful tool for numerical simulation, thorough analysis and design of complex dielectric guiding structures.

Numerical cost (variant IEEM; measured)



3.5 Problems already solved by the ISDM

The method (variant IEEM) has been successfully applied to the analysis of the following dielectric guiding structures:

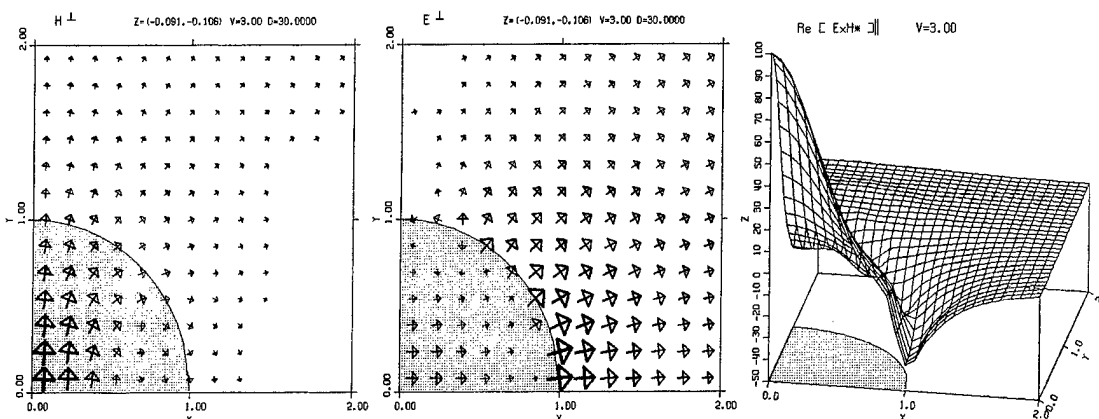
- power profile elliptical fibers with large ellipticity (polarization maintaining fibers);
- anisotropic dielectric waveguides (truly single mode fibers)
- asymmetric double-core waveguides (analysis of wavelength selective coupling)
- multi-core fibers with non-identical cores
- open waveguides with a large core-cladding refractive index difference (complex modes in open lossless dielectric waveguides)
- optical fibers with a lossy core or/and cladding
- birefringent structures with lossy intrusions (dichroic polarizers)
- optical monomode fiber couplers with lossy separating layer of arbitrary refractive index (operating as switches or sensors)
- polarization selective couplers (polarizers and polarization beamsplitters)
- rectangular shielded waveguides loaded with dielectric slabs

4 Selected examples of computed mode fields

4.1 Complex mode in a lossless waveguide

The possibility of existence of complex modes with decaying at infinity fields in lossless isotropic and inhomogeneously filled dielectric waveguides follows from nonselfadjointness of the operator corresponding to the propagation eigenproblem. Nonselfadjointness is a consequence of inhomogeneity of the permittivity in the waveguide cross-section. In the regions of permittivity variation the coupling of the electric and magnetic field components of hybrid modes takes place. At low frequencies, in structures with a large core-cladding index difference this coupling can cause the hybrid mode to become complex [7].

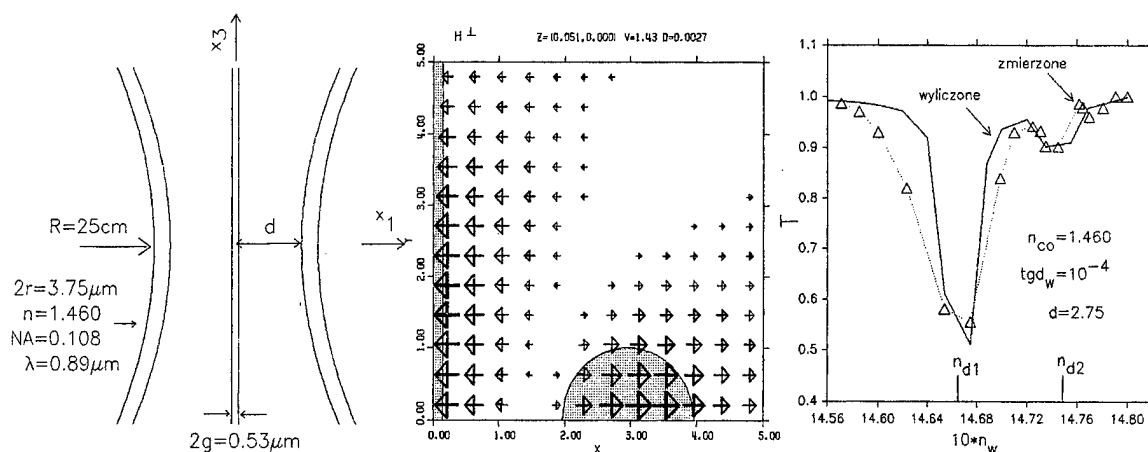
Below, the example of complex EH_{11} mode is shown, namely the transversal field components H_{\perp} , E_{\perp} and the distribution of the energy flow ($\text{Re}\{(E \times \bar{H}) \cdot \vec{x}_3\}$) in the cross-sectional plane of the waveguide at the normalized frequency $V = 3.0$.



4.2 Fiber coupler with a separating layer

The monomode fiber coupler with a separating layer of arbitrary refractive index and geometry shown below has been analyzed in terms of global in the cross-sectional plane, vectorial modes. The coupler is treated as a triple-core structure that is locally homogeneous along the direction of propagation. The global transversal modes contain full information about coupling and attenuation of the fields in each cross-section of the coupler.

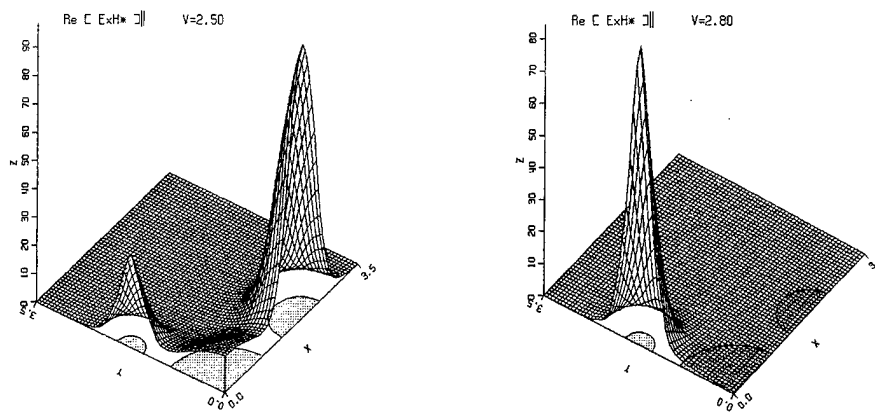
The layer can drain some energy from the fibers (a different quantity for each polarization state), especially when the refractive index of the layer and of the fiber core are more nearly the same. The h_{\perp} field component of the mode that is responsible for the energy transfer to the layer is shown below.



Here we also present the result of the severe, energetical test – computed (continuous curve) and measured (triangle-dotted curve) transmission coefficient T of the coupler versus the refractive index n_w of the layer.

4.3 Multicore fiber with non-identical cores

In such guiding structures the wavelength selective coupling may occur. An example of the mode power density distribution (the real part of the longitudinal component of the Poynting's vector) over the cross-section of a multi-core fiber for different normalized frequencies V is shown below.



5 Conclusions

The effectiveness and versatility of the ISDM are the benefits from applying functional analysis techniques. The method has been successfully applied to a wide class of dielectric guiding structures. The ISDM turned out to be particularly useful as a tool for numerical simulation, thorough modal analysis and design of waveguides with complicated geometry and of various opto-electronic devices including couplers, switches, sensors and resonators.

References

- [1] C. C. Su. A combined method for dielectric waveguides using the the finite-element technique and the surface integral equations method. *IEEE Trans. Microwave Theory Tech.*, MTT-34:1140–1146, November 1986.
- [2] K. Bierwirth, N. Shultz, and F. Arndt. Finite-difference analysis of rectangular dielectric waveguide structures. *IEEE Trans. Microwave Theory Tech.*, MTT-34:1104–1113, November 1986.
- [3] S. F. Kawalko and P. L. E. Uslenghi. A method for the analysis of biaxial graded-index optical fibers. *IEEE Trans. Microwave Theory Tech.*, 39(6):961–968, June 1991.
- [4] T. F. Jabłoński and M. J. Sowiński. Analysis of dielectric guiding structures by the iterative eigenfunction expansion method. *IEEE Trans. Microwave Theory Tech.*, MTT-37:63–70, January 1989.
- [5] T. F. Jabłoński. Iterative eigenfunction expansion method for monomode gradient index fibers with arbitrary cross-section. In *Proc. URSI Int. Symp. E. M. Theory, part B*, pages 415–417, 1986.
- [6] T. F. Jabłoński. *Iterative Spectral Decomposition Method and Its Application to the Analysis of Dielectric Guiding Structures*. PhD thesis, Polish Academy of Sciences, Institute of Fundamental Technological Research, Warsaw, Poland, 1991.
- [7] T. F. Jabłoński. Complex modes in open lossless dielectric waveguides. *J. Opt. Soc. Amer. A*, 11:1272–1282, April 1994.

A SIMPLE METHOD INVERTING LIGHT-SCATTERING DATA OF A DIFFUSIVE SYSTEM INTO THE PARTICLE SIZE DISTRIBUTION FUNCTION

Kusiel S. Shifrin

College of Oceanic & Atmospheric Sciences, Oregon State University
104 Ocean Admin Bldg
Corvallis, OR 97331-5503, USA
Office: 541-737-2016, Fax: 541-737-2064, Home: 541-713-7442
E-mail: shifrink@ucs.orst.edu

1. Introduction

It is known that optical characteristics of diffusive system (OCOS) are related to the particle size distribution function (PSDF) $f(a)$ (a is the particle radius) by a linear integral equation of the first kind. The equation usually has the following form:

$$S(x) = \int_0^{\infty} s(x, a) f(a) da, \quad (1)$$

where $S(x)$ is an experimental OCDS; $s(x, a)$ is the same characteristic related to a single particle. The essence of the problem of inverting lightscattering data into PSDF is to determine $f(a)$ from a given kernel $s(x, a)$ of Eq. (1) and from an experimental $S(x)$ obtained with an error $\Delta S(x)$ (including computational errors)

$$S(x) = \overline{S(x)} \pm \Delta S(x) \quad (2)$$

The quantity $|\Delta S(x)|$ determines the number of Fourier harmonics that can be retrieved by inverting Eq. (1). The harmonics of frequencies $\omega > \omega_o$, where ω_o is some limiting frequency, just disappear in measurement noises of the function $S(x)$. The frequency ω_o is determined from the following formula (see [1]):

$$\Delta S = \int_0^{\infty} S(x, a) e^{i\omega_o a} da. \quad (3)$$

The requirement for measurement and calculation error to be small $\left(\eta \ll 1, \quad \eta = \frac{|\Delta S|}{S} \right)$ is, however, not enough to construct a stable solution to Eq. (1). This is obvious from the following.

The simplest method of solving (1) is to transform it into a system of linear algebraic equations of the following form:

$$\alpha_{ik} x_k = y_i. \quad (4)$$

This method is, however, unsuccessful as a rule, because the systems obtained in such a manner turn out to be ill-conditioned.

The reason has to do with peculiarities of some integral equations of the first kind; these equations are ill-defined, that is to say, they are very sensitive to the choice of linearization points, and to measurement and computation errors. In order to solve the problem, one has to "regularize" it. The regularization amounts to invoking additional information about properties of the sought-for solution to Eq. (1). This additional information makes the problem stable. Strictly speaking, by invoking additional information, one changes one problem for another. It

is important for the substitution not to lead us too far away from our original goal. In other words, solutions to the regularized system should be close to the solutions of the initial physical problem. The regularization has to help us to get rid of computational instability of the problem without changing its physical essence.

The simplest regularization method is to assume that the sought-for PSDF belongs to a certain family of functions. The parameters of the distribution are chosen so that the system (4) is satisfied. Let us denote the frequencies (or scattering angles) at which the function S is measured as γ_i . We denote the sought-for parameters of our family of functions as ν_k . In this case, the determination of the parameters ν_k of the family reduces to solving the following set of equations:

$$S(\gamma_i, \nu_k) = C_i, \quad i = 1, 2, \dots, n. \quad (5)$$

The number n of equations must be no fewer than the number k of the parameters in the sought-for family. In spite of seeming simplicity, the system (5) is, as a rule, also poorly conditioned, so the method does not help much in constructing solutions to Eq. (1).

The principal idea of the method suggested here is to accept $n \gg k$. This means that we will deal with significantly overdefined systems. This will make it possible to improve essentially the determination accuracy of the parameters ν_k . This idea is similar to the method of least squares. Recall that the error $\Delta \varepsilon$ of the mean over n measurements is equal to

$$\Delta \varepsilon = \frac{|\Delta \varepsilon_0|}{\sqrt{n(n-1)}}, \quad (6)$$

and so it is smaller than the error of a single measurement $\Delta \varepsilon_0$ approximately by a factor of n .

2. An example of appreciation of the method suggested.

One of the examples of method applications is discussed in [2]. According to recent experimental data, the function $f(a)$ can be represented as a sum of two components: fine and large ones. Each component has a lognormal distribution that can be described by three parameters: the particle concentration density n_i ($\text{cm}^{-3} \mu\text{m}^{-1}$), the distribution mode r_i (μm), and the distribution variance s_i ($i=1, 2$ for the fine and large components respectively).

It is more common to use two other parameters instead of n_1 and n_2 : $N = n_1 + n_2$, and $c = \frac{n_1}{n_2}$,

where N is the total particle concentration density, and c is the ratio of concentrations of the fine and large components. In [2], the authors fix N and c and examine the sensitivity of aerosol two-component models to variations of the remaining four parameters r_i and s_i . Using different values of r_i and s_i and Eq. (1), it is possible to obtain an unlimited number of two-component models. In order to limit this number, certain intervals for r_i and s_i and for the quantization step are set. The limits of mode radius variations are set basing on data in [3]. For r_1 this interval is $\Delta r_1 = 0.02 - 0.06 \mu\text{m}$; for r_2 it is $\square r_2 = 0.15 - 0.75 \mu\text{m}$.

It is commonly assumed in aerosol models that the value of standard deviation s_i is approximately equal to 0.3. This value is taken for setting intervals for s_i . It is presumed that s_i varies from approximately 50% to 200% of the magnitude. As a result, the interval for s_i can be specified as $\square s_1 = 0.15 - 0.55$; for s_2 , $\square s_2 = 0.1 - 0.7$.

The possibility of retrieving $f(a)$ from the spectral attenuation $\sigma(\lambda)$ is considered in [2]. The spectral attenuation σ /particle was calculated by the Mie formulas for 77 wavelengths that were spaced evenly throughout the extended visible range from 0.3 to $1.06 \mu\text{m}$. It was assumed when doing this that the complex refractive index $m(\lambda)$ of the fine component

coincided with that of the rural component in [3], whereas $m(\lambda)$ of the large component was identical to that of the oceanic component in the same work. The data for m were taken for a relative humidity of 70%.

For each component, 25 values of r_i and 27 values of s_i were used in such a manner that they were spaced evenly throughout their intervals. Matrices of 25×27 elements were constructed in this way for the spectral attenuation $\sigma(\lambda)$ for each of 77 wavelengths λ [distributed evenly throughout the 0.3-1.06 μm range]. As a result, 675 models for each component were obtained for 77 wavelengths. These data arrays of σ constituted the basis for a further analysis.

In order to identify aerosol models satisfying optical data, two optical characteristics were chosen: the Ångström parameter α and the attenuation σ_0 /particle at $\lambda=0.55\mu\text{m}$. These two parameters can fully describe the curve of spectral attenuation in the visible range.

The aerosol models were compared with experimental data for σ_0 and α . It was assumed, in accordance with numerous publications, that the aerosol optical thickness τ_0 of the marine atmosphere in clean oceanic regions varies between 0.07 and 0.09; the value of the Ångström parameter α for the same conditions can change from 0.4 to 0.8.

As a result, it was taken for σ (0.55) and α to satisfy the following inequalities (see [2] for more details):

$$\begin{aligned} 0.9 \times 10^{-4} \text{km}^{-1} \text{cm}^3 \leq \sigma \leq 1.1 \times 10^{-4} \text{km}^{-1} \text{cm}^3, \\ 0.3 \leq \alpha \leq 0.5 \end{aligned} \quad (7)$$

Using these inequalities, the authors of [2] calculated the basic optical characteristics of the above-described 675×675 two-component models. From this set, the models were selected whose σ_0 (0.55) and α satisfy the inequalities (7). At a chosen step of quantization, the number of such models amounted to 5292.

Next, particle size distributions for each model were calculated, and the maximum and minimal values of each distribution were determined for every particle size. It turned out that individual distributions differ between themselves quite significantly, which corresponds to the range of natural variability of the basic optical characteristics. For some intervals of particle radii, distributions differ by orders of magnitude. However, all the selected models were found to be close to each other within the 0.02-1.0 μm particle radius interval. This interval (optically active interval) is responsible for 93% of attenuation in the visible range.

The mean particle size distribution for the active interval was constructed. The relative mean-square error of this distribution grows with the particle radius; for particles of radii of 0.02-0.2 μm , the error does not exceed 20%; for the 0.2-1 μm radius range, it is no higher than 40%; it gradually grows from 40% to 95% as the particle radius changes from 1 to 3 μm . These results make it possible to estimate the retrieval accuracy of the aerosol particle size distribution from an optical data set at different particle size intervals.

It follows that by specifying the interval of basic optical characteristics, one can determine with the above-stated accuracy, an optically active and quite stable set of PSDF. It should be noted that data on the spectral attenuation alone measured in a limited spectral range is not enough to determine PSDF over the entire particle size interval, because differently-sized particles affect the radiative transmittance differently. So, small particles, numerous as they are, possess weak extinction properties, whereas large particles are strong attenuators, although they are few.

3. Conclusions

The information content of data for the spectral attenuation σ at $\lambda=0.55\mu\text{m}$ and for the Ångström parameter α in the visible range for the marine atmosphere was examined for the use in the reconstruction of the aerosol particle size spectrum. The particle size distribution curve was parameterized by a sum of two log-normal distributions, which means that it contained six unknown parameters to be determined from the two measured characteristics. Some parameters were fixed at their typical values in order to diminish the uncertainty of the problem. In the example illustrating the procedure, the total particle concentration and the fraction of the fine and large component were fixed. The number of members of the ensemble was great, because the answer was ambiguous. It is remarkable, however, that in the active particle interval, different members of the ensemble have close distribution curves, so it is natural to accept an average curve as a solution to the problem. In spite of the small body of initial information, the accuracy of the procedure was quite reasonable. It can also be seen how the error grows with the particle radius.

The most important for the method is a correct choice of the initial function in Eq. (1) and of the interval of parameter values. One can expect, for example, that by applying the described procedure directly to some nonaverage atmospheric conditions (such as storms and fogs), one would obtain much worse results. For these conditions, one could possibly vary both the initial formula in Eq. (1) and, more importantly, the intervals of the parameter variability.

References

1. K. S. Shifrin, *Physical Optics of Ocean Water*, American Institute of Physics Translation Series (American Institute of Physics, New York, 1988), p. 285.
2. K. S. Shifrin and I. G. Zolotov, "Information content of the spectral transmittance of the marine atmospheric boundary layer", *Appl. Opt.* **35**, N24, pp. 4835-4842, 1996.
3. E. P. Shettle and R. W. Fenn, "Models for aerosols in the lower atmosphere and the effects of humidity variations on their optical properties", AFGL-TR-79-0214 (U.S. Air Force Geophysics Laboratory, Hanscomb Air Force Base, Mass., 1979), p. 94.

Time-domain solvers versus analytical regularisation in the integral-equation analysis of canonical scatterers.

P.D. Smith *Department of Mathematics, University of Dundee, Dundee DD1 4HN, Scotland, UK*

Introduction.

In the analysis and measurement of electromagnetic systems, much emphasis has been placed on their characterisation in the frequency domain. Although this is entirely appropriate for those systems which are narrow band, an increasing number of practical systems are wideband or ultrawideband (UWB), spanning several octaves of frequency in operation. The advances in UWB pulsed source performance over the last decade have given rise to several novel applications, including UWB radar [1], ground penetrating radar [2], and ultrawideband synthetic aperture radar [3]. Current source technology, providing pulsed waveform risetimes of the order of 100 picoseconds, is reviewed in [4], whilst other faster rise time applications, albeit of lower power, are reviewed in [5]. The book [6] reviews present approaches to UWB studies.

Ultrawideband radar requires the faithful radiation, and reception, of a temporally compact, ultrawideband pulse of some pre-determined waveform, coupled with analysis of the target scattered signature, both in the early time and the late time. In the early time, scattering by features such as edges is important, whereas the later time response is predominantly of a damped, oscillatory nature which can be described in terms of the so called "complex resonances" or "poles" of the Singularity Expansion Method [7]. These later time features may be strongly pronounced for structures with cavities, especially if the Q factor of the cavity is high, so that one or more oscillation has relatively long duration. Determination of the corresponding poles has been explored as the basis of target identification algorithms [6].

In other areas as diverse as personal communications and satellite communications, attempts to circumvent various physical constraints, such as antenna size, have lead to the increasing deployment of wideband antennas in the form of multiband antennas. A novel antenna is the fractal antenna recently examined in [8]. Electromagnetic interference (EMI) and electromagnetic compatability(EMC) continue to grow in importance as the operating frequency of devices increases and the spectrum becomes increasingly crowded. Wideband antennas are central in the effective location and assessment of sources of EMI, and in the determination of both in-band and out-of-band responses of radiating devices.

Time domain techniques are especially attractive to the wideband community. The impulse response of a radiator or scatterer theoretically contains the complete frequency spectral response; in practice, the finite risetime of sources and measurement systems restricts attention to the smoothed impulse response stimulated by a transient pulse of short duration (such as the "Gaussian" pulse), which then provides (via a Fourier transform) a wideband system response, up to a maximal frequency inversely proportional to the pulse duration. For these reasons, numerical simulations often calculate a smoothed impulse response to assess the corresponding finite bandwidth response.

Whether it is obtained directly (by measurement or simulation), or by transformation of frequency domain data, the time domain response of a scatterer, to transient incident illumination, has a direct physical interpretation, which is invaluable in discerning such features such as the specular return, creeping wave phenomena, and cavity resonances.

Let us consider the available analytical and numerical techniques for obtaining the time domain response, and, by implication, the wideband frequency response, of a scatterer.

Analytical and Numerical Time Domain Techniques.

Analytical techniques find their greatest success on narrowly restricted classes of problems. Examples include the Mie series solution of scattering by a sphere (and other such "separation of variables" solutions for canonical scatterers), low frequency (Rayleigh) scattering, and canonical problems soluble by the Wiener-Hopf technique [9]. Techniques applicable to wide classes of scatterers are invariably numerical. At high frequency, ray techniques, such as the geometrical theory of diffraction (GTD) and its extensions [10], can provide good approximations for relatively large scatterers. For the smaller and intermediate wavelength regime, integral equation approaches have been successfully used for the numerical calculation of electromagnetic wave interaction with scatterers, both in the time domain [11] and the frequency domain [12]. We will briefly describe how integral equation methods can be efficiently exploited to obtain scattering signatures across a broad band of frequencies, particularly focussing on the time domain form. The scope and advantages of frequency domain techniques are well explored in [12]. In this regime, other possible approaches include finite difference time domain (FDTD) schemes [13] and finite element methods (FEM), resulting from the direct discretisation of Maxwell's equations. Of course, none of these techniques exists in isolation, and various hybrid schemes, combining analytical approximations and numerical attacks, have been devised. A discussion of these issues is in [14, 15].

Between the extremes of purely analytical and purely numerical techniques lies the Method of Regularisation (MoR). This (frequency domain) method is based upon exact inversion of a singular part of the original equation, which is often identifiable as a "static" part. In the process a system of first kind equations is converted to a set of second kind equations, enjoying various beneficial properties such as guaranteed rates of convergence; the resultant system of equations can be solved vastly more efficiently than with the general purpose numerical schemes mentioned above. It is perhaps the only available method, of some limited generality, that is capable of providing a truly wideband response for a restricted class of scatterers, spanning the frequency range from quasi-static to quasi-optical. This method works well when scattering problems are posed as *mixed* boundary value problems in coordinate systems in which the scattering surfaces form portions of level surfaces (in which one coordinate is held constant). Usually the scattering problem is formulated in terms of the eigenfunctions associated with separation of variables for the Helmholtz equation giving rise to dual or triple series equations, although the basic idea can be applied to the first kind integral equations arising for these problems [16]. The class of scatterers to which the method applies includes objects of some complexity, with edges and cavities, and is therefore extremely valuable in providing rigorous solutions to "benchmark" scattering problems for testing more general purpose numerical codes. Indeed complex scatterers remain the ultimate challenge for electromagnetic signature characterisation [17].

In the next section we consider time domain integral equation. If the incident field is taken to be a Gaussian pulse (i.e. a smoothed impulse), the smoothed impulse response can be calculated. After a Fourier transform the bistatic response as a function of frequency is obtained; the highest frequency in this broadband response is dictated solely by the effective frequency content of the pulse. Although a frequency domain integral equation approach might be considered for such broadband calculations, the time domain approach is often more efficient. The computational complexity grows substantially as the surface area (in square wavelengths) of the scatterer increases, so that whilst the integral equation approach is formally correct for all frequencies, it is of practical use only for scatterers up to several wavelengths in linear dimensions. (The computational complexity of differential equation methods is determined by the volume (in cubic wavelengths) of the truncated free space grid in which the scatterer resides.) The time domain integral equation approach and other "resonance" regime methods therefore complement high frequency methods. As well as accurately determining the response at longer wavelengths, it enables one to determine the scattered response in the transition regime where the accuracy of results obtained by GTD and other methods is less certain.

Time Domain Integral Equation Methods.

In free space, an incident electromagnetic field \bar{E}^i, \bar{H}^i induces currents \bar{J} and charges ρ on the surface S of a perfectly conducting object. In turn these set up a Maxwellian scattered field \bar{E}^s, \bar{H}^s satisfying

$$\nabla \times \bar{E}^s = -\mu \frac{\partial \bar{H}^s}{\partial t}, \quad \nabla \times \bar{H}^s = \epsilon \frac{\partial \bar{E}^s}{\partial t} + \bar{J} \quad (1)$$

A standard approach expresses the fields in terms of a scalar potential ϕ and a vector potential \bar{A} via

$$\bar{H}^s = \mu^{-1} \nabla \times \bar{A}, \quad \bar{E}^s = -\frac{\partial \bar{A}}{\partial t} - \nabla \phi \quad (2)$$

where, in the Lorentz gauge, the potentials may be constrained so that

$$\nabla \cdot \bar{A} + \epsilon \mu \frac{\partial \phi}{\partial t} = 0 \quad (3)$$

This choice is convenient because individual components of \bar{A} and ϕ satisfy the scalar wave equation. A continuity equation connects the surface currents and charges

$$\frac{\partial \rho}{\partial t}(\bar{r}, t) + \nabla_S \cdot \bar{J}(\bar{r}, t) = 0, \quad (4)$$

where ∇_S is the surface divergence on S . The potentials are then given by:

$$\phi(\bar{r}, t) = \frac{1}{4\pi\epsilon} \int_S \frac{\rho(\bar{r}', \tau)}{|\bar{r} - \bar{r}'|} dS', \quad \bar{A}(\bar{r}, t) = \frac{\mu}{4\pi} \int_S \frac{\bar{J}(\bar{r}', \tau)}{|\bar{r} - \bar{r}'|} dS', \quad (5)$$

where $\tau = t - |\bar{r} - \bar{r}'|/c$ is *retarded* time, and c is the speed of light. The electric field integral equation (EFIE) arises by setting the electric field component tangential to S , $(\bar{E}^i + \bar{E}^s)^{tan}$, to zero:

$$\bar{E}^i(\bar{r}, t)^{tan} = \left[\nabla \phi(\bar{r}, t) + \frac{\partial \bar{A}}{\partial t}(\bar{r}, t) \right]^{tan} \quad (6)$$

This holds at every point of the surface S and is valid for surfaces, open or closed. It is worth noting that the Sommerfeld radiation condition is automatically satisfied. The equations (4), (5), (6) are central to our numerical scattering calculations. As explained in [11], a choice of basis functions can be defined on a triangular mesh which approximates a dissection of the arbitrary scattering surface S , and utilises the equations so that present current and charge values are calculable in terms of previous values. This principle can be easily explained by considering the related magnetic field integral equation (MFIE), which is valid only for closed surfaces (without apertures or edges); it is derived (see [18]) by examining the components of the magnetic field tangential to the surface (that is, $n \times \bar{H} = \bar{J}$), obtained from the curl of the vector potential, and has the form

$$\frac{1}{2} \bar{J}(\bar{r}, t) - n \times \frac{1}{4\pi} \int_S \left(\bar{J}(\bar{r}', \tau) + \frac{|\bar{r} - \bar{r}'|}{c} \frac{\partial \bar{J}(\bar{r}', \tau)}{\partial t} \right) \times \left(\nabla' \times \frac{1}{|\bar{r} - \bar{r}'|} \right) dS' = n \times \bar{H}^i \quad (7)$$

It is now transparent that the value of the surface current, at a particular point \bar{r} on the surface and at present time t , is formed from a (weighted) sum of surface currents at every other point on the surface, but taken at times *earlier* than t : specifically the contribution from point \bar{r}' is retarded by an amount equal to the travel time of light, namely $|\bar{r} - \bar{r}'|/c$.

This forms the basis for a numerical discretisation scheme, in which the surface S is divided into N flat patches S_1, \dots, S_N with centroids $\bar{r}_1, \dots, \bar{r}_N$ and unit outward normals n_1, \dots, n_N . The current is assumed constant on each patch. A discrete time step Δt is chosen, and we set $\bar{J}_{i,k} = \bar{J}(\bar{r}_i, k\Delta t)$. If

the time step is chosen to be less than the minimum travel time of signals between any two centroids, and linear interpolation is used to approximate $\bar{J}(\bar{r}_i, t')$ when t' is not an integral time step value, then the discrete solution value $\bar{J}_{i,k+1}$ is a linear combination of the solution values at earlier time steps $k\Delta t, (k-1)\Delta t, \dots$, and the exciting field. The self patch contribution

$$-n_i \times \frac{1}{4\pi} \int_{S_i} (\bar{J}(\bar{r}', \tau) + \frac{|\bar{r}_i - \bar{r}'|}{c} \frac{\partial}{\partial \tau} \bar{J}(\bar{r}', \tau)) \times (\nabla' \times \frac{1}{|\bar{r}_i - \bar{r}'|}) dS' \quad (8)$$

is normally approximated by zero.

The system is supposed quiescent before the transient pulsed illumination arrives, at, say, time zero: $\bar{J}_{i,k} = 0, k \leq 0$. Subsequently, the discrete surface current values are updated at each time step in terms of the values previously calculated by this scheme. Both this scheme, and the more sophisticated scheme described in [11] for the EFIE, work well once a stabilising device is employed. Typical results based upon the MFIE appear in [19]; a variety of problems arising in the study of wideband antennas and their impedance, radar polarimetry and calibration, and scattering problems, including obstacles with a surface impedance coating, are described in [11, 20, 21, 22].

Time Domain Response of Canonical Scatterers via MoR.

Canonical problems involving thin perfectly conducting shells are amenable to the frequency domain solution technique known as the method of regularisation (MoR) or semi-inversion method. Although the shells should coincide with part of one or more coordinate surfaces of spherical or spheroidal or other special geometries, within this constraint a wide variety of diffraction problems has been solved, including the spherical reflector antenna [23], a sphere with one or two holes [24], a spheroid with one or two holes [25], spherical or spheroidal shells enclosing interior shells, and such structures enclosing multilayer dielectric shells [26].

Consider the wave diffracted by a thin, perfectly conducting, spheroidal shell, which possesses two symmetrically placed circular holes to form a hollow spheroidal cylinder, in which the axially aligned source is a vertically polarised electric dipole. A rigorous formulation of Maxwell's equations with boundary and edge conditions, produces a triple series set of equations of the first kind [25]. The MoR technique analytically transforms the set, via a form of Abel's integral equation, to an infinite matrix equation of the second kind. The Fredholm nature of the equation so obtained ensures the existence of a unique solution. The numerical solution algorithm is always stable, and converges to the exact solution with increasing truncation numbers. For practical accuracy, a matrix of the order slightly greater than the electrical size of spheroid should be solved. Two noteworthy advantages gained by this approach are great reductions in computational complexity (compared to the more general methods described above) as well as reliable quantification of edge scattering and cavity effects.

The frequency dependence of radiation patterns was computed in the resonance range $0 < kb < 20$ (b denoting the semi-major axis of the spheroid and k the wave number) for spheroidal shells with axial ratios in the range $0.1 < q < 0.999$ that corresponds to changing the form from practically cylindrical to spherical. It is instructive to examine, via an inverse Fourier transform, the *time domain* response of such cavities to a finite duration pulse: it is convenient to employ the Gaussian time dependence $\exp(-b_1^2(ct/2\pi b)^2)$, whose duration depends the dimensionless parameter b_1 . The radiated response for a *closed* sphere at 10° off axis is shown in figure 1a, in which the incident pulse is initially visible, followed quickly by the specular return, then the creeping wave response followed by very small amplitude late time oscillations. New electromagnetic features appear when the closed sphere is opened up as a cavity, most notably the occurrence of lightly damped (high Q) oscillations which are identifiable as internal cavity oscillations whose frequency is slightly shifted from the frequencies at which the *closed* spherical cavity would oscillate. In the frequency domain response these appear precisely as near resonant features. Two such oscillations are visible in figure 1b (note the incident pulse is broader).

These results were compared with those obtained by the time domain EFIE code discussed above. For the closed structure, the results are in good agreement ; for the unclosed structure the cavity oscillation frequencies (obtained by Fourier analysis) are correctly predicted but are more strongly damped. The accurate prediction of the cavity Q factor is thus perhaps the most demanding test of a general purpose time domain numerical code. On the other hand, care must be taken in frequency domain calculations to resolve such features adequately as a function of frequency, otherwise *acausal* features will appear in the transformed time domain response.

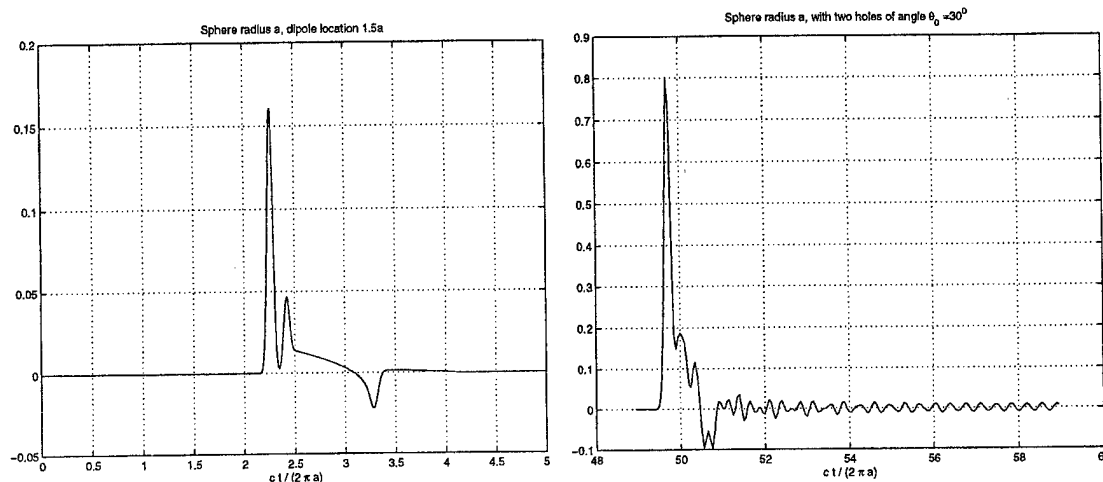


Figure 1: Radiated field at 10° off-axis for the closed sphere (a) and the spherical cavity (b).

Conclusion.

Our understanding of diffraction phenomena is enhanced by examining both time and frequency domain aspects, particularly when complex scatterers, incorporating edges and cavities, are involved. Some features such as high Q resonances are better perceived in the frequency domain, whilst other broadband features such as specular returns and creeping waves appear more clearly in the time domain. This article discussed the relative merits of several low and high frequency general purpose techniques, concentrating upon time domain integral equation techniques. The validity of codes based upon these techniques can be established by comparison with rigorous solution techniques for classes of canonical problems, such as spheroidal shells, which include the required features of interest (such as cavities). In this context the method of regularisation herein discussed is particularly useful. More results will be presented at the Symposium.

References.

- [1] D.M. Parkes, M.F. Lewis, R.L.S. Devine, K. Trafford & D. Richardson, *Practical measurements using ultrawideband radar*, Proc. International Society for Optical Engineering (SPIE), Los Angeles, USA, Jan. 1992, SPIE Vol 1631, pp 232-242 (1992).
- [2] D.J. Daniels, *Surface-Penetrating Radar*, IEE (1996).
- [3] S. Cloude, A. Milne, C. Thornhill & G. Crisp, *Early time signature analysis of dielectric targets using UWB radar*, In : *Ultrawideband Short Pulse Electromagnetics 3*, Edited by C. Baum, L. Carin & A. Stone, 255-262, Plenum Press (1997).
- [4] D.M. Parkes, *Ultrawideband pulser technology*, In : *Ultrawideband Short Pulse Electromagnetics 3*, Edited by C. Baum, L. Carin & A. Stone, 25-29, Plenum Press (1997).
- [5] E.E. Funk & C.H. Lee, *Free-space power combining and beam steering of ultrawideband radiation using an array of laser-triggered antennas*, IEEE Trans. Microwave Theory & Techniques, MTT-44, 2039-44 (1996).

- [6] J.D. Taylor (Editor), *Introduction to Ultrawideband Radar Systems*, CRC Press (1995).
- [7] C.E. Baum, *The singularity expansion method*, In : *Transient Electromagnetic Fields*, Edited by L.R. Felsen, Springer-Verlag (1976).
- [8] J. Fornieles Callejon, A. Rubio Bretones & R. Gomez Martin, *On the application of parametric models to the transient analysis of resonant and multiband antennas* To appear IEEE Trans. Antennas Propag., AP-46 (1998).
- [9] H.A. Serbest & S.R. Cloude (Editors), *Direct and inverse Electromagnetic Scattering*, Chapters II and III, Pitman Research Notes in Mathematics **361**, Addison Wesley Longman (1996).
- [10] R.C.Hansen (Editor), *Geometric Theory of Diffraction*, IEEE Press (1981).
- [11] P.D. Smith, *Time domain integral equation techniques in electromagnetic scattering*, In : *Direct and inverse Electromagnetic Scattering*, Edited by H.A. Serbest & S.R. Cloude, Pitman Research Notes in Mathematics **361**, 171-188, Addison Wesley Longman (1996).
- [12] E.K. Miller, L. Medgyesi-Mitschang & E.H. Newman, *Computational Electromagnetics*, IEEE Press (1992).
- [13] P.G. Petropoulos, *Fourth order accurate staggered finite difference schemes for the time dependent Maxwell equations*, In : *Ordinary and Partial Differential Equations V*, Edited by P.D. Smith & R.J. Jarvis, Pitman Research Notes in Mathematics **370**, 85-106, Addison Wesley Longman (1997).
- [14] E.K. Miller, *A selective survey of computational electromagnetics*, IEEE Trans. Antennas Propag., AP-36, 1281-1305 (1988).
- [15] E.K. Miller, *Time domain modelling in electromagnetics*, J. Electromag. Waves Applic., **8**, 1125-1172 (1994).
- [16] A.I. Nosich, *The Method of Regularisation in wave scattering and eigenvalue problems: Foundations and Review of Solutions*, Preprint (1998).
- [17] W.R. Stone (Editor), *Radar Cross section of Complex Objects*, IEEE Press (1990).
- [18] D.S. Jones, *Methods in Electromagnetic Wave Propagation*, 2nd Ed. OUP (1994).
- [19] P.D. Smith, *Instabilities in time marching methods for scattering : cause and rectification*, Electromagnetics, **10**, 439-451 (1990).
- [20] S.M. Booker, P.D. Smith & S.R. Cloude, *A time domain integral equation approach to the calibration of dihedral reflectors*, Proc. 3èmes Journées Internationales de la Polarimétrie Radar (JIPR), Vol 1, 153-164, Nantes, France (1995).
- [21] S.M. Booker, A.P. Lambert & P.D. Smith, *A numerical calculation of surface impedance effects on transient antenna radiation*, Radio Science, **31**, 1663-1669 (1996).
- [22] S.M. Booker, P.D. Smith & A.P. Lambert, *A numerical determination of transient antenna impedance via near-field integration*, J. Electromag. Waves Applic. **12**, 199-223 (1998).
- [23] S.S. Vinogradov & V.P. Shestopalov, *Solution of a vectorial scattering problem for a sphere with a hole*, Sov. Physics Doklady, **237** (1) (1977).
- [24] S.S. Vinogradov, *Reflectivity of a spherical shield*, Radiophys. & Quant. Electronics, **26**(1) (1983).
- [25] E.D. Vinogradova & P.D. Smith, *Impact of a hollow spheroidal cylinder on electric dipole radiation features*, Proc. Math. Methods in Electromag. Theory (MMET'98), Kharkov, Ukraine June 1998.
- [26] P.D. Smith & S.S. Vinogradov, *A rigorous treatment of electromagnetic scattering by the Luneberg lens reflector*, Proc. Electromag. Theory Symp. (URSI Commission B), Thessaloniki, May 1998.

Galerkin methods in solving integral equations with applications to scattering problems

A. Chakrabarti

Department of Mathematics, Indian Institute of Science
Bangalore - 560012, India

Abstract

The Galerkin methods of obtaining approximate solutions of integral equations and their applications to problems of scattering of electromagnetic and surface water waves are examined. Two typical problems, one occurring in electromagnetic wave propagation and the other in the propagation of two dimensional surface water waves, are taken up as illustrative examples of the methods.

1. Introduction

Varieties of mixed boundary value problems (see Sneddon [6]), of Mathematical Physics are solved by first reducing them to those of solving integral equations of various types and forms. It is only in some specially simple situations that exact closed form solutions of the integral equations can be determined completely, and, in the cases of integral equations with complicated looking kernels or otherwise, only approximate solutions of certain types can be worked out successfully. Of all such approximate methods for solving integral equations, the Galerkin methods (see Jones [4], Evans and Morris [2],[3], Banerjee and Mandal [1], Mandal and Das [5], and others) appear to be extremely powerful, in the sense that certain practical results of high accuracy can be recovered with appropriate choice of certain sets of independent functions, to be described in section 2 of the present paper.

After explaining the major mathematical ideas behind the Galerkin methods in section 2, we have taken up in section 3, two different mathematical problems of scattering, occurring in Electromagnetic theory and in the theory of water waves respectively, and have reduced each of these problems to those of solving two integral equations of first kind, with two different kernels. In section 4, we have presented the approximate solutions of the integral equations formulated in section 3, by employing just one term Galerkin approximations and in section 5, we have derived approximate results for certain special quantities of practical interest for both the problems considered in section 3.

2. The major Mathematical ideas

In many practical situations, like the ones considered in the present work, the principal mathematical problems turn out to be those of solving some linear operator equations (linear integral equations, for the problems considered here) of the type

$$(Lf)(x) = l(x), \quad x \in A, \quad (2.1)$$

where L is a linear operator from a certain inner product space S to itself and $A \subset \mathbb{R}$ (can be \mathbb{R}^n , in general), where f and l are real valued functions. It may also be required (as in the problems considered here) to determine the inner product :

$$[l, f] \equiv [f, l] := \int_A f(x)l(x)dx, \quad (2.2)$$

Whenever the mathematical problems at hand are expressible in the forms of the two relations (2.1) and (2.2) we can resolve them, approximately, by utilizing the following senses and ideas:

Definition: A real valued function $F(x) \in S$ is said to solve the equation (2.1), approximately, if and only if

$$[LF, \lambda] \equiv [\lambda, LF] \approx [\lambda, l], \quad (2.3)$$

where the symbol \approx means "approximately equal to" and we shall write: $f \approx F$, in the sense that

$$[Lf, \lambda] \approx [LF, \lambda], \quad (2.4)$$

for all $\lambda(x) \in S$.

Then, using the approximate solution F of the equation (2.1), we can derive an approximate value of the inner product $[f, l]$, as given by the relation (2.2), in the form:

$$[f, l] \approx [F, l]. \quad (2.5)$$

In the Galerkin methods which can be successfully utilized for many problems (especially for the problems considered here), we express the approximate solution $F(x)$, in the form:

$$F(x) = \sum_{j=1}^n c_j \phi_j(x), \quad (2.6)$$

where $\{\phi_j(x)\}_{j=1}^n$ denotes a set of n linearly independent functions (not necessarily orthogonal) in S and c_j 's are n constants to be determined, as desired below.

Using the relation (2.6) in the relation (2.3), after choosing $\lambda(x) = \phi_k(x)$, for a fixed k ($1 \leq k \leq n$), we obtain the following set of approximate linear relations

$$\sum_{j=1}^n c_j [L\phi_j(x), \phi_k(x)] \approx [l(x), \phi_k(x)], \quad (k = 1, 2, \dots, n). \quad (2.7)$$

Treating the above approximate relations (2.7) as a set of n linear equations, we can determine the constants c_j 's ($j = 1, 2, \dots, n$) and then the determination of the approximate solution $F(x)$, can be completed by using the relation (2.6).

Also, the approximate evaluation of the inner product $[f, l]$ can be completed and we obtain

$$[f, l] \approx \sum_{j=1}^n c_j [\phi_j, l]. \quad (2.8)$$

As an example, by taking $n = 1$ only, we obtain

$$f(x) \approx F(x) = \frac{[l, \phi_1]}{L\phi_1, \phi_1} \phi_1(x), \quad [f, l] = \frac{[l, \phi_1]^2}{[L\phi_1, \phi_1]}. \quad (2.9)$$

It is obvious from the above discussion that varieties of Galerkin methods can be developed by varying ϕ_j 's and n .

The methods for which $n = 1$ are called (see Evans and Morris [2,3]) "single-term" methods, whereas for values of $n > 1$ the corresponding methods are referred to as "multi-term" methods (see Banerjee and Mandal [1] and others). In the present work we shall concentrate only on "single-term" Galerkin approximations.

We shall now make the following observations:

We have

$$\begin{aligned} (i) \quad & [F, LF] \approx [F, l], \quad (ii) \quad [f, l] = [l, f] = [l, f] + [l, f - F], \\ (iii) \quad & [l, f - F] \approx [Lf, f] - 2[LF, F] + [F, LF], \quad (\text{by using } (i)) \\ (iv) \quad & [f - F, L(f - F)] \approx [Lf, f] - 2[LF, F] + [F, LF]. \end{aligned}$$

By using the results (iii) and (iv) we find that

$$[l, f - F] \approx [f - F, L(f - F)], \quad (2.10)$$

and then one of the following two cases hold good.

Case (a): If L is a positive semi-definite linear operator, i.e. if $[h, Lh] \geq 0$, for all $h \in S$, then

$$[l, F] \leq [l, f], \quad (2.11)$$

and

Case (b): If L is a negative semi-definite linear operator, i.e. if $[h, Lh] \leq 0$, for all $h \in S$, then

$$[l, F] \geq [l, f]. \quad (2.12)$$

The above results (2.11) and (2.12) imply that the "approximate" value $[l, F]$, computed with the aid of the "approximate" solution F of the equation (2.1), provides a lower bound for the actual quantity $[l, f]$ in Case (a) whereas $[l, F]$ will provide an upper bound for $[l, f]$ in Case (b).

The above observations clearly help in obtaining estimates of the quantity $[l, f]$ in many practical problems, and in sections 4 and 5 we have demonstrated the applications of these ideas to the two problems of scattering, considered in section 3.

3. Two mathematical problems of scattering theory

Problem 1:

A problem occurring in Scattering of Electromagnetic Waves (See Jones [4])

To solve

$$\frac{\partial^2 \phi}{\partial x^2} + \frac{\partial^2 \phi}{\partial y^2} + \frac{\partial^2 \phi}{\partial z^2} + k^2 \phi = 0, \quad (k > 0), \quad \text{for } -\infty < z < \infty, \quad 0 < x < a, \quad 0 < y < b, \quad (3.1)$$

with $\frac{\pi}{a} < k$, such that

$$\begin{aligned} (i) \quad & \phi = 0, \quad \text{on } x = 0 \text{ and } x = a, \quad (ii) \quad \frac{\partial \phi}{\partial y} = 0, \quad \text{on } y = 0 \text{ and } y = b \\ (iii) \quad & \phi \longrightarrow \begin{cases} (e^{-i\lambda z} + Re^{i\lambda z}) \sin\left(\frac{\pi x}{a}\right), & \text{as } z \longrightarrow -\infty, \lambda > 0 \text{ (a known constant)} \\ Te^{-i\lambda z} \sin\left(\frac{\pi x}{a}\right), & \text{as } z \longrightarrow \infty, \lambda > 0 \text{ (a known constant)} \end{cases} \end{aligned}$$

(Note that R and T are unknown complex constants to be determined).

$$(iv) \quad \begin{cases} (A) \quad \frac{\partial \phi}{\partial z} = 0, \text{ on } z = 0^\pm, \text{ for } d < y < b, 0 < x < a, \\ (B) \quad \phi|_{z=0^+} = \phi|_{z=0^-}, \text{ for } 0 < y < d, 0 < x < a, \\ (C) \quad \frac{\partial \phi}{\partial z}\bigg|_{z=0^+} = \frac{\partial \phi}{\partial z}\bigg|_{z=0^-}, \text{ for } 0 < y < d, 0 < x < a, \end{cases}$$

along with the edge condition that $\nabla \phi$ possesses a square-root singularity at the edge $y = d$.
Note: The forms of ϕ as given by (iii), suggest that

$$-\lambda^2 - \frac{\pi^2}{a^2} + k^2 = 0 \implies \lambda^2 = \left(k^2 - \frac{\pi^2}{a^2}\right) > 0,$$

along with the equation (2.1).

Reduction to two integral equations.

Setting

$$\phi(x, y, z) = \psi(y, z) \sin\left(\frac{\pi x}{a}\right), \quad (3.2)$$

with

$$\psi(y, z) = e^{-i\kappa_0 z} - \sum_{n=0}^{\infty} a_n e^{-i\kappa_n |z|} \text{Sgn}(z) \cos\left(\frac{n\pi y}{b}\right), \quad (\text{Sgn}(z) = \pm 1, \quad (3.3)$$

according as $z > 0$ or $z < 0$),

with

$$\kappa_n = -i\mu_n, \quad \mu_n = \left(\frac{n^2\pi^2}{b^2} - \lambda^2\right) > 0, \quad (\text{assumed}), \quad \text{and } \kappa_0 = \lambda, \quad (3.4)$$

where $a_0 = R = (1 - T)$ and a_n 's ($n \geq 1$) are unknown constants, we find that all the conditions of the problem1 are met with, except the two conditions (A) and (B) of (iv), which lead to the following DUAL SERIES RELATIONS, for the determination of the constants a_n :

$$\sum_{n=0}^{\infty} a_n \cos\left(\frac{n\pi y}{b}\right) = 0, \quad \text{for } 0 < y < d, \quad (3.5)$$

and

$$-\kappa_0 + \sum_{n=0}^{\infty} \kappa_n a_n \cos\left(\frac{n\pi y}{b}\right) = 0, \quad \text{for } d < y < b. \quad (3.6)$$

These dual relations can be easily reduced to two integral equations, in the following manner:

Firstly, setting the left side of the relation (3.6) as equal to $\frac{i}{2}a_0\kappa_0bg(y)$, and noting that $g(y) = 0$, for $d < y < b$, we can easily determine the Fourier coefficients, in terms of $g(y)$ and then the relation (3.5) easily gives rise to the integral equation:

$$\int_0^d K(y, t)g(t)dt = \frac{1}{\kappa_0}, \quad (0 < y < d), \quad (3.7)$$

with

$$K(y, t) := \sum_{n=1}^{\infty} \mu_n^{-1} \cos\left(\frac{n\pi y}{b}\right) \cos\left(\frac{n\pi t}{b}\right) \quad (3.8)$$

We also find that a quantity H can be defined as :

$$H := \frac{1}{2i} \left(\frac{1 - a_0}{a_0} \right) = -\frac{1}{4} \int_0^d g(t) dt. \quad (3.9)$$

As a second approach, setting the left side of the relation (3.5), as equal to $-\frac{i\kappa_0}{2} (1 - a_0)bg_1(y)$, and noting that $g_1(y) = 0$, for $0 < y < d$, we can again determine the Fourier coefficients easily in terms of $g_1(y)$ and then the relation (3.6) gives rise to the following integral equation:

$$1 + \int_d^b K_1(y, t)g_1(t)dt = 0, \quad (d < y < b), \quad (3.10)$$

with

$$K_1(y, t) := \lim_{\epsilon \rightarrow 0} \sum_{n=1}^{\infty} e^{-\epsilon n} \cos\left(\frac{n\pi y}{b}\right) \cos\left(\frac{n\pi t}{b}\right). \quad (3.11)$$

We also find that

$$\frac{1}{H} \equiv \frac{2ia_0}{1 - a_0} = \kappa_0 \int_d^b g_1(t)dt. \quad (3.12)$$

We have thus reduced the problem 1 to that of solving either of the integral equations (3.7) and (3.10), along with either of the two relations (3.9) and (3.12), respectively, which determines an "important" quantity H . It should be emphasized that knowing either $g(y)$ or $g_1(y)$, the problem 1 can be solved completely. However, the kernels K and K_1 are complicated and hence, we will adopt approximate methods (Galerkin methods) as explained in section 4. We also make the observations that the functions g , g_1 and the constant H are real, since the functions K and K_1 are so.

Problem 2:

A Problem occurring in Scattering of Surface Water Waves,

(see Evans and Morris [2])

To solve

$$\frac{\partial^2 \phi}{\partial x^2} + \frac{\partial^2 \phi}{\partial y^2} + \frac{\partial^2 \phi}{\partial z^2} = 0, \text{ for } -\infty < x < \infty, y > 0, -\infty < z < \infty, \quad (3.13)$$

such that

$$\begin{aligned} (i) \quad & K\phi + \frac{\partial \phi}{\partial y} = 0, \text{ on } y = 0 \text{ and } -\infty < x < \infty, \\ & -\infty < z < \infty, (K > 0, \text{ a known constant}) \\ (ii) \quad & \begin{cases} (A) \quad \frac{\partial \phi}{\partial x} = 0, \text{ on and } 0 < y < a, & (B) \quad \frac{\partial \phi}{\partial x} \Big|_{x=0^+} = \frac{\partial \phi}{\partial x} \Big|_{x=0^-}, \text{ for } y > a, \\ (C) \quad \phi|_{x=0^+} = \phi|_{x=0^-} \text{ for } y > a \end{cases} \end{aligned}$$

$$(iii) \quad \phi \longrightarrow \begin{cases} e^{-Ky+ipz}(e^{-imx} + Re^{imx}), \text{ as } x \longrightarrow \infty, \\ Te^{-Ky+ipz}e^{-imx}, \text{ as } x \longrightarrow -\infty, \\ \text{where } p = K \sin(\alpha), m = K \cos(\alpha), (0 < \alpha < \frac{\pi}{2}) \\ (R \text{ and } T \text{ are unknown complex constants to be determined}). \end{cases}$$

$$(iv) \quad \phi, \nabla \phi \longrightarrow 0, \text{ as } y \longrightarrow \infty$$

along with the edge conditions that $\nabla \phi$ possesses a square root singularity at the edge $y = a$, ensuring uniqueness of the solution of the problem.

Reduction to integral equations

Setting

$$\phi(x, y, z) = \psi(x, y)e^{ipz}, \quad (3.14)$$

with

$$\psi(x, y) = e^{-Ky-imx} + R \operatorname{Sgn}(x)e^{-Ky+im|x|} + \int_0^\infty \frac{b(k) \operatorname{Sgn}(x)(k \cos(ky) - K \sin(ky))e^{-k_1|x|}}{k_1(k^2 + K^2)} dk, \quad (3.15)$$

where $k_1 = (k^2 + p^2)^{\frac{1}{2}}$ and $R = (1 - T)$ and $b(k)$ are unknowns, we find that all the conditions of the problem are satisfied, except the conditions (A) and (C) of (ii), giving rise to the following "DUAL INTEGRAL EQUATIONS" for the determination of the function $b(k)$:

$$-\int_0^\infty \frac{b(k)(k \cos(ky) - K \sin(ky))}{k^2 + K^2} dk + im(R - 1)e^{-Ky} = 0, (0 < y < a), \quad (3.16)$$

and

$$\int_0^\infty \frac{b(k)(k \cos(ky) - K \sin(ky))}{k_1(k^2 + K^2)} dk + Re^{-Ky} = 0, (y > a) \quad (3.17)$$

in which R is also an unknown constant.

The above dual integral equations can be reduced to two separate integral equations, by employing a trick, similar to the one used for the problem 1, along with the use of the Havelock's expansion theorem (see Ursell [7]). In fact, this has already been done by Evans and Morris [2].

Firstly, setting the left side of the relation (3.16), as equal to $\frac{\pi R}{2}f(y)$, and noting that $f(y) = 0$, for $0 < y < a$, we can determine $b(k)$ in terms of $f(y)$, by using Havelock's expansion theorem, and then the relation (3.17) gives rise to the integral equation:

$$\int_a^\infty f(t)L(y, t)dt = e^{-Ky}, \text{ for } y > a, \quad (3.18)$$

where

$$L(y, t) = \int_0^\infty \frac{(k \cos(ky) - K \sin(ky))(k \cos(kt) - K \sin(kt))}{k_1(k^2 + K^2)} dk, \quad (3.19)$$

along with the defining relation:

$$A := \frac{im(1 - R)}{\pi KR} = \int_a^\infty f(t)e^{-Kt}dt. \quad (3.20)$$

Secondly, setting the left side of the relation (3.17), as equal to $-\frac{\pi i}{2}(1-R)f_1(y)$, and noting that $f_1(y) = 0$, for $y > a$, we can determine $b(k)$ in terms of $f_1(y)$, by using Havelock's expansion theorem, and then the relation (3.16) gives rise to the integral equation:

$$\int_0^a f_1(t)M(y,t)dt = e^{-Ky}, \text{ for } 0 < y < a, \quad (3.21)$$

where

$$M(y,t) := \lim_{\delta \rightarrow 0} \int_0^\infty \frac{k_1(k \cos(ky) - K \sin(ky))(k \cos(kt) - K \sin(kt))}{(k^2 + K^2)} e^{-k\delta} dk, \quad (3.22)$$

along with the relation

$$\frac{1}{\pi^2 K^2 A} = \int_0^a f_1(t) e^{-Kt} dt. \quad (3.23)$$

We note that f , f_1 and A are all real quantities, since L and M are real.

From the above discussion it follows that the problem under consideration can be solved completely, either by solving the integral equation (3.18) along with the use of the relation (3.20), or by solving the integral equation (3.21), along with the relation (3.23).

4. Approximate solutions of the integral equations.

In this section, we shall employ "single-term"-Galerkin methods to obtain approximate solutions of the integral equations (3.7) and (3.10), derived for the Problem 1, as well as of the integral equations (3.18) and (3.21), derived for the Problem 2. In fact these solutions have also been presented earlier by Jones [4] and Evans and Morris [2], respectively.

For the equation (3.7) we assume a "single-term" Galerkin approximation as given by

$$g(y) \approx b_0 \text{ (a constant)}, \quad (4.1)$$

in the light of the relation (2.6), with

$$b_0 = \frac{d}{\kappa_0 \int_0^d \int_0^d K(y,t) dt dy} = \frac{d}{\kappa_0 \frac{b^2}{\pi^2} \sum_{n=1}^{\infty} (n^2 \mu_n)^{-1} \sin^2 \left(\frac{n\pi d}{b} \right)}, \quad (4.2)$$

in the light of the first of the relations (2.9).

Similarly, we assume a "single-term" galerkin approximation to the solution of the integral equation (3.10), as given by

$$g_1(y) \approx C_0 \cos \left(\frac{\pi}{2} \left(\frac{b-y}{b-d} \right) \right), \quad (4.3)$$

with

$$C_0 = -8(b-d)^3 \pi \left[\frac{1}{\sum_{n=1}^{\infty} \mu_n \left\{ \frac{1}{4(b-d)^2} - \frac{n^2}{b^2} \right\}^{-2} \cos^2 \left(\frac{n\pi d}{b} \right)} \right]. \quad (4.4)$$

Again, for the solution of the integral equations (3.18) and (3.21), we assume the following "single-term" Galerkin approximations (see Evans and Morris [2]) :

$$f(y) \approx C_1 \hat{f}(y) = C_1 \frac{d}{dy} \left[e^{-Ky} \int_a^y \frac{ue^{Ku}}{(u^2 - a^2)^{\frac{1}{2}}} du \right], \text{ for } a < y < \infty, \quad (4.5)$$

and

$$f_1(y) \approx C'_1 \hat{f}_1(y) = C'_1 e^{-Ky} \int_y^a \frac{ue^{Ku}}{(a^2 - u^2)^{\frac{1}{2}}} du, \text{ for } 0 < y < a, \quad (4.6)$$

where C_1 and C'_1 are to be calculated by using the first of the relations (2.9), giving

$$C_1 = \frac{\int_a^\infty e^{-Ky} \hat{f}(y) dy}{\int_a^\infty \int_a^\infty L(y, t) \hat{f}(t) \hat{f}(y) dy dt} \quad (4.7)$$

and

$$C'_1 = \frac{\int_0^a e^{-Ky} \hat{f}_1(y) dy}{\int_0^a \int_0^a M(y, t) \hat{f}_1(t) \hat{f}_1(y) dy dt} \quad (4.8)$$

5. Some approximate results

In this section we shall explain about the derivation of some approximate results for the quantities H and A associated with the two problems 1 and 2, considered in section 3, which represent important quantities of practical interest in the theory of electromagnetism (see Jones[4]) and in surface water wave theory (see Evans and Morris [2]), respectively.

By using the relations (3.9) and the approximate solution for $g(y)$ as given by the relations (4.1) and (4.2), we can easily determine H approximately. We find that in the particular situation, when $d = \frac{b}{2}$ and $\mu_n \approx \frac{n\pi}{b}$ (i.e when $\kappa_0 b \ll \pi$), we obtain

$$H \approx -\frac{\pi^3}{16\kappa_0 b \sum_{n=0}^{\infty} \frac{1}{(2n+1)^3}} \approx -0.59 \frac{\pi}{\kappa_0 b}. \quad (5.1)$$

Similarly, by using the relation (3.12), along with the approximate solution for $g_1(y)$ as given by the relations (4.3) and (4.4), we can determine an approximate value for the quantity H .

We find that when $d = \frac{b}{2}$ and $\mu_n = \frac{n\pi}{b}$, we have

$$H \approx -\frac{\pi}{\kappa_0 b} \left(\frac{\pi^2}{16} + \sum_{n=1}^{\infty} \frac{2n}{(4n^2 - 1)^2} \right) \approx -0.87 \frac{\pi}{\kappa_0 b} \quad (5.2)$$

From the theory that has been explained in section 2, we find that the two results in the relations (5.1) and (5.2) provide some upper and lower bounds respectively, for the quantity H , and, we find that the average of these two bounds gives the value $-0.73 \frac{\pi}{\kappa_0 b}$, which, according to Jones [4], is very near the actual value $-0.71 \frac{\pi}{\kappa_0 b}$.

Also, by using the approximate solutions as given by the relations (4.5), (4.6), (4.7) and (4.8), into the relations (3.20) and (3.23), we can determine two values of A , approximately, which provide some upper and lower bounds, A_1 and A_2 respectively, for this quantity. Then, with the aid of the defining relation (3.20), we find that

$$|R| = (1 + \pi^2 A^2 \sec^2(\alpha))^{-\frac{1}{2}} \quad (5.3)$$

The numerical values of $|R|$ have been worked out by Evans and Morris [2], by using the two bounds for A_1 and A_2 of A as described above, and we give below a representative table for $\alpha = 30^\circ$, for the purpose of completion of this article. The table clearly shows the closeness of the bounds of $|R|$, i.e. $|R_1|$ and $|R_2|$, which must be attributed to the particular choice of the "single-term" Galerkin approximations as suggested in the relations (4.5) and (4.6).

Table

$ R / \mu$	0.2	0.4	0.6	0.8	1.0	1.4	1.8
$ R_1 $	0.0569	0.2432	0.5389	0.7971	0.9252	0.9900	0.9984
$ R_2 $	0.0569	0.2430	0.5382	0.7961	0.9246	0.9898	0.9984

Table of values of $|R_j| = (1 + \pi^2 A_j^2 \sec^2(\alpha))^{-\frac{1}{2}}$, $j = 1, 2$,
for $\alpha = 30^\circ$, $\mu = Ka$.

References

- [1] Banerjee S. and Mandal B. N., "Scattering of water waves by a submerged thin vertical wall with a gap", *J. Aust. Math. Soc., Ser B*, **38**, pp. 1-5, (1997)
- [2] Evans D. V. and Morris C. A. N., "The effect of a fixed vertical barrier on obliquely incident surface waves in deep water", *J. Inst. Maths. Applies*, **9**, pp. 198-204, (1972 a)
- [3] Evans D. V. and Morris C. A. N., "Complementary approximations to the solution of a problem in water waves", *J. Inst. Maths. Applies*, **10**, pp. 1-9, (1972 b)
- [4] Jones D. S., *Theory of Electromagnetism*, Pergamon Press, (1964)
- [5] Mandal B. N. and Das P., "Oblique diffraction of surface waves by a submerged vertical plate", *J. Engng. Math.*, **30**, pp. 459-470, (1996)
- [6] Sneddon I. N., *Mixed Boundary Value Problems*, North Holland, (1966).
- [7] Ursell F., "The effect of a fixed vertical barrier on surface waves in deep water", *Proc. Camb. Phil. Soc.*, **43**, pp. 374-382, (1947)

Analytic Solutions to Maxwell's Equations: Sinusoidal Steady - State and Transient Space - Time Problems in Transverse Magnetic and Transverse Electric Field Analysis

Sergey Edward Lyshevski

Department of Electrical Engineering
Purdue University at Indianapolis
723 West Michigan Street, SL 160B
Indianapolis, Indiana 46202-5132, USA
lyshevs@enr.iupui.edu

Abstract

Maxwell's equations form the basis in electromagnetic field theory. The electromagnetic field, if it exists, satisfies Maxwell's equations and the boundary conditions associated. These equations are simple in the form but contain the variations of the field quantities throughout three-dimensional space (rectangular, cylindrical, and spherical coordinate systems are used) and time. The general solution to Maxwell's equations is usually difficult to find. However, analysis of electromagnetic fields requires to find the general solution without simplifications and assumptions, and our goal is to obtain explicit analytic solutions to Maxwell's equations with the corresponding boundary conditions. This paper researches methods and reports a straightforward mathematical foundation for solving Maxwell's equations in analysis of transverse magnetic (TM) and transverse electric (TE) fields.

1. Introduction

The electromagnetic field model is governed by four Maxwell's equations, which are given in the point form for time-varying fields as

$$\begin{aligned}\nabla \times E(x, y, z, t) &= -\mu \frac{\partial H(x, y, z, t)}{\partial t}, \\ \nabla \times H(x, y, z, t) &= \sigma E(x, y, z, t) + \varepsilon \frac{\partial E(x, y, z, t)}{\partial t} + J(x, y, z, t), \\ \nabla \cdot E(x, y, z, t) &= \frac{\rho(x, y, z, t)}{\varepsilon}, \quad \nabla \cdot H(x, y, z, t) = 0,\end{aligned}$$

where E is the electric field intensity; H is the magnetic field intensity; J is the current density; ρ is the charge density.

The development of analytic methods to solve Maxwell's equations in the coordinate systems used is our particular interest. The common coordinate systems applied (rectangular, circularly cylindrical, and spherical) are studied, and complete analytic solutions to Maxwell's equations are given. The rectangular and cylindrical coordinate systems are commonly used. This paper demonstrates that an analytic solution to Maxwell's equations, if it exists, can be found in the chosen coordinate system by the superposition of TM and TE fields, and the reciprocity theorem can be used. In the circularly cylindrical system, the TM and TE potentials satisfy the Helmholtz equation, and the first-, second-, and third-kind Bessel functions are applied. Only the spherical coordinate system has

complete coordinate surfaces of finite size, and therefore, in this system the boundary value problem can be solved. Hence, the spheroidal configuration, which has ϕ -symmetry, is of a great importance. The wave or Helmholtz equation for the field quantities (E or H) in terms of the time-varying sources can be expressed and solved in the spherical coordinate system.

2. General Methods of Solution

For time-varying fields, the sinusoidal steady-state behavior of the field vectors is our interest. We assume that the E and H components are varying sinusoidally; in particular,

$$E(x, y, z, t) = E_x(x, y, z, t)a_x + E_y(x, y, z, t)a_y + E_z(x, y, z, t)a_z,$$

where $E_x(x, y, z, t) = E_{mx} \cos(\omega t + \psi_x)$, $E_y(x, y, z, t) = E_{my} \cos(\omega t + \psi_y)$, $E_z(x, y, z, t) = E_{mz} \cos(\omega t + \psi_z)$;

$$H(x, y, z, t) = H_x(x, y, z, t)a_x + H_y(x, y, z, t)a_y + H_z(x, y, z, t)a_z.$$

where $H_x(x, y, z, t) = H_{mx} \cos(\omega t + \psi_x)$, $H_y(x, y, z, t) = H_{my} \cos(\omega t + \psi_y)$, $H_z(x, y, z, t) = H_{mz} \cos(\omega t + \psi_z)$.

The magnitudes E_{mx} , E_{my} , E_{mz} , H_{mx} , H_{my} , H_{mz} and phase angles are independent of time, however they depend on the spatial coordinates.

By using complex phasor quantities of E and H , and canceling the $e^{j\omega t}$ term which is common to the right and left sides of equations, one obtains the time-domain form of Maxwell's equations. In particular, the electromagnetic field satisfies the following equations in the point phasor form

$$\begin{aligned} \nabla \times H &= j\omega \epsilon E + J, \quad \nabla \times E = -j\omega \mu H, \\ \nabla \cdot E &= \frac{\rho}{\epsilon}, \quad \nabla \cdot H = 0, \end{aligned} \quad (1)$$

which should be solved.

It has to be emphasized that the permittivity, permeability and conductivity are nonlinear functions of frequency.

By defining $H_2 = H - H_1$, $E_1 = E - E_2$ and $J = J_1 + J_2$, we have

$$\nabla \times (H_1 + H_2) = j\omega \epsilon (E_1 + E_2) + (J_1 + J_2),$$

$$\nabla \times (E_1 + E_2) = -j\omega \mu (H_1 + H_2).$$

A set of equations is found to be

$$\nabla \times H_1 = j\omega \epsilon E_1 + J_1, \quad \nabla \times E_1 = -j\omega \mu H_1,$$

$$\nabla \times H_2 = j\omega \epsilon E_2 + J_2, \quad \nabla \times E_2 = -j\omega \mu H_2. \quad (2)$$

Compare to equations (1), equations (2) can be easily solved because the divergence is zero. That is, H can be represented by a vector potential P , which is given in terms of its components along and perpendicular to the coordinates used. Hence,

$$H = \nabla \times P, \quad P = P_{TM} a_i + P_t.$$

Here, $P_t = \nabla \times P_{TE1} a_i$ is transverse (perpendicular) to the unit vectors a_i ; P_{TM} and P_{TE} are the scalar potentials.

We obtain

$$H = \nabla \times P_{TM} a_i + \nabla \times \nabla \times P_{TE} a_i.$$

Using $H_1 = \nabla \times P_{TM} a_i$ in $\nabla \times H = j\omega \epsilon E + J$, one finds

$$\nabla \times \nabla \times P_{TM} a_i = j\omega \epsilon E_1 + J.$$

$$\text{Furthermore, } \nabla \times (E_1 + j\omega \mu P_{TM} a_i) = 0,$$

and hence

$$E_1 = -j\omega\mu P_{TM} a_i + \nabla p.$$

By making use of E_1 , the following equations result

$$H_1 = \nabla \times P_{TM} a_i, \quad E_1 = \frac{\nabla \times \nabla \times P_{TM} a_i - J_1}{j\omega\epsilon},$$

$$\nabla \times H_2 = j\omega\epsilon E_2, \quad \nabla \times E_2 = -j\omega\mu H_2 - M_2.$$

From equation

$$E_2 = \nabla \times P_{TE} a_i,$$

one finds P_{TE} by solving equation

$$\nabla^2 P_{TE} a_i = \gamma^2 P_{TE} a_i + M_2.$$

The thorough analysis performed indicates, that for TM and TE fields the equations

$$H_1 = \nabla \times P_{TM} a_i$$

$$\text{and } E_2 = \nabla \times P_{TE} a_i$$

should be solved by using the following procedure. In the Cartesian coordinate systems, as one obtains P_{TM} and P_{TE} , H_1 and E_2 results. Furthermore, E_1 can be found by solving

$$\nabla \times H_1 = j\omega\epsilon E_1 + J_1, \quad E_1 = -j\omega\mu P_{TM} a_i + \frac{\nabla \left(\frac{\partial P_{TM}}{\partial x_i} \right)}{j\omega\epsilon},$$

while E_2 is obtained using P_{TE} , and H_2 is found from

$$\nabla \times E_2 = -j\omega\mu H_2, \quad H_2 = j\omega\epsilon P_{TE} a_i - \frac{\nabla \left(\frac{\partial P_{TE}}{\partial x_i} \right)}{j\omega\mu}.$$

In the cylindrical coordinate system, which is given in terms ρ, ϕ, z , the TM and TE field equations are

$$H = \nabla \times P_{TM} a_i$$

$$\text{and } E = \nabla \times P_{TE} a_i,$$

and the scalar potential satisfies Helmholtz equations are given by

$$\nabla^2 P_{TM} = \gamma^2 P_{TM}, \quad \gamma^2 = -\omega^2 \mu \epsilon.$$

The following partial differential equation for P_{TM} results

$$\frac{1}{\rho} \frac{\partial}{\partial \rho} \left(\rho \frac{\partial P_{TM}}{\partial \rho} \right) + \frac{1}{\rho^2} \frac{\partial^2 P_{TM}}{\partial \phi^2} + \frac{\partial^2 P_{TM}}{\partial z^2} - \gamma^2 P_{TM} = J_i,$$

and the solution of this equation is found using hyperbolic functions. In particular,

$$P_{TM} = \Phi_\rho(\rho) \Phi_\phi(\phi) \Phi_z(z),$$

where $\Phi_\rho(\rho)$, $\Phi_\phi(\phi)$ and $\Phi_z(z)$ are the Bessel functions.

If the spherical coordinate system is used, the field components are found for TM fields as

$$H_\phi = -\frac{1}{r} \frac{\partial P_{TM}}{\partial \theta}, \quad H_\theta = \frac{1}{r \sin \theta} \frac{\partial P_{TM}}{\partial \phi},$$

$$E_\theta = \frac{1}{j\omega\epsilon r} \frac{\partial^2 P_{TM}}{\partial \theta \partial r}, \quad E_r = \frac{1}{j\omega\epsilon} \left(\frac{\partial^2 P_{TM}}{\partial r^2} + \beta^2 P_{TM} \right), \quad E_\phi = \frac{1}{j\omega\epsilon r \sin \theta} \frac{\partial^2 P_{TM}}{\partial \phi \partial r},$$

and for TE fields we have

$$E_\phi = -\frac{1}{r} \frac{\partial P_{TE}}{\partial \theta}, \quad E_\theta = \frac{1}{r \sin \theta} \frac{\partial P_{TE}}{\partial \phi},$$

$$H_\theta = -\frac{1}{j\omega\mu r} \frac{\partial^2 P_{TE}}{\partial \theta \partial r}, \quad H_r = -\frac{1}{j\omega\mu} \left(\frac{\partial^2 P_{TE}}{\partial r^2} + \beta^2 P_{TE} \right), \quad H_\phi = -\frac{1}{j\omega\mu \sin \theta} \frac{\partial^2 P_{TE}}{\partial \phi \partial r}.$$

The corresponding Helmholtz equation is

$$\frac{1}{r^2} \frac{\partial}{\partial r} \left(r^2 \frac{\partial \left(\frac{1}{r} P_{TM} \right)}{\partial r} \right) + \frac{1}{r^2 \sin \theta} \frac{\partial}{\partial \theta} \left(\sin \theta \frac{\partial \left(\frac{1}{r} P_{TM} \right)}{\partial \theta} \right) + \frac{1}{r^2 \sin^2 \theta} \frac{\partial}{\partial \phi} \frac{\partial^2 \left(\frac{1}{r} P_{TM} \right)}{\partial \phi^2} + \beta^2 \left(\frac{1}{r} P_{TM} \right) = J_i.$$

Transient space-time problem should be solved in many applications. Consider the following equations

$$\nabla \times E(x, y, z, t) = -\mu \frac{\partial H(x, y, z, t)}{\partial t}, \quad \nabla \times H(x, y, z, t) = \sigma E(x, y, z, t) + \varepsilon \frac{\partial E(x, y, z, t)}{\partial t} + J(x, y, z, t),$$

$$\nabla \cdot E(x, y, z, t) = \frac{\rho(x, y, z, t)}{\varepsilon}, \quad \nabla \cdot H(x, y, z, t) = 0,$$

assuming that the excitation is a known function of time. To solve the problem, the Fourier or Laplace transforms can be used. The solution is not trivial, and the particular scenario should be considered to solve the problem.

3. Duality of Solution

If the field varies sinusoidally with time, the time can be eliminated from the fundamental equations; that is, the solution is obtained in terms of complex vectors. Assume that the electromagnetic field satisfies the following two equations

$$\nabla \times H_1 = j\omega \varepsilon_1 E_1 + J_1, \quad \nabla \times E_1 = -j\omega \mu_1 H_1 \quad (3)$$

with the corresponding boundary conditions.

If the solution of these equations is known, one can solve

$$\nabla \times H_2 = j\omega \varepsilon_2 E_2, \quad \nabla \times E_2 = -j\omega \mu_2 H_2 - M_2 \quad (4)$$

by using the transformations

$$E_1 = -H_2, \quad H_1 = E_2, \quad J_1 = -M_2, \quad \varepsilon_1 = \mu_2, \quad \mu_1 = \varepsilon_2,$$

$$\text{or} \quad E_1 = H_2, \quad H_1 = -E_2, \quad J_1 = M_2, \quad \varepsilon_1 = \mu_2, \quad \mu_1 = \varepsilon_2,$$

$$\text{or} \quad E_1 = H_2, \quad H_1 = E_2, \quad J_1 = -M_2, \quad \varepsilon_1 = -\mu_2, \quad \mu_1 = -\varepsilon_2.$$

In particular, by applying these transformations, solution of (4) is identical to (3).

4. Conclusions

This paper addresses the problem of solution of Maxwell's equations in the rectangular, cylindrical and spherical coordinate systems. Sinusoidal steady-state and transient space-time problems have been researched. By using the results, it is shown that Maxwell's equations can be solved, and important problems have been focused and solved. In particular, the complexity of the solution depends on the coordinate system used, and spherical coordinate system has advantages to find analytic solutions to Maxwell's equations.

RECENT DEVELOPMENTS IN FAST-MULTIPOLE BASED FREQUENCY AND TIME DOMAIN SOLVERS

E. Michielssen, W. Chew, A. Ergin, V. Jandhyala, B. Shanker, and J. Song
 Center for Computational Electromagnetics
 Department of Electrical and Computer Engineering
 University of Illinois at Urbana-Champaign
 Urbana, IL 61801

Abstract: This paper reviews the state of the art in fast integral equation techniques for solving large scale electromagnetic scattering and radiation problems. The Multilevel Fast Multipole Algorithm and its frequency and time domain derivatives are discussed. These techniques permit the rapid evaluation of fields due to known sources and hence accelerate the solution of boundary value problems arising in the analysis of a wide variety of electromagnetic phenomena. Specifically, the application of the Steepest Descent Fast Multipole Method to the frequency domain analysis of radiation from quasi planar structures, e.g., rough surfaces and finite microstrip structures, is described. In addition, the extension of the fast multipole concept to the Plane Wave Time Domain algorithm that permits the efficient analysis of transient phenomena is outlined.

INTRODUCTION

Surface integral equations coupled with Method Of Moments (MOM) based solution algorithms have long been conceived as very accurate, but computationally expensive schemes for analyzing electromagnetic radiation and scattering phenomena. Unlike finite difference and finite element techniques which require the discretization of the entire volume of the structure under study, surface integral equation techniques utilize basis functions only on interfaces between homogeneous regions, thereby resulting in fewer unknowns. However, in contrast to these differential equation techniques, the application of the MOM to the solution of surface integral equations leads to a matrix equation involving a dense matrix. As a consequence, for large problems, the solution of the MOM equations using direct inversion is impractical due to the large CPU time and memory requirements associated with this procedure. The iterative solution of the MOM system is also a time consuming process, with both the number of operations per iteration and the memory cost associated with storing the matrix scaling as $O(N_s^2)$, where N_s is the number of spatial degrees of freedom of the discretized surface current, i.e., the dimension of the system. Integral equation techniques for analyzing surface scattering and radiation phenomena have been developed as well. Unfortunately, their computational complexity scales as $O(N_t N_s^2)$, where N_t denotes the number of temporal steps in the analysis, and prohibits their application to the analysis of large-scale scattering phenomena.

To expedite the iterative solution of electromagnetic boundary value problems, researchers have exploited the underlying structure of the Green's function kernel and developed techniques that facilitate the fast computation of MOM matrix-vector products [1-5]. We have recently developed a host of fast multipole based algorithms for analyzing large-scale radiation and

scattering phenomena [6-7]. In this paper, we report on the implementation of the Multilevel Fast Multipole Algorithm (MLFMA), and a derivative of the latter, the Steepest Descent Fast Multipole Method (SDFMM). These algorithms accelerate the iterative solution of surface integral equations that are pertinent to the analysis of scattering and radiation from arbitrarily shaped three-dimensional and quasi-planar structures, respectively. The computational cost per iteration and memory requirements of the MLFMA and SDFMM scale as $O(N_s \log N_s)$ and $O(N_s)$, respectively. In addition, the extension of the fast multipole concept to the analysis of transient scattering phenomena is described. Fast time domain integral equation based schemes, reminiscent of the frequency domain fast multipole methods, further termed Plane Wave Time Domain (PWTD) schemes, permit the efficient analysis of transient scattering phenomena in $O(N_t N_s \log N_s)$ operations.

THE MULTILEVEL FAST MULTIPOLE ALGORITHM

The MLFMA constitutes an efficient technique for analyzing 3D electromagnetic interaction phenomena [3,6,7]. The algorithm relies on a multilevel divide and conquer strategy and has been implemented in FISC (Fast Illinois Solver Code) technology. The MLFMA is designed to accelerate a matrix-vector multiply that arises in the iterative solution of the MOM equations resulting from a discretization of the boundary integral equations pertinent electromagnetic scattering and radiation analysis. In the MLFMA, the object under study is first subdivided into subscatterers, also termed groups. Fields generated by sources residing in separate source groups are characterized through each group's far-field radiation pattern, measured with respect to the group's center. Then, the addition theorem is used to translate the plane wave components that characterize each source group's far-field pattern to the centers of all other, receiving groups. Fields received at a group center are then redistributed to the individual receivers residing in the group.

Whereas a matrix-vector multiply involving a dense matrix and a dense vector requires $O(N_s^{1.5})$ operations, a matrix-vector multiply carried out using a two-level fast multipole algorithm only requires $O(N_s^{1.5})$ operations. An analogy with a telephone network is in order. Assume that N telephones are connected to one another with direct connections. The number of network wires is N^2 . However, if "hubs" are introduced in the network, then the number of connections can be reduced (Fig. 1(b)). However, the hub structure implies a three-stage connection process. Similarly, in the two-level fast multipole scheme described above, a multiplication is effected through three separate translation procedures: from source to source group center, from the center of the source group to that of the receiving group, and from the receiving group center to the receiver. All these translations can be carried out efficiently by representing all fields in terms of a plane wave basis. The plane wave basis is suitable for translating fields as it gives rise to diagonal translation operators. In other words, when relying on the fast multipole method, the interaction between two basis functions can be represented as

$$\langle \mathbf{j}_r(\mathbf{r}), G_f(\mathbf{r}, \mathbf{r}') \mathbf{j}_s(\mathbf{r}) \rangle = \int_{\mathbf{k}_h} \int_{S_r} \mathbf{j}_r(\mathbf{r}) e^{-j\mathbf{k}_h \cdot (\mathbf{r} - \mathbf{r}_r)} d\mathbf{r} \left[T(\mathbf{k}_h, \mathbf{r}_r, \mathbf{r}_s) \int_{S_s} \mathbf{j}_s(\mathbf{r}) e^{j\mathbf{k}_h \cdot (\mathbf{r} - \mathbf{r}_s)} d\mathbf{r} \right] d\mathbf{k}_h \quad (1)$$

In Eq. (1), the outer integration is over all real \mathbf{k}_h vectors that characterize homogeneous plane waves propagating away from the structure under study. Also, \mathbf{r}_r and \mathbf{r}_s denote the center of the receiver and source group, respectively, and $G_f(\mathbf{r}, \mathbf{r}')$ denotes the free space Green's function. Finally, $T(\mathbf{k}_h, \mathbf{r}_r, \mathbf{r}_s)$ is the diagonal plane wave translator from the source to the observation sphere.

Unfortunately, the above described technique for computing receiver fields only applies to non-overlapping source and observer groups; Hence, all "near-field" interactions, i.e., interactions between sources and observers that reside in the same or in neighboring groups are always accounted for using classical MOM techniques.

By nesting a smaller problem within a larger one, the Multilevel Fast Multipole Algorithm (MLFMA) is obtained. The MLFMA is characterized by $O(N_s \log N_s)$ computational complexity per iteration and memory requirements. The MLFMA uses the two-level fast multipole method as a primitive and transitions between distinct levels in the multilevel tree structure are effected through interpolation and antinterpolation operators. We have implemented this algorithm in two and three dimensions, and the resulting codes are capable of analyzing arbitrarily shaped conductor systems comprised of surfaces and wires. To date, FISC MLFMA technology has been primarily applied to the analysis of large-scale scattering phenomena. As an example, Figure 1 shows the surface currents on a car illuminated by a plane wave at 1 GHz.

83 Camaro Model, $f = 1$ GHz, V-pol.

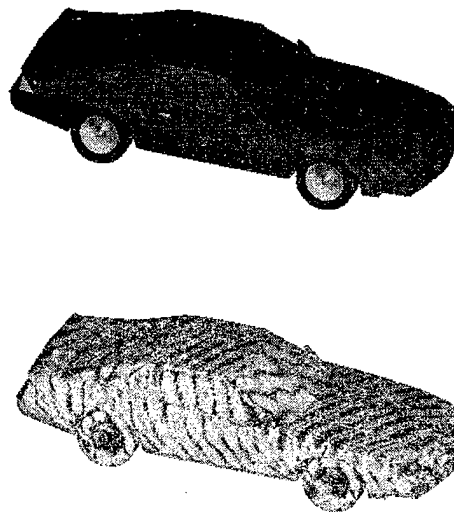


Figure 1. Surface currents on a car illuminated by a plane wave at 1 GHz

THE STEEPEST DESCENT FAST MULTIPOLE METHOD

Although the aforementioned MLFMA permits a very efficient analysis of radiation and scattering from arbitrarily shaped structures, further savings are possible if the application domain is restricted to the class of quasi-planar structures. The SDFMM is a multilevel solver that permits the rapid analysis of radiation and scattering from microstrip traces and patches. The SDFMM is in spirit identical to the above-described MLFMA [8,9]. However, the SDFMM exploits the quasi planarity of a microstrip structure to further accelerate the solution process. This is achieved by casting terms arising in a MOM matrix-vector product in the form of discrete inhomogeneous plane-wave expansions, as opposed to a homogeneous plane wave expansion for the MLFMA. This representation arises from a representation of the pertinent Green's function along a steepest descent path and from the use of the fast multipole method in the transverse plane. The difference w.r.t. the standard MLFMA lies in the use of complex wave vectors and a modified translator operator. These modifications result in significant CPU cost and memory savings over the standard MLFMA. Indeed, the computational cost and memory requirements of

the SDFMM scale as $O(N_s)$, as opposed to $O(N_s \log N_s)$ in the standard MLFMA. Other FMM-like approaches for analyzing microstrip structures are described in [10,11].

We have developed a general purpose SDFMM solver, capable of analyzing a large class of quasi-planar microstrip structures that reside on a finite substrate and ground plane. This solver is based upon a multiregion MOM formulation that features both electric and magnetic surface currents. These currents model fields tangential to perfectly conducting microstrip elements as well as those tangential to penetrable substrate interfaces. The code can handle not only surface elements, but also accommodates bond wires and probe feeds [12].

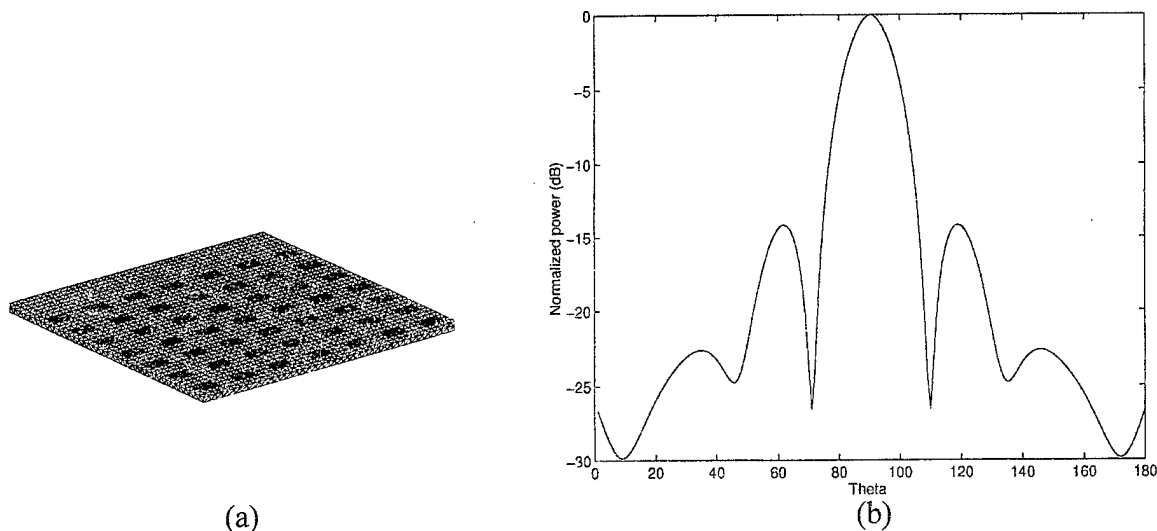


Figure 2: (a) 7 by 7 array of microstrip patches residing on a finite substrate and ground plane. A probe feed connects each patch to the ground plane, (b) Radiation pattern of the 7 by 7 array shown in (a).

The SDFMM permits the analysis of scattering and radiation from extremely large and complex structures within realistic times. To illustrate the capabilities of our SDFMM solver, consider the 7 by 7 array of microstrip patches shown in Figure 2. Each patch is probe fed (in phase). Equivalent currents on the patches, probes, and on the ground plane and the penetrable interfaces are modeled using $N=92,280$ unknowns. Figure 3 shows the pattern of the array computed using the SDFMM. To date, the SDFMM has been applied to microstrip structures modeled in terms of as many as 130,000 unknowns.

TIME DOMAIN FAST MULTIPOLE METHODS: PLANE WAVE TIME DOMAIN SOLVERS

Recently, we have developed a fast time-domain integral equation solver [14]. This fast solver permits the rapid analysis of transient scattering and radiation phenomena involving electromagnetically large surface structures and can be considered the time-domain analogue of the frequency domain multilevel fast multipole solver described above. The cost associated with the electromagnetic analysis of a surface structure that is modeled in terms of N_s spatial unknowns for a total duration of N_t time steps scales as $O(N_t N_s \log N_s)$ using the new solver, as opposed to $O(N_t N_s^2)$ for classical time domain integral equation algorithms. The solver

derives its optimal scaling properties from a time domain plane wave representation of the scattered fields, which is exploited through a multilevel divide and conquer framework. This representation naturally gives rise to windowed diagonal translation operators. These translation operators require convolution of polynomial translation functions with the transient plane wave spectrum of the source distribution, characterized in terms of the source's slant stack transform. To date, the technique has been applied to the analysis of acoustic and electromagnetic scattering from large, three-dimensional surfaces. The application of the solver to the analysis of broadband wire antenna structures, nonlinear phenomena, and electromagnetic compatibility problems is being studied.

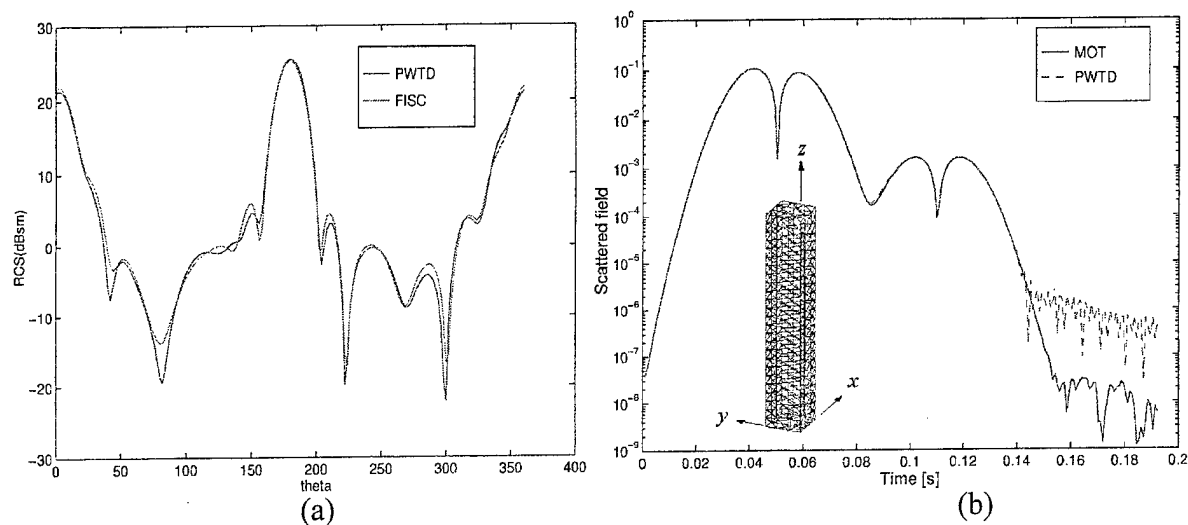


Figure 3. (a) Electromagnetic RCS of a NASA almond, comparison between PWTd (frequency domain parameters extracted from time domain solver) and FISC, (b) temporal fields on top of a rectangular cylinder, comparison between classical time domain integral equation and PWTd results.

CONCLUSIONS

This paper described three different multilevel integral equation solvers: The MLFMA, the SDFMM, and the PWTd. The MLFMA is suited for analyzing scattering and radiation from electrically large, arbitrarily shaped structures. The SDFMM constitutes an MLFMA variant designed to accelerate the analysis of electromagnetic phenomena involving quasi-planar structures, e.g., rough surfaces, optical gratings, and large-scale microstrip structures residing on finite ground planes. Finally, the PWTd schemes are extensions of the MLFMA to the time domain. Hence, the PWTd permits the broadband characterization of scatterers and radiators and is applicable to the analysis of nonlinear phenomena.

ACKNOWLEDGEMENTS

This work was supported in part by a grant from United States AFOSR via the MURI Program under contract no F49620-96-1-0025.

REFERENCES

- [1] C. R. Anderson, "An implementation of the fast multipole method without multipole," *SIAM J. Sci. Statist. Comput.*, vol. 13, no. 4, pp. 923-947, July 1992.
- [2] V. Rokhlin, "Rapid solution of integral equations of scattering theory in two dimensions," *J. Comput. Phys.*, vol. 36, no. 2, pp. 414-439, 1990.
- [3] W. C. Chew and C. C. Lu, "A fast algorithm to compute the wave-scattering solution of a large strip," *Computational Physics*, vol. 107, no. 2, pp. 378-387, Aug. 1993.
- [4] A. Brandt, "Multilevel Computations of integral transforms and particle interactions with oscillatory kernels," *Comput. Phys. Commun.*, vol. 65, pp. 24-38, 1991.
- [5] E. Michielssen and W.C. Chew, "The fast steepest descent path algorithm for analyzing scattering from two-dimensional objects," *Radio Science*, vol. 31, no. 5, pp. 1215-1224, September-October 1996.
- [6] C. C. Lu, and W. C. Chew, "A multilevel algorithm for solving a boundary integral equation of wave scattering," *Micro. Opt. Tech. Lett.*, vol. 7, no. 10, pp. 456-470, July 1994.
- [7] J. M. Song and W. C. Chew, "Multilevel fast-multipole algorithm for solving combined field integral equations of electromagnetic scattering," *Micro. Opt. Tech. Lett.*, vol. 10, no. 1, pp. 14-19, Sept. 1995.
- [8] V. Jandhyala, E. Michielssen, B. Shanker, and W. C. Chew, "A combined steepest descent--fast multipole algorithm for the fast analysis of three-dimensional scattering by rough surfaces", Center for Computational Electromagnetics Research Report, No.: CCEM 3-97, March 31, 1997.
- [9] V. Jandhyala, B. Shanker, E. Michielssen, and W. C. Chew, "Analysis of scattering from dielectric rough surfaces using an $O(N)$ multilevel iterative solver," *Journal of the Optical Society of America*, Accepted for publication, 1997.
- [10] V. Jandhyala, E. Michielssen, and R. Mittra, "Multipole-accelerated capacitance computation for 3-d structures in a stratified dielectric medium using a closed form Green's function," Special issue on Microwave Packages and Interconnects, *Int. J. Microwave and Millimeter-Wave Computer -Aided Engg.*, vol. 5, pp. 68-78, May 1995.
- [11] L. Gurel, M. I. Aksun, "Electromagnetic scattering solution of conducting strips in layered media using the fast multipole method," *IEEE Microwave Guided Wave Letters*, vol. 6, no. 8, pp. 277-279, Aug 1996.
- [12] E. Yip and B. Dembart, "Matrix assembly in FMM-MOM codes," Tech. Rep. ISSTECH-97-002, The Boeing Company, Seattle, WA, 1997
- [13] J.S. Zhao, W.C. Chew, C.C. Lu, J.M. Song, and E. Michielssen, "The thin stratified medium fast multipole method for analyzing microstrip structures," *IEEE Trans. Microwave Theory and Techniques*, Accepted for publication, 1997.
- [14] A. Ergin, B. Shanker, and E. Michielssen, "Diagonal translation operators for transient wave fields," *Journal of Computational Physics*, Accepted for Publication, 1997.

WAVEGUIDING AND ANOMALOUS PROPERTIES OF A KNIFE-TYPE PERIODIC STRIP GRATING

Sukhinin S. V.

Lavrentyev Institute of Hydrodynamics, Siberian Division Russian Academy of Sciences
Lavrentyev prospect, 15, Novosibirsk, 630090, RUSSIA
E-mail sukhinin@hydro.nsk.su

Demonstrated here, are the periodical knife-types gratings always having the waveguiding properties. Discovered here, are the existence criteria of the waveguiding properties of periodic plate grating for different waveguiding modes. Dispersion relations are obtained and investigated, pass and stop bands are determined. The asymptotic form of dispersion relations at the infinite increase of a grating elements sizes and the wave number decrease was derived. The anomalous oscillations near the periodic plate gratings are discovered and investigated. It was proved, that such oscillations always exist. The influence of the geometric characteristics and knife-type grating mode on the oscillation frequency, number and type of waveguiding and cycle modes was investigated. Waveguiding and cycle modes of oscillations are classified by groups of allowed symmetries of a problem. The comparison with known experimental and numerical study was carried out.

Waveguiding property is an existence of the generalized eigen function of the corresponding selfadjoint extension of the Laplace operator, localized in the vicinity of periodic structure. Investigation of the waveguiding properties is embarrassed with those fact, that the corresponding selfadjoint extensions of the Laplace operator have the continuous spectrum filling in all the positive semi-axis.

An existence of the waveguiding properties of the periodic knife-type grating was proved in paper [1] for large enough sizes of grating elements. The approximated investigations of waveguiding properties, dispersion conditions, type of waveguiding functions are in [2, 3], in these papers one can also see the further bibliography.

Formulation and symmetry properties of the problem

If another is not fixed, then it is supposed, that all the profiles of grating elements are consisted of straight line segment, all elements are parallel with each other, periodically repeated and perpendicular to the periodicity direction. Such gratings are of knife-type periodic strip grating. Grating types and corresponding terminology are on Fig. 1.

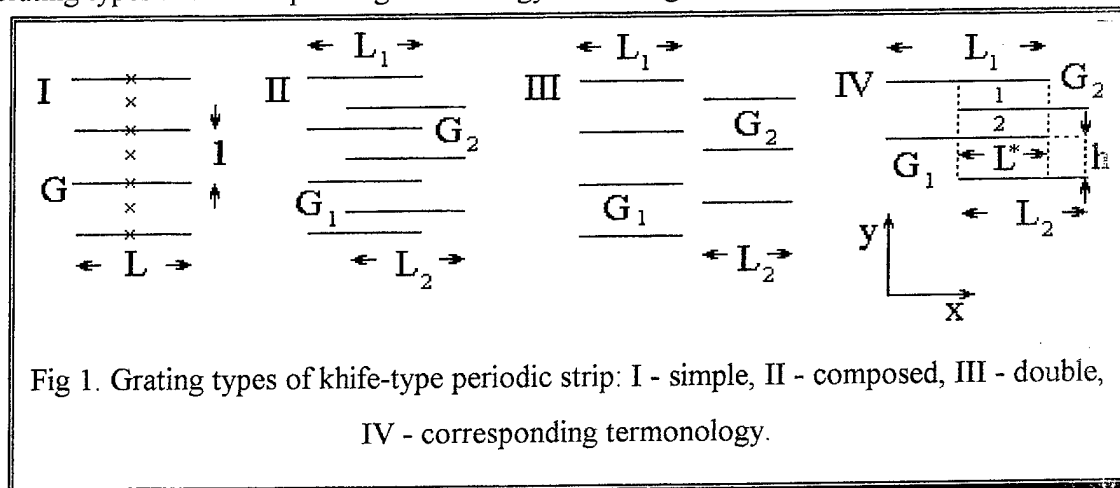


Fig 1. Grating types of knife-type periodic strip: I - simple, II - composed, III - double, IV - corresponding terminology.

The steady-state oscillations near the grating are described by the $u(x,y)$ function whose physical content is determined by the investigated problem

$$\begin{aligned} u_{xx} + u_{yy} + \lambda^2 u &= 0, \\ \partial u / \partial \bar{n} &= 0 \text{ on } G. \end{aligned}$$

Here λ is considered to be the nondimensional frequency of oscillations, easier to commit to paper it is supposed, that $\lambda > 0$. If ω , L_p , H - are the natural frequency of oscillations, natural length of the grating element and natural period of grating correspondingly, then for the corresponding nondimensional magnitudes expressions $\lambda = \omega H / c$, $L = L_p / H$ are correct, the dimensional period of grating in nondimensional variables equals to 1. In any bounded area Ω_b , which is the subarea of whole domain of oscillations Ω , the next condition of local finity of oscillation energy should be fulfilled

$$E(u, \Omega_b) = \int_{\Omega_b} [u^2 + (\nabla u)^2] d\Omega_b < \infty,$$

$E(u, \Omega_b)$ is the nondimensional energy of oscillations in the area Ω_b .

Operator Δ is invariant under any symmetries of space, so the grating symmetry will determine the symmetry of corresponding boundary problem.

As the symmetry group of the one-dimensional periodic structure obligatory consists the subgroup T of translations along the y -axe, so only the next non-trivial sub-groups of the allowed symmetry group are possible: D_1 is the dihedron group with one axe of bilateral symmetry. The next two types of bilateral symmetry are possible: D_1^x axe of bilateral symmetry is parallel to axe x ; D_1^y axe of bilateral symmetry is parallel to axe y ; D_2 is the dihedron group (with two axes of bilateral symmetry); C_2 is the rotation group by π angle; T_σ is the group of gliding symmetry. Symmetry of plate grating permits an expansion of the allowed solution space in invariant subspaces by transformation of this group of symmetry.

As group of translations T is commutative and its representation $\tau(T)$ in the space of allowed solutions of problem is unitary, so the space of solutions can be expanded in invariant one-dimensional subspaces by group T . Functions $u(x,y)$ belonging to these subspaces satisfies the condition $u(x, y+1) = e^{i\epsilon_y} u(x, y)$ and consequently are as the next:

$$u(x, y) = e^{i\epsilon_y} v(x, y), \quad v(x, y+1) = v(x, y).$$

Waveguiding properties

Definition 1. Waveguiding function of a problem is the generalized eigen function localized in the vicinity of plate grating. Corresponding frequency is called the waveguiding frequency.

Classification and type of waveguiding functions.

Definition 2. If a one-directionally periodic structure has the D_1^y - type symmetry, then the even (symmetrical) and uneven (antisymmetrical) functions with respect to variable x will be named α and β waveguiding modes correspondingly. Waveguiding function is α or β mode.

With the help of discrete isometric transform, the group of grating symmetry space of admissible solutions has been restricted and the existence of guiding and anomalous waves has been proved. Pass bands modes have been classified with the help of grating symmetry group.

Existence of the waveguiding property.

To investigate the existence of waveguiding eigen frequencies the "D-N fork" method was used [3]. The following theorem was proved.

Theorem 1. The simple knife-type grating always has the waveguiding property.

Composed and double gratings G can be considered as the disturbance of simple knife-type grating G_1 , caused by a disposition of the additional elements of grating G_2 .

Theorem 2. Composed and double gratings G always have the waveguiding property for any profile lengths and non-zero values of parameter ξ .

Dispersion relations.

Dimensionless waveguiding frequency λ are the function of wave number parameter ξ , these dependences are so-called dispersion correlations. For large sizes of grating elements the approximated dispersion relations are presented in [5]. In the present work these relations are presented for the committing to be entire and being defined more precisely.

Exact dispersion relations for waveguiding frequencies and corresponding wave numbers of the problems are impossible to be written down, even as implicit ones. However, it is possible to indicate some their approximations.

$$\sin[\Theta(\lambda, \xi)] = 0,$$

$$\Theta(\lambda, \xi) = \left\{ \lambda L - 2 \frac{\lambda \ln(2)}{\pi} - \frac{\lambda}{\pi} \left[\Psi\left(\frac{2N\pi + 2\pi + \xi}{2\pi}\right) + \Psi\left(\frac{2N\pi + 2\pi - \xi}{2\pi}\right) - 2\Psi(2N+1) - \right. \right. \\ \left. \left. - \Psi\left(\frac{2\pi + \xi}{2\pi}\right) - \Psi\left(\frac{2\pi - \xi}{2\pi}\right) + 2\Psi\left(\frac{\xi}{2\pi}\right) + \operatorname{ctg}\left(\frac{\xi}{2}\right) \right] + \right. \\ \left. + 2 \arcsin\left(\frac{\lambda}{\xi}\right) + 2 \sum_{n=1}^N \left[\arcsin\left(\frac{\lambda}{2n\pi + \xi}\right) + \arcsin\left(\frac{\lambda}{2n\pi - \xi}\right) \right] - 2 \sum_{n=1}^{2N} \left[\arcsin\left(\frac{\lambda}{n\pi}\right) \right] - \frac{2\lambda}{\xi} \right\}.$$

Here N is natural number, $\Psi(\cdot)$ is the logarithmic derivate of Gamma function. Numerical and theoretic results allow making the next statement:

Statement. For any lengths L of the knife-type grating elements the finite number of waveguiding modes exists.

The above statements refine and correspond with results obtained by other methods and at the "physical"-strict level of rigourousity [5].

At the infinite lengthening of grating elements the dispersion relation allow determination the behavior of waveguiding frequencies $\lambda^{(k)} = \lambda^{(k)}(\xi, L)$ ($k=1 \dots K$) of problem for primar waveguiding modes. Statements where γ is the Euler constant and $L \gg 1$ are correct:

$$\lambda^{(k)}(\xi, L) = \frac{k\pi^2 \operatorname{tg}\left(\frac{\xi}{2}\right)}{L\pi \operatorname{tg}\left(\frac{\xi}{2}\right) - \pi - 2\Psi\left(\frac{\xi}{2\pi}\right) \operatorname{tg}\left(\frac{\xi}{2}\right) - 2\ln(2) \operatorname{tg}\left(\frac{\xi}{2}\right) - 2\gamma \operatorname{tg}\left(\frac{\xi}{2}\right)}.$$

For the primar waveguiding mode for $\xi \ll 1$ the next expression follows from dispersion relations: $\lambda^{(1)}(\xi) = \xi + (2\ln(2) - L\pi)\xi^2/\pi^2$.

This describes the dependence of waveguiding frequencies of primar mode on the oscillation phase shear in the neighbouring fundamental areas of the translation group. This expression is correct for those suppositions in whose framework the dispersion relations are obtained.

Anomalous properties.

The statement about the existance of waveguiding property is proved only for the non-zero phase shear of oscillations ($\xi \neq 0$) in the neighbouring fundamental areas of the translation group. In this connection the question arises, if the generalized eigen functions of problem exist, localized in the vicinity of simple knife-type grating with the periodicity condition correlating with the zero shear of oscillation phase in the neighbouring fundamental areas of the translation group? The answer to this question is positive.

Definition 3. Generalized eigen functions (frequencies) of problem with the periodicity condition localized in the vicinity of knife-type grating, will be named futher an anomalous functions (frequencies) of the problem. If the one-directional periodical structure has a symmetry of the D_1^y - type, then even or uneven by a variable x anomalous functions will be named γ or δ anomalous modes correspondingly.

For waveguiding and anomalous oscillation frequencies near the simple knife-type grating the next system of inequalities is correct: $\alpha_1(\xi) < \beta_1(\xi) < \dots < \alpha_k(\xi) < \beta_k(\xi) < \dots < \pi < \gamma_1 < \delta_1 < \dots < \gamma_m < \delta_m < 2\pi$. Here $\alpha_k(\xi)$, $\beta_k(\xi)$, γ_m , δ_m are frequencies of corresponding mode. The numeration is given according to the frequencies increase.

Existence of the anomalous property of simple grating.

Lemma. Non-trivial anomalous functions of problem, even by an axe passing through some profile of plate grating do not exist. Anomalous function of problem is uneven by every axe parallel to the abscissa axe and passing through point of symmetry of the dihedron group of the problem.

The statements formulated in the lemma allow pointing out signatures of the waveguiding mode α and β and anomalous modes γ and δ in inter-profile channel, presented on Fig. 2.

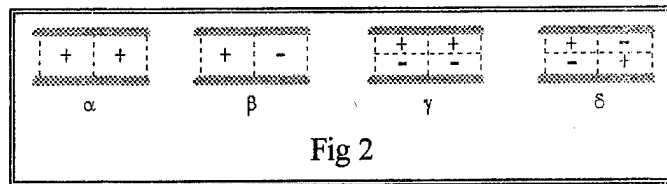


Fig 2

Theorem 3. Non-trivial anomalous frequencies and anomalous functions of problem exist for any profile lengths of the simple knife-type grating, anomalous frequencies belong to the interval $(\pi, 2\pi)$.

Existence of the anomalous property of composed grating.

Composed and double plate gratings can be considered as the disturbance of a simple grating. In the common case they allow more restricted group of symmetries then the simple grating. That's why the method of restriction the allowed class of solutions, based on symmetry of the problem can not be applied to prove the existence of anomalous oscillations near the simple knife-type grating.

If solution u^* of the problem, localized in the vicinity of grating exists, then for all values λ it should satisfy the nessary condition $\int_{\Omega_0} \exp(ix\lambda) u^* d\Omega_0 = 0$, which will be fulfilled if and only if

for all values x the identity $\int_0^1 u^*(x, y) dy = 0$ is correct, Ω_0 - is the fundamental domain of the translation group T . With the help of these condition the following theorem was proved.

Theorem 4. Composed (double) grating has the anomalous property. If length L^* of common part of simple knife-type gratings G_1 and G_2 , composing G does not equal to zero ($L^* \neq 0$), then anomalous oscillation frequencies belong to the interval $(0, 2\pi)$. If $L^* = 0$ (double grating), then anomalous frequencies belong to the interval $(\pi, 2\pi)$.

Fine structure of the spectrum.

The carried out investigations of anomalous oscillation frequencies allow an elaboration of fine

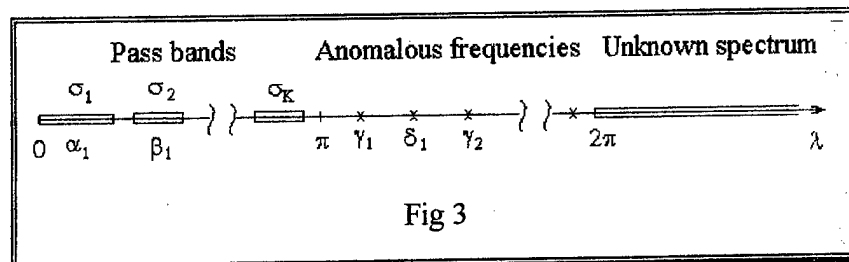


Fig 3

structure of the spectrum of problem for the simple knife-type grating of plates. By the existence theorems of waveguiding and anomalous modes of oscillations the spectrum of problem always consists at least one pass band for the α_1 mode and the anomalous oscillation

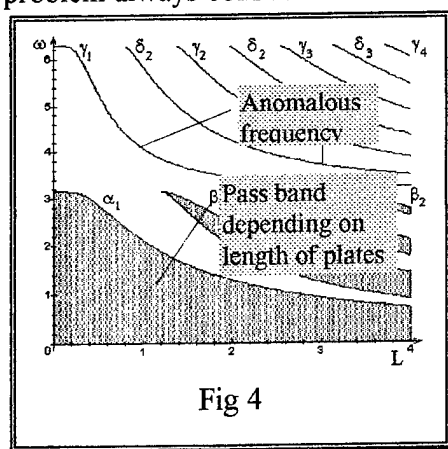


Fig 4

frequency for the γ_1 mode. Presented on Fig. 3, is the scheme of fine structure of the problem spectrum in terms of nondimensional frequencies of oscillations. It is necessary to point out, that for every pass band the mode (α or β) of corresponding waveguiding function and a pass band type is determined. Types of pass bands and anomalous frequencies alternate. The dependence of the geometrical properties of gratings on guiding phenomena has been calculated (Fig. 4).

Type of anomalous functions. Oscillation physics.

Oscillation physics near the knife-type grating of plates, described by waveguiding functions is known [5] and correlates with mechanic analogues, discrete chains of coupled oscillators. This can not be said about anomalous oscillations. To clarify their oscillation physics it is necessary to investigate the outlook of anomalous functions. Presented on Fig. 4 for the case $L=2$, are the velocity field, level lines and pressure field for modes γ_1 , δ_1 , γ_2 of anomalous oscillations in interprofile channel $0 < y < 1$. It is necessary to point out, that velocity field flow from one interprofile channel into another one doesn't happen as distinct from waveguiding oscillations.

From Fig. 5 it is possible to understand the mechanical analogue of anomalous modes, these are oscillations of some connected chains of connected oscillations. Despite of this mechanic analogue being approximated, it allows understanding the oscillation physics: γ_1 are synphase

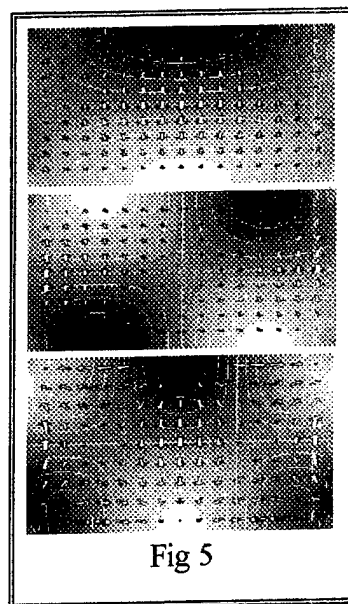


Fig 5

oscillations of one chain, δ_1 are synphase oscillations of two connected chains (chains oscillate in antiphase about each other), γ_2 are synphase oscillations of three connected chains. It is necessary to point out the considerable difference of anomalous oscillations near the plate grating from synphase oscillations of chain of connected oscillators.

Comparison with experimental investigations

It is necessary to remark that [3] and later [2] pioneered in investigating the dependence of waveguiding frequencies on geometrical parameters of the knife-type plates in appliance to electromagnetic waves. Theoretical and experimental investigations of acoustic resonance and waveguiding phenomena near plates in the channel and cyclic gratings of plates were performed independently but later, a comparison with the previously obtained results was not undertaken.

Experimentally investigated in [5, 6], are the acoustic eigen oscillations near the plate gratings in a channel, allowing simulation in the framework of the two-dimensional formulation of the problem and simulating the cyclic grating (the "mirror" effect [6] is applicable). The experimental results [5] are presented in table 1 of paper [7]. Performed on this base, is the comparison of experimental data and numerical investigations of disperse relations dependences of anomalous oscillation frequencies on geometric grating parameters. The comparison with experimental and numerical investigations are shown on Fig. 5. The

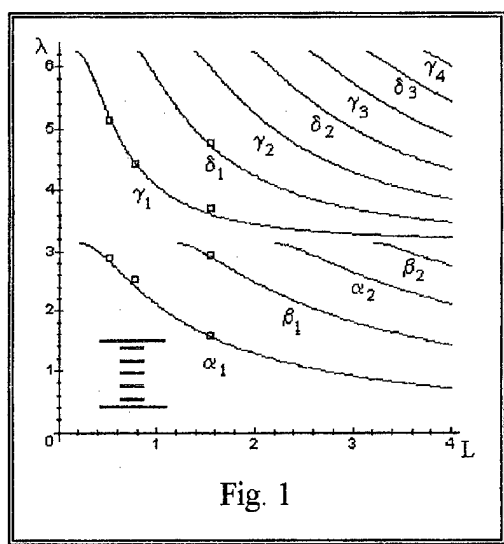


Fig. 1

experimentally obtained results [7], which are nondimensional, are marked with box, continuous curves are the numerical results, obtained with the help of dispersion relations. The satisfactory coinciding of the results can be remarked.

Unsolved problems. The author is not aware, if waveguiding or anomalous frequencies of problem more than 2π exist or not. As eigen oscillations are always connected to the latent symmetry of the problem, so on the basis of the carried out investigation it is possible to advance the next hypothesis: waveguiding and anomalous frequencies of the simple knife-type grating higher than 2π do not exist.

References:

- [1]. Sukhinin S.V. Waveguide effect.//PMTF.-1989.-No 2, p. 92-102.
- [2]. Mittra R., Lee S. Analytical methods of waveguide theory.
- [3]. Brillouin L. Parodi M. Propagation des ondes dans les milieux periodiques, 1956,.
- [4]. Reed M., Simon B. Methods of modern mathematical physics. V. 4, Academic press.
- [5]. Parker R. Resonance Effects in Wake Shedding from Parallel Plates, Some Experimental Observations.// Journal of Sound and Vibration, V. 4, N.1, 1966, pp. 62-72.
- [6]. Cumpsty N.A., Whitehead D.S. The Excitation of Acoustic Resonances by Vortex Shedding.// Journal of Sound and Vibration, V. 18, N.3, 1971, p. 353-369.
- [7]. Parker R. Resonance Effects in Wake Shedding from Parallel Plates: Calculation of Resonant Frequencies.// Journal of Sound and Vibration, V. 5, N.2, 1967, p. 330-343.

THE COST OF PLEASURE: ABOUT SOME CATASTROPHES IN TIME-HARMONIC WAVE SCATTERING

Alexander I. Nosich

Institute of Radio Physics and Electronics, National Academy of Sciences
Kharkov 310085, Ukraine email: alex@emt.kharkov.ua

The paper is concerned with a review of several situations taking place in the time-harmonic wave scattering ($\sim e^{-i\omega t}$), when solutions to certain wave scattering problems do not exist. Each of these situations is closely tied to the violation of solution uniqueness, due to a presence of an eigenvalue, in terms of either natural frequency or propagation constant, simple or multiple, coinciding with the corresponding parameter of the excitation field. Then the reason of solution non-existence can be easily understood based, for example, on the Fredholm Alternative [1,2]. From the physical point of view, the mentioned catastrophes are always a result of joint action of several major assumptions, such as harmonic time-dependence, absence of losses or nonlinearities, and infinite extension of the scatterer. Thus, a loss of solution existence, at certain discrete values of parameters, is the cost of the pleasure of working with a simplified problem.

1. The first of the considered situations occurs when attempting to analyze the scattering of time-harmonic waves from so-called "active" scatterers. The latter are the dielectric or impedance objects characterized by a negative absorption. This is commonly done by introducing a complex-value dielectric constant with a negative imaginary part, or a surface impedance with a negative real part [3]. Such a scatterer can be considered as an approximate model of, e.g., a light-emitting particle in the inversed population conditions, provided that one neglects the effect of saturation due to non-linear character of the light emission. The study of the scattering behavior of active objects has attracted attention since the late 70's, due to a simplicity of analysis and an opportunity to use all the experience accumulated before when studying the scattering from the lossy and passive objects. In the previous works it has been noted a variety of exotic features of active scatterers, like "invisibility", negative scattering and extinction cross-sections, and extraordinarily sharp resonances [3].

However, if looking closely at the mathematical formulation of the problem, one may notice that a negative absorption leads to the violation of the conditions that guarantee the solution uniqueness, and hence, its existence. In fact, the presence of a negative loss shifts the complex natural frequencies of a formerly passive scatterer towards the real axis in the complex k -plane. It may even happen that one of them, say k_0 , comes to the real k -axis. Then the solution will not exist at this frequency due to a pole of the field function. In the pole's vicinity the far-field scattering pattern, the surface current, etc., can change drastically due to a small variation of the frequency. The situation described above is illustrated by the known results for an active-dielectric cylindrical particle and an active-resistivity reflector antenna. It is emphasized that turning to the transient scattering results in a formally unique solution, but showing a non-physical behavior of the unlimited growth in time. Hence the conclusion is that there is no much (if any)

sense in studying the *scattering* problem for an active object. Instead, there is a more clear sense in a search of the conditions for a natural frequency to turn real, by solving an eigenvalue problem of a special sort.

2. The second catastrophic situation occurs when considering an infinitely extended open structure able to support a natural guided surface-wave mode, excited by a surface-wave incident field. The latter can be originated by a modulated electron flow or by a dielectric-slab waveguide, and is assumed to be fixed, i.e. experience a negligible influence of the scatterer. Such problems appear, e.g., in the linear theories of vacuum electron oscillators like BWO and orotron, and the Cherenkov laser. However, if studying the matter of solution uniqueness, one sees that the presence of a natural guided mode leads to the existence of a pole $h_0 > k$ on the real axis of the h -plane, h being the longitudinal wavenumber. When the incident field wavenumber $h^{in} > k$ and comes to a pole, the solution does not exist. The situation is illustrated by a surface-wave excitation of a regular dielectric slab as the simplest open waveguide. Periodic waveguide excitation is also discussed. It is known that groove gratings and other types of periodic structures can support non-attenuating natural modes propagating along the direction of periodicity [4]. When trying to solve the problem of excitation of groove grating by a periodically-modulated electron flow, whose velocity is naturally lower than the light velocity, one comes to the non-existence of solution in the case of synchronization. Introducing the losses shifts the h -poles off the real axis, thus returning the situation to the existence of a unique solution. However, in general, it appears that the problem should be re-considered as an eigenvalue problem for the natural modes of a more complicated open structure consisting of a pair of interacting infinite waveguides.

3. The third kind of catastrophe due to solution non-uniqueness is observed if a local scatterer or a source is embedded in a waveguide able to support not only the natural guided modes, but also *associated* guided modes. The latter may appear due to the multiple roots of the dispersion equation. Then the Fourier-transform of the solution has a multiple pole at the real axis of the h -plane. However, neither a "parent" natural guided mode nor the associated guided modes of the corresponding finite chain carry any power. This eliminates the only reasonable way to determine the sign of the corresponding wavenumber. Hence, there is no way to extract out a physically meaningful unique solution of a lossless-waveguide scattering problem [5]. To avoid this, one has either to switch to the transient scattering or to introduce the losses.

1. C. Muller, *Foundations of the Mathematical Theory of Electromagnetic Waves*, Springer-Verlag, 1969.

2. D. C. Jones, *Methods in Electromagnetic Wave Propagation*, Oxford: Clarendon Press, 1994.

3. M. Kerker, Resonances in electromagnetic scattering by objects with negative absorption, *Applied Optics*, 1979, vol. 18, no 8, pp. 1180-1189.

4. D. Maystre, General study of grating anomalies from electromagnetic surface modes, in A. D. Boardman (Ed.), *Electromagnetic Surface Modes*, NY: Wiley, 1982.

5. A. I. Nosich, Radiation conditions, limiting absorption principle and general relations in open waveguide scattering, *J. Electromagnetic Waves and Applications*, 1995, vol. 8, no 3, pp. 329-354.

BEAM PROPAGATION METHOD MODELLING OF LIGHT PROPAGATION IN OPTICAL WAVEGUIDES

Marian Marciniak

*Institute of Telecommunications, Fibre Telecommunications Department,
1 Szachowa Str., 04-894 Warsaw, Poland,
and Kielce University of Technology, Electronics and Telecommunications Chair,
Al. 1000-lecia PP 7, 25-314 Kielce, Poland
E-mail: mmarcin@jtl.waw.pl*

Beam-Propagation Method (BPM) is now a widely used tool for computer simulation of light propagation in transparent media including optical waveguiding structures. The method was introduced in 1976 by Fleck, Morris and Feit for modelling of laser beam propagation in non-homogeneous atmosphere [1]. In 1979-1980 the method was adopted by Feit and Fleck for modelling of light propagation in optical waveguides in a series of papers in *Applied Optics* [2, 3, 4]. Since then, the method has been successfully applied to analyze various optical waveguide structures, including glass fibres and integrated optic waveguides.

The paper reports some recent activities in BPM modelling of light propagation in optical waveguides that have been carried out in the framework of COST 240 European Project: *Techniques for Modelling and Measuring Advanced Photonic Telecommunications Components, Working Group 2, Waveguide Devices*. In particular, the results of an investigation of a guide with a balance of gain and loss has been reported, and a model for simulation of Second Harmonic Generation (SHG) process in optical waveguides is presented.

The author acknowledges the co-operation and fruitful discussions with his colleagues from COST 240 Project. He also wishes to express his special thanks to COST 240 Chairman, prof. George Guekos from ETH Zurich, Switzerland. The support of COST 240 activities by General Department DG XIII of the European Commission in Brussels is kindly acknowledged.

I. BPM ANALYSIS OF A PLANAR WAVEGUIDE WITH A BALANCE OF GAIN AND LOSS

The problem of light propagation in a planar waveguide with a balance of gain and loss of a geometry as in Fig.1 has been proposed by Hans-Peter Nolting [5], and formerly has been analyzed with the eigenmode formalism through the use of programs resolving numerically wave equation like Mode Solver. Then the interest has been shifted to BPM studies of the problem starting with the results of BPM simulation of the structure by the author of this paper [6]. BPM which is a nonmodal method can serve very well for the purpose of modeling phenomena of light propagation in such waveguides. A BPM benchmark test for waveguide problem with a balance between loss and gain has been proposed [7] and its results are reported below.

A. Light propagation in a waveguide with gain and loss

The waveguide structure of interest is shown in Fig. 1: two layers with mutually complex conjugate refractive indices are surrounded with a medium of a slightly lower real refractive index. The exact values of all parameters are given in Tab. 2. The imaginary parts of refractive indices of guiding layers vary in a very broad range: in terms of the power absorption (gain) coefficient α , between zero and $\pm 10^4 \text{ cm}^{-1}$. The wavelength $\lambda = 1.55 \mu\text{m}$ is assumed.

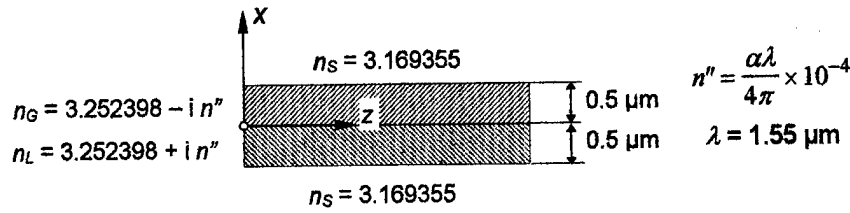


Fig. 1. The geometry of a two-layer waveguide with gain and loss

B. Notation

The attenuation or amplification of light propagating in a transparent medium may be accounted for via a complex-valued refractive index

$$n = n' - i n'' \quad (1)$$

and a complex relative permittivity

$$\epsilon = n^2 = \epsilon' - i \epsilon'' \quad (2)$$

The relation between the power absorption (gain) coefficient α and the imaginary part of refractive index is

$$n'' = \frac{\alpha \lambda}{4\pi} \times 10^{-4} \quad (3)$$

where α is in cm^{-1} and λ is in μm .

Dispersion equation of the waveguide was numerically solved in the complex ϵ_{eff} plane by the Newton method [7]. The calculated dependencies of real and imaginary parts of effective refractive indices versus the absorption coefficient α are plotted in

Fig. 2.

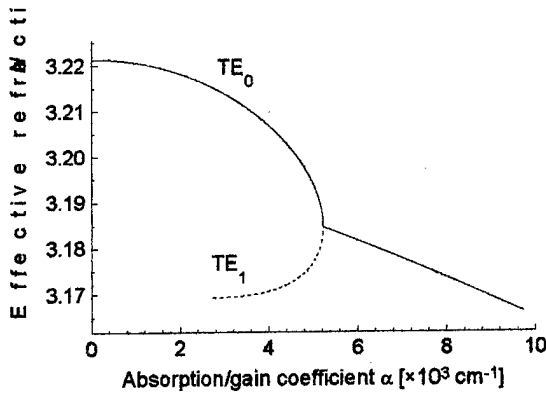


Fig. 2. Effective refractive indices $\text{Re}\{N_{\text{eff}}\}$ (a) and $\alpha_{\text{eff}} = (4\pi/\lambda)\text{Im}\{N_{\text{eff}}\}$ (b) versus attenuation/amplification coefficient α
 a) for $\alpha < \alpha_{\text{branch}}$: lossless modes,
 b) for $\alpha = \alpha_{\text{branch}}$: one degenerate lossless mode,
 c) for $\alpha > \alpha_{\text{branch}}$: the amplified mode is concentrated mainly in the region with gain, while the attenuated mode is concentrated mainly in the lossy region.

C. Beam-Propagation Method

For a planar isotropic waveguide a scalar wave equation is valid. Standard beam-propagation algorithms deal with a solution to hyperbolic Helmholtz equation

$$E(z) = E_0 \exp \left[i z \sqrt{\frac{\partial^2}{\partial x^2} + k_0^2 n_r^2} + i k_0 (n - n_r) z \right] \quad (4)$$

or with a solution to Fresnel parabolic equation

$$E(z) = E_0 \exp \left\{ \frac{-iz}{2k_r} \left[\frac{\partial^2}{\partial x^2} + k_0^2 (n^2 - n_r^2) \right] \right\} \quad (5)$$

where z is the direction of propagation, E_0 is the initial field distribution at a cross section $z = 0$, $n = n(x, z)$ is the refractive index distribution in the waveguide, and n_r is the index of refraction of a reference medium in which the free-space propagation steps are to be carried out. It is assumed that the value of n_r is real and close to those of the media constituting the system. $E(x, z)$ is a slowly-varying field amplitude, and k_r is the wavenumber in the reference medium, $k_r = n_r \omega / c$.

The occurrence of loss or gain in a medium may be automatically accounted for in the phase compensation steps, by an appropriate exponential change (increase for gain, decrease for loss) of the field amplitude according to the imaginary part of the refractive index n [8].

D. Problem set

A problem has been set to determine the branching point α_{branch} value with different BPM programs and approaches. For α approaching α_{branch} there are two different effective refractive index values, they differ in real part for $\alpha < \alpha_{branch}$ or in imaginary part for $\alpha > \alpha_{branch}$. Close to α_{branch} :

$$N \approx N_B - \frac{\Phi_{\alpha\epsilon}''}{2N_B\Phi_\epsilon''}(\alpha - \alpha_B) \pm \frac{i}{2N_B} \sqrt{\frac{2\Phi_\alpha'}{\Phi_\epsilon''}}(\alpha - \alpha_B)^{1/2} \quad (6)$$

Therefore, the difference of mode effective indices scales with square root of $\alpha > \alpha_{branch}$.

Thus, if we restrict ourselves to a two-mode system only, we may expect two kinds of interference effects:

- for $\alpha < \alpha_{branch}$, as the modes differ only in phase velocity in this case, the result is a periodic beating with a spatial period Λ proportional inversely to the (real) effective index difference, which in turn is proportional to square root of $(\alpha_{branch} - \alpha)$. Thus we expect a linear dependence

$$\frac{1}{\Lambda^2} = \text{const.} \times (\alpha - \alpha_{branch}), \quad \alpha < \alpha_{branch}; \quad (7)$$

- for $\alpha > \alpha_{branch}$ the modes have the same phase velocity, but they differ in a way that one is attenuated while the other is amplified. At long distances of propagation, the domination of the mode with gain is obvious. Therefore, a constant growth of the field is the result of two-mode interference. Thus, the effective two-mode beam power amplification coefficient at long distances is a linear function of gain-loss coefficient α , which in turn is proportional to square root of $\alpha - \alpha_{branch}$. Thus we expect a linear dependence of the form of

$$\alpha_{eff}^2 = \text{const.} \times (\alpha - \alpha_{branch}), \quad \alpha > \alpha_{branch}; \quad (8)$$

The task consists of three parts, all of them are to calculate branching point α_{branch} value.

E. Contributors and used methods

The contributors and their algorithms are listed in Table 1.

Table 1. LIST OF CONTRIBUTORS

Institution	Equation	Numerical method	Boundary conditions	Propagation step size
HHI		FE/FD BPM		
Un. Hagen		MoL		-
Un. Twente		FD	Efficient	1 μm
Ac. Comm.	Helmholtz	FFT BPM	Absorber	1/8 μm
Un. Roma		MoL	Absorber	-

F. Discussion of the Results

The resulting values of α_{branch} are reported in Table 2. The differences with respect to the analytic solution do not necessarily mean errors of the method, because the propagated beam is not a combination of two guided modes of the active guide only, but also of a radiation field of this guide.

The participants to the task have done much of numerical effort to avoid inaccuracies due to numerical errors, thus the observed discrepancies should be attributed to different physical models modelled by the BPM programs used. In other words, every method used has analysed very accurately a little different situation.

Table 2. VALUES OF α_{branch} OBTAINED BY THE PARTICIPANTS TO THE BENCHMARK TEST WITH COMPARISON TO ANALYTIC VALUE $\alpha_{\text{branch anal.}} = 5226.3/\text{cm}$

Contributor	α_{branch} , 1/cm	$\alpha_{\text{branch}} - \alpha_{\text{branch anal.}}$, 1/cm
HHI	5306	79.7
Un. Hagen	5236.87	10.57
Un. Twente	5226.5	0.2
Un. Twente	5226.9	0.6
Ac. Comm.	5500	273.7
Un. Roma I	5242.5	16.2

II. BPM MODELLING OF SHG IN A WAVEGUIDE

This part is devoted to an adaptation of Beam-Propagation Method (BPM) for modelling of Second Harmonic Generation (SHG) process in quasi-periodically corrugated planar waveguides. A type I (eoo) of SHG has been chosen as a working example. A model of split-step formalism of SHG has been developed. The model involves propagation of two beams: the fundamental (pump) beam and second harmonic beam, and is outlined below.

As a starting point the following coupled set of governing equations has been adopted [9]:

$$j \frac{\partial a_1}{\partial \xi} + \frac{1}{2} \frac{\partial^2 a_1}{\partial s^2} + a_1^* a_2 \exp(-j\Delta\beta\xi) = 0; \quad j \frac{\partial a_2}{\partial \xi} - \frac{\alpha}{2} \frac{\partial^2 a_2}{\partial s^2} + a_1^2 \exp(+j\Delta\beta\xi) = 0$$

The adopted numerical model of two beams propagation consists of a sequence of two steps: propagation step, and compensation step.

Step 1 involves propagation of the beams only, and diffraction effects. The beams are propagated separately, and SHG process is not included in this step. This is equivalent to uncouple the governing equations by assuming the other's wave amplitude = 0:

$$j \frac{\partial a_1}{\partial \xi} + \frac{1}{2} \frac{\partial^2 a_1}{\partial \xi^2} + 0 = 0, \quad (a_2 = 0); \quad j \frac{\partial a_2}{\partial \xi} - 0 + a_1^2 \exp(+j\Delta\beta\xi) = 0$$

Step 2 involves nonlinear compensation of the amplitudes and phases of both beams. Simultaneously, no diffraction occurs, what follows from an assumption of vanishing transverse variation of the beams, i.e. $\partial^2/\partial x^2 = 0$. This is equivalent to plane wave propagation.

$$j \frac{\partial a_1}{\partial \xi} + 0 + a_1^* a_2 \exp(-j\Delta\beta\xi) = 0; \quad j \frac{\partial a_2}{\partial \xi} - \frac{j}{2} \frac{\partial^2 a_2}{\partial \xi^2} + 0 = 0, \quad (a_1 = 0)$$

The propagation step of the beams can be easily modelled via standard BPM techniques. The nonlinear compensation step involves more difficulty. Under assumed conditions, the fundamental (ω) and second harmonic (2ω) field amplitudes are a subject of following nonlinear changes [10]:

$$|\tilde{A}_\omega(z)| = \left[\frac{8\pi}{n_\omega c} I_{\omega 0} - \frac{n_{2\omega}}{n_\omega} U_\omega^- \text{sn}^2 \left(\frac{K(m)}{\tilde{L}_{\omega NL}} z | m \right) \right]^{1/2}$$

$$|\tilde{A}_{2\omega}(z)| = \sqrt{U_\omega^-} \left| \text{sn} \left(\frac{K(m)}{\tilde{L}_{\omega NL}} z | m \right) \right|$$

where the notation of [10] has been adopted. The above amplitude changes are explicitly given and do not present difficulty in calculations.

Similarly, phases of the waves change in the following way [10]: The fundamental and second harmonic wave phases are:

$$\Phi_\omega(z) = \Phi_{\omega 0} - \frac{4\pi\Delta q}{cn_\omega} I_{\omega 0} \int_0^z \frac{dz}{\frac{8\pi}{n_\omega c} I_\omega - \frac{n_{2\omega}}{n_\omega} U_\omega^- \text{sn}^2 \left(\frac{K(m)}{\tilde{L}_{\omega NL}} z | m \right)}$$

$$\Phi_{2\omega}(z) = \Phi_{2\omega 0} + \pi \sum_{l=1}^{\infty} \text{step}(z - 2l\tilde{L}_{\omega NL})$$

Of the above, the first only the first expression for fundamental wave phase change is given not explicitly, since it contains an integral. The integral has to be evaluated numerically.

In quasi-periodical planar waveguide the phase mismatch $\Delta\beta$ varies according to the local thickness in a given section of the waveguide. Since in realistic corrugated waveguides the thickness variation is very small, this may be considered as an perturbation in a homogeneous waveguide. This issue and its impact on the amount of reflections at the boundaries is currently under study. It is believed that one could neglect the reflections.

In the analysed problem the beams propagate in a planar waveguide, which is a one-dimensional free space for the beams. This means that without nonlinear effects the propagation step length might be arbitrarily long. However, as the SGH process is sensitive to amplitudes and phases of the interacting beams, the propagation step should not involve significant amplitude and phase changes. Thus carry has to be taken out that propagation steps are not to long in order to properly model the SHG process.

As in a standard BPM, for achieving better accuracy with given propagation step, the calculation should be started with an initial half-step propagation. For keeping the accuracy of the modelling and also to shorten the computational time needed for device modelling, it might be necessary to use an adaptive propagation step length. This is due to the dependence of efficiency of SHG on both the waves amplitudes, and phase relations.

For checking the accuracy of SHG modelling in a given waveguide structure it is necessary to compare the results with an analytical solution for the geometry considered. Such solutions are available when second harmonic beam has zero amplitude at the starting point [11].

The above two-beam propagation procedure is actually a subject of further development COST 240 laboratories in University Roma 1 "La Sapienza", Dipartimento di Electronica, and Institute of Telecommunications, Department of Fibre Telecommunications, Warsaw, in order to obtain an efficient tool for SHG modelling in planar waveguides, including quasi-periodic corrugation of the guides along the propagation.

III. CONCLUSION

Beam Propagation Method has been successfully applied to analyze non-modal beam propagation in a waveguide with a balance of gain and loss. A model of SHG modelling in a waveguide with BPM has been presented.

REFERENCES

1. J.A. Fleck, Jr., J.R. Morris, M.D. Feit. "Time-Dependent Propagation of High Energy Laser Beams through the Atmosphere", *Applied Physics* 10 No.2/1976, pp.129÷160
2. M.D. Feit, J.A. Fleck, Jr. "Light Propagation in graded-index optical fibers", *Applied Optics* 17, 1978, pp.3990÷3998
3. M.D. Feit, J.A. Fleck, Jr. "Calculation of dispersion in graded-index multimode fibers by a propagating-beam method", *Applied Optics* 18, No.16/1979, pp.2843÷2851
4. M.D. Feit, J.A. Fleck, Jr. "Computation of mode properties in optical fiber waveguides by a propagating-beam method", *Applied Optics* 19, No.7/1980, pp.1154÷1164
5. H.-P. Nolting, COST 240 Meeting, Dublin, March 1995
6. M. Marciniak, COST 240 Meeting, Porto, October 1995
7. H.-P. Nolting, G. Sztefka, M. Grawert, and J. Ctyroky, "Wave Propagation in a Waveguide with a Balance of Gain and Loss," IPR 96
8. M. Marciniak, "Light propagation in optical waveguides with complex refractive indices", *Optica Applicata*, Vol. XXVI, No.4, p.359-368, 1996
9. R. Cerioni, C. Sibilia, M. Bertolotti, J. Dekker, "Spatial control of pulses in quadratic non-linear materials", *Optical and Quantum Electronics*, Special Issue on Optical Waveguide Theory and Numerical Modelling, 1998
10. G. D'Aguanno, C. Sibilia, E. Fazio, E. Ferrari and M. Bertolotti, "Fields phase modulation and input phase and intensity dependence in a nonlinear second order interaction", accepted for *Journal of Modern Optics*, 1998
11. A. Re, C. Sibilia, E. Fazio and M. Bertolotti, "Field dependent effects in a quadratic nonlinear medium", *Journal of Modern Optics*, 1995, Vol. 42. No.4, 823-839

Inverse and Synthesis Problems

MICROWAVE METHOD FOR THE STEP-LIKE RECONSTRUCTION OF LOSSLESS MULTILAYERED DIELECTRICS

V. Mikhnev and A. Palto

Institute of Applied Physics, Akademicheskaya 16, 220072 Minsk, Belarus

Abstract

A novel one-dimensional microwave imaging approach based on successive reconstruction of dielectric interfaces using the complex reflection coefficient data collected over some standard waveguide band is described. The method is valid for highly contrasted discontinuous profiles and shows low sensitivity to the practical measurement error. Some numerical examples are presented.

Introduction

Development of microwave reconstruction methods has drawn attention of notable number of researchers during past decade. Existing inversion algorithms are based on perturbative Born-type approach or optimization schemes applied to exact integral equations. Unfortunately, all these algorithms suffer from serious problems when discontinuous profiles of high contrast are to be reconstructed. Besides, they usually require the input data to be given in an infinite frequency band (at least, starting from zero frequency). It cannot be realized in practice, because for each frequency band special measuring equipment and antennas should be used.

In this paper, a new method of step-like reconstruction, which is intended, for reconstruction of the profiles of high contrast is presented. The complex reflection coefficient of normally incident wave obtained in a frequency band essentially limited both from upper and lower frequencies is used as input information for the reconstruction process.

Reconstruction algorithm

The algorithm is based on the Newton – Kantorovich procedure applied to the inversion of the boundary problem for the Riccati equation [1]. Let the normally incident electromagnetic wave with the wavenumber k_0 is reflected from the interface between air and the inhomogeneous half-space. The reflection coefficient $r(k_0, x)$ and the refractive index profile $n(x)$ are related by the Riccati nonlinear differential equation:

$$\frac{dr(k_0, x)}{dx} = 2ik_0 \cdot n(x) \cdot r(k_0, x) + \frac{1 - r^2(k_0, x)}{2n(x)} \cdot \frac{dn(x)}{dx}. \quad (1)$$

$$\text{Let's introduce a new variable } t = \int_0^x n(x') dx', \quad (2)$$

which represents the optical path length in the medium.

When applying the Newton – Kantorovich optimization algorithm to (1) transformed with the use of (2), one can compute a correcting term $\Delta n(t)$ to some initial profile $n(t)$ [1]. Successive application of the same scheme using the corrected profile function $n(t) + \Delta n(t)$ as initial profile allows to obtain the solution of the inverse problem after a few iterations.

Unfortunately, this approach works well when the input data are given in some frequency band starting from zero frequency. In case the frequency band of operation does not contain low frequencies, the solution becomes unstable. Nevertheless, it was found that the maximal derivative of the correcting term $\Delta n(t)$ corresponds to the point of the greatest change of the profile (e.g. interface between layers). Hence, a step can be installed in the initial profile at the point of the maximal derivative of $\Delta n(t)$ in such way to provide minimization of the maximal modulus of the reflection coefficient at large depth for all frequencies, i.e. minimax criterion is used. In short, the computational scheme can be summarized as follows:

- 1 calculation of $r(k_0, t)$ for some initial profile $n(t)$ at all frequencies from the given frequency band by numerical solution of (1)-(2)
- 2 calculation of $\Delta n(t)$ using the Newton – Kantorovich iterative procedure. Installation of the step into the initial profile at a point of the most rapid change of $\Delta n(t)$ ensuring minimization of the maximum of $|r(k_0, t)|$ at large depth over all operating frequencies
- 3 updating the profile. Then return to step 1, with the initial profile being replaced by the corrected one. The calculations are stopped, when $\max(|r(k_0, t)|)$ at large depth over the frequency band of operation is less than desirable error
- 4 return to the geometrical depth using reverse coordinate transformation (2).

Numerical examples

In this section, the results of numerical experiments are presented. The reflection coefficients calculated in the frequency band of 26 to 37 GHz in steps of 0.2 GHz were used as input information.

Fig.1 shows results of reconstruction of a three-layered highly contrasted structure on a substrate. The quality of reconstruction is seen to be good enough.

The stability of the method was investigated by adding a uniformly distributed random noise to the input data. The magnitude of noise was chosen to simulate measurements with an accuracy of 20%. The results of reconstruction of a two-layered dielectric structure on a substrate for the case when there is a noise in the input data shown in Fig.2 demonstrate good stability of the solution. Therefore, the method is suitable for practical applications.

The method like others has some limitations. Two most important of them derived from numerical simulations are as follows. First, the best convergence of the solution is achieved when the reconstruction depth is close to $\Delta t = c/2\Delta f$, where Δf is the frequency step.

The resolution of the method can be estimated as $t_0 = c/2F$, where c is the light velocity and F is the bandwidth.

Reference

1. V.A. Mikhnev, P. Vainikainen, Profile inversion of stratified dielectric media using the two-step reconstruction, *Proc. of the 27th European Microwave Conf.*, Jerusalem, 1997, pp. 584-588.

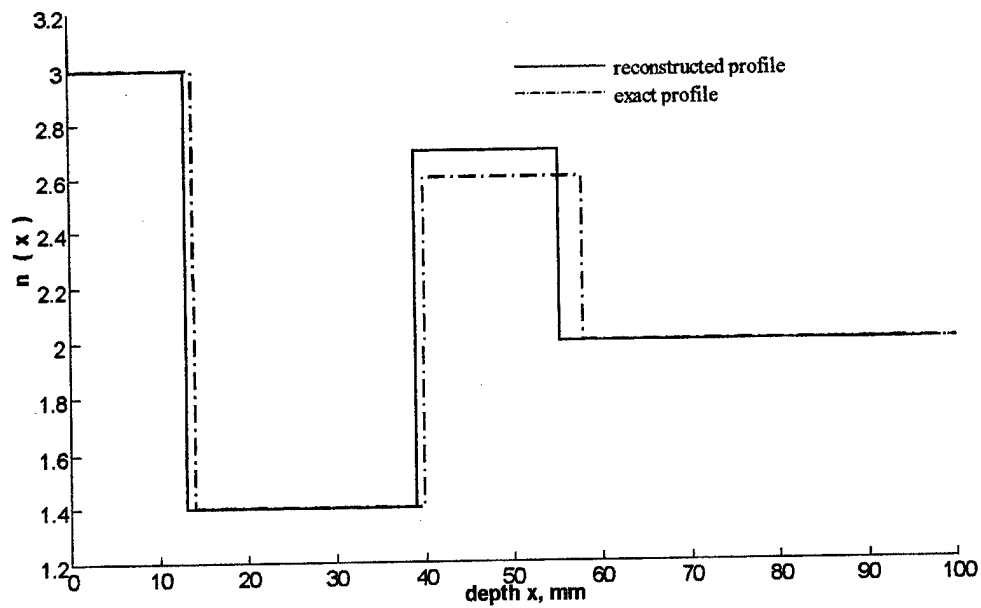


Fig. 1

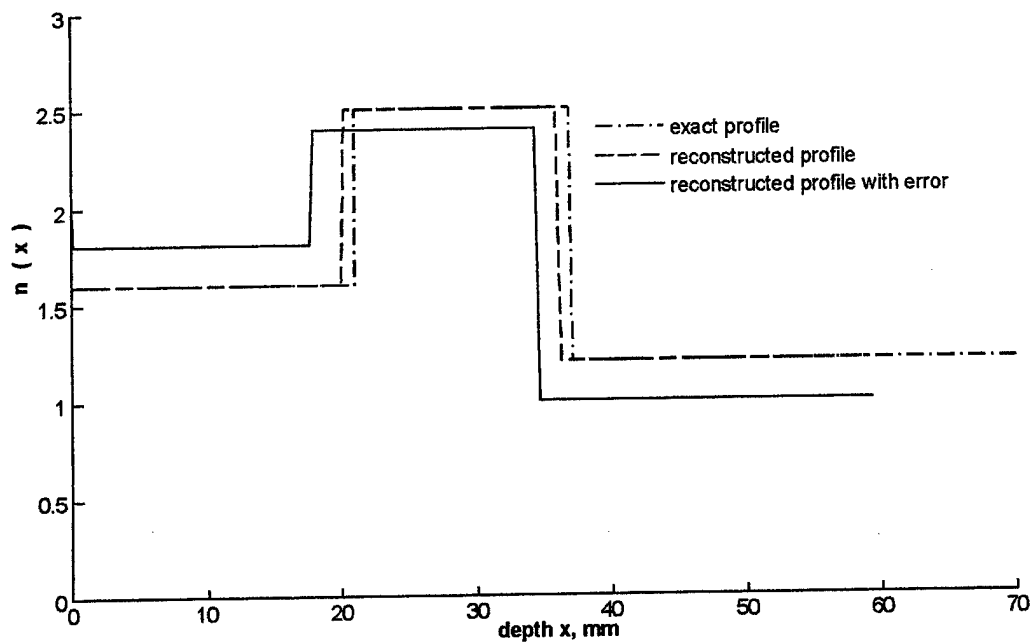


Fig. 2

ANALYSIS AND SYNTHESIS OF IMPEDANCE PLANE

Yuriy V. Yukhanov

Taganrog State University of Radio Engineering, Taganrog, Russia
email: airpu@tsure.ru

Abstract. The problem of synthesis of impedance plane reflecting a plane homogeneous wave in a given direction is solved. The law of distribution of impedance is found in analytical form. The restrictions on the class of the allowable scattering patterns are formulated. Rigorous solution of the problem of the wave scattering by a plane with non-uniform periodic reactance is obtained in analytically closed form for the first time.

Consider solving a two-dimensional problem of the synthesis of an impedance plane in the following statement. Suppose that a plane H-polarized electromagnetic wave (Fig.1) is incident on the plane S from the direction φ_n . At the surface S, the Leontovich impedance boundary conditions are imposed:

$$E_x = Z(x)H_z. \quad (1)$$

It is necessary to find the law of distribution of passive surface impedance Z ensuring the reflection of the plane wave in the given direction φ_0 .

Analytical representation of the incident and the scattered fields as the homogeneous plane waves has the following form in half-space $y \geq 0$:

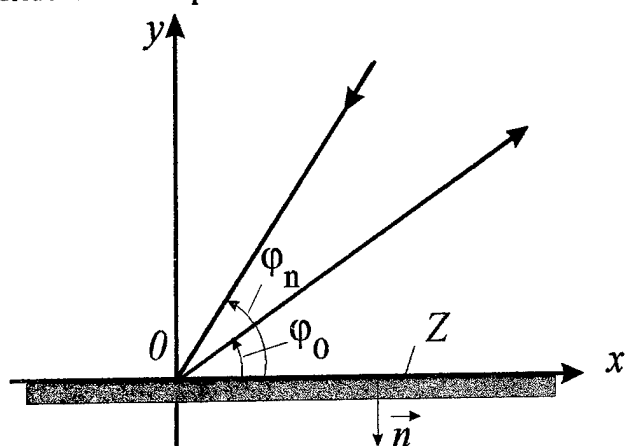


Fig.1

$$H_z^n = e^{ik(x \cos \varphi_n + y \sin \varphi_n)}, \quad H_z^s = e^{-ik(x \cos \varphi_0 + y \sin \varphi_0)} \quad (2)$$

This enables us to find the required law of impedance distribution directly from the boundary conditions (1)

$$Z_M = 0.5 \{ (\cos \gamma_n - \cos \gamma_0) + i(\cos \gamma_n + \cos \gamma_0) \operatorname{tg} \eta x \}, \quad (3)$$

where $\eta = k(\cos \varphi_n + \cos \varphi_0)/2$; $\cos \gamma_n = \sin \varphi_n$; $\cos \gamma_0 = \sin \varphi_0$; γ_n, γ_0 are the angles of incidence and reflection, respectively.

The condition of physical realizability of the real part of passive impedance function defines the restriction on the class of the allowable scattering patterns: *The passive impedance ($\operatorname{Re} Z \geq 0$) provides a total reflection of a homogeneous plane wave only in the following angular sectors: $\varphi_0 \leq \varphi_n$; $\varphi_0 \geq \pi - \varphi_n$. The reactance can ensure such a translation only in the backward, $\varphi_0 = \varphi_n$ ($Z = i \cos \gamma_n \operatorname{tg}(kx \cos \varphi_n)$), or the specular $\varphi_0 = \pi - \varphi_n$ ($Z = 0$) directions.*

The question on an opportunity of efficient reflection of a plane wave in any desired direction with the aid of reactance is of a special interest. The analysis has shown that the reactance determined by the following equation

$$Z = iZ_0 \operatorname{tg}(kx \cos \varphi_n), \quad (4)$$

creates also a reflected beam in the direction φ_0 but besides there is still a whole spectrum of reflected waves, both spatial and surface ones. If the following condition: $Z_0 = \sin \varphi_0$, is satisfied, then, in the reflected field, only two spatial harmonics: homogeneous plane waves in the given direction φ_0 and in the specular (mirror) direction $\pi - \varphi_n$ are present, with amplitudes

$$H_0 = 2 \cos \gamma_n / (\cos \gamma_n + \cos \gamma_0); \quad H_s = (\cos \gamma_n - \cos \gamma_0) / (\cos \gamma_n + \cos \gamma_0).$$

The given solution of the synthesis problem enables ones to derive the formulas for the reflection coefficient P from a plane with variable impedance Z

$$P = \frac{\cos \gamma_0 (3 \cos \gamma_n - \cos \gamma_0) - Z (\cos \gamma_n + \cos \gamma_0)}{(\cos \gamma_n + \cos \gamma_0) (\cos \gamma_0 + Z)}, \quad (5)$$

which transforms to the well-known expression if $Z = \text{const}$.

Advantages of the new reflection coefficients are especially clearly displayed in the vicinity of the angles of observation $\varphi = \arccos(2 \cos \varphi_0 + \cos \varphi_n)$.

Consider now a rigorous solution of the problem of scattering of an H-polarized wave by the plane $y = 0$ with a reactance given by equation (4). Note that publications containing a rigorous solution of this scattering problem in the closed form are absent for a plane with periodic variable impedance (4).

From the Lorentz lemma, we obtain a Fredholm second-kind integral equation for the z -component $H_z(x)$ of the total magnetic field:

$$H_z(x) = -\frac{ik}{2\pi} \int_{-\infty}^{\infty} Z(x') H_z(x') \int_{-\infty}^{\infty} \frac{e^{-ik(x-x')}}{\sqrt{\kappa^2 - k^2}} d\kappa dx' + 2H_z^n(x). \quad (6)$$

By presenting the required function as $H_z(x) = \cos \eta x H(x)$ and using the spectral expansion of $H(x)$ we obtain the solution of the integral equation (6) analytically:

$$H_z(x) = 0.5X \left\{ 1 + A + 2Z_0 \sum \theta_{m-1} G_m / D_m e^{-i2m\eta x} - 2Z_0 A \sum h_{m-1} G_{-m} / C_{-m} e^{i2m\eta x} \right\} e^{i\eta_n x}, \quad (7)$$

where $X = 4/(D_0 + AC_0)$; and factor A is determined from the equation of balance of energy at the reactive surface $y = 0$.

Thus, a discrete spectrum of plane waves travels along the impedance structure. We study the scattered field of such a structure. For a fragment of impedance plane of the length $2L$, the scattered field pattern takes the following form:

$$F(\varphi) = \frac{kLX}{4} \left\{ [(1+A) \sin \varphi - Z_0(1-A)] \frac{\sin U_0}{U_0} + \frac{2Z_0}{D_1} (1 + G_1 \sin \varphi) \frac{\sin U_1}{U_1} - \right.$$

$$\begin{aligned}
& -\frac{2AZ_0}{C_{-1}}(1+G_{-1}\sin\varphi)\frac{\sin U_{-1}}{U_{-1}} + 2Z_0\sum\frac{\theta_{m-1}}{D_m}(1+G_m\sin\varphi)\frac{\sin U_m}{U_m} - \\
& -2AZ_0\sum\frac{h_{m-1}}{C_{-m}}(1+G_{-m}\sin\varphi)\frac{\sin U_{-m}}{U_{-m}} \Big\}, \quad (8)
\end{aligned}$$

where $U_m = L(k\cos\varphi - [2m\eta - \eta_n])$. Thus the field $H_z(x)$ is the same as for an infinite plane.

In the expression (8), the first two terms are the specular F_s and the synthesized F_0 beams launched by the plane S in the directions $\varphi=\pi-\varphi_n$ and $\varphi=\varphi_0$. With normal incidence of the wave, the third term represents the beam F_{s0} , which is specular with respect to the synthesized beam $\varphi=\pi-\varphi_0$. In this case factor A has a simple analytical representation via Z_0

$$A = \pm(1 - Z_0G_I)^2/(1 + Z_0G_I)^2.$$

As we see, the amplitudes of the beams of a complex image depend on the value of Z_0 .

Hence, with the aid of Z_0 it is possible to control the amplitudes of various beams of the scattering pattern. So, the expression for Z_0 , ensuring a maximum $|F_0(\varphi_0)|$ of the synthesized beam is as follows:

$$Z_0 = \sin\varphi_0(\sqrt{2(1+\sin\varphi_0)}/\sin\varphi_0 - 1).$$

Zero amplitude of the specular beam $|F_s(\pi-\varphi_n)|$ is provided by the following condition:

$$Z_0 = \sqrt{(2 - \sin\varphi_0)\sin\varphi_0}. \quad (9)$$

In Fig.2, the scattering pattern of a fragment of reactance plane of the width 8λ that reflects a normally incident wave in the direction of $\varphi_0=30^\circ$, is given, for the value of Z_0 designed after formula (9) (curve 1). Curve 2 corresponds to the scattering pattern of an equivalent conducting strip tilted by the angle $0.5(\varphi_n-\varphi_0)$ with respect to the angle φ_n of the wave incidence.

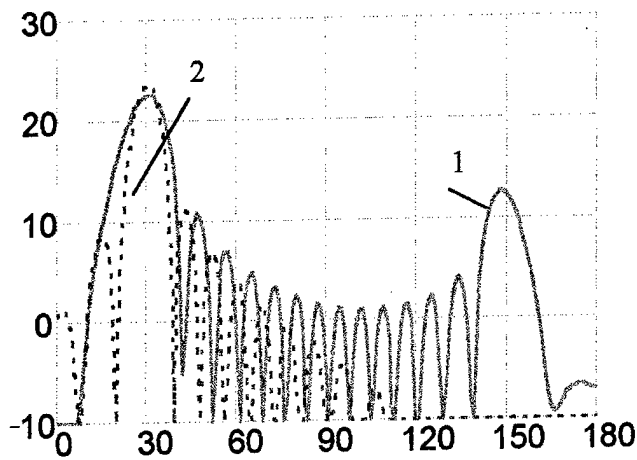


Fig.2

The obtained analytical solution of the wave scattering by a plane with variable periodic impedance (4) can be used for determining the total field (7) on the curved surface of a body of arbitrary shape, if combined with the Physical Optics approach approximate solutions.

SYNTHESIS OF THE ADAPTED HYBRID REFLECTOR ANTENNAS

Bohdan Podlevskyi, Petro Savenko, Myroslava Tkach
 Institute of Applied Problems of Mechanics and Mathematics of NASU
 3"b" Naukova Str., Lviv-601, 290601, Ukraine
 e-mail:kalynjak@ippmm.lviv.ua

Abstract. One approach of solving the synthesis problems of the adapted hybrid reflector antennas (HRA) is proposed. It consists in solving of both problems, the synthesis problem of HRA according to the prescribed directivity pattern (DP) and the problem of forming the deep gap in DP according to the given direction. The variational formulations the synthesis problems are used. The mean-square deviation of the given magnitude and the synthesized one is chosen as the optimization criterion.

The suggested approach permits to synthesize the adapted HRA of the different structure. In particular, the cuttings from reflectors can be both symmetrical and non-symmetrical, and irradiating feed array can have arbitrary configuration. The partial directivity patterns of the elements of the array can be different for each of them.

1. Statement of the problem. The spacecraft hybrid antenna systems are used, in particular, for the construction of the modern systems satellite communication of multi-functional purpose. As rule, they consist of the non-symmetrical paraboloid reflector (a some cutting from paraboloidal reflector) and the control irradiating feed array. It is supposed that the reflector is situated in the far zone in relation to the separate feed element and in the near zone in relation to the feed array as a whole.

Let the field in the far zone is described, using the coordinates of the satellite antenna by the angle of elevation ϑ and the angle of azimuth φ . We assume that the field (partial DP) of the n -th separate beam in the point of observation (ϑ_i, φ_i) , excited by the unit level of power and zero phase, can be presented by the complex vector $\vec{f}_n(\vartheta_i, \varphi_i)$. The feed array in our research may have general configuration in the sense that the position and orientation of each n -th feed element is specified independently. The excitation coefficients and the type of the radiation (a $\cos^p \vartheta$ feed) may also vary from element to element.

We designate the complex factor of excitation of n -th feed element as I_n . Then, the electromagnetic field of whole system is considered as a sum of the partial fields, and the total directivity pattern is given by

$$\vec{F}(\vartheta, \varphi) = A\vec{I} = \sum_{n=1}^N I_n \vec{f}_n(\vartheta, \varphi). \quad (1)$$

The value \vec{f}_n is determined by the physical optics methods.

2. The synthesis problem of HRA according to the prescribed magnitude pattern At first, the synthesis problem of HRA according to the prescribed DP \vec{F}_0 is considered. It is assumed that the magnitude pattern \vec{F}_0 is given in some region Ω of angles ϑ and φ , and $\vec{F}_0=0$ outside of this region. If the geometry of the feed array and the partial directivity patterns of the separate radiators of array are known, then it is required to determine the amplitudes and phases of

excitation of the radiators ($\vec{I} = \{I_1, I_2, \dots, I_n\}$ - is the vector of excitation of the feed elements). Therefore, the synthesis problem consists in a finding the vector \vec{I} minimizing the functional being the mean-square deviation of the synthesized and given magnitudes in a some region Ω . Thus, the criterion of optimization is writtern as

$$\sigma = \iint_{\Omega} [F_0^g - |F^g|^2] d\Omega + \iint_{\Omega} [F_0^p - |F^p|^2] d\Omega + \beta \sum_{n=1}^N |I_n|^2, \quad (2)$$

where F_0^g , F_0^p and F^g , F^p are components of vectors \vec{F}_0 and \vec{F} accordingly in a spherical system of coordinates, N is a quantity of feed elements and $\beta > 0$ is a some real parameter.

The condition of stationary of the functional (2) results in the nonlinear system of algebraic equations, which in the operator form is defined by

$$(\beta \mathbf{E} + \mathbf{B}) \vec{I} = q(\vec{I}), \quad (3)$$

here \mathbf{B} is a matrix, the elements of which do not depend from I (\mathbf{E} is a unit matrix). It permits to construct the following iterative process of the system solution

$$I^{(v)} = (\beta \mathbf{E} + \mathbf{B})^{-1} q(I^{(v-1)}), \quad (4)$$

where v is the number of iteration, $(\beta \mathbf{E} + \mathbf{B})^{-1}$ is the inverse matrix. Numerically the obtained system of equations is solved by the successive approximation method. The considered problem is essentially nonlinear problem and may possess non-unique solution.

3. The synthesis of the adapted HRA. It is assumed the problem of forming the deep gaps in the DP according to the prescribed directions as basis of the synthesis problem of the adapted HRA. Let the amplitude-phase distribution (APD) in irradiating feed array is given and directivity pattern of HRA is writtern by formula (1).

The zero synthesis problem in the DP of the HRA according to the prescribed direction Q_* ($Q = (\xi_1, \xi_2) = (\sin \vartheta \cos \varphi, \sin \vartheta \sin \varphi)$ are generalized angle coordinates) consists in finding such a vector APD \vec{I} , forming DP close to the output in the whole range of visible angles Ω , and equal zero in the direction Q_* . Last demand can be formulated as an inequality $|\vec{f}(Q_*)| < \varepsilon$, where ε is a small prescribed constant.

Introduce in consideration the function

$$\vec{\Phi}(Q) = \vec{F}_0(Q) - \vec{F}_0(Q_*) = \sum_{n=1}^N I_n^{(0)} [f_n(Q) - f_n(Q_*)], \quad (5)$$

where $\vec{I}^{(0)}$ is the APD forming output (nonperturbed) DP \vec{F}_0 . Obviously, that $\vec{F}(Q)$ in all points $Q \in \Omega$ coincides with the output DP and $\vec{\Phi}(Q_*) = 0$. In the space of vector-valued functions H_f we introduce Euclidean metrics determined by the scalar product and norm:

$$(\vec{f}_1, \vec{f}_2) = \iint_{\Omega} [f_1^g(Q) \overline{f_2^g(Q)} + f_1^p(Q) \overline{f_2^p(Q)}] dQ, \quad \|\vec{f}\| = (\vec{f}, \vec{f})^{1/2}.$$

Hence, the synthesis problem consists in finding the vector $\vec{I} \in H_f$ minimizing the following functional:

$$\sigma = \|\vec{\Phi} - A\vec{I}\|^2. \quad (6)$$

The operator A is determined in accordance with (1).

Assuming that the system of partial DP of HRA $\{\vec{f}_n\}$ is linearly independent we apply the orthogonalization process to it. After certain transformations we get the representation of the DP array in the orthogonalized basis

$$\vec{F}(Q) = \sum_{n=1}^N \beta_n \vec{g}_n(Q), \quad (7)$$

here $\{\vec{g}_n\}$ - is the orthogonalized system of the functions;

$$\beta_n = \sum_{j=n}^N \tilde{\alpha}_{jn} I_j, \quad (n = \overline{1, N}), \quad (8)$$

where

$$\tilde{\alpha}_{jn} = \begin{cases} -\alpha_{jn} = (\vec{f}_j, \vec{g}_n), & j = \overline{1, n-1}, \\ d_n = \left\| \vec{f}_n(Q) + \sum_{j=1}^{n-1} \alpha_{nj} \vec{g}_j(Q) \right\|, & j = n. \end{cases}$$

Introducing (7) into (6) and on the base of minimum of the functional σ we obtain the expressions for the optimal coefficients:

$$\beta_n = (\vec{\Phi}, \vec{g}_n) \quad (9)$$

or

$$\beta_n = \beta_n^0 - \left(\vec{F}_0(Q_*), \iint_{\Omega} \vec{g}_n(Q) dQ \right), \quad (n = \overline{1, N}), \quad (10)$$

here the coefficients β_n^0 are determined on the base of output vector \vec{I}_0 by the formula (8). If the coefficients β_n are found according to the form (10) for DP $\vec{F}(Q_*)$ and they satisfy the condition (5), then the problem is solved. The known vector \vec{I} forming DP with the created gap is determined as the solution of linear equations system (8) with triangle matrix. In the inverse case we find coefficients using the following iterative process

$$\beta_n^{(j+1)} = \beta_n^{(j)} - \left(\vec{F}^{(j)}(Q_*), \iint_{\Omega} \vec{g}_n(Q) dQ \right), \quad (n = \overline{1, N}), \quad (11)$$

where j is the iteration number.

The offered approach and developed algorithms permit to solve the synthesis problems of the adapted hybrid reflector antennas with simultaneous forming the deep gap (zero) in the directivity pattern according to the prescribed directions. This investigations are proved by the numerical results.

References

1. P.O. Savenko, M.D.Tkach The numerical solution of synthesis deep gaps problem in the directivity pattern of conformal antenna arrays. Proc. of the seminar/workshop "DIPED-97", Lviv, pp.-78-80.

THE METHOD OF AUXILIARY SOURCES FOR INVESTIGATION OF SCATTERED FIELDS SINGULARITIES AND ITS APPLICATION FOR INVERSE PROBLEMS

R. Zaridze, G. Bit-Babik, K. Tavzarashvili.

Tbilisi State University, Tbilisi, Georgia, e-mail: lae@resonan.ge

Abstract. A simple method for investigation of the scattered fields singularities is presented. It is shown how this technique can be applied to the synthesis problem of "well-matched" antenna with predefined pattern. The basic idea is that the wave field corresponding to the desired pattern must have a domain of singularities, and it is determined by these singularities in a unique way.

I. Introduction

It is known that any wave field carrying the energy into infinity must have the centers of radiation, i.e., the singularities in some domain. Otherwise the wave field function must be everywhere identically equal to zero [1]. In this paper attention is paid to localization of these singularities under assumption that every wave field is determined by its own singularities in a unique fashion. Investigations have shown that these singularities are distributed as bright spots and the distance between them depends on frequency. Based on these concepts and on the Method of Auxiliary Sources (MAS) [2] a simple numerical method for the field reconstruction after its given singularities is suggested. The corresponding mathematical justification can be found in [3]. For localization of the wave field singularities, the functions characterizing the converging and diverging waves are used.

The localization of singularities is used for optimization of the inverse problems solution. It is known that the inverse problems do not have a unique solution. For example, for a specific pattern the different current distributions on the different surfaces can be introduced and there fields differ from each other by the reactive part in the near zone. The main problem is to obtain such currents distribution that occupies a minimum volume and produces the minimum of reactive field in near zone so that the whole feeding energy is transmitted into propagating wave. Such antenna is called the "well matched antenna".

It is assumed that any pattern of the field radiated to infinity should have its own unique singularities in a limited domain. On the other hand it is known that a propagating wave is analytical everywhere except the domain of its excitation. This is the domain of singularities of the radiated field, which forms the propagating wave and its pattern. So the problem is to find out the location of these field singularities.

II. General Algorithm of Near Field Reconstruction

The problem to be solved is to design a "well-matched antenna" that will produce a given far field pattern. This is equivalent to the determination of the singularities of the specific pattern. Thus the near field has to be determined as it has been discussed previously.

For this purpose an auxiliary circular antenna is introduced. The far field of this antenna is calculated and matched with the given far field pattern by distributing the auxiliary sources on the auxiliary surface inside the auxiliary antenna. It is obvious that the near field of this auxiliary sources can be easily calculated, therefore using the method of visualization of

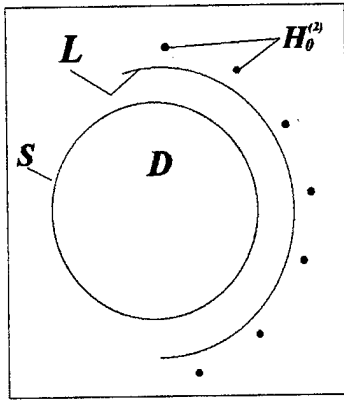


Figure 1: The geometry of the near field reconstructing algorithm.

scattered field singularities described before the singularities of the given pattern (e.g. the location of the antenna dipoles) is determined.

We consider in detail a 2D case, of antenna with a pattern $F(\varphi)$ to be designed. First of all it is necessary to obtain the near field corresponding to the specified pattern $F(\varphi)$. This could be done by distributing N sources of $H_0^{(1)}(kr)$ type on some curve S enclosing an area D (fig. 1). In this case, S is chosen to be the circle of diameter d . Here it should be noted that diameter d must not be less than some definite value to provide the necessary width of the main lobe. This condition is: $d > \lambda/\Theta$, where λ is the wavelength and Θ is the width of the main lobe. The field radiated by these sources will be:

$$E(r) = \sum_{n=0}^N a_n H_0^{(1)}(k(r - r_n)), \quad (1)$$

while the far field pattern will be determined by the asymptotic approach of the expression (1). So, (1) becomes:

$$\lim_{r \rightarrow \infty} E(r) = \sqrt{\frac{2}{\pi kr}} \sum_{n=0}^N a_n e^{-ik(x_n \cos(\varphi) + y_n \sin(\varphi)) + i\frac{\pi}{4}} \quad (2)$$

By using the collocation method to bind the radiated field of these sources in M directions with the given one in far zone, the system of linear equations is obtained

$$\sum_{n=0}^N a_n e^{-ik(x_n \cos \varphi_m - y_n \sin \varphi_m)} = F(\varphi_m) \quad M = 1, 2, \dots, m. \quad (3)$$

On solving the system of linear equations (3), the coefficients can be determined. They are the complex amplitudes of the sources that generate the desired diagram. The accuracy of this solution depends on the number N of collocation points. So after obtaining the pattern with a desirable accuracy, the field of such sources is known everywhere outside the area D including the near field (1). It must be noted that the reactive field of these sources decreases as the diameter d increases, since no standing wave is described by these sources. Hence, area D should be taken large enough to provide low reactive part of the field in near zone.

As the near field is known outside the area D , the second step is to continue it analytically inside D using the following scheme. Taking into account all mentioned above, the continuation of the near field will be also unique up to the singularities regarding the chosen area D . Let us choose some curve L outside D , where the near field is known. Assume that N sources $H_0^{(2)}(kr)$ are placed at some distance from the curve L . These sources act as absorbers of the wave, traveling from the area D to infinity. The N chosen sources will reconstruct the field at the curve L if

$$\sum_{n=1}^N b_n H_0^{(2)}(k(r_n - r_m)) = E(r_m), \quad (4)$$

where b_n is the complex amplitude of the n -th source, and $E(r_m)$ is the near field value at the corresponding point on the curve L . If the number N is large enough, the reconstructed field

approximates the real one. Since there is a matching of fields on the curve L, there must be also matching inside the area D up to the area of singularities of the given near field. So the numerical analytical continuation of the near field will be found inside area D.

III. Example of the Inverse Problem Solution

Consider one more example of optimizing the inverse problem solution. The aim is to synthesize a given radiation pattern, originally generated by two electromagnetic wave sources placed at a distance of several wavelengths from each other. The corresponding pattern is

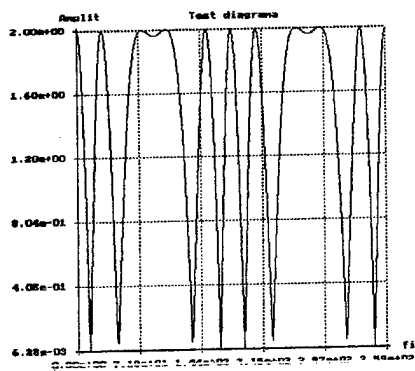


Figure 2.: Suggested pattern

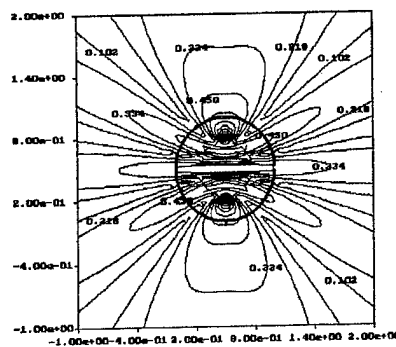


Figure 3.: Field corresponding to the given pattern

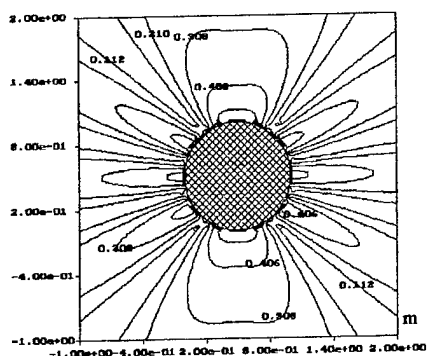


Figure 4.: Reconstructed field.

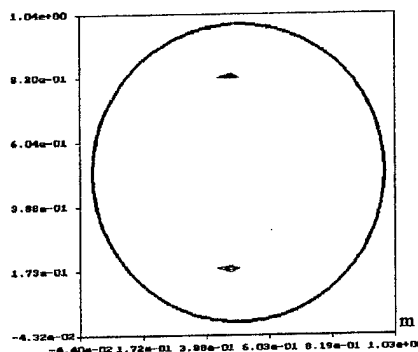


Figure 5.: Reconstructed coordinates of the sources to be found.

shown in Fig.2. and the near field in Fig. 3. With the sources placed at the circle, it is possible to reconstruct this radiation pattern, as it has been described above (see formulas (1) and (4)). The result is shown in Fig. 4. Then using a set of absorbing sources, the near field is continued inside the circle. The field obtained in such a way gives two sharp maxima near the area where the original sources were placed (Fig 5.). Therefore the information about the field singularities is generated: the latter are actually at the points of original sources, and one can note that this information was obtained only after consideration of the radiation pattern without a previous knowledge of original sources. It is now obvious that by placing in two sources at the corresponding point, the desired radiation pattern can be obtained in the most optimal way.

References:

1. V. Kupradze, Method of Integral Equations in the Theory of Diffraction, Moscow-Leningrad, 1935 (in Russian)
2. R., Zaridze D. Karkashadze, et al, The Method of Auxiliary Sources in Applied Electrodynamics, *Proc. Int. URSI Symp. On MTT Theory*, Budapest, 1986, 102-106 pp.
3. D. S. Jones, Methods in Electromagnetic Wave Propagation, Oxford Univ. Press, 1995.

INVESTIGATION OF THE SOLUTIONS OF THE NONLINEAR ANTENNA SYNTHESIS PROBLEMS

M. I. Andriychuk

Pidstryhach Institute of Applied Problems of Mechanics and Mathematics
Ukrainian National Academy of Sciences
3"b" Naukova str., Lviv, 290601, Ukraine
E-mail: voi@ippmm.lviv.ua

Abstract - The antenna synthesis problems according to the prescribed amplitude radiation pattern are considered. The variational statement of the problems is used. The correspond nonlinear Eulerian equations can have nonunique solution. The finding these solutions and investigation of their properties carried out using numerical approach.

The considered problems concern to inverse problems with the partially given information on the radiation pattern (RP). The incomplete complex RP but only its amplitude is accepted as initial RP. Thus the choice freedom of the RP phase is used as additional possibility for better approximation to the prescribed amplitude RP. The variational statement of the problems is used [1], namely it is required the incomplete coincidence of the received amplitude RP with the given one, i. e. only the best approximation to it.

We consider the functional

$$\kappa = (F, |f|)_f / \|u\| \quad (1)$$

as a criterion of the optimization. Here F is the prescribed amplitude RP (real positive function), $|f|$ is the module of the synthesized RP. The functions F and f concern to Hilbertian space H_f of the radiation patterns, $(\cdot, \cdot)_f$ is the inner product in this space, $\|u\|$ is the current norm in the Hilbertian space H_u of the currents.

The radiation pattern f and forming its current u in the antenna are related by the formula

$$f = Au. \quad (2)$$

A is the known linear limited operator. In the case of the plane curvilinear antenna the operator A has the form [2]

$$f = Au \equiv \int_S u(S) \exp(ikr(\varphi') \cos(\varphi - \varphi')) dS_{\varphi'} \quad (3)$$

The inner product $(\cdot, \cdot)_f$ in the Hilbertian space H_f is determined as

$$(f, f)_f = \int_0^{2\pi} p(\varphi) f(\varphi) f^*(\varphi) d\varphi, \quad (4)$$

$p(\varphi) \geq 0$ is the weight function, φ is the angular coordinate in far zone. The inner product $(u, u)_u$ in the Hilbertian space H_u , is determined as

$$(u, u)_u = \int_S u(S) u^*(S) dS_\varphi, \quad (5)$$

where $dS_\varphi = \sqrt{r^2 + (dr/d\varphi)^2} d\varphi$, φ is the angular coordinate in the antenna.

The complete complex function u is necessary to determine in the amplitude-phase synthesis problems, but only its phase ψ in the phase synthesis problems is determined, here $u = |u| \exp(i\psi)$. We receive the corresponding nonlinear Eulerian equations

$$u = \frac{\|u\|}{\kappa} A^*(F \exp(i \arg Au)), \quad (6)$$

$$\psi = \arg(A^*(F \exp(i \arg Au))) \quad (7)$$

for the amplitude-phase and phase problems respectively using the standard technique of the variational calculation. In the equation (7) the nonessential positive multiplier $\frac{\|u\|}{\kappa}$ is omitted.

The operator A^* is adjoint to A , it is determined from the condition

$$(Au, f)_f = (u, A^*f)_u. \quad (8)$$

The equation (6), (7) are nonlinear integral Hammerstein equations [3], if operators A and A^* are determined by formulas (3) and (8) respectively.

The changing of the characteristic electrophysical parameter of the equations (6), (7), contained in their kernel, leads to the appearance of the several solutions. The analytical investigation of a number of these solutions and their properties is difficult problem (particularly for the equation (7)), therefore the numerical approach is used. For the numerical solving these equations the successive approximation method is applied. The calculation carried out by the formulas

$$u_{n+1} = \frac{\|u_n\|}{\kappa_n} A^*(F \exp(i \arg Au_n)), \quad (9)$$

$$\psi_{n+1} = \arg(A^*(F \exp(i \arg Au_n))). \quad (10)$$

The successive approximation method is applied to the various types of the initial approximations for reception of the various solutions [4].

The numerical calculations were carried out for plane circular antenna ($r(\varphi) = a$, a is the antenna radius). The results are presented for the phase synthesis problem. The prescribed amplitude RP were $F_1(\varphi) = \sin^2(\varphi/2)$ (a) and $F_2(\varphi) = \sin^8(\varphi/2)$ (b). As the initial

approximations for the desired phase distributions next functions were prescribed: 1 - $\psi = 0$; 2 - $\psi = 0$, $(0 < \varphi' \leq \pi)$, $\psi = \pi$ $(\pi < \varphi' \leq 2\pi)$; 3 - $\psi = \sin(\varphi')$; 4 - $\psi = \cos(\varphi')$; the amplitude distribution of current $|u| \equiv 1$. In Fig. 1a, b are presented normalized values of κ functional which correspond to solutions of (7). These solutions are obtained using the iterative process (10) (the curves 1-4 correspond to various types of the initial approximation). At the small values of ka for the prescribed amplitude RP F_1 and F_2 exist two and three solutions respectively. The new solutions appear if the value of ka increases. For more exact determination of the branch point of solutions is necessary to apply analytical approach.

The synthesized amplitude RP $|f|$ corresponding to the curves 1 and 2 in Fig. 1a, b respectively and the prescribed amplitude RP F are presented in Fig. 2a, b for $ka = 5$.

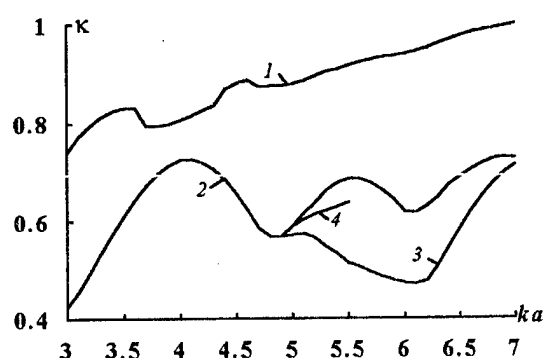


Fig. 1a.

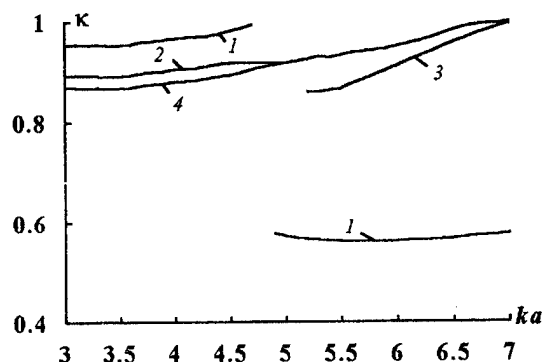


Fig. 1b.

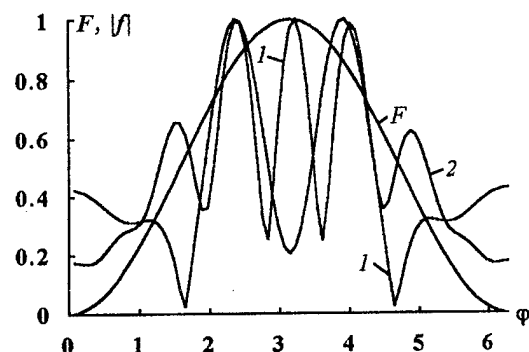


Fig. 2a.

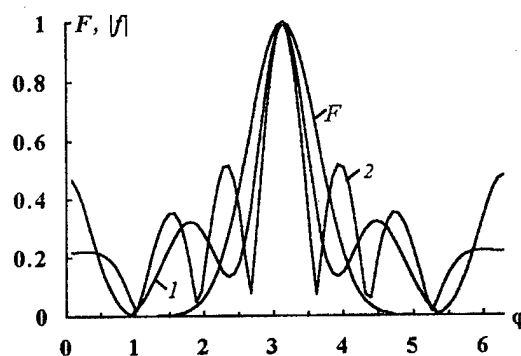


Fig. 2b.

REFERENCES

1. Andriychuk M. I., Voitovich N. N., Savenko P. A., Tkachuk V. P. The antenna synthesis according to the amplitude radiation pattern. Numerical methods and algorithms. *Naukova Dumka Pub.*, 1993. 256 p. (In Russian).
2. Katsenelenbaum B. Z. High-frequency electrodynamics. Moscow, *Nauka Pub.*, 1966. 240 p. (In Russian)
3. Weinberg M. M., Trenogin W. A. Theory of the solution branching of the nonlinear equations. Moscow, *Nauka Pub.*, 1969. 528 p. (In Russian).
4. Andriychuk M. I. About non-uniqueness of the solutions of phase synthesis problems according to the prescribed amplitude directivity pattern. *Proc. of Second Int. Conf. on Antenna Theory and Techniques*. Kyiv, 20-22 May, 1997. Kyiv, NTU "Kyiv Polytechnical Institute", 1997. p. 368-369.

SYNTHESIS OF IMPEDANCE REFLECTOR WITH GIVEN SCATTERING CHARACTERISTICS

Yuri V. Yukhanov, Sergey N. Sorokin

Taganrog State University of Radio Engineering, Taganrog, Russia, airpu@tsure.ru

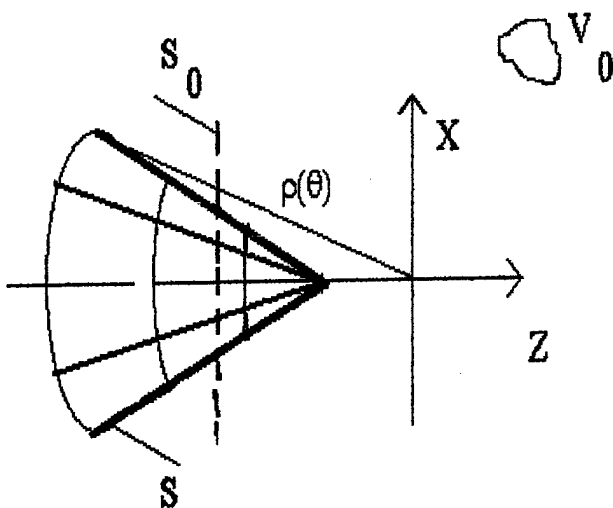
Abstract - The problem of synthesis of an impedance reflector having, at the working wavelength, the same radar cross-section as some perfectly conducting reflector is considered. Analytical expressions for determining the distribution of components of tensor of surface impedance for the synthesized reflector are obtained. The influence of the shape of reflector on its frequency-selective properties is investigated.

We shall consider a problem of synthesis of a reflector with the given radar cross-section (RCS) and frequency properties in the following statement.

Suppose that, in the free space, a three-dimensional reflector is located, on whose surface the Leontovich impedance boundary conditions are imposed. The surface of impedance reflector is assumed to be a body of rotation, the contour of whose longitudinal section is described by the equation $\rho(\theta)$. The tensor of surface impedance, in order to eliminate thermal losses, is assumed as corresponding to a closely spaced mesh of purely reactive strips (Fig.1). In some volume V_0 , located in the far zone of reflector, there distributed are electrical and magnetic currents. They generate, in space V , a locally plane electromagnetic wave that propagates along the direction (θ_p, φ_p) and excites the impedance reflector. It is required thus to determine a distribution of components of tensor of surface impedance, such that in the backward scattering direction the RCS of the synthesized reflector is same as RCS of some reference perfectly conducting reflector with a surface S_0 .

As a reference reflector, another body of rotation is used, the contour of whose longitudinal section is given by the equation $\rho_0(\theta_0)$. The reference reflector is located coaxially with the impedance reflector.

The formulated above problem is solved by the method developed in [1]. For the solution it is necessary that the radius of curvature of reflector is much greater than the wavelength. It enables us to use the Physical Optics approximations. A natural way of solving the problem implies introducing a local system of



coordinates $\{\vec{n}, \vec{v}, \vec{i}_\varphi\}$. Here \vec{n} is the normal vector to the surface of reflector, \vec{v} is the

tangential vector to the contour of the surface longitudinal section, \vec{i}_φ is the unit vector of the spherical system of coordinates centered at the axis of symmetry of reflector at some distance from its top. In this case the tensor of surface impedance takes a diagonal form. For determining the distribution of components of this tensor of impedance we shall act as follows.

First we derive the expressions characterizing the fields scattered by impedance and reference reflectors. By equating them in the direction of backward propagation, we obtain an integral relation for the unknown components of impedance tensor. Then we shall find these components based on the condition of identity of phase factors in the integrand functions. As a result, we shall come to a set of two equations, which appear not solvable analytically for an arbitrary direction of propagation of the incident field or if the reflector surface is not a body of rotation [1]. The analysis of the obtained equations shows that for an arbitrary direction of propagation of the incident wave, the distribution of components of the tensor of surface impedance Z_{11}, Z_{22} depends on the both of angular coordinates θ and φ in a complicated manner.

In the most important for practice case, when the incident wave propagates along the axis of symmetry of reflector, the derived set of equations splits into two independent equations:

$$X_{11} = \operatorname{tg}(\Delta_0 / 2) / \cos \gamma_p; \quad X_{22} = \cos \gamma_p \operatorname{tg}(\Delta_0 / 2),$$

$$\text{where } \cos \gamma_p = n_\theta \sin \theta - n_r \cos \theta; \quad \Delta_0 = 2k(\rho \cos \theta - \rho_0 \cos \theta_0)$$

$$X_{11} = Z_{11} / W, X_{22} = Z_{22} / W, \quad W = 120\pi \text{ Ohm is the free space impedance,}$$

n_r, n_θ are the projections of a unit normal vector to the surface of reflector on the vectors of the spherical system of coordinates; $k = 2\pi / \lambda$. The angles θ, θ_0 are connected by the equation $\rho \sin \theta = \rho_0 \sin \theta_0$.

The analysis of the obtained equations shows that with an axial direction of propagation of the incident wave, the distribution of components of the tensor Z depends solely on one angular coordinate θ , as the impedance and the reference reflectors are the coaxial bodies of rotation. The results of computations enable us to make a conclusion that if using an impedance reflector shaped as a body of rotation, the distribution of components of tensor of the surface impedance quickly changes along the generator of reflector. The period of variation of components of impedance tensor and its uniformity along the generator of reflector is determined the shape of the latter. So, in the case of circular cone used as reflector, the period of variation of the impedance-tensor component remains constant along the reflector generator.

The obtained formulas were used in the computations of the monostatic scattering characteristics of the reference and impedance reflectors. So, for a flat impedance reflector simulating a conical reflector with the tip angle of 90 degrees, the sector of angles of competitive values of the RCS patterns is $\pm 2^\circ$. Further we investigated an opportunity to simulate a flat perfectly conducting disk by an impedance conical reflector. The analysis of the obtained results shows that within the approach of Physical Optics, in the axial direction RCS of impedance reflector is equal to RCS of a perfectly conducting disk. The sector of angles of close values of the scattering characteristics is $\pm 5^\circ$. For the estimation of sector of angles of

competitive levels of the scattering characteristics, in the case of axial excitation of reflectors, the following analytical formula was derived:

$$\Delta\theta \leq 2 \arcsin \sqrt{\pi/16 k \sup |\rho_0 \cos \theta_0 - \rho \cos \theta|},$$

where *sup* means the upper limiting value of a function.

The analysis of the latter expression shows that the sector of angles of concurrence of the patterns is determined by the difference between the shapes of reflectors. It is visible that a reduction of shape difference between the impedance and the reference reflectors leads to a growth of the size $\Delta\theta$. The results given by this formula are in good agreement with estimations obtained by means of computing the scattering characteristics.

The properties of the synthesized reflectors were further investigated in a frequency range. It was supposed that the obtained distributions of components of surface impedance tensor were realized by a closely spaced system of grooves of variable depth. It has been shown that the frequency-selective properties of an impedance reflector are determined by its shape. For reducing the RCS of a reflector outside of a working band of frequencies, it should be fabricated as an elongated body, for example as a circular cone with a small tip angle. Reflector frequency characteristics in this case have a resonant character. Its width is determined by the tip angle value of a conic reflector. A variation in the wavelength of the incident field results in the deformation of scattering characteristics of impedance reflector. The character of deformation is determined by the shape of impedance reflector and the change of frequency.

Interesting results were obtained for an impedance disk simulating a conical reflector with a small tip angle. It is known that RCS of a conical reflector in the axial direction decreases with a reduction of the reflector tip angle. The analysis has shown that RCS of an impedance reflector at the working wavelength of the incident field is the same as that of a reference perfectly conducting reflector. However, changing the wavelength of the incident wave results in a growth of RCS of impedance reflector. The latter can be explained by the fact that the obtained distribution of components of surface impedance tensor at the working wavelength results in a mutual cancellation of the fields scattered by various elements of the surface of a reflector. With a change of the frequency of the incident field, the phase differences between the fields scattered by various sections of the surface of reflector experience disturbances that results in the growth of RCS. In the opposite case, when impedance cone is used for modeling a perfectly conducting disk, the obtained distribution of components of surface impedance tensor should provide, in the axial direction, an addition of the fields scattered by the elements of a reflector surface. Therefore a change of the wavelength of the incident field results in reduction of reflector RCS.

References

1. Y. V. Yukhanov, A. S. Potapenko, Excitation of impedance non-isotropic rotation body, *Scattering of Electromagnetic Waves*, Taganrog: TSURE Press, 1989, vol. 7 (in Russian).

NEW RIGOROUS SOLUTION OF SOME ANTENNA SYNTHESIS PROBLEMS ACCORDING TO PRESCRIBED AMPLITUDE RADIATION PATTERN

N. N. Voitovich, O. M. Gis, O. O. Reshnyak, Yu. P. Topolyuk.

Institute of Applied Problems of Mechanics and Mathematics of National Academy of Sciences. Naukova str. 3"b", 290601 Lviv, Ukraine. E-mail: voi@ippmm.lviv.ua

Abstract. The problem of the least-square minimization of the difference between the prescribed and obtained amplitude patterns is solved for the linear antenna in the closed form with a limited number of complex parameters which are calculated from the set of transcendental equations. The number of parameters depends on the electrical length of antenna. Numerical results concerning two concrete problems are presented. The method is extended to the equidistant linear antenna arrays.

The results may be applied to other problems described by the continuous or discrete Fourier transformation.

One of the approaches to the antenna synthesis problem according to the amplitude radiation pattern consists in the least-square minimization of difference between the prescribed and obtained amplitude patterns. This problem was formerly reduced to a non-linear integral equation [1]. The equation has nonunique solutions branching out when the electrical antenna size increases. This equation was solved and analyzed numerically.

For the case of linear antenna, the above problem may be analytically reduced to a finite set of transcendental equations in some unknown complex parameters [2]. In this case the functional to be minimized has the form

$$\sigma = \int_{-\infty}^{\infty} (F(\xi) - |f(\xi)|)^2 d\xi \quad (1)$$

where $F(\xi)$ is the given amplitude pattern (a finite positive function with the support $[-1, 1]$), $f(\xi)$ is the obtained radiation pattern

$$f(\xi) = \int_{-c}^c u(x) e^{ix\xi} dx, \quad (2)$$

$c = ka \sin \alpha$ is a dimensionless parameter of the problem, $u(x)$ is the current distribution at the antenna, $\xi = \sin \vartheta / \sin \alpha$ is a generalized angle coordinate, 2α is the angle outside which $F(\xi) = 0$. The problem is reduced to the nonlinear integral equation

$$f(\xi) = \frac{1}{\pi} \int_{-1}^1 \frac{\sin \alpha(\xi - \xi')}{\xi - \xi'} F(\xi') e^{i \arg f(\xi')} d\xi'. \quad (3)$$

The current distribution at the antenna is calculated according to the solution of (3) by a simple formula [1].

It is proved that

$$e^{i \arg f(\xi)} = g(\xi) P_N(\xi) / |P_N(\xi)| \quad (4)$$

where $g(\xi) = \prod_j \text{sign}(\xi - \xi_j)$, ξ_j are possible zeros of $f(\xi)$,

$$P_N(\xi) = \prod_{n=1}^N (1 - \eta_n \xi), \quad (5)$$

N is some integer dependent on c , $\eta_n - \bar{\eta}_m \neq 0$, $n, m = 1, 2, \dots, N$.

The complex parameters η_n satisfy the following set of transcendental equations:

$$\int_{-1}^1 F(\xi)g(\xi)\xi^n \sin c\xi / |P_N(\xi)| d\xi = 0, \quad (6a)$$

$$\int_{-1}^1 F(\xi)g(\xi)\xi^n \cos c\xi / |P_N(\xi)| d\xi = 0, \quad (6b)$$

$n=0,1,\dots,N-1$. Relation between the number of multipliers in (4) and parameter c is described by a simple inequality.

The branching points of the solutions are such values of c at which the equations (5) are satisfied for different values of N simultaneously.

In Figs. 1-3 the results concerning two cases, $F_1(\xi)=1/\sqrt{2}$, $g_1(\xi)=1$ and $F_2(\xi)=\sin 3|\xi|$, $g_2(\xi)=\text{sign}\xi$, are presented. Typical dependences $\text{Re } \eta_n$ (solid lines) and $\text{Im } \eta_n$ (dotted lines) on c is given in Fig.1 for the first case. The curves are indicated by numbers equal to the values of N in (5). Fig. 2 shows the optimal values of σ (solid lines) and values σ_0 of the functional at $\text{Im } f(\xi)=0$ (dashed lines). Dotted lines denote borders between intervals with different values of N in the optimal solution. Numbers at the curves are the same as the subscript of F . Dependence of the "synthesis effectivity" $Q(c)=(c_0-c)/c$ on c , where c_0 satisfies the equation $\sigma(c)=\sigma_0(c_0)$, is presented in Fig.3. This value shows how much the antenna can be shorted due to choosing the phase pattern.

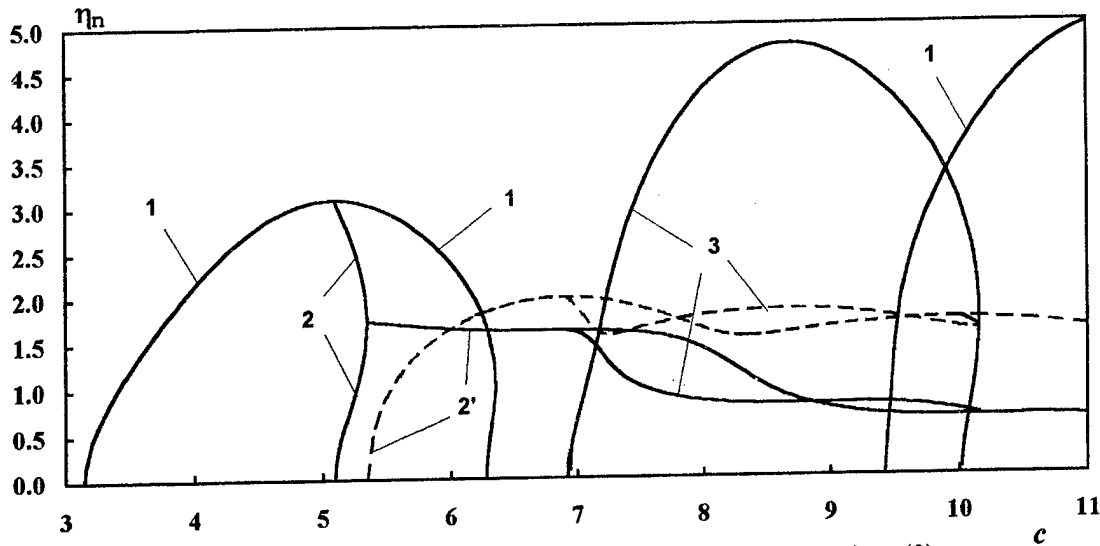


Fig. 1. Parameters in solutions of nonlinear equation (3)

The results are generalized to the equidistant linear antenna array with d as the distance between its elements. In this case the functional to be minimized has the form (1) with integration over $(-\pi/c, \pi/c)$ where $c=kd \sin \alpha$. In this case the integral equation for the optimal pattern is [1]

$$f(\xi') = \frac{c}{2\pi} \int_{-1}^1 \frac{\sin(Mc(\xi - \xi')/2)}{\sin(c(\xi - \xi')/2)} F(\xi) e^{j \arg f(\xi)} d\xi \quad (7)$$

where M is the number of elements in the array. Formula (4) is substituted for

$$e^{j \arg f(\xi)} = g(\xi) P_N(\tau) / |P_N(\tau)| \quad (8)$$

with $\tau = \tan(c\xi/2)$. Accordingly, the equations (6) are substituted for

$$\int_{-1}^1 F(\xi)g(\xi)\tau^n \sin(cM\xi/2)\sqrt{1+\tau^2}/|P_N(\tau)|d\xi=0 \quad (9a)$$

$$\int_{-1}^1 F(\xi)g(\xi)\tau^n \cos(cM\xi/2)\sqrt{1+\tau^2}/|P_N(\tau)|d\xi=0. \quad (9b)$$

REFERENCE

1. M. I. Andriychuk, N. N. Voitovich, P. A. Savenko, V. P. Tkachuk. Synthesis of antennas according to amplitude radiation pattern. Numerical methods and algorithms. Naukova Dumka Publ. Kyiv, 1993. (In Russian).
2. N. N. Voitovich, Yu. P. Topoluk. Antenna synthesis according to prescribed amplitude radiation pattern and the phase problem. Direct and inverse problems of electromagnetic and acoustic wave theory (DIPED-97), Lviv, 1997, p.90-92.

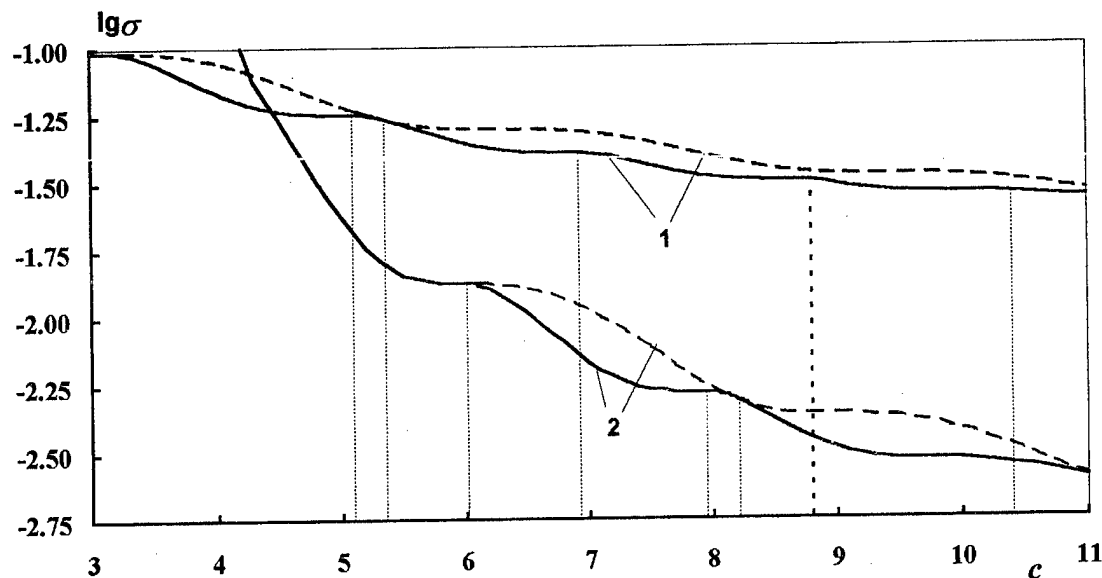


Fig. 2. Value of functional at optimal and synphase patterns

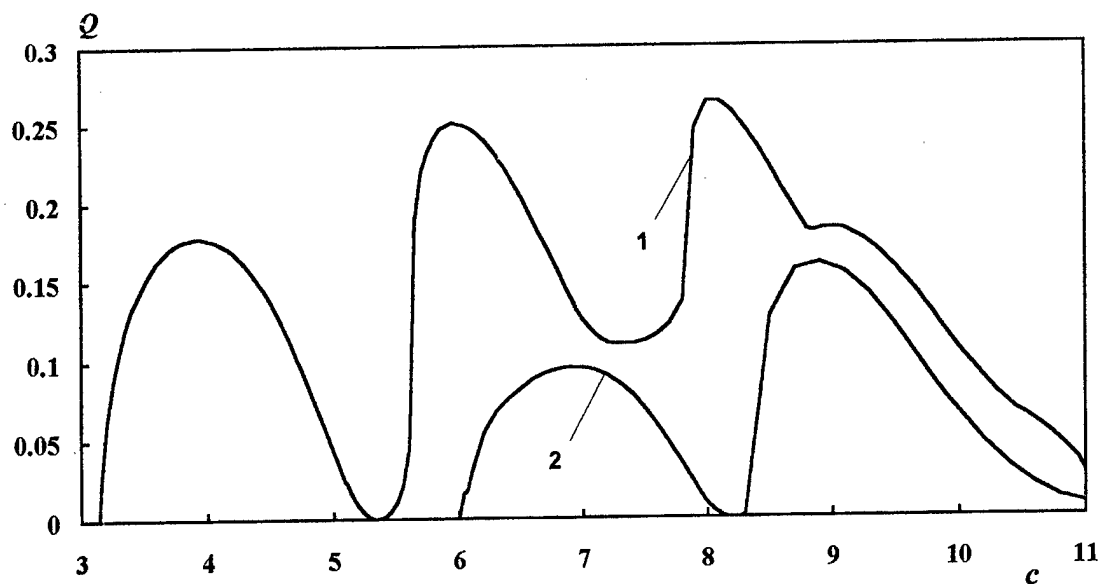


Fig.3. Synthesis effectivity

ARBITRARY GEOMETRY PHASED ARRAY PATTERN SYNTHESIS PROCEDURE

V. A. Obukhovets

Radio Engineering Faculty, Taganrog State University of Radio Engineering
44 Nekrasovsky street, GSP-17A, Taganrog, 347928 Russia
e-mail: decan@vao.rnd.su

ABSTRACT.

Universal phased array pattern synthesis procedure is considered. Radiating elements mutual coupling is taken into account by using the array impedance matrix. The procedure is applicable to arbitrary array geometry with N radiators of any arbitrary sort. The required array pattern is specified at M prescribed points with a restricted sidelobe level. The pattern synthesis is considered as a gain maximization process with arbitrary additional conditions. The variational principles are used to obtain the initial approximation, then this solution is to be corrected by using some iterative process. Only the active part of the impedance matrix is needed to be known for the problem solving.

1. INTRODUCTION.

There are three main kinds of the antenna array synthesis problems. They are the problems of approximation, interpolation and optimization.

The first ones appear when it is necessary to provide a required beam shape. In this case the required pattern is stated as a function, which is determined in the whole angular domain and includes the sidelobes. That is why rather large computational efforts are needed for minimizing the aim function in the whole angular domain. For example, the Chebyshev-synthesized pattern has one and the same sidelobe level even for the far lobes. This is the reason of a gain value decreasing. For the practical needs, important parameter is only the level of the sidelobes but not their shapes.

Interpolation synthesis problems are somewhat closer to the practical needs because their solutions provide the pattern control at several prescribed points. If the number of elementary array radiators is large, it is possible to tune the sidelobe level by choosing prescribed points in the sidelobe domain. However, the intervals between these points cannot be controlled. Introducing an additional number of points increases the problem «dimension» and hence the computing expenses. Besides, interpolation problem solutions do not enable one to minimize the radiated power (i.e., the norm of currents).

The most realistic problem formulation is to determine the distribution of the currents that provides a coincidence between the required and the realized patterns at a finite number of points and satisfies a prescribed sidelobe level restrictions. This formulation implies only the upper sidelobe level restrictions and does not require the coincidence of the patterns at the sidelobe domain.

2. PROBLEM SOLUTION

The first step in the problem solution is the pattern synthesis procedure, which provides a maximum directive gain and coincides with the required pattern at M prescribed points:

$$(1) \quad G(\theta_1, \varphi_1) \rightarrow \max, \quad \text{with} \quad F(\theta_m, \varphi_m) = a_m, \quad (m = 1, 2, \dots, M).$$

The first condition in (1) is equivalent to $F(\theta_1, \varphi_1) = 1$ and $P_{input} = \langle i^* \cdot [r] \cdot r \rangle$; where $G(\theta_1, \varphi_1)$ is the array gain, $F(\theta_m, \varphi_m)$ are the pattern values at prescribed points, P_{input} is the array input power, $\langle i^*$ is the row-matrix of conjugate current distributions, $i \rangle$ is the column current matrix, $[r]$ is the rectangular matrix of the real parts of input impedances.

This problem can be treated in the variational sense, i.e. as minimization of the functional given by

$$(2) \quad \Psi(i) = \langle i^* \cdot [r] \cdot i \rangle + \sum_{m=1}^M \mu_m \cdot \langle f(\theta_m, \varphi_m) \cdot i \rangle,$$

μ_m are the Lagrange factors, $\langle f(\theta_m, \varphi_m) \cdot i \rangle$ is the row-matrix of array radiators at (θ_m, φ_m) -directions. In the minimum of (2) its first variation is zero. That yields the following current matrix:

$$(3) \quad i \rangle = - \sum_{m=1}^M \mu_m^* \cdot [r]^{-1} \cdot f^*(\theta_m, \varphi_m).$$

Unknown expansion coefficients μ_m can be calculated by solving the following set of linear algebraic equations:

$$(4) \quad \sum_{m=1}^M \mu_m^* \cdot \langle f^*(\theta_k, \varphi_k) \cdot f(\theta_m, \varphi_m) \rangle = -a_m, \quad (k = 1, 2, \dots, M).$$

The realized pattern is the following one:

$$(5) \quad F(\theta, \varphi) = - \sum_{m=1}^M \mu_m^* \cdot \langle f^*(\theta_m, \varphi_m) \cdot [r]^{-1} \cdot f(\theta, \varphi) \rangle.$$

This pattern can have the sidelobe amplitudes higher than the prescribed limit value t .

So the next step in the solution is to correct the «initial» pattern (5) by adding some new control points (θ_m, φ_m) to the synthesis conditions (1). The prescribed pattern values at these points must be equal to t . Then the procedure is reiterated. To solve the

set (4), the number of control points M can not exceed the number of array radiators N minus one.

Proposed synthesis procedure, in the simplest case when the number of prescribed points $M = 1$, provides a pattern with maximum gain in the direction (θ_1, φ_1) without any other restriction [1]. For $M > 1$, the current distribution (3) can be treated as a linear combination of the several simplest (i.e., corresponding to $M = 1$) distributions. Each of them provides maximum gain in the corresponding direction (θ_m, φ_m) . In the iterative process, such «partial» patterns develop a minimum distortion of the initial pattern. By using functional analysis techniques one can prove the iterative procedure convergence. A great number of sample synthesis computations have shown that normally only several iterations are needed for problem solving.

If $M = N$, the pattern (5) coincides with prescribed values at the points (θ_m, φ_m) without any gain maximization. For $M > N$, only a mean square approximation can be provided. The same conclusions can be done in the case of traditional interpolation synthesis problems.

One of the main features of the proposed synthesis procedure is that it takes into account the array elements mutual coupling. Only real part of the impedance array matrix is needed for the problem solving. Its computation is much easier than a full complex matrix determination.

There are no any limitations either on the radiator type or on the array geometry. Polarization properties can be calculated if the radiator pattern is a vector function. Several examples of numerical synthesis of cylindrical array patterns, both in the azimuthal and in the axial planes, with specific shapes and differently limited sidelobe levels in different angular sectors will be presented.

3. CONCLUSIONS

Effective iterative procedure has been proposed for an arbitrary antenna array synthesis based on the gain optimization process with some additional restrictions.

References

1. A.W. Rudge, K. Milne, A. D. Olver, P. Knight, *The Handbook of Antenna Design*, London: Peter Peregrinus, 1983.

ON THE STRUCTURE OF THE SOLUTIONS OF THE ANTENNA SYNTHESIS PROBLEMS ACCORDING TO THE PRESCRIBED AMPLITUDE DIRECTIVITY PATTERN USING THE REGULARIZATION FUNCTIONALS

Petro O. Savenko

Institute of Applied Problems of Mechanics and Mathematics of NASU
3"b" Naukova Str., Lviv, 290601, Ukraine
E-mail: voi@ippmm.lviv.ua

Abstract. It is known, that the antenna synthesis problems according to the prescribed amplitude directivity pattern belong to the class of essentially incorrect problems. The absence of the demands to the phase directivity pattern under the conditions of the problem should be used as the additional possibility to improve the approximation of the synthesized directivity pattern (DP) to the given one. At the same time, the nonlinearity of the problem leads to the nonuniqueness of the solutions that complicates the process of numerical searching the solutions. In this report the investigations of the quantity and quality characteristics of the existing solutions, based on the methods of functional analysis, is given in the cases of the linear antenna and the antennas with plane aperture and their discrete analogy (antenna grids). It turns out, that the quantity and the quality of the solutions depend on the value of the electrical size of the aperture, on the value of the space angle (where the DP is given), and on the quality of DP.

Statement and Solution of the Problem. Let \tilde{f} be the DP of the radiating system, prescribed by the linear quite uninterrupted operator $A(c)$ acting from the Hilbert space of the apertured functions H_U into the space of the realized DP H_f

$$\tilde{f} = A\tilde{U} \equiv A_g\tilde{U} + A_\varphi\tilde{U}. \quad (1)$$

The form and the properties of the operator $A(c) = \{A_g, A_\varphi\}$ depend on the type and geometry of the radiating system. The parameters characterizing the electrical size of the aperture (named as the main parameters of the synthesis problem) are contained in the operator A nonlinearly, as a rule. The variational problem consists in searching such function of the amplitude-phase distribution of the fields (currents) \tilde{U} on the aperture, minimizing the regularization functional

$$\sigma_\beta = \|F_g - A_g\tilde{U}\|^2 + \|F_\varphi - A_\varphi\tilde{U}\|^2 + \beta\|U\|^2. \quad (2)$$

It consists of the mean-square deviation of modules of the synthesized DP $|\tilde{f}| = (f_g^2 + f_\varphi^2)^{1/2}$ and given one $|F| = (F_g^2 + F_\varphi^2)^{1/2}$, and limiting the norm of the aperture function.

The problem of searching the points of minimum is reduced to finding the solutions of Euler's equations of the regularization functional σ_β relative to either optimal amplitude-phase distribution (APD)

$$\beta\tilde{U} = -A_g^*A_g\tilde{U} - A_\varphi^*A_\varphi\tilde{U} + A_g^*(F_g e^{i \arg A_g \tilde{U}}) + A_\varphi^*(F_\varphi e^{i \arg A_\varphi \tilde{U}}) \quad (3)$$

of the fields (currents) or optimal synthesized DP \tilde{f}

$$\begin{aligned}\beta f_g &= -A_g A_g^* f_g - A_g A_\varphi^* f + A_g A_g^* (F_g e^{i \arg f_g}) + A_g A_\varphi^* (F_g e^{i \arg f_\varphi}), \\ \beta f_\varphi &= -A_\varphi A_g^* f_g - A_\varphi A_\varphi^* f + A_\varphi A_g^* (F_g e^{i \arg f_g}) + A_\varphi A_\varphi^* (F_g e^{i \arg f_\varphi})\end{aligned}\quad (4)$$

These equations are the equivalent ones. They include besides the nonlinear operator of Hammerstein's type the self-adjoint negative halfdefined linear operator in the right parts.

It should be noted, that for the analytical investigations the equation (4) in regard to synthesized DP is more simple. The equation (3) relative to the optimal APD is preferred for searching the numerical solutions for the antenna grids.

The existence of the solutions of the equations (3), (4) is proved by the following theorem.

Theorem. Let the operator A acts from the complex Hilbertian space of the vector-valued functions H_U into the complex space of the uninterrupted functions H_f with introduced integral metric, and it is quite uninterrupted. Then, the functional σ_β take on the minimal value at some element of the space H_U , the equation (3) in the space H_U and the equation (4) in the space H_f each has at least one solution.

It is shown, that in the case of arbitrary positive value of the main parameters c of the problem the Euler's equation (4) has at least two solutions \tilde{f}_1, \tilde{f}_2 in the region of the real-valued functions. We shall name these solutions as primary ones of the first (\tilde{f}_1) and second (\tilde{f}_2) type. The solutions for the linear antennas and for the grids should be written in the evident form. The characteristic peculiarity of the primary solution of the second type is that at some points of the region Ω , in which the main lobe of the necessary amplitude DP is given, it becomes equal to zero. When the main parameters of the problem are little, the primary solutions minimize the researched functional (2). The efficiency of the primary solutions depends on the properties of the given DP F . If the given DP at some internal points of Ω , the region of its definition, equals to zero, it is more effective to use the primary solution of the second-type \tilde{f}_2 .

With the growth of the value of the main parameter c , the complex solutions which are more effective (in the sense of the value of functional (2)) than the primary ones, are branching from the real primary solutions. The branching points of the solutions can be found by solving either the corresponding systems of transcendental equations or the generalized eigen-value problem with the nonlinear spectral parameter. The corresponding iterative processes are built and their convergence is proved. It is shown, that the branching points of two types exist for every primary solution. The results of investigations of branching the solutions at every point are given.

The general structure of the solutions can be shown in the form of two "trees" of the solutions. The "trunks" correspond to the primary solutions and the "branches" to the branching solutions of a certain type. The "tree" of the solutions of the linear antenna synthesis problem is shown in the fig. 1, in the case when DP has form $F(\xi) = 1$. The primary solution is denoted by $f_1(\xi, c)$, and the branching

solutions are denoted by $f_{1,2}^{(n)}(\xi, c)$ ($n=1,2,3$). The points of branching of the first and the second types are denoted by $c_1^{(j)}, c_2^{(j)}$, where j is the number of the corresponding branching points, $\tilde{c}_1^{(1)}$ is the branching point of the first branched solution.

The investigations of the solutions of Euler's equation (4) for the antennas with plane aperture in special cases is based on modelling the problem of synthesis of a plane aperture by two independent synthesis problems of linear aperture. The dependence of the number of the solutions, branched from the first primary solution of the synthesis problem of the antenna with plane rectangular aperture, on the main problem parameters, is shown in fig. 2. The given amplitude DP has two planes of symmetry, $c_1^{(j)}, c_2^{(j)}$ are the points of branching of the primary solutions.

The equations (3) are solved numerically by the successive approximation method according to the implicit scheme

$$\beta \vec{U}_{n+1} + A_g^* A_g \vec{U}_{n+1} + A_\varphi^* A_\varphi \vec{U}_{n+1} = A_g^* (F_g e^{i \arg A_g \vec{U}_{n+1}}) + A_\varphi^* (F_\varphi e^{i \arg A_\varphi \vec{U}_{n+1}}). \quad (5)$$

The convergence of iterative process is proved. To receive the solution of either type, the initial approach of it should be taken in a certain way. The numerical examples of synthesis of some given DP and the structure of their solutions are presented.

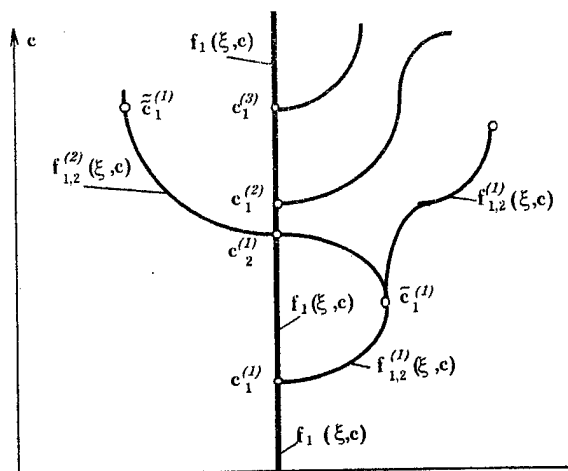


Fig. 1.

c_2	7	21	35	35	49
$c_{2,1}^{(2)}$	5	15	25	25	35
$c_{2,2}^{(2)}$	5	15	25	25	35
$\tilde{c}_{2,1}^{(1)}$	3	9	15	15	21
$c_{2,1}^{(1)}$	1	3	5	5	7
0					
	0	$c_{1,1}^{(1)}$	$c_{1,1}^{(1)}$	$c_{1,2}^{(2)}$	$c_{1,1}^{(2)}$
					c_1

Fig. 2.

References

1. P. O. Savenko. On branching of problem of antenna synthesis for a given amplitude directivity pattern with using of regularization functional // Izvestija vyssh. uchebn. zaveden. Radioelektronika. (In Russian) - 1996. -39, N 2. - p.p. 35-50.

NONLINEAR INVERSE PROBLEMS OF TIME-HARMONIC WAVE SUPPRESSION IN REGULAR WAVEGUIDES

G.V. Alekseev, D.V. Panov, V.G. Sinko

Institute of Applied Mathematics, Far Eastern Branch
of Russian Academy of Science, Radio 7, Vladivostok, 690041, Russia

A.S. Panasyuk

Sankt-Peterburg State University, S. Peterburg, 199034, Russia

Abstract. The paper deals with a theoretical and numerical study of nonlinear inverse problems of time-harmonic wave suppression in regular three-dimensional waveguides. In these problems the field, which is generated by a primary source is given and it is required to suppress it completely or to minimize it by the action of secondary sources. The problems are considered as the minimization problems of some cost functionals. The power radiated to the far zone of the waveguide or the potential energy of the field in some bounded domain of the waveguide are used as these functionals. The coordinates and amplitudes of the secondary antennas play the role of controls. Each of the mentioned functionals is a quadratic function of the complex intensity and a nonconvex general function of the point source coordinates. Efficient numerical method for solution of these problems is developed and some results of numerical experiments are discussed.

Suppose that $D=D_H=\{\mathbf{x}=(x, y, z) \in \mathbb{R}^3 : 0 < z < H, -d/2 < y < d/2, -\infty < x < \infty\}$ is a regular three-dimensional acoustic waveguide of the depth H with a pressure-free upper boundary $z=0$ and rigid other boundaries. Other parameters are: the frequency $\omega > 0$, constant density $\rho > 0$, and the variable sound velocity $c(z) \in L^\infty(0, H)$. Denote by (\mathbf{x}_j, q_j) a point monopole with a center $\mathbf{x}_j = (x_j, y_j, z_j) \in D$ and a complex amplitude q_j . Direct problem of the sound radiation in the waveguide D , generated by N monopoles (\mathbf{x}_j, q_j) , $j=1, 2, \dots, N$, consists of finding a solution (acoustic pressure) p of the Helmholtz equation

$$\frac{\partial^2 p}{\partial x^2} + \frac{\partial^2 p}{\partial y^2} + \frac{\partial^2 p}{\partial z^2} + k^2(z)p = -\sum_{j=1}^N q_j \delta(\mathbf{x} - \mathbf{x}_j), \quad k^2 = \frac{\omega^2}{c^2} \quad (1)$$

in D , satisfying the radiation condition as $x \rightarrow \infty$ and the boundary conditions

$$p = 0 \text{ at } z = 0, \quad \frac{\partial p}{\partial z} = 0 \text{ at } z = H, \quad \frac{\partial p}{\partial y} = 0 \text{ at } y = \pm d/2. \quad (2)$$

If we set $D^+ = \{\mathbf{x} \in D : x > x^+ > x_j, j = 1, 2, \dots, N\}$, $\Gamma^+ = \{\mathbf{x} \in D : x = x^+\}$ then, by using the Fourier method, the solution of the direct problem can be represented in D^+ as [1]

$$p(x, y, z) = i \sum_{n,m=1}^{\infty} \sum_{j=1}^N \zeta_{mn}^{-1} q_j \varphi_n(z_j) \varphi_n(z) \chi_m(y_i) \chi_m(y) \exp(i\zeta_{mn}(x - x_j)). \quad (3)$$

Here $\eta_m = (m-1)\pi/d$, $\chi_1(y) = (1/d)^{1/2}$, $\chi_m(y) = \sqrt{2/d} \cos[\eta_m(y + d/2)]$, $\zeta_{mn}^2 = \xi_n^2 - \eta_m^2$, ξ_n^2 and φ_n are the eigenvalues and normed eigenfunctions of the spectral problem:

$$\varphi''(z) + [k^2(z) - \xi^2] \varphi = 0, \quad \varphi(0) = 0, \quad \varphi'(H) = 0. \quad (4)$$

It is well-known that $\xi_1^2 > \xi_2^2 > \dots > \xi_n^2 \rightarrow -\infty$ as $n \rightarrow \infty$. Also, we assume that

$$\text{Im} \zeta_{mn} \geq 0 \text{ and } \zeta_{mn}^2 \equiv \xi_n^2 - \eta_m^2 \neq 0, \quad \forall (m, n) \in \mathbb{N} \times \mathbb{N}.$$

Suppose that L is a number of all pairs $(m, n) \in \mathbb{N} \times \mathbb{N}$ for which $\xi_n^2 - \eta_m^2 > 0$, and every such pair (m, n) corresponds to a single subscript l which varies from 1 to L . Denote by $A = A(\mathbf{x}_j)$ the

rectangular $L \times N$ - matrix with the components $\alpha_{ij} = \zeta_{mn}^{-1/2} \varphi_n(z_j) \chi_m(y_j) \exp(-i\zeta_{mn} x_j)$, and $\mathbf{q} = (q_1, q_2, \dots, q_N)$. If in D^+ , besides of the field (3), there is a (primary) field

$$p_b(x, y, z) = -i \sum_{m,n=1}^{\infty} \frac{\beta_{mn}}{\sqrt{\zeta_{mn}}} \varphi_n(z) \chi_m(y) \exp(i\zeta_n x) \quad (5)$$

with given coefficients β_{mn} generated by a noise source, then the powers $P(p)$ of the field p , P_b of the field p_b and $P(p+p_b)$ in D^+ are determined respectively by [1]

$$P(p) = \frac{1}{2\omega} \|A\mathbf{q}\|_{C^L}^2, \quad P_b = \frac{1}{2\omega} \|\mathbf{b}\|_{C^L}^2, \quad P(p+p_b) = \frac{1}{2\omega} \|A\mathbf{q} - \mathbf{b}\|_{C^L}^2, \quad \mathbf{b} = (\beta_1, \beta_2, \dots, \beta_L).$$

The analysis of the formula for $P(p+p_b)$ shows that this formula contains $4N+L$ parameters: N complex amplitudes q_j , L complex coefficients β_j and $3N$ coordinates x_j, y_j, z_j of the point sources. Denote the $3 \times N$ matrix (lattice), which consists of coordinates $x_j, y_j, z_j, j=1, \dots, N$ of considered monopoles, by \mathbf{Z} and the corresponding discrete antenna by (\mathbf{Z}, \mathbf{q}) . So one can write, in particular, that $P(p+p_b) \equiv J_1(\mathbf{Z}, \mathbf{q}, \mathbf{b})$. Hence, we can pose several inverse extremal problems, each of them corresponds to a case when a part of the parameters is fixed while the others are to be determined. For example an interesting problem is to minimize the power $P(p+p_b)$ in D^+ . This problem is the inverse problem of active minimization (suppression) of the time-harmonic acoustic fields that has a great practical importance [1,2]. Another control problems are connected with minimization of the functional $J_2(\mathbf{Z}, \mathbf{q}, \mathbf{b})$ which describes the total time-average acoustic potential energy, and the functional $J_3(\mathbf{Z}, \mathbf{q}, \mathbf{b})$ which describes the sum of the squared sound pressures at a number of discrete locations. The role of controls is played by the array \mathbf{Z} and the strength vector \mathbf{q} for all these functionals.

Now we formulate mathematically some inverse extremum problems. Let $\Omega_\delta = [0 \leq x \leq x^+] \times [-d/2 + \delta \leq y \leq d/2 - \delta] \times [\delta \leq z \leq H - \delta]$, where $\delta > 0$ be fixed. By B we denote a set in C^N formed by the vectors $\mathbf{q} = (q_1, \dots, q_N)$ for which $\|\mathbf{q}\|_{C^N}^2 = |q_1|^2 + \dots + |q_N|^2 \leq Q_0^2$. Here Q_0 is a parameter which has a sense of restriction to the power supplied to the antenna (\mathbf{Z}, \mathbf{q}) . Let J is any functional of J_1, J_2, J_3 . We are interested in the following minimization problems:

Problem 1. Given an integer N , and a vector \mathbf{b} in C^L , find a discrete antenna (\mathbf{Z}, \mathbf{q}) , $\mathbf{Z} \in \Omega_\delta^N$, $\mathbf{q} \in B$ such that $J(\mathbf{Z}, \mathbf{q}, \mathbf{b}) \rightarrow \inf$.

Problem 2. Given an integer N , a vector $\mathbf{b} \in C^L$ and an array $\mathbf{Z}_0 \in \Omega_\delta^N$, find a vector $\mathbf{q} \in B$ such that $J(\mathbf{Z}_0, \mathbf{q}, \mathbf{b}) \rightarrow \inf$.

The last problem in which the coordinates of the secondary point sources are fixed, and it is required to find the complex amplitudes q_j by minimizing the corresponding quadratic functional, has been studied in [1]. An efficient stable method based on regularization method and incomplete singular factorization has been developed. Using this method we have developed the algorithm (Algorithm 1) for solving nonquadratic Problem 1 for the two-dimensional waveguides in [3-5]. It is based on using the enumeration type technique with respect to coordinates of monopoles on some two-dimensional grid and the above method with respect to monopole amplitudes. Here we investigate the capabilities of Algorithm 1 for a three-dimensional homogeneous waveguide D with the parameters $c=1450$ m/sec, $\omega=20\pi$ taken from [1], in the case when the primary field is generated by a unit monopole located at the point $(0,0,z_0)$ with $z_0=H/2$. For Problem 2, the secondary array was in the form of a vertical one $\mathbf{Z} = \{0,0,z_0 - jh: j=1,2,\dots,N, h=20 \text{ m}\}$, located at the z axis. The results of solving Problem 2 are shown in Fig. 1a where the curves 1, 2 and 3 describe the dependence of the magnitude of the power suppression (in decibels) $|\Delta P|_{\text{dB}} = 10|\log[P(p+p_b)/P_b]|$ on N for the depth

$H=1000\text{m}$ and Q_0^2 equal to 1, 3 and 10 respectively. The results of solving Problem 1 by using Algorithm 1 are shown in Fig. 1b where curves 1, 2 and 3 characterize the dependence of $|\Delta P|_{\text{dB}}$ on N for $Q_0^2=3$, for three values of the depth H equal to 400, 500 and 700 m, respectively.

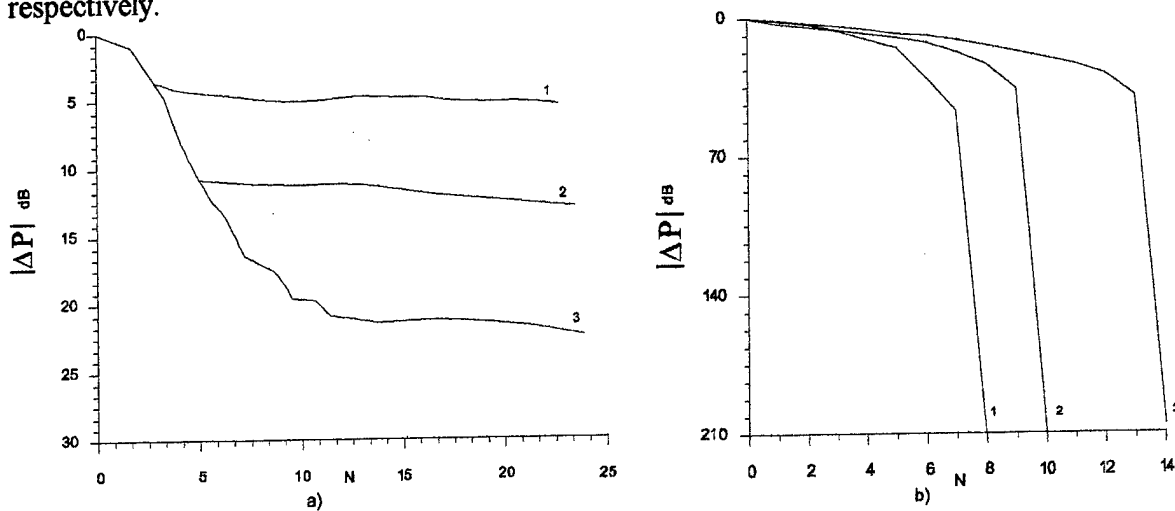


Fig. 1.

Analysis of Fig. 1a and other results of solving Problem 2 (see e.g. [1]) shows that, for a fixed antenna configuration, the maximum value of suppressed power output strongly depends on the arrangement of primary source and secondary antenna and usually does not exceed 20 - 25 dB even for the relatively large values of the number N of secondary point sources. On the other hand, if one implements the power output suppression by combining an optimal allocation and a choice of monopole amplitudes by using Algorithm 1 of solving Problem 1, then the substantial reduction in the power output of a primary noise source having the order of 100 dB and higher can be achieved even for a relatively small number N of point sources. In fact, we can see from Fig. 1b that a complete (200 dB) suppression of the primary source power is achieved at $N=8$ for the depth 400 m when $L=19$, at $N=10$ for the depth 500 m ($L=23$) and at $N=14$ for the depth 700 m ($L=33$). It is worth noting that this fact has been observed in a wide range of depths H (or frequencies ω) of the waveguide D and distances $|x_0|$ to the primary source. Together with the results of [3-5], this demonstrates a high accuracy and robustness of Algorithm 1 when solving nonquadratic active minimization Problem 1.

Acknowledgments

The work was supported by the Competition Center for Basic Research at St.-Petersburg State University under Grant #95-0-4.2-97 and by the Federal Goal Program "State Support of Integration of Higher Education and Fundamental Science", under Project 97-723: Education-Scientific Center for Study of Resources and Monitoring of the Pacific Ocean.

References

1. Alekseev, G.V. and Komarov, P.A. Inverse Extremal Problems of Acoustic Radiation in a Three-Dimensional Waveguide. *J. Inv. Ill-Posed Problems* (1994). 2, N2, 85-108.
2. Elliott, S.J. and Nelson, P.A. Active Minimization of Acoustic Fields. *J. Méc. Theor. Appl.* (1987). 6, (special issue), 39-98.
3. Alekseev, G.V. and Komarov, E.G. Numerical Study of Nonlinear Inverse Extremal Problems of Sound Radiation in a Two Dimensional Waveguide. *J. Inv. Ill-Posed Problems* (1996). 4, N1, 1-21.
4. Alekseev, G.V. Nonlinear Problems of Active Noise Control in Two-Dimensional Layered Inhomogeneous Waveguides. *Acoust. Phys.* (1997). 43, N6, 639-645.
5. Alekseev, G.V. and Komarov, E.G. Nonlinear Inverse Problems of Active Sound Control in Two-Dimensional Waveguides. *Dokl. Akad. Nauk Russia.* (1998). 358, N1, 27-31.

PERMITTIVITY PROFILE SYNTHESIS OF PLANAR BURIED WAVEGUIDES

N.E.Nikolaev, V.V.Shevchenko
Russian Peoples' Friendship University
Mikluho-Maklaya, 6, Moscow, 117198, Russia
E-mail: nnikolaev@mx.pfu.edu.ru

Abstract The method of finding the permittivity profile of graded-index single-mode planar waveguide after the given mode parameters is described. For solving this inverse problem the some universal mathematical model of profile is proposed. It has the shape of double truncated exponential-power function. Each set of function parameters corresponds to a particular distribution of permittivity in the waveguide. Solution of direct problem by the shift formula method yields the mode parameters of the waveguide [1]. Multiply repeated numerical solution of direct problem by special algorithm using the least-square method enables us to select the function parameters for a certain set of mode parameters. As a result of the procedure, the profile function in question is synthesized.

1. For describing the permittivity profile in a waveguide, the authors propose a reasonably universal function [1]. It has the following form (see Figure):

$$\varepsilon(y) = \varepsilon_g [1 - 2\Delta_j f_j(y)], \quad (1)$$

where

$$f_j = \left\{ \frac{1 - \exp q_j \varphi_j(y)}{1 - \exp q_j} \right\}^{p_j}, \quad (2)$$

$$j = 1, \text{ when } 0 \leq y < r; \quad j = 2, \text{ when } r < y \leq 1,$$

$$\Delta_1 = \frac{\varepsilon_g - \varepsilon_b}{2\varepsilon_g}, \quad \Delta_2 = \frac{\varepsilon_g - \varepsilon_s}{2\varepsilon_g}, \quad \varphi_1 = 1 - \frac{y}{r}, \quad \varphi_2 = 1 - \frac{1-y}{1-r}. \quad (3)$$

Here $\varepsilon(y) = \varepsilon_b$, if $y = 0$; $\varepsilon(y) = \varepsilon_g$, if $y = r$; $\varepsilon(y) = \varepsilon_s$, if $y = 1$.

According to this double truncated exponential-power function, the permittivity distribution in the waveguide is determined by 9 parameters. Such a model can be used for the studies of the waveguides of vastly different types. By solving the direct problem it is possible to get the values of cutoff frequencies and dispersion characteristics of the waveguides with practically arbitrary permittivity profile. Such a versatility of the model makes it convenient for solving the inverse problem, i.e. the problem of the permittivity profile reconstruction after the mode parameters.

Generally, for solving the inverse problem a knowledge of the propagation constants of several waveguide modes is required [2-6]. However, in case of a single-mode waveguide the known methods (such as WKB-method) cannot be used. In this work the authors propose a method for solving the inverse problem for such waveguides.

2. The proposed method is based on the representation of permittivity profile using the double truncated exponential-power function. As stated above, the profile is determined by 9 parameters. Usually some of them can be specified beforehand considering the implantation process of fabricating the buried waveguides [7]. So the problem of profile reconstruction reduces to finding the parameters p_1, q_1, p_2, q_2 . The difficulty of the problem lies in the fact

that the knowledge of at least two values of propagation constants is required. It is possible to get them by considering the operation of the waveguide at two frequencies within the limits of single-mode operating regime.

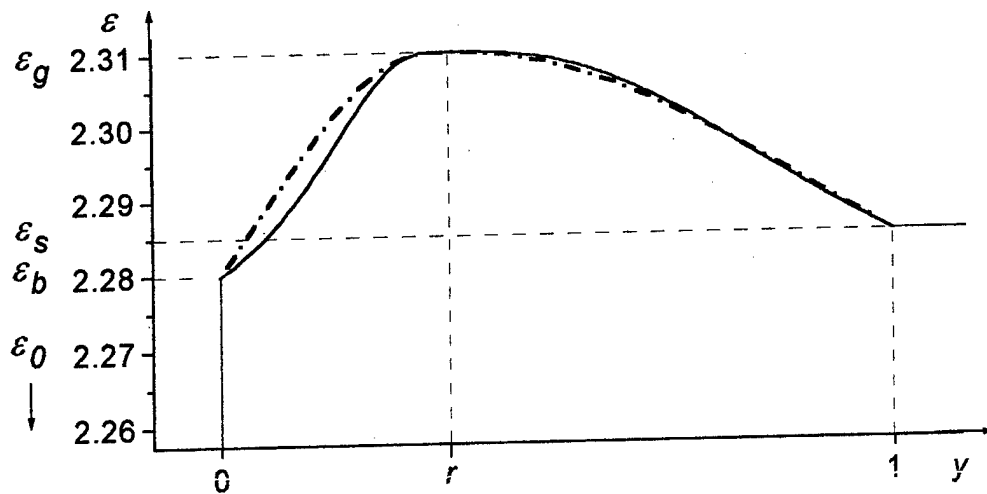


Fig. Permittivity profiles of two waveguides with the parameters:

solid line: $q_1 = -3.0$, $q_2 = -2.0$, $p_1 = p_2 = 4.0$.

dash-dotted line: $q_1' = q_2' = -1.15$, $p_1' = p_2' = 2.66$

3. In order to study the details of solution, the conditions of the problem were simplified: the respective parameters in both parts of the profile were assumed to be equal, i.e. $q_1 = q_2 = q$ and $p_1 = p_2 = p$. Firstly, a basic profile with the preset parameters was chosen. For this waveguide the normalized propagation constants B_1 , B_2 at two normalized frequencies V_1 , V_2 [8] were calculated. The frequencies V_1 , V_2 were within the limits of a single-mode regime. Furthermore it was assumed that only these modal parameters were known. The aim was to find the profile parameters p , q . The way to solve this problem is described below. Some arbitrary profile parameters are chosen. The propagation constants are calculated at two frequencies V_1 , V_2 . Then they are compared with propagation constants of the waveguide with basic profile. The difference between the values of propagation constants was estimated by the least-square method. If the values were not equal to each other, new profile parameters were chosen. At the first step this is made rather voluntarily. Direction of profile parameters change is chosen so that the sum of deviation squares becomes smaller. The use of the direct problem solution results [1] and some experience made the procedure easy to realize and it could be automated.

However the least-square method appears to give not sufficient criterion for the selection of parameters. So, in addition one more criterion was used: the closeness of the value $(B_2 - B_1)/(V_2 - V_1)$ calculated for the modes of basic waveguide and that of the waveguide under consideration.

Simultaneous application of both criteria gives good accuracy in the selection of profile parameters. For instance, in the case of the basic waveguide with the parameters: $q = -2.0$, $p =$

4.0, $\varepsilon_0=1$, $\varepsilon_b=2.280$, $\varepsilon_s=2.285$, $\varepsilon_g=2.310$, $r=0.33$ the selection gave the same parameters, i.e. $q_1=q_2=-2.0$ and $p_1=p_2=4.0$.

4. At the next step of study, the basic waveguide had the profile parameters of which one pair was different: $q_1=-3.0$, $q_2=-2.0$, $p_1=p_2=4.0$, $\varepsilon_b=2.280$, $\varepsilon_s=2.285$, $\varepsilon_g=2.310$, $r=0.33$. For this profile at the frequencies $V_1=3.0$, $V_2=5.0$ within the limits of the single-mode regime, the normalized propagation constants $B_1=0.19599$, $B_2=0.51072$ were calculated.

In this case the procedure of parameters selection is similar but still slightly differs when compared with the procedure conducted before. For the previous profile the parameters of the basic waveguide in the both parts of the profile were equal ($q_1=q_2$, $p_1=p_2$). The parameters of the waveguide to be synthesized were also selected on the basis of their equality. Now one pair of parameters differed ($q_1 \neq q_2$) whereas the selection of parameters was performed on the basis of the previous assumption of their equality. Under these conditions the calculations gave the following results: $q_1'=q_2'=-1.15$, $p_1'=p_2'=2.66$.

The propagation constants of the waveguides with profile parameters $q_1'=q_2'$, $p_1'=p_2'$ at the set frequencies coincide with the propagation constants of the waveguide with basic profile with parameters q_1 , q_2 , p_1 , p_2 . So, it can be stated that the waveguides with different profile parameters exist, each satisfying the conditions of the problem. The difference between the waveguide parameters makes their profiles different, but this difference is relatively small. Figure shows the profiles of the waveguides with parameters: 1): $q_1=-3.0$, $q_2=-2.0$, $p_1=p_2=4.0$; 2): $q_1'=q_2'=-1.15$, $p_1'=p_2'=2.66$. It should be noted that despite the difference in parameters the waveguides are equivalent to each other if their dispersive characteristics are considered, at least in the interval of frequencies between V_1 and V_2 .

References

1. N.E. Nikolaev, V.V. Shevchenko, *Radiotekhn. i Elektron.*, 1997, v.42, No.8, p.901.
2. D. Marcuse, *IEEE J. Quantum Electr.*, 1973, v.QE-9, No.10, p.1000.
3. J. Janta, J. Ctyroky, *Optics Comm.*, 1978, v.25, No.1, p.49.
4. J.M. White, P.F. Heidrich, *Appl. Opt.*, 1976, v.15, No.1, p.151.
5. L.M. Andrushko, *Dielectric Inhomogeneous Waveguides of Optical Range*, Kiev: Tekhnika, 1983.
6. N. Espinosa-Ortiz, V.V. Shevchenko, *Radiotekhn. i Elektron.*, 1994, v.39, No.3, p.394.
7. M.L. Von Bibra, A. Roberts, *J. Lightwave Techn.*, 1997, v.15, No.9, p.1695.
8. T. Tamir, *Guided-Wave Optoelectronics*, Springer-Verlag Berlin Heidelberg, 1988.

INHOMOGENEOUS TRANSIENT CONDUCTIVE HALF-SPACE: RECONSTRUCTION OF CONDUCTIVITY TIME-DEPENDENCE BY SCATTERED FIELD

Irena Yu. Vorgul

Kharkov State University, 4 Svoboda Sq., Kharkov 310077, Ukraine

e-mail: ira@unicom.kharkov.ua

Alexander G. Nerukh

Kharkov Technical University of Radio Electronics, 14 Lenin Av., Kharkov 310726, Ukraine

Abstract. Inverse problems for a half-space with time-varying conductivity are solved. Determination of conductivity time-dependence after the scattered field is carried out in assumption of the half-space homogeneity, for a propagating conductivity change and for the transient conductivity inhomogeneous in one dimension. Analytical solutions for the conductivity are obtained from integral equations and can be used for the diagnostics problems or for determination of the conductivity time-dependence providing the required field transformation.

Introduction

The present work is devoted to solving the inverse problem for media with time-varying conductivity. Time-varying conductivity can appear as a result of atmospheric fluctuation, nuclear or chemical explosion, or environmental changes, or can be deliberately created, for example in some types of semiconductors. Electromagnetic field transformation in the media with specific time-dependences of conductivity was investigated for harmonic wave and harmonic conductivity [1], and for the opposite case of rectangular pulse and time jump of conductivity [2,3]. Recently, a splash in the studies of inverse problems for conducting media in time domain was marked [4-5]. However, although the transient fields were considered, the problems were solved only for stationary media.

Common formulation of the problems

In this work we consider a sequence of transient problems in the order of their increasing complexity. Their common formulation is in determination of conductivity time-dependence in a half-space $x > 0$ by initial and scattered fields.

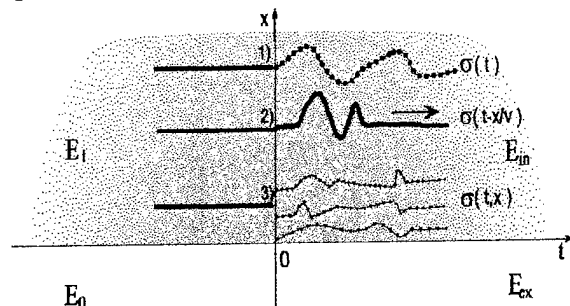


Fig.1

It is considered that the unknown conductivity change starts at the moment $t = 0$ (Fig.1). Before this moment, the conductivity value (if it was constant) or time-dependence (if it changed) are assumed known, and the fields for $t < 0$ and for $t > 0$ are called the initial and scattered fields, correspondingly. The fields are considered to have only those components, which are normal to the x -axis and independent on the y - and z - coordinates. Thus we solve one-space-

dimensional problems.

Three cases are considered there: the case of a homogeneous transient half-space, the case of a propagating conductivity change and the case of an inhomogeneous half-space with transient conductivity. For each problem an analytical expression for the conductivity time-dependence is obtained. The external region is assumed to be a stationary homogeneous lossless medium.

Mathematically, the problems are formulated in terms of the Volterra integral equation for the electrical component of electromagnetic field [6], which has the following form for the internal field (inside the transient region) for $t > 0$, $x > 0$:

$$E_m(t, x) = A(t, x) - \frac{2\pi}{\epsilon v} \theta(vt - x) \int_{t-x/v}^t dt' \sigma(t', x - v(t-t')) E_m(t', x - v(t-t')) - \frac{2\pi}{\epsilon v} \theta(x - vt) \int_0^t dt' \sigma(t', x - v(t-t')) E_m(t', x - v(t-t')) - \frac{2\pi}{\epsilon v} \int_0^t dt' \sigma(t', x + v(t-t')) E_m(t', x + v(t-t')) \quad (1)$$

and for the external field for $t > 0, x < 0$:

$$E_{ex}(t, x) = B(t, x) - \frac{2\pi}{\epsilon v} \theta(vt + x) \int_0^{t+x/v} dt' \sigma(t', v(t-t') + x) E_{in}(t', v(t-t') + x) \quad (2)$$

where the terms A and B are determined by the initial field and prehistory of its interaction with the media, ϵ is the dielectric permittivity, $v = c / \sqrt{\epsilon}$ is the light velocity in considered medium and the conductivity time-dependence (or time-spatial dependence) $\sigma(t, x)$ is a function to be found.

Homogeneous half-space with unknown transient conductivity

Inside the transient half-space, there are two spatial-temporal zones: $x > vt$ and $x < vt$, where integral equations for the fields and the fields themselves are different. For $x > vt$ the transformed field is not influenced by the boundary and the processes and formulas here are the same as those in the unbounded-domain case. For $x < vt$, the boundary influence changes the transformed field. But instead of this the differential equations for $\sigma(t)$ turned out to be the same as those for the unbounded-domain problem and for $x > vt$. Their solution is:

$$\sigma(t) E_{in}(t, x) = \frac{\epsilon v^3}{4\pi} \int_0^t \frac{\partial^2}{\partial x^2} [E_{in}(t', x) - A(t', x)] dt' - \frac{\epsilon v}{4\pi} \frac{\partial}{\partial t} [E_{in}(t, x) - A(t, x)]. \quad (3)$$

The conductivity time-dependence in (3) is determined by the initial and internal transformed fields. In the most of applications such as remote sensing, one usually knows not the internal but only the external field. So we try to obtain an expression for conductivity depending only on the external and initial fields.

Introduce a new function F of one variable as:

$$F(t) = -\frac{2\pi}{\epsilon v} \int_0^t dt' \sigma(t', v(t-t')) E_{in}(t', v(t-t')), \text{ which determines the external field in the external}$$

region $-vt < x < 0$ by the expression $E_{ex}(t, x) - B(t, x) = F(t + x/v)$, and a new function $\Phi(t, x) \equiv E_{in}(t - x/v, x) - A(t - x/v, x)$ for $0 < x < vt$, satisfying the following equation obtained from (1):

$$\Phi_x'(t, x) + \frac{2}{v} \Phi_t'(t, x) = -\frac{4\pi}{\epsilon v} \frac{\partial}{\partial t} \int_0^{t-x/v} dt' \sigma(t', v(t-t')) E_{in}(t', v(t-t')) \quad (4)$$

with the boundary and initial conditions $\Phi(t, 0) = F(t)$, and $\Phi(x/v, x) = E_{in}(0, x) - A(0, x) = 0$.

Knowing the external field at any point, the field in the whole external region can be determined, including the region close to the boundary. So it would be enough to obtain the solution for the conductivity determined by the external field at the points where $|x| \ll vt$. Under this approximation, we can solve the equation (4), hence expressing the internal field through the external one, because the integral at the right-hand part of (4) will be equal to $F(t)$:

$$\Phi_x'(t, x) + \frac{2}{v} \Phi_t'(t, x) \approx 2F'(t), \quad (5)$$

After substitution of this equation solution into (7) we obtain the conductivity time-dependence in the half-space determined by the scattered field:

$$\sigma(t) (E_{ex}(t - x/v, x) - E_0(t - x/v, x) + E_0(t, 0)) = \sigma_0 A(0, 0), \quad (6)$$

where $\sigma_0 = \sigma(0)$ is the known value of initial conductivity, and x means an arbitrary point coordinate (not only $|x| \ll vt$) inside the external region $-vt < x < 0$.

The obtained expression (6) for the conductivity determination corresponds to the effect of current freezing-in at the boundary, by analogy with that for plasma. This formula enables one to

reconstruct the conductivity after the scattered field only if the initial conductivity is not zero, as one can see from (6).

To demonstrate the obtained solution implementation, we calculate the conductivity time-variation which causes a transformation of initial field as a rectangular pulse into the external field taken as a set of pulses (Fig.2(a)).

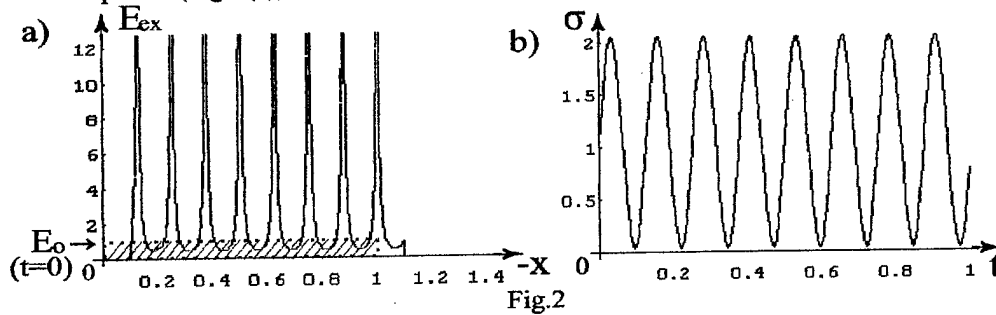


Fig.2

The calculated conductivity, shown in Fig.2(b), turns out to be time-harmonic.

Inhomogeneous time-varying conductivity.

When the conductivity in the half-space $x > 0$ depends not only on time but also on space coordinate x , the reasoning analogous to the above for a homogeneous half-space leads to the solution for the conductivity time-dependence on the boundary:

$$\sigma(t, 0) (E_{ex}(t + x/v, -x) - E_0(t + x/v, -x) + E_0(t, 0)) = \sigma_0 A(0, 0) \quad (7)$$

1) Assuming that the conductivity does not change in the whole half-space simultaneously but its change is propagating with a velocity v_1 , that is $\sigma(t, x) \equiv \sigma(t \pm x/v_1)$, we can reconstruct this dependence by

$$\sigma(t \pm x/v_1) (E_{ex}(t \pm x/v_1 + z/v, -z) - E_0(t \pm x/v_1 + z/v, -z) + E_0(t \pm x/v_1, 0)) = \sigma_0 A(0, 0)$$

This formula corresponds to a wave of conductivity change as well as to the conductive half-space uniform motion along the x -axis.

2) To reconstruct not only the conductivity time-dependence at the boundary but also its spatial distribution, we expand the right-hand part of (6) in terms of the full Taylor series:

$$\Phi_x'(t, x) + \frac{2}{v} \Phi_t'(t, x) = F(t) + \sigma(t) E_{in}(t, 0) x + \dots \left[\sigma(t - x/v, x) E_{in}(t - x/v, x) \right]_x^{(n)} \Big|_{x=0} \frac{x^n}{n!} + \dots \quad (8)$$

Starting from the boundary conductivity time-dependence determined by (7), we imbed by iterations into the transient half-space, substituting the conductivity spatial-temporal dependence determined at the previous step into (8) and finding then the internal field and the conductivity for the next x value. The deeper we imbed in the half-space, the more terms in (8) we need to provide the required accuracy.

Electromagnetic field interaction with a transient conductive half-space enables one to reconstruct the conductivity temporal-spatial dependence after the scattered field. The obtained results could be useful for remote sensing and other diagnostic problems, and for carrying out new field transformers based on the time-varying material conductivity.

1. F.A.Harfoush and A.Taflov, *Scattering of electromagnetic waves by a material half-space with time-varying conductivity*. IEEE Trans. Antennas Propagat., Vol.39, N 7, 1991, pp.898-906.
2. A.G. Nerukh, I.Yu.Shavorykina, *Electromagnetic impulse return from a conductive medium which has come into being*. Proc. Int. Symp. Antennas Propagat., Vol.2, 1992, pp.585-588.
3. A.G.Nerukh, I.Yu.Shavorykina, *Transformation of radiation pulse in nonstationary conducting medium*". Radiophysics and Quantum Electronics(Engl.Transl.), Vol.35, 1992, N 3-4, pp.203-209.
4. G.Kristensson, R.J.Krueger and R.C.Winther. *Existence and construction of solutions of dissipative inverse problems*, J. Math. Anal. Appl., Vol.157 (2), 1991, pp.542-554.
5. T. Melamed and E.Heyman, *Local Time Domain Inverse Scattering Using Pulsed Beams*, Proc. URSI Int. Symp. on EM Theory, 1995, pp.157-161
6. A.G.Nerukh, N.A.Khizhnjak, *Modern Problems of Transient Macroscopic Electrodynamics*, Test-Radio Publ., Kharkov, 1991 (in Russian).

Limb-Viewing Refraction Inverse Problem in Duct Case¹

K.P. Gaikovich, M.B. Tchernyaeva

*Radiophysical Research Institute, B. Pecherskaya st., 25,
Nizhny Novgorod, Russia, 603600,*

Phone: 8312 367294, Fax: 8312 369902, E-mail: gai@nirfi.nnov.su

*Nizhny Novgorod State University, Gagarina, 23
Nizhny Novgorod, Russia, 603600,*

Abstract - The limb-viewing refraction inverse problem for retrieval of refraction index with spherical symmetry distribution in the Earth atmosphere is solved as an ill-posed problem, supposing that the retrieval height interval is wider than the height interval for ray perigee in which the refraction is given. The problem is solved for the most important case of duct presence.

Introduction

Limb-viewing refraction measurements have been used for investigation of all the planet atmospheres in the Sun System [1]. Limb-viewing measurements are the measurements of refraction in dependence on the ray perigee height above the planet surface. The corresponding inverse problem consist of the solution of the Abel-type integral equation on the basis of its well-known inverse transformation. The refraction index height profile is determined as the integral of measured refraction dependence.

In the present paper this inverse problem is considered supposing that the retrieval height interval is wider than the height interval for ray perigee in which the refraction is given. Such a formulation leads to an ill-posed inverse problem. There are various possibilities of this problem formulation. The most important case from the practical point of view is the case when the refraction dependence is given from the lower retrieval level up to some determined height level, and the refraction index height profile should be retrieved not only in this layer but also in the height region above this layer. This case is to be considered here for the Earth atmosphere. It is also possible to solve this problem when the refraction dependence is given in two or more height intervals. In all such cases the exact solution of Abel equation is not applicable, and we have the ill-posed inverse problem for integral equation of the 1-st kind.

Problem formulation

For limb-viewing measurements the refraction inverse problem can be expressed by the following integral equation:

$$10^{-6} \int_{r_h}^{r_{\max}} \frac{dN}{dh}(r) \frac{-2r}{\sqrt{(nr)^2 - (n_h r_h)^2}} dr = \mathcal{E}(r_h), \quad r_0 \leq r_h \leq r_{\max} \quad (1)$$

where $r = r_0 + h$, r_0 is Earth radius, $N = 10^6(n-1)$ is refraction index, n is refractive index, $n_h = n(r_h)$. In the case of duct absence the nonlinear equation (1) can be expressed in a linear form:

¹ This work was supported under grant of Education Ministry of Russian Federation

$$10^{-6} \int_{p_h}^{p_{\max}} \frac{dN}{dp}(p) \frac{-2p}{\sqrt{p^2 - p_h^2}} dp = \mathfrak{E}(p_h), \quad p_0 \leq p_h \leq p_{\max} \quad (2)$$

$p = nr$, $n_0 = n(r_0)$, $p_0 = n_0 r_0$. In the well-posed case, when the refraction dependence is given on the all the retrieval interval, this equation has the known exact solution:

$$N(p) = \int_p^{p_{\max}} \mathfrak{E}(p_h) \frac{dp_h}{\pi \sqrt{p_h^2 - p^2}}, \quad p_0 \leq p \leq p_{\max} \quad (3)$$

Using the relationship $h = \frac{p}{1 + 10^{-6} N(p)} - r_0$ the profile $N(p)$ could be converted into

height profile $N(h)$. There is a finest point in this inverse problem, which hasn't been mentioned before. It is easy to see from (1), which depends on derivative of refraction index, that the solution is determined in reality up to arbitrary constant shift. This fact becomes important in the case of numerical solution of (1). To obtain the solution (2), the condition $N(p_{\max}) = 0$ is necessary to use in addition.

Let us consider the equation (1) in the case when its right side is given in the region $0 \leq h \leq h_1$, $h_1 \leq h_{\max}$. The solution of the equation (1) for the region $h_1 \leq h \leq h_{\max}$ is the typical ill-posed problem, the same type as the astronomical refraction inverse problem in the case of ground-based measurements considered in [2]. It is easy to show that this problem is more complicated than the solution of the Fredholm equation of the 1-st kind. Really, if the refraction index profile $N(p)$ is also considered as known in the region $p_0 \leq p \leq p_1$, it is easy reduce the problem to Fredholm integral equation of the 1-st kind. To retrieve the refraction index in the region $0 \leq h \leq h_{\max}$ by refraction measurements in $0 \leq h \leq h_1$ the equation (1) is solved numerically on the basis of Tikhonov's general discrepancy method [3], which uses the belonging of exact solution to the set of square-integrable functions with square-integrable derivatives. The results of numerical simulation give us the retrieval accuracy at various levels of the refraction error.

Results

In the Fig.1 it is possible to see an example of real typical sonde refraction index profile retrieval by refraction measurements in the region $0 \leq h \leq 5$ km at the error level $\delta\epsilon = 5''$ on the basis of linear equation (2). The specific character of the profile above the upper level of measurements ($h_1 = 5$ km) is retrieved with a good quality.

The most interesting is the case, when there is the region of the atmosphere duct above the upper level of refraction measurements. In this region the refraction measurements are absent or distorted because of strong diffraction. Moreover, the linear equation (1) is inapplicable in the presence of duct region. So, it is necessary to use in the solution iteration procedure for nonlinear equation (1).

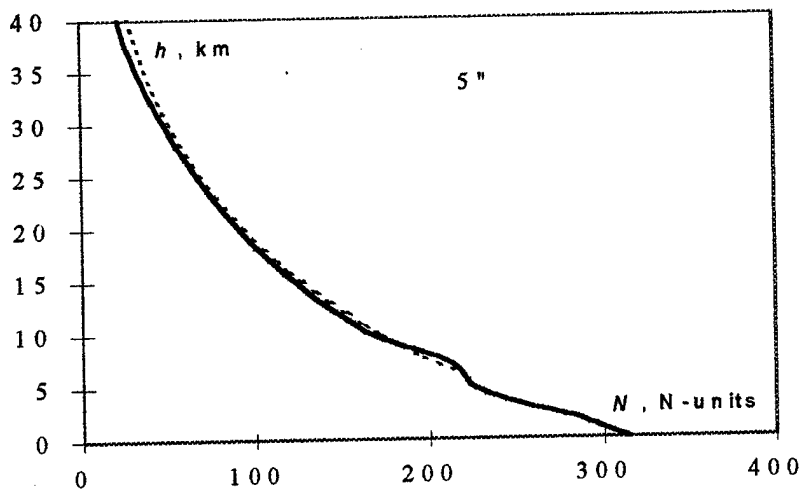


Fig.1.

An example of the retrieval from nonlinear equation (1) in the case of duct stratification is shown in the Fig.2. The duct refraction index distribution is successfully retrieved at $\delta\epsilon = 15''$.

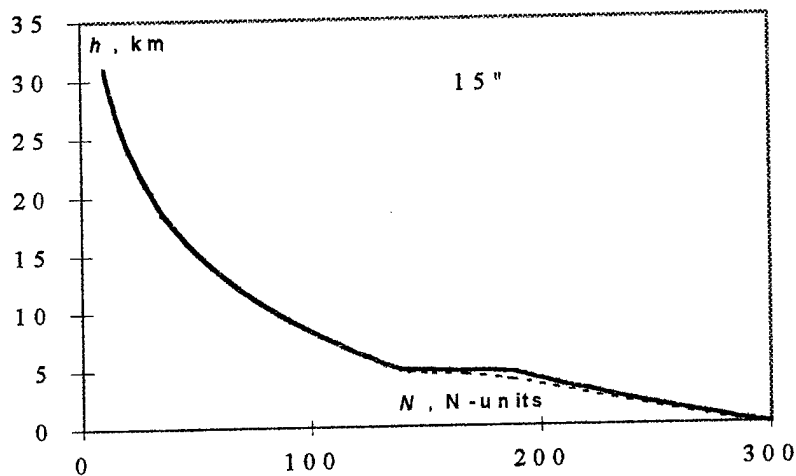


Fig.2.

References

1. Kliore A.J., Gain D.L., Levy G.S., Eshelman V.R. Astronaut and aeronaut, 1965, No. T-7, p.72.
2. Gaikovich K.P. Radiophysics and quantum electronics, 1992, v.35, No.3-4, p.149.
3. Tikhonov A.N., Goncharsky A.V., Stepanov V.V., Yagola A.G. Regularization algorithms and *a priori* information. Moscow, Nauka, 1983.

Regularization algorithms for inverse problems in the radio wave probing of the ionospheric plasma

L. F. Chernogor, K. P. Garmash, V. T. Rozumenko

Department of Space Radio Physics, Kharkiv State University,
4 Svobody Square, Kharkiv 310077, Ukraine
E-mail: *Leonid.F.Chernogor@univer.kharkov.ua*

Inversion problems in radio wave probing of the ionospheric plasma amount to solving integral equations the right-hand part of which originate from measurements. Therefore, the solutions to such equations are unstable and require the application of regularization algorithms. As an example, we consider the partial reflection technique.

The theory of partial reflection yields the following relation between the estimated from measurements profile $R(z)$ and the electron number density profile $N(z)$ to be obtained:

$$\int_{z_0}^z K(z', \nu(z')) N(z') dz' = \ln \frac{R_0(z)}{R(z)} \quad (1)$$

where: $K(z')$ is the kernel of the integral equation, $R_0(z)$ is the function known from the theory of the partial reflection technique, z_0 is the altitude of the lower edge of the ionosphere.

Earlier, profiles $N(z)$ were derived by differentiating (1) with respect to z . The quality of the profiles obtained depend on random errors of estimates of $R(z)$, as well as on the stability of an algorithm of numerical differentiation.

Since the inversion problem of the partial reflection technique is ill-posed, the Tikhonov regularization algorithm is employed in this study. The collision frequency profile is taken from well-known models.

The algorithm of regularization suggest determining $N(z)$ by minimizing the functional:

$$\Phi[N, R, \alpha] = \left\| \int_{z_0}^z K(z') N(z') dz' - R(z) \right\|^2 + \alpha \Omega[N] \quad (2)$$

where: α is the parameter of regularization, Ω is the stabilizer.

It has turned out that the applying of this regularization algorithm allows to reduce (3 to 5 times) the effects of measurement errors on the restoration of $N(z)$ from $R(z)$ and extend the altitude range by approximately 10 km. It should be added that the optimization of estimating $R(z)$ is achieved at the values of smoothing intervals ΔT of the order of 5 to 10 min.

Errors in the derived $N(z)$ profiles decrease from 50% to 30% when the integration time increases from 5 to 10 min, respectively. We have managed to obtain N profile in a $z \sim 75$ to 85 km altitude range; at greater and lower altitudes the signal-to-noise ratios are too small.

The results of modeling efforts are illustrated in Figures 1 and 2.

The authors have been supported by Science and Technology Center in Ukraine Grant No. 471.

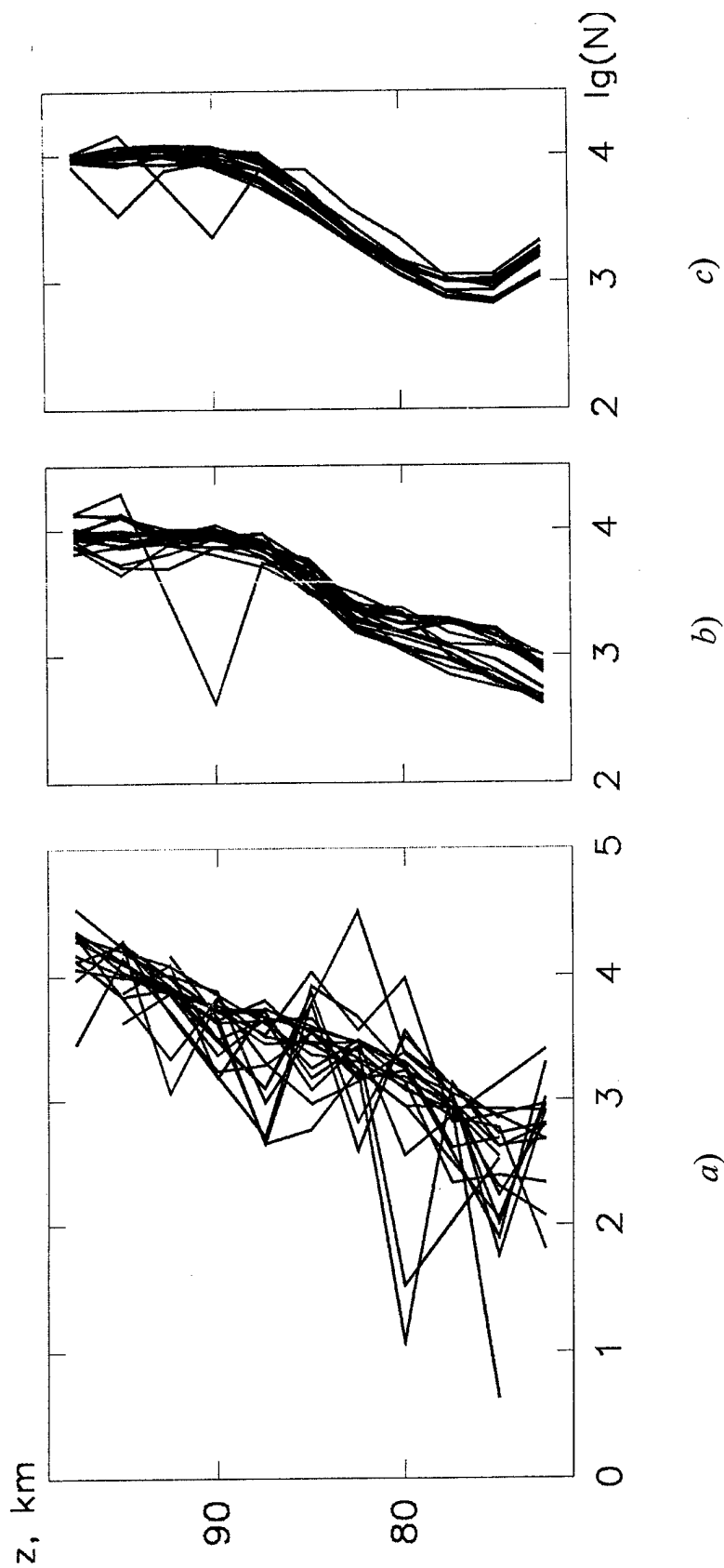


Figure 1. Sequence of 20 profiles $N(z)$ obtained in the vicinity of Nizhni Novgorod consecutively at 10:00 through 13:20 LT on March 2, 1991, in the 2.5 km height step and averaged over 10 min intervals: *a* - algorithm of numerical differentiation; *b* and *c* - regularization algorithm with different initial approximations.

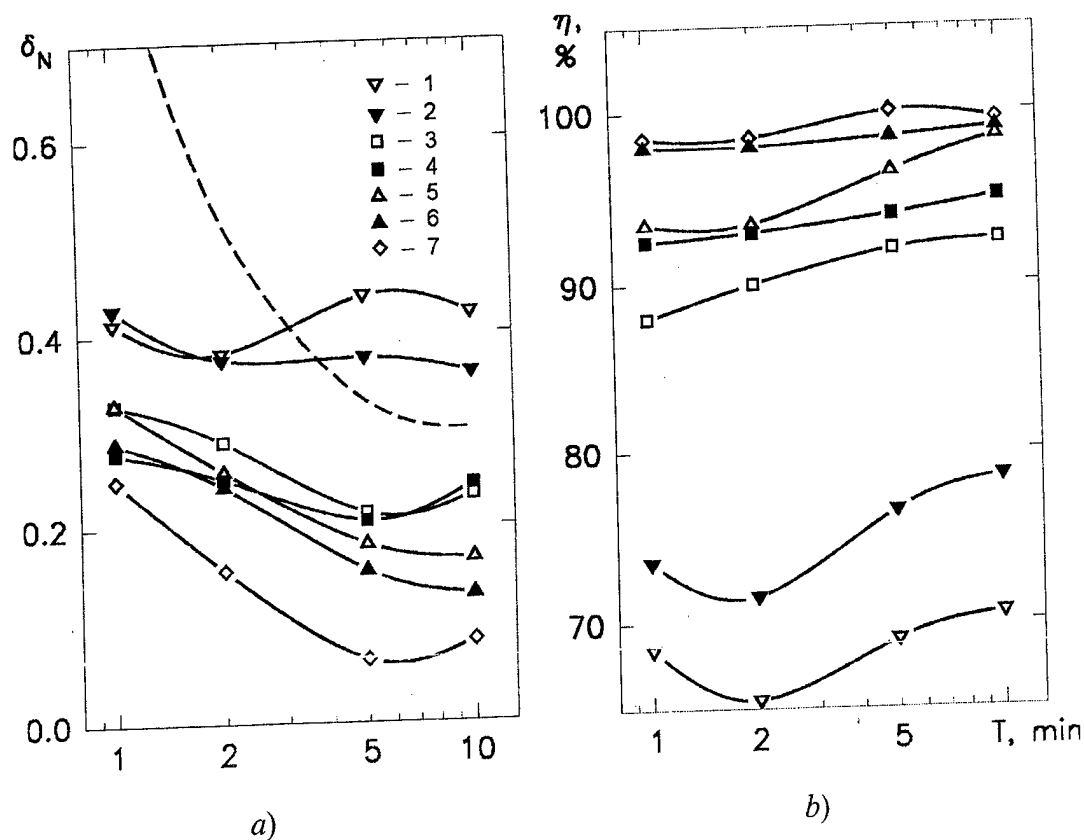


Figure 2. Dependences of errors and quality of the solution on the interval of averaging for different algorithms employed: *a* - relative root-mean square deviations in profiles $N(z)$; *b* - mean percentage of positive values of N in the profiles: 1, 2 - algorithm of numerical differentiation; 3, 4, 5 and 6 - regularization algorithm with different initial approximations; the light marks are for the 1.25 km height step, the dark marks and 7 are for the 2.5 km height step.

NUMERICAL TECHNIQUE FOR INVERSE PROBLEMS OF GEOMETRICAL OPTICS OF INHOMOGENEOUS MEDIA

V. A. Kaloshin, A. S. Venetsky

Institute of Radioengineering and Electronics, Russian Academy of Sciences
Moscow, Mohovaya 11, 103907, Russia
E-mail: vak@mail.cplire.ru

Abstract

The synthesis of inhomogeneous lenses, the problems of phase tomography of one-dimensional gradient media in geometrical optics approximation, etc., can be reduced to nonlinear integral equations relatively to an unknown function of the index of refraction [1]. These equations have closed-form solutions in a small number of particular cases. In this work, a new technique to solve these problems is proposed. According to this technique, we analyze a layered medium instead of inhomogeneous one. As a result, we have a stepped-law function of the index of refraction variation. It is possible to decrease a difference between the stepped and the continuous-law functions by increasing the number of layers. Three modifications of this technique: ray, phase and combined, are used to investigate inhomogeneous media where index of refraction is a function of a Cartesian coordinate or radius. Two latter of them provide a desired accuracy.

1. In the first case we analyze a medium with spherical symmetry. We suppose that it consists of m spherically uniform layers (Fig. 1). We know the phase front of the source of radiation (spherical one) and the phase front of the scattered field. Our problem is to determine the indices of refraction of the layers, n_i

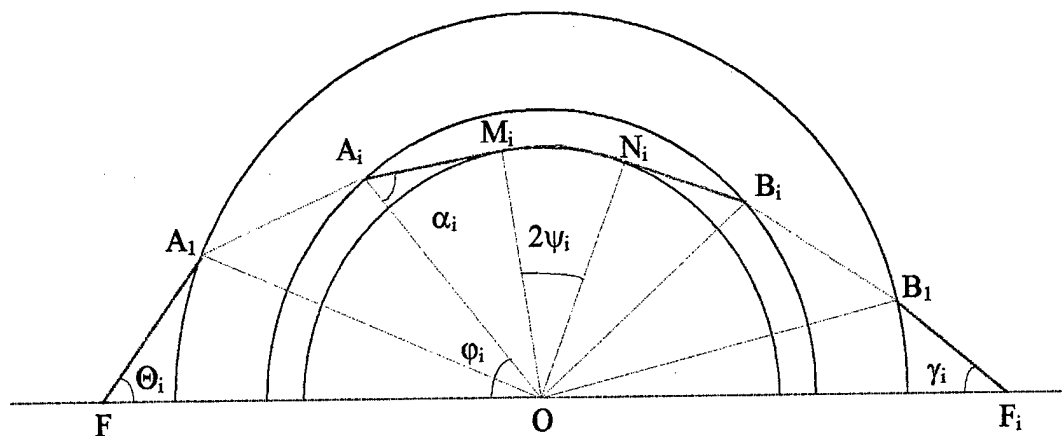


Fig. 1.

At the first step, we suppose that the indices of refraction and the widths of the 1, 2, ..., $i-1$ -st layers are known already. We shall trace the path of ray which comes out of the source at the angle $\Theta_i = \Theta_a - i\Delta\Theta$, where $\Theta_a = \arcsin(R_1/F)$, $\Delta\Theta = \Theta_a/m$, R_1 is the radius of the medium, F is the distance from the center of the medium to the source (Fig.1). After passing through the $i-1$ layers the ray gets to the i -th layer. We suppose that the ray touches the inner boundary of that layer, $R = R_{i+1}$, at the point M_i , slides along the boundary, and takes off it at the point N_i . The ray path in this case consists of three parts: two lines $A_i M_i$, $N_i B_i$ and the arc $M_i N_i$. The phase of the ray at the point B_i is:

$$\Phi(F, B_i) = |FA_i| + \Phi(A_i, A_i) + \Phi(B_i, B_i) + |A_i M_i| n_i + 2|OA_i| \sin \alpha_i n_i \psi_i + |N_i B_i| n_i$$

where $\Phi(A_i, A_i) = \Phi(B_i, B_i)$ are the optical distances.

From the law of refraction:

$$n_i \sin \alpha_i = n_{i-1} \sin \alpha_{i-1} = q,$$

and geometrical relations we can get the equation:

$$(1) \quad |FA_i| + 2\Phi(A_i, A_i) + 2R_i q (\operatorname{ctg} \alpha_i + \psi_i) = \Phi(F, B_i),$$

where $\alpha_i = 1/2\theta_i - 1/2\gamma_i + \varphi_i + \psi_i$, and γ_i can be found from the equation:

$$F \sin \theta_i = F_i \sin \gamma_i$$

On determining ψ_i from equation (1) by some numerical technique we obtain:

$$n_i = q / \sin \alpha_i, \quad R_{i+1} = R_i \sin \alpha_i$$

The same procedure can be used to determine n_1 , if the index of refraction in the outer space, n_0 , is known. Applying this procedure to find n_1, n_2, n_3, \dots , we obtain, as a result, a quasi-continuous law of the index of refraction variation relatively to n_0 .

2. Instead of a medium with the index of refraction being a function of some Cartesian coordinate, for example, $n = n(y)$, we shall analyze now a layered medium (Fig. 2).

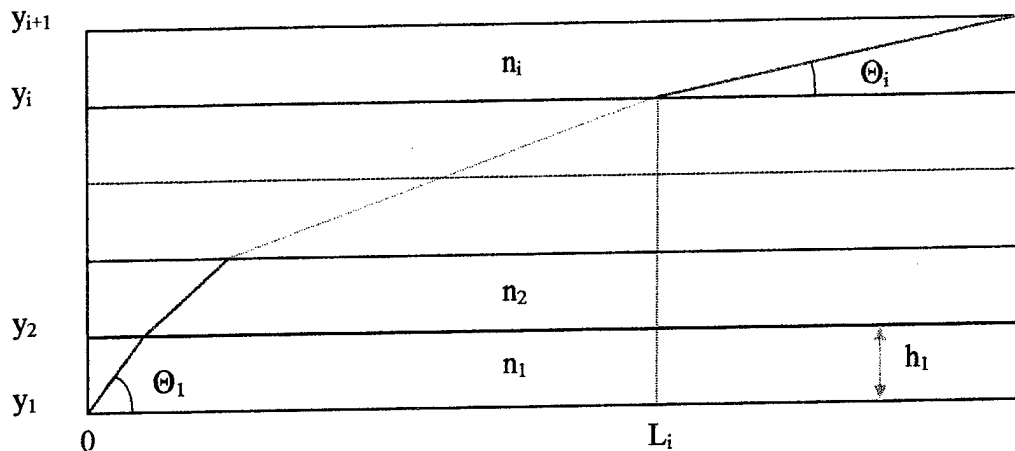


Fig. 2.

We suppose that $n(y)$ has an extremum and the indices of refraction and the widths of the $i-1$ layers are known, n_1 being the value of extremum. Tracing the ray which comes out of the source at the angle $\theta_1 = i\Delta\theta$, we can find the phase at the output point ($y_{i+1} = y_i + h_i$):

$$(2) \quad \Phi(y_{i+1}) = \sum_{j=1}^{i-1} \frac{h_j}{\sin \theta_j} n_j + \frac{(1-L_i)}{\cos \theta_i} n_i$$

Here h_j is the width of the j -th layer, n_j is the index of refraction, θ_j is the angle between the ray in the j -th layer and the X-axis, y_i and L_i are the coordinates of the entrance point of ray into the layer number i . We suppose that h_j, n_j, θ_j and y_j are known if $j < i$. Taking into account the law of refraction

$$(3) \quad n_i \cos \theta_i = n_{i-1} \cos \theta_{i-1} = \dots = n_1 \cos \theta_1 = q,$$

and the geometrical relations:

$$L_i = \sum_{j=1}^{i-1} h_j \operatorname{ctg} \theta_j$$

$$h_i = (1 - L_i) \operatorname{tg} \theta_i$$

we obtain that

$$(4) \quad A + (1 - L_i) / \cos^2 \theta_i = \Phi(y_i + h_i),$$

where

$$A = \sum_{j=1}^{i-1} \frac{h_j}{\sin \theta_j} n_j$$

Equation (4), relatively to θ_i , can be solved by any numerical technique. Using a linear approximation of the phase front:

$$\Phi(y_i + h_i) = \Phi(y_i) + k_i(1 - L_i) \operatorname{tg} \theta_i,$$

we can obtain the closed-form solution:

$$\operatorname{tg} \theta_i = \frac{1}{2p} (r + \sqrt{r^2 - 4p(p+C)})$$

where

$$p = (1 - L_i)q,$$

$$C = A - \Phi(y_i),$$

$$R = k_i(1 - L_i),$$

After that we have:

$$n_i = q / \cos \theta_i$$

$$h_i = (1 - L_i) \operatorname{tg} \theta_i$$

So, the parameters of the layer number i have been found. However we have to know the index of refraction of the first layer, n_1 , to start the iterations. Applying this procedure to finding n_2, n_3, \dots , we obtain eventually a quasi-continuous law of the index of refraction variation relatively to n_1 .

References

- [1] S. Cornbleet, *Microwave Optics*, Academic Press, 1976.

ON GROUNDING ONE CLASS OF NONLINEAR INVERSE PROBLEMS OF MATHEMATICAL PHYSICS

Volodymyr Anokhin*, Petro Savenko**

* State University "L'vivs'ka politekhnika". St. Bandery St., 12, L'viv, Ukraine

** Pidstryhach Institute of Applied Problems of Mechanics and Mathematics of Ukrainian National Academy of Sciences, Naukova St. 3-b, 290601, L'viv, Ukraine, e-mail: kalyniak@ippmm.lviv.ua

The theorems, that ground the statements and numerical methods for solutions of the synthesis problem of the plane aperture shape and amplitude-phase distribution of the field in the aperture for a given power pattern are presented. It is known [1], that the vector directivity pattern $\vec{f}(Q)$ of the plane aperture D , which is outlined by a continuous function $\rho(\psi)$, $\psi \in [0; 2\pi)$ is given as $\vec{f} = f_x \vec{i}_x + f_y \vec{i}_y = A(\rho, I_x) \vec{i}_x + A(\rho, I_y) \vec{i}_y$, where $(I_x(P), I_y(P))^T \in L^2(D) \times L^2(D)$ are the components of distribution of electromagnetic field in the aperture,

$$A(\rho, I_v) = \int_0^{2\pi} \int_0^{\rho(\psi)} I_v(r, \psi) \exp[-ik(Q, P)] dP, \quad v=x, y. \quad (1)$$

The inverse problem - the problem of synthesis - consists in approximation of components of the given real vector function, i.e. a power pattern $\vec{F} = (F_x, F_y)^T \in L^2(R^2) \times L^2(R^2)$, by the magnitude of the synthesis directivity pattern. The variational statement of the problem considers:

$$\sigma(I_x, I_y, \rho) = \sum_{v=x, y} \|F_v - |A_v \vec{u}|\|_{L^2(R^2)}^2 + \frac{\gamma}{2} \|\rho\|_{L^2(D)}^2, \quad (2)$$

where the last addition provides the minimum of the area of the aperture. Iteration process of numerical minimization of the functional (2) is based on the method, which is analogous to the coordinate descent method. Let (I_x^0, I_y^0, ρ^0) be a point of initial approximation, which is located in a certain area of the minimum point (I_x^*, I_y^*, ρ^*) . We'll find a function $\rho_0(\psi)$, which describes the outline of initial aperture D^0 . Let's consider the narrowing of functional (2):

$$\tilde{\sigma}(I_x, I_y) \equiv \sigma(I_x, I_y, \rho^0). \quad (3)$$

Theorem 1. Let F_x, F_y be the positive functions, that are continuous on the limited area Ω and are equal to zero outside it. Then the functional (3) arrives at the minimum value on a certain element of $L^2(D) \times L^2(D)$.

The necessary condition of the functional minimum leads to the Euler equation with regard to both functions I_x and I_y :

$$I_v(P) = \left(\frac{k}{2\pi}\right)^2 \iint_{\Omega} F_v(Q) \exp[i \arg f_v(Q)] \exp[-ik(Q, P)] dQ, \quad v=x, y. \quad (4)$$

The unknown functions I_x and I_y enter the right part of the equation (4) through the definitions of functions $f_v = A(\rho, I_v)$. After substitution (4) to (1) and non-complicated transformations the equations concerning the synthesized directivity pattern are obtained:

$$f_v(Q) = B(f_v(Q)) \equiv \left(\frac{k}{2\pi}\right)^2 \iint_{\Omega} F_v(Q') K(Q, Q', k) \exp[i \arg f_v(Q')] dQ', \quad v = x, y, \quad (5)$$

where $K(Q, Q', k)$ is a kernel. It should be noticed, that equations (5) are independent.

The solutions of equations (5) has been found on the basis of successive approximations method:

$$f_v^{(n+1)}(Q) = B(f_v^{(n)}(Q)) \quad v = x, y, \quad n = 0, 1, 2, \dots \quad (6)$$

Theorem 2. *The numerical sequence of the values of the functional (3) is convergent on the steps of the iterative process (6).*

Now we'll fix the functions I_x^1 and I_y^1 , which are obtained after substitution of solutions of equation (5) into the formula (4). Let's consider the narrowing of functional (2):

$$\tilde{\sigma}(\rho) \equiv \sigma(I_x^1, I_y^1, \rho). \quad (7)$$

Theorem 3. *Let F_x, F_y be the positive functions, which are continuous on the limited area Ω and are equal to zero outside it. Then the functional (7) arrives at the minimum value on a certain element of $L^2[0; 2\pi)$ when $\gamma > 0$.*

The necessary conditions of the functional minimum leads to the nonlinear integral equation:

$$G(\rho) \equiv \sum_{v=x,y} |I_v(\rho(\psi), \psi)|^2 - \gamma \left(\frac{k}{2\pi}\right)^2 = 0. \quad (8)$$

Equation (8) has a simple geometrical interpretation. The solution of this equation is the projection of the level lines $\gamma \left(\frac{k}{2\pi}\right)^2$ of the function $\sum_{v=x,y} |I_v(\rho(\psi), \psi)|^2$ on XOY plane.

The solution of the equation (8) has been found on the basis of Newton-Kantorovich method:

$$G'(\rho_k) \Delta \rho_k = -G(\rho_k), \quad (9)$$

$$\rho_{k+1}(\psi) = \rho_k(\psi) + \Delta \rho_k(\psi), \quad k = 0, 1, 2, 3, \dots,$$

where G' is the Freshet derivative of G operator. The theorem of convergence of iterative process (9) in the sense of convergence of numerical sequence of functional (7) values on the steps of proposed iterative processes are proved.

If we'll continue the successive minimization of the functional (2) with regard to (I_x, I_y) and ρ when the solutions of the previous iterative processes are fixed, we'll arrive at the minimum point (I_x^*, I_y^*, ρ^*) .

The numerical examples of synthesis of contour directivity pattern of complicated forms are presented. The given power pattern is shown in Fig. 1 and Fig. 2 by solid line. The level of the necessary radiation is equal to 1 inside this contour and it's equal to 0 outside it. The synthesized amplitude directivity pattern of the fixed circle non-optimal aperture is shown in Fig. 1. Synthesized amplitude directivity pattern after optimization of the shape of the aperture is presented in Fig. 2. It should be noticed that the square of the optimal aperture (Fig. 3, regular line) is equal to square of the circle aperture (Fig. 3, solid line). Amplitude of the field distribution on the optimal aperture is presented in Fig. 4.

Finally we shall notice, that the given approach can be used for grounding the convergence and for building the iterative methods for solution of a system

of potential integral equations with the unknown function on the limit of integration.

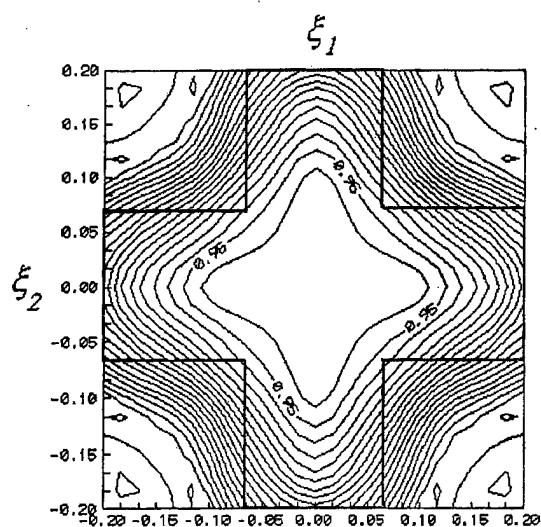


Fig. 1

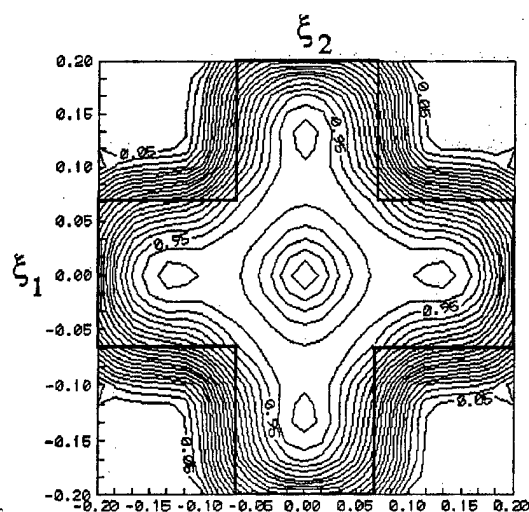


Fig. 2

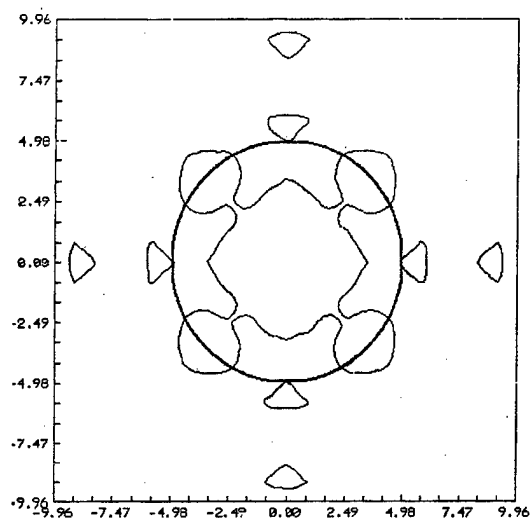


Fig. 3

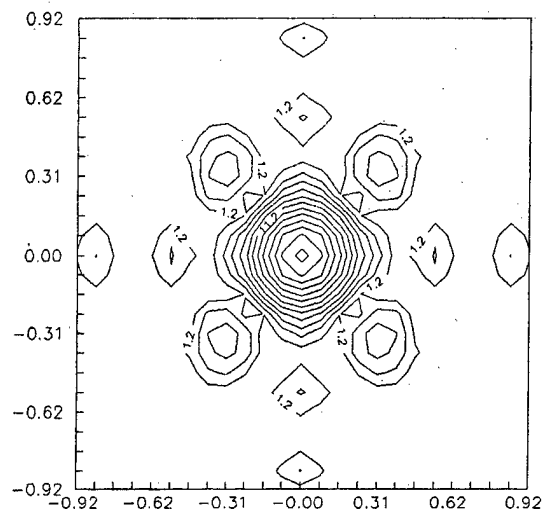


Fig. 4

Reference

1. Zelkin E. G., Sokolov V. G. The methods of the antennas synthesis .- M. Sov. radio, 1980 - 250p.

IMPROVED ALGORITHM BASED ON RYTOV APPROXIMATION FOR THREE-DIMENSIONAL STRUCTURE DETERMINATION OF BIOLOGICAL OBJECTS

C. Kechribaris, K. S. Nikita and N. K. Uzunoglu
 Department of Electrical and Computer Engineering
 National Technical University of Athens
 9, Iroon Polytechniou str., 15773 Athens – Greece
 E-mail: knikita@cc.ece.ntua.gr

An inverse scattering formulation is developed for large size - low contrast dielectric objects, based on Rytov approximation and optimization techniques for three dimensional (3D) scalar waves, providing an efficient solution to the diffraction tomography problem associated with the imaging of soft tissues in biomedical engineering applications. The developed algorithm is based on the following assumptions:

a) The unknown object function $o(\underline{r}') = n^2(\underline{r}') - 1$, where $n(\underline{r})$ is the diffraction index of the object to be imaged, is described in terms of superposition of Gaussian pulses placed on a rectangular grid array with unknown weighting coefficients a_i to be determined as follows:

$$o(\underline{r}') = \sum_{i=1}^N a_i \exp(-p^2 |\underline{r} - \underline{r}'|^2) \quad (1)$$

where p is a constant, depending on the grid cell size.

b) A Rytov type approximation to describe the field $\Psi(\underline{r})$ inside the scatterer is adopted, leading into an analytic expression,

$$\Psi(\underline{r}) = \Psi_0(\underline{r}) \exp \left[jk_0^2 \Psi_0^{-1}(\underline{r}) \int_{V_s} G(\underline{r}/\underline{r}') o(\underline{r}') \Psi_0(\underline{r}') d\underline{r}' \right] \quad (2)$$

where $\Psi_0(\underline{r})$ is the incident wave exciting the scatterer, $G(\underline{r}/\underline{r}')$ the free space Green's function and k_0 the propagation constant of the infinite medium surrounding the scatterer to be imaged. The integral in eq. (2) is computed over the scatterer volume.

Following the above assumptions, the scattering amplitude $F(\hat{s})$ measured along the \hat{s} unit vector direction, for an incident plane wave impinging from the \hat{s}_0 direction is computed using the well known relation,

$$F(\hat{s}) = C_0 \int_{V_s} e^{jk_0 \hat{s} \cdot \underline{r}'} o(\underline{r}') \Psi(\underline{r}') d\underline{r}' \quad (3)$$

where C_0 is a constant. On substituting eq. (1), (2) into (3), after a series of analytical manipulations, the $F(\hat{s})$ scattering amplitude is described in terms of the unknown coefficients a_i (see eq. (1)) in the following form,

$$F(\hat{s}) = \sum_{i=1}^N a_i \Phi(a_i, \hat{s}_0, \hat{s}) \quad (4)$$

where Φ is a non - linear function of the a_i coefficients.

In order to determine the a_i coefficients, an experimental system has been set up. The object to be imaged is immersed in a water tank and is interrogated by an appropriate transmitter with a series of incident waves from various directions. The scattering amplitude is measured at different positions of a receiver and at every view of the object. The receiver is scanned by stepping motors, controlled by a PC. The components of the complex wave field are detected, amplified, filtered and stored in the same PC. The unknown object function of eq.(1) is determined by solving the non-linear optimization problem,

$$\min_{a_i} \|F(\hat{s}) - F_{measured}\| \quad (5)$$

for $\hat{s} = \hat{s}_1, \hat{s}_2, \dots, \hat{s}_N$

and $\hat{s}_0 = \hat{s}_{01}, \hat{s}_{02}, \dots, \hat{s}_{0M}$

In equation (5), $F_{measured}$, $F(\hat{s})$ denote the experimental and the estimated, as given by equation (4), values of the scattering amplitude, respectively.

QUASI-OPTICAL DIFFRACTION TOMOGRAPHY

A. A. Vertiy ^{(1),(2),(3)}, S.P. Gavrilov ^{(1),(2),(3)}, I. V. Voinovskiy ⁽³⁾,
V. N. Stepanuyk ⁽³⁾

1. TÜBITAK -M.R.C. , Turkish- Ukrainian Joint Research Laboratory,
P.K. 21, 41470, Gebze- Kocaeli, Turkey,
phone: 90(262)6412300, e-mail: alex@mam.gov.tr
2. IRE, National Academy of Science of Ukraine, 12 Acad. Proskura St.,
Kharkov, Ukraine.
3. State Research Center " Fonon " , 37 Pobedy Ave., 252056, Kiev,
Ukraine.

ABSTRACT

Tomographical methods of image reconstruction of two-dimensional cross-sections of volumetric objects in millimeter wavelengths band are suggested and considered. Experimental images obtained using antennas of dielectric type and radiation frequency $f \approx 136\text{GHz}$ are represented. Volumetric dielectric objects have been taken as objects under investigation.

It is shown that in the frequency band under consideration, the images of investigated objects with characteristic dimension $A \approx 7\lambda \div 15\lambda$ may be obtained by first-order diffraction tomography method (Born, Rytov or high frequency approximation of the first-order for scattered electromagnetic field).

1. INTRODUCTION

There is a large number of publications on applied and theoretical tomography. In the case of UHF radiowaves, for instance, microwaves, important problems of nondestructive testing of materials and industrial products, surface and subsurface sensing, receiving of microwave images of inhomogeneous bodies in medicine and others may be solved.

To receive quasioptic tomographic image in the case of diffraction (scattering of electromagnetic wave by a sample), methods of diffraction tomography may be used. If the object weakly scatters the electromagnetic wave and the scattered field is described by Born or Rytov approximations of the first order [1,2], Fourier diffraction project theorem is employed.

In the present paper methods of the first-order diffraction tomography are considered.

2. OBTAINING IMAGES BY FIRST-ORDER DIFFRACTION TOMOGRAPHY

The basic equation of the diffraction tomography may be obtained as a result of solution of an inverse problem of scattering of a plane electromagnetic wave on the object under investigation [1,2]. We consider a scattering object characterizing by refractive index $n(\vec{r}) = 1 + f(\vec{r})$, where f is equal to zero outside the refracting object. A plane harmonic $\exp(-i\omega t)$ wave $U_I(\vec{r}) = \exp[ik(\vec{\theta} \cdot \vec{r})]$ incidents on the object; $\vec{\theta}$ is a unit vector pointing the direction of the wave propagation; $k = \omega/c$; ω is radiation frequency; c is light velocity. In the case of direct scattering, the total field $U = U_I + U_S$ (where $U_S(\vec{r})$ is a scattered wave) satisfies the given wave equation

$$\Delta u + k^2 (1 + f)^2 u = 0 \quad (1)$$

and the boundary condition in infinity. The scattered field U_S may be found using equation (1) in the first-order Born approximation. Equation (1) may be also solved in the framework of Rytov approximation of the first order. In inverse scattering problem, function f should be found with known scattered field U_S . Solution of such

problem allows us to obtain the main equation of diffraction tomography [1]. After that we may find functions $f(\vec{r})$.

Let the incident wave propagate along a positive direction of η axis of the rectangular Cartesian coordinate system ξ, η where measurements of phase and amplitude of electromagnetic fields U, U_I and straight line $\eta = \text{const} > OB$ are carried out. Let the center of another rectangular Cartesian coordinate system x, y connected with the investigated object coaxed with the center of ξ, η coordinate system and with the center of circle O with radius OB. The investigated object is characterized by function $f(\vec{r})$ which is different from zero in a certain region inside circle O. Then by rotating the ξ, η coordinate system relatively x, y coordinate system and using measured data of U and U_I , Fourier image of function in frequency domain in circle with radius not less than k may be found. Analogous result may be obtained, if system of data collection remains immovable and the object under investigation is rotating relatively the center O (Fig.1) and, hence, x, y coordinate system rotates relatively ξ, η coordinate system.

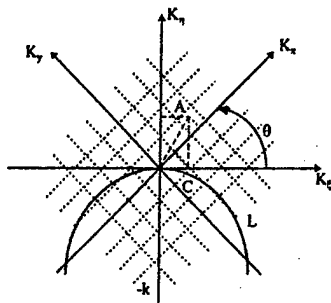


Fig.1. Finding of Fourier image of the object function.

From Fig.1 one can see that, by changing the angle θ , it is possible to find positions when each of the pointed points will be located on circle L at values $K_x \geq 0$ of vector \vec{K}_C projection on axis K_x . If we will know the values of K_x and angle θ we will be able to calculate Fourier image of the object.

3. EXPERIMENTAL SET-UP AND RECONSTRUCTION

Millimeter wave tomography set up^(*) allowing to measure phase and amplitude of U and U_I fields at straight line $\eta = \text{const}$ in ξ, η coordinate system is shown in Fig. 2. Signal from oscillator 1 with operating frequency 136 GHz is divided by directional branch into two signals. One of these signals is given to up-converter 2, and the other to down-converter 8. Signal from reference generator 10 with frequency 160 Hz is also supplied to up-converter 2. As a result a signal radiated by antenna 3 which is represented by an end of a dielectric waveguide (electric vector \vec{E} of the wave is directed along straight line 6) is shifted up by frequency at 160 Hz relatively to operating frequency of oscillator 1. Sample 5 may be rotated round its axis and move along straight line 6 (step motors are used to move and rotate). The signal received by antenna 7 in the absence of the sample is given to down-converter 8.

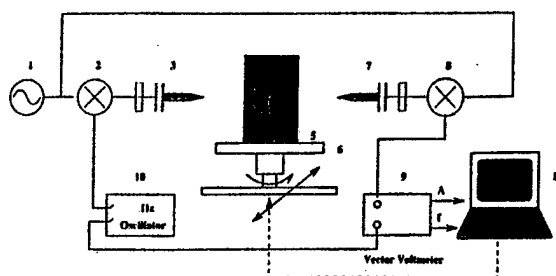


Fig.2. Scheme of tomograph with dielectric antennas.

The signal from the operating oscillator 1 is given to the same down-converter, with the result that signal at the output of device 8 is shifted "down" and its frequency 160 Hz. This signal is fed then to vector voltmeter 9. A signal from generator 10 of frequency 160 Hz is supplied to the same voltmeter. Amplitude A and phase Φ measured by vector voltmeter 9 are taken to be equal to amplitude and phase of the incident field U_I at straight line 6. Analogue signals corresponding to the measured amplitude and phase of the field U_I are given then to system 11 of processing and obtaining of image which also manages the stepping motors.

In this case when an object weakly scatters an incident wave and Rytov or Born approximations for scattering field, the measured signal will correspond to the total field U received by antenna 7 in line 6. As this takes place, U_I measured in the straight line 6 is substituted into formula for the diffraction tomography equation instead of plane wave field e^{ink} in the straight line $\eta = \text{const}$ at $0 \leq \theta \leq 2\pi$; $\Delta\theta = \pi/6$. All measurements were carried out at $\eta \approx 7.9\lambda$.

Fig. 3-4 shown images of $|Q(\vec{r})|$ cross sections of the objects under experimental investigations: Fig.3- cylinders with approximately circle cross-section manufactured from a paper and having the following dimensions: height $h = 20\lambda$ ($\lambda \approx 2$ mm); diameter $D = 12.5\lambda$. The thickness of the wall is $t = 0.05\lambda$. Fig.4 shows the same cylinder but it has two slots (12 and 7 mm) in the wall

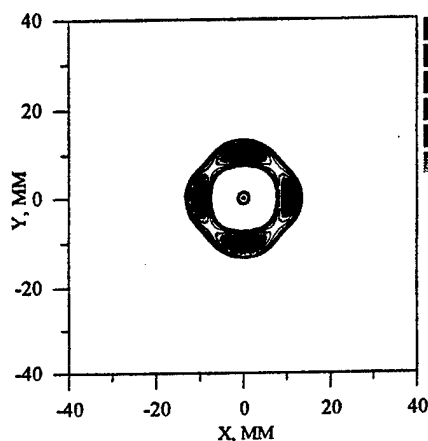


Fig. 3.

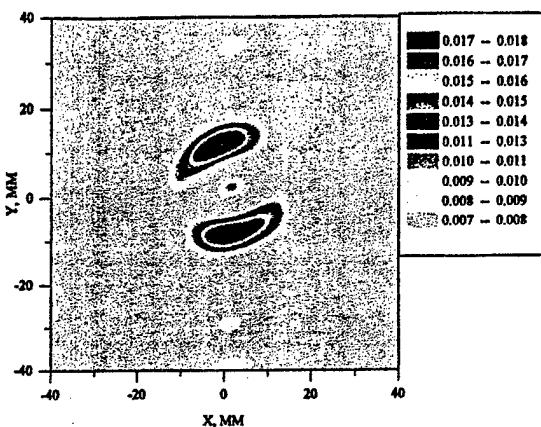


Fig. 4.

Fig. 3-4. Images of cross sections of the objects under experimental investigations.

5. CONCLUSION

Thus, an image is a reconstructed distribution function in the region of investigated cross-section of the object of one of its electrodynamical parameters. The images are obtained using methods of first-order diffraction tomography for weakly scattering objects having a simple structure. Reconstruction of images has shown that at millimeter waves the high frequency approximation in the basic equation of diffraction tomography may be assumed.

The investigations carried out have showed that there are difficulties when reconstructing the object images with complicated structure (several short-range located inhomogeneities in the object). In this case, there may be observed a multi-scattering and the methods of first-order diffraction tomography do not allow to reconstruct the function to be found sufficiently accurately.

REFERENCES

1. F. Natterer. The Mathematics of computerized tomography. - M.: Mir, 1990. - 288p., (in Russian).
2. Malcolm Slaney, Avinash C. Kak, and Lawrence E. Larsen. Limitations of Imaging with First- Order Diffraction Tomography. - IEEE Transactions on Microwave Theory and Techniques, vol. MTT-32, № 8, p.p. 860-874, 1984.

(*) Components have been represented by Quasi-Optical Dept. of IRE NASU, Kharkov, Ukraine.

SOLUTION OF INVERSE PROBLEM FOR A CHARGE COMBINED WITH A POINT-LIKE DIPOLE

V. Ya. Epp and T. G. Mitrofanova

Tomsk Pedagogical University, Tomsk, Russia; e-mail: epp@tspi.tomsk.su

The inverse problems in electrodynamics are not sufficiently advanced from our point of view though they are of certain theoretical interest and practical implementation. Inverse problem of radiation of a relativistic charged particle has been solved in [1-3]. Here we propose a particular inverse problem of electrostatics.

It is well known that the field induced by electric charge arbitrary distributed within a finite area is in the far-field approximation equal to the field of a point-like charge and dipole momentum. Calculation of the field produced by a given charge or dipole momentum is referred to as a direct problem. The inverse problem solved in this paper is as follows. Suppose we know that some electric field is generated by a distant point-like charge combined with an electric dipole momentum. The problem is to restore the position and the value of charge and dipole momentum. It is evident that the knowledge of three components of the electric field \vec{E} is not enough to find seven unknown quantities: position of the charge and momentum \vec{r} , vector of dipole momentum \vec{d} and the value of the charge e . Thus, we assume that we know the electric field vector \vec{E} and a three-dimensional tensor of first derivatives $E_{ij} = \partial E_i / \partial x_j$. It follows from the Maxwell equations that $\text{rot} \vec{E} = 0$ and $\text{div} \vec{E} = 0$, which yields $E_{ij} = E_{ji}$ and $E_{11} + E_{22} + E_{33} = 0$, respectively. Hence, only five independent components of E_{ij} remain. Besides, the considered field is axially symmetric. In cylindrical coordinate system ρ, ϕ, z we have three additional conditions: $E_\phi = 0$, $\partial E_\rho / \partial \phi = \partial E_z / \partial \phi = 0$ leaving five independent unknown quantities: two components of \vec{E} and three components of E_{ij} .

Let the origin of a Cartesian coordinate system x', y', z' be at the point where the vector $\vec{E} = (E'_x, E'_y, E'_z)$ and tensor E'_{ij} are known. It is convenient to use a special coordinate system x, y, z which we define as follows: the axis x is directed along the vector \vec{E} , the axis y along the principal normal and the axis z along the binormal to the field line. The principal normal \vec{n} is given by the equation [4]:

$$\vec{n} = \frac{1}{kE} \frac{\partial \vec{E}}{\partial s},$$

where $E = |\vec{E}|$, k is the principal curvature of the field line, and s is the coordinate along the line. After simple algebra we derive the normal \vec{n} and binormal \vec{b} :

$$\vec{n} = \frac{1}{kE^4} [\vec{E} \times [\vec{D} \times \vec{E}]], \quad \vec{b} = \frac{1}{kE^3} [\vec{E} \times \vec{D}], \quad (1)$$

where $\vec{D} = (\vec{E} \nabla) \vec{E}$, $D'_i = E'_j E'_{ji}$ and $k^2 = [\vec{E} \times \vec{D}]^2 / E^6$. Now we transform the vector $\vec{E} = (E'_x, E'_y, E'_z)$ and tensor E'_{ij} into the new coordinate system in a standard way

$$E_i = \alpha_{ik} E'_k, \quad E_{ij} = \alpha_{ik} \alpha_{js} E'_{ks}, \quad (2)$$

where the transformation matrix α_{ik} can be found from (1):

$$\alpha_{1k} = \delta_{1k}, \quad \alpha_{2k} = \frac{1}{kE^4} E_k E_j (E_j E_{ik} - E_i E_{kj}), \quad \alpha_{3k} = \frac{1}{kE^3} \epsilon_{klm} E_l D_m, \quad (3)$$

δ_{ik} is the Kronecker symbol. The result looks like follows

$$\vec{E} = (E, 0, 0), \quad E_{ij} = \begin{pmatrix} E_{11} & E_{12} & 0 \\ E_{21} & E_{22} & 0 \\ 0 & 0 & E_{33} \end{pmatrix}. \quad (4)$$

In particular, $E_{12} = k = E^{-3} \sqrt{E^2 D^2 - (E'_i D'_i)^2}$.

We consider only those points of the field where $k \neq 0$. Now let us proceed to the solution of the problem. The field of a charge and dipole momentum is (see [5]):

$$\vec{E} = \frac{e\vec{R}}{R^3} + \frac{3(\vec{R}\vec{d})\vec{R} - R^2\vec{d}}{R^5} \quad (5)$$

with \vec{R} being the vector from the charge to the point where the field is determined. Taking the derivatives we obtain

$$E_{ij} = \frac{\partial E_i}{\partial x_j} = \delta_{ij} \left[\frac{e}{R^3} + 3 \frac{\vec{R}\vec{d}}{R^5} \right] + 3 \frac{d_j R_i + d_i R_j}{R^5} - 3 R_i R_j \left[\frac{e}{R^5} + 5 \frac{\vec{R}\vec{d}}{R^7} \right]. \quad (6)$$

In the coordinate system x, y, z we replace $\vec{R} = -\vec{r} = -(x, y, 0)$ and $\vec{d} = (d_x, d_y, 0)$. Then (1), (2) take the form

$$E = -\frac{ex}{r^3} + \frac{3(\vec{r}\vec{d})x - r^2 d_x}{r^5}, \quad 0 = -\frac{ey}{r^3} + \frac{3(\vec{r}\vec{d})y - r^2 d_y}{r^5}, \quad (7)$$

$$E_{11} = \frac{e}{r^3} - 3 \frac{(\vec{r}\vec{d})}{r^5} - 6 \frac{d_x x}{r^5} - 3x^2 \left[\frac{e}{r^5} - 5 \frac{(\vec{r}\vec{d})}{r^7} \right], \quad (8)$$

$$E_{12} = -3 \frac{d_x y + d_y x}{r^5} - 3xy \left[\frac{e}{r^5} - 5 \frac{(\vec{r}\vec{d})}{r^7} \right], \quad E_{33} = \frac{e}{r^3} - 3 \frac{(\vec{r}\vec{d})}{r^5}. \quad (9)$$

We have got five equations for five unknown quantities: x, y, d_x, d_y, e . First we use (7) and the last of (9) to find the value of the charge and dipole momentum

$$d_x = -r^3(E + E_{33}x), \quad d_y = -r^3 y E_{33}, \quad e = -2r^3 E_{33} - 3xrE. \quad (10)$$

Substituting this into (8) and the first of (9), we obtain

$$\begin{aligned} x^2(2E_{33} + E_{11}) + y^2(E_{33} - E_{11}) + 2yx E_{12} &= 0, \\ -xy(E_{33} + 2E_{11}) - y^2 E_{12} + x^2 E_{12} + 3yE &= 0. \end{aligned} \quad (11)$$

This set of quadratic equations has the following solution:

$$x = \frac{3E}{4E_{12}^2 + F_3^2} \left[F_3 \pm \frac{E_{12}(F_1 - F_2)}{S} \right], \quad y = \frac{3E}{4E_{12}^2 + F_3^2} \left[2E_{12} \pm \frac{2E_{12}^2 - F_1 F_3}{S} \right], \quad (12)$$

where $F_1 = E_{22} - E_{33}$, $F_2 = E_{33} - E_{11}$, $F_3 = E_{11} - E_{22}$, $S = \sqrt{E_{12}^2 + F_1 F_2}$. Substitution of (12) into (10) yields the value of the charge and dipole momentum. We see that (7) - (9) have two different solutions. It means that the same field with its derivatives can be created by two different sources. Now the solution of the problem can be easily transformed back into the original coordinate system by means of the inverse to (2) transformations.

References

1. V.G. Bagrov, M.M. Nikitin, N.I. Fedosov, and V.Ya. Epp, *Radiophysisc Quantum Electronics*, **27**, 1984, p. 1287.
2. V.G. Bagrov, M.M. Nikitin, N.I. Fedosov, V.F. Zalmez and V.Ya. Epp, *Nucl. Instr. and Meth.*, **A239**, 1985, p. 579.
- 3 E.G. Bessonov, Preprint N. 162, Lebedev Physics Institute, Moscow, 1988 (in Russian).
4. G. Korn and T. Korn, *Mathematical Handbook*, McGraw-Hill, N.Y., 1968.
5. L.D. Landau and E.M. Lifshitz, *The Classical Theory of Fields*, Pergamon, Oxford, 1980.

***Gratings and
Frequency-Selective
Surfaces***

VALIDITY OF APPROXIMATE BOUNDARY CONDITIONS FOR PERIODIC STRIPS ON CYLINDRICAL SUBSTRATES

Zvonimir Sipus, Radovan Zentner and Juraj Bartolic
Faculty of Electrical Engineering and Computing
University of Zagreb
Unska 3, HR-10000 Zagreb, Croatia

Abstract

The strip gratings on dielectric cylinders are analyzed by using two types of approximate boundary conditions and by the moment method (MoM). The used approximate boundary conditions are the boundary conditions obtained by the homogenization method (BCHM), where the local planar approximation was applied, and the asymptotic strip boundary conditions (ASBC). The results show that the both approximate boundary conditions give good results when the period of the strips is small compared to the wavelength. However, BCHM gives more accurate results, and practically there is no difference between the MoM results and the results obtained by BCHM method if the periodicity is small enough. Furthermore, the ASBC cannot predict the coupling of the incident wave to the waveguide modes of the strip-loaded dielectric cylinder, which is predicted both by the MoM and the BCHM methods. The numerical results are also compared to measurements showing a very good agreement.

Introduction: Strip gratings are well known for their polarization properties. Incident waves with the electric field parallel to the strips are mainly reflected, and waves with the electric field orthogonal to the strips mainly pass through the grating. In the present paper we analyze strip gratings located on the dielectric cylinder (Fig. 1). The analysis can be easily extended for strips located between any two layers inside cylindrical multilayer structures.

Analysis: We have performed accurate analysis of periodic strips inside a multilayer structure by expanding the currents on the strips in basis functions, and the amplitudes of the basis functions are determined numerically by the moment method (MoM) [1]. The electromagnetic field is in the form of Floquet modes due to the periodicity of the structure. It is sufficient to determine the current on one strip, since the currents on the other strips are identical except for a phase difference.

If the source excites a full spectrum of plane or cylindrical waves, such as a dipole, the Floquet-mode expansion/MoM is a laborious process. A simpler approach is to use approximate boundary conditions. We have used two types of approximate boundary conditions: the asymptotic strip boundary conditions (ASBC) [2], [3] which in the planar case correspond to modeling the strips as a unidirectional conducting screen [4], and boundary conditions obtained by the homogenization method (BCHM), i.e. by averaging the fields of the fundamental Floquet mode [5].

In the BCHM case we have used a local planar approximation, that means we suppose that the surface where the strips are located is locally a plane surface. By this we can easily transform the boundary conditions from the rectangular coordinate system [5] to the cylindrical one. For example, for φ -directed strips we have

$$E_{\phi}^{+} = E_{\phi}^{-}, \quad E_z^{+} = E_z^{-}, \quad (1)$$

$$E_{\phi} = -\frac{l_e}{2} \left[j\omega \frac{2\mu^{+}\mu^{-}}{\mu^{+} + \mu^{-}} (H_z^{+} - H_z^{-}) - \frac{2}{\varepsilon^{+} + \varepsilon^{-}} \frac{1}{\rho} \frac{\partial}{\partial \phi} (\varepsilon^{+} E_{\rho}^{+} - \varepsilon^{-} E_{\rho}^{-}) \right] \quad (2)$$

$$H_{\phi}^{+} - H_{\phi}^{-} = 2l_h \left[j\omega \frac{\epsilon^{+} + \epsilon^{-}}{2} E_z + \frac{\mu^{+} + \mu^{-}}{2\mu^{+}\mu^{-}} \frac{1}{\rho} \frac{\partial B_{\rho}}{\partial \phi} \right] \quad (3)$$

where superscripts + and - denote the E- and H-fields and permittivity/permeability above and below the strips, respectively. Parameters l_e and l_h are defined by

$$l_e = \frac{P}{\pi} \ln \csc \frac{\pi W}{2P}, \quad l_h = \frac{P}{\pi} \ln \sec \frac{\pi W}{2P}, \quad (4)$$

where P and W are the periodicity and the width of the strips (Fig. 1).

The ASBC are more general, and they do not depend on the geometry. Theoretically, the surface with the strips can be of any shape, and the strips can be nonperiodical provided that the distance between strips is small enough. For φ -directed strips the ASBC are

$$E_{\phi}^{+} = 0, \quad E_{\phi}^{-} = 0, \quad (5)$$

$$E_z^{+} = E_z^{-}, \quad H_{\phi}^{+} = H_{\phi}^{-}. \quad (6)$$

Note that the ASBC can be obtained from BCHM by letting $P \rightarrow 0$ and by keeping the ratio P/W constant.

Results: Fig. 2 shows the calculated scattered field from the dielectric cylinder loaded with periodic circumferential strips. The results are obtained by the MoM (accurate results), and by the ASBC and the BCHM methods. The radius and the relative permittivity of the cylinder are $\rho = 1.2$ cm and $\epsilon_r = 2.1$. The frequency is 10 GHz, and the periodicity and the width of the strips are $P = 0.8$ cm and $W = 0.3$ cm, i.e. $0.27 \lambda_0$ and $0.1 \lambda_0$, respectively. The incident wave is TM_z polarized, and angle of incidence is $\theta = 90^\circ$ (normal incidence). The shown scattered field is normalized to $E_i \sqrt{2j / \pi k \rho} \exp(-jk\rho)$. Both ASBC and BCHM results show a good agreement with MoM results. However, the BCHM method is more accurate and practically there is no difference between MoM and BCHM results.

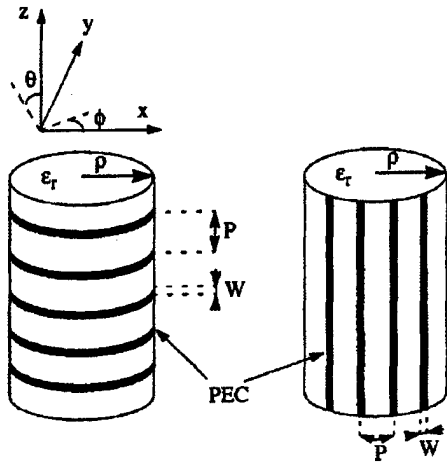


Figure 1. Geometry and coordinates of strip grids on dielectric cylinder.

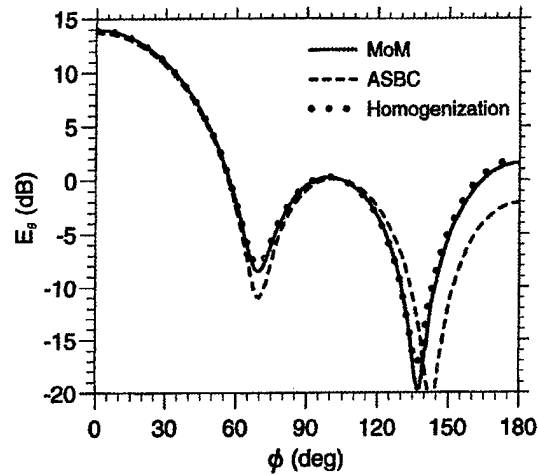


Figure 2. Scattered field from a dielectric cylinder loaded with periodic circumferential strips.

Fig 3. shows the equivalent blockage width of the scatterer from the previous example. The equivalent blockage is a complex parameter showing how wide the cylinder appears for electromagnetic waves, and it is obtained from the forward scattered field [2]. The incident wave is TE_z polarized, and the results for two incident angles are shown : $\theta = 60^\circ$ and $\theta = 90^\circ$. The numerical results are also compared to the measurements. The results again show that both the ASBC and the BCHM are accurate approximations, and that the BCHM method is more accurate (as in Fig. 2, there is no difference between MoM and BCHM results). Furthermore, the ASBC cannot predict the coupling of the incident wave to the waveguide modes of the strip-loaded dielectric cylinder, which can be seen in measured results and in the calculated results by the MoM and the BCHM methods. It is interesting to mention that although the cylinder has a relatively small radius ($0.42 \lambda_0$ at 10 GHz) the local planar approximation used in the BCHM method works very well.

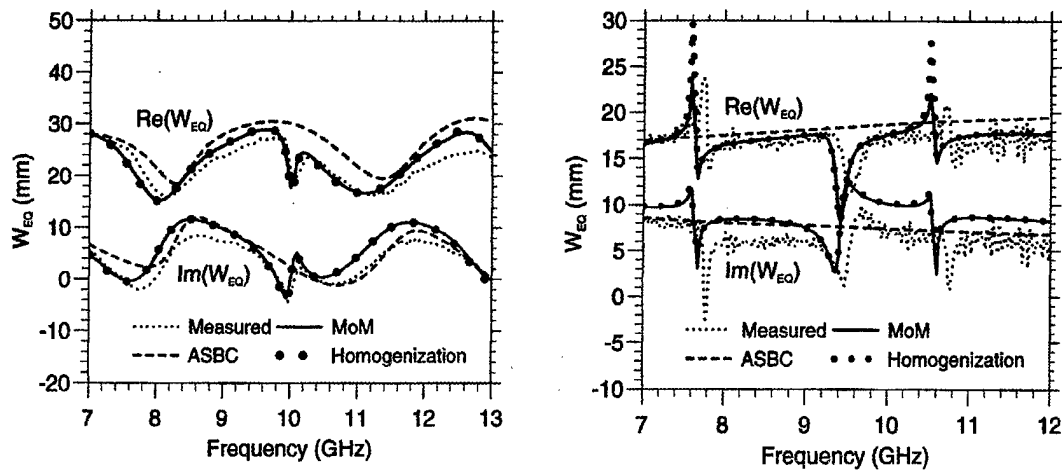


Figure 3. The equivalent blockage width of a dielectric cylinder loaded with periodic circumferential strips. (a) $\theta = 60^\circ$, (b) $\theta = 90^\circ$.

Acknowledgment: The authors would like to thank Prof. Edward F. Kuester and Prof. Per-Simon Kildal for inspiring this research, and B. Eng. Audun Tengs for providing the measurement results.

References:

- [1] Z. Sipus, S. Raffaelli, and P.-S. Kildal, "Periodic strips on planar and circular cylindrical substrates: exact and asymptotic analysis," *Microwave Opt. Technol. Lett.*, Vol. 17, pp. 173-178, Feb 1998.
- [2] A. A. Kishk and P.-S. Kildal, "Asymptotic boundary conditions for strip-loaded scatters applied to cylinders under oblique incidence," *IEEE Trans. Antennas Propagat.*, Vol. 45, pp. 51-56, Jan. 1997.
- [3] P.-S. Kildal, A. A. Kishk, and Z. Sipus, "Asymptotic boundary conditions for strip-loaded and corrugated surfaces," *Microwave Opt. Technol. Lett.*, Vol. 14, pp. 99-101, Feb 1997.
- [4] F. C. Karal and S. N. Karp, "Propagation of electromagnetic waves along unidirectional screens," in *Electromagnetics Waves*, E. C. Jordan, Pergamon, New York, pp. 967-980, 1963.
- [5] F. H. Bellamine, E. F. Kuester, "Guided waves along a metal grating on the surface of a grounded dielectric slab," *IEEE Trans. Microwave Theory Tech.*, Vol. 42, pp. 1190-1197, July 1994.

DIFFRACTION OF ELECTROMAGNETIC WAVES BY GRATINGS WITH PIECEWISE SMOOTH BOUNDARIES

E. K. Lipachev

Kazan State University, Kazan, Russia

email: evgeny.lipachev@ksu.ru

We consider a boundary value problem for the Helmholtz equation that arises in the mathematical modeling of the scattering of a plane electromagnetic wave by infinite perfectly conducting gratings with an arbitrary piecewise-smooth profile of finite size.

In the Hilbert space of the square-integrable functions we find the solution of this problem as a potential whose density represents a solution of a weakly singular integral equation.

1. Statement of the Problem and Notations. Consider the problem of finding the field scattered due to a plane electromagnetic wave incident (at the angle θ with respect to the axis z) onto a conducting grating [1]. The geometry of such a grating is characterized by the curve $\gamma = \{(x, f(x)) : x \in [-a, a]\} \cup (\mathbb{R} \setminus [-a, a])$, where f is a piecewise-smooth function, $\Omega = \{\Omega_j\}_{j=1}^m$ is the set of boundary edges.

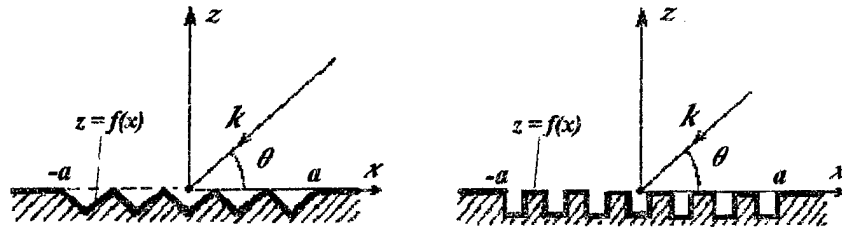


Figure 1: Geometry of the gratings

This problem can be reduced to the following boundary value problem. Find a function

$$v(x, z) := \begin{cases} E_y(x, z) & , \text{ in the } E\text{-polarization,} \\ H_y(x, z) & , \text{ in the } H\text{-polarization,} \end{cases}$$

which satisfies the two-dimensional Helmholtz equation:

$$\Delta v(x, z) + k^2 v(x, z) = 0, \quad \text{Im } k \geq 0,$$

with the following boundary conditions:

$$v(x, z) = -u_0(x, z), \quad (x, z) \in \gamma \setminus \Omega, \quad - \text{ in the } E\text{-polarization,}$$

and

$$\frac{\partial v}{\partial \vec{n}}(x, z) := \frac{\partial u_0}{\partial \vec{n}}(x, z), \quad (x, z) \in \gamma \setminus \Omega, \quad - \text{ in the } H\text{-polarization,}$$

where u_0 is the incident field.

We assume that the function v satisfies the edge condition [2] at the points Ω_j and the radiation condition at infinity:

$$v^* = e^{ikr} O\left(\frac{1}{\sqrt{r}}\right), \quad \frac{\partial v^*}{\partial r} - ikv^* = e^{ikr} o\left(\frac{1}{\sqrt{r}}\right), \quad \text{Im } k \geq 0,$$

where $r = \sqrt{x^2 + z^2}$, $z > 0$, $v^*(x, z) = v(x, z) - \tilde{v}(x, z)$,

$$\tilde{v}(x, z) = e^{-ik(\alpha x + \beta z)} + \zeta e^{-ik(\alpha x - \beta z)}, \quad \zeta = \begin{cases} -1 & \text{in the } E\text{-polarization,} \\ 1 & \text{in the } H\text{-polarization,} \end{cases}$$

$$g(x) = f(x), x \in [-a, a]; \quad g(x) = 0, x \notin [-a, a].$$

2. Approximation method. In [3], the solvability of the scattering problem in $C^{(2)}(S) \cap C(S \cup \gamma)$ ($S = \{(x, z) : z > g(x)\}$) for a smooth boundary has been proved. With the aid of this one can prove the uniqueness of solution of our problem in the Hilbert space of square-integrable functions.

By using the integral equation method [4], this problem can be reduced to solving the following set of integral equations:

$$\psi(x) = \chi(x) + (B_1 \psi)(x) + (B_2 \psi)(x),$$

where

$$(B_1 \psi)(x) = -\frac{ik}{2} \int_{-a}^a H_1^{(1)}(kr) h_1(x, x') \psi(x') dx',$$

$$(B_2 \psi)(x) = -\frac{ik}{2} \int_{-a}^a H_1^{(1)}(kr^*) h_2(x, x') \psi(x') dx',$$

$$h_1(x, x') = \frac{1}{r_{PP'}} \{(x - x') f'_{x'}(x') - (g(x) - f(x'))\},$$

$$h_2(x, x') = \frac{1}{r_{PP'}^*} \{(x - x') f'_{x'}(x') + (g(x) + f(x'))\},$$

in the case of E -polarization, and

$$\varphi(x) = \rho(x) + (D_1 \varphi)(x) + (D_2 \varphi)(x),$$

where

$$(D_1 \varphi)(x) = -\frac{ik}{2} \int_{-a}^a H_1^{(1)}(kr) q_1(x, x') \varphi(x') dx',$$

$$(D_2 \varphi)(x) = -\frac{ik}{2} \int_{-a}^a H_1^{(1)}(kr^*) q_2(x, x') \varphi(x') dx',$$

$$q_1(x, x') = \frac{1}{r_{PP'}} \{(g(x) - f(x')) - (x - x') f'_{x'}(x')\},$$

$$q_2(x, x') = \frac{1}{r_{PP'}^*} \{ (g(x) + f(x')) - (x - x') f'_x(x') \},$$

in the case of *TH*-polarization.

Solutions of these integral equations are approximated by splines whose coefficients are determined via the mean-values of the input data [5]. A computer algorithm for solving the problem has been developed.

References

1. V. I. Kas'yanov, E. K. Lipachev, *Numerical realization of integral equation methods of diffraction theory*, Kazan State University Press, 1993 (in Russian).
2. Y. Hayashi, The Dirichlet problem for the two-dimensional Helmholtz equation for an open boundary, *J. Math. Anal. Appl.*, 1973, vol. 44, pp. 489-530.
3. E. K. Lipachev, Solvability of the scattering problem for a groove structure of finite size, *Proc. Conf. Algebra Analysis*, Kazan, 1997, pp. 135-137 (in Russian).
4. D. Colton, R. Kress, *Integral Equation Methods in Scattering Theory*, New York: Wiley, 1983.
5. B. G. Gabdulkhaev, *Numerical Analysis of Singular Integral Equations. Selected Chapters*, Kazan State University Press, 1996 (in Russian).

MODEL SYNTHESIS OF EFFICIENTLY ABSORBING STRUCTURES WITH DIFFRACTION GRATINGS

L. G. Velichko

*Institute of Radiophysics and Electronics, National Academy of Sciences of Ukraine
12 Acad. Proskura St., Kharkov, 310085, Ukraine*

In this paper we consider certain problems related to the synthesis of the efficiently absorbing structure (perfectly conducting periodic grating covered with a dielectric layer having complex-valued permittivity ε). The optimization of absorbing properties of this structure is carried out. As a result, analytical relations between absorbed (reflected) energy and electromagnetic and geometric characteristics of the system under study are derived. These parameters form the input data set in the synthesis problem. Some algorithms for solving relevant inverse problems are suggested in the paper.

1. Optimization of absorbing properties of coatings

Let us consider a perfectly conducting grating covered with a dielectric layer of depth $2\pi\theta$ (Fig.1). The absorbing ability of the coating material is determined by the imaginary part of the complex-valued relative permittivity $\varepsilon = \text{Re}\varepsilon + i\text{Im}\varepsilon$, $\text{Re}\varepsilon \geq 1$, $\text{Im}\varepsilon > 0$. Let $\text{Im}\varepsilon$ be fixed and a plane E -polarized wave $U^0(y, z) = \exp[i(\Phi_0 y - \Gamma_0 z)]$ be incident upon the structure (with the angle of incidence φ). Here, $\Gamma_n = \sqrt{\kappa^2 - \Phi_n^2}$, $\text{Re}\Gamma_n \geq 0$, $\text{Im}\Gamma_n \geq 0$, $\Phi_n = n + \kappa \sin \varphi$, κ is a dimensionless frequency parameter (the ratio of 2π to the incident wavelength). The series representation of the total field $U(y, z)$ has the form:

$$U(y, z) = \begin{cases} U^0 + \sum_{n=-\infty}^{\infty} a_n e^{i(\Phi_n y + \Gamma_n z)}, & z \geq 0, \\ \sum_{n=-\infty}^{\infty} (d_n e^{-i\Gamma_n^e z} + c_n e^{i\Gamma_n^e(z+2\pi\theta)}) e^{i\Phi_n y}, & -2\pi\theta < z < 0, \end{cases} \quad (1)$$

where $\Gamma_n^e = \sqrt{\kappa^2 \varepsilon - \Phi_n^2}$, $\text{Im}\Gamma_n^e \geq 0$, $\text{Re}\Gamma_n^e \geq 0$. To determine the complex scattering amplitudes

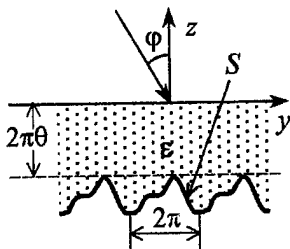


Fig.1

a_n , we apply the method of generalized scattering matrices at the boundaries of partial regions (in the planes $z = 0$ and $z = -2\pi\theta$). Consider that the generalized scattering matrix $R = \{r_{np}\}_{n,p}$ of the grating, placed in the medium with parameters $\varepsilon_0 \varepsilon$ and μ_0 , is known [1]. Further we shall use so-called generalized characteristic $\{N, M\}$ of the scattering phenomenon [1]. Here, $N = \sum_n |\Gamma_n|^{-1} \text{Re}\Gamma_n$ is the number of

the scattered harmonics propagating without decay. M is the similar characteristic for ε -layer as $\text{Im}\varepsilon = 0$. It is obvious that it determines the number of waves that are «deeply» involved in the energy exchange between the grating and the radiation region

$z > 0$. $W_n^a = |a_n|^2 \Gamma_0^{-1} \text{Re}\Gamma_n$ is the relative part of the scattered energy carried away from the grating by the wave with the complex amplitude a_n .

Consider now the ranges of parameters κ , Φ , and ε that are characterized by vector $\{N, M\}$

with $N = M = 1$. Without considering the fields decaying exponentially in a layer even with $\text{Im } \varepsilon = 0$, we get

$$W_0^a = \frac{|\nu_0|^2 + |K|^2 + 2|\nu_0||K|\cos(\arg K - \arg \nu_0)}{1 + |\nu_0|^2 + |K|^2 + 2|\nu_0||K|\cos(\arg K + \arg \nu_0)}, \quad 0 \leq \arg(\dots) < 2\pi, \quad (2)$$

where $K = r_{00} e^{i2\pi\theta\Gamma_0^s}$, $\nu_0 = (\Gamma_0 - \Gamma_0^s)/(\Gamma_0 + \Gamma_0^s)$.

Minimizing (2) as a function of $\arg K$, we obtain the following estimation of the reflected energy:

$$W_0^a < (|\nu_0| - |K|)^2 (1 + |\nu_0||K|)^{-2} \quad (3)$$

as

$$\cos(\arg K - \arg \nu_0) = -1. \quad (4)$$

Condition (4) can be written in terms of electromagnetic and geometric parameters of the structure as follows

$$4\pi\theta \text{Re } \Gamma_0^s + \arg r_{00} - \arg \nu_0 = -\pi + 2\pi m, \quad m = 0, 1, 2, \dots \quad (5)$$

For $\arg \nu_0$ approaching π (when the value of $\text{Im } \varepsilon$ is not very high), (5) is coincident with a longitudinal resonance condition for the zeroth harmonic in the layer separating free space and the grating. In the interval

$$0 < |K| = |r_{00}| \exp(-4\pi\theta \text{Im } \Gamma_0^s) < 2|\nu_0|(1 + |\nu_0|^2)^{-1}, \quad (6)$$

under conditions (5), the structure has higher absorbing ability than the dielectric half-space, that is $W_0^a < |\nu_0|^2$. The total minimum of the reflected energy is reached at the same conditions for $|r_{00}| = |\nu_0| \exp(4\pi\theta \text{Im } \Gamma_0^s)$.

Disregarding condition (5) we obtain from (2) that $W_0^a < |\nu_0|^2$ provided that

$$|K| = |r_{00}| \exp(-4\pi\theta \text{Im } \Gamma_0^s) < \frac{2|\nu_0|[-\cos(\arg K - \arg \nu_0)]}{1 + |\nu_0|^2}. \quad (7)$$

In the case of a plane perfectly conducting underlayer, $|K|$ can be reduced to a satisfactory value only through increasing the layer depth ($|K| = \exp(-4\pi\theta \text{Im } \Gamma_0^s)$). In order for (5) to be realized, the depth of the layer has to be equal to an odd number of quarters of wavelength λ_s in ε -medium ($2\pi\theta/\lambda_s = (2m-1)/4$, $m = 1, 2, \dots$). The use of gratings allows to solve the optimization problem for absorbing coatings more efficiently. In the first place, it is achieved through choosing the proper values of $\arg r_{00}$ «accelerating» the wave (the depth of the layer can be reduced substantially); in addition, we can select the parameters and operation conditions of a grating in such a way that $|r_{00}|$ gets into a required interval at a minimum layer depth $2\pi\theta$.

An important point is that such satisfactory selection can be realized not only for discrete sets of values of κ and Φ , but also if the angle of incidence and the incident wavelength are varied through a

wide range. Similar analysis has been performed for $N > 1$, $M > 1$, when harmonics «locked» within the layer come into existence.

2. On algorithms for solving inverse synthesis problems

The conducted optimization of the absorbing properties of a coating allows one to consider the problem of synthesis of a grating ensuring the desired characteristics of a coating. To do this, the period of the structure, the depth of the layer, and the relative permittivity of material are settled. We set also the ranges of incident angles and frequencies as well as the relevant maximum value of the reflected energy, $\max W_0^a = W$. The algorithms for solving the associated inverse problems of synthesis of a periodic structure in a frequency band are suggested. These schemes are based on the integral representations relating the complex scattered amplitudes a_n with the continuous current density $\eta(y)$ on the boundary S (the function $f(y)$ describes a profile of the grating):

$$\begin{cases} a_n \\ \delta_n^0 \end{cases} = \frac{i}{4\pi\Gamma_n} \int_0^{2\pi} \eta(y_0) e^{\{\pm\}i\Gamma_n f(y_0)} e^{-iny_0} dy_0, \quad n = 0, \pm 1, \dots \quad (8)$$

If we have P amplitudes $a_{n_1}, a_{n_2}, \dots, a_{n_P}$ of the scattered field on the frequency interval $[\kappa_1, \kappa_2]$, then one of the possible solutions of the inverse synthesis problem have the form:

$$f(y) = \text{Re} \left(- \frac{i}{2\Gamma_0(\kappa_2 - \kappa_1)} \int_{\kappa_1}^{\kappa_2} \sum_{m=1}^P (a_{n_m} + \delta_{n_m}^0) e^{im y} d\kappa \right). \quad (9)$$

Numerical examples of the use of this algorithm for different P are presented in Fig.2. The problem is to synthesize a periodic structure having scattered characteristics closely approximating the given complex amplitudes $a_{n_m}(\kappa)$ (curve 1 in Fig.2) at $0.652 < \kappa < 0.952$ and $\varphi = 10^\circ$. As input data for solving the inverse problem the solutions (complex amplitudes) of a direct problem for perfectly conducting grating from semicylinders are used. The diffraction characteristics of the synthesized structures (by the example of «-1» scattered harmonic) are depicted in Fig.2 by curves 2–4. The sets of input data $\{a_{-1}(\kappa), a_0(\kappa), P=2\}$, $\{a_{\pm 1}(\kappa), a_0(\kappa), P=3\}$, and $\{a_{-5}(\kappa), \dots, a_5(\kappa), P=11\}$ correspond to curves 2, 3, and 4, respectively. The detailed description of the algorithms we have given in [2].

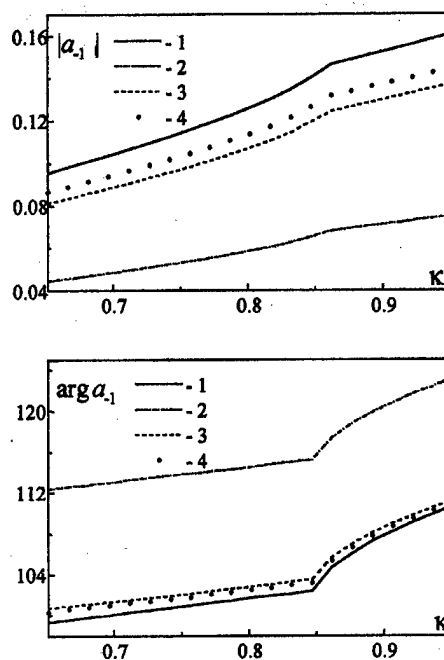


Fig.2

REFERENCES

- [1] V.P.Shestopalov, A.A.Kirilenko, S.A.Masalov, Y.K.Sirenko, Resonant Wave Scattering, V.1, Diffraction Gratings, Kyiv: Naukova Dumka, 1986 (in Russian)
- [2] L.G.Velichko, Y.K.Sirenko, Synthesis of reflecting gratings with arbitrary profile, Radiofizika i Radioastronomija, 1997, V.2, N2, p.214-219 (in Russian)

ELECTROMAGNETIC WAVE SCATTERING BY SEMI-INFINITE GRATING CONSISTING OF METAL STRIPS PLACED IN MAGNETIC-DIELECTRIC HALF SPACE

Sergy N. Vorobiov and Dmitry L. Litvinenko

Institute of Radio Astronomy of National Academy of Sciences of Ukraine

4, Chervonopraporna St., Kharkiv 310002, Ukraine

Phone: +38-0572-448-503 Fax: +38-0572-476-506 E-mail: prosvirnin@rian.kharkov.ua

The problem of electromagnetic wave diffraction by semi-infinite gratings is of particular interest in physics and mathematics. On the one hand this structure is almost infinite (far from its first element) and should have properties inherent to periodic gratings: discrete spectrum, Wood's anomalies, etc., and on the other hand it is a quite finite structure (near its beginning) and should have continuous spectrum, cylindrical-type wave propagating (if 2-D problem is considered) in this zone, etc. Dealing with the semi-infinite grating consisting of thin metal scatterers, it is obvious that surface current distributions on the scatterers will differ not only in a phase shift (i.e. the Floquet theorem can't be used). There is another interesting question concerning the previous: at what number of scatterer (counting from the first) its surface current distribution will correspond, with the given accuracy, to the one on the scatterer placed in the infinite grating having the same geometry and conditions of excitation?

Moreover, one can find here some mathematical difficulties through the semi-infinity of the structure. The Poisson formula in its classic well-known form can't be applied, but summing up in the scattered field representation still remains infinite at its upper limit while terms to be summed decrease rather slowly. That is why the solution of the mentioned above diffraction problem with the spectral method and the method of moments was not yet successful.

Consider the grating consisting of thin perfectly conducting strips which are placed periodically in the magnetic-dielectric half-space beginning at some distance from its surface and extending to infinity. The incident wave comes from the free space and illuminates the structure (see figure).

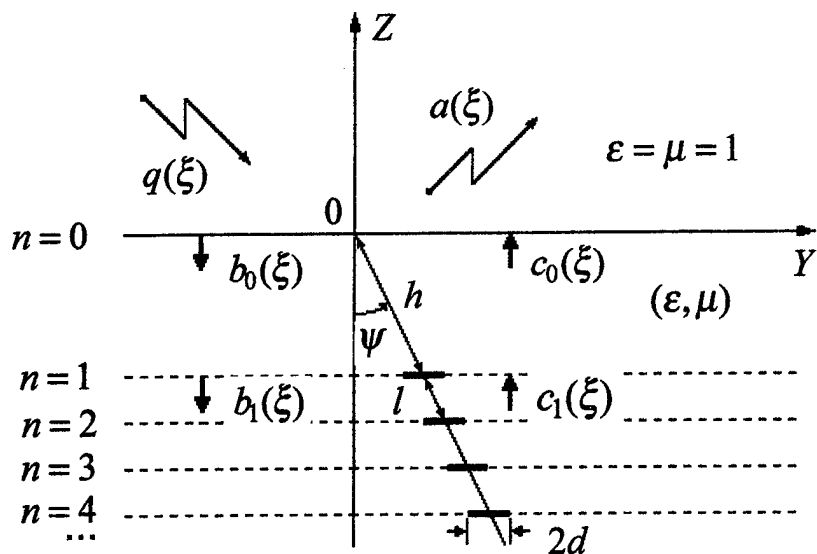


Figure. Geometry of the wave scattering by semi-infinite grating.

This electromagnetic wave diffraction problem is solved in the present paper using the operator method.

Working with the operator method one has to deal with the Fourier-amplitudes of reflected and transmitted fields existing in some domains and to build operator relations with respect to these amplitudes at the boundaries separating mentioned domains. Thus, the fields above the structure and between the strips are represented in the form of Fourier integrals. Time dependence is assumed to be

$\exp(-i\omega t)$ and omitted. Requested operators for the relations to be obtained at the interface of the magnetic-dielectric (in the plane $Z = 0$) and between neighbouring strips are as follows:

r_0^\pm and t_0^\pm are reflection and transmission operators of the boundary $Z = 0$ (if the wave propagation occurs in the direction $Z > 0$ then the sign plus should be used and, on the contrary, if the direction is $Z < 0$ the sign minus must be chosen);

r and t are reflection and transmission operators of a single thin metal strip placed in the magnetic-dielectric medium (ϵ, μ) ;

e_{zh} and e_{zl} are operators describing phase variations when shifting along the OZ axis in the direction of wave propagation takes place (e_{zh} in the domain beginning from the magnetic-dielectric surface up to the plane where the first strip of the grating is placed, and e_{zl} in the domains between the planes where neighbouring strips of the grating are placed);

e_{yh}^\pm and e_{yl}^\pm are operators describing phase variations when shifting along the OY axis occurs (the sign plus should be used if shifting takes place in the positive direction along the OY axis and the sign minus must be chosen if the shift occurs in the negative OY direction; subscripts h and l denote the same domains as in the previous case);

R is the reflection operator of the semi-infinite strip grating placed in the magnetic-dielectric medium (ϵ, μ) . The operator R has translation properties, this means that the operator R is invariant to the position of the strip which is taken as the beginning of the semi-infinite grating.

Introduce the definition of the integral operator F which acts on some analytic function $g(\zeta)$ converting it into the function $d(\xi)$:

$$d(\xi) = (F \cdot g)(\xi) = \int_{-\infty}^{\infty} F(\xi, \zeta) g(\zeta) d\zeta.$$

The function of two variables $F(\xi, \zeta)$ is the kernel of this operator F . Now it is feasible to give the analytical representation of kernels for integral operators mentioned above. For the sake of definiteness and shortness, assume the incident field to be H -polarised (i.e. to have nonzero components H_x , E_y and E_z). The kernels of operators r_0^\pm and t_0^\pm , r and t , e_{zh} and e_{zl} , e_{yh}^\pm and e_{yl}^\pm are as follows:

$$r_0^\pm(\xi, \zeta) = \pm \frac{\gamma^-(\zeta) - \epsilon \gamma(\zeta)}{w(\zeta)} \cdot \delta(\xi - \zeta), \quad w(\zeta) = \gamma^-(\zeta) + \epsilon \gamma(\zeta),$$

$$t_0^+(\xi, \zeta) = \frac{2\epsilon \gamma^-(\zeta)}{w(\zeta)} \cdot \delta(\xi - \zeta), \quad t_0^-(\xi, \zeta) = \frac{2\gamma(\zeta)}{w(\zeta)} \cdot \delta(\xi - \zeta),$$

$$\gamma^-(\zeta) = \sqrt{k_0^2 \epsilon \mu - \zeta^2}, \quad (z \leq 0), \quad \gamma(\zeta) = \sqrt{k_0^2 - \zeta^2}, \quad (z \geq 0).$$

$$r(\xi, \zeta) = \sum_{s=1}^{\infty} r_{1s}(\xi) r_{2s}(\zeta), \quad r_{2s}(\zeta) = i \frac{\gamma^-(\zeta)}{\zeta} \sum_{r=1}^{\infty} Q_{rs} \sqrt{r} J_r(\zeta),$$

$$r_{1s}(\xi) = \sqrt{s} J_s(\xi) / \xi, \quad \text{the matrix } Q \text{ has the form } Q = (A - I)^{-1},$$

and the matrix A elements are expressed in the form:

$$A_{rs} = \sqrt{rs} (1 + (-1)^{r+s}) \int_0^{\infty} J_r(\vartheta) J_s(\vartheta) \left(1 + \frac{i}{\vartheta} \sqrt{\eta^2 \epsilon \mu - \vartheta^2} \right) \frac{d\vartheta}{\vartheta}.$$

Here $\delta(\xi - \zeta)$ is the delta-function, $J_s(\vartheta)$ is the Bessel function of the first kind and s -order, $\eta = k_0 d$ is the dimensionless half-width of one strip.

The kernels of operators \mathbf{r} and \mathbf{t} obey the equality: $t(\xi, \zeta) = \delta(\xi - \zeta) - r(\xi, \zeta)$.

$$e_{zh}(\xi, \zeta) = \exp(i\gamma^-(\zeta)h \cos \psi) \cdot \delta(\xi - \zeta), \quad e_{zl}(\xi, \zeta) = \exp(i\gamma^-(\zeta)l \cos \psi) \cdot \delta(\xi - \zeta),$$

$$e_{yh}^\pm(\xi, \zeta) = \exp(\pm i\zeta h \sin \psi) \cdot \delta(\xi - \zeta), \quad e_{yl}^\pm(\xi, \zeta) = \exp(\pm i\zeta l \sin \psi) \cdot \delta(\xi - \zeta).$$

Connections between the Fourier-amplitudes in the planes $Z = 0$ and $Z = -h \cos \psi$ bring the following six operator relations: $a(\xi) = r_0^+ q(\xi) + t_0^+ c_0(\xi)$, $b_0(\xi) = t_0^- q(\xi) + r_0^- c_0(\xi)$,

$$c_0(\xi) = e_{yh}^- e_{zh} R e_{yh}^+ e_{zh} b_0(\xi), \quad c_0(\xi) = e_{yh}^- e_{zh} (t c_1(\xi) + r e_{yh}^+ e_{zh} b_0(\xi)),$$

$$b_1(\xi) = r c_1(\xi) + t e_{yh}^+ e_{zh} b_0(\xi), \quad c_1(\xi) = e_{yl}^- e_{zl} R e_{yl}^+ e_{zl} b_1(\xi).$$

It would be mentioned that such an approach has been applied successfully to the analysis of the semi-infinite structure consisting of plane infinite periodical gratings [1].

On using four last operator relations and after some transformations, the operator equation with respect to the reflection operator of the semi-infinite grating \mathbf{R} is obtained as a result:

$$f(\mathbf{R}) = \mathbf{R} - \mathbf{r} - (\mathbf{I} - \mathbf{E}_l^- \mathbf{R} \mathbf{E}_l^+ \mathbf{r})^{-1} \mathbf{E}_l^- \mathbf{R} \mathbf{E}_l^+ \mathbf{t} = 0, \quad \text{where } \mathbf{E}_l^\pm = \mathbf{e}_{yl}^\pm \cdot \mathbf{e}_{zl}.$$

This is non-linear in \mathbf{R} operator equation, it might be solved by using the Newton iterative technique. The $(n+1)$ -th iteration corresponding to the Newton method is expressed as follows:

$$\mathbf{R}_{n+1} = \mathbf{R}_n - \left(\frac{d}{d\mathbf{R}} f(\mathbf{R}) \right)^{-1} f(\mathbf{R})|_{\mathbf{R}=\mathbf{R}_n}.$$

Transformations of the first three operator relations lead to the expression for obtaining the Fourier-amplitude of the scattered field above the magnetic-dielectric ($Z > 0$):

$$a(\xi) = (\mathbf{r} + \mathbf{t} (\mathbf{I} - \mathbf{E}_l^- \mathbf{R} \mathbf{E}_l^+ \mathbf{r})^{-1} \mathbf{E}_l^- \mathbf{R} \mathbf{E}_l^+ \mathbf{t}) q(\xi).$$

The generalised criteria of the accuracy of calculations of the reflection operator \mathbf{R} and Fourier-amplitudes $a(\xi)$ of the electromagnetic field in free space is the energy conservation law. In the dimensionless form the power conservation law is expressed as follows:

$$\int_{-1}^1 (|a(k_0 \zeta)|^2 - |q(k_0 \zeta)|^2) \sqrt{1 - \zeta^2} d\zeta = \frac{1}{\varepsilon} \int_{-\sqrt{\varepsilon \mu}}^{\sqrt{\varepsilon \mu}} (|b_0(k_0 \zeta)|^2 - |c_0(k_0 \zeta)|^2) \sqrt{\varepsilon \mu - \zeta^2} d\zeta,$$

$$\text{where } b_0(\xi) = (\mathbf{I} - \mathbf{r}_0^- \mathbf{E}_h^- \mathbf{R} \mathbf{E}_h^+)^{-1} \mathbf{t}_0^- q(\xi), \quad \mathbf{E}_h^\pm = \mathbf{e}_{yh}^\pm \cdot \mathbf{e}_{zh},$$

$$c_0(\xi) = \mathbf{E}_h^- \mathbf{R} \mathbf{E}_h^+ b_0(\xi) = \mathbf{E}_h^- \mathbf{R} \mathbf{E}_h^+ (\mathbf{I} - \mathbf{r}_0^- \mathbf{E}_h^- \mathbf{R} \mathbf{E}_h^+)^{-1} \mathbf{t}_0^- q(\xi).$$

If the energy identity is not satisfied with a desirable accuracy then some additional iterations should be done to determine the operator \mathbf{R} more precisely.

Solution of the wave diffraction problem for the semi-infinite strip grating is of specific interest not only due to its "middle" position between infinite and finite structures. This problem has physical applications also, for example, such as detection and determination of periodical metal inclusions in magnetic-dielectric medium by analysing of their scattered fields rather far from the magnetic-dielectric.

1. Litvinenko L.N., Reznik I.I. and Litvinenko D.L. Wave diffraction by semi-infinite periodical structures, Reports of Academy of Sciences of Ukr.SSR, 1991, No.6, p. 62-67 (in Russian).

WAVEGUIDING AND ANOMALOUS PROPERTIES OF PERIODIC SLANTING STRIP GRATING

Shirnen A. A.

Novosibirsk State University

Faculty of Mathematics and Mechanics, Department of Hydrodynamics
Novosibirsk, 630090 Pirogova str.2, RUSSIA

It has been shown that periodic slanting strip grating possesses guiding and anomalous properties. The dependence of guiding frequency on the geometrical parameters of gratings has been investigated. With the help of discrete isometric transform group of grating symmetry space of admissible solutions has been restricted and the existence of guiding and anomalous waves has been proved. Pass bands modes have been classified with the help of grating symmetry group. Fine structure of the spectrum has been investigated.

Statement of problems.

Steady-state oscillations near the strip grating are described by the function u , which satisfies the following conditions:

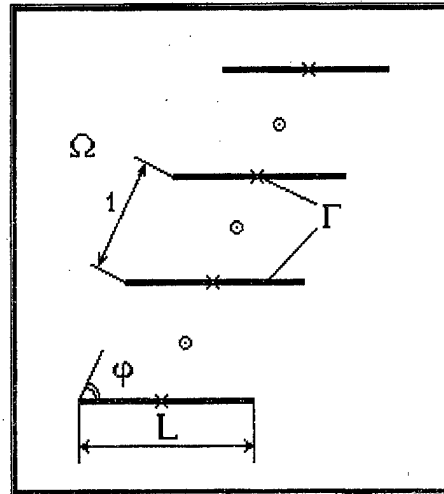
$$\left. \begin{aligned} u_{xx} + u_{yy} + \lambda^2 u &= 0 - \text{oscillation equation,} \\ \frac{\partial u}{\partial \vec{n}} \Big|_{\Gamma} &= 0 - \text{boundary condition,} \\ \int_{\Omega} (|\nabla u|^2 + u^2) d\Omega &< \infty - \text{energy finiteness.} \end{aligned} \right\} \quad (B)$$

φ —angle of grating incline, L —length of plate, λ —non-dimensional frequency, \odot and \times are points which have rotation symmetry by π angle.

Since the translation group is commutative and its representation in the space of admissible solutions is unitary, the space of solution can be expanded into invariant one-dimensional spaces, the functions from which are

$$u(x + \cos(\varphi), y + \sin(\varphi)) = e^{i\theta} u(x, y), \quad (|\theta| < \pi) \quad (1)$$

The problem B with the condition (1) is called the problem $B(\theta)$. On the ground of translational symmetry this problem can be considered only for $\Omega' = \{(x, y): 0 < y < \sin(\varphi)\}$.



Waveguiding properties.

Definition 1

The waveguiding function is defined as the solution $u(x, y)$ of problem $B(\theta)$, which is a generalized function of Laplace operator. One-directional periodic structure possesses waveguiding property, if non-trivial waveguiding function of problem $B(\theta)$ exist.

The basic difficulty of investigation of waveguiding property of periodic strip grating is that waveguiding and free frequencies of problem $B(\theta)$ can coincide, in spite of the difference of free and waveguiding functions. Let the free and waveguiding frequencies be positive. It follows from the condition (1) that the continuous spectrum $[0, \infty)$.

Theorem 1. (Existence of waveguiding property)

Slanting periodic strip grating possesses waveguiding property.

Proof The proof is carried out by the method of "Dirichlet - Neumann fork". Let Dirichlet conditions (the problem B(DR)) or Neumann condition (the problem B(DR)) be fulfilled in addition to the boundary conditions of problem B(θ) for $x=R$ ($R > 0$). For $\lambda(DR)$ - eigenvalues of problem B(DR) and $\lambda(NR)$ - eigenvalues of problem B(NR) the following system of inequalities $\lambda(NR) < \lambda < \lambda(DR)$ is right.

(follows from the variational statement of problem), hence it is enough to prove, that for $\forall L > \cos(\varphi) \exists R$ that the inequalities $0 < \lambda(NR) < \lambda(DR) < \theta$.

$\lambda > 0$. It follows from connectedness of Ω and condition (1).

$\lambda < \theta$. Any solution u in domain Ω represent as $u = u + u$, where $u[r]$ is function discontinuous in the set G , continued with 0 outside the plate grating, $u[n]$ is function discontinuous in the whole domain, satisfies all relations of problem B(DR), except the Neumann condition on the plate. For all values C - constant the relation

$$\lambda_{DR}^2 \leq \frac{\int_{\Omega_R} |\nabla u|^2 d\Omega_R}{\int_{\Omega_R} |u|^2 d\Omega_R} = \mu^2(C, R)$$

is right. Here $\Omega = \Omega \cap \{(x, y) : |x| < R\}$. For big values R the asymptotic representation

$$\mu^2(C, R) = \theta^2 + \frac{A}{R} + \frac{B}{R^2} + o\left(\frac{1}{R^3}\right)$$

is right. Since the values A and B depend on C , the values of A are negative for corresponding choice of constant C , hence for enough big values of R $\mu < \theta$. The theorem is proven.

Dispersion relation.

Due to the radiation condition, the general representation of wave guiding solution of problem B(θ) are, accordingly for symmetrical oscillations (symmetry rotation of angle is equal to πn) and anty - symmetrical oscillations

$$u_1(x, y) = \sum_{n=0}^{\infty} A_n \left(\cos\left(\frac{n\pi y}{\sin(\varphi)}\right) \cosh(\alpha_n x) + \sin\left(\frac{n\pi y}{\sin(\varphi)}\right) \sinh(\alpha_n x) \right) \quad (\text{in } \Omega_1) - \text{for}$$

simmetrical oscillations,

$$u_1(x, y) = \sum_{n=0}^{\infty} A_n \left(\cos\left(\frac{n\pi y}{\sin(\varphi)}\right) \sinh(\alpha_n x) + \sin\left(\frac{n\pi y}{\sin(\varphi)}\right) \cosh(\alpha_n x) \right) \quad (\text{in } \Omega_1) - \text{for}$$

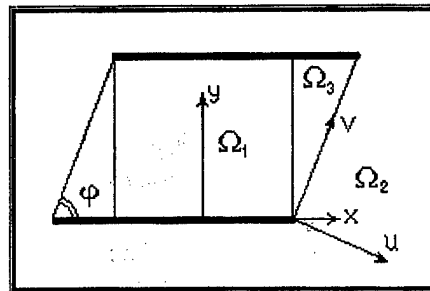
anty - symmetrical oscillations,

$$u_2(u, v) = \sum_{n=-\infty}^{\infty} B_n e^{i(2m+\theta)v} e^{-\alpha_n |u|},$$

$$\alpha_n = \sqrt{(\pi n / \sin(\varphi))^2 - \lambda^2}, \quad \beta_n = \sqrt{(2\pi m + \theta)^2 - \lambda^2}.$$

For these functions in order to be solutions of problem B(θ) on the boundaries of domains Ω ($j=1, 2, 3$), the conditions of continuity of solution and its normal derivative must be fulfilled Grin's formula.

The endless system of equations, which has been received from this Grin's formula, has been investigated numerically.



One can consider that parameter θ , from relation (1) is a wave number for waveguiding function of periodic grating G. Non – dimensional waveguiding frequencies λ depend on θ , these dependencies are dispersion relations. In the article, some its approximations have been investigated. In particular, the case of little deviation of angel φ for $\pi/2$ have been considered.

Anomalous properties.

Definition 2

Anomalous functions are defined as generalized eigenfunctions of problem B, localized in the neighborhood of slanting strip grating, satisfying the periodicity condition (2).

$$u(x + \cos(\varphi), y + \sin(\varphi)) = u(x, y) \quad (2)$$

Since the slanting periodic grating accepts the more narrow symmetry group then the simple grating, it's necessary to add the condition

$$\int_{\Omega} (uY) d\Omega = 0 \quad (3)$$

to the conditions of problem B, where Y – generalized eigenwave. Thus all anomalous functions must be orthogonal to ingoing generalized eigenwave (the direction of propagation Y and plane of plates are parallel). This conditions restricted the space of admissible solutions of problem. The problem 'B' with the condition (3) is called the problem 'A'. Continuous spectrum of Laplace operator, corresponding to free eigenfunctions of problem 'A' represents the set $\sigma = [4\pi^2, \infty)$, or in terms of non-dimensional frequency $[2\pi, \infty)$.

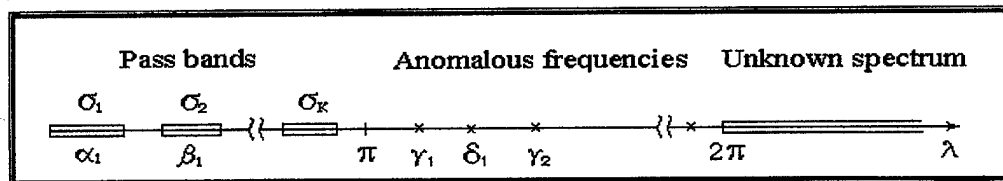
Theorem 2 (Existence of anomalous property)

Slanting periodic strip grating possesses anomalous property, then $\cos(\varphi) < L$.

The theorem is proved through the method of "Dirichlet – Neumann fork".

Fine structure of the spectrum.

By the existence theorems of waveguiding and anomalous properties the spectrum of problem consist of pass bands (α mode – symmetrical waveguiding function, β mode – anti-symmetrical waveguiding function), anomalous frequencies (γ and δ modes) and unknown spectrum.



Acknowledgment.

I am indebted to Dr. S. V. Sukhinin who guides my research.

References.

- [1] Sukhinin S. V. Waveguidings and anomalous properties of knife-type periodic strip grating.- Institute of hydrodynamics, 1998.
- [2] Sukhinin S.V. Waveguiding effect. – Applied mechanics and technical physics magazine, № 2, 1989.
- [3] Mitra R., Lee S.W. Analytical techniques in the theory of guided waves.- M.: Mir, 1974.

Moment - method analysis of electromagnetic wave scattering by plane array of chiral strip elements

Sergey Prosvirnin and Tatyana Vasilyeva

Institute of Radio Astronomy National Academy of Sciences of Ukraine
4 Chervonopraporna St., Kharkiv, 310002, Ukraine; e-mail: prosvirnin@rian.kharkov.ua

A numerical method of electromagnetic modelling of scattering by 2-D periodical array consisting of metal strip elements which have complex shape is presented. The method is applied to the characterisation of chiral arrays. Scattering characteristics of periodical arrays placed in free space and microstrip arrays are analysed.

Chiral mediums are well known as mediums that have optical activity. Electromagnetic wave transforms its polarisation propagated through such medium slab. There are no natural media which have properties of optical activity in microwave frequency region. That is why a design and a mathematical modelling of artificial media or electromagnetic structures, properties of which are similar to optical activity, are a subject of a great interest [1]. It is natural to include chiral resonant-size particles, in microwave frequency region, in these structures.

Recently plane structures have been suggested that consist of two-dimensional chiral particles and mathematical models were created for the characterisation of electromagnetic wave scattering by some structures [2, 3]. Plane chiral structures have typical properties of three-dimensional artificial chiral medium but are more feasible in manufacturing.

In this paper we consider mathematical modelling of plane electromagnetic wave diffraction and scattering by periodical structures consisting of strip metal elements having complex shape, particularly chirality shape. To the characterisation of microstrip array the algorithms were developed and numerical analysis was carried out, i.e. the array which elements are placed on magneto-dielectric slab with metal ground plane (see Fig. 1), and diffraction array in free space. Arrays are periodical in two orthogonal in the plane directions. The elements of arrays are plane metal strips of complex shape, particularly chiral S-shape and C-shape.

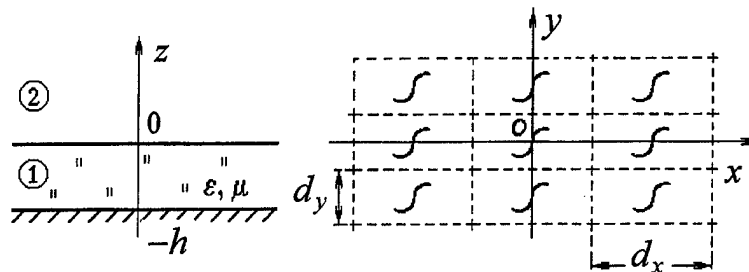


Fig. 1. Microstrip array.

In each case the solution of boundary value problem was reduced to a moment-method solution of integral equation for unknown surface current density on the strip elements of array. Spectral representation of Green's functions were used in the both cases: microstrip array and array in free space. Integral equations were obtained under the assumption that surface current flows along the strip element only, i.e. the width of the strip which can be variable is so small that current density cross component can be neglected. The cross current density distribution is given by a single moment-method basis function with the necessary

singularities for the current distribution at the strip edges. The expansion of the current density along the curved strip is made by using the roof-top basis functions.

Such array scattering characteristics have the resonant behaviour versus frequency. Resonances arise at frequencies when a half-wave-length in the free space or the microstrip line equals approximately to the strip length. Essential variations of the amplitude and polarization of reflected and transmitted fields occur at the wave resonant conditions.

For simplicity, we shall consider the normal incidence of a plane electromagnetic wave on the array: $\mathbf{E}^i = \mathbf{p}e^{ikz}$. Both periods of array are assumed smaller than the wavelength: $d_x / \lambda < 1$ and $d_y / \lambda < 1$. Then there is only one space harmonic in the reflected and transmitted fields: $\mathbf{E}^r = \mathbf{r}e^{-ikz}$, $\mathbf{E}^t = \mathbf{t}e^{ikz}$. In each pair, the vectors \mathbf{r} , \mathbf{p} and \mathbf{t} , \mathbf{p} are connected by the operators of reflection and transmission: $\mathbf{r} = \mathbf{S}\mathbf{p}$, $\mathbf{t} = \mathbf{T}\mathbf{p}$. When bases are formed by the unit vectors \mathbf{e}_x and \mathbf{e}_y , the matrices of \mathbf{S} and \mathbf{T} tensors as follows

$$\mathbf{S} = \begin{pmatrix} s_{xx} & s_{xy} \\ s_{yx} & s_{yy} \end{pmatrix}, \quad \mathbf{T} = \begin{pmatrix} t_{xx} & t_{xy} \\ t_{yx} & t_{yy} \end{pmatrix}.$$

The identities $s_{xy} = s_{yx}$ and $t_{xy} = t_{yx}$ follow from Lorenz's lemma and energy conservation law. The relations $T = 0$ and $|s_{xx}| = |s_{yy}|$ hold true in the case of a microstrip array as well.

The reflection field has an elliptic polarization in usual case of normally incident plane line polarized electromagnetic wave on a microstrip array consisting of S-shape elements in the regime of the propagation of a single partial harmonic. However the reflected field has linear polarization that is orthogonal to the incident field in the certain resonant conditions. Such microstrip screen can be as fully transparent for a linear polarization transmitting-receiving antennas in the certain conditions.

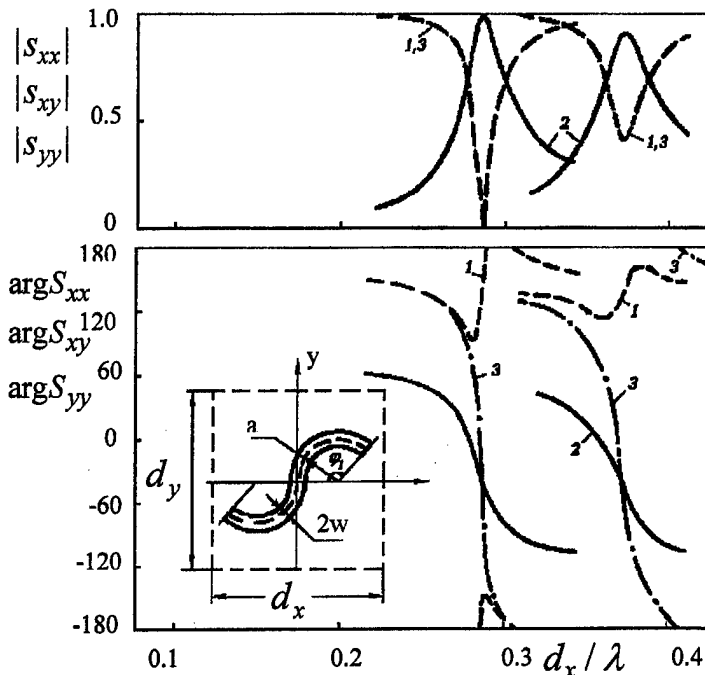


Fig. 2. The elements of reflection matrices versus d_x / λ ratio ($d_x = d_y$, $\epsilon = 2$, $\mu = 1$, $a / d_x = 0.3$, $w / d_x = 0.005$, $h / d_x = 0.15$; the curves near $d_x / \lambda = 0.285$

correspond to $\varphi_1 = 120^\circ$; the curves near $d_x / \lambda = 0.37$ correspond to $\varphi_1 = 90^\circ$).

Figure 2 shows the dependence of the elements of the reflection tensor versus period to wavelength ratio for the case of microstrip array consisting of S-shape strips. Such array is a chiral structure that has pronounced resonant dispersion characteristics.

If the angular dimension φ_1 is such that there are some parts on the strip with mutually orthogonal current directions, then the diagonal matrix elements of \mathbf{S} might tend to zero (see Fig. 2, $\varphi_1 = 120^\circ$). Let us consider the incidence of a wave that has a linear polarization along

one of directions of periodicity of array. The reflected wave is orthogonally polarized to an incident wave at the corresponding frequencies in above-mentioned conditions.

In the case of array placed in free space it is possible that a circularly polarized normally incident wave can be transformed to the approximately equal (by amplitudes) reflected and transmitted linearly polarized fields at the resonant dimension of S-shape element (see Fig. 3). Turning of polarization plane or transformation to elliptic polarisation of transmitted field occur in the case of linear polarization of the incident field in the resonant conditions.

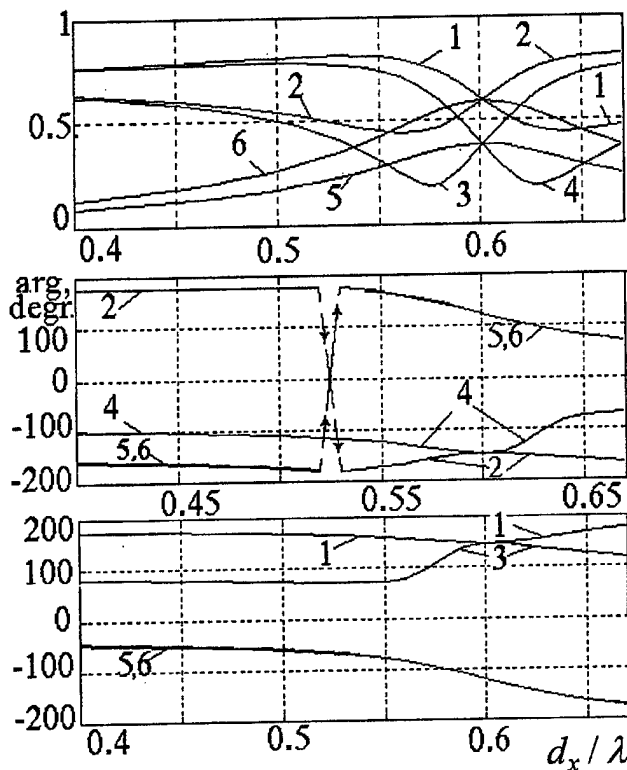


Fig. 3. Dependence of amplitudes and phases of transmitted and reflected fields in the case of left (-) and right (+) circularly polarized incident wave versus ratio d_x / λ . Normal incidence. The S-shape strip array in a free space ($d_x = d_y, w/d_x = 0.005, a/d_x = 0.3$, $\varphi_1 = 90^\circ$): 1 - t_x^- , 2 - t_x^+ , 3 - t_y^- , 4 - t_y^+ , 5 - r_x^-, r_x^+ , ($r_x^- \cong r_x^+$), 6 - r_y^-, r_y^+ , ($r_y^- \cong r_y^+$).

- [1] F. Mariotte, S.A.Tretyakov, B. Sauviac, Modelling effective properties of chiral composites, IEEE Antennas and Propagation Magazine, v.38, no.2, April 1996, pp.22-32.
- [2] L.R. Arnaut, L.E. Davis, On planar chiral structures, Proceedings, Progress in Electromagnetic Research Symposium (PIERS 1995), (24-28 July 1995, Seattle, WA), p. 165.
- [3] L.R. Arnaut, Mutual coupling in arrays of planar chiral structures, in the book, A.Priou et al. (eds.) "Advances in Complex Electromagnetic Materials", Kluwer Academic Publishers, Printed in the Netherlands, 1997, pp. 293-309.

ELECTROMAGNETIC WAVE SCATTERING ON TRANSPARENT WAVY INTERFACE

A. S. Ilinski and T. N. Galishnikova

Faculty of Computational Mathematics and Cybernetics, Moscow State University,
Vorobievsky Gory, V-234 Moscow, 119899 Russia.
Phone: 939-38-57, 939-17-76; Fax: 939-25-96, E-mail: celd@cs.msu.su

The method of observation of the earth surface by various technical tools is one of the most widespread methods for the investigation of the environment. Radar stations of survey of the earth surface are of great importance among such tools. We consider the practical problem of remote sensing of the sea water. The most important for applications is the inverse problem of determination of the reflecting surface boundary. To solve the inverse problem it is necessary to have an efficient numerical method for the direct problem solving.

In this paper we consider the numerical procedures for analysis of the diffraction problem of a plane electromagnetic wave incident on a wavy interface between two different media. An infinite periodical cylindrical surface as well as the cylindrical surface differed from the plane on a bounded part of it is discussed here. In the case of an illuminated region wide compared to the wavelength of the incident field, the choice of periodic model of reflecting surface is justified.

Several accurate and approximate methods for solving the problems of reflecting gratings have been proposed. We would like to emphasize the methods of Kirchhoff [1], of small perturbations [2], and of small inclinations [3] among the approximate methods of solving diffraction problems for an undulate surface. Approximate methods may have not only high but also low accuracy depending on the range of variation of input parameters. These questions are discussed in [4,5]. Approximate methods of solving the diffraction problems for reflecting gratings have been thoroughly reviewed in [4]. For a grating with rectangular profile, a rigorous method of partial regions was developed and resonant features of such a reflecting grating were studied in the works by L. Deryugin. Systematic investigation of gratings with saw-tooth profile was carried out at the Kharkov school of radiophysics [6].

We investigate a full electromagnetic formulation of the problem of plane wave diffraction by a periodic wavy interface between two different media, on whose surface either the continuity conditions of the tangential components of electric and magnetic fields or the Leontovich conditions are satisfied. Boundary value problem for the Maxwell set of equations in the half-space is reduced to a set of integral equations over a finite portion of the boundary by selecting appropriate fundamental solutions. The authors of this paper have developed the method of integral equations in [7]. Perfectly conducting structures have been studied by the method of integral equations in [8].

Consider diffraction problem in the following formulation. Suppose that S is the interface between two media D_1 and D_2 with dielectric and magnetic permeabilities ϵ_1, μ_1 and ϵ_2, μ_2 , respectively ($\text{Im } \epsilon_1 = 0$). Suppose that cylindrical surface S is periodic along the x axis, its generatrix is parallel to the z axis and given by the equation $y = f(x)$. A plane wave is incident from D_1 onto S . Its time dependence is $\exp(-i\omega t)$, with $k_{1,2} = \omega \sqrt{\epsilon_{1,2} \mu_{1,2}}$, where ω is the frequency. Let us denote, by $\mathbf{E}_0(x, y, z)$, $\mathbf{H}_0(x, y, z)$, the incident field of the plane wave, which has the form:

$$\mathbf{E}_0(x, y, z) = \mathbf{E}_0 \exp(-i\alpha_0 x - i\beta_0 y + i\gamma_0 z), \quad \mathbf{H}_0(x, y, z) = \sqrt{\epsilon_1 / \mu_1} \mathbf{E}_0(x, y, z). \quad (1)$$

Here $\alpha_0 = k_1 \sin \varphi_0 \sin \vartheta_0$, $\beta_0 = k_1 \sin \varphi_0 \cos \vartheta_0$, $\gamma_0 = k_1 \cos \varphi_0$, where φ_0 is the angle between the z axis and the propagation direction of the incident field, ϑ_0 is the angle between the negative direction of the y axis and the projection on the plane $z=0$ of the propagation direction of the incident field.

In the domains D_1 and D_2 , we seek a solution to the uniform set of the Maxwell equations with the boundary conditions of continuity of the tangential components of electromagnetic field across the media interface S . The scattered field satisfies the radiation conditions. We shall assume that the total electromagnetic field has the dependence on the z -coordinate as $\exp(i\gamma_0 z)$. It can be shown that diffraction problem is reduced to the determination of the projection on the z -axis of the field $\mathbf{E}(x, y)$ and $\mathbf{H}(x, y)$, which satisfy a uniform two-dimensional Helmholtz equation with coefficients $(k_{1,2}^2 - \gamma_0^2)$ in the domains D_1 and D_2 . The boundary conditions couple the tangential components of the electromagnetic field.

In order to derive the integral equations let us introduce two-dimensional quasi-periodic fundamental solutions $g_{1,2}(M, P)$ to the Helmholtz equation in the domains $D_{1,2}$ that satisfy the radiation conditions, and shown in the work [7]. By using the Green's formulas, the properties of surface potentials, and the quasi-periodic fundamental solutions $g_{1,2}(M, P)$, diffraction problem is reduced to a set of four integral equations for $u(P) = E_z^{(1)}(P)$, $v(P) = H_z^{(1)}(P)$, $\partial u(P)/\partial n$, $\partial v(P)/\partial n$ over a finite portion S_0 of the surface S [7]. The values of $\partial u(P)/\partial \tau$, $\partial v(P)/\partial \tau$, for a numerical solution of this integral equation set, are substituted by $u(P)$ and $v(P)$ on S_0 .

In the particular case if wave incident in the xy -plane ($\gamma_0 = 0$), boundary conditions can be simplified, and the set of four equations splits into two independent systems of integral equations of the form

$$\begin{aligned} \hat{u}(M) = & \frac{1}{2\pi} \int_{S_0} \left[\hat{u}(P) \frac{\partial}{\partial n_P} (g_2(M, P) - g_1(M, P)) + \frac{\partial \hat{u}(P)}{\partial n} (g_1(M, P) - \alpha g_2(M, P)) \right] ds_P + \hat{u}_0(M), \\ \frac{1}{2}(1+\alpha) \frac{\partial \hat{u}(M)}{\partial n} = & \frac{1}{2\pi} \int_{S_0} \left[\hat{u}(P) \frac{\partial^2}{\partial n_M \partial n_P} (g_2(M, P) - g_1(M, P)) - \right. \\ & \left. - \frac{\partial \hat{u}(P)}{\partial n_P} \frac{\partial}{\partial n_M} (\alpha g_2(M, P) - g_1(M, P)) \right] ds_P + \frac{\partial \hat{u}_0(M)}{\partial n_M}, \quad M \in S_0, \end{aligned} \quad (2)$$

where $\alpha = 1$, $\hat{u}(P) = u(P) = E_z^{(1)}(P)$, in the E -polarization, or $\alpha = \varepsilon_2 / \varepsilon_1$, $\hat{u}(P) = v(P) = H_z^{(1)}(P)$ in the H -polarization. Integral equations are further solved by discretization (2). Algorithms have been constructed based on explicit representation of the logarithmic singularity contained in the equation kernels.

In the case of the media D_2 having a strong conductivity, the Leontovich boundary conditions are valid on the surface S : $[\mathbf{n} \times \mathbf{E}] = -W_2[\mathbf{n} \times [\mathbf{n} \times \mathbf{H}]]$. These conditions for the electromagnetic field, which satisfies the set of the Maxwell equations and has a dependence on the z -coordinate as $\exp(i\gamma_0 z)$ can be written as

$$E_z = \frac{W_2}{\beta_1^2} \left[-i\gamma_0 \frac{\partial H_z}{\partial \tau} - i\omega\varepsilon_1 \frac{\partial E_z}{\partial n} \right], \quad H_z = \frac{1}{W_2\beta_1^2} \left[i\gamma_0 \frac{\partial E_z}{\partial \tau} - i\omega\mu_1 \frac{\partial H_z}{\partial n} \right]. \quad (3)$$

To solve the diffraction problem, the set of two integral equations for the unknown functions $\partial u(P)/\partial n$, $\partial v(P)/\partial \tau$ on S_0 is obtained. If $\gamma_0 = 0$, i.e. if the plane wave propagates in the xy -plane, the boundary conditions (3) become simpler, and a single integral equation for $\partial u(P)/\partial n$ can be obtained instead of the set of two equations. An integral equations set with respect to $\partial u(P)/\partial \tau$ and $v(P)$ can be derived analogously. In the case of $\gamma_0 = 0$ we obtain the integral equation for $v(P)$.

A similar consideration has been developed for a plane wave diffraction problem on the surface differing from the plane on a bounded part of it. The sets of integral equations have been obtained for the interface between two different media and for the surface with the Leontovich boundary conditions.

REFERENCES

1. F.G.Bass and I.M.Fuks, *Wave Scattering by Statistically Rough Surface*, Moscow, 1972, (in Russian).
2. B.Z.Katsenelenbaum, "Electromagnetic field perturbation for small deformation of metal," *Zh. Tekhnich. Fiziki*, vol. 25, No. 2, pp. 542-557, 1955, (in Russian).
3. A.G.Voronovich, "Small-inclination approximation in the theory of wave diffraction by rough surfaces," *Zh. Eksp. Teor Fiz.*, vol. 89, No. 1(7), pp. 116-125, 1985, (in Russian).
4. V.A.Korneev, A.G.Mikheev, E.Yu.Rabotnova, and A.S.Shamaev, "Accuracy comparison of numerical and asymptotic methods in the problem of plane electromagnetic wave diffraction by a periodic perfectly conducting surface," *Radiotekhnika i Elektronika*, vol. 35, No. 2, pp. 258-266, 1990, (in Russian).
5. Yu.P.Lysanov, "The wave scattering theory by periodically rough surfaces," *Akustich. Zhurnal*, vol. 4, No. 1, pp. 3-12, 1958, (in Russian).
6. V.P.Shestopalov, L.N.Litvinenko, S.A.Masalov, and V.G.Sologub, *Wave Diffraction by Gratings* (in Russian), Kharkov, 1973, (in Russian).
7. T.N.Galishnikova and A.S.Ilinski, "The Scattering of the Plane Wave by the Wavy Surface," Moscow, MSU-Press, pp.86-111, 1995, (in Russian).
8. Yu.I.Krutin', Yu.A.Tuchkin, and V.P.Shestopalov, "Diffraction of E-polarized electromagnetic wave by a periodic smooth wavy surface," *Radioelektronika*, vol. 37, No. 2, pp. 202-208, 1992, (in Russian).

ELECTROMAGNETIC WAVE SCATTERING BY RECTANGULAR-CELL DOUBLE-PERIODIC MAGNETO-DIELECTRIC GRATINGS

N.V.Ryazantseva and V.V.Yachin
Institute of Radio Astronomy
of the National Academy of Sciences of Ukraine,
4, Krasnoznamennaya str., 310002 Kharkov, Ukraine

Abstract

The problem of electromagnetic waves scattering by a double-periodic grating is solved by the new method based on the rigorous volume integro-differential equations. The Galerkin method is applied to reduce this volume integro-differential equation to a set of second-order differential ones with constant coefficients in functionals. Numerical solution was obtained for the simplest double-periodic magneto-dielectric rectangular-cell grating as an example of a structure with translational symmetry.

Introduction

Periodic screens are used in many applications as a filter of electromagnetic waves. The purpose of this paper is to present a simple transformation from the integral equations to the differential ones that leads to efficient way of solving the scattering problem for waves arbitrary incident on a double-periodic structure. We shall analyze the case of the rectangular-cell magneto-dielectric grating shown in Fig. 1.

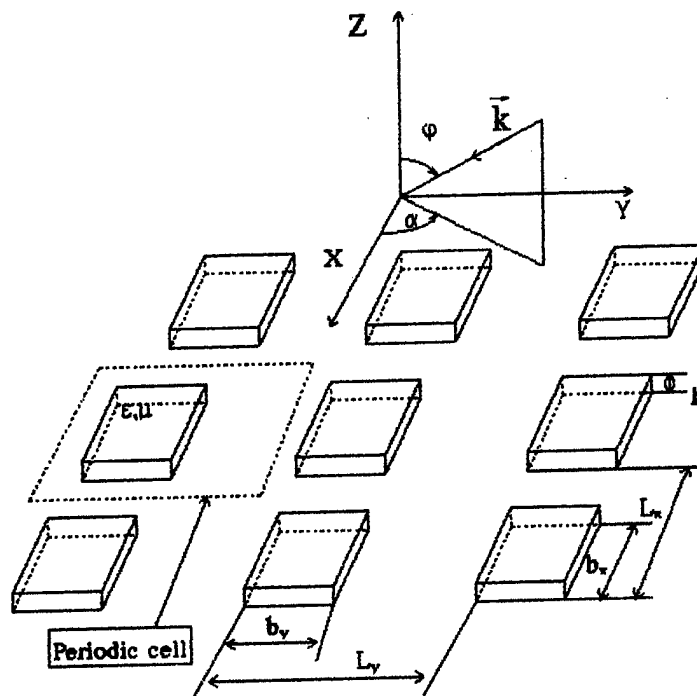


Fig. 1. Geometry of free-standing surface.

Method

The most general set of integro-differential equations for the electromagnetic field can be written in the form borrowed from [1]:

$$\begin{aligned}\vec{E}(\vec{r}) = \vec{E}_0(\vec{r}) + \frac{1}{4\pi}(\nabla\nabla + k^2) \int_V (\hat{\epsilon} - 1) \vec{E}(\vec{r}') G(|\vec{r} - \vec{r}'|) d\vec{r}' - \\ - \frac{ik}{4\pi} \nabla \times \int_V (\hat{\mu} - 1) \vec{H}(\vec{r}') G(|\vec{r} - \vec{r}'|) d\vec{r}',\end{aligned}\quad (1)$$

$$\begin{aligned}\vec{H}(\vec{r}) = \vec{H}_0(\vec{r}) + \frac{1}{4\pi}(\nabla\nabla + k^2) \int_V (\hat{\mu} - 1) \vec{H}(\vec{r}') G(|\vec{r} - \vec{r}'|) d\vec{r}' + \\ + \frac{ik}{4\pi} \nabla \times \int_V (\hat{\epsilon} - 1) \vec{E}(\vec{r}') G(|\vec{r} - \vec{r}'|) d\vec{r}',\end{aligned}\quad (2)$$

where ∇ acts on \vec{r} , $G(r-r')$ is the Green's function. The material of the medium is characterized by the relative permittivity tensor $\hat{\epsilon}$ and the relative permeability tensor $\hat{\mu}$, V is the volume of scatterer, $\vec{E}_0(\vec{r})$ and $\vec{H}_0(\vec{r})$ are the electric and magnetic components of the incident field. Time dependence of the field is assumed to be $\exp(-i\omega t)$ and suppressed throughout this paper.

Taking into account the scattering structure geometry and characteristics of the incident field we can rewrite equation (1)-(2), where the Green's function can be represented in the integral form as:

$$G(r, r') = \frac{1}{2\pi} \int_{-\infty}^{\infty} \int_{-\infty}^{\infty} \frac{e^{i\omega(x-x') + i\gamma(y-y') + i(z-z')\sqrt{k^2 - \gamma^2 - \omega^2}}}{\sqrt{k^2 - \gamma^2 - \omega^2}} d\omega d\gamma$$

and the field inside the grating is expanded in terms of the Floquet modes (see e.g. [2]):

$$\begin{aligned}E(x, y, z) = \sum_{m=-\infty}^{\infty} \sum_{n=-\infty}^{\infty} E_{mn}(z) e^{i(k_x + \frac{2\pi m}{L_x})x} e^{i(k_y + \frac{2\pi n}{L_y})y}, \\ E_{mn}(z) = \frac{1}{L_x L_y} \int_0^{L_x} \int_0^{L_y} E(x', y', z') e^{-i(k_x + \frac{2\pi m}{L_x})x'} e^{-i(k_y + \frac{2\pi n}{L_y})y'} dx' dy', \\ H(x, y, z) = \sum_{m=-\infty}^{\infty} \sum_{n=-\infty}^{\infty} H_{mn}(z) e^{i(k_x + \frac{2\pi m}{L_x})x} e^{i(k_y + \frac{2\pi n}{L_y})y}, \\ H_{mn}(z) = \frac{1}{L_x L_y} \int_0^{L_x} \int_0^{L_y} H(x', y', z') e^{-i(k_x + \frac{2\pi m}{L_x})x'} e^{-i(k_y + \frac{2\pi n}{L_y})y'} dx' dy'.$$

After substituting these expansions into (1), (2) the obtained expression is integrated over all possible variables of integration and differentiated with respect to x and y . Then we act on the left and right-hand sides of these equations by the finite integration operator:

$$\hat{A}_{nl} = \frac{1}{L_x L_y} \int_0^{b_y} \int_0^{b_x} e^{-i(k_x + \frac{2\pi m}{L_x})x} e^{-i(k_y + \frac{2\pi n}{L_y})y} dx dy$$

Eventually, using the easily derivable relations:

$$E_x(z) = \frac{\partial^2 I_x(z)}{\partial^2 z} + \chi_x^2 I_x, \quad H_x(z) = \frac{\partial^2 M_x(z)}{\partial^2 z} + \chi_x^2 M_x,$$

where $I_x(z) = \frac{1}{2i\chi_x} \int_0^h E_x(z') e^{i(k_x - \chi_x z')/L_x} dz'$, $M_x(z) = \frac{1}{2i\chi_x} \int_0^h H_x(z') e^{i(k_x - \chi_x z')/L_x} dz'$ and

$\chi_x = \sqrt{k^2 - (k_x + 2\pi m/L_x)^2 - (k_y + 2\pi n/L_y)^2}$ one can obtain linear differential equations of the second order with constant coefficients in the functionals I_x, M_x . Then, following [3], the transmitted field can be determined:

$$E_x^T(x, y, z) = \frac{1}{4} \sum_m \sum_n \frac{e^{i(\psi_m x + \theta_n y + \chi_{mn}(z-h))}}{\chi'_{mn}} \sum_s e^{\lambda_s h} C_s (\lambda'_s + i\chi'_{mn}) [(1 - \psi_m'^2) W_1 - \psi_m' \theta_n' W_2 - \theta_n' W_5 + \chi'_{mn} W_4 - \psi_s' \chi'_{mn} W_6],$$

$$E_y^T(x, y, z) = \frac{1}{4} \sum_m \sum_n \frac{e^{i(\psi_m x + \theta_n y + \chi_{mn}(z-h))}}{\chi'_{mn}} \sum_s e^{\lambda_s h} C_s (\lambda'_s + i\chi'_{mn}) [(1 - \psi_m'^2) W_2 - \psi_m' \theta_n' W_1 + \psi_m' W_5 - \chi'_{mn} W_3 - \theta_n' \chi'_{mn} W_6],$$

$$E_z^T(x, y, z) = \frac{1}{4} \sum_m \sum_n \frac{e^{i(\psi_m x + \theta_n y + \chi_{mn}(z-h))}}{\chi'_{mn}} \sum_s e^{\lambda_s h} C_s (\lambda'_s + i\chi'_{mn}) [(1 - \psi_m'^2) W_6 - \psi_m' \chi'_{mn} W_1 - \theta_n' \chi'_{mn} W_2 - \psi_m' W_4 + \theta_n' W_3],$$

where $k\psi_m' = \psi_m = k_x + 2\pi m/L_x$, $k\theta_n' = \theta_n = k_y + 2\pi n/L_y$ are the propagation constants of the medium, C_s are the coefficients of the expansion, λ_s, W_j are the eigen values and associated eigen vectors of the structure.

References

1. N.A.Khizhnyak, The Integral Equations of Macroscopic Electrodynamics, Kiev, Naukova Dumka, 1986, (in Russian).
2. N.Amitay, V.Galindo and C.P.Wu, Theory and Analysis of Phased Array Antennas, New York, Wiley, 1972.
3. V.V.Yachin, N.V.Ryazantseva and N.A.Khizhnyak, The scattering of electromagnetic waves by periodic magnetodielectric structures with arbitrary profiles and inhomogeneous media // Journal of electromagnetic waves and applications, Vol. 11, No 10, p.p. 1349-1366, 1997.

PLANE WAVE SCATTERING BY A CASCADED DIFFRACTION GRATING (H-CASE)

Z.Nazarchuk, O.Ovsyannikov, T.Senyk

Physico-Mechanical Institute of National Academy of Sciences of Ukraine

5 Naukova St., Lviv 290601, Ukraine

e-mail: nazarch@ipm.lviv.ua, oleg@ipm.lviv.ua, star@ipm.lviv.ua

ABSTRACT. The problem of a plane wave scattering on a multielement diffraction grating is considered in the paper. The diffracted field is sought for as a double-layer potential. The technique of integration contour deformation is utilized for Green function's calculation. An accounting for a singularity of an integrand on a specially chosen part of the integration contour is adopted to derive a numerical solution. To reduce the computation time for Sommerfeld-type integral calculations essentially a Lagrange-type interpolation polynomial of several variables is constructed. By an integration contour deformation and accounting for residues from poles the estimation of the Green's function at infinity is provided. A two-layered grating of two curvilinear screens on the period was considered.

The correct modeling and engineering of radiowave equipment in the superhigh frequency range require accounting of resonance effects. The high merit of such effects leads to rigorous methods in their investigation, in particular – to integral equation technique. Cascaded diffraction grating often is a resonance element of such equipment. Effects of resonance interaction of electromagnetic waves with such grating are known. But electromagnetic wave diffraction by cascaded grating with shape close to an open planar waveguide is not widely presented in papers yet. This paper is devoted to the last case.

Consider multielement d -periodic grating in homogeneous isotropic media with wave number χ . One period of the grating may contain N cylindrical perfectly conducting screens with generatrices parallel to Oz axis. Cross-sections of the screens by xOy plane are open smooth Lyapunov-type contours L_k , $k = \overline{1, N}$. The grating is irradiated by a unit-amplitude plane electromagnetic wave with $\exp[-i\omega t]$ time dependence incident at β angle to Oz axis. Such problem is reducible to Helmholtz equation solution which satisfies the following conditions: of Dirichlet (E -polarization) or Neumann (H -polarization) on the arcs L_k , $k = \overline{1, N}$; of Meixner-type near the screens' ribs (L_k arc end-points); of absence of wave propagating from infinity (except the exciting one). Consider only the H -case now.

The diffracted field is sought for as a double-layer potential. Using Floquet periodic condition a Green function of such periodic problem is obtained

$$G(t_k, z) = \frac{i}{4} H_0^{(1)}(\chi r_k) + \frac{i}{4} \sum_{\substack{u=-\infty \\ u \neq 0}}^{+\infty} H_0^{(1)}(\chi |t_k + ud - z|) \exp[i\chi du \sin \beta], \quad (1)$$

$r_k = |t_k - z|$, $t_k = t_k(s_k) = x_k(s_k) + iy_k(s_k)$, s_k - arc abscissa of contour L_k , $z = x + iy$ - complex view-point coordinate, u - period number.

The evaluation of function (1) requires convolution of weakly convergent series. The series in (1) are diverging in grazing points and direct convolution of the series is unjustified. That is why the known [1] integral presentation of Hankel function and the future special integral's contour deformation is used [2,3] which lead to:

$$\begin{aligned} G(t_k, z) &= \frac{i}{4} H_0^{(1)}(\chi r_k) + S_+(t_k, z) + S_-(t_k, z); \\ S_+(t_k, z) &= e^{-i\chi d \sin \beta} \frac{1}{4\pi} \int_{\Gamma_m} \frac{1}{v(1 - e^{id(\xi - \chi \sin \beta)})} e^{-[\Im\{t_k - z\}v - i\xi \Re\{t_k - d - z\}]d\xi}, \\ S_-(t_k, z) &= e^{i\chi d \sin \beta} \frac{1}{4\pi} \int_{\Gamma_m} \frac{1}{v(1 - e^{id(\xi + \chi \sin \beta)})} e^{-[\Im\{t_k - z\}v + i\xi \Re\{t_k + d - z\}]d\xi}. \end{aligned} \quad (2)$$

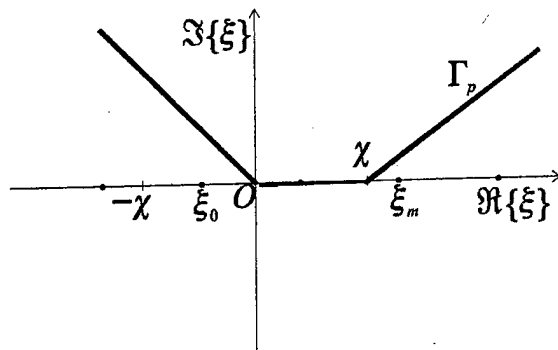
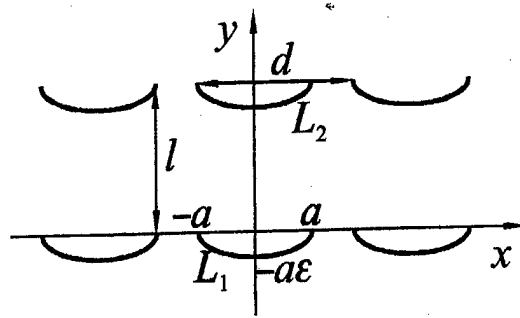
Fig. 1. Account for existing of poles ξ_l .

Fig. 2. Cascaded grating with two curvilinear screens on the period.

Calculation of integrals (2) requires accounting for a logarithmic singularity in functions $S_{\pm}(t_k, z)$

$$S_{\pm}(t_k, z) = e^{\mp i\chi d \sin \beta} \frac{i}{4} (H_0^{(1)}(\chi |z - t_k \pm d|) + S_{\pm}(t_k \mp d, z)). \quad (3)$$

To reduce the computation time essentially for Sommerfeld-type integral calculations when repeated many times a Lagrange-type interpolation polynomial of several variables is constructed [4].

To provide estimation of function $G(t, z)$ at infinity it is necessary to change contour Γ_m like in Fig. 1 accounting for poles ξ_m on real axis Ox . Accounting for residues from them derives to:

$$G^{\infty} = \frac{i}{2\chi d} \sum_{m=-n}^{n_k} \frac{e^{i\chi \{ \Im\{z-t_k\} \cos^* (\beta, m) + \Re\{z-t_k\} \sin^* (\beta, m) \}}}{\cos^* (\beta, m)}, \quad (4)$$

$$\cos^* (\beta, m) = \sqrt{\cos^2 \beta - \frac{4\pi m}{\chi d} \sin \beta - \left(\frac{2\pi}{d} m \right)^2}, \quad \Im\{\cos^* (\beta, m)\} \geq 0, \quad \sin^* (\beta, m) = \frac{2\pi}{\chi d} m + \sin \beta$$

Angle θ is established under condition of the fastest decaying of the integrand function. Then, the field at infinity may be obtained as [5]

$$H^s(z) \Big|_{\Im\{z\} \rightarrow \pm\infty} = \frac{\pi i}{\chi d \cos \beta} \sum_{k=1}^N \int_{L_k} j_k(t_k) \frac{\partial}{\partial n_k} \times \\ \times \frac{\partial}{\partial n_k} (\exp[i\chi (\pm \Im\{z-t_k\} \cos \beta + \Re\{z-t_k\} \sin \beta)]) ds_k$$

To receive the solution of the problem construct the integral equation system by satisfying the conditions on the contours L_k , $k = 1, N$. The systems are solved by the mechanical quadrature method [3].

As an example, consider the case when one grating's period contains two screens. Contours L_k are parabolic arcs with end-points $a+il(k-1)$ and vertexes $-ib+il(k-1)$ (Fig. 2). Parametric arc's equations in complex plane $z=x+iy$ look like

$$t_k(\tau) = a(\tau + i\varepsilon(1-\tau^2)) + il(k-1), \quad \tau \in [-1; 1], \quad \varepsilon = b/a, \quad k = 1, 2 \quad (5)$$

where l is distance between screens. The wave number χ is postulated to be real. Such cascaded grating may be considered as an open waveguide.

Fig. 3 presents behaviour of reflection coefficient [5]

$$R = H^s(z) \Big|_{\Im\{z\} \rightarrow +\infty} \cdot \exp[-i\chi \{ \Im\{z\} \cos \beta + \Re\{z\} \sin \beta \}]$$

depending on l and β (incident angle influence). Here we assume that $d=\pi/2$, $a=d/2$, and $\mathbb{M}_1=\mathbb{M}_2=0.0$. The grating is irradiated by H -polarized plane wave. In the case of $l=0.35d$ the grating is nearly transparent. The increasing of l leads to increasing of R . The reflection minimum migrates to the larger l values correspondingly with the incident angle increasing.

Figs. 4,6 present behaviour of reflection coefficient of the same grating but the screens' camber is nonzero. Here we assume that $d=\pi/2$, $a=d/2$, $\mathbb{M}_1=\mathbb{M}_2=0.25$ at Fig. 4 and $\mathbb{M}_1=-\mathbb{M}_2=0.25$ at Fig. 6. In general the influence of screens' camber leads to the smoothing of the grating's reflects coefficient (Fig. 4) and to the

increasing of the incident angle influence (Fig. 6). The reflection minimum shifts from $l=0.35d$ at Fig. 3 to $l=0.40d$ at Fig. 4 and $l=0.45d$ at Fig. 6. So, with the higher screens' camber the considered waveguide seems to be wider. It is also worth to mention the increasing of the reflection coefficient at the high incidence angles ($\beta > 80^\circ$).

Fig. 5 presents the "incidence angle – screens' camber" dependencies of the reflection coefficient of the same grating. Here we assume that $d=\pi/2$, $a=d/2$, $l=0.351d$ (the case of the reflection minimum at Fig. 3).

As a conclusion of the paper one can say that the integral representation of periodic Green function that presented here allowed increasing noticeably the calculation accuracy. The application of interpolation polynomial to Green function approximation significantly decreased the amount of that calculations. That allows to construct efficient from a computer-resource point view algorithm of solution of scalar problem of plane electromagnetic wave diffraction on a multielement grating consisting from arbitrary-profiled screens and to provide an accurate numerical analysis of its scattering features in the resonance range.

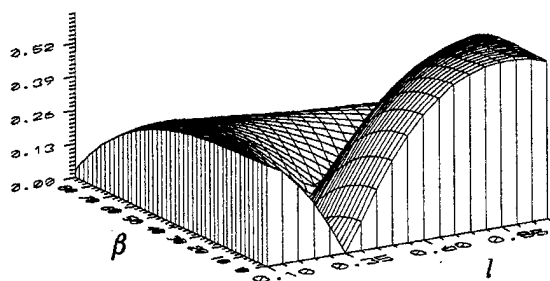


Fig. 3. Reflection coefficient of a two-layered plane grating.

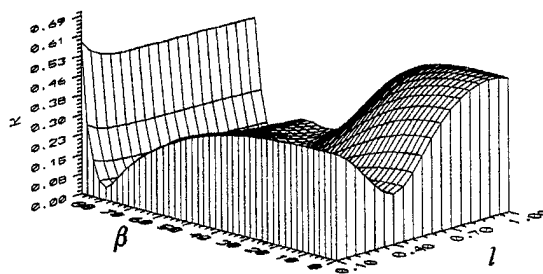


Fig. 4. Reflection coefficient of a two-layered curvilinear grating ($m_1=m_2=0.25$).

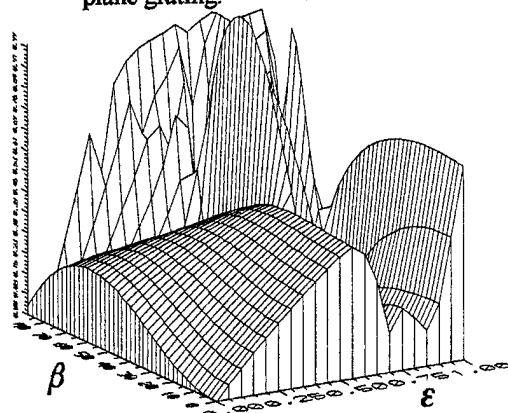


Fig. 5. Reflection coefficient of a two-layered curvilinear grating ($l=0.351d$)

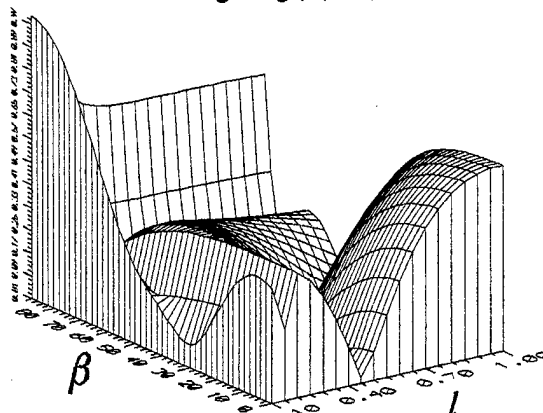


Fig. 6. Reflection coefficient of a two-layered curvilinear grating ($m_1=-m_2=0.25$).

REFERENCES

1. Lüneberg E. Diffraction by an infinite set of parallel half-planes and by an infinite strip grating: comparison of different methods, *Analytical and numerical methods in electromagnetic wave theory*. – Tokyo: Science House Co., 1993, P.317 –372.
2. Z. Nazarchuk, O. Ovsyannikov, T. Senyk, Plane Wave Scattering by a Multilayer Diffraction Grating, *Journées Internationales De Nice Sur Les Antennes*, Nice, 1994, pp. 302–305.
3. V.V. Panasyuk, M.P. Savruk., Z.T. Nazarchuk, Method of Singular Integral Equations in Two-Dimensional Diffraction Problems, Kyiv: Nauk. dumka, 1984, 344p (in Russian).
4. Z. Nazarchuk, O. Ovsyannikov, T. Senyk, Interpolation Method for Evaluation of Periodic Green Function in the Problem of Diffraction, *Radiophysics and Radioastronomy*. V.1, 1996, pp.32–36.
5. Z. Nazarchuk, O. Ovsyannikov, Electromagnetic Wave Diffraction by a Multielement Diffraction Grating, *Reports of AS of Ukraine*, 1994, A, №7, pp.79-84 (in Russian).

Analysis of the scattered field from the grating of resistive dipoles

J. Ziemelis, P. Chertov

Riga Technical University

Abstract—Microwire gratings may be used as a component of absorbing structures, so it's important to study different gratings consisting of resistive materials. Scattering of electromagnetic waves from a two-dimensional regular grating is investigated. The microwires are coated with a glass sheath. It effects little on electromagnetic properties but may effect pretty much on the process of heat exchange in strong electromagnetic fields.

A simulation methodology with reference of different parameters of gratings is worked out. Also, a degree of microwire heating is estimated with different intensities of the incident field.

Resistive microwires are thin cylinders with diameter over a range from some tenth of a micron to some microns. The cylinder consists of an amorphous material and coated with a glass sheath [1]. Microwires properties are specified by a value of the resistance per unit length, which may vary over a wide range. Such microwires may be used as a component of absorbing structures [2]. While the analysis methodology of infinite gratings is well known [3], few works concern gratings with elements of finite size and specific resistive properties. A method of computer simulation for the analysis of the field scattered from gratings with different parameters is to be worked out.

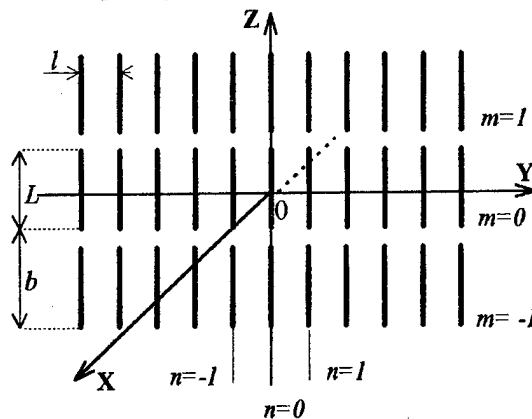


Fig. 1.

The analysed grating [Fig.1] consists of dipoles of equal length L which are parallel to z -axis. Let b denote the grating's period along z -axis and l - along y -axis. The dipoles are labeled with indexes m (along z -axis) and n (along y -axis). The dipole with zero index is located in the origin of coordinates.

For simplicity, the case of normal incidence is considered. Solution of the electric field integral equation (EFIE) is done by the Method of Moments. Electric field is a result from incident and scattered field intensities. Scattered field intensity is excited by the current in microwires.

$$\vec{I}_{ekv} = \int_S \vec{J}_{ekv} \cdot dS = i\omega \int_S (\epsilon - \epsilon_0) \cdot \vec{E} \cdot dS$$

Vector potential of the scattered field is a result from all dipole currents. Due to a very small cross-section and conductivity of the microwires, current density in the cross-section could be assumed constant, thus simplifying solutions of the vector potential:

$$\vec{\Pi} = \vec{e}_z \sum_{n=-\infty}^{\infty} \sum_{m=-\infty}^{\infty} \int_0^L \frac{I_{ekvz} \cdot e^{-ika_{nm}}}{4\pi \cdot a_{nm}} \cdot ds, \quad (1)$$

where $a_{nm} = \sqrt{(z-s-m \cdot b)^2 + (y-n \cdot l)^2 + x^2}$.

Scattered field intensities:

$$\vec{E} = \frac{1}{i\omega\epsilon_0} \cdot (k^2 + \text{grad div}) \vec{\Pi}; \quad \vec{H} = \text{rot} \vec{\Pi}. \quad (2)$$

The current distribution is found in the form of the Fourier series

$$I_{ekvz}(s) = \sum_{v=1}^{35} p_v \cdot \sin\left(\frac{\pi \cdot v \cdot s}{L}\right).$$

The expansion coefficients we get by writing equations on the surface of the microwire:

$$Z \cdot \sum_{v=1} p_v \cdot \sin\left(\frac{\pi v z}{L}\right) = E_{0z} + \frac{1}{i\omega\epsilon_0} \left(k^2 + \frac{\partial^2}{\partial z^2}\right) \sum_{v=1} p_v \sum_{n=-\infty}^{\infty} \sum_{m=-\infty}^{\infty} \int_0^L \frac{e^{-ika_{nm}}}{4\pi a_{nm}} \cdot \sin\left(\frac{\pi v s}{L}\right) \cdot ds, \quad (3)$$

where Z is the impedance per unit length of the microwire and E_{0z} - incident field intensity.

Using orthogonality of the trigonometric functions, from (3), we obtain system of equations determining current's coefficients. Also, using integral relation

$$\frac{e^{-ika_{nm}}}{a_{nm}} = \int_0^{\infty} \frac{J_0\left(t\sqrt{(y-n \cdot l)^2 + x^2}\right)}{\sqrt{t^2 - k^2}} \cdot e^{-|z-s-m \cdot b| \cdot \sqrt{t^2 - k^2}} \cdot t \cdot dt$$

and Poisson's summation formula, Fourier series sum and majority of the integrals principal values we can write analytically.

We used magnetic field to obtain scattered field in the far zone. Components of the magnetic field produced by this current (the scattered field from the dipole with indexes m, n)

$$H_{xnm} = \frac{\partial}{\partial y} \int_0^L I_{ekvz}(s) \frac{\exp(-ika_{nm})}{a_{nm}} \cdot ds \quad H_{ynm} = -\frac{\partial}{\partial x} \int_0^L I_{ekvz}(s) \frac{\exp(-ika_{nm})}{a_{nm}} \cdot ds \quad (4)$$

The total scattered field

$$H_x = \sum_{n=-\infty}^{\infty} \sum_{m=-\infty}^{\infty} H_{xnm}; \quad H_y = \sum_{n=-\infty}^{\infty} \sum_{m=-\infty}^{\infty} H_{ynm}. \quad (5)$$

Since the argument of the exponential function may be substituted with square root approximation in the far zone ($x \gg \lambda$), integrals in (4) may be expressed in terms of the Fresnel integrals. In case of great distances to the view point $|m \cdot b| \gg L$, the results may be expressed in terms of elementary functions. Performing integration in (4), for the harmonic of the current with number v

$$R_{vnm} = \frac{A_{nm}^2 \cdot (\pi \cdot v / L)}{A_{nm}^2 \cdot (\pi \cdot v / L)^2 - k^2 \cdot (m \cdot b - z)^2} \cdot \left\{ 1 - (-1)^v \cdot \exp\left[-ikL \cdot (m \cdot b - z) / A_{nm}\right] \right\}$$

where $A_{nm} = \sqrt{(z-m \cdot b)^2 + (y-n \cdot l)^2 + x^2}$.

Differentiating the obtained expressions, one may show that the double series converge according to the Cauchy integral criterion.

Summing the double series with respect of m , a sum over n is derived with its module decreasing as $n^{-3/2}$. Observing changes of arguments of complex terms, it's possible to evaluate the result of summation. Since the magnetic field in the far zone almost completely formed by its transversal component, the electric field intensity may be found from corresponding expressions for a plane wave.

The simulation were carried out with following parameters of microwires: radius $5[\mu\text{m}]$, resistance per unit length $R_p=1[\text{k}\Omega/\text{cm}]$ and intensity of the incident field $E_0=1[\text{V/m}]$. In order to compare results, those values were taken for the length of the dipoles $L=1[\text{cm}]$ and wavelength $\lambda=3[\text{cm}]$. For convenience, the origin of coordinates is shifted to the lower end of the dipole labeled $m=0, n=0$.

Numerical results:

1. $b=1.5[\text{cm}]$, $l=2[\text{cm}]$. The view point coordinates $x=100[\text{cm}]$, $y=0[\text{cm}]$, $z=0.5[\text{cm}]$. Evaluated intensity of the scattered field $E_s=2.8032 \cdot \exp(i \cdot 0.18227)[\text{mV/m}]$.

2. $b=1.5[\text{cm}]$, $l=2[\text{cm}]$, $x=1[\text{m}]$, $y=0[\text{cm}]$, $z=0[\text{cm}]$, $E_s=2.8035 \cdot \exp(i \cdot 0.18223)[\text{mV/m}]$.

3. $b=1.5[\text{cm}]$, $l=2[\text{cm}]$, $x=10[\text{m}]$, $y=0[\text{cm}]$, $z=0.5[\text{cm}]$, $E_s=2.7981 \cdot \exp(i \cdot 0.18178)[\text{mV/m}]$.

4. $b=1.5[\text{cm}]$, $l=0.1[\text{cm}]$, $x=100[\text{cm}]$, $y=0[\text{cm}]$, $z=0.5[\text{cm}]$, $E_s=22.172 \cdot \exp(i \cdot 0.74566)[\text{mV/m}]$.

Estimating approximate value of absorbed power, mutual resistance of dipoles in the grating isn't taken into consideration. For cylindrical conductors their impedance per unit length is

$$Z = \frac{k_1 r}{2} \cdot \frac{J_0(k_1 r)}{J_1(k_1 r)} \cdot \frac{1}{\pi \cdot r^2 \cdot \sigma_1} \quad \text{where } k_1 = \frac{2\pi}{\lambda} \cdot \sqrt{1 - i \frac{\sigma_1}{\omega \cdot \epsilon_0}}.$$

With this approximation the absorbed power is

$$P = 0.5 \cdot \int_0^L |I(s)|^2 \cdot \text{Re}(Z) \cdot ds$$

which includes the active power of radiation. Therefore, the radiation resistance should be subtracted from $\text{Re}(Z)$ evaluating the power of losses. In the simplest way its value may be estimated by comparing with radiation resistance of the Hertz dipole ($87.7 [\Omega]$). In our case, it is small part of the resistance and may be neglected in the first approximation.

Outside radius of the glass coating $r_2=10[\text{m}]$. Estimating the process of heat exchange, we assume that the temperature doesn't increase outside the glass sheath. In that case, the amount of heat emitted by the conductor is equal to the amount of heat emitted outside the glass coating. Its thermal conductivity $=1.13[\text{W/m} \cdot \text{grad}]$. Heat amount emitted per unit time outside the glass coating in the stationary case must be set equal to absorbed power

$$\frac{2 \cdot \pi \cdot \eta \cdot L \cdot (T_1 - T_0)}{\ln(r_2/r)} = P. \quad (6)$$

Expression (6) allows us to find the temperature of the dipoles and change the value of their resistance per unit length if necessary. For $E_0=1 [\text{kV/m}]$, the value of absorbed power $P=0.25[\text{mW}]$, that changes the temperature of the dipoles approximately for $\Delta T=2.4 \cdot 10^{-3}$. However, with intensities of the incident field higher than $1 [\text{kV/m}]$, behaviour of the impedance per unit length becomes non-linear and other methods are needed considering this problem.

Conclusions. Values of the magnetic field intensities calculated for different x and z indicates that the shape of the scattered field corresponds to a plane wave. For sparse gratings, intensity of the scattered field as well as the reflection coefficient of plane waves are negligible. For dense gratings ($l=1[\text{mm}]$), intensity of the scattered field increases considerably. Thus, microwires are effective scatterers with little space filling. The idea of warming dipoles up with medium intensities of the incident field is groundless.

References

1. Бадинтер Е.А., Берман Н.Р. и др. Литой микропровод и его свойства. Кишинев: ШТННЦА, 1973.
2. V.Lazarev, J.Semenako. Electromagnetic waves absorber. Patent of the Republic of Latvia HP01Q17/00, 1994.g.
3. Шестопалов В.П., Кириленко А.А., Масалов С.А., Сиренко Ю.К. Дифракционные решетки. Киев: Наукова думка, 1986, 232с.
4. Computer techniques for electromagnetics. Edited by R.Mitra. Pergamon Press, 1973, 486 p.
5. Кутателадзе С.С. Основы теплообмена. Москва: Атомиздат, 1979, 45с.

EXAMPLES OF "FAKED UNITARITY" IN DIFFRACTION GRATING COMPUTATIONS

Sergey Yu. Sadv

Keldysh Institute of Applied Mathematics, Moscow, 125047, Russia
and

Department of Physics and Astronomy, University of Manitoba
Winnipeg, MB, R3T 2N2, Canada

Abstract. The energy balance criterion is the most widely used tool for verification of diffraction computations. Two examples are given, in which numerical methods imply that the criterion is fulfilled exactly, but results are incorrect: in the first case due to problem's parameters lying beyond the region of the method's validity, in the second case due to a programming error.

1. Introduction. There exist many methods for solving electromagnetic diffraction problems, in particular, grating problems (see e.g. [1,2]), but very few ways to confirm the correctness of numerical results. In the author's opinion, the following three approaches have a good reputation and may be recommended:

- (1) varying the algorithm's parameter(s) like a stepsize until the results stabilize;
- (2) comparison of results obtained by independent methods;
- (3) for conservative problems — checking the energy balance.

See [3] for critique of some other verification methods.

Methods (1) and (2) require a series of (at least two) calculations for the same problem. Besides, (1) meets practical difficulties for certain diffraction grating algorithms realized with the limited-precision arithmetics. For example, in the Rayleigh point-matching method, decreasing the stepsize leads to a poor-conditioned matrix.

Consequently, the energy balance criterion, if applicable, is widely used to determine the validity and to evaluate the precision of a solution *directly*.

Usually one assumes a *real number* to be the criterion's output. That number is, however, just one of the diagonal entries of a quadratic complex matrix S^*S , where S is the *scattering matrix* [2]. It is useful (especially in test computations) to have the whole matrix S^*S computed and to compare it to the identity matrix. In case of the S -matrix's size greater than 1, this approach increases the probability of error detection — or the confidence in the correctness of results.

The energy balance (or the unitarity) criterion is a helpful and, in general, a reliable tool. However, in this paper we draw the reader's attention to possible misleading conclusions that may be caused by a blind belief in this criterion.

In our first example we deal with the Rayleigh point-matching method. This method has well-known, theoretically argued bounds of applicability [1],[3]. We show, however, that the numerical scheme inherently satisfies the energy balance criterion in case of normal incidence of a long wave, no matter what is the profile height and the stepsize. The second example, from the programming practice [4], concerns a hard-to-detect program bug. Despite of the bug, the calculation demonstrates the convergence and exactly satisfies the unitarity criterion. In both examples we avoid complications and consider the simplest versions of scattering problems: scalar fields, 2D geometry, Dirichlet's boundary conditions.

2. Notation and Problems. Put the grating period $d = 2\pi$, angle of incidence θ , wave number k . Coordinates: x (along the grating), z (upright). The field $U(x, z)$ is

considered above the grating (Reflection Problems, abbr. RP) or above and under the grating (Reflection-Refraction Problems, abbr. RRP). It satisfies the Helmholtz equation $\Delta U + k^2 U = 0$ outside the grating. For RP, $k^2 = \text{const}$ above the grating; for RRP, we have two different constants k^2 and \tilde{k}^2 , above and under the grating. A problem formulation includes: a boundary condition, the quasiperiodicity condition $U(x + d, z) = U(x, z)e^{i\alpha}$, $\alpha = \sin \theta$, and the radiation condition, which we replace by a direct definition of the scattering matrix. In our examples boundary conditions are the Dirichlet conditions at the grating surface: for RP, $U = 0$; for RRP, U and $\partial U / \partial n$ to be continuous.

Denote, for $n \in \mathbb{Z}$: $\alpha_n = \alpha + n$, $\mathcal{P} = \{n \in \mathbb{Z} : |\alpha_n| < k\}$, $\mathcal{E} = \mathbb{Z} \setminus \mathcal{P}$. (\mathcal{P} stands for propagating waves, \mathcal{E} for evanescent waves). Next, $\beta_n = (k^2 - \alpha_n^2)^{1/2}$; square root sign rule: $\beta_n > 0$ for $n \in \mathcal{P}$, $\text{Im} \beta_n > 0$ for $n \in \mathcal{E}$. For RRP, we introduce, in addition, the notation $\tilde{\mathcal{P}}$, $\tilde{\mathcal{E}}$ and $\tilde{\beta}_n$ corresponding to \tilde{k} .

Scattering matrix — RP. The field above the top of grating consists of incident (–), reflected (+) and evanescent (0) waves:

$$U(x, z) = \sum_{n \in \mathcal{P}} A_n^{(\pm)} \exp(i\alpha_n x \pm i\beta_n z) + \sum_{n \in \mathcal{E}} A_n^{(0)} \exp(i\alpha_n x - |\beta_n z|).$$

(1) *There exists a one-to-one linear correspondence between the set of coefficients $\{A_n^{(+)}\}$ and $\{A_n^{(-)}\}$:*

$$\beta_n^{-1/2} A_n^{(+)} = \sum_{m \in \mathcal{P}} S_{nm} \beta_m^{-1/2} A_m^{(-)}. \quad (2) \text{Complex numbers}$$

S_{nm} constitute the *scattering matrix*. It is the goal of a computation.

Scattering matrix — RRP. In addition to the latter paragraph, the structure of the field under the bottom of grating is described by Eq. (1) with tilded notation: $\tilde{A}_n^{(+/-/0)}$, $\tilde{\mathcal{P}}$, $\tilde{\mathcal{E}}$, $\tilde{\beta}_n$. Now $\tilde{A}_n^{(-)}$ are the amplitudes of refracted waves, $\tilde{A}_n^{(+)}$ the amplitudes of the waves incident from below. The *reflection matrix* R and the *transmission matrix* T relate the coefficient sets $\{A_n^{(-)}\}$, $\{A_n^{(+)}\}$ and $\{\tilde{A}_n^{(-)}\}$ under the condition $\tilde{A}_n^{(+)} = 0$, $n \in \tilde{\mathcal{P}}$:

$$\begin{aligned} \beta_n^{-1/2} A_n^{(+)} &= \sum_{m \in \mathcal{P}} R_{nm} \beta_m^{-1/2} A_m^{(-)}, & n \in \mathcal{P}, \\ \tilde{\beta}_n^{-1/2} \tilde{A}_n^{(-)} &= \sum_{m \in \mathcal{P}} T_{nm} \beta_m^{-1/2} A_m^{(-)}, & n \in \tilde{\mathcal{P}}. \end{aligned}$$

To define the reflection \tilde{R} and transmission \tilde{T} matrices w.r.t. incidence from below the grating, one exchanges the symbols with and without tildes. The whole scattering matrix consists of four blocks $R, T, \tilde{R}, \tilde{T}$.

3. Example 1: Faked unitarity in Rayleigh's point matching method. Recall the simplest version of the Rayleigh method for solving the Reflection Problem. The expansion (1) is supposed to be valid up to the boundary. The infinite series over $n \in \mathcal{E}$ is truncated at $n = \pm N$; points (x_j, z_j) on the boundary are chosen. Given coefficients $A_n^{(-)}$, the system of linear equations $U(x_j, z_j) = 0$ is solved w.r.t. unknowns $\{A_n^{(+)}\}$, $\{A_n^{(0)}\}$.

Consider a normally incident long wave: $k < 1$. Only one diffraction order exists, and the scattering matrix reduces to the complex number $S_{00} = A_0^{(+)} / A_0^{(-)}$.

Theorem. *Let $k < 1$ and $\alpha = 0$. Then the Rayleigh method with symmetric truncation always brings to a unitary scattering amplitude $|S_{00}| = 1$.*

Proof. Consider matrices $A = (a_{jn})$ and $A' = (a'_{jn})$ defined by

$$\begin{aligned} a_{jn} &= \exp(i\alpha_n x_j + i\beta_n z_j), & -N \leq j, n \leq N, \\ a'_{jn} &= a_{jn} \quad (n \neq 0), & a'_{j0} = -\exp(i\alpha_n x_j - i\beta_0 z_j), & -N \leq j \leq N. \end{aligned}$$

By Kramer's rule, $S_{00} = \det A' / \det A$.

Denote by B the $(2N+1) \times 2N$ matrix obtained from A by means of exclusion of the 0-th column. The mirror permutation ($n \leftrightarrow -n$) of the columns of the matrix B gives us the matrix \hat{B} . Since $\alpha = 0$, we have $\alpha_n = n$, $\beta_n = \beta_{-n}$. Consequently, $a_{jn} = \bar{a}_{j,-n}$ ($1 \leq n \leq N$), and $\hat{B} = \bar{B}$ (bar stands for complex conjugation). Hence, all of $(2N+1)$ minors M_n of order $2N$ of the matrix B possess the property $M_n = (-1)^N \bar{M}_n$, i.e. M_n are either all real or purely imaginary. Now,

$$\det A = \sum_{-N \leq n \leq N} (-1)^n \exp(i\beta_0 z_n) M_n, \quad \det A' = - \sum_{-N \leq n \leq N} (-1)^n \exp(-i\beta_0 z_n) M_n.$$

Since all M_n have the same complex arguments, we obtain $|\det A| = |\det A'|$. Q.E.D.

4. Example 2: Faked unitarity in a wrong realization of the differential method. The *differential method* [1] for the Reflection-Refraction problem consists in the following. The field is expanded in quasi-periodic Fourier series

$$U(x, z) = \sum U_n(z) \exp(i\alpha_n x).$$

Using the Helmholtz equation and the boundary condition, an infinite system of second order ordinary differential equations w.r.t. the functions $U_n(z)$ is derived. The system is truncated at $n = \pm N$. Then one subsequently assigns the Cauchy data under the bottom of the grating corresponding to sole refracted and evanescent waves (but not to the waves incident from below) and solves the ODE system to the top of the grating. So, for $z \ll 0$ we have: $U_n(z) = \delta_{nj} \exp(i\tilde{\beta}_j z)$ for $j \in \tilde{\mathcal{P}}$; $U_n(z) = \delta_{nj} \exp(|\tilde{\beta}_j|z)$ for $j \in \tilde{\mathcal{E}}$. For the j -th set of data, we obtain as $z \gg 0$:

$$U_n(z) = M_{nj}^+ \exp(i\beta_j z) + M_{nj}^- \exp(-i\beta_j z).$$

From the matrices M^+ and M^- we derive the reflection matrix R : it is the submatrix of $(M^-)^{-1} M^+$ whose column and row indices belong to the set \mathcal{P} . Other blocks of the scattering matrix are calculated similarly.

Now, what happened once to a computer program. Because of a typing error, the Cauchy data corresponding to the exponents $\exp(i\tilde{\beta}_j z)$, $j \in \tilde{\mathcal{P}}$, were replaced by the data corresponding to the real exponents $\exp(\tilde{\beta}_j z)$. Matrices M^+ and M^- appeared to be complex conjugate, and the matrix R was always unitary, that was considered as an excellent result in the case of *total internal reflection*. However, the unitarity of the R -matrix was unexpectedly observed beyond that case as well. It ultimately made the programmer to seek an error.

Acknowledgements. The author is grateful to Dr. A.S. Shamaev, Dr. M.A. Gilman, and Mr. M. Smith for discussions regarding grating computations. This work was supported by a Postdoctoral Fellowship from the University of Manitoba, which became possible due to the initiative of Dr. K.A. McGreer.

REFERENCES

- [1]. Electromagnetic theory of gratings, R. Petit ed., Springer, Topics in Current Physics, **22**, 1980.
- [2]. A.G. Voronovich, Wave scattering from rough surfaces, Springer, Series in Wave Phenomena, **17**, 1994
- [3]. A. Wirgin, Reflection by a grating: Rayleigh methods: Comments, JOSA L **72**:7, 1982, 963-969
- [4]. M. Smith, Personal communication, 1998

CLASSIFICATION OF WAVE INSTABILITIES PRODUCED BY INTERACTION OF GRATING MODES

Yu. Terent'ev

*Radiophysics Department, Dnepropetrovsk State University,
Dnepropetrovsk 320625, Ukraine*

Phone: +380-562-43-36-30, e-mail: vytovtov@apl.net-rff.dsu.dp.ua

Here we present the criteria and the main results of the wave instability studies in a phase grating containing space harmonic set. It is now generally accepted that all instabilities may be reduced to those of Bragg's kind. The Bragg's correlations pertain, however, barely to special case periodical system. Now we assume that the dielectric permittivity takes the grating form

$$\varepsilon(x) = \varepsilon\{1 + hg(x)\}; \quad h \ll 1, \quad (1)$$

where

$$g(x) = \sum_{i=1}^M C_i \cos(k_i x). \quad (2)$$

Any common relations between k_i are assumed.

Consider the appropriate differential equation

$$U''(x) + a\{1 + hg(x)\}U(x) = 0. \quad (3)$$

We expand the acceptable solution $U(x)$ in a power series in h

$$U(x) = \sum_{i=0}^{\infty} h^i U_i(x). \quad (4)$$

A similar presentation we apply to $a(h)$:

$$a(x) = \sum_{i=0}^{\infty} h^i a_i. \quad (5)$$

by substitution, differential equation takes the form of an infinite set of differential equations. The left-hand side of any equation has a simple form:

$$\hat{L}U = U'' + a_0 U. \quad (6)$$

Combining (3), (4), (5), we obtain

$$\begin{cases} U_0'' + a_0 U_0 = 0 \\ U_1'' + a_0 U_1 = -g a_0 U_0 - a_1 U_0 \\ U_2'' + a_0 U_2 = -g a_0 U_2 - g a_1 U_0 - a_1 U_1 - a_2 U_0 \\ \dots\dots\dots \\ U_n'' + a_0 U_n = -g \sum_{i=1}^{n-1} a_i U_{n-i-1} - \sum_{j=1}^n a_j U_{n-j} \end{cases} \quad (7)$$

The presence of divergence, i.e. resonance terms in the right-hand side of the n -th order linear equation, in this set is accounted for by the parametric wave instability. The order of instability will be depending upon the order of the linear equation.

For any chosen value a_0 we solve the set of equation by integrations.

Removing the secular member at the n -th order we get the pair $a_n^{(1)}, a_n^{(2)}$

$$a_n^{(2)} > a_n^{(1)}. \quad (8)$$

The center of the instability band is settled near

$$a_0 \approx k_g \sqrt{\varepsilon}. \quad (9)$$

For the band of the instability we obtain

$$\sum_{n=0}^{\infty} a_n^{(1)} h^n \leq a \leq \sum_{n=0}^{\infty} a_n^{(2)} h^n. \quad (10)$$

In the most mere situation condition of instability has the following form:

$$2k_g \sqrt{\varepsilon} = |k_i - k_j|; \quad i, j=1, 2 \dots M \quad (11)$$

So, this instability is formed by the difference of grating modes. Sum of grating modes forms the instability

$$2k_g \sqrt{\varepsilon} = |k_i + k_j|; \quad i, j=1, 2 \dots M \quad (12)$$

The width of the band Δk can be written as

$$\Delta k \sqrt{\varepsilon} \cong h^2 C_i C_j. \quad (13)$$

For the even order such an instability takes the form

$$2k_g \sqrt{\varepsilon} = n|k_i - k_j|; \quad n=1, 2 \dots; \quad i, j=1, 2 \dots M \quad (14)$$

and

$$2k_g \sqrt{\varepsilon} = n|k_i + k_j|; \quad n=1, 2 \dots; \quad i, j=1, 2 \dots M \quad (15)$$

with

$$\Delta k \cong h^{2n}. \quad (16)$$

For the simple instabilities at odd order we got the condition:

$$2k_g \sqrt{\varepsilon} = |2k_i - k_j|; \quad i, j=1, 2 \dots M, \quad (17)$$

and, respectively,

$$2k_g \sqrt{\varepsilon} = |2k_i + k_j|; \quad i, j=1, 2 \dots M, \quad (18)$$

where

$$\Delta k \cong h^3 C_j C_i^n. \quad (19)$$

We have carried out similar calculations in the band of instability. Suitable unknown function $U(x)$ is defined as

$$U(x) = V(x) e^{\mu x}, \quad (20)$$

where q is expanded in a power series in h

$$\mu(h) = \sum_{l=0}^{\infty} h^l \mu_l. \quad (21)$$

As above we may calculate the solution by means of iteration procedure.

In summary, the existence on instabilities is due to interaction between electromagnetic wave and phase grating modes. Periodicity of grating, i.e. $g(x)$ function periodicity, is likely to be unimportant.

Combining our analytical studies with model calculations may lead to a better understanding of wave instabilities.

DIFFRACTION OF PLANE WAVE ON DIELECTRIC GROOVE

Katerina Yu. Kramarenko, Nikolay A. Khizhnyak

*Chair of Applied Electrodynamics, Kharkov State University, Svobody sq. 4
Kharkov 310077, Ukraine*

Consider a diffraction of a plane wave on dielectric groove by the method, which was used, for example, in [1,2] for theoretical study of similar problems (Fig. 1).

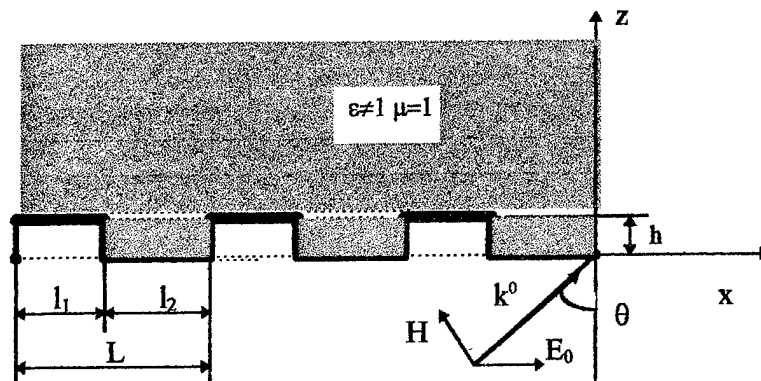


Fig. 1

We divide the whole domain into two sub-domains: I - $z < 0$, $z > h$ i. e. , uniform medium; II - $0 < z < h$ a dielectric layer with periodically varying dielectric constant. For the perpendicular (transverse magnetic, TM- mode) polarization assumed here, the tangential components of the electric and magnetic fields below the groove ($z < 0$) are given, respectively, by

$$E_x = \frac{k_z^0}{k^0} H^0 e^{-i(k_x^0 x + k_z^0 z)} - \sum_{n=-\infty}^{\infty} A_n \frac{c_n}{k^0} e^{-i(s_n x - c_n z)} \quad (1)$$

$$H_y = H^0 e^{-i(k_x^0 x + k_z^0 z)} + \sum_{n=-\infty}^{\infty} A_n e^{-i(s_n x - c_n z)}, \quad (2)$$

where H^0 is the amplitude of the incident wave and $s_n = k^0 \sin \theta + (2\pi n / L)$, $c_n^2 = (k^0)^2 - s_n^2$. Time dependence $\exp(i\omega t)$ is assumed and suppressed.

The reflected field is represented as a sum of Floquet harmonics. The terms A_n in (1) and (2) denote the amplitudes of the diffracted wave Floquet harmonics of the reflected field, while θ is the incidence angle and $k^0 = \omega(\mu_0 \epsilon_0)^{1/2}$ with ϵ_0 and μ_0 being the permittivity and permeability of the air, respectively.

The transmitted field above the grating ($z > h$) is similarly given by

$$E_x = \sum_{n=-\infty}^{\infty} B_n \frac{d_n}{k^0 \varepsilon} e^{-i(s_n x + d_n(z-h))} \quad (3)$$

$$H_y = \sum_{n=-\infty}^{\infty} B_n e^{-i(s_n x + d_n(z-h))}, \quad (4)$$

where $d_n^2 = (k^0)^2 \varepsilon - s_n^2$.

In the periodic layer ($0 < z < h$), the field is represented as a sum of the groove modes:

$$E_x = \sum_{m=-\infty}^{\infty} \frac{k_m}{k^0} \left[\frac{1}{\varepsilon} U_1(x) + \frac{e^{-i\psi} - U_1(L)}{U_2(L)} \frac{1}{\varepsilon} U_2(x) \right] (C_m e^{-ik_m z} - F_m e^{ik_m z}) \quad (5)$$

$$H_y = \sum_{m=-\infty}^{\infty} \left[\frac{1}{\varepsilon} U_1(x) + \frac{e^{-i\psi} - U_1(L)}{U_2(L)} \frac{1}{\varepsilon} U_2(x) \right] (C_m e^{-ik_m z} + F_m e^{ik_m z}), \quad (6)$$

where functions $U_1(x)$ and $U_2(x)$ are the fundamental solutions of the equation

$$\varepsilon(x) \frac{d}{dx} \left(\frac{1}{\varepsilon(x)} \frac{dD_x}{dx} \right) + ((k^0)^2 \varepsilon(x) - k_m^2) D_x = 0 \text{ with the corresponding boundary conditions}$$

$$u_1(0) = 1, \frac{1}{\varepsilon} \frac{du_1(0)}{dx} = 0, u_2(0) = 0, \frac{1}{\varepsilon} \frac{du_2(0)}{dx} = 1.$$

Values of k_m are assumed to be known for any given combination of ε, l_1 and l_2 . These quantities are found by solving an eigenvalue problem for the modes in infinite ($h \rightarrow \infty$) periodic medium, by following, for example, the analysis in [3]. The values of k_m are the complex roots of the dispersion equation:

$$\cos s_n L = \cos p_1 l_1 \cos p_2 l_2 - \frac{1}{2} \left(\frac{p_1 \varepsilon}{p_2} + \frac{p_2}{p_1 \varepsilon} \right) \sin p_1 l_1 \sin p_2 l_2 \quad (7)$$

where $p_1^2 = (k^0)^2 - k_m^2$, $p_2^2 = (k^0)^2 \varepsilon - k_m^2$. An infinite number of s_n corresponds to each value of k_m ($s_n L$ is the phase shift of the waves during the period).

To determine the scattered amplitudes A_n, B_n and the modal amplitudes F_m, C_m we impose continuity conditions for E_x and H_y at $z = 0$ and $z = h$:

$$H^0 \delta_{0n} + A_n = \sum_{m=-\infty}^{\infty} S_{nm} (C_m + F_m) \quad (8)$$

$$k_z^0 H^0 \delta_{0n} - c_n A_n = \sum_{m=-\infty}^{\infty} S'_{nm} k_m (C_m - F_m) \quad (9)$$

$$B_n = \sum_{m=-\infty}^{\infty} S_{nm} (C_m e^{-ik_m h} + F_m e^{ik_m h}) \quad (10)$$

$$\frac{d_n}{\varepsilon} B_n = \sum_{m=-\infty}^{\infty} S'_{nm} k_m (C_m e^{-ik_m h} - F_m e^{ik_m h}) \quad (11)$$

$$\text{where: } S_{nm} = \frac{1}{L} \int_0^L \left[U_1(x) + \frac{e^{-i\psi} - U_1(L)}{U_2(L)} U_2(x) \right] \exp(is_n x) dx$$

$$S'_{nm} = \frac{1}{L} \int_0^L \left[\frac{1}{\varepsilon} U_1(x) + \frac{e^{-i\psi} - U_1(L)}{U_2(L)} \frac{1}{\varepsilon} U_2(x) \right] \exp(is_n x) dx$$

Equations (8)-(11) can be solved for the unknowns A_n, B_n, F_m and C_m by truncating the infinite sums. The resulting set of linear equations can be manipulated by various standard methods.

Consider the electromagnetic field under the groove. It consists of the incident and the reflected fields. The behaviour of the reflected field depends on the harmonic amplitudes and the propagating constants. There are a few real values of c_n and an infinite number of imaginary ones. The imaginary values of c_n correspond to the guided waves propagating along the x axes with the amplitudes vanishing along z as $e^{-c_n z}$. The waves propagating constants s_n along x-axes more than the propagating constant of the incident wave.

If $\lambda \gg L$, only $c_0 = \frac{2\pi}{\lambda} \sqrt{1 - \sin^2 \theta}$ is real, and only one mode in second sub-domain has the real wavenumber $k_0 = k^0 \left(\frac{\epsilon_1(\epsilon_1 - \sin^2 \theta)}{\epsilon_1} \right)^{1/2}$, $\epsilon_1 = \frac{\epsilon L}{\epsilon l_1 + l_2}$, $\epsilon_1 = \frac{\epsilon l_2 + l_1}{L}$. The ratio of the reflected wave amplitude to the incident wave amplitude is the following:

$$\eta = 1 - \frac{2S_{00}S'_{00} \frac{k_0}{k_z} \cos k_0 h + 2iS_{00}^{1/2} \frac{k_0^2 \epsilon}{k_z^0 d_0} \sin k_0 h}{S_{00}S'_{00} \left(\frac{k_0 \epsilon}{d_0} + \frac{k_0}{k_z^0} \right) \cos k_0 h + i \left(S_{00}^2 + S_{00}^{1/2} \frac{k_0^2 \epsilon}{k_z^0 d_0} \right) \sin k_0 h} \quad (12)$$

As for the waves, propagating in dielectric ($z > h$), for $\lambda \gg L$ and $\epsilon < \frac{\lambda}{L}$ only one propagating constant has the real value $d_0 = \frac{2\pi}{\lambda} \sqrt{\epsilon - \sin^2 \theta}$, and the ratio of the amplitude of wave transmitted in dielectric to the incident wave amplitude is

$$\mu = \frac{2S_{00}S'_{00} \frac{k_0 \epsilon}{d_0}}{S_{00}S'_{00} \left(\frac{k_0 \epsilon}{d_0} + \frac{k_0}{k_z^0} \right) \cos k_0 h + i \left(S_{00}^2 + S_{00}^{1/2} \frac{k_0^2 \epsilon}{k_z^0 d_0} \right) \sin k_0 h} \quad (13)$$

To conserve power, the sum of the reflection and transmission coefficients $|\eta|^2 + |\mu|^2$ must be equal to unit. This is the condition of truncating the infinite sums (8)-(11).

Using such an approach enables one to extract the situation when the most part of the energy of the incident field transforms into the one guided wave propagating along the x-axes.

1. Theory and calculation of linear accelerators. The collection of articles. Gosatomizdat, Moscow, 1962.
2. Henry L. Bertoni, Li-Hsiang S. Cheo, Theodor Tamir. *Frequency-selective reflection and transmission by a periodic dielectric layer*, IEEE Transactions on antennas and propagation, V.37, N. 1, pp.78-83, 1989.
- [3]. N.A. Khizhnyak, K. Yu. Kramarenko, *Propagation of electromagnetic waves in space periodic structures with dual periodicity*. Ukrainian Journal of Physics, N 10, V.42, 1997, pp.1256-1259

SCATTERING AND ABSORPTION OF A VIDEO PULSE BY A SET OF ALTERNATED LAYERS WITH RESISTIVE FILMS

Vladimir V. Podlozny

Chair of Theoretical Radiophysics, Kharkov State University, 310077, Kharkov, Ukraine

ABSTRACT

Presented paper deals with a videopulse reflection from a periodic layered structure with resistive films. The role of resistive films under the videopulse-structure interaction is described. Influence of the number of periodic composite cells is discussed.

INTRODUCTION

Layered structures based on the alternated magnitodielectric layers with dissipative elements are simple in manufacturing and have wide electromagnetic applications. Periodicity of these structures permits to simplify significantly the treatment of their scattering characteristics [1]. An effective investigation method based on the matrix polynomial theory [2] was presented in [3]. In this work, a monochromatic wave diffraction problem on a set of the alternated magnitodielectric layers with resistive films has been solved. The solution of this problem is presented as direct analytical formulas for reflection and transmission coefficients. These formulas stay simple for arbitrary number of the basic elements and structure load. Such a solution avoids large volume of calculations. These features permit us to employ this method for numerical investigation of a videopulse diffraction problem using the Fast Fourier Transform.

FORMULATION OF A PROBLEM

The structure consists of a consecutive set of N identical composite cells (periods). The half-spaces before and after the structure have arbitrary wave conductivities (Y_0, Y_T). The composite cells contain two dielectric layers of different width (d_j) ($d_1 + d_2 = L$), permittivity (ϵ_j) and permeability (μ_j). There is a thin resistive film of conductivity Y_σ between them (Fig.1).

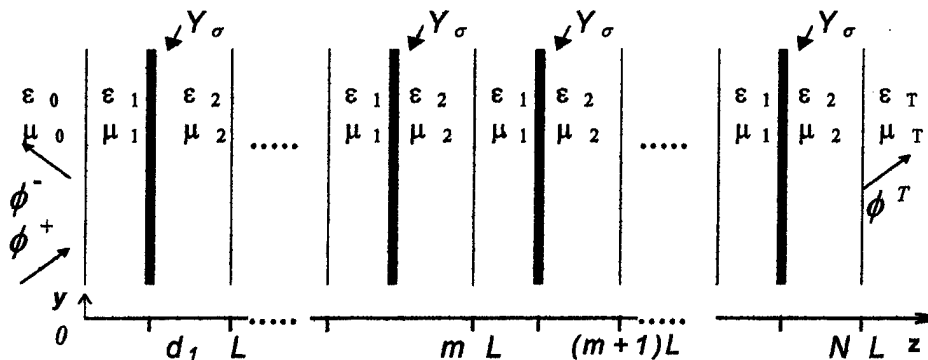


Fig.1 Multilayered structure.

The videopulse

$$\phi^+(t) = (\exp(-a_1 t) - \exp(-a_2 t)) / (\exp(-a_1 T_f) - \exp(-a_2 T_f)) \quad (1)$$

is incident from the half-space $z < 0$. T_f is the interval of the pulse front, a_1, a_2 are the constants. By varying a_2/a_1 , we can change the videopulse form in a wide range [4]. The question is: what kind of pulse will be reflected and what part of the videopulse energy will be absorbed?

METHOD OF ANALYSIS AND NUMERICAL RESULTS

We use analytical formula of the reflection coefficient [3] and the direct and inverse discrete Fourier transforms to calculate the reflected field in the following principal cases.

To describe the role of resistive films in videopulse reflection, we shall consider a set of resistive films on a metal screen (Fig. 1, 2). For this configuration, we assume that the common width of the structure is constant: addition to the structure the resistive films leads to decrease of the spaces (d_j) between them.

For one film ($N=1$), the reflected pulse has three main negative peaks (Fig. 2.). The first peak is caused by resistive film. Its response time interval is $\Delta\tau_1 \approx 0.66 \times 10^{-10}$ sec. This and any other time intervals can be easily calculated by using the following formulas:

$$\tau_j = \sum_{j=1}^N \Delta\tau_j, \text{ where } \Delta\tau_j = 2d_j \sqrt{\varepsilon_j} / c, \text{ } c \text{ is the light velocity, } j \text{ is the index of the layer. The}$$

second peak is caused by the metal screen. It has the maximum amplitude. The third peak is coming up after the double reflection between the film and the metal screen. After the third peak, we can observe vanishing peaks due to the film-screen multireflections.

For the five films ($N=5$) we obtain a smoothed time dependence (Fig. 2.) with a low level of amplitude. Increasing number of resistive films results in the reflection, which is similar to the metal screen one. Therefore, we can note that: there exists an optimum number of the resistive films, which provide a low level of reflection. Moreover, such a number of resistive films masks the peak from metal screen.

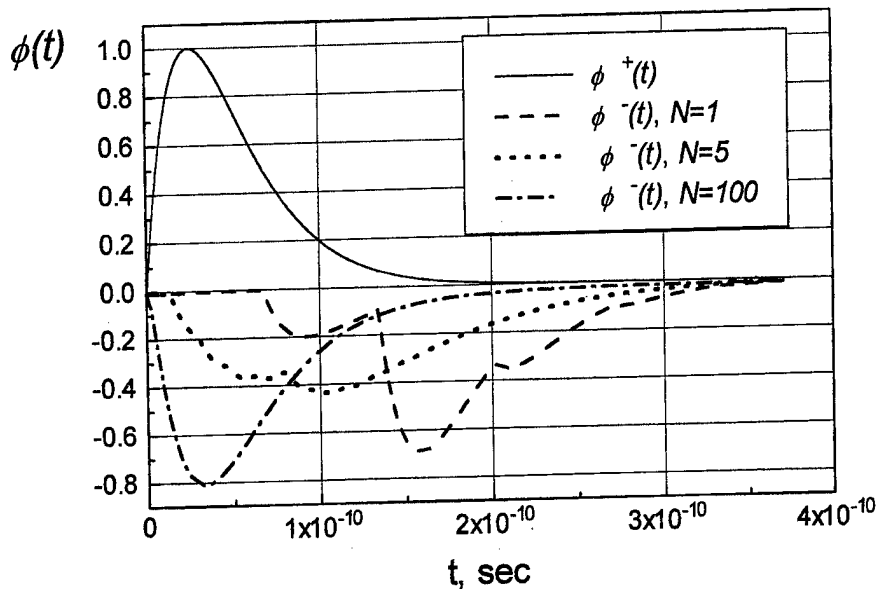


Fig. 2. Time dependences of diffracted field, $T_f = 0.25 \times 10^{-10}$ (sec), $a_2/a_1 = 1.0001$, $\varepsilon_{0,1,2} = \mu_{0,1,2} = 1$, $d_1 = d_2 = (0.01)/N$ (m), $Y_\sigma = 0.5$, $Y_T \rightarrow \infty$.

To specify the conditions of the maximum absorption, we have investigated the absorption dependences from the number of resistive films (N) and their conductivity (Y_σ). The energy of the incident and reflected videopulse can be presented as: $W^{+(-)} = \sum_{i=1}^K [\varphi^{+(-)}(t_i) \Delta t_i]^2$, where t_i are the elements of discrete time observation interval, Δt_i is the step of discretization. Then, the absorbed fraction of energy is: $S = 1 - W^-/W^+$.

Fig. 3 shows the existence of maximum absorption zones for different configurations of the structure. Decreasing the conductivity of resistive films leads to a growth in their number at the fixed level of absorption.

These features of the structure open a way to construct the high-efficient absorbers and successfully resolve the problems of electromagnetic compatibility and ecology.

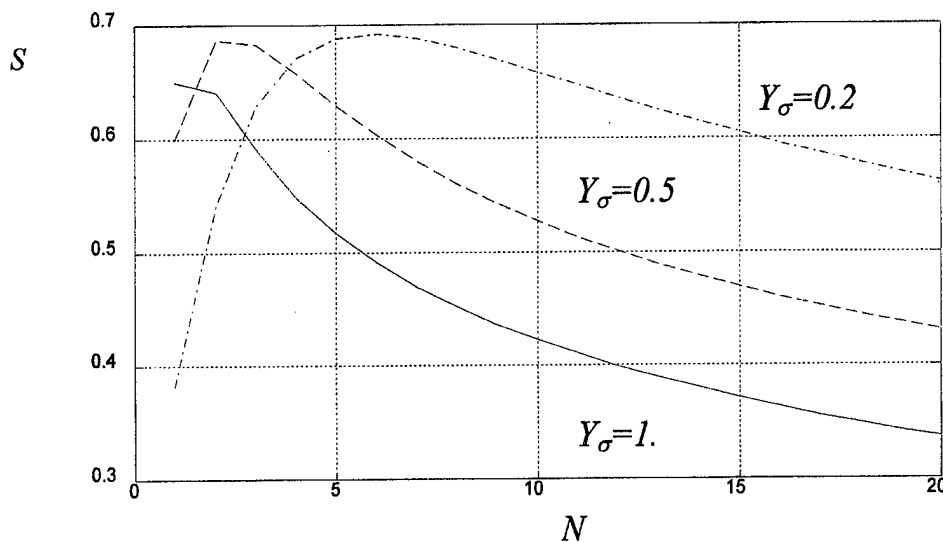


Fig. 3. Absorption in the structure, $\varepsilon_{0,2}=\mu_{0,1,2}=1$, $\varepsilon_1=2$, $d_1=d_2=0.01$ (m), $T_f=0.5 \cdot 10^{-10}$ (sec), $Y_T \rightarrow \infty$.

CONCLUSION

Periodic structures with resistive films can be used in the design of low-reflecting absorbing coatings. A pulse method is efficient in non-destructive testing of such structures.

REFERENCES

1. V. B. Kazanskiy, V. V. Podlozny, Quasiperiodic layered structure with resistive film, *Electromagnetics*, pp. 131-145, no. 2, vol. 17, 1997.
2. H. Levine, *Unidirectional Wave Motions*, Amsterdam, 1978.
3. V. B. Kazanskiy, V. V. Podlozny, Investigation of periodic finite structures by using Mauguin polynomials, *Dopovidi Akademii Nauk Ukrainy*, pp.86-91, no.3, 1998 (in Russian.)
4. S. A. Masalov, A. O. Puzanov, A. I. Timchenko, Non-stationary excitation of layered dielectric structures. *Radiowaves Propagation in Millimeter and Submillimeter Band.*, IRE NAS, Kharkov, pp.178-193, 1995 (in Russian).

SIMULATION OF CONTROLLABLE SOLID-STATE STRUCTURES

V. A. Obukhovets, A. O. Kasyanov, S. V. Piven

Taganrog State University of Radio Engineering, 44 Nekrasovsky st., Taganrog, 347928 Russia
Phone +7(86344) 61883. E-mail: decan@vao.rnd.su

Abstract - New class of controllable reflective type antenna arrays is considered, made as microstrip integrated circuits with arbitrary-shape microstrip radiators and controlled elements (crystal diodes). Electromagnetic characteristics of the array are varied by tuning the diode bias voltages. For a digital control possibility, all microstrip radiators are divided into several groups (modules). Each module can be at least in two electromagnetic conditions which are defined by the diodes states (open or closed one). The array controlling is carried out by a microprocessor. The digital array probable states number is proportional to the number of modules and each module allowable conditions number. Digital diffraction reflect-array has a set of microwave radar images whose changing enables one to create so called "intellectual covers" capable to adapt for radar-tracking environment.

The report is devoted to theoretical modeling of controllable microstrip arrays. Microstrip arrays have many applications in radomes, frequency selective surfaces and artificial dielectrics. High price of arrays and their complicated experimental research cause a significant interest to development of their mathematical models. The most known models describe the array in the radiation mode when its element excitation is carried out by feed source currents. At the same time the questions of analysis of microstrip diffraction arrays, which serve as a basis of low-cost reflective type antenna arrays with an optical feeding system, remain less investigated. Practical requirements of microstrip diffraction array applications alongside with phased antenna arrays include the design of antenna reflectors, frequency and angular filters, wave converters and antenna radomes, traveling wave systems, etc. The microstrip diffraction arrays perspective applications are the multireflector antennas for space communication systems, in which the microstrip diffraction arrays are used as the frequency-selective surfaces.

Proposed mathematical model is based on the periodical structure concept and integral equation system solution. Vector integral equations are formulated after the Lorentz lemma. The application of periodicity condition has allowed reducing the solution domain to one Floquet channel. The column matrix of magnetic current density components at the array aperture $J^M(q)$, and electrical currents in controllable elements $I_j^3(z')$ have to be determined from the set of integral equations obtained based on the boundary conditions [1]:

$$\int_{S_A} \langle K^{MM}(p/q) \rangle \cdot J^M(q) dS_q - i2\pi a \sum_{j=1}^N \int_{-h}^0 I_j^3(z') \cdot \langle K^{M3}(p/q_j, z') \rangle dz' = \sum_{j=1}^N R_j^{(1)}(p);$$

$$\int_{S_A} \langle K^{3M}(p_i, z/q) \rangle \cdot J^M(q) dS_q - 2\pi a \sum_{j=1}^N \int_{-h}^0 I_j^3(z') \cdot \langle K^{33}(p_i, z/q_j, z') \rangle dz' = \sum_{j=1}^N r_{ij}(z),$$

where $i = 1, 2, \dots, N$. $z \in [-h; 0]$, h is the thickness of the array substrate, a is the shunts radius; S_A is the aperture surface. The kernel of the integral equation is a square matrix. This row-matrix blocks $\langle K^{3M}(p/q) \rangle$ describe interaction between electrical and magnetic currents. Right-hand parts of equa-

tions are formed by the excitation fields. Several possible ways of the microstrip elements excitation are considered including a plane wave one and feeding by periodical system of coaxial probes.

The first equation represents the condition of the field tangential components continuity at the array aperture. The N remaining equations ($i = 1, 2, 3, \dots, N$) are Poklington's type equations on the N controllable element surfaces. Those elements are simulated as conducting shunts with impedance loads. Let us consider that impedance distribution functions along each shunt are known. The moment method is used for integral equation numerical solution. The sub-domain rooftop function set is used as the basis functions for the current approximation [2]. The model does not impose restrictions on the microstrip element shape or substrate parameters. The crystal diodes are simulated as the loads with controllable surface impedance providing the digital control of microstrip array parameters. Every load is connected with the elementary microstrip patch. Such loads can execute a role of either phase shifters, or switching elements. The substrate can be a crystalline semiconductor. In this case the diodes became an integrated parts of a substrate. This electromagnetic structure is of a solid-state construction. Some ways of such microstrip array application has been proposed.

It is known that solid-state reflective type microstrip arrays can be applied as high directivity antennas [3]. These arrays are capable to compete with conventional parabolic antennas for DBS (Domestic Broadcasting Systems). Such a reflective type antenna consists of a flat microstrip diffraction array as reflector and an offset feed system. Wider opportunities can be provided by using microstrip radiators with switching diodes. The array electromagnetic characteristics are varied by changing the diode bias voltages. Diodes are positioned at various points of each microstrip element and are used as digital phase shifters. The array controlling is carried out by a microprocessor. This controllable impedance load application in microstrip reflective arrays is investigated in the paper. Such elements can be applied both for beam scanning and for fixed phase delay «pedestal» creating.

Besides of reflective antennas, flat microstrip lenses are investigated in the paper. The most perspective type of such antennas is a lens with electrically controlled radiation pattern. Controllable lenses can be considered as media with electrically changed refraction coefficient, so called «RADANT» [4]. Its main disadvantage is the great number of diodes used in the array. A modified lens «RADANT» [5] has no this disadvantage because the H-shaped microstrip elements are used in it. We have calculated this array scattering characteristics applying the above-mentioned mathematical model. The other perspective application is in the multireflector antennas for space communication systems where microstrip diffraction arrays are used as a frequency-selective surfaces [6]. Such structures are promising as twist reflectors. The numerical analyses have enabled us to design broadband microstrip twist reflectors. The experimental measurements of the array models have proved almost complete adequacy between theoretical and measured characteristics [7]. The application of controllable microstrip arrays as a binary microstrip polarizing [8] modulator is discussed. The physical parameters of the binary modulator are determined from the numerical experiments. Besides, many other types of artificial media, frequency selective surfaces, "invisible" anti-radar covers, chiral cover structures, angular filters can be designed by means of created mathematical model.

REFERENCES

1. A. O. Kasyanov, V. A. Obukhovets, *Radiotekhnika*, 1995, no 12, pp 32-6 (in Russian).
2. A. W. Glisson, D. R. Wilton, *IEEE Trans. Antennas Propagat.*, vol. AP-25, 1980, pp. 593-607.
3. V. A. Obukhovets, A. O. Kasyanov, *Proc. Int. Conf. Antennas, Radio Commun. Systems and Means*, (ICARSM'97), Voronezh: VSU, 1997, Vol. 1. p. 174-178.
4. C. Chekroun, D. Herrick, *Microwave Journal*, 1981, vol. 24, No. 2, pp. 45 - 53.
5. J. J. H. Wang, *Proc. Int. Symp. on Antennas and Propagation*, Kyoto, 1985, vol. 3, pp. 743 - 746.
6. V. A. Obukhovet, A. O. Kasyanov, *Development Directions of Radio Communication Systems and Means*, *Proc. Conf. Antennas, Radio Commun. Systems & Means*, Voronezh: VSU, 1995, pp. 144-149.
7. A. O. Kasyanov, A. I. Semenikhin, I. V. Iliin, *Electromagnetic Wave Scattering*, Taganrog: TSURE, no 8, pp. 113-119 (in Russian).
8. K. G. Guisev, A. D. Filatov, A. P. Sopolev, *Polarization Modulation*, Moscow: Radio i Svyaz, 1974 (in Russian).

LOW-FREQUENCY ASYMPTOTICS IN THE DIFFRACTION OF WAVES BY ECHELETTE

I. L. Verbitskii

Kharkov State Pedagogical University, Kharkov, Ukraine
Tel: 380-(572)-47-14-92, e-mail: verb@reg.kharkov.ua

The subject of this communication is the H-polarized plane wave diffraction from a symmetrical metallic echelette Γ whose dimensions are small comparing to the wavelength (see fig. 1).

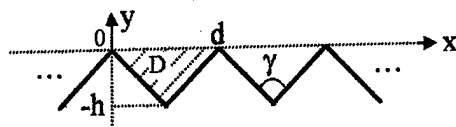


Fig.1 Domain Ω with boundary Γ .

Mathematical formulation of the problem is the Helmholtz equation for the H_z component of field, denoted as u :

$$\Delta u + k^2 u = 0 \quad (1)$$

with the Neumann boundary condition

$$\left. \frac{\partial u}{\partial n} \right|_{\Gamma} = 0, \quad (2)$$

condition of quasi-periodicity (Floquet)

$$u(x+d, y) = e^{i\beta d} u(x, y), \quad (3)$$

condition of radiation or limiting absorption at $y \rightarrow \infty$, and Meixner conditions near the edge points. The incident wave is $u^{(0)} = A e^{i\beta x + \alpha y}$, where $\beta = k \sin \varphi$, $\alpha = -ik \cos \varphi$, $k = \frac{2\pi}{\lambda} = \frac{\omega}{c}$ is the wave number, φ is the angle of incidence.

To solve the problem, we apply the Quasistatic Green Function Method developed in [1]. From this method it follows that the solution of the general diffraction problem on the periodical surface can be represented in the form

$$u = A f^+(x, y) + \sum_{n=-\infty}^{\infty} C_n f_n(x, y) + \sum_{m=0}^{\infty} B_m g_m(x, y), \quad (4)$$

where

$$f^+(x, y) = -k^2 \int_0^d dx' \int_0^\infty G(x, y, x', y') e^{i\beta x' + \alpha y'} dy', \quad (5)$$

$$f_n(x, y) = -k^2 \int_0^d dx' \int_0^\infty G(x, y, x', y') e^{i\beta_n x' - \alpha_n y'} dy', \quad (6)$$

$$g_m(x, y) = -k^2 \int_0^d dx' \int_0^\infty G(x, y, x', y') u_m(x', y') dy', \quad (7)$$

and

$$G = - \sum_{n=-\infty}^{\infty} e^{i\beta_n(\xi-\xi')} \frac{e^{-|\beta_n||\eta-\eta'|} + e^{-|\beta_n||\eta+\eta'|}}{2|\beta_n|d}, \quad (8)$$

is the quasistatic Green's function, $\beta_n = \beta + 2n\pi/d$, $\alpha_n = \sqrt{\beta_n^2 - k^2}$, $\beta_0 = \beta$, $\alpha_0 = \alpha$, $\xi = \xi + i\eta$ is the function conformally mapping Ω onto the halfplane $\eta > 0$, $\{u_n(x, y)\}_{m=0}^{\infty}$ is any complete in D set of functions. The coefficients C_n and B_m are the Fourier coefficients of u according to $\{e^{i\beta_n x}\}$ and $\{u_m(x, y)\}$ respectively. They can be found from the fast convergent set of linear algebraic equations. As it has been shown in [2], functions f_n and f^* can be represented in the form

$$f_n(x, y; \alpha_n) = e^{i\beta_n x} (e^{-\alpha_n y} - e^{-|\beta_n|y}) \Theta(y) + (\alpha_n - |\beta_n|) K_n, \quad f^* = f_0(x, y; -\alpha), \quad (9)$$

where

$$\Theta(y) = \begin{cases} 1, & y > 0 \\ 0, & y < 0 \end{cases},$$

$$K_n(x, y) = e^{i\beta_n x} \frac{\sinh \beta_n y}{\beta_n} \Theta(y) + \begin{cases} \sum_{p=0}^n e^{i\beta_p x} \frac{\cosh \beta_p \eta}{\beta_p} a_{np}, & n \geq 0 \\ + \sum_{p=n}^{-1} e^{i\beta_p x} \frac{\cosh \beta_p \eta}{\beta_p} b_{np}, & n < 0 \end{cases}, \quad (10)$$

a_{np} and b_{np} are known coefficients. It is clear from (9) that if $(d/\lambda)^2 \ll 1$, one can neglect in the first sum of (4), all the terms except $C_0 f_0$, so we have:

$$u \cong A f^+(x, y) + C_0 f_0(x, y) + \sum_{m=0}^{\infty} B_m g_m(x, y). \quad (11)$$

To simplify the second sum, we must at first choose the functions u_m . In case in question we can take for those coming out from separating of variables in D : $u_m = J_\lambda(k\rho) \cos \lambda \varphi$, where $\lambda = m\pi/\gamma$, and ρ, φ are the polar coordinates with origin O' at $(d/2, -h)$ and axis along the side of D . Then for the small $|k\rho|$ we can neglect all u_m except u_0 , and take $u_0 = 1$ as the first approximation. So we obtain:

$$u \cong A f^+(x, y) + C_0 f_0(x, y) - B_0 k^2 \iint_D G(x, y, x', y') dx' dy'. \quad (12)$$

Then equations for C_0 and B_0 take the form

$$C_0 + A = \frac{A}{d} \int_0^d f^+(x, 0) e^{-i\beta x} dx + \frac{C_0}{d} \int_0^d f_0(x, 0) e^{-i\beta x} dx - B_0 k^2 \iint_D \left[\frac{1}{d} \int_0^d G(x, 0, x', y') e^{-i\beta x} dx \right] dx' dy' \quad (13)$$

$$B_0 = \frac{1}{\gamma} \int_0^\gamma [A f^+(x, y) + C_0 f_0(x, y) - B_0 k^2 \iint_D G dx' dy'] d\varphi$$

where one must take $\rho \leq h$ in the second of equations (13). In [2], the following results have been obtained:

$$f_0 = \frac{\beta - \alpha}{\beta} e^{i\beta(\zeta - z)} \operatorname{ch} \beta \eta, \quad \frac{1}{d} \int_0^d f_0(x, 0) e^{-i\beta x} dx = \frac{\beta - \alpha}{\beta} \frac{1 + |e^{i\beta \chi}|^2}{2}, \text{ and}$$

$$\frac{1}{d} \int_0^d G(x, 0, x', y') e^{-i\beta x} dx = -\frac{e^{-i\beta \zeta'} + e^{-i\beta \bar{\zeta}'}}{2\beta d} e^{i\beta \chi}, \text{ where } \chi = \lim(\zeta - z), y \rightarrow \infty.$$

Accordingly to the accepted approximation, we can take in (13) that

$$\frac{1 + |e^{i\beta \chi}|^2}{2} \cong 1 - \beta \operatorname{Im} \chi; \quad \frac{1}{d} \int_0^d G(x, 0, x', y') e^{-i\beta x} dx \cong -\frac{1}{\beta d};$$

$$G \cong -\frac{1}{\beta d}, \quad \text{and } f_0 \cong \frac{\beta - \alpha}{\beta} (1 + i\beta \operatorname{Im} \chi).$$

It gives after some calculations for the reflection coefficient $R = C_0/A$:

$$R = \frac{\cos \varphi - k[(e^{i\varphi} \sin \varphi) \operatorname{Im} \chi - \frac{ih}{2}]}{\cos \varphi - k[(e^{-i\varphi} \sin \varphi) \operatorname{Im} \chi + \frac{ih}{2}]}, \quad (14)$$

Conformal mapping of the halfplane $\eta > 0$ onto Ω can be expressed explicitly with the aid of the Schwarz-Christoffel formula, and after some algebra we obtain:

$$\chi = \frac{id}{\pi} \left[\frac{\psi(\Theta) + C}{2} + \ln 2 + \frac{\pi h}{d} \right], \quad (15)$$

where $\Psi(\theta)$ is digamma function and $C = 0.5772\dots$ is the Euler constant. Substituting (15) into (14) we obtain finally:

$$R = \frac{\cos \varphi - k \left\{ \frac{d}{2\pi} (e^{i\varphi} \sin \varphi) [\psi(\Theta) + C + 2 \ln 2 + \frac{2\pi h}{d}] - \frac{ih}{2} \right\}}{\cos \varphi - k \left\{ \frac{d}{2\pi} (e^{-i\varphi} \sin \varphi) [\psi(\Theta) + C + 2 \ln 2 + \frac{2\pi h}{d}] + \frac{ih}{2} \right\}}, \quad (16)$$

The problem of low-frequency diffraction on the general periodic surface has been studied in the works [3] and [4] where some expressions for R have been proposed. In the limiting cases of normal incidence ($\varphi = 0$) and grazing incidence ($\varphi = \pi/2$), the values of R obtained from these expressions are in agreement with those obtained from (16):

$R = \frac{1 + ikh/2}{1 - ikh/2} \cong e^{ikh}$ and $R = -1$. However, for the other values of φ they do not coincide with the rigorous result (16), so they turn out to be incorrect in general case.

References

1. L. Verbitskii, On one method of solving the Helmholtz equation, I, *J. Math. Phys.*, 1981, vol. 22, no. 1, p. 32-38.
2. L. Verbitskii, *ibid*, II, 1982, vol. 23, no. 4, p. 510-516.
3. V. M. Astapenko, Sound reflection from impedance goffered surface, *Doklady Akademii Nauk SSSR*, 1970, vol. 195, no. 6, p. 1286-1289. (in Russian)
4. E. I. Nefedov, A. N. Sivov, *Electrodynamics of periodic structures*, Moscow: Nauka, 1977 (in Russian).

Electromagnetic Theory

NEW DESCRIPTION OF SPATIAL HARMONICS OF SURFACE WAVES

Vladimir Onufrienko

Zaporizhzhya State Technical University
Zhukovsky Str., 64, Zaporizhzhya, 330600, SP-39, Ukraine

Abstract. In the paper, one idea concerning potentialities of fractional calculus: description of spatial harmonics of surface waves by means of the α -features, is considered. The application of the boundary conditions for determining the α -features of a field is discussed. Numerical solution of one particular scattering problem for an electromagnetic wave incident on an impedance and edged surface is outlined.

Introduction

Impedance boundary conditions and their classical variant: the Shchukin-Leontovich condition, are widely applied to the description of processes of interaction of an electromagnetic field with surfaces. These conditions are based on a number of physical assumptions, which simplify the statement and solution of a problem [1]. However these assumptions impose restrictions on some geometrical characteristics of contours and surfaces.

Considering a surface of the unit of media as fractal, we propose to take into account its impedance properties at the expense of representations about such its structure, when all points statistically are similar to each other.

It is interesting to find out, in what extent the use of the recently developed differintegrals technique (see, for example, [2]) allows to take into account a fractal structure of both ideal and real conductors. It can be easily done by considering an incidence of a plane wave on the interface between two media.

Differintegral boundary conditions

For the solution of a particular scattering problem, when the required field can be considered as independent on one of the Cartesian coordinates, let us consider, instead of a scalar potential function, its α -features as a differintegral $(D_{a+}^{-\alpha} u^{\alpha})(x, y)$ satisfying the Helmholtz equation on the plane

$$\nabla_{xy}^2 (D_{a+}^{-\alpha} u^{\alpha})(x, y) + k^2 (D_{a+}^{-\alpha} u^{\alpha})(x, y) = 0, \quad 0 < \alpha < 1, \quad k = 2\pi / \lambda \quad (1)$$

and boundary conditions on the surface Γ

$$\sum_{i=1}^2 a_i (D_{a+}^{-\alpha_i} u^{\alpha_i})|_{\Gamma} = g(M), \quad M \in \Gamma, \quad (2)$$

which characterize reflection and transmission of the wave at the surface completely.

It is obvious that with $a_1 = 1, \alpha_1 = 0, a_2 = j\delta, \alpha_2 = 1$ we have a statement of a problem about a field of magnetic polarization ($\delta = Z / kW_0$, Z is the surface impedance, $W_0 = 120 \pi \Omega$ is the free-space impedance). With $a_1 = 1, \alpha_1 = 1, a_2 = j\eta, \alpha_2 = 0$, we have a problem about a field of electrical polarization ($\eta = kZ / W_0$).

The problem as (1), (2) is stated mathematically correctly. It is possible to prove rigorously its solution existence and uniqueness (following, for example, [3]).

The introduction of the differintegrals α -features satisfying the boundary conditions (2), enables us to work with components of the field as with smooth regular functions. It is essential while considering fractal boundaries that have breaks and edges. Thus the differ-integration not only keeps, but also essentially improves the properties of the functions.

Examples of solution of particular scattering problems

We shall further consider examples of the solution of the problems about the scattering of an electromagnetic wave from an impedance flat surface and with an edged surface, in new statement.

1). Consider a particular scattering problem about the propagation of a slow electric wave above a flat surface in the direction of the axis Oz .

The solution of equation (1) concerning the α -features of longitudinal component of electric field, E_z^α , is obtained as follows:

$$E_z^\alpha / E_{zmax} = \frac{I^\alpha e^{-kx\sqrt{n_{ph}^2-1}}}{\left(kx\sqrt{n_{ph}^2-1}\right)^\alpha};$$

(3)

where $n_{ph} = \frac{\beta}{k} = \sqrt{1 + \frac{\tau^2}{k^2}}$ is the deceleration factor of the phase velocity,

$$k^2 = g^2 + \beta^2, \quad g = i\tau, \quad I^\alpha \text{ is the scale multiplier.}$$

With $\alpha = 0$, a classical result is obtained from (3) (compare, for example, with [4]).

In Fig. 1, the longitudinal z -component of the E -wave, above the impedance plane, is shown as a function of the normalized distance kx (curve f1 corresponds to parameter $\alpha = 0.1$; curve f2 to $\alpha = 0.9$; curve g1 to $\alpha = 0$; $n_{ph} = 2$).

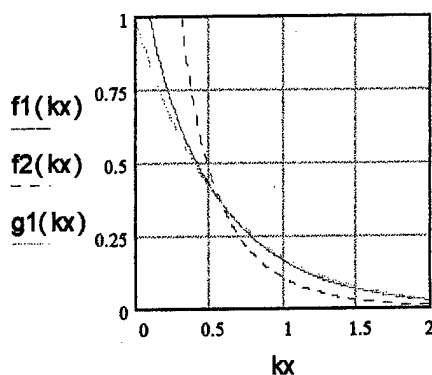


Fig.1

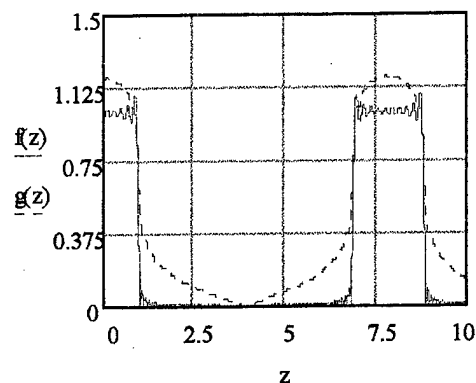


Fig.2

2). Consider now an impedance surface, which is formed by the metallic plane at $x = 0$ with the grooves (a gratings with period L). Suppose that the α -features of the field

component E_z transform to zero on the surface of metal.
From (1) we obtain that

$$E_z^\alpha / E_{z \max} = \sum_{p=-\infty}^{\infty} E_z^\alpha p = \sum_{p=-\infty}^{\infty} \frac{I^\alpha \frac{d}{L} M_p e^{-kx\sqrt{n_{ph}^2-1}}}{\left(kx\sqrt{n_{ph}^2-1}\right)^\alpha},$$

(4)

where $M_p = \frac{\sin(\beta_p d/2)}{\beta_p d/2}$ is the amplitude factor of harmonic (structure form-factor)

The distribution of the electrical component of the field, $E_z^\alpha / E_{z \max}$, along the axis Oz is shown in Fig.2 (curves $f(z)$ and $g(z)$ here correspond to the 0- and 0.33-features of field; $k=0.2$; $L=k\pi/4$; $d=0.5 L$). If $\alpha = 0$ (the structure of the ridged surface of a fractal structure is not taken into account), a complete coincidence of our results of numerical solution with the known data is observed (see, e.g. [4]).

Conclusion

In this paper, we have briefly outlined some of the applications of differintegrals in electromagnetics. Since fractional differintegrals are in fact an intermediate case between the conventional integer-order differentiation/integration, one may speculate that the use of these fractional operators may result in obtaining interesting novel solutions in electromagnetics.

The application of fractional calculus enables one to estimate interaction of electromagnetic waves with fractals surfaces with the help of the classical Maxwell equations without introduction in them any additional specific addendum, that inevitably follows the attempts of construction of adequate physical model.

As well as in the case of approximate boundary conditions of the Shchukin-Leontovich type, the boundary conditions (2) allow to take into account the presence of a fractal surface and neglect the field inside a body (the same properties take place for the boundary conditions on an perfectly conducting surface). Some other cases, such as fractionalization of the internal and external boundary problems, are currently under study by the author.

References

- [1] A. S. Il'inskiy, G. Ya. Slepyan, Impedance boundary conditions and their application for calculating the absorption of electromagnetic waves in conducting media, *Radiotekhnika i Elektronika*, 1990, vol. 35, no 6, pp.1121-1139 (in Russian).
- [2] D. Colton, R. Kress, *Integral Equation Methods in Scattering Theory*, New York, 1983.
- [3] N. Engheta, On Fractional Calculus and Fractional Multipoles in Electromagnetism, *IEEE Trans. Antennas Propagat.*, 1996, vol. 44, no 4, pp.554-556.
- [4] V.I. Volman, Y. V. Pimenov, *Technical Electrodynamics*, Moscow: Svyaz, 1971 (in Russian).

Analytical Expression Transformation for the Engineering Calculation of Parametric Absorption Effect

Svetlana A. Gayvoronskaja, Victor I. Sergeev

Voronezh Construction Bureau of Antenna Design
Russia, 394000, Voronezh, P. O. Box 175, VCB AD
tel/fax (073-2) 33-29-92, e-mail: sergeev@vcb-ad.vrn.ru

Recently the investigations of the effect of electromagnetic wave energy parametric absorption by the material objects, its consequences and practical applications have been increasing steadily [1, 2].

In the previous works, the analytical expressions which took into account the fact that the irradiated object was dielectric, were proposed. In the engineering design, in the case of the practical (radar) implementation of the known expressions characterizing the effect of parametric absorption, it was revealed a necessity to modify the mentioned expressions for a material object constructed of metals (lossy conductors) but not dielectrics.

In this paper we present the transformed analytical expressions for the engineering calculation of the parametric absorption effect under interaction of an electromagnetic wave and an object made of conducting materials.

The original analytical expressions for determining the irradiation parameters (the irradiation power and the maximum value of absorbed energy, respectively) have the following form [1]:

$$P_0 = \left[1 + L'_0 \left(\frac{1}{\sqrt{\varepsilon_1 \mu_1^3}} + \sqrt{\varepsilon \mu^3} \right) \right] \sqrt{\varepsilon \mu^3} \left\{ F1 \times \exp \left[\frac{2\pi L_0(i-1)}{\lambda_{np}} \sqrt{\frac{1}{2}(\sqrt{tg^2 \delta + 1} - 1)} \right] \right\}^{1/i} P_n^{(i-1)/i} \quad (1)$$

$$E_M = S_n \pm \frac{iQ_A^{i-1} \exp \left[\frac{2\pi L_0(i-1)}{\lambda_{np}} \sqrt{\frac{1}{2}(\sqrt{tg^2 \delta + 1} - 1)} \right] P_0 \tau_v}{k^2 \pi^2 \left\{ \left[1 + L'_0 \left(\frac{1}{\sqrt{\varepsilon_1 \mu_1^3}} + \sqrt{\varepsilon \mu^3} \right) \right] \sqrt{\varepsilon \mu^3} \right\} S_k}, \quad (2)$$

where P_0 is the power irradiating a material object that is sufficient for the display of the parametric energy absorption effect; L'_0 is the dimension-less value, numerically equal to L_0 that is the length of the closed curve of the refracted wave propagating in object; ε , μ are the dielectric and magnetic

refracted wave propagating in object; ε , μ are the dielectric and magnetic constants of the propagation layer (external layer); ε_1 , μ_1 are the dielectric and magnetic constants of the reflecting layers (internal layers); i is the quantity of the microwave pulses in the irradiation packet; τ_v is the single pulse duration; F_1 is the multifunctional parameter determining the interrelation of irradiating parameters and resonant and physical properties of the object; λ_{mp} is the wavelength of the refracted wave; Q_A is the quality factor; $\tan \delta$ is the loss tangent; S_k is a linear coefficient characterizing the pulse form; P_H is the normalization factor; E_1 is the maximum value of the absorbed energy; S_e is the coefficient having the energy dimension and corresponding to the manner of the observation object reaction on the high-power outer influence.

The expressions for determining the irradiation power and the maximum value of energy required to compensate for the arisen shortage contain the parameters characterizing the electromagnetic wave circulation and attenuation in the material object. A requirement to modify the expression for the engineering calculation is connected with the fact that when irradiating the object constructed of the conducting materials one can not use the expressions having the parameters characterizing the dielectric medium. For instance, the loss tangent for the dielectrics is less than 1, while the conductor loss tangent is much greater than 1. As a result, the expressions for the attenuation ratio of dielectrics and lossy conductors are different.

Attenuation ratio for dielectrics is commonly defined as follows [3]:

$$k \approx \frac{\omega}{c} \sqrt{\frac{1}{2} \left(-1 + \sqrt{tg^2 \delta + 1} \right)}. \quad (3)$$

Whereas the expression for a lossy conductor attenuation ratio differs from the written above, namely [3]:

$$k \approx \frac{\omega}{c} \sqrt{\varepsilon' \mu'} \sqrt{\frac{tg \delta}{2}}, \quad (4)$$

where ε' , μ' are the real parts of the parameters ε , μ . Instead of ε' и μ' , it is necessary to take $|\varepsilon|$ and $|\mu|$, because in the considered case $|\varepsilon| \approx \varepsilon'$, $|\mu| \approx \mu'$. In our work we had accepted the notations: $|\varepsilon| = \varepsilon$, where $\varepsilon = \varepsilon_a / \varepsilon_o$ and $|\mu| = \mu$, where $\mu = \mu_a / \mu_o$.

In the given expressions such a value as quality factor (Q-factor), which is equal to the inverse value of the loss factor, is present. For good dielectrics Q-factor reaches large values, while for lossy conductors it is small.

All the listed above reasons point out to a necessity of the transformation, which is, for instance, in the substitution of the dielectric attenuation ratio for the conductor attenuation ratio. As a result, the expressions for the calculation of the irradiation parameters (irradiation power and absorbed energy maximum value) of the material object made of lossy metals (conducting materials) were obtained as follows:

$$P_o = \left[1 + L'_o \left(\frac{1}{\sqrt{\varepsilon_1 \mu_1^3}} + \sqrt{\varepsilon \mu^3} \right) \right] \sqrt{\varepsilon \mu^3} \left\{ F1 \times \exp \left[\frac{2\pi L_o (i-1)}{\lambda_{np}} \sqrt{\varepsilon \mu} \sqrt{\frac{tg \delta}{2}} \right]^{1/i} P_H^{(i-1)/i} \right\} \quad (5)$$

$$E_M = S_n \pm \frac{i Q_A^{i-1} \exp \left[\frac{2\pi L_o (i-1)}{\lambda_{np}} \sqrt{\varepsilon \mu} \sqrt{\frac{tg \delta}{2}} \right] P_o \tau_v}{k^2 \pi^2 \left\{ \left[1 + L'_o \left(\frac{1}{\sqrt{\varepsilon_1 \mu_1^3}} + \sqrt{\varepsilon \mu^3} \right) \right] \sqrt{\varepsilon \mu^3} \right\} S_k}, \quad (6)$$

The engineering calculation performed for a material object made of a lossy conductor (Aluminium) has confirmed the necessity and validity of the introduced modifications.

Summarizing, in our paper we have shown that the transformation of the analytical expressions for the engineering calculation of the parametric absorption effect widens the range of applicability of the presented expressions and improves the agreement of modeling and experimental data.

References

1. Chesnokov, et al., Radar recognition of the stealth objects with the usage of the principles of non-linear radar and new physical hypotheses, *Proc. Int. Conf. Antennas, Radio Communication Systems and Means*, Voronezh: VGU Press, 1997.
2. V. I. Sergeev, About a possibility of microlevel interpretation of electromagnetic wave energy absorbtion parametrical effect. *Proc. Int. Conf. Actual Problems of Electronic Instrument-making*, Saratov, 1996 (in Russian).
3. V. V. Nikolsky, T. I. Nikolskaya, *Electromagnetics and Radio Wave Propagation*, Moscow: Nauka Publ., 1989 (in Russian).

Numerical calculation of the electron distribution function with the goal of simulating a current drive

I.O.Girka*, N.B.Marushchenko**, I.V.Pavlenko*

*Kharkiv State University, Svobody sq.4, 310077 Kharkiv, Ukraine

**Institute of Plasma Physics, NSC KIPT, Akademicheskaja 1,
310108 Kharkov, Ukraine

The results of numerical simulation of the current drive via solving the Fokker-Planck equation are presented. The problem of numerical instabilities is discussed.

1. Introduction. The numerical simulation of any kinetic problem associated with auxiliary plasma heating and current drive requires the solution of a Fokker-Planck type equation. As well known, one of the main numerical problems of kinetic equation solving consists in that of conservative formulation, that is not so trivial especially for the Coulomb operator. There is a number of tricks designed especially for avoiding the numerical instabilities (as example of the most common one see [1]), but these tricks are not so general and the problem still requests a great care. Another problem of numerical solving the kinetic equation, which describes the quasilinear interaction with launched into plasma RF fields and collisional relaxation of the induced perturbation, is the difference in kinds of symmetries of the relevant differential operators. While the most natural representation of the Coulomb operator is that in spherical coordinates, the quasilinear operator has as native cylindrical ones. Moreover, the quasilinear diffusive operator describes a diffusive process exactly along a given resonant lines, being actually one-dimensional (curvilinear) operator. This means that no one chosen coordinate system can exclude an appearance of so-called crossed derivatives in total diffusive operator (i.e. aggregated Coulomb and quasilinear ones), which usually are one from the main sources of numerical inaccuracy appearance.

Report presents the results of numerical simulations of some problem associated with producing the current drive by lower hybrid heating (LHCD). Fokker-Planck kinetic equation is solving by the finite difference method with the help of the developed FPTM code [2]. In the following, we show the results of successful application of the developed code to the one specific problem with appearance of a plateau on the distribution function in the resonance region.

2. Formulation of problem. Apart from omitted small number of relativistic particles such as running-away electrons and α -particles, for the typical plasma parameters in tokamaks the basic assumption about time-scales is that $\tau_B \ll \tau_c \sim \tau_{ql} \ll \tau_{neo}, \tau_a$ holds, where $\tau_B \equiv \oint ds/v_{||}$ is the period of bounce oscillations, τ_c and τ_{ql} are the character times of collisions and quasilinear heating, respectively, evaluated in order of magnitude from $(\partial f/\partial t)_{coll,ql} \sim f/\tau_{c,ql}$; τ_{neo} and τ_a are the character times of neoclassical and anomalous transport, respectively. This relation means that having so far separated the rates of redistribution of any perturbation in velocity and real spaces and being interested only by kinetic effects of RF heating we can neglect the process of any space diffusion and solve the kinetic equation for the given magnetic surface with given plasma parameters. Bounce averaged Fokker-Planck equation can be written then as [3,4]

$$\frac{\partial f_{\alpha 0}}{\partial t} + \frac{Z_{\alpha} e}{m_{\alpha}} \langle E_{||} \frac{\partial f_{\alpha 0}}{\partial v_{||}} \rangle_B = \sum_{\beta=i,e} \langle C^{\alpha/\beta} [f_{\beta}, f_{\alpha 0}] \rangle_B + \langle L^{RF} [f_{\alpha 0}] \rangle_B. \quad (1)$$

Here and below index "0" is related to the point of minimum of the steady magnetic field absolute value B for the given magnetic surface situated at the equatorial plane. Usually, the collision operator $C^{\alpha/\beta}$ is defined for maxwellian distribution functions of "ground" particles $f_{\beta} = f_{\beta, Max}$, and for the most kind of problems this approach has a high accuracy. Only

simulations of resistivity or another similar problems related to the electron current require to use a more complete model. The operator L^{RF} describes a quasilinear diffusion of electrons in velocity space during lower hybrid heating and has usual for it form (see, for example, [5]). Below, the set of spherical coordinates is used, which turns the Coulomb operator to the diagonal form.

In fact, equation (1) is a system of equations for passing, co-passing and trapped particles, coupled by boundary conditions along those lines in velocity space which separate these populations. These equations can be also coupled by Coulomb operator $C^{\alpha/\alpha}$ (depending upon the type of the model used). In the set of dimensionless variables $u = v/v_{th}$ and θ_0 (pitch angle computed in the minimum of B) this system, labeled by index m , can be expressed in dimensionless and conservative form as

$$\lambda \frac{\partial f_0^m}{\partial t} = \frac{1}{u^2} \frac{\partial}{\partial u} (u^2 S_u^m) + \frac{1}{u^2 \sin \theta_0} \frac{\partial}{\partial \theta_0} (\sin \theta_0 S_{\theta_0}^m), \quad (2)$$

where $\lambda \equiv v\tau_B |\cos \theta_0| / \oint ds B_{\min}/B(s)$, and S_{u,θ_0}^m are the fluxes in velocity space in "u" and "θ₀" directions, respectively:

$$S_u^m = D_{uu}^m \frac{\partial f_0^m}{\partial u} + D_{u\theta_0}^m \frac{\partial f_0^m}{\partial \theta_0} + F_u^m f_0^m, \quad S_{\theta_0}^m = D_{\theta_0\theta_0}^m \frac{\partial f_0^m}{\partial \theta_0} + D_{\theta_0 u}^m \frac{\partial f_0^m}{\partial u} + F_{\theta_0}^m f_0^m. \quad (3)$$

To discretize the equations the accurate and absolutely stable difference scheme of Karetkina (see [6]) is used. Formally this procedure is executed by integration of eqn. (2) with weight $u^2 \sin \theta_0$ over the mesh unit cell $u_{i-1/2} \leq u \leq u_{i+1/2}$, $\theta_{j-1/2} \leq \theta_0 \leq \theta_{j+1/2}$. In the approach of Karetkina the flux term (3) is rewritten as [2] (for brevity here and below only "u" component of flux is shown)

$$S_{u,i+1/2}^m = F_{u,i+1/2}^m (\alpha_i^m f_i^m + \beta_i^m f_{i+1}^m) + D_{uu,i+1/2}^m \frac{f_{i+1}^m - f_i^m}{\Delta u} + \left(D_{u\theta_0}^m \frac{\partial f_0^m}{\partial \theta_0} \right)_{i+1/2}, \quad (4)$$

where the weight coefficients α_i and β_i are

$$\alpha_i^m = \frac{1}{\omega_i^m} \left(1 - 1/t_{i+1/2}^m \right), \quad \beta_i^m = \frac{1}{\omega_i^m} (t_{i+1}^m - 1), \quad \omega_i^m = \Delta u \frac{F_{u,i+1/2}^m}{D_{uu,i+1/2}^m}, \quad (5)$$

$$t_{i+1/2}^m = \exp \int_{u_i}^{u_{i+1/2}} \frac{F_u^m}{D_{uu}^m} du \approx \exp \left[\frac{\Delta u}{4} \left(\frac{F_u^m}{D_{uu,i}^m} + \frac{F_u^m}{D_{uu,i+1/2}^m} \right) \right].$$

In comparison with the most commonly used scheme of discretization of Chang and Cooper [1] the approach (4)-(5) has much more generality and does not request any "physical" assumptions to define the weight coefficients α_i^m and β_i^m .

A conservative, finite-difference, two-step operator splitting algorithm [3,6] is used for the time advancement (between the l th and the $(l+1)$ th time steps) of $f_{i,j}^{m,l} \equiv f_0^m(u_i, \theta_{0,j}, t_l)$,

$$\lambda_j \left(\frac{f_{i,j}^{m,l+1/2} - f_{i,j}^{m,l}}{\Delta t/2} \right) = \Lambda_{uu}^{m,l} [f_0^{m,l+1/2}] + \Lambda_{u\theta_0}^{m,l} [f_0^{m,l}], \quad (6)$$

$$\lambda_j \left(\frac{f_{i,j}^{m,l+1} - f_{i,j}^{m,l+1/2}}{\Delta t/2} \right) = \Lambda_{\theta_0 u}^{m,l} [f_0^{m,l+1/2}] + \Lambda_{\theta_0\theta_0}^{m,l} [f_0^{m,l+1}],$$

Δt being the time step. The operators Λ^m incorporates the collisions, the quasilinear heating and the Ohmic terms. One can see that this scheme is implicit one only for diagonal operators, while other ones in equation are written as explicit part. To suppress inaccuracy produced by the explicit part of the differential operator the time step Δt has to be kept as enough small.

3. Applications. The triangular spectra model [5] is one of the most commonly used for the description of LHCD problem. We apply this model too, studying current drive for

the wide set of plasma parameters. A tokamak configuration with circular magnetic surfaces was used and all calculations were done for the given inverted aspect ratio $\epsilon = 0.8$. As mostly sensitive for quasilinear heating, the case of low density plasma was studied, with the following parameters of plasma: $n_e = n_i = 10^{13} \text{ cm}^{-3}$, $Z_{eff} = 1$, $T_e = T_i = 2 \text{ keV}$, which are typical for the middle size tokamaks. To cover as much as possible number of cases suitable for any analytical estimations the launched power was varied in very wide area from small 0.05 W/cm^3 up to almost irreal 10 W/cm^3 . Comparison of the forms of the distribution functions calculated with taking into account the existence of trapped particles (Fig.1a) and without it (Fig.1b) shows that the visible part of the moment got from external wave packet is lost due to collisions with trapped particles, which are excluded from those not contributing to the current. This is also illustrated at the Fig.2, where the dependence of efficiency versus launched power is shown.

Note by the way that, in the formal consequence with appearance of the plateau, the order of the solved equation degrades locally in the region of the plateau (at least the leading term becomes small). This fact often can be the reason of some numerical instabilities. The approach of the conservative discretization holding is a good guarantee from any numerical instabilities of this kind.

This work was partly supported by the Ukrainian Ministry of Science and Technologies.

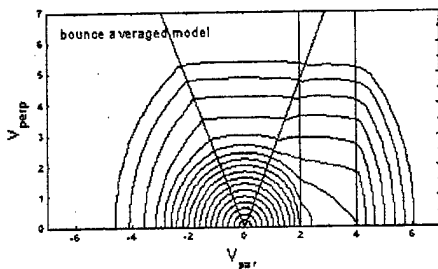


Fig.1a

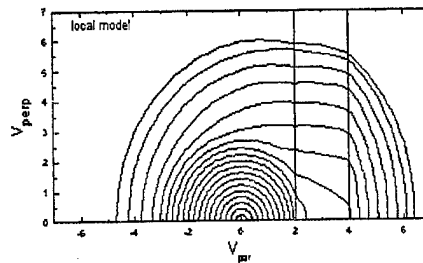


Fig.1b

Fig.1a. Contour lines of the electron distribution function with taken into account an existence of trapped electrons (bounce averaged model).

Fig.1b. Contour lines for the local model, i.e. obtained in assumption of absence any trapped electrons.

Fig.2. Dependence of the efficiency of current drive producing on launched power.

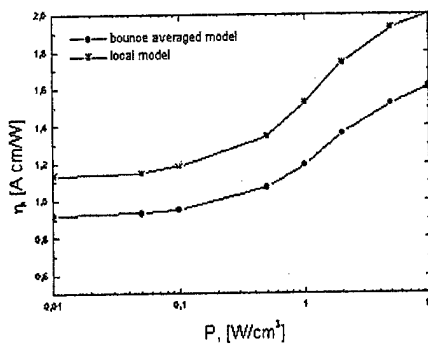


Fig.2

References

- [1]. J.Chang and G.Cooper, J. Comput. Phys. 6 (1970) 1.
- [2]. N.Marushchenko, U.Gasparino, H.Maassberg, M.Rome, Comput. Phys. Comm., 103 (1997) 145.
- [3]. J.Killeen, G.D.Kerbel, M.G.McCoy, A.A.Mirin, *Computational Methods for Kinetic Models of Magnetically Confined Plasmas*. Springer-Verlag, New York Inc., 1986.
- [4]. M.R.O'Brien, M.Cox, D.F.H.Start, Nuclear Fusion, 26, 1625 (1986).
- [5]. N.J.Fish and C.F.F.Karney, Phys. Fluids 28, 3107 (1985)
- [6]. Ju.N. Dnestrovskiy, D.P. Kostomarov, *Mathematical Simulation of Plasma*, Springer-Verlag, New York Inc., 1985.

Electrodynamics of Superconducting Structures

Viktor F. Kravchenko

Institute of Radio Engineering and Electronics, Russian Academy of Sciences, ul. Mokhovaya, 11,
Moscow, Center, GSP - 3, 103907 Russia.

Department of General and Applied Physics, Nonlinear Physics Laboratory, Moscow Institute of
Physics and Technology, Institutskii Pereulok, dom 9, Dolgoprudnyi, Moscow Region, 141700
Russia.

Phone: +7 (095) 9214837, 4086772, 9024737(home). Fax: +7 (095) 9259241

E-mail: kvf@mx.rphys.mipt.ru, kazarov@aha.ru, postmaster@nonlin.mipt.ru OR
zaoiprzhr@glasnet.ru

Introduction.

The present report is devoted to developing the electrodynamic theory of superconducting structures and its application to the technique of the microwave band. The actuality of the given problem lies in the fact that nowadays there is no any acceptable mathematical methods, by means of which it would be possible to investigate in sufficient details and give designers of the radioelectronic equipment practical recommendations on solving internal and external boundary value problems (stationary and nonstationary), associated with excitation, scattering and propagation of electromagnetic waves on the superconducting (SC) objects of simple and complex shape. Therefore the developing of the electrodynamic foundations of SC structures for external and internal problems with the methods of the spectral theory is important practical task in antenna and waveguide technique. **The report consists of three parts.**

In the first part solution of internal problems of the electrodynamics with boundary conditions of the third kind in contexts of methods of the spectral theory is considered. It's known that when studying such problems an important role plays the superconductor impedance [1]. Therefore the attention should be paid to selection and grounding the physical models for the surface impedance of the superconductors (stationary and nonstationary models). A number of particular boundary value problems has been solved: excitation and propagation of the electromagnetic waves (EW) in superconducting waveguides, cavity and open resonators of the ordinary and complex shape. For certain devices the numerical experiments have been carried out. The physical analysis of these results enable us to make a conclusion about the efficiency of the proposed methods. New approximate boundary conditions for superconducting structures with time-periodical electrodynamic characteristics will be developed.

In the second part the algorithms for external boundary value problems for the first time will be obtained and justified. These model problems can be used in practice [2-22], for example, for calculating the basic electrodynamic characteristics of superconducting superdirectional antennas, superconducting spiral antennas, superconducting planar printed antennas for the satellite communications and television, superconducting RSA used for remote sounding of underlying surfaces of different nature, as well as integrated circuits and microelectronic devices based on superconductors.

In the third part solutions of nonstationary boundary value problems on waveguide and antenna technique will be obtained. An analysis of the results obtained will be made and practical recommendations for constructing particular superconducting microwave devices will be given [22].

Modeling of Physical Processes in Various Superconducting Structures.

We consider the cycle of problems on excitation, diffraction and scattering of the electromagnetic waves by superconducting structures. Such structures are the plane, the strip, the system of strips, the circular and elliptic cylinders, the sphere, the thin shell and a number of other bodies. Such wide range of problems was considered in works of the author [1,9-22]. Investigations associated with the scattering and propagation of the electromagnetic waves in the superconducting structures are caused first of the progress toward the microelectronics and advances in the different solid-state superconducting devices. The practical success that was achieved in low-temperature and high-temperature superconductivity [1] within the last years made it possible to obtain quantitatively new results on determination of the basic electrodynamic characteristics of the different microwave devices and structural elements. The mathematical modeling of physical processes performed by author and his colleagues when solving the wide class of boundary value problems of the third kind (internal and

external) is based on the superconductor surface impedance mentioned in [1]. New mathematical methods for solving the boundary value problems of this kind are developed and justified are based on the theory of spectral operators. These enabled us to solve a number of the important application problems. Following the practical purpose of these or those radiotechnical systems and devices we could emphasize several groups of such problems. First of all are the problems associated with scattering and propagation of electromagnetic waves along the boundary between the free space and superconductor. To the same class of explored structures can be attributed the scattering of the electromagnetic waves on one, two and system of superconducting tapes. Here also should be regarded problems on the propagation of electromagnetic waves in waveguides with "sandwich" type walls, determination of the basic electrodynamical characteristics of the microstrip superconducting resonators and cavity resonators of complex shape. The second group of problems deals with the excitation and scattering of electromagnetic waves on the superconducting disk and two disks, cylinder, sphere, rough wedge and so on. Hereto problems group adjoin the many problems of the antenna and waveguide technique, microwave microelectronics. Finally, the third group of problems, when solving them it is expedient to use the superconductor surface impedance, concerns developing of the theory of open superconducting resonators. To basic scientific results can be attributed: solution of the diffraction boundary value problem on two thin superconducting tapes which represent the open resonator and results of the study of open superconducting resonators, formed by rectangular and circular planar, cylindrical and spherical mirrors. Many of the mentioned problems should be solved in nonstationary approximation.

Theory and Its Applications.

Developed and grounded mathematical methods for solving of stated in [1-22] scientific and technical problems are perspective and can find wide applications in various fields of the physics and technique of the microwave band. Mention some of them. The creation of the advanced radar and radiomeasuring systems on the element base of the superconductors will permit one to solve the next major problems: in space communication, location and ship navigation, search and detection of heat-radiating objects, remote measurement of temperatures, spectral analysis of temperatures, spectral analysis of the planetary atmosphere, medicine, microelectronics, fundamental metrology. So in [20] for the first time the research in the refinement of the fundamental physical constant (FPC) the velocity of light on the basis of superconducting circular cavity resonators have been carried out. The performed numerical experiments on refinement and determination of the FPC the velocity of light by two different mathematical methods (the perturbation technique and the method of the generalized natural oscillations) on the basis of cavity resonators are reference to building the theory of open superconducting resonators. In such a way a principle possibility, having created this theory, to obtain the algorithm and the programs software for its refinement on the basis of superconducting open resonators appears for the first time. Besides on the basis of these relationships for particular physical models of the open superconducting resonators (for example, confocal) the real possibility appears to perform experimental studies concerning the determination of the velocity of light. Note that the theory of open superconducting resonators represents the new scientific research area in modern electrodynamics [2,4,5,11,12]. How it follows from the analysis of the results obtained, it is clear that they will find wide application in electronics, instrumentation and antenna technique of the microwave band.

REFERENCES

1. Kravchenko, V. F. and Kazarov, A. B., Surface Impedance of Superconductors and Its Applications in Physics and Engineering, Foreign Radio Electronics. Advances in Modern Radio Science. 1997, no. 11, pp. 59-77.
2. Kravchenko, V. F., Electromagnetics of Superconducting Structures and Its Application to the Problems of Antenna and Waveguide Technique, Proceedings of the Second International Conference on Antenna Theory and Techniques, May 20-22, 1997, Kyiv, Ukraine, pp.1-4.
3. Kravchenko, V. F. and Kazarov, A. B., Scattering of the Electromagnetic Wave by the Rough Superconducting Strip, Proceedings of the 1st Workshop on Electromagnetic and Light Scattering: Theory and Applications, May 27-28, 1997, Moscow, Russia, p. 143-146.
4. Kravchenko, V. F. and Kazarov, A. B., Determination of Electrodynamical Characteristics of Superconducting Open Resonators, Proceedings of 6th Russian Workshop "Physics and Microwave Applications", Krasnovidovo, Moscow Region, May 26-31, 1997, pp. 31-33.

5. Kravchenko, V. F. and Kazarov, A. B., To the Theory of Superconducting Open Resonators, Extended Abstracts – ISEC'97, 6-th Int. Superconductive Electronics Conference, June 25-28, 1997, Berlin, Germany, vol. 3, pp. 281-283.
6. Kravchenko, V. F. and Kazarov, A. B., Electromagnetic Wave Scattering by a Dielectric Half-Plane Covered by a Superconducting Film with Surface Roughness, Proceedings of PIERS'97 Progress in Electromagnetic Research Symposium, July 7-11, 1997, Cambridge, Massachusetts, USA, p. 262.
7. Kravchenko, V. F. and Kazarov, A. B., Electromagnetic Wave Interaction with HTSC Thin Film, Proceedings of ISRAMT'97, 6th International Symposium on Recent Advances in Microwave Technology, August 4-7, 1997, Beijing, China.
8. Kravchenko, V. F., Integral Methods and Some of its Applications to Boundary Value Problems of Diffraction of Electromagnetic Waves on Superconducting Structures, Proceedings of IMA Conference on Boundary Integral Methods: Theory and Applications. September 15-18, 1997, University of Salford, UK, p. 76-77.
9. Kravchenko, V. F. and Tyutyukin, R. G., New Method for Determination the Electrodynamical Characteristics of the Superconducting Disk Being Excited by Electrical Dipole, Radiotekhnika, 1997, no. 2, pp. 8-16.
10. Kravchenko, V. F. and Kazarov, A. B., Electrodynamical Characteristics of Superconducting Disk Open Resonators, Dokl. Akad. Nauk, 1997, vol. 356, no. 5 pp.620-624.
11. Kravchenko, V. F. and Kazarov, A. B., Superconducting Open Resonators with Planar Rectangular and Circular Mirrors, Radiotekhnika, 1997, no. 9, pp. 21-27.
12. Gandel', Yu. V., Kravchenko, V. F. and Morozova, N. N., Diffraction of Electromagnetic Waves on Superconducting Thin Stripes Grating, Electromagnetic Waves and Electronic Systems, Moscow, Publishing House of Journal "Radiotekhnika", 1997, vol. 2, no. 1, pp. 4-15.
13. Kravchenko, V. F., Excitation of a Superconducting Spherical Resonator by a Dipole in the Center of the Sphere, Dokl. Akad. Nauk USSR, 1982, Ser. A, no. 1, pp. 63-66.
14. Kravchenko, V. F., Rvachev, V. L., and Taldykin, I. V., On a Method of Electromagnetic Boundary Value Problem Solution for the Complex Shape Inhomogeneous Impedance Region, Dokl. Akad. Nauk SSSR, 1988, vol. 302, no. 1, pp. 72-74.
15. Kravchenko, V. F., Rvachev, V. L., and Chaplin, A. F., Electromagnetic Field of Superconducting Antenna Arrays, Dokl. Akad. Nauk, 1993, vol. 333, no. 6, pp. 725-726.
16. Kravchenko, V. F. and Erofeenko, V. T., Diffraction of Electromagnetic Waves on a Thin Superconducting Cylindrical Shells., Dokl. Akad. Nauk, 1994, vol. 337, no. 1, pp. 25-27.
17. Kravchenko, V. F., Erofeenko, V. T., and Pustovoi, V. I., Diffraction of Electromagnetic Waves on Two Hollow of Superconducting Spherical Shells, Dokl. Akad. Nauk , 1994, vol. 339, no. 2, pp. 166-170.
18. Gandel', Yu. V., Kravchenko, V. F., and Sidelnikov, G. L., Excitation of Planar Superconducting Waveguide by System of Parallel Straight Cuts, Radiotekhnika i Elektronika, 1997, vol.42, no.11, pp.1312-1319.
19. Gandel', Yu. V., Kravchenko, V. F., and Pustovoi, V. I., Scattering of Electromagnetic Waves by a Thin Superconducting Band, Doklady Mathematics, 1996, vol. 54, no. 3, pp. 959-961. (Translated from Dokl. Acad. Nauk, 1996, vol. 351, pp. 462-464).
20. Kravchenko, V. F., Method for Determination of the Speed of Light Based on the Impedance Measurements of Superconductors, Radiotekhnika (Electromagnetic Waves, no. 4), 1995, no. 12, pp. 108-117.
21. Kravchenko, V. F., Erofeenko, V. T. Scattering of Electromagnetic Waves by Two Superconducting Bands, Electromagnetic Waves and Electronic Systems, 1996, vol. 1, no. 1, pp.4-13. Publishing House of the Journal "Radiotekhnika", Moscow.
22. Kravchenko, V. F., Approximate Boundary Conditions for Superconducting Structures with Time-Periodical Electrodynamical Characteristics, Electromagnetic Waves and Electronic Systems, 1998, (to be published). Publishing House of the Journal "Radiotekhnika", Moscow.

Evolution of a Magnetic Resonance Line Under Microwave Field of High Intensity

A. M. Zabolotskiy^{*)}, S. I. Tarapov^{**)}

^{*)} 1, Vavilov St., Maysky, Belgorod, RUSSIA, Belgorod State Agricultural Academy.

<sup>**) 12, Ak. Proskura St., Kharkov, UKRAINE, Institute of Radiophysics and Electronics of
NAS of Ukraine.</sup>

1. The classical description of the Electron Spin Resonance (ESR) phenomenon is based on the known Bloch equation [1] for a motion of a vector magnetization \mathbf{J} in a variable magnetic field $H(t)$:

$$d\mathbf{J}/dt = \gamma[\mathbf{J}, \mathbf{H}] + \mathbf{R} \quad (1)$$

here γ is the gyromagnetic ratio, $\mathbf{R} = \{J_x/\tau_2; J_y/\tau_2; (J_z - J_0)/\tau_1\}$ is the dissipative term, whose components contain the times of the longitudinal (τ_1) and cross (τ_2) relaxation. The dependence $H(t)$ usually is chosen in a form

$$H_x = H_0 \sin(\omega t), \quad H_y = H_0 \sin(\omega t + \varphi), \quad H_z = \text{const.} \quad (2)$$

At $\varphi = \pm\pi/2$ it is possible to determine the periodic solution of (1) in an analytical form, which corresponds to the stationary mode of oscillation of the vector $\mathbf{J}(t)$. Here, the dependence of the amplitude J_{xy} of magnetization in XOY plane on the detuning value (δ) of a microwave field frequency is given by the expression:

$$J_{xy}(\delta) = \sqrt{J_x^2 + J_y^2} = \frac{q\sqrt{1+\delta^2}}{1+Q^2+\delta^2} J_0, \quad (3)$$

where

$$\delta = (\omega - \gamma H_z) \tau_2, \quad q = \gamma H_0 \tau_2, \quad Q = \gamma H_0 \sqrt{\tau_1 \tau_2}.$$

The function $J_{xy}(\delta)$ determines the shape and the structure of the ESR line. It is easy to see that depending on the value of parameter Q it has either one (at $Q < 1$), or two maxima (at $Q > 1$). Thus, for large enough intensity of the microwave field, the splitting of the ESR line to two components is observed, when the intensity of the variable field H_0 exceeds the critical value, H_{cr} , determined from the condition $Q = 1$:

$$H_{cr} = 1/\gamma\sqrt{\tau_1 \tau_2} \quad (4)$$

Using (3), it is easy to see also that at the resonant frequency $\omega = \gamma H_z$ the magnetization J_{xy} decreases with growing of intensity of the microwave field, if $H_0 > H_{cr}$. But it is difficult to explain physical nature of this phenomenon within the framework of the classical model.

2. In order to study the magnetic relaxation mechanism of ESR phenomenon observed in the high-intensity microwave field, the authors developed a statistical method of the process simulation. Here the paramagnetic medium is represented by a system of elementary magnetic moments M_i ($i=1, 2, \dots, n$), which interact with phonons of a crystal lattice in the random moments of time (ν_{ik}). In the time intervals $\nu_{ik} < t < \nu_{i,k+1}$ the motion of the moments M_i is determined by the equation

$$dM_i/dt = \gamma [M_i, H] \quad (5)$$

The description of interaction of magnetic moments with phonons is based on the following assumptions:

a) a sequence of values of energy $E_i = -M_i H$ at the moments of time ν_{ik} after interaction with phonon will form the homogeneous Markov process [2], which has the Boltzman type stationary distribution;

b) the intervals of time $\Delta \nu_{ik} = \nu_{i,k+1} - \nu_{ik}$ have an exponential kind of distribution with parameter $\lambda = 1/\tau$, where τ is the average interval of time between interactions (magnetic relaxation time).

Thus, in the presented model, magnetic moments M_i are the randomly oriented vectors having regular trajectories in space $\{M_x, M_y, M_z\}$, which are broken by the random perturbations at the moment of time ν_{ik} according with the equation (5).

A computer program realizing numerical algorithm of solution of (5) and simulating the interaction of magnetic moments with phonons using the Monte-Carlo method [3] in accordance with the conditions a) and b) has been developed. For simplicity the absolute values of the magnetic moments were assumed identical.

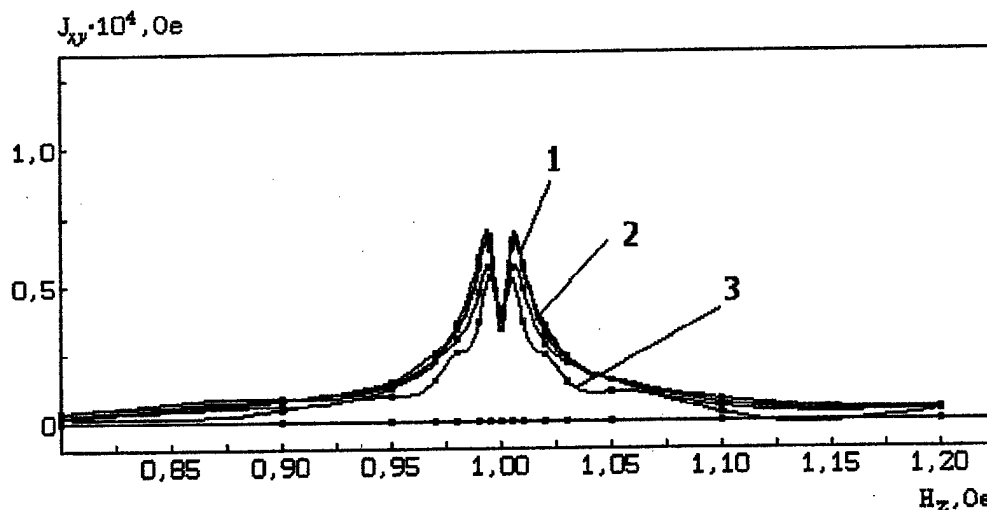


Fig.1. Formation of a resonance line versus the amplitude of the microwave field ($H_0^{(3)} > H_0^{(2)} > H_0^{(1)} > H_{cr}$).

3. Numerical experiments performed on the basis of statistical method demonstrate the effect of splitting of magnetic resonance line to two components, as well as the solution of phenomenological equation (1). In Fig.1 the dependencies of the magnetization J_{xy} on the

static magnetic field H_z , for different values of $H_0^{(0)} > H_{cr}$ are presented. One can see the reduction of magnetization with growing the intensity H_0 of the microwave field under the condition of resonance $\omega = \gamma H_z$. The analysis of dynamics of this process demonstrates that this phenomenon is caused by the fact that in the vicinity of the resonant frequency, at $H_0 > H_{cr}$, the system of magnetic moments splits on two subsystems with opposite orientations of vectors M_i . This phenomenon leads to the reduction of the medium magnetization in the XOY plane.

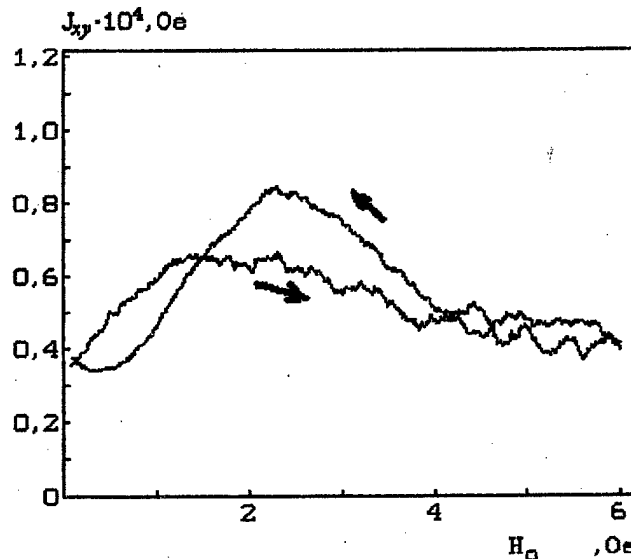


Fig.2. Dependence of the magnetization value J_{xy} on the intensity H_0 at the resonant frequency $\omega = \gamma H_z$.

The ESR phenomenon was also simulated under the conditions of amplitude modulation of microwave field. Here the variation of the value of H_0 in time is linear. As calculations show, for a high intensity H_0 and incomplete magnetic relaxation the double loop of hysteresis caused by the effect of the resonant line splitting is formed on the diagram $J_{xy} - H_0$ (Fig.2). As far as the width of the hysteresis loop is one-to-one connected with the relaxation time, this phenomenon can be used as a basis for the development of an independent method of definition of magnetic relaxation time.

Thus the statistical method, whose opportunities are discussed here, appears to be rather efficient method of simulation of dynamic processes in magnetics. The analysis of the calculations of magnetoresonance absorption evolution demonstrates that by taking into account the crystal fields and exchange interaction it will be possible to apply this method for the research of more complicated magnetic structures such as ferromagnetics, asperomagnetics, spin-glasses, etc.

References

1. Bloch F., Nuclear Induction. Phys. Rev., v70, N7, 1946, P.460-472.
2. Gihman I.I., Skorohod A.V., The randomized processes theory. Ch.2, M., Nauka, 1973 (in Russian).
3. Sobol I.M., Numerical Monte-Carlo methods, M., Nauka, 1973 (in Russian).

ANALYSIS OF METHODS OF CALCULATION OF ELECTRIC FIELD IN GRANULAR MATERIAL

B.I.Nevzlin, Y.Y.Dyachenko

East Ukrainian State University, Department of Electromechanics
348034 Lugansk, kv. Molodezhniy, 20A, Ukraine
E-mail: root@vugu.lumsi.lugansk.ua

Abstract - The methods of calculation of electric field in granular materials are analyzed: classical, conformal mappings and breakdown into sections. A conclusion about necessity of solution of the Laplace equation for the exact description of a field in granular material is done.

The measurement of humidity is important in many industrial and agricultural applications. Wide class the media, whose humidity is necessary to monitor, are granular materials (GM). They are: seeds of grain cultures (wheat, rye, etc.), crushed coal and ores of minerals, various powders: from mould mixtures in foundry shops up to raw material for obtaining electrotechnical ceramics.

For an operational and non-destructive control of GM humidity, a high-frequency method is applied, which provides definition of humidity of a material by the analysis of its parameters in alternating electric field with frequency 5 kHz...50 MHz. In most cases empirical dependences specific only to one type of GM are used.

For obtaining the generalized characteristics of an electric field in GM used in the process of design and graduation of moisturemeters, it is necessary to consider the character of electric field in GM.

In [1] it is simply assumed that all the particles of GM have identical and definite form and are packed in a cubic lattice.

For a single spherical particle, an exact solution of the problem of calculation of a can be obtained with the aid of the Laplace equation [2, p. 250]:

$$\nabla^2 \phi = 0.$$

Thus the field inside a particle is represented as uniform, that is true only in the case of absence of active conductivity. In calculation of the field for a group of particles of GM, it is necessary to take into consideration the fact that each particle GM is surrounded by other particles, which distort the field. That is to accept the following boundary conditions: the particle is limited by two tangents equipotential planes, which are perpendicular to force lines of the uniform (before depositing a particle) electrical field. Such a solution has not been obtained yet.

However a portrait of the field can be obtained, under some assumptions, without a solution of the Laplace equation.

According to [1] a particle and the medium enclosing it are divided into two zones: the first is the conductivity zone and the second is the contact one (Fig. 1). Thus the boundary between the zones is assumed as an equipotential plane and in each zone the field is calculated separately.

We shall assume that the specific resistance of the particle material ρ_p is significantly smaller then of the medium ρ_m (the space between particles is filled by air), that is, with $\rho_p \ll \rho_m$, considered in [3]. As a dump particle has not only reactive (capacity), but also active part of conductivity, a picture of a current field enables us to consider the force lines in

the zone of contact of a particle as the straight lines [4] outgoing from the point of contact; in the zone of conductivity the force lines are the arcs of ellipses [5, p. 10].

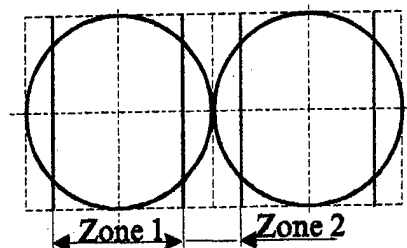
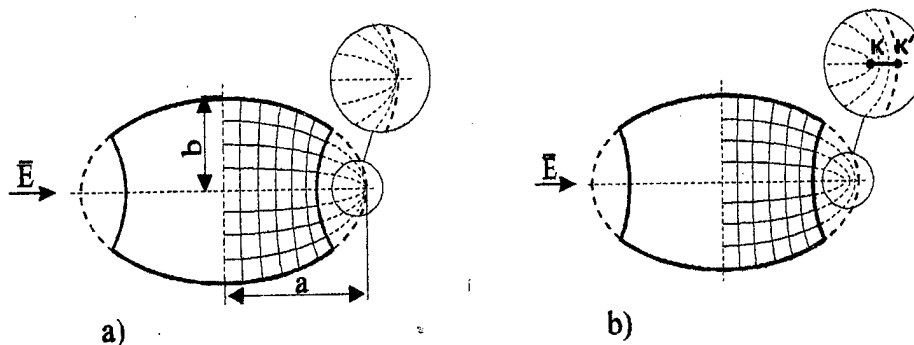


Fig. 1. The scheme of decomposition of a particle into zones

Several ways of calculation of the field in the zone of conductivity for the shaped as ellipsoid of rotation, with $\rho_p \ll \rho_m$, are possible.

In [6], calculation is carried out by the Roters method with the mentioned assumptions on the picture of the field (Fig. 2a). In case of the picture of the field after [6], the boundary between zones should have, approximately, the shape of a part of a sphere.



With a picture of the field after [7], see Fig. 2b, the calculation of the field is done by the method of conformal mappings, thus the boundary between zones is a sort of a hyperboloid of rotation. Essential difference, except for the boundary of zones, is that in the second variant the force lines converge not at a point of contact, but on the line KK' that does not correspond to a real picture.

The relative difference of values of active resistances at the computation after [6] and after [7] with a relation of semiaxes of an ellipsoid of rotation a/b from 1.5 up to 10.0 decreases from 33 % up to 0.4 % with insignificant change of absolute difference. It happens for two reasons:

- a) the forms of force lines with an increase of a/b draw together;
- b) the influence of the different forms of boundaries between zones insignificantly depends on a/b , and is reduced with the growth of a/b .

Thus, for the final solution of a problem about a choice of the picture of the field in the zones of conductivity and contact, and, correspondingly, the form of the boundary between zones, the solution of the Laplace equation for a group of particles of GM is necessary.

REFERENCES

1. N.S. Dubrov, E.S. Krichevsky, B.I. Nevzlin, Multiparametric Moisture-Meters for Granular Materials, Moscow: Mashinostroenie, 1980 (in Russian)
2. V.E. Kuzmichev, Laws and Formulas of Physics, Kiev: Naukova Dumka, 1989 (in Russian)
3. R. Holm, Electrical Contacts, Moscow: Inost. Literatura, 1961 (in Russian)
4. A.V. Isakova, Study of Inhomogeneous Contact Elements of the Low-Current Circuits, Ph.D. Dissertation, Kharkov, 1968 (in Russian)
5. V.T. Omelchenko, Theory of the Contact Processes, Kharkov: Visha Shkola, 1979 (in Russian)
6. B.I. Nevzlin, Yu.Yu. Diachenko, Calculation of Electric Conductivity of Granular Bulk Medium with Cubic Packing, Visnyk SUDU, 1997, vol. 4(8), pp. 244-252, (in Russian)
7. Yu.Yu. Diachenko, Application of Conformal Mapping to the Calculation of Conductivity of a Particle of Granular Material, Visnyk SUDU, 1997, vol. 6(10), (in Russian)

FORCES OF INTERACTION BETWEEN MACROSCOPIC OBJECTS IN THE FIELD OF ELECTROMAGNETIC WAVE

Nikolay G.Kokody

Kharkov State University, Radio Physics Department,
Kharkov, 310077, Ukraine

Mechanical action of electromagnetic radiation on material objects (pressure or rotation) is exhibited in many physical phenomena. It plays an important role in the processes inside the stars. It influences on the orbits of small particles which move in the space. In the physics of condensed media the electromagnetic (ponderomotive) forces are exhibited in the electrostriction effect. The radiation pressure plays great role in the interaction of laser pulses with plasma in the laser-heating nuclear fusion machine. It is used for the measurement of the power of microwave and laser radiation.

Ponderomotive action of electromagnetic field on the isolated objects in free space has been investigated well, both theoretically and experimentally. It is not so, however, when there are two or more objects. P. N. Lebedev made such experiments. He had not finished them, however. There are modern publications on the research of the radiation pressure on a system, which contains several dipoles in a waveguide. They investigate the case when $\lambda/a \gg 1$ (λ is the wavelength, a is the size of the dipole), however.

Ponderomotive forces in the system for two circular cylinders, which are placed in the field of a plane electromagnetic wave are found in the present work. It is a simple case but its results can be used for a system of other objects.

It is necessary to find the electromagnetic field in the neighbourhood of each cylinder for determining the ponderomotive forces. This problem was solved for two identical cylinders with the radius a and the complex-valued refraction index m , placed at the distance d from each other. The wave is incident normally to the plane, in which the cylinders are located. The ratio λ/a can be arbitrary.

The addition theorem for cylindrical functions was used for solving of the problem. The formulas representing the sum of fields of the incident wave and the waves which are scattered by cylinders are found:

$$E_z = E_0 \sum_{n=-\infty}^{\infty} i^{-n} \left[J_n(kr) - b_n H_n^{(2)}(kr) + J_n(kr) \sum_{l=-\infty}^{\infty} b_l H_{l+n}^{(2)}(\delta) \right] e^{-in\varphi},$$

$$H_\varphi = -\frac{i}{\omega\mu_0} \frac{\partial E_z}{\partial r}, \quad H_r = \frac{i}{\omega\mu_0 r} \frac{\partial E_z}{\partial \varphi},$$

where $\delta = 2\pi d/\lambda$,

$$b_n = b_{0,n} \left[1 - \sum_{l=-\infty}^{\infty} b_l H_{l+n}^{(2)}(\delta) \right],$$

$b_{0,n}$ is coefficient for a single cylinder.

It is necessary to solve an infinite matrix equation for finding the expansion coefficients b_n . One can limit the number of equations based on the physical conditions: radius of cylinders, distance between them and wavelength of the radiation. For this problem $l_{max} \approx 2\rho$, $\rho = 2\pi a/\lambda$.

The longitudinal F_l and transversal F_t the forces acting on the cylinders were calculated through the components of the Maxwell stress tensor T_{rr} and $T_{r\varphi}$ by using the results of the solution of the previous problem[1,2]:

$$F_l = \int_0^{2\pi} (T_{rr} \cos \varphi - T_{r\varphi} \sin \varphi) a d\varphi = \frac{P}{c} Q_{pl},$$

$$F_t = \int_0^{2\pi} (T_{rr} \sin \varphi + T_{r\varphi} \cos \varphi) a d\varphi = \frac{P}{c} Q_{pt},$$

where

$$T_{rr} = -\frac{\epsilon_0}{4} E_z E_z^* + \frac{\mu_0}{4} (H_r H_r^* - H_\varphi H_\varphi^*),$$

$$T_{r\varphi} = \frac{\mu_0}{2} \operatorname{Re} (H_r H_\varphi^*),$$

P is the power of radiation incident on the cylinder, c is the light velocity, Q_{pl} and Q_{pt} are the efficiency factors of the radiation pressure.

The functions of Q_{pl} and Q_{pt} versus the distance $\delta = 2\pi d/\lambda$ are shown in Figs. 1 and 2. The cylinders are perfectly reflecting ($m \rightarrow \infty$). The electric vector of the wave is parallel to the axes of cylinders.

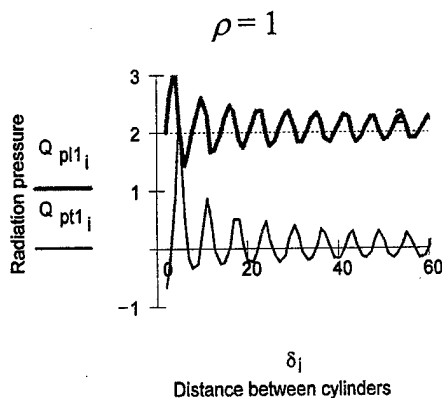


Figure 1

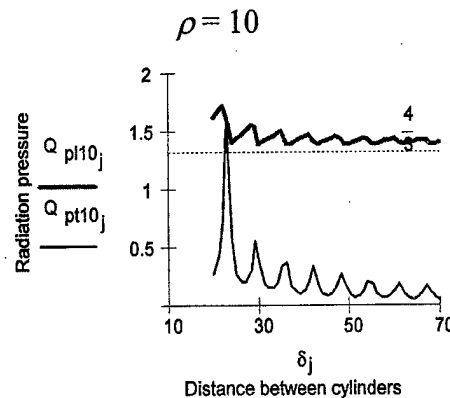


Figure 2

The dependence of the longitudinal force F_l oscillates about the asymptote, which is corresponding to a single cylinder. The amplitude of oscillations decreases very slowly. It is still large even with $\delta = 60$.

The character of transversal forces F_t depends on the value ρ . The cylinders, which have small value of ρ , can attract or push away from each other at the different distances δ between them (see Fig. 1 for $\rho = 1$). The direction of the force depends on the function of distribution of currents on the surfaces of the cylinders. These currents interact with the magnetic field of the wave. On the surface of a single cylinder this function is symmetric about the direction of the wave vector. The symmetry disappears with the appearance of the wave scattered by the neighbouring cylinder. The maximum of the current may be on the inner or the outer part of the surface of cylinder. The sum of transversal forces is directed outside (in the first case) or inside (in the second case) of the cylinders, which are pushed away or attracted, respectively.

When $\rho \gg 1$, the cylinders are pushed away only (see Fig. 2 for $\rho = 10$), since the wave scattered by one cylinder does not circle the surface of the second cylinder. The maximum of the surface current is always on the inner part of the surface of the cylinder.

The efficiency factors of the radiation pressure are well approximated by the following formulas:

$$Q_{pl} = \frac{4}{3} + \frac{4}{5} \frac{\rho^2}{\delta^2}, \quad Q_{pt} = \frac{\rho}{2\delta}.$$

The magnitude of the transversal forces decreases as $1/d$.

General behavior of the forces remains the same for the other polarization of the wave and in the cases when the cylinders have a finite real or complex-valued refraction index. Only the magnitudes of the forces vary.

REFERENCES

1. I. E. Tamm, Foundations of the Theory of Electricity, Moscow: Nauka Publ., 1966 (in Russian).
2. N. G. Kokody, Extinction, scattering and radiation pressure efficiency factors of thick cylinders, *Optika i Spektroskopiya*, 1994, v. 77, No. 4.

ANALYSIS OF THE OERSTED EXPERIMENTS

Yu.A. Branspiz, A.A. Kovalevsky

East Ukrainian State University
sq. Molodegnyi, 20-a, Lugansk, 348034, Ukraine

Abstract Analytical solution is given of the problem about an angle of deviation of magnetic arrow for want of modification of a distance between it and conductor with a current in experience of Oersted. Existence of a maximum in the dependence of the indicated angle on the distance is revealed.

The experiments of Oersted on the force acting due to a conductor with current on magnetic arrow are considered now mainly as a historical fact [1-3]. The mentioning the Oersted experiments is present basically in the textbooks where attention is paid purely to the fact of the force action of magnetic field of a current on the magnetized substance. However, the experiments of Oersted by no means should be "given up" to the history. They contain an interesting material for the problems, which can be included in the modern teaching of the theory of electromagnetism. A review of one of such problems, namely the problem about a force action of conductor with current on magnetic arrow parallel to the conductor (in the absence of current) is given in this work. Analytical approach to a solution of this problem enables us to obtain new results about the angle of deviation of magnetic arrow due to the indicated force action.

Oersted himself wrote the following about the angle of deviation of magnetic arrow originally parallel to a conductor with current, [3]: " If the distance from a wire up to arrow does not exceed 3/4 inches, the deviation makes about 45° . If a distance to increase, the angle proportionally decreases... "

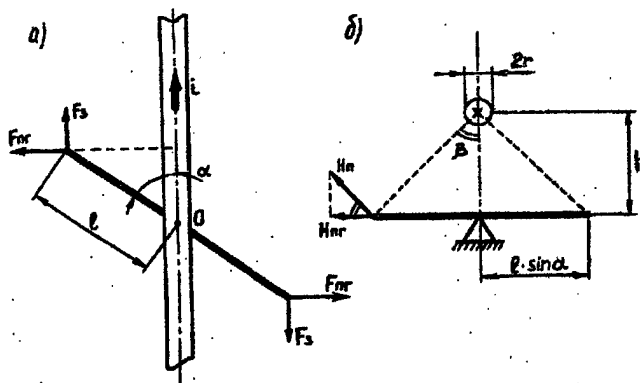


FIG. 1

Our goal is to update this qualitative solution. To this end we model a magnetic arrow as two magnetic charges of opposite sign (fictitious charges) located on the arrow tips, that quite corresponds to the modern representations about permanent magnets with homogeneous magnetization [4]. Then, the force action of magnetic field of a conductor with current on the magnetic arrow of length $2l$, located at the distance h from conductor, is equivalent to the

force actions of this magnetic field (force F_{mz}) onto the indicated fictitious magnetic charges. This force action is counterbalanced by the force action of magnetic field of the ground (force F_s) onto the active magnetic charges of the arrow.

In Fig.1 the top view (Fig.1, a) and axial aspect (Fig.1, b) of an equilibrium of magnetic arrow in the horizontal plane (we neglect the earth magnetic field tilt) is shown. Equilibrium is achieved under condition of moment equality of indicated forces concerning a

central suspension of magnetic arrow (point About in Fig.1):

$$F_{\text{III}} \cdot \ell \cdot \cos \alpha = F_3 \cdot \ell \cdot \sin \alpha. \quad (1)$$

If one takes into account that the forces F_{nz} and F_3 are proportional to the strength of magnetic field (H_{nz} and H_3 respectively, Fig.1) then instead of (1) it is possible to write

$$H_{\text{III}} \cdot \cos \alpha = H_3 \cdot \sin \alpha. \quad (2)$$

If we consider equality (2) as an equation concerning the angle α , then on solving it we can obtain the dependence of the angle α on all the parameters of the problem including the distance h . However, a direct solution of (2) for α , is rather complicated and inconvenient for the analysis. These inconveniences can be avoided if we consider the relation (2) as an equation for the distance h that brings us to the following equation:

$$h^2 - \frac{i}{2\pi H_3} \operatorname{ctg} \alpha \cdot h + \ell^2 \cdot \sin^2 \alpha = 0, \quad (3)$$

whose solution is given by

$$h = \frac{i}{4\pi H_3} \operatorname{ctg} \alpha \pm \sqrt{\left(\frac{i}{4\pi H_3} \operatorname{ctg} \alpha\right)^2 - \ell^2 \sin^2 \alpha}. \quad (4)$$

This solution enables us to construct the function $h = h(\alpha)$, whose inverse is the required dependence $\alpha = \alpha(h)$. So the properties of the dependence $\alpha(h)$ are determined by the properties of the right-hand part of the formula (4). In particular, it is possible to deduce from it the existence of a limiting angle $\alpha = \alpha_0$, for which the formula (4) is meaningful. This limiting angle α_0 is determined by equaling to zero the radical in this formula:

$$\alpha_0 = \arcsin \left(\sqrt{\left(\frac{i}{4\pi H_3 \ell}\right)^2 + \frac{1}{4} - \frac{1}{2}} \right). \quad (5)$$

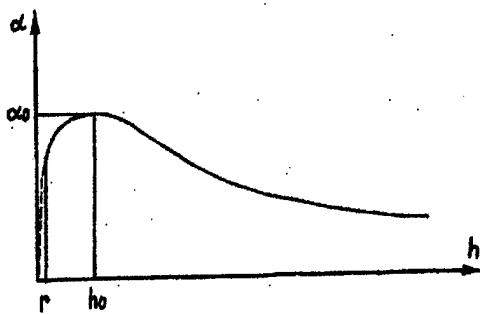


FIG. 2

From the form of the right-hand part of the formula (4) it is possible also to see the following. If the distance h is varied in a leg of a diminution after some large value (it means that the increase of h reduces in a diminution α), the angle α will at first increase, and then, after some distance h_0 (the value α_0 corresponds to this case), it will decrease. This qualitative description of the dependence of the angle α on the distance h is presented in Fig.2.

The value of the distance h ($h = h_0$), for which the angle α has maximum value, is

determined by the equation (see(4)):

$$h_0 = \ell \cdot \sin \alpha_0. \quad (6)$$

Note that, according to Fig.1, from the formula (6) it follows that in the considered

experiment there is always an angle of a maximum deviation of magnetic arrow from the direction of the axis of the wire. It is achieved if the angle β (Fig.1,b) is 45° , as in this case ($\alpha = \alpha_0$) the distance h_0 is equal to the horizontal deviation of the top of the arrow from initial position.

This feature of the dependence $\alpha = \alpha(h)$ corresponds to what had been noted in the Oersted experiments, only for rather large distances h (i.e., for small A). So, from the formula (4), it is easy to obtain the following dependence of the angle of deviation on the distance h , provided that h is large:

$$\alpha \approx \frac{i}{2\pi H_3} \cdot \frac{1}{h}, \quad (7)$$

This fact was noted by Oersted as a decrease of the angle of deviation of magnetic arrow from its initial position when increasing the distance between conductor and this arrow [3].

Concluding, we remark that the first of the authors of the given work made an experiment with magnetic arrow of a tourist compass and a conductor of diameter of 6 mm (in isolation) with the current of 4 to 8 A. Stabilization of the angle α from distance of 10 to 15 mm and up to a maximum approaching of magnetic arrow to conductor was observed. To detect the effect of decrease of the angle A when decreasing further the distance h in this experiment was not possible.

References

1. B.I. Spassky, History of Physics, Moscow: Vysshaya Shkola, 1977, part.2 (in Russian)
2. V.P. Kartsev, Magnet for Three Millenia, Moscow: Energoatomizdat, 1988, (in Russian)
3. G.-Ch. Oersted, Experiments on the Action of Electric Current on Magnetic Arrow, in G.M. Golin, S.P. Filonovich (Eds.), Classics of Physical Science, Moscow: Vysshaya Shkola, 1989, pp. 308 – 312 (in Russian)
4. I.E. Tamm, Fundamentals of the Theory of Electricity, Moscow: Nauka, 1976 (in Russian)

METHOD OF ASYMPTOTIC PERTURBATION OF FUNDAMENTAL SOLUTION AND ITS APPLICATION TO PROBLEMS OF WAVE FIELD INVESTIGATION

Victor I. Selin

Lenin st., 210-22, Obninsk, 249020, Russia
Tel/fax: +7-(8439)-73637, E-mail: iate@storm.iasnet

Abstract. Major points of a new method of calculation of integrals containing the Bessel function are summarized. On the basis of the method of asymptotic perturbations of the fundamental solution the results of the analysis of fields in a layered structure are obtained. The leading terms of the asymptotic behavior of the fields in layered structure are obtained.

Many problems of mathematical physics, including the problems of calculation of fields in a layered medium, are reduced to the calculation of integrals of the following type [1,2]:

$$I(r, z) = \int_0^{\infty} J_0(\lambda r) F(\lambda, z) d\lambda, \quad (1)$$

where $J_0(z, r)$ is the cylindrical Bessel function of the first kind and zero order, $F(\lambda, z)$ is a function determined from the solution of a boundary value problem for an ordinary differential equation.

In work [3], the method of calculation of integrals (1), based on their consideration as integral representations (perturbed by the differential in general sense operators) of the fundamental solution of the operator of mathematical physics was offered. With a reference to the problems associated with the Laplace operators, we formulate such an approach as the following

Theorem 1.

Suppose that it is possible to decompose the function $F(\lambda, z)$ in (1) in terms of the series:

$$F(\lambda, z) = \exp(-\lambda z) f(\lambda) = \exp(-\lambda z) \begin{cases} \sum_{n=0}^{\infty} \alpha_n \lambda^n, 0 \leq \lambda < \lambda^* \\ \sum_{n=1}^{\infty} \frac{\alpha_{-n}}{\lambda^n}, \lambda^* \leq \lambda \end{cases} \quad (2)$$

Then (1) can be presented as an operator function:

$$\int_0^{\infty} J_0(\lambda r) \exp(-\lambda z) f(\lambda) d\lambda = \begin{cases} f\left(\frac{\partial}{\partial z}\right) \frac{1}{R} = \sum_{n=0}^{\infty} (-1)^n \alpha_n \frac{\partial^n}{\partial z^n} \frac{1}{\sqrt{z^2 + r^2}}, & 1 < \sqrt{z^2 + r^2} \\ f\left(\int_0^z dt\right) \frac{1}{R} = \sum_{n=1}^{\infty} \frac{(-1)^n \alpha_{-n}}{(n-1)!} \int_0^z \frac{(z-t)^{n-1}}{\sqrt{t^2 + r^2}} dt, & 0 < \sqrt{z^2 + r^2} < 1 \end{cases} \quad (3)$$

Inside its domain of convergence, series (3) can be differentiated in term by term manner.

Representations (2), (3) are down in a limiting form valid if the function $F(\lambda, z)$ is infinitely differentiable function. Request now that $F(\lambda, z)$ has n continuous derivatives, and the $(n+1)$ -st

derivative is bounded. Then the infinite series in (2) and (3) should be replaced by finite sums. In this specific case, when $z=0$ in the area $r>1$ of (3), we shall obtain the result known from the basic A. N. Tyhonov theorem of his work [4].

Further we write down the representations similar to (2) and (3) for the integral (1) in problems with the Helmholtz operator.

Theorem 2.

Suppose that it is possible to decompose function $F(\lambda, z)$ in (1) in terms of the series:

$$F(\lambda, z) = \frac{\exp(-\eta z) \lambda}{\eta} f(\eta) = \frac{\exp(-\eta z) \lambda}{\eta} \begin{cases} \sum_{n=0}^{\infty} \alpha_n \eta^n, & 0 \leq \eta < \eta^* \\ \sum_{n=1}^{\infty} \frac{\alpha_{-n}}{\eta^n}, & \eta^* \leq \eta \end{cases} \quad (4)$$

Then (1) can be presented as an operator function:

$$\int_0^{\infty} J_0(\lambda r) \frac{\exp(-\eta z) \lambda}{\eta} f(\eta) d\lambda = \begin{cases} f\left(\frac{\partial}{\partial z}\right) \frac{\exp(ikR)}{R} = \sum_{n=0}^{\infty} (-1)^n \alpha_n \frac{\partial^n}{\partial z^n} \frac{\exp(ikR)}{R}, & 1 < kR \\ f\left(\int_0^z dt\right) \frac{\exp(ikR)}{R} = \sum_{n=1}^{\infty} \frac{(-1)^n \alpha_{-n}}{(n-1)!} \int_0^z (z-t)^{n-1} \frac{\exp(ik\sqrt{t^2+r^2})}{\sqrt{t^2+r^2}} dt, & 0 < kR < 1 \end{cases} \quad (5)$$

where $\eta = \sqrt{\lambda^2 - k^2}$, k is a constant value, $R = \sqrt{z^2 + r^2}$.

Inside its domain of convergence series (5) can be differentiated in term by term manner.

The series (3), (5) are analogous to the Taylor series with reference to the integrals, which are solutions of boundary value problems for the operators of mathematical physics. In this sense the representation (3) and (5), in the domain of their convergence, are identities. With reference to the problems of wave field investigation these formulas serve as a generalization of the principles of Huygens and of superposition of waves.

In practice, one uses a finite number of terms from (3), (5). For finding the asymptotic behavior of integrals (1), sometimes it is sufficient a knowledge of the first term of the series (5) only. For calculation of surface waves along the interface of media, it is possible restrict the analysis by the quadrupole ($n=2$ in (5)) approximation of the fundamental solution of the wave equation with the Helmholtz operator. In some cases the fundamental solution corresponding to $n=0$ in (5) is enough.

As an analysis model, we shall consider the structure presented in Fig.1. Integral $V(r, z)$ corresponds to the single non-zero z -component of the Green's tensor function of the layered medium. The principal values of the integrals $V(r, +0)$ and $V(r, -H-0)$ determine the surface waves at the part of external interface of the layered structure. It is possible to calculate these integrals, $V(r, +0)$ and $V(r, -H-0)$, in the quadrupole approximation of the fundamental solution of the wave equation. The values of $V(r, +0)$ and $V(r, -H-0)$ decrease with distance as $1/r^2$. Integral $V(r, z)$ with a source at the interface: $z' \rightarrow +0$ at $z \in [0, -H]$, can be calculated in the approximation of the

fundamental solution of the wave equation. This approximation determines a communication wave of the layered medium

$$V_c(r, z) = \frac{\varepsilon_1}{\left(1 + \varepsilon_1 \sqrt{\varepsilon_1 - 1} \quad k_0 H + \frac{\varepsilon_2 \sqrt{\varepsilon_1 - 1}}{\sqrt{\varepsilon_1 - \varepsilon_2}}\right)} \left[\frac{\exp\left(ik_1 \sqrt{z^2 + r^2}\right)}{\sqrt{z^2 + r^2}} - \frac{\exp\left(ik_1 \sqrt{(z + 2H)^2 + r^2}\right)}{\sqrt{(z + 2H)^2 + r^2}} \right] + O\left(\frac{z + 2H}{(z + 2H)^2 + r^2}\right), z \in [0, -H].$$

If $z \rightarrow -0$, V_c becomes a communication surface wave of a layer at the interface with a source

$$V_c(r, -0) = \frac{\varepsilon_1}{\left(1 + \varepsilon_1 \sqrt{\varepsilon_1 - 1} \quad k_0 H + \frac{\varepsilon_2 \sqrt{\varepsilon_1 - 1}}{\sqrt{\varepsilon_1 - \varepsilon_2}}\right)} \left[\frac{\exp(ik_1 r)}{r} - \frac{\exp(ik_1 \sqrt{4H^2 + r^2})}{\sqrt{4H^2 + r^2}} \right] + O\left(\frac{2H}{4H^2 + r^2}\right).$$

The presence of the interface of the media at $z = -H$ results in the behavior of the field on the internal interface of a layer with a source as $\sim 1/r$.

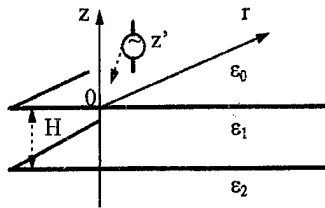


Fig. 1. Model of layered media with one layer.

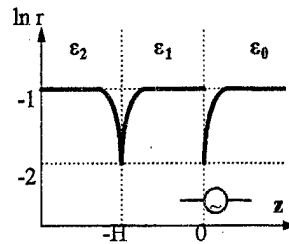


Fig. 2. Scheme of the principal-value integrals $V(r)$ of layered structure.

In Fig. 2, the behavior of the principal value of integral $V(r)$ of the layered structure is shown, depending on the position of coordinate z of the point of observation. This scheme shows the domains of communication, Geometric Optics field ($\ln r = -1$), and that of the field decreasing according to the law $\sim 1/r^2$ ($\ln r = -2$), including surface waves of layered structure. The scheme clearly demonstrates the properties and the essence of the concept of communication waves in a layered media.

REFERENCES

1. A. N. Tihonov, D. N. Shahsuvarov, *Izvestiya Akademii Nauk SSSR Geofizika*, 1956, no 3, p. 245 (in Russian).
2. V. I. Dmitriev, *Electromagnetic Fields in Non-uniform Media*, Moscow University Press, 1969 (in Russian).
3. V. I. Selin, *Integral Transforms and Special Functions*, 1997, vol. 1, no 3 (in Russian).
4. A. N. Tihonov, *Doklady Akademii Nauk SSSR*, 1959, vol. 125, no 5, p. 982 (in Russian).

SIMPLE APPROXIMATE FORMULAS FOR EVALUATING SOMMERFELD TYPE INTEGRALS

Peter L. Tokarsky, Vladimir V. Dolzhikov
Kharkiv State Technical University of Radio Electronics,
14, Lenin Av., Kharkiv, 310726, Ukraine

Tel: +380 572 409 430, Fax: +380 572 409 113, E-mail shifrin@kture.kharkov.ua

Introduction. Analysis of antennas and scatterers, located in a close proximity to the air/ground interface is concerned with calculation of Sommerfeld type improper integrals [1]. This problem has no rigorous solution in a closed form, therefore it is solved either by numerical integration or with the use of approximation. Among the latter, widespread are the methods of the high-contrast approximation (HCA) [2] and of the reflection coefficient (RCM) [3], which are convenient for application but always have not a high accuracy. The purpose of the present paper is development of more accurate expressions for evaluating near fields of an infinitesimal electric dipole located over the lossy half-space. We assume that the dipole is located at a point $M'(0,0,h>0)$ in the cylindrical coordinate system (r,φ,z) , and the plane $z=0$ separates the homogeneous material half-spaces. The upper half-space ($z>0$) is a medium 1 with the permittivity ϵ_1 , permeability μ_1 and conductivity $\sigma_1=0$ (air), and the lower half-space ($z<0$) is a medium 2 with the electrical parameters $\epsilon_2, \mu_2, \sigma_2$ (ground). Besides, it is assumed that the dipole current has a unit amplitude with a harmonic time dependence $\exp(j\omega t)$. We examine the radiated field from an electric dipole into the medium 1 and take account of two dipole orientation cases: one is along the axis z (vertical dipole) and the other is along the radius r at $\varphi=0$ (horizontal dipole).

Vertical electric dipole (VED). The Hertzian potential of the VED field has a z -component only [1]:

$$\tilde{\Pi}(M) = \tilde{z}^0 \Pi_{zz}, \quad \text{where} \quad \Pi_{zz}(M) = G(R_1) + G(R_2) + \Delta \Pi_{zz}, \quad \Delta \Pi_{zz} = -\frac{1}{4\pi} \int_0^\infty f_{zz}(v) J_0(vr) \exp(-\gamma_1 \zeta) dv,$$

$$f_{zz}(v) = \frac{2k_1^2 \gamma_2}{k_2^2 \gamma_1 + k_1^2 \gamma_2} \frac{v}{\gamma_1}, \quad R_1 = \sqrt{r^2 + (z-h)^2}, \quad R_2 = \sqrt{r^2 + \zeta^2}, \quad \zeta = z+h, \quad \gamma_{1,2} = \sqrt{v^2 - k_{1,2}^2}, \quad k_1 = \omega \sqrt{\epsilon_1 \mu_1},$$

$k_2 = \omega \sqrt{\epsilon_2(1 - j\sigma_2/\omega\epsilon_2)\mu_2}$, $G(R) = \frac{1}{4\pi} \frac{\exp(-jk_1 R)}{R}$ is the Green function of the free space, $J_m(x)$ is the Bessel function of order m , (r, φ, z) are coordinates of an observation point M . The correction term $\Delta \Pi_{zz}$ is expressed through the Sommerfeld type integral, where the integrand has two branch-points $v=k_1$ and $v=k_2$, in the vicinities of which the sharp bursts are observed. When $|k_2| > |k_1|$ it can be presumed that the contribution of the point $v=k_2$ to the integral value is considerably smaller than of the point $v=k_1$ due to the decreasing exponential factor. Taking this into account, we reduce the algebraic factor of integrand to the following form:

$$f_{zz}(v) \approx \frac{2k_1^2 \cdot jk_2 \cdot v}{k_2^2 \gamma_1^2 [1 + (k_1^2 \cdot jk_2) / (k_2^2 \cdot jk_1)]} = j \frac{2k_1}{n+1} \frac{v}{\gamma_1^2}, \quad \text{where } n = k_2/k_1,$$

that enables the integral in the expression for $\Delta \Pi_{zz}$ to be transformed as follows [2]:

$$I(r, R_2) = \frac{1}{4\pi} \int_0^\infty J_0(vr) \exp(-\gamma_1 \zeta) \frac{v}{\gamma_1^2} dv = \frac{1}{4\pi} \int_1^\infty \frac{\exp(-jk_1 R_2 t)}{\sqrt{t^2 - (r/R_2)^2}} dt.$$

We expand the denominator of the integrand in the latter expression in the power series and then we can find the required expression for $\Delta \Pi_{zz}$

$$\Delta \Pi_{zz} \approx -j \frac{2k_1}{n+1} I(r, R_2), \quad (1)$$

$$\text{where } I(r, R_2) = \frac{1}{4\pi} \sum_{m=0}^\infty A_m E_{2m+1}(jk_1 R_2), \quad A_m = \frac{1 \cdot 3 \cdot 5 \dots (2m-1)}{2 \cdot 4 \cdot 6 \dots 2m} \left(\frac{r}{R_2} \right)^{2m} \quad \text{end} \quad E_m(z) = \int_1^\infty \frac{\exp(-zt)}{t^m} dt$$

is the exponential integral [4]. The series (1) is fast convergent and its calculation usually requires no more than 3 or 4 terms. The general term can be easily obtained using the recurrent formulas:

$$E_{2m+1}(jkR) = \frac{\exp(-jkR)}{2m} \left(1 - \frac{jkR}{2m-1} \right) - \frac{(kR)^2}{2m(2m-1)} E_{2m-1}(jkR), \quad A_m = \frac{2m-1}{2m} \left(\frac{r}{R_2} \right)^2 A_{m-1}, \quad A_0 = 1,$$

$E_1(jkR) = -\text{ci}(kR) + j\text{si}(kR)$, $\text{si}(x)$ and $\text{ci}(x)$ are the sine and cosine integrals.

Horizontal electrical dipole (HED). The Hertzian potential of the HED field has two components: $\vec{\Pi} = \vec{x}^0 \Pi_{xx} + \vec{z}^0 \Pi_{zz}$. We consider first the vertical component of the Hertzian potential, that is defined by the equation [1]:

$$\Pi_{zz}(M) = -\frac{\cos \varphi}{4\pi} \int_0^\infty f_{zz}(v) J_1(vr) \exp(\gamma_1 \zeta) dv, \text{ where } f_{zz}(v) = 2v^2 \frac{\gamma_1 - \gamma_2}{k_2^2 \gamma_1 + k_1^2 \gamma_2}.$$

We shall simplify the function $f_{zz}(v)$ in two ways. At first we proceed the same way as in the VED case:

$$f'_{zz}(v) \approx 2v^2 \frac{jk_1 - jk_2}{k_2^2 \gamma_1 [1 + (k_1/k_2)]} = -j \frac{2}{k_2} \frac{n-1}{n+1} \frac{v^2}{\gamma_1}.$$

The substitution of this approximation in the integral yields:

$$\Pi'_{zz}(M) = -j \frac{\cos \varphi}{4\pi} \frac{2}{k_2} \frac{n-1}{n+1} \int_0^\infty J_1(vr) \exp(\gamma_1 \zeta) \frac{v^2 dv}{\gamma_1} = -j \cos \varphi \frac{2}{k_2} \frac{n-1}{n+1} \frac{\partial}{\partial r} G(R_2). \quad (2)$$

In the second way, before a simplification of the function $f_{zz}(v)$, we present its denominator as the sum of the squares:

$$f''_{zz}(v) = 2v^2 \frac{\gamma_1 - \gamma_2}{k_2^2 \gamma_1 + k_1^2 \gamma_2} \frac{k_2^2 \gamma_1 - k_1^2 \gamma_2}{k_2^2 \gamma_1 + k_1^2 \gamma_2} \approx \frac{2}{k_2^2} \frac{n^2 + 1}{n^2 - 1} v^2 - j \frac{2}{k_2} \frac{n^2 + 1}{n^2 - 1} \frac{v^2}{\gamma_1} - \frac{2}{n^2} \frac{v^2}{\gamma_1^2}$$

and obtain
$$\Pi''_{zz}(M) = -\cos \varphi \frac{2}{k_2^2} \left\{ \frac{n^2 + 1}{n^2 - 1} \left[jk_2 \frac{\partial}{\partial r} + \frac{\partial^2}{\partial r \partial \zeta} \right] G(R_2) + k_1^2 \frac{\partial}{\partial r} I(r, R_2) \right\}. \quad (3)$$

By using expansion of the integral $I(r, R_2)$ in the series (2) it is easily shown that

$$\frac{\partial}{\partial r} I(r, R_2) = -\frac{r}{R_2} \left[\left(1 + \sqrt{1 - (r/R_2)^2} \right)^{-1} G(R_2) + j \frac{k_1}{4\pi} \sum_{m=0}^\infty \frac{2m-1}{2m} A_{m-1} E_{2m}(jk_1 R_2) \right].$$

Calculations with the use the formulas (2) and (3) enabled us to establish that the deviations of $\Pi'_{zz}(M)$ and $\Pi''_{zz}(M)$ from the exact value are rather close in magnitude but have opposite signs, so the best approximation is given by their mean value:

$$\Pi_{zz}(M) = 0.5 [\Pi'_{zz}(M) + \Pi''_{zz}(M)]. \quad (4)$$

The horizontal component of Hertzian potential of the HED field is expressed in the following form [1]:

$$\Pi_{xx}(M) = G(R_1) - G(R_2) + \Delta \Pi_{xx}, \quad \Delta \Pi_{xx} = \frac{1}{4\pi} \int_0^\infty f_{xx}(v) J_0(vr) \exp(-\gamma_1 \zeta) dv \quad f_{xx}(v) = \frac{2v}{\gamma_1 + \gamma_2}$$

The function $f_{xx}(v)$ can be approximated in two ways as well:

$$f'_{xx}(v) \approx -j \frac{2v}{k_1(n+1)} \quad \text{and} \quad f''_{xx}(v) = \frac{2v}{\gamma_1 + \gamma_2} \frac{\gamma_1 - \gamma_2}{\gamma_1 - \gamma_2} \approx \frac{2\gamma_1 v - j2k_2 v}{k_1^2(n^2 - 1)},$$

from which it follows that

$$\Delta \Pi'_{xx}(M) = j \frac{2}{k_1(n+1)} \frac{\partial}{\partial \zeta} G(R_2) \quad (5)$$

and

$$\Delta \Pi''_{xx}(M) = \frac{2}{k_1^2(n^2 - 1)} \left[jk_2 \frac{\partial}{\partial \zeta} + \frac{\partial^2}{\partial \zeta^2} \right] G(R_2). \quad (6)$$

Expression (6) is equivalent to similar one in [7], where it was obtained by using the Fourier transform method (FTM).

Numerical results. The calculations were carried out for the case well known from the literature [5,6]: $\epsilon_1 = \epsilon_0$, $\epsilon_2/\epsilon_1 = 10$, $\mu_2 = \mu_1 = \mu_0$, $\sigma_2 = 0.01(\Omega \cdot \text{m})^{-1}$, $R_2 = 10\text{m}$, $\theta_2 = \arctan(r/\zeta) = 10^\circ$, $\varphi = 0$. The results of calculation of $\Delta \Pi_{zz}$ by (1), Π_{zz} by (3), (4) and $\Delta \Pi_{xx}$ by (5), (6) are presented in the Tabs.1–3. For a comparison, here are given also the exact values obtained by a numerical integration method and the results of calculation by using of the HCA-method [2]. Besides, numerical results of calculation by the RCM and FTM methods are taken from [5], [6] included in Tabs.2, 3.

Conclusions. Comparative analysis of the numerical results shows that the derived formulas ensure rather high accuracy of the Hertzian potential calculations for the vertical or horizontal electric dipoles over the lossy half-space. Simplicity of the formulas and absence of numerical integrations makes them convenient for many electromagnetic applications.

Table 1. The correction term $\Delta\Pi_{zz}$ for Z-component of the VED Hertzian potential

F, MHz	R_2/λ	RCM, from [5] $\times 10^4$	HCA $\times 10^4$	Present, eqn. (1) $\times 10^4$	Exact results $\times 10^4$
1.0	0.033	-10.0 -j 5.45	- 0.76 -j 4.12	- 0.90 -j 3.88	- 1.00 -j 4.16
2.0	0.05	-15.2 -j 3.81	- 4.46 -j 7.16	- 4.55 -j 6.39	- 4.93 -j 6.87
3.0	0.1	-18.8 +j 0.05	- 9.48 -j 7.77	- 9.15 -j 6.46	- 9.95 -j 6.92
6.0	0.2	-18.7 +j16.6	-21.16 +j 3.86	-18.20 +j 4.97	-19.56 +j 5.82
9.0	0.3	-4.08 +j28.5	-15.93 +j23.30	-11.75 +j20.97	-11.80 +j22.90
12.0	0.4	16.3 +j26.7	5.00 +j32.76	6.52 +j26.83	8.09 +j28.14
15.0	0.5	31.1 +j11.2	28.26 +j23.53	24.67 +j17.30	26.69 +j16.98
18.0	0.6	32.5 -j10.8	39.46 -j 0.48	31.82 -j 2.85	32.96 -j 4.48
21.0	0.7	19.5 -j29.3	31.62 -j26.87	23.76 -j23.32	23.45 -j25.18
24.0	0.8	-2.43 -j35.7	7.92 -j42.31	4.06 -j34.05	2.65 -j35.14
27.0	0.9	-23.9 -j27.3	-20.74 -j39.08	-18.31 -j29.89	-19.98 -j29.78
30.0	1.0	-35.9 -j 7.42	-41.31 -j18.30	-33.37 -j12.54	-34.48 -j11.43

Table 2. Z-component Π_{zz} of the HED Hertzian potential

F, MHz	HCA $\times 10^5$	FTM, from [6] $\times 10^5$	Present, eqn. (2) $\times 10^5$	Present, eqn. (4) $\times 10^5$	Exact results $\times 10^5$
3.0	-39.54 +j53.60	-45.0 +j19.6	-24.75 +j48.90	-34.82 +j33.84	-34.51 +j28.69
6.0	-16.54 +j60.59	-20.1 +j41.6	- 2.59 +j47.05	-11.80 +j44.04	-14.08 +j43.14
9.0	16.26 +j64.13	9.95 +j45.6	21.21 +j41.04	15.03 +j43.56	13.90 +j44.36
12.0	51.68 +j47.29	36.2 +j30.6	40.34 +j22.56	38.03 +j27.01	37.95 +j27.81
15.0	72.77 +j 9.50	47.6 +j 2.87	46.08 -j 4.42	46.93 -j 0.58	47.21 -j 0.19
18.0	66.91 -j36.11	40.0 -j25.7	35.10 -j30.20	37.59 -j28.24	37.86 -j28.13
21.0	33.61 -j70.49	16.9 -j43.7	11.04 -j44.93	13.66 -j44.95	13.85 -j44.94
24.0	-14.96 -j78.28	-12.2 -j44.2	-17.07 -j42.90	-15.45 -j44.26	-15.29 -j44.30
27.0	-59.38 -j55.02	-36.0 -j27.3	-38.92 -j24.78	-38.46 -j26.60	-38.33 -j26.70
30.0	-81.43 -j 9.19	-45.2 +j0.42	-45.99 +j 2.62	-46.63 +j 1.13	-46.56 +j 0.97

Table 3. The correction term $\Delta\Pi_{xx}$ for X-component of the HED Hertzian potential

F, MHz	RCM, from [6] $\times 10^4$	HCA $\times 10^4$	Present, eqn. (5) $\times 10^4$	Present, eqn. (6) $\times 10^4$	Exact results $\times 10^4$
3.0	18.30 +j0.0076	22.42 -j30.40	18.23 -j29.07	24.40 -j17.29	21.45 -j19.75
6.0	18.30 -j16.1	9.38 -j34.36	5.43 -j30.52	11.56 -j26.64	9.98 -j27.24
9.0	4.11 -j27.7	-9.22 -j36.37	-10.63 -j29.82	-5.27 -j29.88	-6.48 -j29.82
12.0	-15.70 -j26.2	-29.31 -j26.82	-26.09 -j19.81	-22.51 -j22.39	-23.38 -j21.83
15.0	-30.30 -j11.1	-41.27 -j 5.39	-33.70 -j 1.44	-32.53 -j 5.09	-32.91 -j 4.22
18.0	-31.80 +j10.4	-37.95 +j20.48	-28.93 +j18.80	-30.05 +j15.60	-29.86 +j16.45
21.0	-19.20 +j28.5	-19.06 +j39.98	-12.66 +j32.73	-15.22 +j31.05	-14.60 +j31.59
24.0	2.15 +j34.9	8.48 +j44.40	9.11 +j34.36	6.33 +j34.58	7.10 +j34.62
27.0	23.20 +j26.9	33.68 +j31.20	27.87 +j22.63	25.98 +j24.34	26.57 +j23.93
30.0	35.10 +j 7.5	46.18 +j 5.21	36.13 +j 1.86	35.71 +j 4.18	35.91 +j 3.54

References

1. A.Sommerfeld, "Partielle Differentialgleichungen der Physik", Leipzig, 1948.
2. G.A.Lavrov, A.S.Knyasev, "Prizemnyye i podzemnyye anteny", Sovetskoye Radio, Moscow, 1965. (In Russian).
3. P.R.Bannister, "Application of complex image theory", Radio Science, Vol.21, No.4, pp.605-616, 1986.
4. M.Abramovitz, I.A.Stegun (Eds.), "Handbook of Mathematical Functions with Formulas, Graphs and Mathematical Tables", NBS, Applied Mathematics Series - 55, 1964.
5. A.Karwowski, "A Comparison of Three Techniques for Evaluating the Vector Potential of a Vertical Current Element Radiating over the Lossy Half-Space", Proc. IEEE 1985 Inter. Symp. on Electromagnetic Compatibility, New York, N.Y., pp. 82-84, 1985.
6. R.Mitra, P.Parhami, Y.Rahmat-Samii, "Solving the Current Element Problem over Lossy Half-Space Without Sommerfeld Integrals", IEEE Trans. on Antennas and Propagation, Vol. AP-27, No.6, pp. 778-782, 1979.

NONLINEAR THEORY OF RELATIVISTIC MICROWAVE ELECTRON DEVICES

V. Chursin, E. Odarenko, A. Shmat'ko
Dept. of Radiophysics, Kharkov State University,
Svobody Sq., 4, 310077, Kharkov, Ukraine

1. Introduction

The increase of output power is an important task of the theoretical and experimental research of resonant oscillators of millimeter and submillimeter waves (orotron, diffraction radiation generator, laddertron, ledatron, etc.). It is well known that the application of relativistic voltages for acceleration of electron beams in millimeter wave oscillators allows to obtain high levels of output power of radiation. Dynamic relativistic variation of the electron mass can considerably change the character of the electron-wave interaction process. This effect is essential if the magnetic guide field strength is limited or dc focusing field is nonuniform. In this case the transverse electron-wave interaction and to motion of electrons in the transverse direction should be taken into account, and for a theoretical description of the device a multi-dimensional model should be applied.

2. Theoretical model

We consider the following model of a resonant relativistic oscillator. A sheet electron beam is passing through the resonator (cavity or open one) near to the slow-wave structure surface. The electron beam is subjected to the dc longitudinal magnetic field applied in the y direction. The focusing field can be nonuniform in general case. The rf field is assumed to have fixed spatial structure and change slowly in the scale of the electron transit time through the resonator. This is justified if the oscillatory system has sufficiently large value of the quality factor.

For a self-consistent description of the electron-wave interaction process, we start from the Maxwell-Lorentz equations, which can be written assuming the ordinary for resonant devices approximations in the following form [1]:

$$-\frac{dC_s}{dt} + i(\omega - \omega_s)C_s = \frac{1}{2N_s\pi} \int_V \int_0^{2\pi} \vec{J} \vec{E}_s^* \exp(i\omega t) d(\omega t) dV; \quad (1)$$

$$\frac{d\vec{v}}{dt} = -\frac{|e|\hbar}{m_0\gamma} \left\{ \vec{E} + \vec{v} \times \vec{B} - \frac{\vec{v}}{c^2} (\vec{v} \cdot \vec{E}) \right\}; \quad (2)$$

where C_s is the complex amplitude of rf oscillations of the s -th resonator mode. The components of the electric field strength vector $\vec{E} = (0, E_y, E_z)$ are given by:

$$E_y = C_s f(y) \psi_y(z) \exp[i(\beta y - \omega t)]$$

$$E_z = iC_s f(y) \psi_z(z) \exp[i(\beta y - \omega t)]$$

The functions f and ψ_y, ψ_z define the longitudinal (along the coordinate y) and transverse (along the coordinate z) spatial distribution of the s -th resonator mode field,

respectively; $N_s = \epsilon_0 \int_V |\vec{E}_s|^2 dV$ is the modal norm; $\dot{\omega}_s = \omega'_s + i\omega''_s / 2Q_s$ is the fundamental complex frequency of the s -th mode; Q_s is the resonator quality factor; ω is the generation frequency; \vec{J} is the convection current vector of the beam; e, m_0 are the electron charge and rest mass, respectively; \vec{v} is the velocity vector of the electron; c is the light velocity; $\gamma = (1 - v^2/c^2)^{-1/2}$; \vec{B} is the magnetic displacement vector; $\beta = \omega/v_p$; v_p is the phase velocity of the slow wave.

The equations set (1,2) is resolved numerically. Preliminary results are obtained for different values of magnetic displacement of uniform focusing field.

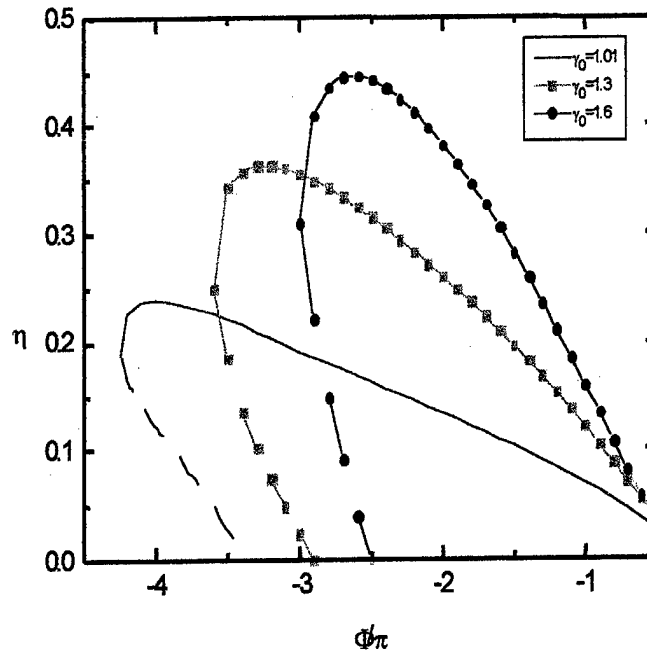


Fig. 1

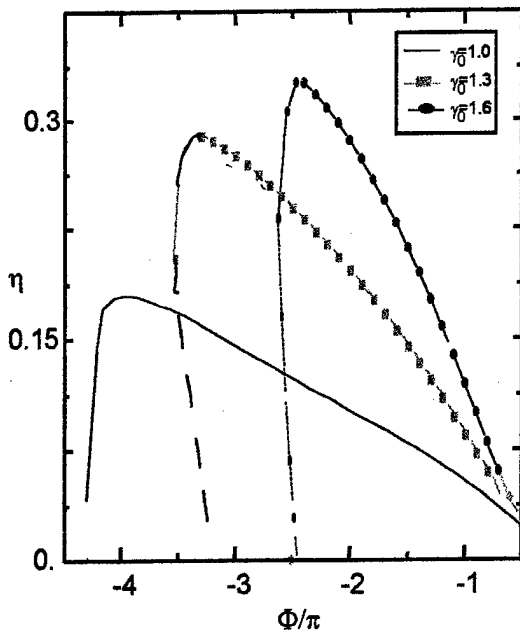


Fig. 2.

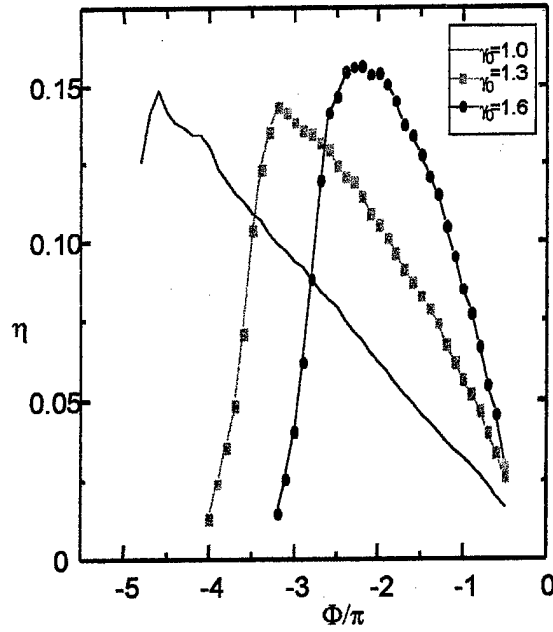


Fig.3.

Discussion

The efficiency dependences upon the parameter $\Phi = (1 - v_0/v_p)\omega L/v_0$ for the different values of γ_0 ($\gamma_0 = \gamma|_{v=v_0}$) and normalized cyclotron frequency $\omega_c/\omega = eB/m\omega$

are shown in Figs. 1, 2 and 3. Solid curves correspond to a drooping regime of the oscillations excitation and dotted curves correspond to a hard regime. All graphs are plotted for the fixed value of the beam current.

Dependences $\eta(\Phi)$ for the value $\omega_c/\omega = 0.4$ are shown in Fig.1. Electron trajectories can be assumed linear in this case. A relativistic factor increase results in the generation zone narrowing and efficiency enhancement. These results correspond to the one-dimensional theory of relativistic resonant oscillator. Hence, the longitudinal electron-wave interaction is the basic energy exchange mechanism between electrons and rf field in the case of $\omega_c/\omega = 0.4$. The cyclotron frequency decrease results in the narrowing of the hard excitation regime domain and efficiency reducing for all the values of relativistic factor (Fig.2, 3). Note that here $\omega_c/\omega = 0.15$ (Fig.2) and $\omega_c/\omega = 0.1$ (Fig.3).

It should also be noted that the maximum efficiency value almost does not depend upon the parameter γ_0 at $\omega_c/\omega = 0.1$ (Fig.3). Furthermore the electron hysteresis (especially nonlinear phenomenon) is absent in this case. The additional calculations showed that the focusing field displacement decrease results in the particles settling onto the slow-wave structure surface. The electrons which interact with the most intensive rf field are settling first. Therefore the settling of the electrons results in the change of relation between the electrons, which interact with damping, and the accelerating rf electric field of the slow wave. Conditions of the electron-wave interaction may be changed significantly in this case and efficiency changes as well. If the electrons interacting with the damping rf field are settling onto the grating, the efficiency decreases. On the other hand, the settling of the accelerated electrons may be a reason of the efficiency enhancement [2].

In the considered situation (uniform focusing field), the electron settling results in the efficiency decrease. To obtain the efficiency enhancement one should use a nonuniform dc magnetic field [2].

3. Conclusions

The efficiency of the relativistic resonant O-type oscillator depends upon the focusing field displacement value.

The settling onto the slow-wave structure surface results in the efficiency decrease. Moreover efficiency reduction is more significant in the relativistic case in comparison with nonrelativistic case.

4. References

1. L.A.Vaynshtein, V.A. Solntcev, Lectures on Ultrahighfrequency Electronics, Moscow: Sov. Radio, 1973.
2. E.N.Odarenko, A.A. Shmat'ko, Nonlinear Theory of O-type Microwave Oscillators with Nonuniform Magnetostatic Field (Two-Dimensional Model), *J. of Communications Techn. and Electronics*, 1994, vol. 39, no 9, p.p. 1-8.

MAGNETIC FIELD DISTRIBUTION FOR SUPERCONDUCTORS WITH ROTATIONAL SYMMETRY

V. Ivaška, V. Jonkus, and V. Palenskis

Vilnius University, Department of Radiophysics, Saulėtekio al. 9, 2040 Vilnius, Lithuania

Abstract. Some studies on the magnetic flux trapped in a hollow superconductor and an applicability of the hollow superconductor for the magnetic shielding are reported.

Superconducting sample with a hole has some different properties than the continuous one. Consider the loop of metallic wire is initially placed in a static magnetic field such that flux threads the hole. After the system reaches the steady state, the field is suddenly turned off. Consequently, as required by Lenz's law, a current will be induced in the wire to resist the change of the flux. From elementary circuit theory, we know that the current will decay in the exponential fashion with the time constant $\tau=L/R$. In case of superconducting wire $R=0$ and $\tau \rightarrow \infty$; this means, that a persistent current will flow in the superconducting loop and the magnetic field it produces will never be observed to decay as long as the loop remains in superconducting state. Because of this property superconductor with a hole may act as steady magnet or can be applied for magnetic field shielding.

In [1–5], the investigated samples were made of type-II high- T_c materials and had a shape of a hollow cylinder. In some papers the critical currents were investigated, evaluating them from the magnetic field strength measurements [1, 2], and an applicability of the superconducting hollow cylinder for the magnetic field shielding [3–5]. The case with a hollow superconductor forces to use an approximate formula or numerical modelling. In a hollow superconductor (in other word multiply connected) it is observed magnetic flux trapping phenomenon. Moreover, this magnetic flux is quantized.

In this paper we present the numerical solution method. This method is suitable for evaluation of magnetic field and surface current distributions. We only assume that superconductor is an ideal diamagnetic and has the rotational symmetry. The external field (if it was switched on) is parallel to rotation axis and assumed to be static. Since the problem assumed to be static, the final field distribution depends on the way the superconductor was cooled down. Therefore the solution takes into account the trapped magnetic flux. Modelling results are given for two cases: a superconducting torus and superconducting hollow cylinder.

Due to rotational symmetry the sheet current and the vector potential have only one component (in cylindrical coordinates $\{\rho, z, \varphi\}$): $\vec{j} = j \vec{e}_\varphi$, $\vec{A} = A_\varphi \vec{e}_\varphi$.

A corresponding vector potential can be expressed by

$$\rho A_\varphi(P) = \int_{\Gamma} j(P') G(P, P') dS' ; \quad (1)$$

where integration region Γ is the superconductor surface in ρ - z plane; kernel $G(P, P')$ is the Green's function; P' and P is the set of source $\{\rho', z'\}$ and field $\{\rho, z\}$ coordinates, respectively; $j(P')$ is unknown sheet current density. Kernel $G(P, P')$ can be calculated analytically [6]. The boundary condition is the continuity of the normal component of the magnetic induction. If one finds such coordinates $\{u, v, \varphi\}$, where $u = \text{const}$ defines the shape of the sample, while v and φ run over its surface boundary condition may be expressed as [6]

$$\left. \frac{\partial(\rho A_\varphi + B_0 \rho^2 / 2)}{\partial \nu} \right|_{u=u_0} = 0. \quad (2)$$

This condition can be reduced to:

$$\left(\rho A_\varphi + B_0 \frac{\rho^2}{2} \right) \Big|_{u=u_0} = f(u) \Big|_{u=u_0} = \text{const} = \frac{\Phi_0}{2\pi}, \quad (3)$$

here quantity Φ_0 is the flux, which threads the hole of the sample. If the sample has no hole then always $\Phi_0=0$. Now, we can write the integral equation for $j(P')$:

$$\begin{cases} \int_{\Gamma} j(P') G(P, P') dS' = -B_0 \frac{\rho^2}{2}, & P \in \Gamma \\ \int_{\Gamma} j(P') dS' = I \end{cases} \quad (4)$$

Besides $j(P')$, in this integral equation the quantities B_0 , Φ_0 and I are involved. Two of them considered to be known. The next one and the $j(P')$ can be found as a solution. Which of three quantities (B_0 , Φ_0 , I) are considered to be known, it depends on the way by which the superconductor is cooled down. For solution of this problem we approximated the integral equation by linear equation set [7].

Magnetic field distribution

Superconducting torus.

1) Let us suppose the torus was cooled down in the zero external magnetic field. When we apply the static magnetic field, then, the induced surface current prevents field penetration into the superconductor and keeps the flux within the hole zero. This property may be used for the magnetic field shielding.

2) Suppose we placed the torus in the external magnetic field at a temperature higher than T_c . After this we lower the temperature and the torus becomes superconducting. If the external wasn't changed, it is no induced persistent current.

3) Let us now examine slightly different case. The superconducting torus was cooled down in the presence of the static external magnetic field as in previous case. After this the external magnetic field is switched off. As required by Lenz's law, the magnetic field change induces the current. Because there is no loss in the superconductor, this current

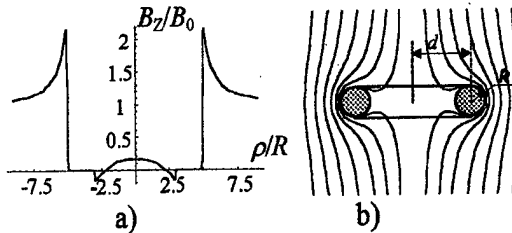


Fig. 1. Superconducting torus ($\Phi_0=0$, $B_0=1$);
(a) magnetic field profile in the central plane ($z=0$);
(b) magnetic field lines.

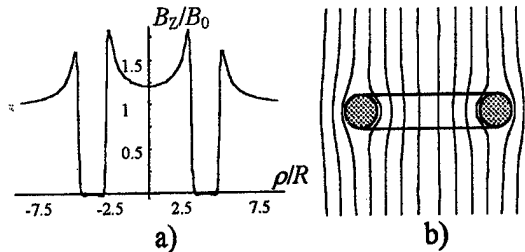


Fig. 2. Superconducting torus ($I=0$, $B_0=1$);
(a) magnetic field profile in the central plane ($z=0$);
(b) magnetic field lines.

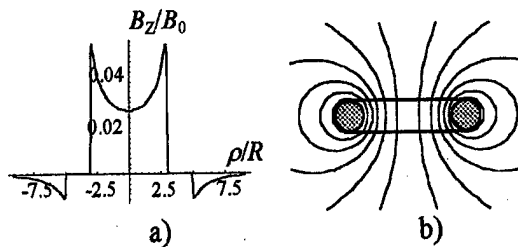


Fig. 3. Superconducting torus ($\Phi_0=1$, $B_0=0$);
(a) magnetic field profile in the central plane ($z=0$);
(b) magnetic field lines.

cannot decay away and the flux is permanently trapped. In this case superconducting torus acts as steady magnet.

Superconducting hollow cylinder. As we can see from Fig. 4, the superconducting hollow cylinder is more suitable for the external field screening than the torus. The magnetic flux density in the inner space of the hole is considerably lower than the external field. In order to increase screening properties of the cylinder we need to increase the height of the cylinder.

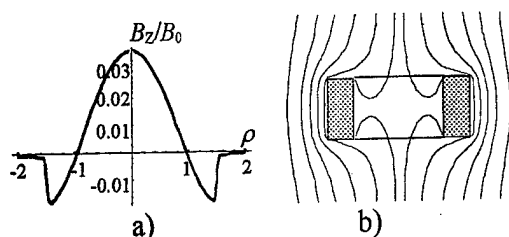


Fig. 4. Superconducting hollow cylinder ($B_0=1$, $\Phi_0=0$);
a) magnetic field profile in the central plane ($z=0$);
b) magnetic field lines.

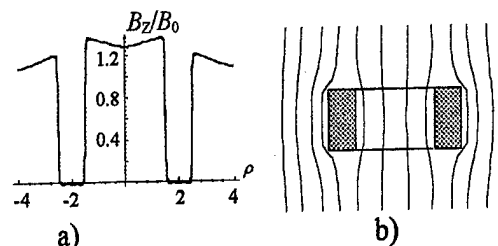


Fig. 5. Superconducting hollow cylinder ($B_0=1$, $I=0$);
a) magnetic field profile in the central plane ($z=0$);
b) magnetic field lines.

Summary

In this paper a method for the magnetic field modelling in the superconductor with rotational symmetry is presented. It is supposed that superconductor is an ideal diamagnetic. This method takes into account magnetic flux trapping phenomenon, which takes place for hollow superconductor. As a solution it is possible to determine the circumferential current and the sheet current density. Therefore this method is suitable for the current evaluation from the field measurement, and for the field distribution investigation inside the hole of the sample.

References

1. M.Polák, M.Majoroš, F.Hanic, J.Pitel, M.Kedrová, P.Kottman, J.Talapa, L.Vencel, "Magnetic field dependence of shielding current density in Y-Ba-Cu-O Rings at 77 K", *Journal of Superconductivity*, V. 2, No. 2, p. 219-233 (1989).
2. А.Г.Лаптев, В.Ф.Мещеряков, "Экранировка и захват магнитного потока полыми цилиндрами из гранулярных ВТСП материалов", *Сверхпроводимость*, Т. 6, No. 2, с. 299-313 (1993).
3. J.O.Willis, M.E.McHenry, M.P.Maley, H.Sheinberg, "Magnetic shielding by superconducting Y-Ba-Cu-O hollow cylinders", *IEEE Trans. on Magn.*, V. 25, No 2, p. 2-5 (1989).
4. J.W.Purpura, T.R.Clem, "The fabrication and characterization of high temperature superconducting magnet shields", *IEEE Trans. on Magn.*, V. 25, No. 2, p. 2506-2510 (1989).
5. T.Okada, K.Takahata, S.Nishijima, S.Yoshida, T.Hanasaka, "Applicability of oxide superconductor to magnetic shielding", *IEEE Trans. on Magn.*, V. 25, No 2, p. 2270-2272 (1989).
6. Ф.М.Морс, Г.Фешбах, *Методы теоретической физики*, (Москва, Издательство Иностранной Литературы, 1960).
7. T.V.Hromadka, Ch.Lai, *The complex variable boundary element method in engineering analysis*, (New York, Springer-Verlag, 1987).

Technique for Determination of RF-Magnetic Field Dependence of the HTS Surface Impedance by Microwave Resonators¹

K.P.Gaikovich¹, A.N.Reznik²

¹ Radiophysical Research Institute, B.Pecherskaya st., 25/14, 603600, N.Novgorod, Russia.

² Institute for Physics of Microstructures of RAS, GSP-105, 603600, N.Novgorod, Russia.

Introduction. The investigations of nonlinear electromagnetic properties of high-temperature superconductors (HTS) in the last years arouse active interest in connection with the prospects of HTS application in various microwave devices (resonators, filters, antennas etc.), with problems of quality control of these materials, with fundamental problems of physics of superconductors. Nonlinearity of HTS is usually characterized by the dependence of a surface impedance Z_S on the amplitude of a variable magnetic field H on HTS surface, i.e. $Z_S(H)$. This dependence is determined by using microwave resonators of various designs [1-5]. The parameters to be measured are nonlinear broadening of the frequency response Δf_B and the resonant frequency shift Δf_0 . The algebraic equations which relate $\Delta f_B, \Delta f_0$ to $R_S(H) = \text{Re } Z_S(H)$, $X_S(H) = \text{Im } Z_S(H)$ are in use. For all resonator types there is a strong inhomogeneity of a field H distribution on a HTS surface. In the present paper it is shown that HTS nonlinearity and fields inhomogeneity lead to essential errors in conventional techniques, and a new approach to the problem of diagnostics of nonlinear microwave properties of HTS is advanced.

The integral equations. The techniques used for determination of $Z_S(H)$, are based on the following equation:

$$\Delta f = \Delta f_0 + (i/2)\Delta f_B = (i/8\pi W) \int_S H^2 Z_S d^2 r, \quad (1)$$

where W is the energy stored into the resonator, and the integration is made on a HTS surface. In the nonlinear resonator the nonuniform field structure leads to an inhomogeneous distribution of $Z_S(H)$ on a HTS surface. In this case we obtain from (1)

$$\Delta f = (i/2)G < Z_S >, \quad (2)$$

where $G = (1/4\pi W) \int_S H^2 d^2 r$ is the geometrical factor which is calculated for each particular resonator or is measured by calibration,

$$< Z_S > = \int_S H^2 Z_S(H) d^2 r / \int_S H^2 d^2 r \quad (3)$$

is the averaged surface impedance. Thus, the use of equation (2), as is done in [1-5], yields $< Z_S >$ rather than Z_S , which largely reduces the value of the obtained results, since $< Z_S >$ depends not only on the properties of HTS material, but also on the resonator type and the excited mode.

We shall assume that the resonator contains one HTS film as a conducting wall whose dependence $Z_S(H)$ is the sought-for parameter. The H field structure on a HTS surface near the resonant frequency is determined by the eigen function of the appropriate mode $\Phi(\vec{r})$:

$$H(\vec{r}) = H_m \Phi(\vec{r}), \quad (4)$$

¹ This work was supported by RFBR under grant 96-02-16997 and by the Russian State Program on Physics of Condensed Matters under grant 96129.

where H_m is the maximum value of H (Φ is normalized so that $\Phi_{\max} = 1$). The field H_m of the nonlinear resonator for each value of the input power is calculated on the basis of the well-known techniques (for example, for a microstrip resonator see [6]). Passing in (3) from integration on the coordinate variable to integration on H with the account of (4) we obtain

$$\langle Z_S(H) \rangle = \int_0^{H_m} K(H_m, H) Z_S(H) dH, \quad (5)$$

where $K(H_m, H)$ is the kernel of the integral equation, which depends on the resonator type and the exited mode ($\int_0^{H_m} K(H_m, H) dH = 1$). We have obtained the expressions for $K(H_m, H)$ for different resonator types: confocal, microstrip, cavity, dielectric.

Using (5), we have calculated a relative excess $R_S(H)$ over $\langle Z_S(H) \rangle$ for various types of resonators and for typical dependencies $R_S(H)$, observable in experiments [1-5]. We have found out that the use of equation (2) gives an underestimated value of $R_S(H)$: 1.3-1.7 times less for cavity-, 2-3 times less for confocal-, and 4.5-7 times less for microstrip resonators.

Method of solution of the inverse problem. The method we offer consists in measurement of $\langle Z_S \rangle$ by a HTS resonator using formula (2) at several input powers. Then $Z_S(H)$ is defined by solution of equation (5). Equation (5) is the integral equation of Volterra of the 1-st kind, whose solution is an ill-posed inverse problem. In the given work the Tikhonov method [7] was applied for solution of (5). We shall rewrite the equation (5) in the operator form

$$\hat{K}R = R_m^\delta, \quad (6)$$

where R_m^δ is the vector of experimental data, obtained with some tool error. In the Tikhonov method the approximate solution is sought for by minimization of the functional

$$M^\alpha(R) = \|\hat{K}R - R_m^\delta\|_{L_2}^2 + \alpha \|R\|_{W_2^1}^2, \quad (7)$$

where $\|f\|_{L_2}^2$ is the norm of function f in space L_2 of square integrable functions, and

$\|f\|_{W_2^1}^2$ is the norm of function f in the space W_2^1 of square integrable functions together with their derivatives. The problem of minimization of functional (7) after appropriate discretization was solved by the method of conjugate gradients [8]. Smoothing of the solution derived from (7) is adjusted by parameter α which, as is shown in [7], is connected with the integrated measure of an inaccuracy of experimental data and is sought as the root of the nonlinear algebraic equation

$$\rho(\alpha) = \|\hat{K}R^\alpha - R_m^\delta\|_{L_2}^2 - \delta^2, \quad (8)$$

where R^α is the solution of (7).

Parameter of an effective error δ in (8) includes all errors of measurements and interpretations. Thus, in the used method smoothing of the solution is determined by an error δ . For high measurement accuracy, the error δ reduces and, hence, there is less smoothing in the obtained solution, i.e., the details of $Z_S(H)$ can be reconstructed.

Results of numerical modelling. The investigation of opportunities of retrieval is carried out on the basis of numerical simulation for typical $R_S(H)$ and limits of tool errors. We

have used the expression for $K(H_m, H)$ in (5) obtained for a rectangular cavity resonator and the power field dependence for R_S , which is met more often in practice. Modeling of the reconstruction procedure was done in the following closed circuit. For the given initial function $R_S(H)$ the exact dependence $\langle R_S(H_m) \rangle$ was calculated from (5), for which a random error with the given rms δR_m was added in discrete points $m = 1, 2, \dots, M$, simulating the measurements errors. Thus obtained "data of measurements" were used for solution of the inverse problem, and the retrieved dependencies were compared with the initial one. For estimation of the efficiency of the Tikhonov method equation (5) was solved also by the method of direct inversion, i.e., by solving a numerical analogue of the integral equation (5), which after appropriate discretization becomes a linear system of algebraic equations.

The results of numerical modeling are presented in Fig.1,2. In Fig.1 one can see an example of retrieval. In Fig.2 the normalized dependencies of an integral measure of inaccuracy $\delta R = [H_{\max}^{-1} \int_0^{H_{\max}} \sigma_R^2(H) dH]^{1/2}$ on a number of experimental points M are shown. It was obtained from the results of numerical simulation that the Tikhonov method provides qualitative reconstruction at $\delta R_m \leq 0.02 \text{ mOhm}$, whereas the direct inversion - only at errors $\delta R_m \leq 0.005 \text{ mOhm}$, close to extreme values, achievable for the state-of-art measurement techniques. We emphasize the existence of optimum value M , at which the error of reconstruction is minimum (Fig.2), and this minimum for the Tikhonov method corresponds to a much smaller error than for the method of the direct inversion, and at smaller values of M .

Conclusions. The method offered here is based on the theory of the solution of the inverse problem for $Z_S(H)$, which allows to take into account the inhomogeneous structure of an electromagnetic field in resonators.

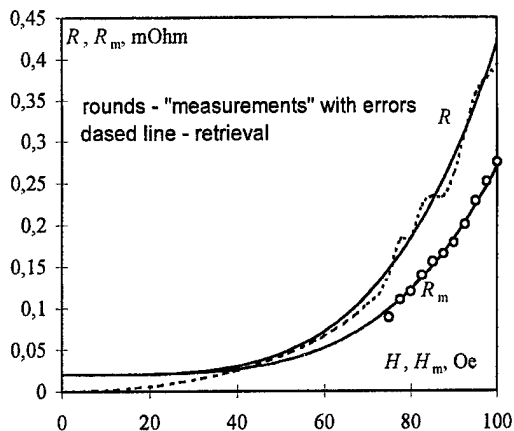


Fig1.

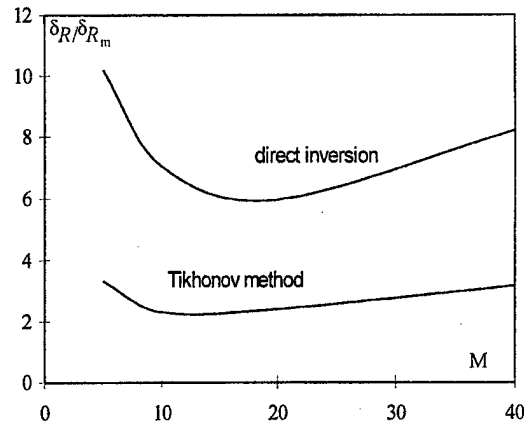


Fig.2.

References

1. Oates D.E. et al. J. Supercond. 1990, v.3, N3, p.251.
2. Cooke D.W. et al. J. Supercond. 1990, v.3, N3, p.261.
3. Shen Z.-Y. et al. IEEE Trans. Microwave Theory Techn. 1992, v.40, p.2424.
4. Golosovsky M.A. et al. Phys. Rev. B. 1995, v.51, p.6462.
5. Hein M. et al. IEEE Trans. Appl. Supercond. 1997, v.7, p.1564.
6. Sheen D.M. et al. IEEE Trans. Appl. Supercond. 1991, v.1, p.108.
7. Tikhonov A.N. et al. Regularization algorithms and a priori information. M.: Nauka, 1983.
8. Vasil'ev F.P. Numerical methods for solution of extreme problems. M.: Nauka, 1981.

MODERN METHODS FOR CALCULATION OF MAGNETIC FIELD FORCE ACTING ON MAGNETICS

M.V.Zagirnyak, Yu.A.Branspiz

East Ukrainian State University
Molodeznuy, 20-a, Lugansk, 348034, Ukraine

Abstract

It is shown, that formulae of the magnetic field action force on ferromagnetic body, corresponding to various models of magnetization of its substance, give the same result while calculating summary action force of the magnetic field on this body, coinciding with a real force.

1. Problem Statement

One of the modern description fundamentals of force action of direct magnetic field on ferromagnetic bodies is the use of volume density \bar{f} of the magnetic field ponderomotive force for which the following main methods of its definitions are known energetic, equivalent magnetic charges, equivalent magnetic moments, equivalent currents of magnetization, Maxwell tensions [1-4]. This work deals with three calculation methods of magnetic field force acting on ferromagnetic, corresponding to three simulation methods of its magnetization: equivalent magnetic charges, equivalent magnetic moments (dipoles), equivalent currents of magnetization. Consideration of these three methods is explained by the fact, that both energetic and tensor methods of volume density determination of the magnetic field ponderomotive force, with rigorous approach, is based on certain formulae for space distribution of ponderomotive force of the magnetic field in magnetic [1,2], that is energetic and tensor methods are secondary with respect to the methods, which allow to determine directly volume density \bar{f} .

In the case of absence of electrical current in ferromagnetics, the given three methods enable one to obtain the following formulas for numerical calculation of specific (per unit of magnetic volume) ponderomotive force of magnetic field:

$$\bar{f}_A = \text{rot}(\bar{M}) \times \bar{B}, \quad (1)$$

$$\bar{f}_P = -\mu_0 \bar{H} \cdot \text{div}(\bar{M}), \quad (2)$$

$$\bar{f}_{MM} = \mu_0 (\bar{M} \times \text{grad}) \bar{H}, \quad (3)$$

where μ_0 - vacuum magnetic permeability; \bar{B} , \bar{H} - vectors corresponding to magnetic field induction and strength; \bar{M} - magnetization vector.

As it is known [1-4], these formulae do not describe real distribution of magnetic field ponderomotive force in the volume of magnetic. But they can be used for determination of sum action of magnetic field on ferromagnetic body.

2. Integral Equivalency of the Formulas of Volume Density of Magnetic Field Ponderomotive Force Acting on the Magnetic for Various Models of its Magnetization

It is to be noted, that the formulas (1-3) are often used in general form when instead of the vectors and the vectors and , are considered which are induction and intensity of the magnetic field source, external in respect to the magnetic [2,4]. For this less general case it is known, that the considered methods of determination of value f are integrally equivalent, giving while calculating summary force, acting on solitary ferromagnetic body, the same result [2,4].

The given work shows that the considered methods of determination \vec{f} , to say more exactly corresponding to them formulae (1-3), are integrally equivalent: the integrals

$$\int_{V_B} \vec{f}_A \cdot dV, \int_{V_B} \vec{f}_P \cdot dV, \int_{V_B} \vec{f}_{MM} \cdot dV \quad (4)$$

are equal to each other (here V_B is the whole volume of solitary magnetic body).

For solving this task we used a special integral ratio:

$$\int_V [(\vec{a} \cdot \text{grad}) \vec{b} + \vec{b} \cdot \text{div} \vec{a}] \cdot dV = \int_S \vec{b} \cdot (\vec{n} \cdot \vec{a}) \cdot dS, \quad (5)$$

valid for any continuous (in volume V) vectors \vec{a} and \vec{b} and reducing the integration over an arbitrary volume V to surface the integration over the surface S of the volume V [5].

As a result we obtain that: all integrals (4) in the process of integration yield the same surface integral. This proves, eventually, the integral equivalency of the formulas (1-3).

3. Correspondence of the Considering Formulae to Real Distribution of Volume Density of Magnetic Field Ponderomotive Force in the Solitary Magnetic

The next step of this work was the determination of the fact, that the formulae (1-3) at volume integration give the result, coinciding with integration of real distribution of volume density of the magnetic field ponderomotive force.

It was taken into account, that all three models of magnetized magnetic material produce outside of it one and the same magnetic field, whose influence on external source is equal and anti-directed to action of the applied (external) magnetic field on the solitary magnetic.

REFERENCES

1. J.A. Stratton, The Theory of Electromagnetism, Moscow, OGIS, 1948, (Russian translation)
2. I.E. Tamm, Fundamentals of Electricity Theory, Moscow, Nauka, 1989, (in Russian)
3. A.I. Ivanov-Smolensky, Electromagnetic Forces and Energy Transformation in Electrical Machines, Moscow, Vischaya shkola, 1989, (in Russian)
4. R. Rosentsveig, Ferrohydrodynamics, -Moscow, Mir, 1989, (in Russian)
5. Yu.V. Abramkin, A.V. Ivanov-Smolenskii, Determination of formulas for specific ponderomotive forces in electromagnetic field on the basis of Maxwell field theory and uniqueness theorem, *Electricity*, 1995, № 9, pp. 52-65, (in Russian).

HOMOGENIZATION THEORY AND IMPURE SUPERCONDUCTORS

Leonid Pankratov

Mathematical Division, Institute for Low Temperature Physics
47 Lenin ave., 310164, Kharkov, Ukraine
e-mail: pankratov@ilt.kharkov.ua

The paper is devoted to the homogenization of the Neumann boundary value problem for the stationary and nonstationary Ginzburg–Landau heat equations in a porous medium consisting of a melange of a superconductor $\Omega^{(s)}$ and a dielectric $Q^{(s)}$ with complicated microstructure. Let us consider, for example, the Ginzburg–Landau heat flow equation :

$$\frac{\partial u}{\partial t} = \Delta u + (1 - |u|^2)u$$

in a porous medium. The so-called weakly connected domain $\Omega^{(s)}$ is taken as a model of the porous medium. The positive integer s characterizes the scale of the microstructure. The domain $\Omega^{(s)}$ consists of two non-intersecting subdomains $\Omega_1^{(s)}$ and $\Omega_2^{(s)}$ that are interconnected by a "thin" set $R^{(s)}$.

In the present paper we study the asymptotical behavior of the solutions $u^{(s)}(x, t)$ of the Neumann boundary value problem for the Ginzburg–Landau heat flow equation in the weakly connected domains $\Omega^{(s)}$ as $s \rightarrow \infty$. It is shown (see [14]) that the first term of the asymptotical expansion of the solution of the initial boundary value problem is described by the solution of the Neumann boundary value problem for a system of two parabolic partial differential equations in the domain Ω (homogenized model) :

$$\begin{aligned} d_1(x) \frac{\partial u_1}{\partial t} &= \sum_{i,j=1}^3 \frac{\partial}{\partial x_i} \left(a_{ij}^1(x) \frac{\partial u_1}{\partial x_j} \right) + d_1(x) u_1 [1 - |u_1|^2] - \gamma(x) [u_1 - u_2]; \\ d_2(x) \frac{\partial u_2}{\partial t} &= \sum_{i,j=1}^3 \frac{\partial}{\partial x_i} \left(a_{ij}^2(x) \frac{\partial u_2}{\partial x_j} \right) + d_2(x) u_2 [1 - |u_2|^2] - \gamma(x) [u_2 - u_1]. \end{aligned}$$

The coefficients of the homogenized equations are obtained by some local characteristics of the domain.

The coupling term appears in the homogenized model because of the structure of the domain $\Omega^{(s)}$ and it is not related to the nonlinearity. For example, the same term appears in the linear case (c.f. also [13]). We can regard this term as an interaction of two "phases" of the complex superconductor. In the particular case of the weakly connected domain, we can calculate all the coefficients of the homogenized system explicitly.

The homogenization problem in weakly connected domains for the linear elliptic and parabolic problems was studied for the first time by E. Khruslov [6].

In the recent years, different boundary value problems related to the Ginzburg–Landau equation have been of great interest not only for physicists but also for mathematicians (see, for instance, [1–4]). The steady-state Ginzburg–Landau equation is

the fundamental model in the theory of superconductivity. On the other hand, the Ginzburg-Landau model characterizes the superconductor near a critical temperature T_c :

$$\frac{T_c - T}{T_c} \ll 1. \quad (1)$$

Within the framework of this theory it is naturally to consider a composite superconductor Ω that is a melange of a superconducting material $\Omega^{(s)} \equiv \Omega \setminus Q^{(s)}$ and a dielectric $Q^{(s)}$ (impure superconductor). Since the current does not penetrate the dielectric, the Neumann boundary condition is true at the dielectric boundary $\partial Q^{(s)}$. In fact, in the absence of the magnetic field we can use such a boundary condition if the temperature of a superconductor satisfies the following inequality:

$$\frac{a}{\xi_0} \ll \left(1 - \frac{T}{T_c}\right)^{1/2}. \quad (2)$$

Here a is an interatomic distance and ξ_0 is a coherence length (see, for example [5]). Thus, our approach works nicely under conditions (1), (2). It is well known that the magnitude of the critical temperature is much smaller than in a pure one. However, in a number of practically important cases we can assume that our conditions are physically reasonable. From the physical point of view these conditions imply the limits of possible applications of our model in the theory of superconductivity. Note that the emphasis in the paper is placed on the asymptotical properties of the abstract mathematical model of such impure superconductors. The dielectric $Q^{(s)}$ is usually a strongly "fine-dispersioned" set. The notion of weakly connected domains appears here as a result of analysis and generalization of the notion of weak connection that is widely used in the superconducting theory. The homogenization results for the steady-state Ginzburg-Landau equation in weakly connected domains and in domains with "traps" were obtained in [8].

The homogenization of non-linear non-stationary equations in the weakly connected domains are also of a great interest. The corresponding results for the scalar nonlinear elliptic and parabolic second-order partial differential equations were proved by the author [11, 12] and also by A. Kovalevsky (see, for example, [9]).

References

- [1] F. Bethuel, H. Brezis, F. Helein, *Ginzburg-Landau vertices*, Birkhäuser, Boston, 1994.
- [2] F. Bethuel, T. Riviere, Vortices for a variational problem related to superconductivity, *Ann. Inst. Poincaré - Analyse non linéaire*, 1995, vol. 12, no 3, pp. 243-303.
- [3] A. Boutet de Monvel-Berthier, V. Georgescu, R. Purice, A boundary value problem related to the Ginzburg-Landau model, *Commun. Math. Phys.*, 1991, vol. 142, pp. 1-23.
- [4] Fang Hua Lin, Solutions of Ginzburg-Landau equations and critical points of the renormalized energy, *Ann. Inst. Poincaré - Analyse non linéaire*, 1995, vol. 12, no 5, pp. 599-622.

- [5] P. G. De Gennes, *Superconductivity of Metals and Alloys*, W. A. Benjamin, Inc., New York–Amsterdam, 1966.
- [6] E. Ya. Khruslov, On convergence of second boundary value problem solutions in weakly connected domains, in *Theory of Operators in Functional Spaces and its Applications*, Naukova Dumka, Kiev, 1981, pp. 129-173 (in Russian).
- [7] E. Ya. Khruslov, *An homogenized model of nonstationary diffusion in cracked-porous media*, Kharkov, Preprint FTINT AN UkrSSR, 1988, No 50–88 (in Russian).
- [8] E. Ya. Khruslov, L. S. Pankratov, Homogenization of boundary problems for Ginzburg–Landau equation in weakly connected domains, in V. A. Marchenko (Ed.), *Spectral Operator Theory and Related Topics*, AMS Providence, 1994, Vol. 19, pp. 233-268.
- [9] A. Kovalevsky, *On some homogenization problems with varying domains*, Preprint 93.10, Donetsk: Institute for Applied Mathematics and Mechanics, 1993 (in Russian).
- [10] O. A. Ladyzhenskaya, V. A. Solonnikov, N. N. Uraltseva, *Linear and quasilinear equations of parabolic type*, AMS, Providence, 1968.
- [11] L. S. Pankratov, Homogenization of nonlinear Neumann elliptic and parabolic problems, *Proc. Int. Conf. Homogenization and Applications to Material Sciences*, Nice, 1995, Gakuto Int. Series, Vol.9 (1997), Gakkōtoshō, Tokyo, pp. 341-353.
- [12] L. S. Pankratov, *Homogenization of quasilinear parabolic equations*, Institut de Mathématiques de Jussieu, 1995, Prépublication 15.
- [13] L. S. Pankratov, Homogenization of semilinear parabolic equations in domains with spherical traps, *Applicable analysis*, 1997, vol. 64, pp. 303-317.
- [14] L. S. Pankratov, Homogenization of the Ginzburg–Landau heat flow equation in a porous medium, *Applicable analysis* (accepted for publication).

NUMERICAL THEORY OF EXCITATION OF AXISYMMETRIC OPEN-ENDED FINITE LENGTH SLOW WAVE STRUCTURE ON THE BASIS OF THE BOUNDARY SINGULAR INTEGRAL EQUATION METHOD

V.A. Shcherbina, G.I. Zaginaylov, S.A. Zhuchenko

Kharkov State University, Svobody sq. 4, Kharkov, 310077, Ukraine

Open-ended axisymmetric slow wave structures (SWS) are commonly used as interaction chambers in high-power microwave (HPM) sources. According to [1], finite length effects and nonuniformity of SWS can be exploited to achieve enhanced output power and frequency tunability. However, they cannot be analyzed with a proper accuracy by conventional theoretical methods [2], and using special simulation codes based on direct numerical analysis appears to be the most preferable approach [3]. In turn, the former so far are associated with a great amount of computations that, occasionally, results in a too high level of numerical noise capable to ruin the accuracy of simulation. Therefore a sophistication or development of alternative methods of study is still very actual.

Below we present a new approach, which appears to combine positive features of both analytical and direct numerical approaches, i.e. it will enable us to consider the same complicated 2D or 3D configurations of electromagnetic structures as those by using special codes, but with considerably lower computational expenses.

Consider an axisymmetric open-ended SWS (see Fig.1) typical for high-power backward wave oscillators (BWO), traveling wave tubes (TWT) and some other HPM sources. Here for simplicity we use the simplest model of the electron beam: thin, annular, magnetized, modulated current of given amplitude: $\vec{I} = (0, 0, I_z(r, z, t))$, $I_z(r, z, t) = I_0 g(r) \exp(ikz / \beta - i\omega t)$, where $k = \omega / c$, $\beta = V / c$, ω is the modulation frequency, V is the beam velocity. The walls of SWS are assumed to be perfectly conducting. The problem of SWS excitation can be formulated in the mathematically rigorous manner as the boundary-value problem:

$$(\Delta + k^2)\vec{E} = -\frac{4\pi ik}{c}\vec{I}, \quad \vec{r} \in \mathcal{R}^3 \setminus S \quad (1)$$

$$E_{\tau}|_S = 0$$

where S is the surface of SWS, $\vec{H} = (1/ik)\nabla \times \vec{E}$, the time factor is omitted.

Representing the solution of (1) in the form: $\vec{E} = \vec{E}_1 + \vec{E}_0$, where \vec{E}_0 is some partial solution of (1) in the space \mathcal{R}^3 , we come to the problem:

$$(\Delta + k^2)\vec{E}_1 = 0, \quad \vec{r} \in \mathcal{R}^3 \setminus S \quad (2)$$

$$E_{1\tau}|_S = -E_{0\tau}|_S \quad (3)$$

We look for the general solution of (2) in the form $\vec{E}_1 = \nabla \times \vec{A}$ where \vec{A} is the superposition of the double and single layer potentials with unknown densities [4]

$$\vec{A}(\vec{r}) = \int_S \left\{ \vec{j}(\vec{r}') \frac{\partial}{\partial \vec{r}'} \frac{e^{ik|\vec{r}-\vec{r}'|}}{|\vec{r}-\vec{r}'|} + \vec{i}(\vec{r}') \frac{e^{ik|\vec{r}-\vec{r}'|}}{|\vec{r}-\vec{r}'|} \right\} ds' \quad (4)$$

Both the first and the second terms in (4) satisfy the radiation condition at infinity and have the jumps across S that can be expressed in terms of the densities $\vec{j}(\vec{r}')$ and $\vec{i}(\vec{r}')$, respectively. Taking into account that E_{1r} must be continuous across S , we can state a simple algebraic relation between $\vec{j}(\vec{r}')$ and $\vec{i}(\vec{r}')$ that cancels the jump in E_{1r} , and furthermore using (3) we obtain a boundary singular integral equation. After integration over the azimuthal angle it becomes one-dimensional:

$$\int_0^L Q(\zeta, z) u(\zeta) d\zeta = f(z), \quad z \in (0, L), \quad (5)$$

where $Q(\zeta, z) = R(\zeta) \left(R'(\zeta) \frac{\partial}{\partial \zeta} - \frac{\partial}{\partial \rho} - \frac{1}{R(\zeta)} \right) \left(R'(z) \frac{\partial}{\partial z} - \frac{\partial}{\partial r} - \frac{1}{R(z)} \right) \Psi(\zeta, z, \rho, r) \Big|_{\rho=R(\zeta), r=R(z)}$,

$$\Psi(\zeta, z, \rho, r) = \int_0^{2\pi} \frac{\cos \varphi \exp[ikl(\zeta, z, \rho, r, \varphi)]}{l(\zeta, z, \rho, r, \varphi)} d\varphi, \quad l(\zeta, z, \rho, r, \varphi) = ((\zeta - z)^2 + \rho^2 + r^2 - 2\rho r \cos \varphi)^{1/2},$$

$$u(z) = j(r, z) \Big|_{r=R(z)}, \quad f(z) = -E_{0r}(r, z) \Big|_{r=R(z)}, \quad R(z) \text{ is the radial profile of SWS.}$$

The kernel of (5) contains strongly singular terms $\propto (\zeta - z)^{-2}$, integration of which must be understood in Adamard's sense. Numerical analysis of (5) has been fulfilled by two ways. One of them is associated with the interpolation quadrature formulae listed in [5], another is based on the original quadrature formulas. The difference between the obtained results is becoming negligible at a sufficiently large number of quadrature terms. In both cases after discretization we obtain the set of linear algebraic equations with dominant diagonal terms expressed through well-tabulated analytical functions (full elliptic integrals) that enables us to construct the computationally efficient algorithms. Results of numerical modeling for $\beta = 0.8$ are shown in Figs. 2-4. The main attention was paid to the study of SWS electromagnetic behavior within the passband of the lowest order symmetric transverse magnetic mode (TM_{01}). The total radiation power as a function of frequency (Fig. 2) has several sharp maxima associated with different axial TM_{01} mode forming due to the end reflections. As it is well known, finite-length SWS with N periods has $N + 1$ different axial modes. In Fig. 2 we can clearly recognize only six of them, possibly because near the upper and lower passband ends they are located very closely, fusing together. The highest of them ($f = \omega / 2\pi = 8.966$ GHz) corresponds to the π -type oscillations and exceeds the others more than ten-fold. It is interesting to point out that in this regime the real part of the surface potential density distribution $u(z)$ is approximately equal to image one taken with the opposite sign (see Fig. 3 a,b), and both are almost symmetrical with respect to $z = L/2$. Radiation pattern in the far zone has only one maximum in both forward and backward directions within the TM_{01} -mode passband that agrees with the radiation features for an open-ended single-mode waveguide [7]. Approaching to the lower end of the passband, the maximum of radiation pattern shifts away from SWS axis (Fig. 4, a,b) up to normal direction at the cutoff frequency (Fig. 4,c). Beyond the TM_{01} -mode passband the level of radiation is much lower than within it, while the radiation pattern drastically changes becoming similar to that for a solid conducting body (see Fig. 4,d).

Thus, application of new approach enables us to reduce the problem of excitation of a realistic electromagnetic structure to a one-dimensional singular integral equation, for which

computationally efficient numerical codes have been developed. Obtained results are in good qualitative agreement with experimental ones [6]. Some difference from the measured resonance frequencies seems to be caused by certain differences of considered SWS from experimental ones and neglecting the ohmic losses.

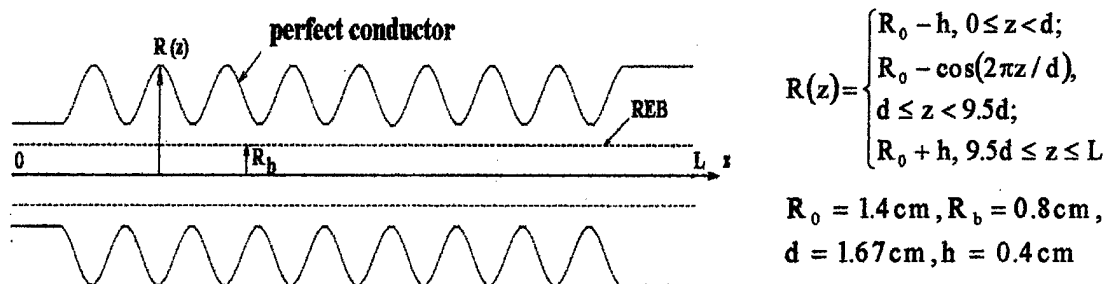


Fig. 1

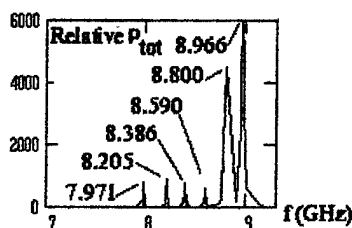


Fig. 2

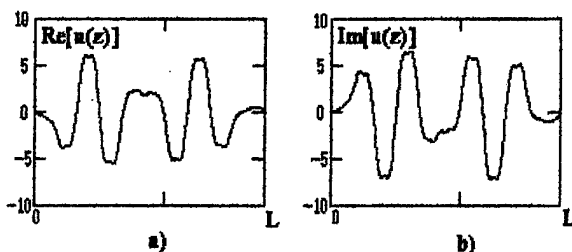


Fig. 3

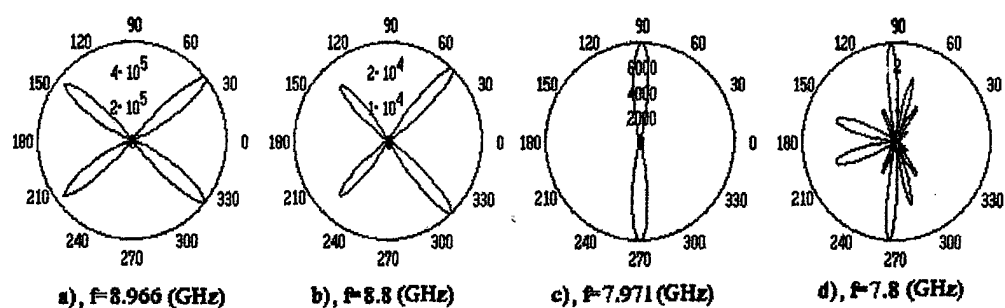


Fig. 4

References

1. L.D. Moreland et al., *IEEE Trans., Plasma Science*, v. 24, no. 3, p. 852-858 (1996).
2. S.M. Miller et al., *Phys. Plasmas*, v. 1, no. 3, p. 730-740 (1994).
3. See, for example B. Goplen et. al., *Comp. Phys. Commun.*, v. 87, p. 54-86 (1995).
4. V.A. Shcherbina, Proc. Int. Conf. "Methods of discrete singularities in aerodynamics, electromagnetics, and diffraction theory", Ukraine, Feodosia, part II, p. 234-235 (1997).
5. Yu.V. Gandel', I.K. Lifanov, and T.S. Polyanskaya, *Differential equations*, v. 31, no. 9, p. 1491-1497 (1995).
6. Y. Carmel et al., *Phys. Rev. Lett.*, v. 69, p. 1652-1655 (1992); W. Main et al., *IEEE Trans., Plasma Science*, v. 22, no. 5, p. 566-576 (1994).
7. L.A. Weinstein, *Open Resonators and Open Waveguides*, Boulder, CO: Golem Press, 1969.

HAMILTONIAN APPROACH TO THE PROBLEM OF WAVE COLLAPSE

Valeriy V. Gushchin

Department of Physics and Technology, Kharkov State University,
Svobody sq. 4, Kharkov, 310077, Ukraine

Formation of singularities in the wave system within a finite time, or, in the other words, a wave collapse is one of the basic phenomena in nonlinear physics. The collapse plays an essential role in various fields of physics. For example, great interest has focused on collapse with application to beam-plasma and laser-plasma experiments, ionospheric modulation, the Earth's foreshock, nonlinear optics, solar wind, etc. [1-3].

Intense, localized, high-frequency waves can modify the medium in which they propagate via excitation of low frequency disturbances by their ponderomotive forces, for example. A common feature is that the collapse involves interaction between high- and low-frequency waves coupled by nonlinear interactions that cause the refractive index of high-frequency waves to increase with increasing the wave intensity. The resulting tendency to focus into regions already of high intensity can then lead to collapse.

The Langmuir waves collapse has been studied most intensively. The main results are obtained in the framework of Zakharov's equations [1]. However, these equations do not take in to account various nonlinear effects of higher order: electron nonlinearity, variations in the wave dispersion law, hydrodynamic ion nonlinearities, etc. Their significance increases with the caverna compression and according to the estimates, all nonlinearities are to be taken into account simultaneously.

A generalization of Zakharov's equations by taking into account additional nonlinearities turns out to be the best if the Hamiltonian formalism (HF) is used. It is necessary to underline that commonly used HF needs an implementation of general variants of canonical transforms [6]. Only after this it enables one to obtain the "improved" dynamic equations, which have the following form:

$$\frac{\partial a_k}{\partial t} + i\omega_k a_k = -i \frac{\delta H_{int}}{\delta a_k^*}, \quad \frac{\partial b_k}{\partial t} + i\Omega_k b_k = -i \frac{\delta H_{int}}{\delta b_k^*}, \quad H_{int} = H_3 + H_4 + \dots \quad (1)$$

Here $a_k \equiv a(\vec{k}, t)$; $b_k \equiv b(\vec{k}, t)$; $\omega_k \equiv \omega(\vec{k})$; $\Omega_k \equiv \Omega(\vec{k})$ are the complex amplitudes, dispersion functions of the high- and low-frequency waves respectively, and H_{int} is the reduced interaction hamiltonian (see the details in the papers [7,8]).

Equations (1), written in the momentum (\vec{k}, ω) representation, can be written in the coordinate (\vec{r}, t) representation by using the inverse Fourier transform. They are significantly more complicated but in the limiting cases can be expressed in terms of the well-known equations studied in [1-3].

In the framework of equations (1), it is possible to obtain the increment of the modulation instability of nonlinear Langmuir wave cluster localized in a cavity. The single isolated cavern can be divided to the parts changing the general scenario for the Langmuir collapse.

Introducing a positively defined value:

$$I \equiv \int d\vec{k} |\partial a_k / \partial \vec{k}|$$

one can write the Talanov theorem [1-3] in the \vec{k} representation with an account of higher nonlinearities, which forbid the existence of well-known automodel solutions.

By using HF for the analysis of stationary solutions, one can prove that the hamiltonian is limited from below for the fixed plasmon number. This fact enables us to conclude about a possibility of existence of stable solutions.

The presented results prove a significant impact of higher nonlinearities on the collapse dynamics. But a deeper understanding of the problem requires further investigations.

References

- [1] Zakharov V.E. in Basic Plasma Physics, edited by M.N.Rosenbluth and R.Z.Sagdeev (North-Holland, Amsterdam, 1984), p.81.
- [2] Shapiro V.D. and Shevchenko V.I. *ibid.*, p.119.
- [3] Goldman M.V. *Rev. Mod. Phys.*, 1984, v.56, p.709.
- [4] Zakharov V.E., Musher S.L., and Rubenchik A.M. *Phys. Reports*, 1985, v.129, p.285.
- [5] Zakharov V.E. and Kuznetsov E.A. *Usp. Fis. Nauk*, 1997, v.167, p.1137.
- [6] Gushin V.V. and Gulenko V.V. *Ukr. Fis. Zh.*, 1994, v.39, N 6, p.763.
- [7] Gushchin V.V. and Gulenko V.V. *Doklady Acad. Sci. Ukraine*, 1994, N 3, p.73
- [8] Gushchin V.V. and Gulenko V.V. *ibid.*, N 4, p.70.

***Ionospheric
Electromagnetics***

A METHOD FOR DERIVATION OF ELECTRIC FIELDS IN THE LOWER IONOSPHERE FROM MEASUREMENTS WITH A PARTIAL REFLECTION FACILITY

Gokov A.M., Martynenko S.I., Rozumenko V.T., Tsymbal A.M., and Tyrnov O.F.

Department of Space Radio Physics, Kharkiv State University, 4 Svobody Square, Kharkiv 310077, Ukraine; e-mail: Oleg.F.Tyrnov@univer.kharkov.ua

Abstract

The distribution of variations in the effective electron collision frequency was obtained at the 60 – 66 km altitude range in the lower ionosphere (experimental errors within this altitude range were less than 50%). A technique for estimating the variations in atmospheric electric fields at the lower boundary of the ionosphere was developed using the experimental values of the effective electron collision frequency. From our measurements follows that the electric field $E > 0.25 \text{ V} \cdot \text{m}^{-1}$ in approximately 70% cases under quiet ionospheric and atmospheric conditions. These facts must be taken into account in the investigations of ionospheric processes, meteorological and propagation effects.

It is well known that electric fields can produce large disturbances in ionospheric parameters of the lower ionosphere. Our experimental results indicate that a possible cause of the appearance of big enough variations in the electron collision frequency is the effect of external electric fields of atmospheric origin. This provides an opportunity to measure electric fields in the lower ionosphere using remote sensing instruments employing radio-wave techniques.

The measurements were made with the Kharkiv State University partial reflection facility during 1978 through 1997 at frequencies of $f = 1.8 - 3.0$ MHz using a 25-micros pulse length.

The data on the effective electron collision frequency, ν , are collected at altitudes of 60, 63, and 66 km. The transcendental equation in ν

$$\frac{\overline{A_-^2}}{\overline{A_+^2}} = \frac{[(\omega + \omega_L)^2 + \nu^2]^2}{[(\omega - \omega_L)^2 + \nu^2]^2} \cdot \frac{(\omega - \omega_L)^2 K_\epsilon^2 \left(\frac{\omega - \omega_L}{\nu} \right) + \nu^2 K_\sigma^2 \left(\frac{\omega - \omega_L}{\nu} \right)}{(\omega + \omega_L)^2 K_\epsilon^2 \left(\frac{\omega + \omega_L}{\nu} \right) + \nu^2 K_\sigma^2 \left(\frac{\omega + \omega_L}{\nu} \right)} \quad (1)$$

is being solved where $\overline{A_-^2}$ is the intensity of the extraordinary mode of partially reflected signals averaged over an 8 to 10 min interval, and $\overline{A_+^2}$ is the intensity of the ordinary mode of partially reflected signals averaged over the same interval, $\omega_L = 2\pi f_L$, f_L is the component of the electron gyrofrequency along the ambient magnetic field direction; in middle latitude experiments, the value of f_L is assumed to be equal 1.35 MHz, K_ϵ and K_σ are the kinetic coefficients which describe the kinetic effects in the permittivity ϵ and conductivity σ of the lower ionosphere. The dependences $K_\epsilon(x)$ and $K_\sigma(x)$ can be approximated with an error of an order of a few per cent by the relations

$$K_\epsilon(x) = 1 + \frac{a_1}{b_1 + x^2}; \quad a_1 = 0.155, \quad b_1 = 0.075, \quad 0.05 \leq x < \infty;$$

$$K_\sigma(x) = 0.89 + \frac{a_2}{b_2 + x^2}; \quad a_2 = 0.027, \quad b_2 = 0.052, \quad 0 \leq x \leq 3.5;$$

$$K_\sigma(x) = 1; \quad 3.5 \leq x < \infty.$$

where $x = (\omega - \omega_L)/\nu$ for the extraordinary mode, and $x = (\omega + \omega_L)/\nu$ for the ordinary mode. Partial reflection random measurement errors in $\nu(z)$ do not exceed the magnitude of the order of 30 – 50% in the altitude range indicated above.

The processing of partial reflection signals have allowed us to establish a database that presently contains data on the electron collision frequency at 60, 63 and 66 km over more than 170 events.

If we take into account the fact that fluctuations in the number density of neutral particles and in their temperature in the ionospheric D region generally are not more than 10 – 20% (in reality their most probable magnitudes are significantly smaller), then the sharp maximum in the ν/ν_m distribution should be expected within a $(1 \pm 0.2)\nu/\nu_m$ value interval (here ν_m is the model value of ν at the same altitude from which partial reflection signals are received; $\nu_m(60\text{km}) = 3.75 \cdot 10^7 \text{sec}^{-1}$, $\nu_m(63\text{km}) = 2.55 \cdot 10^7 \text{sec}^{-1}$, and $\nu_m(66\text{km}) = 1.68 \cdot 10^7 \text{sec}^{-1}$). However, taking into account random measurement errors of 70%, the values of ν/ν_m exceed the above-mentioned threshold for the conditions of our experiment. From our standpoint, a single reasonable explanation of this fact could be the hypothesis that $T_e > T_n$ (where T_e is the electron temperature, and T_n is the temperature of neutral particles) in 70% of cases in the lower part of the D region.

The most probable cause of existence of increased values of T_e can be strong atmospheric electric fields. Supposing this is true, electric field values could be estimated from ν/ν_m measurements. It is natural to suppose that the cases of $\nu = \nu_m$ correspond to the absence of electric fields.

In order to obtain the dependence of E upon ν , let us use the well-known set of balance equations in the electron number density N , the electron temperature T_e , and the number density of positive ions N^+ in a plane D-region weakly ionized plasma, and take into account the condition of quasi-neutrality

$$\frac{\partial N}{\partial t} = q_i + \nu_d \lambda N - \nu_a N - \alpha_r N^2 (1 + \lambda) + \frac{\partial}{\partial z} \left\{ (D_t + D_a) \frac{\partial N}{\partial z} \right\}, \quad (2)$$

$$\frac{\partial N^+}{\partial t} = q_i - \alpha_r N^2 (1 + \lambda) - \alpha_i N^2 \lambda (1 + \lambda) + \frac{\partial}{\partial z} \left\{ (D_t + D_a) \frac{\partial N^+}{\partial z} \right\}, \quad (3)$$

$$\frac{\partial T_e}{\partial t} = \frac{2Q_e}{3kN} - \delta \nu (T_e - T_n), \quad (4)$$

$$N^+ = N + N^-, \quad (5)$$

where t is time, q_i is the total production rate per unit volume of positive ions resulting from the ionization of neutral atmospheric constituents, ν_d is the effective rate at which the negative ions are destroyed by electron detachment, $\lambda = N^-/N$ is the negative ion to electron number density ratio, N^- is the negative ion density, ν_a is the effective rate at which the negative ions are formed by the attachment of electrons to neutral constituents, α_r is the effective ion-electron recombination coefficient for positive ions, D_t is the coefficient of eddy diffusion, D_a is the coefficient of ambipolar diffusion, z is the altitude, α_i is the effective ion-ion recombination coefficient, k is Boltzmann's constant, Q_e/N is the average energy acquired by the electron from an external source of heating (for example, from external electric field), δ is the fractional loss of energy per electron collision, T_n is the neutral constituency temperature. In the ionospheric D region, the disturbances in

the ion temperature are neglected because they are M/m times less than the disturbances in T_e (M is the average ion mass, m is the electron rest mass). For a low-frequency disturbing electric field E (that is when the inequalities $\omega_1^2 \ll \omega_L^2 \ll \nu^2$ hold, where ω_1 is the frequency of the disturbing field), the kinetic coefficient $K_\sigma(|\omega_1 \pm \omega_L|/\nu) \simeq K_\sigma(0) \simeq 1.4$, and $\sigma \simeq 1.4e^2 N/m\nu$ where e is the electron charge. The multiple time-scaling analysis helps considerably simplify the initial set of equations (2)-(5) by introducing the following time scales:

$$t_1 = t_{T_e} = (\delta\nu)^{-1}, \quad t_2 = t'_N = (\nu_d + \nu_a)^{-1}, \quad t_3 = t_N = \{4q_i(\alpha_r + \lambda\alpha_i)/(1 + \lambda)\}^{-1/2},$$

where t_{T_e} is an electron temperature relaxation time, t'_N is the evolution time of the disturbances in N caused by activating attachment processes, t_N is the evolution time of disturbances in N due to changes in the ionization-recombination balance. Note that in the lower ionosphere $t_{T_e} \ll t'_N \ll t_N$.

For $0 < t \leq t_{T_e}$, one can easily derive the following simplified energy balance equation:

$$\frac{d\theta}{dt} = \frac{0.97e^2 E^2}{km\nu_o \theta^{5/6}} - \delta(\theta)\nu_o \theta^{5/6}(\theta - 1)T_{eo},$$

where: $\theta = T_e/T_{eo}$, $\nu = \nu_o \theta^{5/6}$, $\theta(0) = 1$, $E(t < 0) = 0$. This equation is no longer dependent on N and N^+ . As a result, in a quasi-steady case, we readily obtain the following relation between E and ν :

$$E^2 = 1.67 \cdot 10^{-18} T_{eo} \nu^2 \left[1 - \left(\frac{\nu_o}{\nu} \right)^{6/5} \right], \quad (6)$$

where E is measured in $V \cdot m^{-1}$, T_e in K, and ν in sec^{-1} . The subscript "o" stands for parameters of the ionosphere at $E = 0$. When deducing (6), transport processes were neglected for $L \gg 10$ m (L is a characteristic size of the disturbed region) at the heights $z \sim 60 - 70$ km. Using (6), one may determine the atmospheric electric field on the lower ionospheric boundary from the experimental values of ν . If we set $T_n = T_{eo}$, then the well known relation

$$\nu_o = 5.8 \cdot 10^{-11} N_n T_{eo}^{5/6}, \quad (7)$$

where N_n is the neutral particle number density at a particular altitude (in cm^{-3}) allows to determine the undisturbed values of ν . Usually, we assume $\nu_o = \nu_m$, although it is possible to determine ν_o from partial reflection data. The results obtained with relations (1), (6), (7) and our partial reflection data show that on the ionospheric boundary there are electric fields of $E > 0.25 V \cdot m^{-1}$ in about 70% of cases. The analysis of relations (6) and (7) shows that relative random measurement errors in electric field intensity E are due to relative random measurement errors in ν , and in our experiments do not exceed 30-50 %.

The results obtained significantly improve understanding of complicated physics of the disturbed ionospheric D region. The presence of significant electric fields at the lower edge of the ionosphere (when partially reflected signals occur) indicate that an additional source of electron heating should be taken into account while investigating a disturbed ionosphere and radio wave propagation conditions. The technique described here permits the real-time derivation of changes in the electric field intensity at the lower edge of the ionosphere from partial reflection measurements.

The authors have been supported by Science and Technology Center in Ukraine Grant No. 471.

ABOUT POSSIBLE HARBINGERS OF EARTHQUAKES IN CHARACTERISTICS OF VLF SIGNALS OF ELECTROMAGNETIC BACKGROUND

N. A. Kazakova, A. G. Kolesnik, B. M. Shinkevich

Siberian Institute of Physics and Technology
Novo-Sobornaya Sq., 1, Tomsk 643050, Russia
tel: +7-(3822)-412797, fax: +7-(3822)-233034, e-mail: natalia@elefot.tsu.tomsk.su

The problem of searching for forerunners of earthquakes of different intensities numbers tens of years but nowadays is still one of the hot unresolved problems. Recently it has been shown that the processes of preparing the earthquakes that take place in the Earth lithosphere manifest themselves not only on its surface, but in the variations of parameters of the ionosphere plasma as well. This manifestation is ambiguous and, as a rule, is at the level of noise of ionospheric plasma, that does not enable one to use only these effects as practical earthquake forerunners.

It was established by numerous studies in different seismoactive regions of Earth that anomalous changes of intensities of natural electromagnetic radiations (EMR) in the wide range of frequencies preceded a significant number of strong earthquakes. These anomalous changes of intensities of natural radiations are formed, in general, by ionospheric plasma. For the first time such anomalous changes of natural electromagnetic fields before the earthquakes were registered in 1973. They are represented mainly by an increase or reduction of intensity of a natural pulsing electromagnetic signal, in comparison with the background, for several or more hours before the strong underground hits. When generalizing these results, it is necessary to point out to certain general regularities of observed anomalies of the ionosphere parameters connected to the seismic events, in spatial and time scales. In the spatial scale it is:

- "effect of crater": spatial scale of the earthquakes preparation process decreases when approaching to the source;

- latitude-longitude asymmetry: vertical spatial scales of F_2 layer along the parallels are considerably greater than the spatial scales along the meridians.

Besides, two characteristic time scales of manifestation of the earthquake preparation processes are observed in the ionosphere: 1) several hours, and 2) several days before the earthquake.

Based on [1-4], it is possible to note the principal anomalous characteristics of earthquake harbingers (in the range of heights of 90 to 2500 km) according to the results of various observations: by the methods of ground-based, satellite and vertical sounding, VLF-radiographing the wavetide in the Earth ionosphere, reception of ULF radiations, etc., in a wide range of frequencies:

- change of electronic concentration at all the ionospheric levels and height h that causes characteristic variations of $N(h)$ -structures;

- increasement of fluctuations of critical frequencies in ionosphere;

- increasement of variations with $t > 2$ h in the critical frequency f_o of the F_2 layer,

- pulse and noise radio radiation in the range of frequencies of 10Hz to 10kHz and more;

- generation of alternating EM fields in the range of frequencies of 1kHz to 10kHz;

- formation of inhomogeneities of various scales in the whole ionosphere.

The listed harbingers are characteristic for the earthquakes with magnitude $M > 4$ and manifest themselves during several days to hours (tens of minutes) on vast territories at

hundreds and thousands of kilometers. The authors would like to mark that the physical mechanisms connecting the disturbance in ionosphere with the earthquake preparation processes involve both electromagnetics and acoustics, as revealed by research.

A qualitatively new information for the forecast of earthquakes is possible to be obtained by sounding the whole space of ionosphere disturbed by forerunners, i.e. by realizing a monitoring of space-time parameters of the ionosphere in a wide range of heights and vast areas, that is by using ionosphere as a detector of the events accompanying the earthquake preparation process.

In this work, the regular measurements of parameters of VLF-signals along the routes of different orientation and extension, passing near seismoactive regions, and the data of vertical sounding of ionosphere are analyzed. These data were obtained by a receiving-measuring complex of electromagnetic background of environment in different radiobands including the frequencies from 0.01 Hz to 30 MHz. Joint analysis of data has shown that in the time period from 15 minutes to 4 hours before the earthquakes, an increase of amplitude of VLF-signals and a growth of self-wave structure of F₂ layer can be fixed. In Fig.1, the amplitude value of VLF-signal at the frequency of 12.9 kHz along the line Tomsk-Japan on June 9, 1997 are presented. During this period, manifestations of 2 strong earthquakes occurred: 1) at 07.19.48 UT in Xizang, $M=4.5$, and 2) at 09.36.08 UT in Hokkaido, Japan, with $M > 5$. Before the earthquake, an increasement in the signal amplitude was observed. These earthquakes occurred at the magnetoquiet time. It points out to the absence of both planetary sources of electromagnetic radiation and hence the conditions perturbing the propagation of electromagnetic waves, and local anomalies of EMR due to the seismoactive phenomena of earthquake preparation.

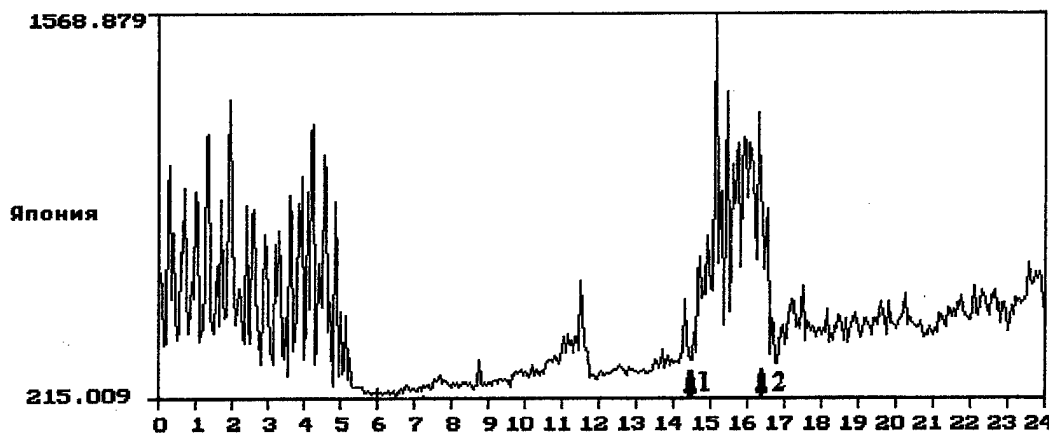


Fig.1 Diurnal variations of amplitude receiving the signal frequency 12.9 kHz of route Tomsk - Susima for 09.06.97 y., arrows show time-start the earthquake

In Fig. 2, an increase the signal amplitude is observed at the frequency 12.9 kHz on the line Tomsk-Japan on November 28, 3 hours before the second earthquake at 06.10.48 UT in the Sea of Okhotsk, with $M > 5.1$.

This earthquake occurred at the background of a strong magnetic storm, i.e. before the earthquake a burst of X-ray class was recorded. Thus, the manifestations of seismic events before earthquakes, in amplitudes of VLF-signals, are observed both in magnetically disturbed periods and in magnetically quiet time, see Fig. 3.

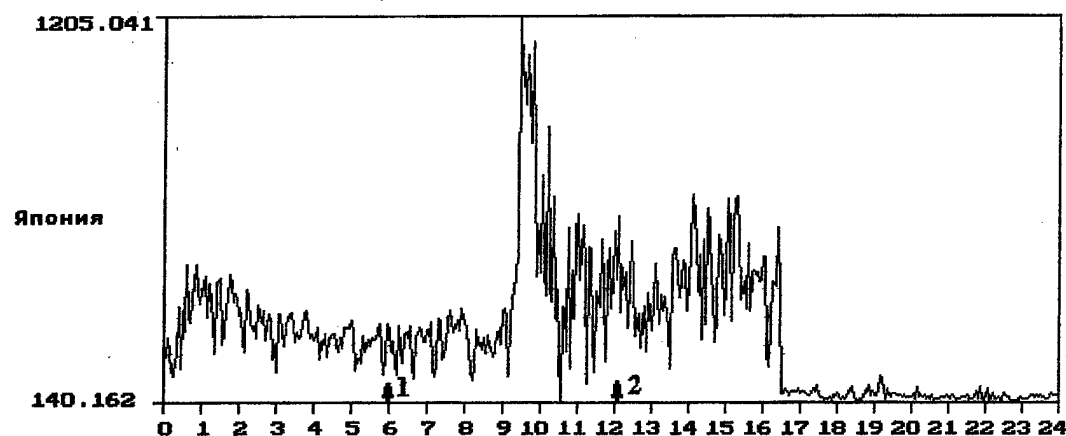


Fig.2 Diurnal variations of amplitude receiving the signal frequency 12.9 kHz of route Tomsk - Susima for 28.11.97 y.

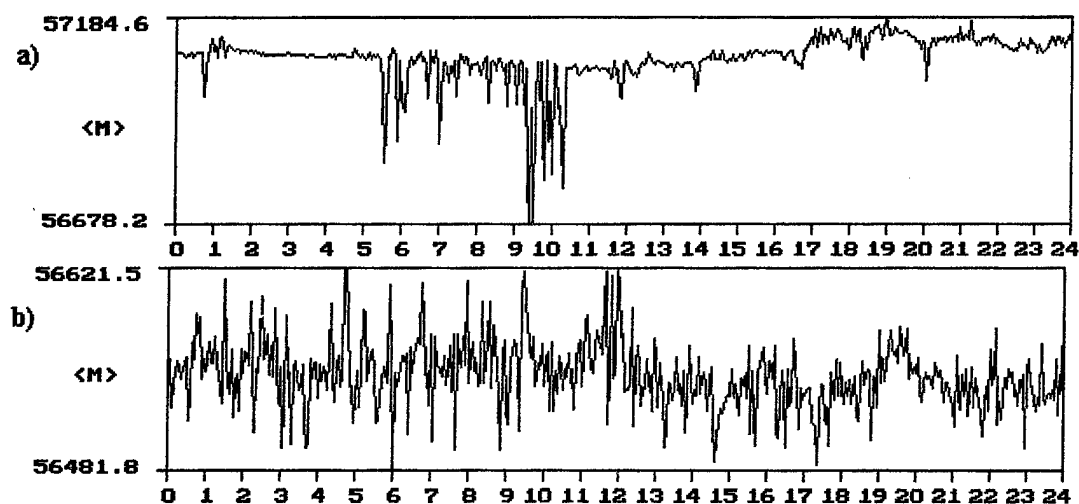


Fig. 3 Diurnal variations of module magnetic field on a) for 09.06.97 y. and on b) for 28.11.97 y

From the additional spectral analysis of fluctuations of critical frequencies of F2-layer it was found out that on the previous day before a group of strong earthquakes with $M > 4.5$, located approximately in one region, the increase of separate spectral peaks (periods 4.8; 1.846; 1.2 and 0.522h.) occurred. This fact can be used as an additional information in determination of electromagnetic forerunners of earthquakes.

References

1. V.A. Liperovskii, O.A. Pokhotelov, C.A. Shalimov, *Ionospheric Earthquake Precursors*, Moscow: Nauka Publ., 1992 (in Russian).
2. I.M. Fuks, R.S. Shubova, *Geomagnetizm and Aeronomiya*, 1994, vol. 34, no , pp.130-136 (in Russian).
3. M.B. Gokhberg, V.A. Morgunov, O.A. Pokhotelov, *Seismo-Electromagnetic Phenomena*, Moscow: Nauka Publ., 1989 (in Russian).
- 4 N.A. Kazakova, B.M. Shinkevich, Monitoring of earthquake electromagnetic forerunners, *Proc. Russian Conf. Physical Problems of Ecology*, Moscow: MGU Press, 1997 (in Russian).

MULTI-SIGNAL STUDYING OF SEISMO-IONOSPHERIC INTER-CONNECTIONS USING VLF OMNIPAL RECEIVER

M. Hayakawa¹, O. A. Molchanov², A. V. Shvets^{3*}, N. Yamamoto¹

¹ The University of Electro-Communications, 1-5-1, Chofugaoka, Chofu shi, Tokyo 182, JAPAN

² NASDA EORC, 1-9-9, Roppongi, Minato-ku, Tokyo 106, JAPAN

³ Institute of Radio Physics and Electronics, 12 Proskury st., Kharkov 310085, UKRAINE

ELF-VLF measurements aimed for the seismo-ionospheric effects studying had been started at the University of Electro-Communications in Chofu, Tokyo from the beginning of 1997. The testing of this field site, placed in a such industrial region as Tokyo is, showed a good quality of measurement with a wide spectrum of electromagnetic phenomena in the ELF-

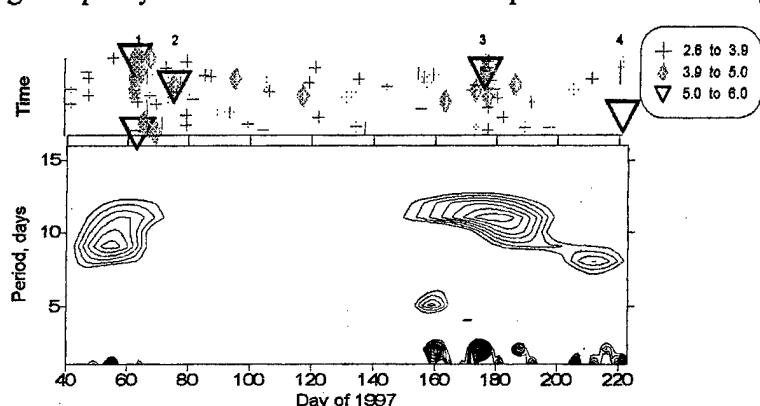


Fig. 1. Wavelet transform amplitude of terminator minimum time variations of Omega Tsushima signal along with earthquake activity within the third Fresnel zone of the corresponded propagation path.

Hayakawa et al. [1996] in which the terminator minimum time method for the searching of earthquake precursors was proposed. The authors found abnormal shift of the terminator

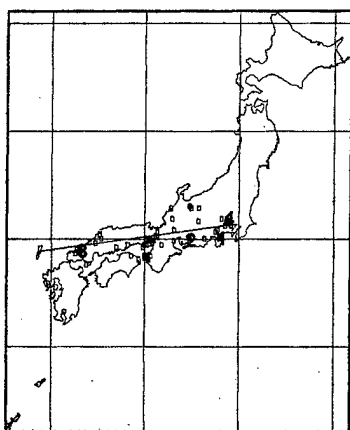


Fig. 2. Earthquakes distribution in the vicinity of the Omega, Tsushima - Chofu, Tokyo propagation path.

minimum time in diurnal dependencies of the Omega (Tsushima) VLF station just few days before the Kobe earthquake ($M = 7.2$, January 17, 1995) and repeated up to the day of the earthquake.

In the present work we apply a new processing technique based on wavelet analysis to clarify the hypothesis about interconnection between an intensification of planetary waves and seismic activity supposed in the original paper by Hayakawa et al. [1996]. An amplitude of a Morlet wavelet transform calculated for a day-to-day dependence of the evening terminator minimum times in diurnal runs of the Omega signal received at Chofu, Tokyo is presented in Fig. 1. The contour map of the wavelet amplitude is combined with a time-date map of the earthquakes occurred along the propagation path during the semi-annual observational period. A geographical distribution of corresponding earthquakes are

VLF ranges (Schumann resonance, Trimpf effect etc.) Electronic data bank was stored with high time resolution (0.1 s) consisting of diurnal runs of narrow-band signals received from Omega, Tsushima (till its stopping); China; NPM, Hawaii; NWC, Australia VLF stations using digital receiver OmniPAL.

This work is a further extension of the study by

* Invited scientist at EORC NASDA of Japan during preparation of this work.

amplitude is combined with a time-date map of the earthquakes occurred along the propagation path during the semi-annual observational period. A geographical distribution of corresponding earthquakes are shown in Fig.2. with the strongest cases ($M > 5$) marked by numbers in both graphs. The contour lines shown begin from 1/3 of the dynamic range of the wavelet transform amplitude. An intensification of some frequency components in this graph can be referred to the periods in March and July with an enhancement of seismic activity included the most strong earthquakes ($M \sim 5.1-5.9$, cases 1-4). It is clearly seen two wide maxima corresponded to periodicity of about 10 days. In the third case the ~ 10 -day oscillations in the lower ionosphere parameters ascribed to the evening terminator time are accompanied in part by ~ 5 -day and ~ 2 -day harmonics. We can also see not so prominent maximum of about 8 days period preceding to the last earthquake (case 4) with $M = 5.1$. A comparison between different station signals show, that the effect of increasing of the 10-day oscillations corresponded to seismic processes is observed rather clearly for relatively short (less than 1000 km) propagation paths, such as Tsushima - Tokyo path is in our case. Nevertheless, some coincidence is observed in the terminator minimum fluctuations of China and NPM station signals within a propagation path of about 3000 km and 6000 km length correspondingly.

In the result of this study on the base of wavelet analysis of VLF data describing the lower ionosphere parameters fluctuations ascribed to the terminator time and covering a semiannual period we can make the next conclusions.

- An enhancement of periodical components in fluctuations of parameters of VLF signal during evening terminator period is observed before relatively strong earthquakes ($M = 5.1 - 5.9$).
- These oscillations arise with periods of about 10, 5, 2 days which are in the range of different modes of the atmospheric planetary waves.
- Data from relatively short propagation paths (less than ~ 1000 km) reveal a better correspondence to seismic activity in comparison with more longer paths.

The signature of planetary waves in the fluctuations of ionospheric parameters observed in our study connected with seismic activity let us to consider the planetary waves as a possible part of a mechanism of triggering of earthquakes. We hope that experimental evidences of a connection between seismic processes and planetary waves found in our study will induce a discussion about this mechanism.

REFERENCES

- Hayakawa, M., Molchanov O. A., Ondoh T., and Kawai E., Precursory Signature of the Kobe Earthquake on VLF Subionospheric Signal. *Journal of Atmospheric Electricity*, Vol. 16, No. 3, pp. 247-257, 1996.

STATISTICAL ANALYSIS OF A DISPLACEMENT OF AUTOCORRELATED FUNCTIONS PROCESSING PROCEDURES BY INCOHERENT SCATTERING IN IONOSPHERE

Mazmanishvili A.S., Rogozhkin E.V., Suriadnyi A.S.

Kharkov State Polytechnic University,
Ukraine, 310002, Kharkov, Frunze str., 21

The new statistical approach to the analysis of data of an incoherent scattering in ionosphere is offered. It consists on accounting the displacement of values of autocorrelated functions estimations. It is shown that with such account the error of estimations of temperatures of ionic and electronic ionosphere components is reduced up to twice.

1. The advantage of the incoherent scattering (IS) method is a possibility to trace the dynamics of ionosphere processes during long periods (solar activity circle, seasonally and daily changes) as well as short periods of time. For want of those it's suggested that hardware observations be conducted correctly, it means that hardware parameter changes take no place or they are post-corrected. The information about ionosphere is being obtained using the values of autocorrelated functions (ACF) of signal scattering spectrum valuation analysis and it still might happen that in conditions of great estimation variance the estimations of ionosphere parameters would be also displaced. Thus the changes of external conditions lead to errors of systematic kind. Therefore the problems that appear are to reveal the fact of displacements existence, to detect the degree of those displacements, to detect the character of errors and to find out how to avoid such errors.

On the nature the IS signal is properly a casual signal with normal rule of amplitudes distribution. Each ordinal value of IS ACF may be considered as a normal random value. When the data are numerically processed one of processing operations is to put an ACF $R(\tau)$ to a standard form when $R(0)=1$. Dividing all the counts of ACF on its zero count approaches this. When estimating necessary ionosphere parameters it is these normalized ACF data to be used.

In this work the question of ACF valuations displacement appearing as a result of normalizing procedure is considered using an example with selected ACF sequences. Meanwhile it's suggested that ACF-valuations are not displaced till the normalization and the noises relevant to all ACF-counts are normal values with zero expectations and fixed variance.

2. Mathematically the problem is being reduced to statistical exposition of a casual value – estimation of \hat{R} which is expressed by the ratio

$$\hat{R} = X_n / X_0, \quad (1)$$

where X_0 - zero ACF-count, and X_n - remaining ACF-counts ($n > 0$). The densities of ACF-counts distribution are given below

$$p_0(x_0) = \frac{1}{\sqrt{2\pi}\sigma_0} \exp\left\{-\frac{(x_0 - k_0)^2}{2\sigma_0^2}\right\}, \quad p_n(x_n) = \frac{1}{\sqrt{2\pi}\sigma_n} \exp\left\{-\frac{(x_n - k_n)^2}{2\sigma_n^2}\right\}, \quad (2)$$

where k_0 - perfect (undisplaced) ACF-value ($n > 0$), σ_0^2 - variance, k_n - perfect ACF-value, σ_n^2 - variance ($n > 0$). The distribution densities of the required ratio equals to the following:

$$f(\hat{r}) = \frac{1}{2\pi\sigma_0\sigma_n} \int_{-\infty}^{\infty} |x_0| \exp \left\{ -\frac{(x_0 - k_0)^2}{2\sigma_0^2} - \frac{(\hat{r}x_0 - k_n)^2}{2\sigma_n^2} \right\} dx_0. \quad (3)$$

For digital accounts realization the following modification of formula (3) is convenient:

$$f(\hat{r}) = \frac{1}{2\pi\sigma_0\sigma_n} \exp \left\{ -\frac{AC - B^2}{A} \right\} \cdot \left\{ \frac{1}{A} \exp \left(-\frac{B^2}{A} \right) + \frac{B\sqrt{\pi}}{A^{3/2}} \operatorname{erf} \left(\frac{B}{\sqrt{A}} \right) \right\}, \quad (4)$$

where $A = \frac{1}{2\sigma_0^2} + \frac{\hat{r}^2}{2\sigma_n^2}$, $B = \frac{k_0}{2\sigma_0^2} + \frac{\hat{r}k_n}{2\sigma_n^2}$, $C = \frac{k_0^2}{2\sigma_0^2} + \frac{k_n^2}{2\sigma_n^2}$, $\operatorname{erf}(\alpha)$ - error function.

In special case, when $k_0 = 0$ and $k_n = 0$ for any n , densities (4) turns into its analogue, which corresponds to a casual value, distributed under the Coshi's law. There are no moments this casual value has, and when estimating by method of maximum approaching it is an argument point used, which gives maximal densities. In this case estimation displacement appears because of $k_0 \neq 0$ and $k_n \neq 0$.

3. To detect the degree of the displacement the modeling numerical experiments were conducted. In those experiments well known ACF-depending were used as perfect values. At fig.1 an example of 45-item densities set is represented $f(\hat{r})$. Account parameters: $T_i = 1000\text{K}$, $T_e = 2000\text{K}$, working wavelength - 2 m, $\sigma_0 = \sigma_n = 3\%$. Estimations according to depending (fig.1) are given at fig.2. The set of estimable depending is taken for a perfect case $\sigma_0 = \sigma_n = 0\%$ (continuous curve) and $\sigma_0 = \sigma_n = 30\%$ (circles). Figures shows that even surplus estimation displacement take place. Using (5) one can show that estimating surplus $\Delta\hat{r}$ we obtained

$$\Delta\hat{r} = k_n\sigma_0^2/k_0^3. \quad (5)$$

At figures 3-6 there are estimation results of selected pairs of ionic and electronic components taken for different variances represented (selected average values and scatter value are specified). The results were obtained conducting modeling numerical experiments (with use of pre-counted ACF-library). It's obvious that surplus account (5) realization (pictures on the right) reduces to diminution of obtained temperature estimations statistical scatter on a comparison with traditional approach (pictures on the left).

4. Thus the distortions of ACF-data appearing during the data zero count normalization are investigated in the work. Assuming parasites normal and signal/noise ratio value small an explicit expression for displacement $\Delta\hat{r}$ of ACF-estimation \hat{R} is obtained. Account of specified displacement will allow to obtain more fiducial information about ionosphere parameters.

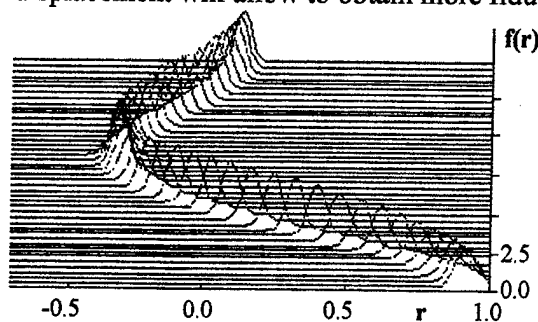


Fig.1. The set of densities $f(\hat{r})$ of casual

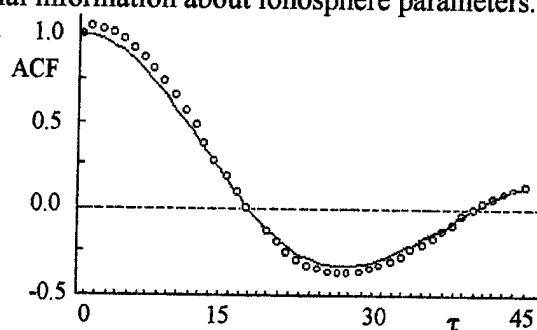


Fig.2. Perfect ACF (continuous line)

estimation for 45-item ACF.

and its \hat{R} estimations (circles).

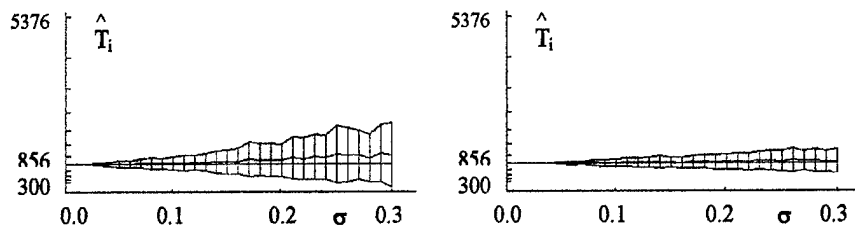


Fig.3. Ionic temperature estimation and scatter ($T_i = 856K; T_e = 856K$).

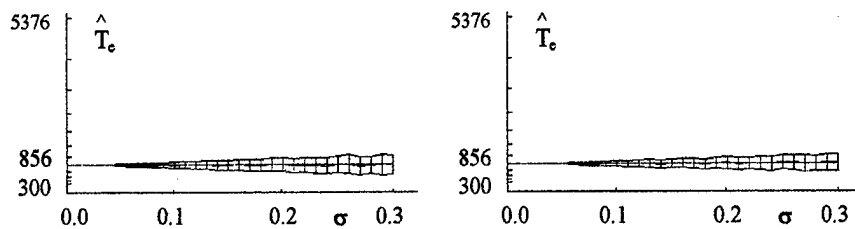


Fig.4. Electronic temperature estimation and scatter ($T_i = 856K; T_e = 856K$).

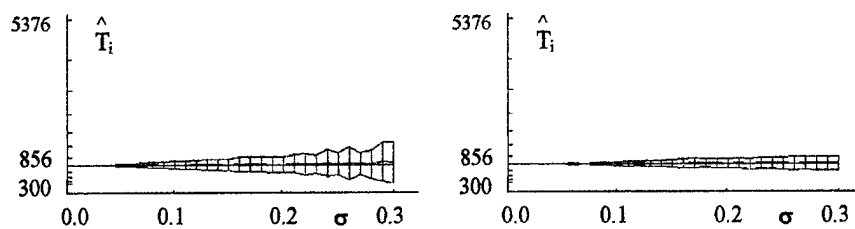


Fig.5. Ionic temperature estimation and scatter ($T_i = 856K; T_e = 3181K$).

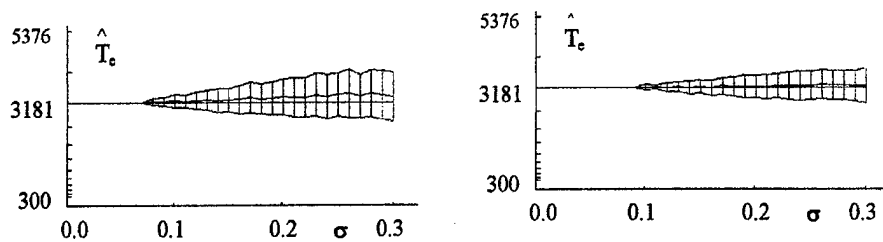


Fig.6. Electronic temperature estimation and scatter ($T_i = 856K; T_e = 3181K$).

VLF SCATTERING FROM RED SPRITES: VERTICAL COLUMNS OF IONISATION IN THE EARTH-IONOSPHERE WAVEGUIDE

Craig J. Rodger (1), James R. Wait (2), and N. R. Thomson (3)

- (1) British Antarctic Survey, Cambridge, United Kingdom
- (2) 2210 East Waverly, Tucson, Arizona, USA
- (3) Physics Department, University of Otago, Dunedin, New Zealand.

Abstract. Red Sprites were discovered by chance in 1989 when a Low Light TV system was pointed above an active thunderstorm. Optically, red sprites are observed as clusters of short-lived (~ 50 ms) pinkish-red luminous columns, stretching from ~ 40 km to ~ 85 km altitude, each about 1 km wide. Red sprite discharges produce columns of ionisation in the Earth-ionosphere waveguide, which can persist for up to ~ 100 s at higher altitudes. The ionised columns have been observed through "VLF Sprites", perturbations of the phase and/or amplitude of subionospheric VLF transmissions, which can be used to study the electrical properties of the red sprite columns. Previous theoretical studies of red sprite columns have simplified the problem by assuming the columns were of infinite length, or inside a "flat-earth" waveguide. We present calculations using well-developed VLF propagation methods to describe a finite length sprite inside a realistic Earth-ionosphere waveguide.

Introduction

Red sprites were discovered by chance in 1989, when a Low Light Level TV (LLTV) system was tested through night-time observations of near-horizon stars. During this time, an active thunderstorm occurred, just over the horizon. The LLTV camera observed a twin upward flash originating in the distant cloud tops lasting over two $1/60$ s TV fields [Franz *et al.*, 1990]. This was the first known observation of this phenomenon, now termed a "red sprite". Optically, red sprites are observed as clusters of short-lived (~ 50 ms) pinkish-red luminous columns, stretching from ~ 40 km to ~ 85 km altitude, each about 1 km wide [see the review by Rodger, 1998]. While the original observation was made with a LLTV camera, red sprites are often visible to the unaided human eye.

Red sprite discharges produce columns of ionisation in the Earth-ionosphere waveguide, which can persist for up to ~ 100 s at higher altitudes. The ionised columns have been observed through "VLF Sprites", perturbations of the phase and/or amplitude of subionospheric VLF transmissions, which can be used to study the electrical properties of the red sprite columns. Previous studies of VLF scattering from red sprites have made a number of simplifying assumptions; for example assuming the columns are infinitely long to examine the scattering from multiple interacting (non-Born) columns, or examining a single column inside a "flat-earth" waveguide. In this paper we make use of a modified form of the theory put forward by Wait [1991], to examine a column of ionisation inside the waveguide, and including the effects of mode conversion at the scatterer. The Wait [1991] expressions are extended to remove the first order Born approximation used to estimate the induced currents on the column.

Scattering from a Column in the Earth-Ionosphere Waveguide

In our scattering situation the Earth's surface is at $r = a$, and the ionosphere at $r = a+h$ in a spherical coordinate system (r, θ, ϕ) , with origin at the Earth's centre. The Earth's surface is characterised by constant surface impedance Z_g and the reflecting boundary of the ionosphere by an effective surface impedance Z_i . The time factor in our analysis is $\exp(+j\omega t)$, where ω is the angular frequency of the primary field. The radial (i.e. vertical) electric field, at great circle distance $s = r\theta$, $\phi = 0$, and $r = a+z'$, is designated $E_r^p(s, z')$, where z' is the height of the observer above the Earth's surface. The scattered field from a radially orientated column of ionisation, stretching from $r = a+z_a$ to $r = a+h$, with conductivity $\sigma(z') = \sigma$ (i.e. constant with z'), cross-sectional area δA , at great circle distance d_1 from the source dipole (and great circle distance d_2 from the observer) is designated $E_r^s(s, z')$. Wait [1991]

shows that the ratio of the scattered field to the primary field at the observer (point P , at great circle distance d from the source dipole and altitude z_2) is:

$$\frac{E_r^s(d, z_2)}{E_r^p(d, z_2)} \cong -j\sigma\omega\mu_0 \delta A \sqrt{\frac{d}{2\pi j k d_1 d_2}} e^{-jk(d_1+d_2-d)} \times \left[\frac{\sum_n \sum_m C_{m,n} \Lambda_n \Lambda_m G_n(y_1) G_m(y_2) e^{-j(t_n \chi_1 + t_m \chi_2)}}{\sum_n \Lambda_n G_n(y_1) G_m(y_2) e^{-j t_n \chi}} \right] \quad (1)$$

where $k = \sqrt{\epsilon_0 \mu_0 \omega}$, $\chi = (ka/2)^{1/3} (d/a)$, $\chi_1 = (ka/2)^{1/3} (d_1/a)$, $\chi_2 = (ka/2)^{1/3} (d_2/a)$,

$y_1 = (ka/2)^{-1/3} k h$, $y_1 = (ka/2)^{-1/3} k z_1$, $y_2 = (ka/2)^{-1/3} k z_2$,

n order number of the primary (incident) waveguide modes,

m order number of the scattered waveguide modes,

G_n, G_m height gain functions, which satisfies the differential equation,

$$d^2 G_n / dy^2 = (t_n - y) G_n$$

for eigenvalues t_n , which satisfy $A(t) B(t) - 1 = 0$ [see Wait, 1991, or Wait, 1995]

Λ_n, Λ_m excitation factors of the waveguide modes,

$C_{m,n}$ mode conversion factor, which in the case of an ionised column from $z = z_a$ to $z = h$ is:

$$C_{m,n} = \frac{1}{h} \int_{z_a}^h G_n(y') G_m(y') dz'$$

A simple modification of the working equations in Wait [1991], is to replace the actual column conductivity $\sigma(z')$ by an effective (complex) conductivity $\sigma_e(z')$. The implementation of this step is:

$$\sigma(z') \delta A \Rightarrow \sigma(z') \pi \hat{a}^2 \Rightarrow \sigma_e(z') \pi \hat{a}^2 \Rightarrow [Z_c(z') + Z_{ex}]^{-1}$$

where \hat{a} is the radius of the conducting column,

$Z_c(z')$ is the axial (z' dependent) internal impedance of the column,

Z_{ex} is the external impedance of the column,

Once again assuming that electrical properties ($\sigma, \epsilon_c, \mu_c$) of the column are independent of z' , the column impedances are given by [Wait, 1986]:

$$Z_c = \left(\frac{1}{2\pi \hat{a}} \right) \sqrt{\frac{j\mu_c \omega}{\sigma + j\epsilon_c \omega}} \frac{I_0(\gamma_c \hat{a})}{I_1(\gamma_c \hat{a})} \quad \text{where} \quad \gamma_c = \sqrt{j\mu_c \omega (\sigma + j\epsilon_c \omega)}$$

I_x is the modified Bessel function of type one and order x ,

$$Z_{ex} = \frac{j\mu_0 \omega}{2\pi} K_0(j k \hat{a}) \quad \text{where } K_0 = \text{modified Bessel function of type two and order zero}$$

Example Calculation

The scattered electric fields from red sprites can be investigated using equation (1), along with the modification detailed above. We investigate the situation appropriate for the VLF transmitter NLK (Seattle, 48° 12' 15" N, 121° 55' 00" W, 24.8 kHz) propagating to Colorado, where several red sprite research campaigns have been conducted. The transmitter-column distance is set to 1000 km, the column radius \hat{a} is 500 m, lowest column altitude 50 km, and column conductivity σ is 10^{-4} S/m. The surface impedance Z_g of the ground (with electrical properties $\sigma_g, \epsilon_g, \mu_g$) is given by:

$$Z_g = (120\pi) \sqrt{\frac{j\epsilon_g \omega}{(\sigma_g + j\epsilon_g \omega)}} \sqrt{1 - \frac{j\epsilon_g \omega}{(\sigma_g + j\epsilon_g \omega)}}$$

Of great importance in any studies of propagation inside the Earth-ionosphere waveguide is the selection of an ionospheric model. We make use of propagation parameters produced by the US Naval

Ocean Systems Center program *Modfinder* to calculate the waveguide mode eigenvalues, and the ionospheric surface impedance Z_p , which is dependent upon the mode order (n , or m). The ionospheric height h is 84 km, which is reasonable for night-time propagation. Given the quite short propagation distances involved in this situation, a large number of modes must be included in the calculations. Guided by the results of *Modfinder*, we include 22 modes in our calculations (although this includes a large degree of redundancy).

Figure 1 shows the magnitude of the ratio given in equation (1). As is clear, there is a large degree of variation in the observability of the scattered signal relative to the primary. However, this is somewhat similar to the results of *Rodger et al.* [1998], where there was large variability in the scattered signals azimuthally around a set of columns. Thus, one can expect large variability in the scattered signals in two situations – when one moves azimuthally around a set of columns, but also when one travels radially away from a set of columns (a red sprite event).

At a great circle distance of 200 km from the column (that is the observer is 200 km from the column and 1200 km from the transmitter), the magnitude of the ratio of scattered field to primary field is -27.2 dB. At 1200 km from NLK (towards Boulder, CO), the primary field strength is 74.15 dB above 1 $\mu\text{V/m}$ (about 5.1 mV/m). Thus the perturbation is 224.4 $\mu\text{V/m}$, which is very small. However, *Rodger et al.* [1998b] have shown that the field from 15 columns (experimentally determined from a red sprite image) can be more than 20 dB higher than that for a single column, resulting in a perturbation of ~ 2.23 mV/m, which will certainly be detectable! *Rodger and Dowden* [1998] estimate a reasonable lower limit for direction finding measurements of VLF sprites from NLK as 30 dB below the primary (the detection limit is more like -40 dB). Figure 1 suggests that VLF sprites should be observable on NLK for most great circle distances from 100 km to 2000 km, but with a small 'blind patch' near 450 km (depending on the number of columns present). *Dowden et al.* [1996] found that the detection efficiency of (optical) red sprites through observations of VLF perturbations was $\sim 95\%$.

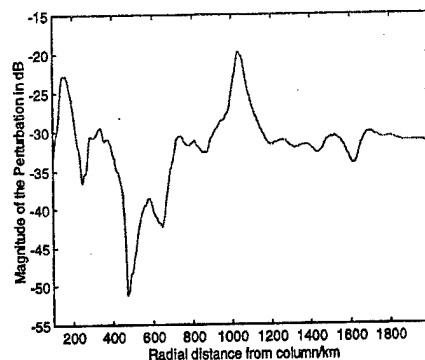


Figure 1. The variation in the magnitude of the ratio of the scattered field to the primary field (as given by a modified equation (1)), with distance from the radiating column.

References

- Dowden, R. L., J. B. Brundell, W. A. Lyons, and T. Nelson, Detection and location of red sprites by VLF scattering of subionospheric transmission, *Geophys. Res. Lett.*, 23, 1737-1740, 1996.
- Franz, R. C., R. J. Nemzek, and J. R. Winckler, Television image of a large upward electrical discharge above a thunderstorm system, *Science*, 249, 48-51, 1990.
- Rodger, C. J., Red Sprites, Vertical Lightning and VLF Perturbations, *Rev. Geophys.*, (in review), 1998.
- Rodger, C. J., and R. L. Dowden, Position determination of red sprites by scattering of VLF subionospheric transmissions, *Geophys. Res. Lett.*, 25(3), 281-284, 1998.
- Rodger, C. J., J. R. Wait, R. L. Dowden, Brief report: Scattering of VLF from an experimentally described sprite, *J. Atmos. Sol.-Terr. Phys.*, (in press), 1998.
- Wait, J. R., *Introduction to antennas and propagation*, Peter Peregrinus, London, 1986.
- Wait, J., EM scattering from a vertical column of ionisation in the earth-ionosphere waveguide, *IEEE Trans. Antennas and Propagation*, 39(7), 1051-1054, 1991.
- Wait, J., *Electromagnetic waves in stratified media*, IEEE Press, New York, 1996.

WAVELET ANALYSIS OF THE ELF SIGNATURES OF GLOBAL THUNDERSTORM ACTIVITY

Vladimir Vinogradov, Galina Litvinenko

Institute of Radio Astronomy National Academy of Sciences of Ukraine
4, Chervonopraporna St., Kharkiv, 310002, Ukraine; e-mail: gallitv@rian.kharkovua

Abstract

In the given work the signals from near and long-distance thunderstorms are considered by the method of wavelet transform with the purpose to check a hypothesis about the presence of the $1/f$ -noise component in the investigated processes. It is shown, that when the thunderstorm center moves up to a reception point, the Schumann or global resonances on a spectral plane decrease, gaining a character of flicker-noise process with a power spectrum $1/f^\gamma$ with γ accepting values in limits [from 1. to 1.2].

Introduction. The radiation from the near and far thunderstorm discharges observed in the spherical Earth-ionosphere cavity forms the natural electromagnetic noise of the Extremely Low Frequency (ELF) range (4-40 Hz). Numerous scientific publications are devoted to a research of this range of frequencies. In the experimental power spectra of ELF noise, the resonance maxima on certain frequencies are clearly observed, a possibility of whose origin for the first time was specified by Schumann [1]. He calculated the spectrum of the Earth-ionosphere resonator eigen frequencies, which were experimentally detected by Balser and Wagner. Such a form of is spectrum with strongly expressed resonance maxima on the frequencies 8, 14, 21, 26, 32 Hz usually called a Schumann spectrum. As it was shown earlier (see for instance [2]), electromagnetic energy of ELF range is connected mainly to a radiation of vertical thunderstorm discharges (discharges between a cloud and the Earth and intracloud discharges). It is necessary to notice that clear Schumann spectra are observed with a measurement of signals from long-distance thunderstorms. As long-distance thunderstorms, it is accepted to name a thunderstorm activity of global scale that happens continuously (~ 100 discharges in 1h) and produces a quasistationary background noise. However, for the observations of a near thunderstorm signals, i.e. when thunderstorm centers are at distances up to 500 km from the receiver, the spectra form is essentially different. Firstly, the signal intensity increases in tens to hundreds times. Secondly, there are no clearly expressed resonance maxima in the energy spectra; with the increase of the frequency the spectral curves smoothly decrease. In view of such spectral character of near thunderstorm signals it has been suggested to analyze whether the given noise process contains a clearly manifested flicker-component. The flicker-noise or, as it is accepted to name it in the modern literature, $1/f$ - noise, is characterized by a spectral density which depends on frequency as $1/f^\gamma$, where γ is a spectral constant accepting the values from 0.8 up to 2. Till now the noise nature of the radiation of thunderstorms has not been investigated in detail.

Observation data. The data analyzed in the present work have been obtained in the Radio Astronomy Institute of the NAS of Ukraine in its Low-frequency Observatory during the summer season of 1997. The experiments have been carried out by a group of the employees of Ionospheric Research Department of the Institute and kindly released to the present authors for research. In experiments, the vertical electrical component of ELF signals was measured, the noise circumstances for which in the range of 4 to 40 Hz are determined by the near

thunderstorm discharges, rainfall and wind. The characteristic feature of a reception tract was in building-up a "rectangular" frequency characteristic in the band of the first five Schumann resonances. The level of noise signals corresponding to the Schumann maxima at the place of reception was $|E_z| \approx (2 \div 4) \cdot 10^{-4}$ V/m that did not contradict with the known from the literature data.

Method of the analysis. Processing of signals from the near and long-distance thunderstorms was carried out by the method of wavelet analysis which is now widely applied in the problems of signal processing. For one-dimensional signals $s(t)$, a wavelet transformation consists in their expansion in terms of obtained from the mother-wavelet $\psi(t)$ basis of functional Hilbert space by the scale transformations and shifts:

$$s(t) = \sum_m \sum_n s_n^m \psi_n^m(t), \quad (1)$$

where $\psi_n^m(t) = 2^{-m/2} \Psi(2^{-m}t - n)$, $m, n \in \{\dots, -2, -1, 0, 1, 2, \dots\}$, M is the scaling index, n is the translation one.

So the wavelet transform performs a time-frequency description of the signal $s(t)$ with the wavelet coefficients s_n^m .

To prove our supposition that ELF signals produced by the near thunderstorms have component with a spectral density proportional to $1/f^\gamma$, algorithm developed in work [3] for determining the spectral parameter γ was used. The indicated algorithm is based on a maximum likelihood estimation for the wavelet coefficients s_n^m . It was supposed that the near thunderstorm signal $s(t)$ can be considered as a superposition of a flicker-component and a white Gaussian noise:

$$s(t) = f(t) + w(t), \quad (2)$$

where $f(t)$ is the flicker-type process, $w(t)$ is the white Gaussian noise. Because of the linearity of the wavelet transformation, the wavelet coefficients s_n^m for (2) are also a sum of two components. Wavelet coefficients s_n^m for (2) were obtained numerically.

Results. Thus we analyzed the signals from long-distance and near thunderstorm centers. A special interest for processing represented a recording, which included both as "quiet" conditions (global thunderstorm activity) and the beginning of a near thunderstorm. For these events in Fig. 1 a histogram of a variation of parameter γ as function of time is constructed. Simultaneously, in Fig. 2 a time dependence of the signal to noise ratio (SNR) is presented (here $f(t)$ was assumed as the signal in (2)), to show the efficiency of $s(t)$ modeling with the flicker noise component. A comparison of the graphs in both Figures shows good correlation in the behaviour of obtained dependences. While a thunderstorm center is moving up to the receiver, substantial increase of the values γ and signal to noise ratio takes place. Estimation of the values γ and SNR from Figs.1 and 2 showed, for a signal of a near thunderstorm, that $\gamma=1 \dots 1.2$ and SNR 27...32 dB that proves the presence of a clearly expressed flicker-component in the investigated signal.

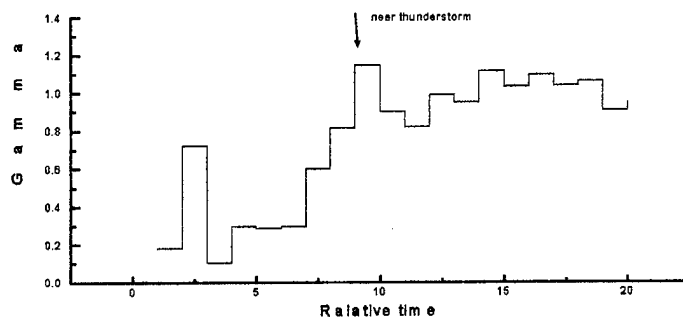


Fig.1

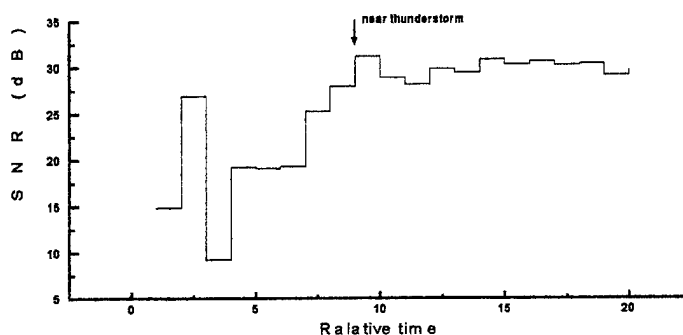


Fig.2

Conclusion. Application of the wavelet analysis method to a research of the noise radiation of ELF range generated long-distance and near thunderstorm discharges has enabled us to determine the presence of a flicker-component in the signals produced by the near thunderstorm center. This result can be used for a determination and classification of noise signals of both terrestrial and extraterrestrial origin. It is necessary also to notice, though by us such a problem has not been considered, that an analysis of mathematical model of the process (for example, the characteristics of the form of the given signal) possessing the $1/f$ - noise, can throw a light on the understanding of the physical mechanism causing the given phenomenon.

References

- [1] Schumann W.O. Über die Strahlungslosen Eigenschwingungen eine leitenden Kugel die von Luftschicht und eine Ionosphärenhülle umgeben ist.-Z. Naturforsch., 1952, 7a, s. 149-154.
- [2] Bliokh P.V., Nikolaenko A.P., and Yu.F. Filippov, Global Electromagnetic Resonances in the Earth-Ionosphere Cavity, Kiev, Naukova Dumka, 1977, (in Russian).
- [3] Ryabov V.B., Stepanov A.V., Usik P.V., Vinogradov V.V., and Yu.F. Yurovsky, From chaotic to $1/f$ processes in solar mcw-bursts, Astron. Astrophys. 324, p. 750-762, 1997 (in Russian).

Cross-Mode Modulation Effect in Schumann Resonances

Yuri M. Yampolski, Vasily S. Beley, Sergey B. Kascheev, Boris V. Lazebny, Vladimir E. Paznukhov, and Anatoly G. Rokhman

Institute of Radio Astronomy, National Academy of Sciences of Ukraine,
4 Chervonopraporna St., Kharkov 310002, Ukraine

1. Introduction

The propagation of radio waves through the ionosphere generally results in nonlinear interactions of the electromagnetic field with the plasma, modifying the electrodynamical characteristics of the latter. The question of principal importance for the observation of such effects is sensitivity of the methods and devices applied for the registrations. It should be noted that the threshold levels of the external fields for stimulating nonlinear effects in the ionospheric plasma are quite low, varying between 10^{-5} and 10^{-2} V/m for different types of the effects at different heights [1]. Active experiments with the "heating" facilities in the USA, the USSR (and later in Russia and Ukraine), and Norway allowed investigating a series of new phenomena in the ionosphere [2]. Obviously, implementation of such experiments is very complicated. Meanwhile, other possibilities exist to investigate nonlinear interactions between natural wave fields and the ionosphere, involving no active (i.e. using dedicated transmitters) experiments. Such an approach was realized by the authors in paper [3], where a cross-modulation effect between the Schumann resonances (SR) and round-the-world HF signals was detected and interpreted.

This paper describes an attempt of detecting nonlinear effects in the ELF band alone (4 to 40 Hz) where the Schumann resonance spectrum belongs. Preparing the investigations we used the following speculations. Passage of a radio signal through a nonlinear "device" (propagation medium) is accompanied by the appearance of combination spectral lines at frequencies f_y , that are either higher-order harmonics of the initial spectral components, i.e. $f_y = j \cdot f_i$ (here i and j are integers and f_i is the i -th spectral component frequency of the initial signal), or sum/difference combinations of the frequencies contained in the signal spectrum, i.e. $f_{y\pm} = f_i \pm f_j$. A distinctive feature of the "new" harmonics is their statistical relation to the initial spectrum components at the frequencies f_i and f_j . It is obvious that the common thermal nonlinearity type would be quite weak at ELF, as far as the Schumann signal power $\sim E_s^2$ is small in comparison with the plasma field power $\sim E_p^2$ in the lower ionosphere. The estimates made in paper [3] show

$$\frac{E_s^2}{E_p^2} \approx 10^{-6}, \quad (1)$$

in the ELF band, and hence direct heating of the ionospheric plasma by the Schumann resonances does not exceed 10^{-4} K. This means that in order to detect the extremely weak combination effects in the band the averaging time should greatly exceed that of observation of the Schumann spectral maxima themselves.

Yet, in spite of the unsatisfactory estimate of equation (1) the band was chosen for a search for natural nonlinearities, the reasons behind being as follows. First, the global Earth - ionosphere resonator exists permanently; second, it is constantly stimulated by the world lightning activity; third, the average parameters of the resonator are quite stable, and, fourth, the Schumann spectrum is of multimode character with well known frequencies of the spectral peaks,

i.e. $F_1 \approx 7.8$ Hz; $F_2 \approx 14.0$ Hz; $F_3 \approx 20.0$ Hz; $F_4 \approx 26.1$ Hz, and $F_5 \approx 31.8$ Hz [4]. In addition, we would note that there is a rather strong natural nonlinearity in the atmosphere and lower ionosphere, caused by super-powerful lightnings, which can play the role of nonlinear transformers of incident electromagnetic fields [5, 6].

2. Measuring technique. Power spectra of the Schumann resonances

The first stage of data processing was computing the average amplitude spectrum of the signal $U(t)$,

$$S(f) = \sqrt{\langle |S_N(f)|^2 \rangle},$$

where $S_i(f)$ is the spectrum for the i -th period of length T , and the angular brackets denote averaging over N realizations.

$$\langle |S_N(f)|^2 \rangle = \frac{1}{N} \sum_{i=1}^N |S_i(f)|^2.$$

The realization length was chosen to be equal to $T \approx 6.8$ s. It is known (see, for example, [4]) that the optimum averaging period is between 5 and 10 minutes which allows calculating distinct SR spectrum. However spectra obtained at such periods contain no sign of nonlinear transformation of the observed signals. For this reason we averaged the spectra over much longer periods (about 2 hours of averaging). Fig. 1 shows typical SR spectra in the cases of low (Fig. 1A) and high (Fig. 1B) external noise circumstances. The interferences are characterized by wide frequency band, with the intensity increasing in the low frequency part of the spectrum, and considerable (tens and hundreds times) excess over the SR level.

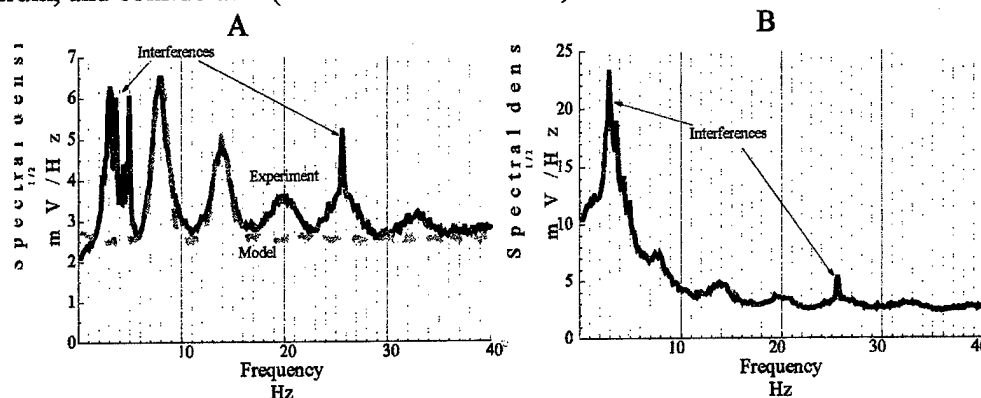


Fig. 1. The SR amplitude spectra under the conditions of low (A) and high (B) level of external interferences.

During two measuring campaigns (July 1996 and July - August 1997) over 100 hours of the SR observational data were accumulated. The amplitude spectra averaged over the intervals from 2 to 4 hours were calculated. Nevertheless, for these long averaging sessions no considerable increases of the spectral density in the vicinity of doubled frequency of the first SR mode $2f_1 = (15.6 \pm 0.5)$ Hz and combination frequencies of the first and second ones $f_{12-} = (6.2 \pm 0.5)$ Hz and $f_{12+} = (21.8 \pm 0.5)$ Hz were detected.

3. Multiplicative algorithm for processing the SR data

To discover the combination lines in the Schumann resonance spectra a special multiplicative algorithm was applied. Its essence is as follows. Let us assume the analyzed signal $U(t)$ to consist of two initial narrow-band components at the frequencies f_1 and f_2 and their combination harmonics at $f_{12-} = f_2 - f_1$ and $f_{12+} = f_2 + f_1$ which raised as the result of a nonlinear inter-

action between the initial components. Using a digital filtering procedure(2), let us pick out the initial components $U_1(t) = A_1 \cdot \cos(2\pi f_1 t - \varphi_1)$, $U_2(t) = A_2 \cdot \cos(2\pi f_2 t - \varphi_2)$ and then multiply them: $U_{12}(t) = U_1(t) \cdot U_2(t)$. It is obvious that this synthesized signal will contain combination harmonics coherent with those in the analyzed signal and, as assumed, born by some natural nonlinear physical process. Now, if we calculate the coherence function between the signals $U(t)$ and $U_{12}(t)$, it will be of non-zero value at the combination frequencies f_{12-} and f_{12+} (3).

$$\Pi(f)_i = \begin{cases} 0, & f < f_i - \Delta f \\ 1, & f_i - \Delta f \leq f \leq f_i + \Delta f \\ 0, & f > f_i + \Delta f \end{cases} \quad (2)$$

Then the output of the filters are $U_i(t) = F^{-1}\{S(f) \cdot \Pi(f)_i\}$. Further the complex spectrum of the product is calculated: $S_{12}(f) = F\{U_1(t) \cdot U_2(t)\}$. At the final stage the coherence function is derived as the result of averaging and normalizing the cross-spectrum:

$$\Gamma(f) = \frac{\langle |S(f) \cdot S_{12}^*(f)| \rangle}{\sqrt{\langle |S(f)|^2 \rangle \cdot \langle |S_{12}(f)|^2 \rangle}}, \quad (3)$$

where asterisk denotes the complex conjugation operator. Here we should note that the algorithm might be considered as a specific particular case of the bispectral analysis method [8].

Let us turn to the results of the data processing. First examine a "quiet" record containing practically no non-stationary interferences (Fig. 1A). In this picture the Schumann resonance modes (up to the fifth one) along with the spectral peaks due to the fundamental power harmonic and low frequency "wind" interferences are seen. The plot in Fig. 2A illustrates presence of coherent components in the region of the first mode doubled (16 Hz) frequency (in this case both digital filters (2) are tuned to $f_1 = f_2 = 8$ Hz with the halfwidth $\Delta f = 1$ Hz). Close to this results were obtained while tuning the filters to frequencies of the SR modes having different numbers (Fig. 2B).

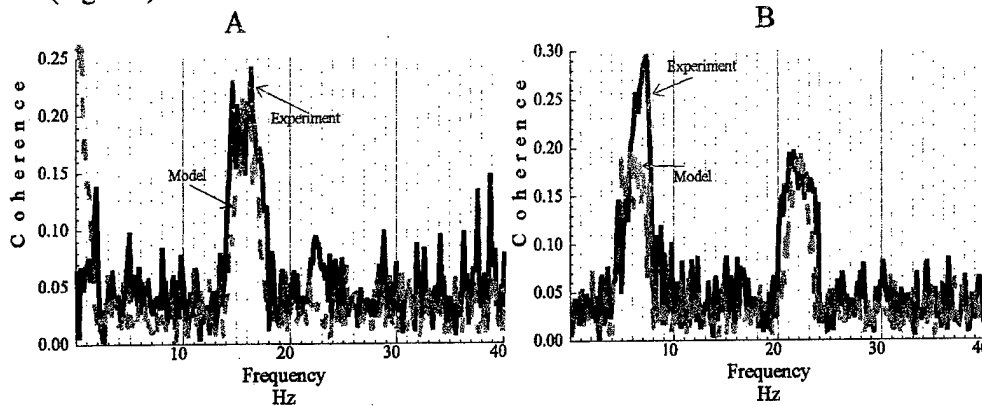


Fig. 2. Coherence of the second harmonic of the first SR mode (A) and the combination harmonic of the first and second ones (B).

Results similar to those shown in figures 2 and 3 were obtained while processing the overwhelming majority of measuring sessions both for day-time and night-time conditions, which allows affirming existence of the nonlinear interaction between the SR modes. After this fact has been established, additional careful tests of the algorithm, the data collection system, and the receiving complex were performed. We should note that in no test experiment any increase of the coherence function level was detected in the band of combination harmonics.

4. Discussion

Currently authors cannot offer a strict physical model which would allow interpreting the discovered fact of nonlinear transformation. Nevertheless, some conclusions can be suggested. For instance, we estimated the transformation factor of the SR energy which is transformed to higher-order and combination harmonics under the influence of presently unknown natural mechanism. The analyzed signal was simulated numerically assuming the nonlinear transformation is described by a quadratic function:

$$U(t) = N(t) + u(t) + K \cdot u^2(t), \quad (4)$$

where $N(t)$ is "white" noise with zero average and dispersion σ_N^2 , and $u(t)$ is superposition of two narrow-band components with Gaussian power spectra. The factor K characterizes "steepness" of the nonlinear transformation. As Fig. 1A shows, the noise level is constant over the analysis band and can be estimated as $2.6 \text{ mV} \cdot \text{Hz}^{-1/2}$. The spectral components S_1 and S_2 simulated two first SR. In this way the model signal having spectrum close to the SR (dashed curve in Fig. 1A) was simulated. The K factor was varied till the coherence function (3) (dashed curves in Fig. 2) became approximately equal to the value calculated from the experimental data. It turned out that in the model (4) the nonlinear transformation factor is constant within accuracy of 10% both for the second harmonics of the two first SR modes and their combination ones f_{12+} : $K \approx 2.4 \cdot 10^{-1} \text{ mV}^{-1}$. Calibrating the value of K on spectral densities of the observed and simulated spectra allows estimating the quantity of stored in the resonator energy which is transformed due to the quadratic nonlinear mechanism (3). According to our calculations about 0.5% of the SR signals power is transformed to the higher-order and combination harmonics.

References

1. Gurevich, A.V. and A.B. Shwartsburg. Nonlinear theory of radio waves propagation in the ionosphere. Moscow, Nauka publish, 1973.
2. Stubbe P. The Ionosphere as Plasma Laboratory. In: Modern Ionospheric Science. Edited by H. Kohl, R. Ruster, and K. Schlegel. European Geophysical Society, Katlenburg-Lindau, FRG 1996, pp. 274 - 345.
3. Yampolski Y., P. Bliokh, V. Beley, V. Galushko, and S. Kascheev. Nonlinear interaction between Schumann resonances and HF signals. Journal of Atmospheric and Solar-Terrestrial Physics, Vol. 59, No. 3, 1997, pp. 335 - 342.
4. Bliokh, P.V., A.P. Nikilaenko, and Y.F. Filippov. Global electromagnetic resonances in the Earth-ionosphere cavity. Kiev, Naukova dumka publish, 1977.
5. Nikolaenko A.P., and M. Hayakawa. Heating of the Lower Ionosphere Electrons by Electromagnetic Radiation of Lightning Discharges. Geophysical Research Letters, Vol. 22, No. 22, 1995, pp. 3015 - 3018.
6. Taranenkov Y.N., U.S. Inan, and T.F. Bell. Interaction with the lower ionosphere of electromagnetic pulses from lightning: heating, attachment, and ionization. Geophysical Research Letters, No. 20, 1993, p. 1539.
7. Rycroft M.J. Resonances of the Earth - ionosphere cavity observed at Cambridge. England Radio Sciences, 69D, Vol. 8, 1965, p. 1071.
8. Wernik A.W. Methods of Data Analysis for Resolving Nonlinear Phenomena. In: Modern Ionospheric Science. Edited by H. Kohl, R. Ruster, and K. Schlegel. European Geophysical Society, Katlenburg-Lindau, FRG 1996, pp. 322 - 345.

CALCULATION OF ATMOSPHERIC ELECTRICITY DAY TREND

V.A. Donchenko, V.T. Kalaida, E.V. Ovcharenko

Radio Physics Faculty, Tomsk State University
Lenin St. 63, Tomsk, 634050 Russian

Abstract. In this paper, we discuss the problems of approximation of the atmospheric electricity day trend. It is shown that for the approximation of the time trend with a 3 to 4 % error, 5 sine harmonics or 10 sine-cosine harmonics are enough.

From the physical viewpoint, average means of tension (AMT) should be in good agreement with the integral value of the electrical field and show the global 24 hour trend alterations of this field. To verify this, the following algorithm was used, under an assumption that the time trend for various realisation of AMT should be correlated with the integral value of AMT. This algorithm was developed for the analysis of the opportunity to design a mathematical simulation tool of the 24-hour trend of the Atmospheric Electricity Day Trend (AEDT). It is based on two groups of methods: spectral and statistical ones. The use of spectral methods is justified by the general purpose (to raise the information efficiency of the spectral research by means of the analyses of spectra containing fast fluctuations). Fast Fourier Transform (FFCT) application is useful here from the point of view of deriving the mean values of AMT. FFT ratios can be calculated by the formula:

$$a(n) = \sum_{j=0}^{N-1} x(j)W_N^{-nj}, \quad (1)$$

where $x(j)$ are the measured tension values, N is the number of values in selection. Then the first member in the frequency dependence, divided by $(N-1)$, will represent the average value of \bar{x} . On using FFT in every selection of 3500 values and dividing the first member of the transform by N , we obtain 72 mean values of AMT. The choice of Vinogradov's method is explained by the independens on the data, unlike that of the "butterfly" one.

With the developed algorithm, several dosens of 24-hour trends have been processed. Polynomial approximation functions have been chosen in the method of the least squares (MLS). MLS is a particular case of the maximum similarity method providing asymptotic non-shifted effective and significant values of the randomly measured data; besides, the function of the tension density distribution is normal. Unknown coefficients C_i were determined at each iteration step. The algorithm calculated the root mean square deviations, σ_j at the points $j=1, \dots, k$ (where k is the number of points)

and the total root mean-square deviations, $\sigma = \sum_{j=1}^k \sigma_j$, for each polynomial of the order N . The

polynomial of the order having the minimum total root mean square deviation was taken as an approximation polynomial. The given approximation error, $\sigma_{\text{ap}} = \frac{\sqrt{\sigma/k}}{\Delta E_{\text{max}}} * 100\%$, where k is the

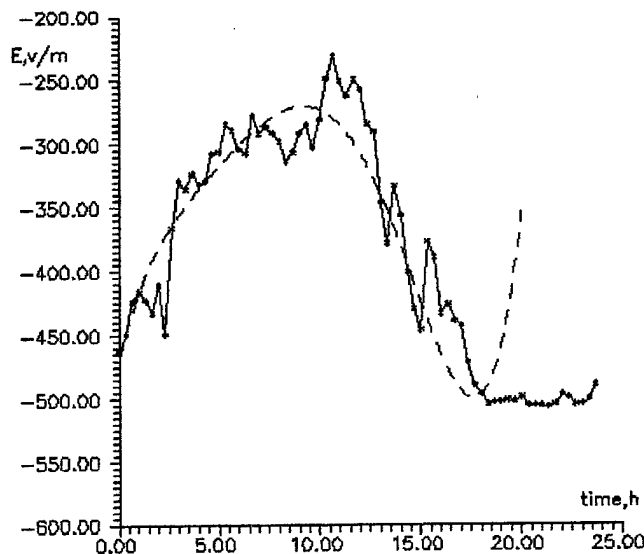
number of points, ΔE_{max} is the maximum scattering of experimental values of E , was also calculated. As a result, from the available trends testing data, we obtained the minimum values of σ and σ_{ap} based on the fifth-degree polynomials, the scattering in the values of σ_{ap} being 5 to 30%.

The calculation revealed a decline in the hypothesis results testing with $N=5$ and 6 during the observation season.

Here, the character of the curves for the same observation seasons and the relative values of the coefficients C for similar degrees agree well enough. Besides, one and two peaked time trend distributions of AMT have been observed, as well as the known from publications integral values. It is a reliable validation of the derived by us time trend and integral distribution law correlation.

However, it should be noted that a demerit of this method is in the considerable discrepancy between the calculated curves and the experimentally obtained ones within the observation period. From our viewpoint, these can be explained by the fact that the representation of the function of AMT, with the application of our technique, was carried out at the starting point of observation, $t=0$, and so it is quite natural that the error increases the farther the point is from the observation start. Evidently this problem solution is in the representation of AMT by a set of orthogonal periodic functions

Representations by the trigonometric functions set are the most probable ones. The calculations show that in almost all the possible cases the time change of AMT can be described by the fifth-order polynomial, the root mean square deviation at the point not exceeding 7%. The calculation results and their comparison with the experiments are shown in the Figure, where time, counted in hours, is marked along the horizontal axis, and the field tension mean value is plotted. Solid curve shows the real 24-hour trend obtained as a result of data processing with automatic measuring complex, dotted curve shows the calculated dependence.



However, the suggested approximation by means of polynomials tends to a noticeable error encrease at the upper limit of approximation interval. The behavior of the Earth electrostatic field trend enabled us to suppose that the most natural kind of approximation will be by the periodic functions.

Here, two problems arise:

- a) about the basic period of periodic series,
- b) about the number of approximation harmonics needed for the trend to be characterized accurately

As it is known from the publications, the 24-hour time is commonly taken as the basic period. However, our experimental data studies did not agree with this. We solved the problem of the basic period determination. The basic period was assumed as an unknown quantity, the random realisation of the experimental data obtained in different seasons being taken as the function.

As a result, we obtained the mathematical expectation of the basic period equal to 9 hours. The second problem deals with a simpler and more accurate approximation convenient in the practical applications. We used the Fourier series with $T=9$ hours and various numbers of harmonics. The analysis has shown that for the approximation of the time trend with a 3 to 4% error, 5 sine harmonics or 10 sine-cosine harmonics are enough. Besides, the obtained approximation, unlike the previous one, has a sufficiently small continuous error throughout the interval observed. We can predict the time progress of the electric field with a sufficiently good accuracy.

Seasonal Drift of the Global Thunderstorms and Schumann Resonance Frequencies

A.P. Nickolaenko

*Institute of Radiophysics and Electronics, Ukrainian National Academy of Sciences
12 Acad. Proskury str., Kharkov 310085, Ukraine*

L.M. Rabinowicz

*Institute of Radio Astronomy, Ukrainian National Academy of Sciences
4, Krasnoznamennaya str., Kharkov 310002, Ukraine*

We discuss an impact of the seasonal north-south drift of the global thunderstorm centers on the results of observation of the first mode Schumann resonance (SR) frequency.

Global electromagnetic resonances were predicted by W.O.Schumann in 1952. The resonance is observed in form of separate peaks in the power spectra of natural EM noise of the Earth-ionosphere cavity, and the global lightning activity is the source of these oscillations. The world-wide thunderstorms are concentrated at the tropics, their maximum follows the Sun and circles the globe during the day producing regular diurnal variations in the SR amplitudes and apparent resonance frequencies. These last occur due to finite conductivity of the cavity boundaries. Frequency characteristics of individual SR modes overlap substantially, and as a result, the particular peak (resonance) frequency depends on the interaction between the given mode and the nearby resonance peaks. Since amplitudes of individual peaks depend on the source-observer distance, the apparent resonance frequencies become modulated on a daily span.

We apply two models of the global thunderstorm distribution. The first is the model of a single compact lightning center. This center is positioned near evening terminator and has the size of some tens of degrees. At solstice period of a year, the center shifts southward (during the winter time in the Northern hemisphere) or northward (during the summer). Its diurnal trace coincides with the equator at equinox conditions. The second model is based on the concept of three global thunderstorm centers situated over Africa, Central America and South-East Asia. Seasonal drifts of the centers are pertinent to the model as well. Physically, the difference between above two models is as follows: the first one suggests the gradually moving (crawling) thunderstorm zone, while the second is based on the model of the lightning activity striding in wide steps from one continent to another during the day.

The main goal of the report is an attempt to interpret the year-to-year variations in the diurnal frequency patterns. It had been established experimentally that the diurnal patterns for a particular month remain very similar the year after year, but they are shifted as a whole by 0.1-0.2 Hz.

There two possible explanations may be suggested for the effect. The simplest one is the global annual change in the lower ionosphere. The second, much more realistic interpretation exploits the year-after-year variations in the spatial distribution of the global thunderstorms. Their positions and size do not coincide for different years, producing relevant changes in the SR signals.

After comparison with the results of the SR monitoring, the first approach allows for a conclusion that the scale factor of the atmospheric conductivity profile should be changed by 5-8 %, while the second shows that the position and/or size of the source undergoes the 5-10° variation from year to year.

Time Domain Solution for the Natural Sub-Ionospheric ELF Pulse

I.G. Kudintseva

Kharkov State University

4 Svobody square, Kharkov 310077, Ukraine

S.V. Myand, A.P. Nickolaenko

Institute of Radiophysics and Electronics Ukrainian National Academy of Sciences

12 Acad. Proskury str., Kharkov 310085, Ukraine

and

L.M. Rabinowicz

Radioastronomical Institute of the Ukrainian National Academy of Sciences

4 Krasnoznamennaya str., Kharkov 310002, Ukraine

We model numerically the sub-ionospheric propagation of an electromagnetic wave in the extremely low frequency (ELF) band from a few hertz to some kilohertz frequency using the time domain presentation for the field. A point vertical electric dipole is the source of the radio wave that arrives to ground based observer through the spherical Earth-ionosphere cavity. We suppose the radiation moment of the source to be the delta-pulse, hence, the solution obtained is the Green's function of the problem. Formal representation for such a function is well-known either for the cases of postulated propagation constant or for a given effective surface impedance of the lower ionosphere. The formal solution is constructed using the zonal harmonic series representation (ZHSR) that applies the Legendre polynomials describing the angular field dependence and spherical Hankel functions accounting for the radial dependence.

The ZHSR is valid in the frequency domain and describes the well-known Schumann resonances (SR). To obtain the fields in the time domain, we had transformed ZHSR applying the Fourier transformation (FT) analytically to each term of the infinite sum. Two cases are treated separately. The first one corresponds to the linear frequency dependence of the propagation constant of the ELF radio wave. The second radio propagation model exploits the linear frequency dependence of the effective surface impedance of the lower ionosphere. After the FT is applied, each term of the ZHSR turns into a standard function that is a time-decaying cosine function representing the response of the Earth-ionosphere cavity on the input delta-pulse. It is shown that the field representation obtained in the time domain converges uniformly and absolutely for arbitrary time $t > 0$.

Results of the ELF field computations are presented for a set of the source-observer distances. A specific feature of the ELF field in the time domain is the 'bouncing' of an electromagnetic pulse from the source antipode and from the point where the source initially had been placed. The ELF pulse width grows with the propagation path due absorption the lower ionosphere.

The main result of the present study is as follows.

- The time domain representation obtained allows computing the electromagnetic pulse everywhere in the Earth-ionosphere cavity for $t > 0$, while the ZHSR diverges at the source point.
- When computing the field in the frequency domain first and applying a FFT algorithm then to obtain the temporal dependence of the field, one fails to describe the field at the source regardless the time.
- When the analytical FT is used first and the time domain field representation is obtained initially, the series describes the pulse everywhere, including these multiply crossed the Earth's circumference.

Schumann Resonance and Global Lightning Activity

A.P. Nickolaenko

*Institute of Radiophysics and Electronics Ukrainian National Academy of Sciences
12 Acad. Proskury str., Kharkov 310085, Ukraine*

M. Hayakawa and Y. Hobara

*The University of Electro-Communications
1-5-1 Chofugaoka, Chofu-city, Tokyo 182, Japan*

Temporal variations of the global lightning activity are deduced from the long-term Schumann resonance (SR) continuous records. The intensities of the horizontal magnetic field component of the first, second, and third SR modes were monitored at the Tottori observatory (35.5° N and 134.33° E). Variations of the effective source-observer distance were estimated from the data using the ratios between intensities of individual SR modes. This allowed us to compensate for the source motion in respect to the observatory and extract from the records the average diurnal variations of the global lightning activity itself. The procedure had been done for every month within the observation period. The results show that estimates for the effective distances between the field-site and the global centers of the lightning activity remain very stable. Simultaneously, the temporal changes of the fields monitored and of the relevant global lightning activity derived from the records demonstrate substantial variability.

The global electromagnetic resonances are named after W.O.Schumann, who predicted the phenomenon in 1952 and estimated the eigen-frequencies of the Earth-ionosphere cavity. The global lightning activity is a source of the oscillations. Resonances are detected as separate peaks observed in the power spectra of the natural electromagnetic radio noise around frequencies of 8, 14, 20, and 26 Hz.

The world-wide lightning activity is concentrated in the tropical zone, and its maximum circles the globe every day producing diurnal variations in the SR amplitudes and apparent resonance frequencies. Amplitude variations depend on both the source-observer effective distance and on the current lightning intensity. This is why the Schumann resonance allows monitoring the world-wide thunderstorm activity from a single field-site.

We use the results of the long-term records carried out at Tottori observatory from 1968 to 1975. A comparison was made between the experimental records and computed data obtained in the framework of two different models of the global lightning distribution. This allowed us to elaborate the signal processing procedure aimed to the evaluation of both the median distance and the level of the world-wide lightning activity.

A magnetic loop antenna had been used to measure the SR field, that is a solenoid about 5 cm in diameter with permalloy core, number of turns is 30,000. The frequency characteristic of the amplifier was made flat in the frequency range from 5 to 35 Hz. The magnetic field intensity has been measured in the frequency bands 2 Hz wide around resonant frequencies of 8, 14, and 20 Hz. Intensities of individual SR modes were recorded on a chart paper, and so we had to read the data first. The tables obtained were used then to plot a survey of the diurnal variations in the intensities of three SR modes. This allowed performing the final check of the experimental time series and eliminate the reading errors together with the omitted changes of the receiver gain.

Natural ELF radio signal is a random succession of electromagnetic pulses that originate from the lightning discharges all over the globe. At ELF, only three field components are detectable at the surface of the ground: the vertical electric and two horizontal magnetic fields. It is assumed usually that the random pulses radiated by the lightning strokes are the Poisson succession. It means that the incoherent summation takes place, and the intensities of individual events are summed up. Since the experimental data were not absolutely calibrated, we did not calculate the absolute field levels.

For the final processing, we applied a single source model, that is characterized with two free parameters: the source-observer distance and the source intensity. Within such a model, variations in the source-observer distance have different impact on the SR amplitudes due to range dependencies of individual resonance modes of the field. To compensate for this kind of variations, we used the ratios of the intensities of individual modes. Such a ratio is independent of the source intensity, as well as of the magnetic antenna angular pattern that is the same for all the SR mode frequencies. After transition to the mode ratios, the effective source-observer distance becomes the single free parameter of the problem to be estimated from the records.

As in any inverse problem, we obtained the ambiguous solution: the distances derived had split into two compact groups. Day-to-day stability of the distances obtained indicates that the global thunderstorms move in a regular way around the observatory. Indeed, from low to severe diurnal variations occurred during the observation period, still, the distances derived remained stable, slightly fluctuating within a 1 Mm gap. This result indicates also the variations in the field recorded were produced predominantly by the changes in the intensity of the global lightning activity.

After evaluating the source-observer distances, we deduced the variations of the source intensity. The procedure was as follows. From the recorded intensities of the SR modes (we took the median value for each hour of a day) we calculated the ratios between the modal intensities and obtained then the source-observer candidate distances (six estimates that fell usually into two clusters). For each set of the distances we computed six fields expected at each SR mode. After dividing the data measured by the fields calculated, we obtain six estimates for the level of the global thunderstorm activity at each mode. These hour-after-hour estimates were sorted into 24 groups and stored. In such a way we obtained 540 estimates for the global lightning activity during a particular time of a day based on the records one month long.

Applying statistical processing of the final estimates we obtained average diurnal variations for a given month together with the standard deviations of the data.

Conclusion

The main results of this study are as follows:

1. The idea is confirmed that the records of the Schumann resonance intensity represent the level of the global thunderstorm activity.
2. From the records of the SR background the diurnal, seasonal and annual variations of the global lightning activity are deduced.
3. Temporal variations may substantially differ for the successive days, while the source-observer distance remains stable.
4. Accuracy of the final estimates for the level of the global thunderstorm activity is approximately 30% for the monthly averaged data and 20% for the median activity over the one year span.
5. Seasonal trends were observed with the SR background data. The level of the global lightning activity does not always return to the value measured the same month during the previous year.

IMPACT OF VARIATIONS IN THE RADIOACTIVE BACKGROUND ABOVE THE EARTH ON THE IONIZATION BALANCE IN THE LOWER IONOSPHERE

S.I.Martynenko¹ and R.S.Shubova²

¹Department of Space Radio Physics, Kharkov State University, 4 Svobody Square, Kharkov 310077, Ukraine;

²Institute of Radio Astronomy of the Ukrainian Academy of Sciences, 4 Krasnoznamennaya Street, Kharkov 310002, Ukraine

Abstract

A lithosphere-ionosphere interaction model is put forward, involving atmospheric vertical conduction electric currents, the variations of which can change the electric potential of the lower ionosphere. The ionospheric parameter variations have been estimated, compared with the gathered data, and both quantitative and qualitative agreement found.

Introduction. One of the most important topics in ionospheric physics is coupling with lower altitudes which focuses on response of the $\sim 60 - 150$ km region to forcing mechanisms originating in lower atmospheric regions, and the transmission of these effects throughout the thermosphere-ionosphere system. Effects are revealed in the ionosphere which are due to earthquakes, volcanic eruptions and anthropogenic impacts: explosions, rocket launches, accidents at nuclear power stations (NPS) accompanied by radioactive materials releases.

Precursors of earthquakes in the D region of the ionosphere are investigated by VLF radio waves in the Earth-lower ionosphere waveguide. Anomalous variations in signal amplitude and phase is an indicator to disturbance. On paths near seismic regions, anomalies in signals appear in a few days before the earthquake and show that the lower boundary of the ionosphere in the disturbed region descends. Similar anomalies were revealed on the VLF paths near the Chernobyl NPS during the accident in April 1986. The fact that two different processes, natural and anthropogenic, result in similar perturbations may be interpreted as that they both are caused by changes in conductivity near ground. The conductivity in this part of the atmosphere is the result of action of nuclear decay in the ground, radioactive contamination in the atmosphere, and space radiation. Before earthquakes the conductivity increases because of enhanced radon emissions, one of the major sources of ionization near ground, and during the Chernobyl accident because of radioactive material release.

Atmosphere-ionosphere interaction. In our analysis, we use a model of the spherical capacitor, the inner plate of which is the negatively charged liquid and solid surface of the Earth and the outer plate is the positively charged ionosphere. The external electric fields produced by thunderstorms cause electric currents, $I = U/R$, to flow between the Earth and its atmosphere over the entire planet. The potential of the upper conductive atmosphere, the outer plate, reaches an equilibrium value of approximately 200 or 300 kV with respect to the surface of the Earth, when the fair weather electric current flowing between the plates balances the electric currents produced by

the thunderstorms. Both these currents are closed through the Earth's surface and the ionosphere at $z \sim 60$ km. The electrical resistance between the Earth and the ionosphere is $R = \int_0^h \rho(z) dz$, its magnitude mainly being determined by the lower layers of the atmosphere up to $z \leq 5$ km. The resistivity is controlled by the Earth's background level of radiation. The increase in the background level of radiation by a factor of several times, which occurs before earthquakes or during nuclear accidents (with the discharge of radioactive material), leads to a proportional increase in the near-Earth atmospheric conductivity, $\sigma = 1/\rho$, and in the current I in the capacitor.

The magnitude of the fair-weather vertical electric field component is about 130 V per meter at the Earth's surface. Electric-field variations observed before an earthquake are sometimes so large that one even observes a change in the direction of the electric field at the Earth's surface. As a result, we may expect that large changes in the electric field intensity will occur at the outer plate of the capacitor, i.e. in the lower ionosphere. Measurements have shown that the magnitude of electric field at the altitude of 60 km is of the order of 1-10 V/m. We suggest that variations of the electric potential of the lower ionosphere may lead to changing lower-ionosphere parameters.

Changes in lower-ionosphere parameters. To estimate the effect of the variations in the electric field intensity, E , on changes in lower-ionosphere parameters, we shall use the well known system of equations, the energy balance equation (in terms of the electron temperature T_e), the two continuity equations in the electron density N and the positive-ion density N^+ in the stratified inhomogeneous weakly-ionized plasma, and the condition of quasi-neutrality:

$$\frac{\partial N}{\partial t} = q_i + \nu_a \lambda N - \nu_a N - \alpha_r N^2 (1 + \lambda) + \frac{\partial}{\partial z} \left\{ (D_t + D_a) \frac{\partial N}{\partial z} \right\}, \quad (1)$$

$$\frac{\partial N^+}{\partial t} = q_i - \alpha_r N^2 (1 + \lambda) - \alpha_i N^2 \lambda (1 + \lambda) + \frac{\partial}{\partial z} \left\{ (D_t + D_a) \frac{\partial N^+}{\partial z} \right\}, \quad (2)$$

$$\frac{\partial T_e}{\partial t} = \frac{2Q_e}{3kN} - \delta \nu (T_e - T_n), \quad (3)$$

$$N^+ = N + N^-, \quad (4)$$

where t is time, q_i is the total production rate per unit volume of positive ions resulting from the ionization of neutral atmospheric constituents, ν_a is the effective rate at which the negative ions are destroyed by electron detachment, $\lambda = N^-/N$ is the negative ion to electron number density ratio, N^- is the negative ion density, ν_a is the effective rate at which the negative ions are formed by the attachment of electrons to neutral constituents, α_r is the effective ion-electron recombination coefficient for positive ions, D_t is the coefficient of eddy diffusion, D_a is the coefficient of ambipolar diffusion, z is the altitude, α_i is the effective ion-ion recombination coefficient, k is Boltzmann's constant, Q_e/N is the average energy acquired by the electron from an external source of heating (for example, from external electric field), δ is the fractional loss of energy per electron collision, ν is the effective electron-neutral collision frequency, T_n is the neutral constituency temperature. In the ionospheric D region, the disturbances in the ion temperature are neglected because they are M/m times less than the disturbances in T_e (M is the average ion mass, m is the electron rest mass).

The initial system of equations (1)-(4) is considerably simplified with the help of the multiple time-scaling analysis by introducing the following time scales:

$$t_1 = t_{Te} = (\delta\nu)^{-1}, \quad t_2 = t'_N = (\nu_d + \nu_a)^{-1}, \quad t_3 = t_N = \{4q_i(\alpha_r + \lambda\alpha_i)/(1 + \lambda)\}^{-1/2},$$

where t_{Te} is the T_e -relaxation time, t'_N is the evolution time of the disturbances in N caused by activating attachment processes, t_N is the evolution time of disturbances in N due to changes in the ionization-recombination balance.

Note that in the lower ionosphere $t_{Te} \ll t'_N \ll t_N$. For $0 < t \leq t_{Te}$, one can easily derive the following simplified energy balance equation:

$$\frac{d\theta}{dt} = \frac{0.97e^2 E^2}{km\nu_o \theta^{5/6}} - \delta(\theta)\nu_o \theta^{5/6}(\theta - 1)T_{eo}, \quad (5)$$

where: $\theta = T_e/T_{eo}$, $\nu = \nu_o \theta^{5/6}$, $\theta(0) = 1$, $E(t < 0) = 0$. The subscript "o" is used to denote the magnitude of the ionospheric parameters in the absence of electric field variations. Equation (5) is no longer dependent on N and N^+ . It has easily been solved using basic integration techniques. Then, neglecting the transport processes, it may be used to find the solution to equations (1) and (2) with respect to N and N^+ , using the expansion of them in the t_2 - and t_3 -scales. The steady state value of the N , caused by the presence of the electric field E , is given by:

$$N_\infty = q_{io}^{1/2} \{(1 + \nu_a(\theta_\infty)/\nu_d)(\alpha_r(\theta_\infty) + \alpha_{io}\nu_a(\theta_\infty)/\nu_d)\}^{-1/2}, \quad (6)$$

where θ_∞ is the quasi-stationary solution of equation (5).

The numerical estimates of the expected changes in the main parameters of the lower ionosphere were made for $E_1 = 1$ V/m and $E_2 = 10$ V/m at the altitude of 60 km. Our calculations show that the decrease in the electric field E and the corresponding ν and N changes lead to a lowering of the ionospheric conduction contour by Δz (for instance, for the level $z = 60$ km under $E_1 = 1$ V/m, we have $\Delta z \leq 5$ km and, under $E_2 = 10$ V/m, we have $\Delta z \leq 10$ km). The main cause of this effect is the ν decrease from ν_∞ to ν_o .

Analysis. Thus, there are some reasons to suggest that during processes before an earthquake or during a nuclear accident, the near-Earth atmospheric conductivity increases, the electric field in the ionosphere decreases, and there is an inhomogeneous region with a lower altitude on the VLF wave-propagation path. In the Earth-ionosphere waveguide, the decrease in the altitude leads to an increase in the phase velocity of the waves and, hence, to a decrease in the phase delay of the signal received in the case of one-mode propagation. The estimates show that in order to match our theoretical results with those obtained experimentally, changing the ionospheric altitude by 5-10 km, the inhomogeneous region along the path should be 600-300 km, respectively. The presence of significant electric fields at the lower boundary of the ionosphere indicate that an additional source of electron heating should be taken into account while investigating a disturbed ionosphere and radio wave propagation conditions. It has been shown that the model of the interaction between the near-Earth atmosphere and the ionosphere (caused by the vertical conduction-current) clearly allows us to explain the cause of the changes in the lower ionosphere occurring before an earthquake and during accidents at a nuclear power station with radioactive releases.

Magnetic field polarimetry of seismic sources

Sergey Prosvirnin

*Institute of Radio Astronomy of National Academy of Sciences of Ukraine
Chervonopraporna Street 4, 310002 Kharkov, Ukraine
Fax: +38-0572-476506. E-mail: prosvirnin@rian.kharkov.ua*

A necessity of investigation of ULF and ELF electromagnetic emission polarization characteristics is grounded in the connection with earthquake precursor problem. The investigation method is suggested.

Introduction

Inhomogeneities in the earth crust are a necessary conditions for an earthquake precursor appearance. Deformations and micro cracks appear before a seismic gap by the reason of inhomogeneities of earth rocks. Each seismic break is unique and has its peculiarities of earthquakes and precursors [1].

Certain seismoelectric transformations appear at the time of deformations of earth crust before the earthquake, and we can detect an electromagnetic emission in a wide frequency band long before a seismic gap. Maximum of electromagnetic emission takes place in ULF and ELF bands, commonly within 0.1 Hz to 20 Hz [2].

Grounding a necessity of studying the electromagnetic emission polarization

Equivalent electromagnetic source has a large size that is approximately equal to the dimension of the area of origin of the possible earthquake. This source is appeared by deformations in the stress field along gaps. Equivalent source is determined as specific structure, which is inherent to this gap, although the currents have chaotic nature in each small volume. Preferential orientation of chaotic currents is important in ULF and ELF bands for a polarization anisotropy appearance of electromagnetic emission. Electromagnetic emission has well determined polarization characteristics that can be called a polarization signature [3].

Polarization characteristics of emission are conditioned in main by the seismic source structure. By this reason they are in average a less varying over a small time interval (minutes and hours) than amplitude variations of electromagnetic field burst. That is why polarization measurements may open a possibility to identify the field burst in some random set that is associated with one source of radiation. On the other hand the variations of polarization characteristics during a longer time interval can be interpreted as essential variations of the source structure in the earthquake origin and the stress field in this region.

Choosing the frequency range

Earth rocks are a medium that has a high conductivity. Electromagnetic radiation penetrates on the earth surface mainly in the frequency range from 0.3 Hz to 10 Hz. There are some sources of electromagnetic emission in this frequency range besides of the seismic sources. We note the main two of them. One magnetic field excitation frequency is associated with the earth rotation in the electric and magnetic environment. A dominant peak is observed in the frequency domain from about 1.2 to about 1.9 Hz [4]. Another magnetic field excitation frequency is associated with the first Shumann resonance. This resonance is dominant near 7.8 Hz. Seismogenic electromagnetic field emission has a peak commonly within 2 to 5 Hz

between the mentioned above major field peaks [4]. This frequency range choosing is worth while for a study of seismic activities.

Requirements to magnetometers

As it is known, magnetic field of geomagnetic pulsations is mainly a horizontally polarized one (H polarized). Shumann resonance electric field is Z-polarized and magnetic field is H- and D- polarized. That is why magnetic field emission sources, which have $B_z / B_H > 1$ and $B_z / B_D > 1$, can be identified as seismic field sources with large probability.

Three-component magnetometers are needed for a study of polarimetric signatures of the seismic magnetic field. Typical magnetic field level is approximately from 0.1 to 10.0 nT. It is necessary to have the sensitivity of a magnetometer near 10^{-4} nT and the dynamic range near 40 dB. The speed of information collection is estimated as 40 counts per second.

Numerical processing of data

It is necessary usual preliminary data processing. After that the goal of processing consists in deducing some polarization characteristics of magnetic field in the frequency range within 2 to 5 Hz. The first of these characteristics is the polarization degree. The polarization stage of fully polarized magnetic field component is characterized by three Stock's parameters. These four parameters can be shown as a polarimetric signature of a seismic source of magnetic field in the chosen seismic region.

Conclusion

Systematic study of electromagnetic emission polarization characteristics and its analysis can give us the possibilities to determine the practical significant polarimetry in the monitoring system of seismic activities. The polarimetric behavior of electromagnetic field then can be implemented for the earthquake hazard mitigation measures.

References

- [1] Mogi Kiyoo, Earthquake prediction. - Academic Press, Tokyo, 1985.
- [2] Boerner W-M., Lanary R., Franceschetti G., Moreira J., Keydel W., Rosen P., Rignot E., Weinman N.R., Teti J., Verdi J.S. Development of multispectral POL-SAR image interferometry and its implementation in environmental stress analysis, i.e. surface deformation, changes in vegetation parameters, etc... - Proc. of the Third Intern. Workshop on Radar Polarimetry. - Nantes, March 21-23, 1995. - Vol. 2, p. 731.
- [3] Boerner W-M., Dea J.Y., Gokhberg M.B., Fraser-Smith A.J., Varatsos P., Green A.W., Yoshino T., Bobb L.C. Ultralow frequency polarimetry in seismo electro/magnetogenic signatures analyses for the development of intermediate to short term earthquake prediction algorithm. - Proc. of the Third Intern. Workshop on Radar Polarimetry. - Nantes, March 21-23, 1995. - Vol. 1, p. 382.
- [4] Van Bise W.L., Rauscher E.A. Ambient electromagnetic fields as possible seismic and volcanic precursors. - Electromagnetic phenomena related to earthquake prediction. - Edited by Hayakawa M. and Fujinawa Y. - Terra Scientific Publishing Company, Tokyo, 1994, pp. 221-242.

Wave Impedance Technique to Derive Distance from Nearby Lightning Discharges

M.A. Korol ¹⁾, A.P. Nickolaenko ²⁾, and A.V. Shvets ²⁾

¹⁾ *Institute of Radio Astronomy, NAS of Ukraine, 4, Krasnoznamennaya st., Kharkov 310002
UKRAINE*

²⁾ *Institute of Radio Physics and Electronics, NAS of Ukraine, 12 Proskury st., Kharkov
310085, UKRAINE*

We discuss the results of application of the ELF-VLF wide-band measurement technique suggested earlier for locating the nearby lightning discharges. The measurements were performed at Singapore from the field site situated on board of the research vessel. Three field components, namely, vertical electric and two orthogonal horizontal magnetic fields, were digitally recorded and used for the analysis then. The distance from the lightning discharge was established using the characteristic frequency dependence of the complex wave impedance spectra pertinent to the nearby lightning discharges of vertical orientation (Korol et al., 1993). The method implies the frequency dependence of the transition range between the static, induction and radiation field components of the wide-band radio signal, similarly to the well-known *E-H* field technique (Ruhnke, 1971; Kononov et al., 1986). The technique suggested is distinguished by the wide-band measurements that include completely the ELF-VLF range. The horizontal Poynting vector components (Rafalsky et al., 1994) were used to find the source bearing. This technique eliminates an ambiguity in the arrival angle automatically. Simultaneously, a product of the electric and magnetic field components integrated over the pulse duration depends only on coherent portions of a signal. This particular feature allows for extraction of the linearly polarised signal, improving the output accuracy of the direction finding. The results of analysis of the atmospheric waveforms recorded agree reasonably well with the concurrent visual observations of the parent lightning discharges.

After the source coordinates were established, we used the spectra of the electric and magnetic field components to reconstruct the spectra of the particular current moments of the lightning observed. It is shown that that the experimental spectra tend to be constant within the frequency range of our studies, i.e. from 1 to 10 kHz, while the model spectra of the current moment usually applied in the range vary as f^{-1} .

REFERENCES

- Kononov, I. I., Petrenko, I. A., and Snegurov, V.S., Radio Techniques for Locating Thunderstorms. Hydrometeoizdat, Moscow, 244 pp., 1986, (in Russian).
- Korol, M. A., and Nickolaenko, A. P., A Technique to derive the distance from near discharges. *Res. Lett. Atmos. Electr.* **13**(1),1, 1993.
- Rafalsky, V. A., Nickolaenko, A. P., Shvets, A. V., and Hayakawa, M. A time-domain direction finding technique for ELF-VLF atmospherics. *J. Atmos. Electr.* **14**, 97, 1994.
- Ruhnke, L.H., Determining distance to lightning strokes from a single station. *NOAA Technical report ERL 195-APCL 16*, Boulder, Colorado, 1971.

REMOTE SENSING BY VLF USING "ABSOLUTE OMNIPAL": 1. INVESTIGATION OF THE DECAY OF SPRITE PLASMA.

R. L. Dowden, J. B. Brundell, University of Otago, Dunedin, New Zealand
C. J. Rodger, British Antarctic Survey, Cambridge, U. K.

Amplitude perturbations, or both amplitude and phase perturbations, of VLF transmissions in the Earth-ionosphere waveguide have been recorded since their discovery by Trimpi in 1963 [Helliwell *et al.*, 1973] after whom such perturbations are named. The amplitude and phase perturbations define the phasor of the perturbed signal. Vector subtraction of the unperturbed signal defines the phasor of the scattered signal [Dowden and Adams, 1988]. This scattered signal can be regarded as the wave scattered off a localized plasma anomaly beneath or extending down from the base of the ionosphere into the Earth-ionosphere waveguide like a stalactite [Dowden and Adams, 1988]. Measurement of the echo phase (phase of the perturbation phasor) simultaneously on two receivers spaced a short distance ($l/2$) apart and broadside to the VLF transmitter enables determination of the direction of arrival of the scattered signal. This can be as much as 180° from the direction of arrival of the direct signal [Dowden *et al.*, 1996a] implying a "hard" scatterer — one in which the incident wave is strongly modified — such as a bundle of highly conducting plasma columns [Rodger *et al.*, 1997].

A close relationship between such "Trimpis", whistlers and electron precipitation [Rycroft, 1973; Voss *et al.*, 1984] lead to the general acceptance that the localized plasma anomaly causing the Trimpi is produced by whistler-induced electron precipitation from the Radiation Belts.

Discovery of the "early/fast" Trimpi [Armstrong, 1983], which onsets too soon ("early") after the initiating lightning to be produced by electron precipitation and reaches full perturbation rapidly ("fast"), showed that such Trimpis are directly caused by lightning. Campaigns monitoring both optical "red sprites" and VLF early/fast Trimpis showed that nearly all sprites within about 300 km of the VLF receivers produced simultaneous early/fast Trimpis on two or more VLF transmissions [Dowden *et al.*, 1996a], showing that the luminous columns of sprites are highly conductive [Dowden *et al.*, 1996b]. Such early/fast Trimpis clearly associated with sprites are called "VLF sprites", though it may be that all early/fast Trimpis have the same cause and so indicate the presence of sprites when optical observations are not available.

Here we consider observations [Dowden *et al.*, 1997a] of very strong early/fast Trimpis or VLF sprites observed at Darwin ($12^\circ 26'S$, $130^\circ 59'E$) only 2,000 km from the US Navy transmitter, NWC ($21^\circ 48'S$, $114^\circ 9'E$). The unperturbed signal strength was about 20 mV/m during the Trimpi observations (at night). The echo amplitudes of the strong Trimpis ranged up to 8 mV/m, some 30 dB stronger than those studied previously in Colorado. The much higher signal/noise ratio enabled accurate measurements of the time variation of the amplitude and phase of the echoes. The illustrations shown at Kharkov in the oral version of this paper cannot be included here but the points made with each illustration are given below in the same order.

1. Immediately before the Trimpi only the direct wave from the transmitter is present at the receiver. Immediately the Trimpi begins, and until it decays, both the direct wave and the wave scattered by the sprite plasma are present and so interfere.

2. The result of this interference, that is, the vector sum of the direct wave and the scattered wave, is the perturbed wave which is defined by the amplitude and phase perturbation (note that both the phase and amplitude perturbations must be measured, as by OmniPAL, to define the vector perturbation). If the direct wave vector is constant, and so given by the unperturbed wave vector, and if the perturbed wave vector is measured, the scattered wave vector is easily found by vector subtraction.
3. The initial Trimpi phase and amplitude perturbations are sensitively dependent on the position of the sprite plasma, the source of the scattered wave. Thus these perturbations can be of any phase/amplitude combination: phase advance or phase retard, amplitude increase or amplitude decrease. However, if the Trimpi phase and amplitude perturbations versus time for the duration of the Trimpi are transformed to scatter wave amplitude and phase versus time, the transformed amplitude and phase variation of very different Trimpis look quite similar. In particular, the scatter wave amplitude decays as the logarithm of time. This implies that the scatter amplitude decays to zero at some time $t = t_0$.
4. This behaviour cannot apply at $t = 0$, for then the scatter amplitude would be infinite, nor for $t > t_0$ for then the scatter amplitude would be negative. However, logarithmic decay is not logically absurd between, say, $t = 1$ s and $t = t_0$. Plotting scatter amplitude on a logarithmic time scale should be strictly linear if decay (on a linear time scale) is strictly logarithmic. Tests show such a linear fit (on a logarithmic time scale) is quite good. Any departures could be attributed to unknown variation of the direct wave vector during the scatter wave decay. Such variation is probably due to other natural perturbations independent of the sprite plasma decay under investigation. If this is so, departures from strictly logarithmic decay should vary from one "VLF Sprite" event to another in a random fashion. How can we test this? A neat way is to normalise all events so that the scatter amplitude at $t = 1$ s is unity and that $\log_{10} t_0 = 1$ so that $t_0 = 10$. Then the normalised decay for all events should fit the same straight line.
5. Four events were superimposed to test this, the different events being distinguished by using different plot symbols and colours. Unfortunately, the result depends on the order of plotting because the earlier plots are overlaid by the later plots. A better test used 12 events plotted as fine line segments without plot symbols. This more clearly showed no consistent departure from logarithmic decay.
6. During the decay of the scatter amplitude, the scatter phase also varies monotonically with random error variations which increase as the scatter amplitude decreases, as expected. The total change over the typically 100-s duration of the Trimpi decay is around 90° . This Doppler shift of some 2 mHz implies movement of the scatter source either horizontally (mesospheric winds [Dowden, 1996]) or vertically (rising scatter altitude). Since the total variation is small, a linear fit is as good as a logarithmic fit. At Darwin in November the scatter phase decreased with time at a rate (Doppler shift) which was much the same from event to event. If we therefore replace the measured scatter amplitude by its best fit logarithmic decay and the measured scatter phase by its best fit Doppler shift, we can synthesise the original "pure" Trimpi perturbation cleaned of its random noise.
7. The mesosphere where sprites occur is too high for balloons and too low for satellites and so inaccessible for *in situ* measurements except by rockets for fleeting times. However, over the last decade or so, atmospheric chemists have established that the plasma decay by attachment is dominant even for sprite plasma which initially is several orders of magnitude denser than ambient. At any given altitude, the sprite plasma decays exponentially with time, but at a rate which decreases rapidly with altitude. Atmospheric chemistry shows that the decay rate is proportional to the product of [O] and [N], each of

which decreases exponentially with the scale height of about 7 km. This means that the sprite plasma decay rate decreases exponentially with altitude with a scale height of 3.5 km. The VLF reflection coefficient of sprite plasma columns remains near unity until the plasma density decays below a critical level for which VLF reflection is insignificant. At any given altitude, at the time when the plasma density has decayed to e^{-1} (37%) of its initial value, plasma at the altitude 3.5 km below will have decayed to e^{-e} (6.6%) of its initial value.

8. Thus at any given time the sprite plasma columns "appear" to the VLF wave from the transmitter as having a well defined bottom whose altitude increases with the logarithm of time, this being the inverse of exponential. The top of optically-observed sprites appears to be well defined so presumable the plasma remaining after the sprite luminosity (electrical discharge) ends has this same well-defined top. If we suppose the VLF scatter amplitude is proportional to the vertical length of the plasma "seen" by the VLF incident wave, then the scatter amplitude will decay with the logarithm of time as observed. The time $t = t_0$ is when the plasma density at the top of the sprite has fallen below critical for VLF scattering. Observed (by OmniPAL) values of t_0 over the range of about 30 s to 500 s agree with optical measurements of the altitude of the top of sprites of 75 to over 80 km.

References

- [1] Armstrong, W. C., Recent advances from studies of the Trimpi effect, *Antarctic J.*, 18, 281-283, 1983.
- [2] Dowden, R. L., Distortion of Trimpi shapes by high-altitude winds, *J. Geophys. Res.*, 101, 315-321, 1996.
- [3] Dowden, R. L., and C. D. D. Adams, Phase and amplitude perturbations on sub-ionospheric signals explained as echoes from lightning induced electron precipitation ionization patches, *J. Geophys. Res.*, 93, 11543 - 11550, 1988.
- [4] Dowden, R. L., J. B. Brundell, W. A. Lyons, and T. Nelson, Detection and location of red sprites by VLF scattering of subionospheric transmission, *Geophys. Res. Lett.*, 23, 1737-1740, 1996a.
- [5] Dowden, Richard, James Brundell, Craig Rodger, Oleg Molchanov, Walter Lyons, and Thomas Nelson, The structure of red sprites determined by VLF scattering, *IEEE Antennas and Prop. Mag.*, 38, 7-15, 1996b.
- [6] Dowden, R. L., J. B. Brundell and C. J. Rodger, Temporal evolution of very strong Trimpi observed at Darwin, Australia, *Geophys. Res. Lett.*, 24, Oct 1, 1997a.
- [7] Helliwell, R. A., J. P. Katsufakis, and M. L. Trimpi, Whistler-induced amplitude perturbation in VLF propagation, *J. Geophys. Res.*, 78, 4679, 1973.
- [8] Rodger, C. J., J. R. Wait, and R. L. Dowden, Electromagnetic scattering from a group of thin conducting cylinders, *Radio Sci.* 32, 907-912, 1997.
- [9] Rycroft, M. J., Enhanced energetic electron intensities at 100 km altitude and a whistler propagating through the plasmasphere, *Planet. Space Sci.*, 21, 239-251, 1973.
- [10] Voss H. D., W. L. Imhof, M. Walt, J. Mobilia, E. E. Gaines, J. B. Reagan, U. S. Inan, R. A. Helliwell, D. L. Carpenter, J. P. Katsufakis, and H. C. Chang, Lightning-induced electron precipitation, *Nature*, 312, 740-742, 1984.

***Time Domain
Electromagnetics***

TIME-DOMAIN NUMERICAL SIMULATION OF EM PULSE PROPAGATION THROUGH A TIME-VARYING SLAB

Igor V. Scherbatko and Alexander G. Nerukh,
*Kharkov Tech Univ. of Radio Electronics,
Lenin Ave. 14, Kharkov, 310726, Ukraine*

I. Introduction

Problems involving time-varying parameters are of interest for the purpose of investigation of electromagnetic wave propagation in ionosphere, for remote sensing of unstable objects by short electromagnetic pulses, etc. A necessity of considering such problems stems also from the investigation of ultrafast electromagnetic phenomena in semiconductor and quantum electronics. For the problem solving in the differential statement, FDTD method has gained a wide recognition. An alternative approach reduces the problem to a perturbation method [1] or integral equations [2]. Using a resolvent method for solving the obtained Volterra integral equations that characterise electromagnetic transients enables us to formulate the evolutionary recursion method [3]. In this paper, a direct numerical time-domain integral equation method is extended to the case of a dissipative dielectric whose permittivity and conductivity change arbitrarily in time.

II. Integral equation

The time-domain solution of the transient wave propagation problem relies on an integral equation technique, which has been used for pulsed EM transient problems recently [3,4]. A starting point is the integral equation for the electric flux density D in an active medium:

$$D(\tau, \xi) = \frac{1}{a^2(\tau, \xi)} D_0(\tau, \xi) - \frac{1}{2} \int_0^\infty d\tau' \frac{a^2(\tau', \xi)}{a^2(\tau, \xi)} \left\{ b(\tau', \xi) + \frac{1 - a^2(\tau', \xi)}{a^2(\tau', \xi)} \frac{\partial}{\partial \tau} \right\} \times \quad (1)$$

$$\theta(\tau - \tau') [D(\tau', \xi + \tau - \tau') + D(\tau', \xi - \tau + \tau')],$$

where ξ and τ are spatial and temporal coordinates respectively; a and b are parameters which are related to the permittivity $\varepsilon_1(\tau, \xi)$ and the conductivity $\bar{\sigma}(\tau, \xi)$, respectively, as:

$a^2(\tau, \xi) = \frac{\varepsilon}{\varepsilon_1(\tau, \xi)}$, $b(\tau, \xi) = \frac{1}{\varepsilon v \kappa} \bar{\sigma}(\tau, \xi)$. The initial values of permittivity, conductivity and electrical flux density before parameter changing are ε , $\bar{\sigma}(\tau < 0, \xi < 0) = 0$ and $D_0(\tau, \xi) = \varepsilon \bar{E}_0(\tau, \xi)$, respectively. $v = 1/\sqrt{\varepsilon \varepsilon_0 \mu_0}$ is the velocity of light in the initial medium, ε_0 , μ_0 are permittivity and permeability of vacuum, κ is the wavelength factor, $\theta(\tau)$ is the Heavyside unit function.

III. Scheme of numerical solution

For the purpose of the equation (1) numerical solution we assume a uniform grid on the coordinate plane (τ, ξ) with equal time $\Delta\tau$ and spatial $\Delta\xi$ steps: $\Delta\tau = \Delta\xi$. This equality is

met with the stability condition for the numerical analysis: $\Delta x \leq v\Delta t$. Then the integration paths in the equation (1) are straight diagonal lines, which pass through nodes of the grid.

The essence of the proposed methodology is the sequence solution of (1) by marching in time step by step. We can find the electric flux density at the specified temporary step $\tau = \tau_n$ by using solutions for previous steps. We would like to avoid the repetitive calculations of integrals that have been calculated along the covered time intervals. Hence we select from the integral in the (1) the integrals over the line segment $[0, \tau_{n-1}]$ introducing new function:

$$B_a(\tau_n, \xi_i) = \int_0^{\tau_{n-1}} \varphi_1(\tau_n, \tau', \xi_i) D(\tau', \xi_i + \tau_n - \tau') d\tau', \quad (2)$$

where $\varphi_1(\tau_n, \tau', \xi_i) = (1 - a^2(\tau', \xi_i + \tau_n - \tau'))$. This enables us to make use of previously calculated values of the integrals over preceding time layers. Since $D(\tau', \xi_i + \tau_n - \tau') = D(\tau', \xi_{i+4} + \tau_{n-4} - \tau')$, then, according to (2), we have the recursive relation:

$$B_a(\tau_n, \xi_i) = B_a(\tau_{n-4}, \xi_{i+4}) + \int_{\tau_{n-5}}^{\tau_{n-1}} \varphi_1(\tau_n, \tau', \xi_i) D(\tau', \xi_i + \tau_n - \tau') d\tau'. \quad (3)$$

On introducing in the same manner the functions: $B_b(\tau_n, \xi_i)$, $B_c(\tau_n, \xi_i)$ and $B_d(\tau_n, \xi_i)$ we can obtain the following equation [4]:

$$D(\tau_n, \xi_i) = D_0(\tau_n, \xi_i) - \frac{1}{2} \left\{ \frac{\partial}{\partial \xi} (B_a(\tau_n, \xi_i) - B_b(\tau_n, \xi_i)) + (B_c(\tau_n, \xi_i) + B_d(\tau_n, \xi_i)) \right\} + \quad (4)$$

$$+ o(\Delta \tau),$$

where $o(\Delta \tau)$ is the contribution of the integral (1) over the segment $[\tau_{n-1}, \tau_n]$ into the electric flux density $D(\tau_n, \xi_i)$. Here it is assumed that this contribution can be neglected. Under such an assumption, we derive a formula for the calculation of the field $D(\tau_n, \xi_i)$ through the mediation of the calculated values of this function on preceding time layers. Depending on the desired observation time period, a simulation run on a Pentium PC with 16 MB of RAM takes from 1 to 10 min. For the case listed below the grid spacing was selected uniform as $\Delta \tau = \Delta \xi = 0.015$.

IV. Discussion of numerical examples

In order to present a visual illustration of developed numerical technique we consider a one-dimension problem of propagation of a TEM square pulse: $D_0(\tau, \xi) = \theta(\tau - \xi + 2) - \theta(\tau - \xi + 1)$ through the dielectric slab with time-varying permittivity and conductivity (parameters a and b respectively). Spatial-temporal distribution of electric flux magnitude is presented in Fig.1. Before $\tau = 1$, when permittivity of the medium ε is still constant and conductivity equals zero ($a=1$ and $b=0$, respectively), the pulse propagates in the positive direction without perturbation. When $\tau = 1$, the permittivity of the slab (medium with $\xi \geq 0$) becomes 1.7 times greater than initial one and the conductivity appears ($a=0.6$ and $b=0.01$, respectively). The pulse transforms into two opposite-propagating pulses. They are well recognisable in Fig.1. The magnitude of backscattered pulse is negative because $a < 0$. The backscattered pulse is incident to the boundary of slab, passes it through and is partially

reflected back. In Fig. 1 this is shown as the third trace which follows in the positive direction from the boundary (dotted line at $\xi = 0$). The different angles of traces correspond to the several

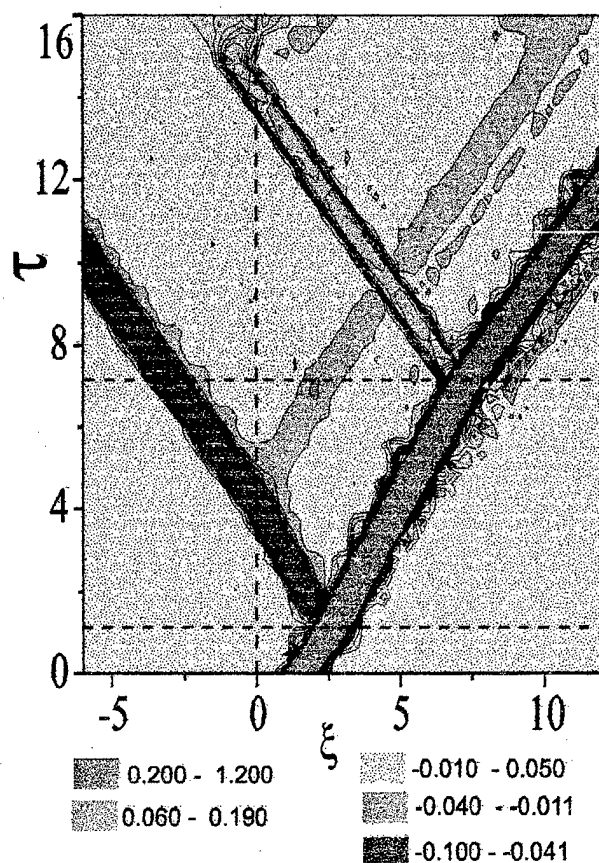


Fig. 1

permittivity and conductivity is presented. This field is described by the time-domain two dimensional Volterra integral equation of the second kind. The algorithm is based on the discrete time scheme and does not impose restrictions on the signal shape and duration, as well as on the time behaviour of the medium parameters. The influence of a jump in the medium parameters on electromagnetic square pulse transformation is shown.

velocities of pulses due to medium parameters changing. The second jump of the medium parameters to initial values appears when $\tau=7$, and then the difference between the left and right half-spaces vanishes. This leads to the splitting all the located in the slab pulses into forward- and back-scattered ones. The results presented here are in a good-agreement with those obtained by the analytical resolvent method [3].

Direct time-domain solution of the integral equation (4) accumulates numerical errors during the time of observation. That is why the last-time distribution of field suffers from "noise". The rough scaling of the level-plot hampers the fine recognition of all details of propagating pulses.

V. Conclusions

An evolutionary algorithm for direct numerical calculation of a nonstationary electromagnetic field in an active (gain or lossy) medium with time-varying

References

1. Harfoush, F.A. and A. Taflov, "Scattering of electromagnetic waves by a material half-space with a time-varying conductivity", IEEE Trans. on Ant. and Prop., V.39, 7, pp. 898, 1991.
2. Pao, H.-Y., S.L. Dvorak and D.G. Dudley, "An accurate and efficient analysis for transient plane waves obliquely incident on a conductive half space", IEEE Trans. on Antennas and Propag., Vol. 44, 7, pp. 918-932, 1996.
3. A.G. Nerukh, and I.Yu. Shavorikina, "Splitting of electromagnetic impulse under a conductivity jump of restricted medium", J. Tehnich. Fisiki, Vol. 62, 5, pp. 108-118, 1992 (in Russian).
4. A.G. Nerukh, I.V. Scherbatko, and O.N. Rybin, "The Direct Numerical Calculation of an Integral Volterra Equation for an Electromagnetic Signal in a Time-Varying Dissipative Medium", J. Electromagn. Waves and Applications, Vol.12, pp.163-176, 1998.

RADIATION OF A LONG CONDUCTOR EXCITED BY A SHORT PULSE

Yu. I. Buyanov, V. I. Koshelev, V. V. Plisko

High Current Electronics Institute RAS
4, Akademicheskoy ave., 634055 Tomsk, Russia
e-mail: koshelev@hcei.tomsk.su

During recent years a great number of papers devoted to the investigation of nonstationary radiation of wire antennas were published, but most of them have a theoretical character. In the well-known experimental works electromagnetic field was radiated and registered near a metal surface. To use ultrawideband (UWB) impulse signals in practical aims, it is required to radiate and receive signals in free space. The study of peculiarities of UWB impulse signal radiation and receiving was carried out taking as an example a long conductor disposed perpendicularly to a metal plate as the most simple for investigation.

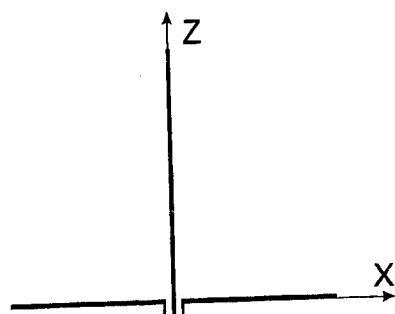


Fig. 1.

For this aim an experimental setup presenting a 1.64-m long and 10-mm diameter conductor installed perpendicularly to a 1.8-m diameter metal plate has been created (Fig. 1). Electrical field was registered by means of a specially developed receiving antenna on the basis of a biconical vibrator having a dimension $2l = 15$ cm with nonuniformity of an amplitude-frequency characteristic in a 400-1200 MHz range no more than ± 3 dB. To excite the conductor, a 2-ns long bipolar pulse was used (Fig. 2a). The choice of a bipolar pulse is conditioned by its sufficiently wide frequency band and absence of a constant constituent in the spectrum.

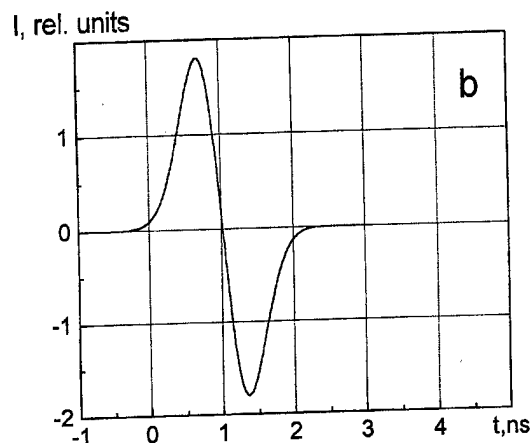
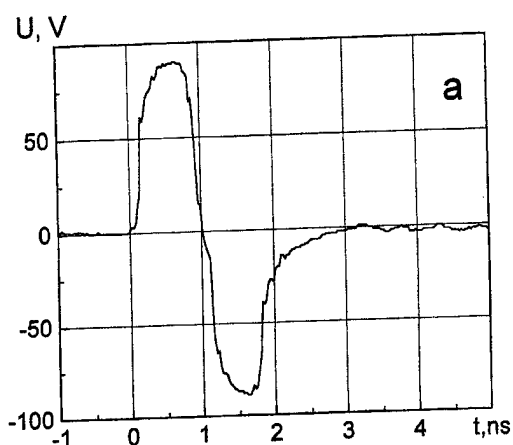


Fig. 2.

At numerical simulation the metal plate was substituted for a system of radially divergent conductors of a corresponding length. The conductors were perfectly conducting. A bipolar pulse was simulated by means of a derivative in time from a gaussoid (Fig. 2b). For numerical calculations of ultrawideband signal radiation a program has been developed on the basis of expression for electromagnetic field of the conductors excited by the given current [1]:

$$\vec{E}(\vec{r}, t) = \frac{1}{4\pi\epsilon_0} \int \left\{ \frac{3(\vec{q}\vec{R})\vec{R} - \vec{q}(\vec{R}\vec{R})}{R^5} + \frac{3(\vec{j}\vec{R})\vec{R} - \vec{j}(\vec{R}\vec{R})}{cR^4} + \frac{(\vec{j}'\vec{R})\vec{R} - \vec{j}'(\vec{R}\vec{R})}{c^2R^3} \right\} dl,$$

where \vec{j} and \vec{j}' are the current and its derivative in time, respectively, $\vec{R} = \vec{r} - \vec{r}'$ is the distance from the conductor surface point to the observation point, $\vec{q}(t) = \int_0^t \vec{j}(t') dt'$, ϵ_0 is the dielectric constant, c is the velocity of light in vacuum.

The obtained simulation results were compared with the results of calculations with application of the program WIRES [2]. Fig. 3 presents the calculation results of the E_z -field component for the point $x = 0.7$ m and $z = 0.84$ m made by means of our program (dashed line) and program WIRES (solid line). The difference in the delays between the first and second pulses is due to the difference of velocities of current pulse propagation along the conductor. In our program this velocity was taken to be equal to the light velocity in vacuum.

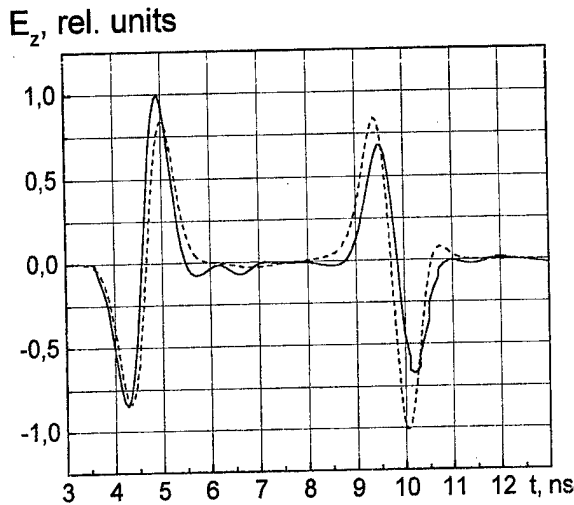


Fig. 3.

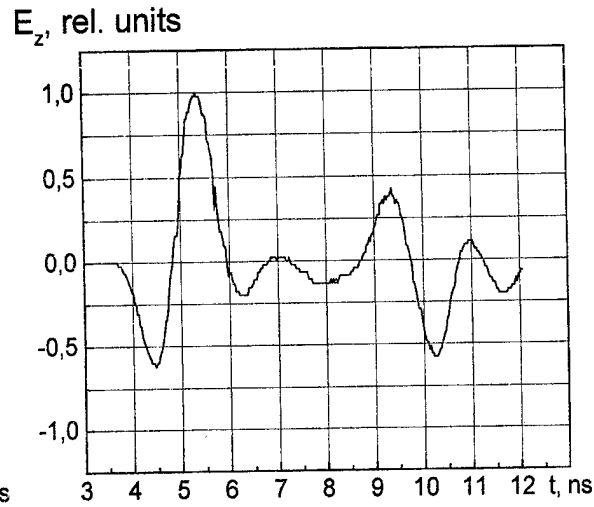


Fig. 4.

In the experiment a z -component of electrical field was measured. For comparison, Fig. 4 presents the field oscillogram in the point $x = 0.7$ m, $z = 0.84$ m. As is follows from the calculations by the program WIRES and from the experiments, the amplitude of the second pulse radiated by the linear conductor end is less than the amplitude of the first one. The difference of the calculations by our program and by WIRES (Fig. 3) is related to the fact that in the first case the conductor diameter is not taken into account and in the second case the conductor diameter is 10 mm. Fig. 5 presents the results of calculation (dashed line) and measurements (solid line) for the point $x = 0.45$ m, $z = 0.08$ m. Theoretical (dashed line) and experimental (solid line) dependencies of maximal ratio of the second and first pulse half-periods on the coordinate z for the $x = 0.45$ m are presented in Fig. 6. The difference in the curves can be explained by the finite frequency band of a receiving antenna and the difference of exciting pulses in the experiment and calculation (Fig. 2).

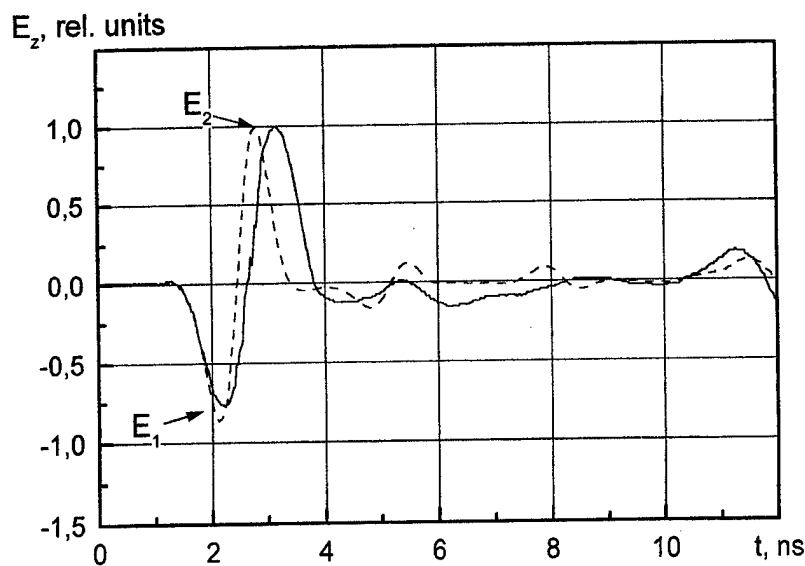


Fig. 5.

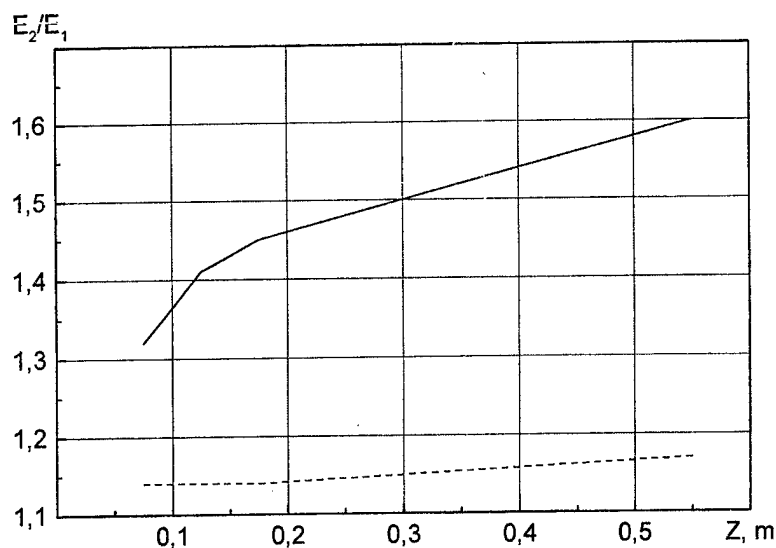


Fig. 6.

As it follows from the obtained results, the main contribution into the radiated field give the currents at the conductor ends and radiation from the plane plate edge can be neglected.

References

1. R. Gomez, J. A. Morente and A. R. Bretones "An approximate analysis of radiation from linear antennas." *Int. J. Electronics*, v.61, №3, pp.343-353, 1986.
2. V. M. Lugovtsov. "Spline-collocation method for numerical analysis of nonstationary electromagnetic radiation and scattering of thin-wired structures." *Radiotekh. Elektron.*, v.38, №9, pp. 1559-1569, 1993.

PULSE SIGNAL SCATTERING BY OBJECT LOCATED NEAR THE EARTH SURFACE

O. I. Sukharevsky, S. A. Gorelyshev, A. V. Muzychenko

Kharkov Military University, Maidan Svobody 6, Kharkov 310043, Ukraine
Tel. +380-(572)-450096

Mathematical simulation of a pulse signal scattering by an object placed above a dielectric media boundary (Fig. 1), for example, air-to-earth interface, is of interest for a number of electromagnetic and radar problems.

Using the Lorenz lemma in the different space regions and combining these results, we can obtain the integral representation for the field scattered by the object S in the direction \vec{R}^0 under a monochromatic illumination:

$$j\omega \vec{p} \left(\vec{E}(\vec{R}^0) - \vec{E}(\vec{R}^0) \right) = \int_S \vec{E}_T(\vec{x}|\vec{R}^0, \vec{p}) \vec{H}_\perp(\vec{x}) d\vec{s} \quad (1)$$

Here $\vec{E}(\vec{x}|\vec{R}^0, \vec{p})$ is the field generated by the plane wave propagating in the $(-\vec{R}^0)$ direction in the presence of only the half-space V^+ (i.e., in the absence of scatterer S); $\vec{E}(\vec{R}^0)$, $\vec{E}(\vec{R}^0)$ are the back scattering patterns of considered structure in the presence and absence of scatterer S , respectively.

The field $\vec{E}(\vec{R}^0)$ scattered in the $(-\vec{R}^0)$ direction can be approximated by zero in the case of oblique (to L) incidence of the plane wave. Finally, considering the phase shifts caused by the reflection from the boundary L , equation (1) can be rewritten as follows:

$$\vec{p} \vec{E}(\vec{R}^0) = -j \frac{\exp(jk_0|x_0|)}{4\pi|x_0|} k_0 \sqrt{\frac{\mu_0}{\epsilon_0}} \times \\ \times \int_S \left[\vec{p} \exp(-jk_0(\vec{R}^0 \cdot \vec{x})) + \vec{p}^1 \exp(-jk_0((\vec{R}^0 - \vec{R}^1) \cdot \vec{x} + \vec{R}^1 \cdot \vec{x})) \right] \times \vec{H}_\perp(\vec{x}) d\vec{s} \quad (2)$$

where $\vec{R}^1 = \vec{R}^0 - 2\vec{n}(\vec{R}^0 \cdot \vec{n})$; \vec{p}^1 is the polarization vector of the plane wave reflected by boundary L , $\vec{n} = \vec{x} - \frac{(\vec{x} \cdot \vec{n}) + h}{(\vec{R}^1 \cdot \vec{n})} \vec{R}^1$; h is the distance from the plane of L to the origin of coordinates associated with object S ; \vec{n} is normal unit vector to boundary L .

Function $\vec{H}_\perp(\vec{x})$ is the surface current density on S generated by the plane wave propagating in the $(-\vec{R}^0)$ direction due to the boundary L of the half-space V^+ . The existence of media interface L leads to the fact that both the wave reflected from L and that propagating in the $(-\vec{R}^1)$ direction are incident together on the object S surface. Therefore, two mutually intersecting (in general case) "lighted regions" S_1 , S_2 regions are present on the object surface (Fig.1). In this case, on using the Physical Optics approach for the surface

current density on S and the known connection (by means of the Fourier-transform) between the object response to the temporal δ -function and the object frequency-domain characteristics (i.e., a response to monochromatic illumination), we can obtain the transient characteristic of the object (response to step-function):

$$\begin{aligned} \hat{E}(t) = & \int_{\Gamma_{11}(t)} \frac{A_0(\vec{x})}{\sqrt{1 - (\vec{R}^0 \cdot \vec{n})^2}} dl + \int_{\Gamma_{12}(t)} \frac{A_1(\vec{x})}{\sqrt{1 - \left(\frac{(\vec{R}^0 + \vec{R}^1) \cdot \vec{n}}{|\vec{R}^0 + \vec{R}^1|} \right)^2}} dl + \\ & + \int_{\Gamma_{21}(t)} \frac{B_0(\vec{x})}{\sqrt{1 - (\vec{R}^1 \cdot \vec{n})^2}} dl + \int_{\Gamma_{22}(t)} \frac{B_1(\vec{x})}{\sqrt{1 - \left(\frac{(\vec{R}^0 + \vec{R}^1) \cdot \vec{n}}{|\vec{R}^0 + \vec{R}^1|} \right)^2}} dl, \end{aligned} \quad (3)$$

where $\Gamma_{ij}(t)$ are the integration contours, i.e., the intersection lines of the "lighted regions" S_1, S_2 and the planes determined by different combinations of vectors \vec{R}^0, \vec{R}^1 , $A_i(\vec{x}), B_i(\vec{x})$ ($i=0,1$) are the functions depending on the mutual configuration of scatterer S , media interface L , and illumination direction and polarization vector of the incident wave.

Thus, the calculation of the transient characteristic $\hat{E}(t)$ of an object near media boundary is reduced to the computation of four integrals. By using the expression for the probing signal $\Omega(t)$, (due to its entire-function character), we can obtain the expression for the response to the pulse probing as follows:

$$\tilde{E}(t) = \int_0^T \Omega'(s) \hat{E}(t-s) ds, \quad (4)$$

where $T = \min\{\tau_u, t\}$, τ_u is the duration of signal $\Omega(t)$.

The proposed approximate method of calculation of back-scattering from perfectly conducting objects near a media boundary can be efficiently applied in the analysis of complicated shape objects, provided that object dimensions are noticeably greater than the signal duration (as measured in the "light" distance units).

When performing numerical studies, a video pulse

$$\Omega(t) = \exp(-t^2 / \tau_u^2) \quad (5)$$

with duration $\tau_u = 1$ ns was chosen as a probing signal. As a result, a number of dependences (on time), of the normalized magnetic-field density in different model illumination conditions and a horizontal polarization of the incident plane wave have been obtained. These results are presented in Figs.2 to 5. The following parameters were taken for the lower half-space: $\varepsilon = 7$, $\mu = 1$. The pulse signal responses at the height of the sphere lower point above the surface, $L = 0,5$ m, for $\theta = 45^\circ$ and $\theta = 15^\circ$, respectively, are shown in Figs.2 and 3. Responses in the case that the sphere touches the L plane, for $\theta = 45^\circ$ and $\theta = 15^\circ$, are shown in Figs.4 and 5, respectively.

In all figures the time (in nanoseconds) is counter along the horizontal axis. The relative response, $2\pi r \times 10 \vec{p} \tilde{E}(t)$, where r is the distance to observation point, \vec{p} is the horizontal polarization unit vector of receiving antenna, is counted along the vertical axis.

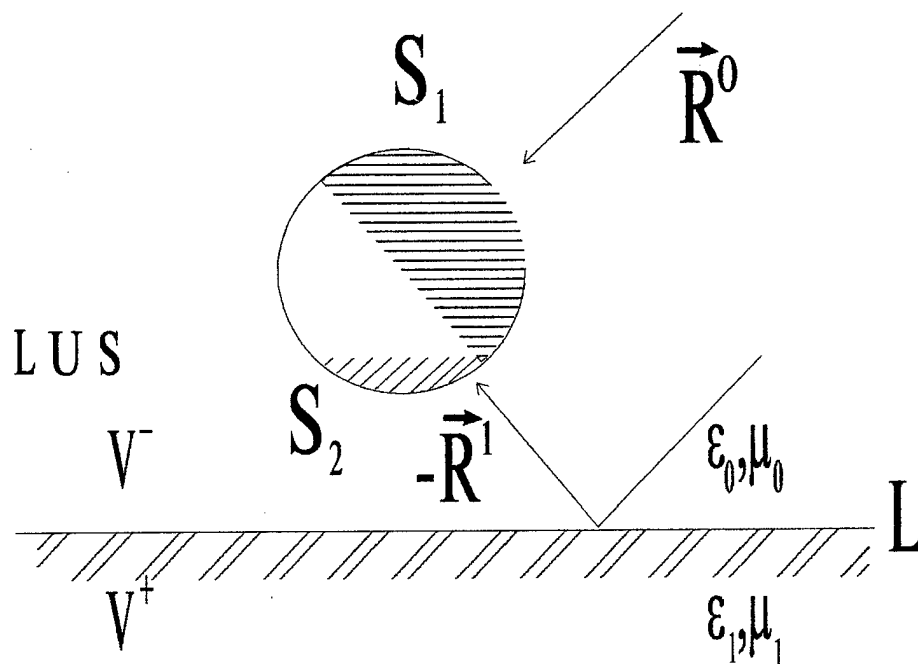


Fig. 1

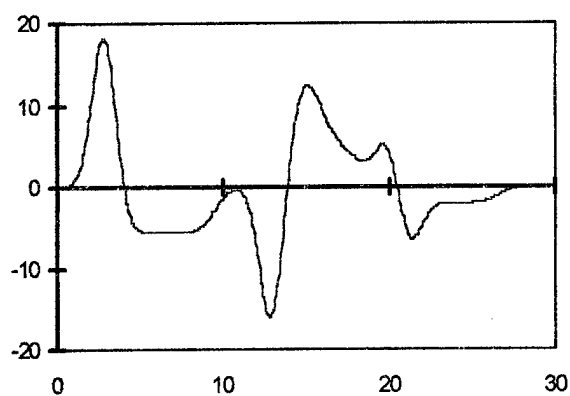


Fig. 2.

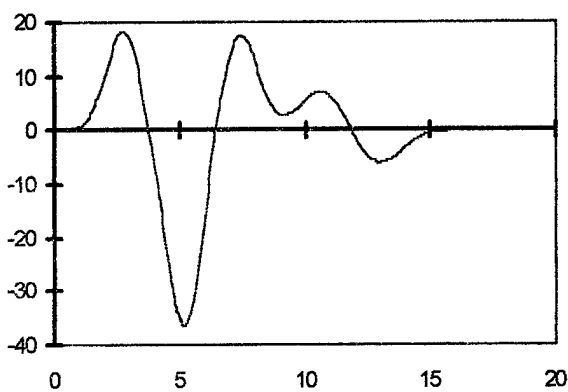


Fig. 3

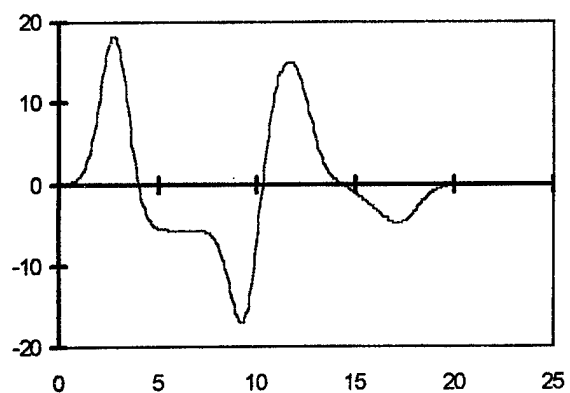


Fig. 4.

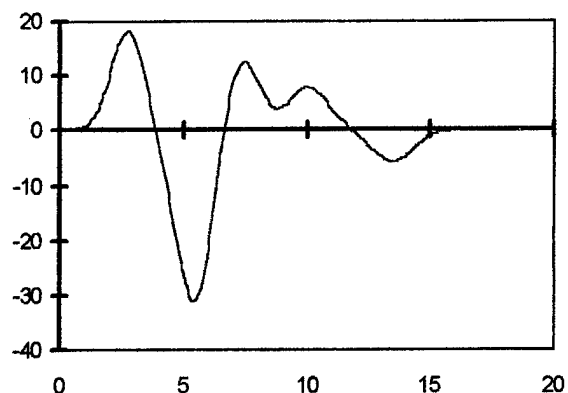


Fig. 5

References

1. R. King, G. Smith, *Antennas in Material Media*, Moscow: Mir Publ., 1984 (Russian transl).

CONSTRUCTION OF BESSEL-TYPE BEAMLIKE SOLUTIONS TO THE MAXWELL EQUATIONS

Victor V. Borisov

Institute of Physics, St. Petersburg University, St. Petersburg, Russia

1. The aim of this report is to construct the transient solutions to Maxwell's equations describing the Bessel type beamlike TM waves in free space. We suppose that the current pulse of special transverse and angular distributions belongs to a plane that is at rest or starts its motion with a constant velocity v at the fixed moment of time. The explicit solutions of the initial-value problem are the transient beamlike modes of the cylindric coordinates system. We discuss peculiarities of these solutions, which describe both transient and steady-state waves. In the previous communications, the beamlike solutions: a scalar steady-state wave [1] and a transient electromagnetic wave of TE type [2] produced by immovable sources, were obtained for the modes of order zero only.

2. At first, we obtain the explicit solution of the scalar problem

$$\nabla^2 \psi - \frac{\partial^2}{\partial \tau^2} \psi = \frac{4\pi}{c} j; \quad \psi = j = 0, \tau < 0. \quad (1)$$

Here $\tau = tc$ is the time variable, c denotes the velocity of light. We suppose that the source of the wave perturbation in the cylindric coordinates ρ, φ, z is given by

$$j = h(\tau) \delta(z - \beta\tau) f(\tau) \exp(im\varphi) J_m(a\rho), \quad \beta = v/c, \quad (2)$$

where $h(z)$ is the Heaviside function, $\delta(x)$ is the Dirac function, $J_m(a\rho)$ is the Bessel function of the first kind, m is an integer, and $a > 0$ is a constant.

Separating the variables φ, ρ and using the Riemann formula, we obtain the solution of the problem (1), (2) in the form

$$\psi = \psi_m = \frac{e^{im\varphi} J_m(a\rho)}{c\sqrt{1-\beta^2}} \int_0^T d\tau' f\left(\frac{\tau'}{\sqrt{1-\beta^2}}\right) J_0\left(a\sqrt{(\tau_\beta - \tau')^2 - z_\beta^2}\right) = e^{im\varphi} J_m(a\rho) \Phi(z_\beta, \tau_\beta), \quad (3)$$

where $\tau_\beta = (1 - \beta^2)^{-1/2}(\tau - \beta z)$, $z_\beta = (1 - \beta^2)^{-1/2}(z - \beta\tau)$, $T = \tau_\beta - z_\beta$ if $z_\beta > 0$, and $T = \tau_\beta + z_\beta$ if $z_\beta < 0$. One can interpret the wavefunctions ψ_m as beamlike modes in cylindrical coordinates having the same profiles for arbitrary time-dependence of the source. It should be noted that the function Φ is a solution of the telegraph equation in 1-D space. Hence, the time-longitudinal structure of the above modes is similar to both the transient plane waves in collisionless plasma and transient guided waves. In particular case of the time dependence $f(\tau) = e^{ik\tau}$ (k is a constant), one can represent Φ by means of Lommel's functions of two variables $U_n(w, z)$ or $V_n(w, z)$ (see [2] for extended consideration).

3. Now express the components of the TM electromagnetic field vectors \vec{E} and \vec{B} via the Bromvich-Borgnis potential Π

$$E_\rho = \frac{\partial^2 \Pi}{\partial \rho \partial z}, E_\varphi = \frac{1}{\rho} \frac{\partial^2 \Pi}{\partial z \partial \varphi}, E_z = \frac{\partial^2 \Pi}{\partial z^2} - \frac{\partial^2 \Pi}{\partial \tau^2}, B_\rho = \frac{1}{\rho} \frac{\partial^2 \Pi}{\partial \varphi \partial \tau}, B_\varphi = -\frac{\partial^2 \Pi}{\partial \rho \partial \tau}, B_z = 0. \quad (4)$$

Then Maxwell's equations together with the initial conditions $\vec{E} = \vec{B} = 0$, $\tau < 0$ yield the scalar problem (1) where $\psi = \frac{\partial \Pi}{\partial \tau}$ and j is the non-zero component of the current density vector $\vec{j} = \vec{e}_z j_z$. Therefore the solution (3) permits us to obtain the components of the magnetic induction vector \vec{B} by differentiating the wavefunction ψ_m with respect to the variables φ or ρ . To calculate the components of the electric field strength, one should integrate solution (3) with respect to the time variable.

4. Consider the limiting case of the current pulse which travels with the velocity of light. When $z_\beta < 0$ and $\beta = 1$ we have from expression (3)

$$\psi_m = \frac{1}{2c} e^{im\varphi} J_m(a\rho) \int_0^{\tau+z} ds f(s/2) J_0\left(a\sqrt{(\tau-z)(\tau+z-s)}\right) = e^{im\varphi} J_m(a\rho) \Phi(\tau, z), \tau \pm z > 0. \quad (5)$$

In the particular case of $f(\tau) = e^{k\tau}$, one gets

$$\Phi(\tau, z) = (1/c k) [U_1(w, z) + iU_2(w, z)], \quad (6)$$

where $w = k(\tau + z)$, and $z = a\sqrt{\tau^2 - z^2}$. We rewrite the above expression using the functions $V_n(w, z)$ [3] as

$$\Phi = (1/c k) \left[e^{\frac{1}{2}(k(\tau+z) + \frac{a^2}{k}(\tau-z)) - \frac{\pi}{2}} + V_1(w, z) + iV_0(w, z) \right] \quad (7)$$

and supposing that $\frac{w}{z} = \frac{k}{a} \sqrt{\frac{\tau+z}{\tau-z}} \gg 1$ obtain the steady-state wavefunctions

$$\psi_m \simeq \frac{1}{ck} e^{im\varphi} J_m(a\rho) e^{\frac{k^2+a^2}{2k}\tau + \frac{k^2-a^2}{2k}z - \frac{\pi}{2}} \quad (8)$$

The condition $\frac{w}{z} > 1$ determines the space-time domain where the steady-state waves exist. Hence the boundary of the above domain is

$$z = \beta_0 \tau, \quad \beta_0 = (a^2 - k^2)(a^2 + k^2)^{-1}, \quad (9)$$

where $\beta_0 > 0$ if $a^2 > k^2$ and $\beta_0 < 0$ when $a^2 < k^2$. It is easy to verify that the equation $\tilde{k}^2 = (\tilde{\omega}/c)^2 - a^2$, where $\tilde{\omega}$ denotes a frequency and \tilde{k} denotes a value of wave-vector, is satisfied if $\tilde{\omega}c = (k^2 + a^2)/(2k)$ and $\tilde{k} = (k^2 - a^2)/(2k)$ or $\tilde{\omega}/c = k$ and $\tilde{k} = \sqrt{k^2 - a^2}$. It should be noted that we do not obtain the localized wave structures of Brittingham's type in the case of a source moving with the velocity of light.

5. Let us discuss the axisymmetric solution of the wave equation (1) for the Gaussian transverse distribution of the immovable source

$$j = (1/2\pi) \delta(z) f(\tau) \exp(-\rho^2/a^2) \quad \tau > 0, j = 0 \quad \tau < 0. \quad (10)$$

One can verify that the function

$$\psi = \frac{1}{ca^2} e^{-\frac{\rho^2 - z^2}{a^2}} \int_0^{\tau-z} d\tau' f(\tau') e^{-\frac{(\tau-\tau')^2}{a^2}} I_0 \left(\frac{2\rho}{a^2} \sqrt{(\tau-\tau')^2 - z^2} \right) \quad (11)$$

is a solution of the problem (1) and (10) in the space domain $z > 0$. Here $I_0(z)$ is the modified Bessel function of the first kind. One can see that the transverse distribution of the above wavefunction has, in general case, a variable profile. Changing the function $\delta(z)$ in (10) to $\delta(\tau - z)$, we obtain the source moving with velocity of light. In this case the solution of the scalar problem (1) describes Brittingham's focus wave mode formation if $f(\tau) = e^{ik\tau}$ (see [4]).

Acknowledgement. This research became possible in part due to the Grant 96-02-17166 from the Russian Foundation for Fundamental Research.

References

- [1] J. Durnin, Exact solution for nondiffracting beams. I. The scalar theory. *J. Opt. Soc. Am. A*, Vol. A 4, no 4, 1987, pp. 651-654.
- [2] V. V. Borisov, *Nonsteady-State Electromagnetic Waves*, Leningrad: Univ. Press, 1987 (in Russian).
- [3] G. N. Watson, *Theory of Bessel Functions*, Cambridge Univ. Press, Cambridge, 1945.
- [4] V. V. Borisov, A. B. Utkin, On formation of focus wave modes, *J. Phys. A: Math. Gen.*, Vol. 27, 1994, p. 2587.

EVOLUTIONARY BASIS AND OPERATORS OF TRANSFORMATION OF NON-STATIONARY WAVES IN PERIODIC STRUCTURES

Andrey O. Perov

Institute of Radiophysics and Electronics of National Academy of Sciences
12 Ac. Proscura str., Kharkov 310085, Ukraine

A new approach to solution of model problems of the linear non-stationary theory of gratings is presented. Its foundation is formed by the operator method in the space of "evolutionary" bases of non-stationary signals.

Development of the spectral theory of gratings [1] made it possible to clarify the basic directions of analysis within the time domain. The problem of development of both the mathematical models adequate to situations dealt with and numerical-analytical methods of their realization has become a high priority one. The proposed method of solution of this problem is based on the description of the scattering properties of periodic structures in terms of the operators of transformation, the latter being qualitatively identical for all the regular sections of the Floquet channel of the "evolutionary" basis of the non-stationary wave.

Consider a model initial-boundary problem (see Fig. 1)

$$\begin{cases} \left[-\varepsilon(g) \frac{\partial^2}{\partial t^2} - \sigma(g) \frac{\partial}{\partial t} + \frac{\partial^2}{\partial z^2} + \frac{\partial^2}{\partial y^2} \right] [U(g, t)] = F(g, t), \quad t > 0, \quad g = \{y, z\} \in Q \\ U(g, t)|_{t=0} = \varphi(g), \quad \frac{\partial}{\partial t} U(g, t)|_{t=0} = \Psi(g); \\ M[U(g, t)]|_{g \in S} = 0, \quad U \left\{ \frac{\partial U}{\partial y} \right\} (2\pi, z, t) = \exp(i\Phi 2\pi) U \left\{ \frac{\partial U}{\partial y} \right\} (0, z, t), \quad t > 0 \end{cases} \quad (1)$$

assuming that the functions $F(g, t)$, $\varphi(g)$, $\Psi(g)$, $\varepsilon(g) - 1$, $\sigma(g)$, which are finite in the domain $Q = R \setminus \overline{\text{int } S}$, $R = \{g \in R^2: 0 < y < 2\pi, |z| < \infty\}$, satisfy the conditions of the theorem of unique solvability of (1) within the $W_2^1(Q^T)$, $Q^T = Q \times (0, T)$, $T < \infty$ energy class (Sobolev space) [2]. Here: M is either an identical operator in the E-polarization case of $U(y, z, t) = E_x$, $H_x = E_y = E_z = 0$, or an operator of differentiation along the outer normal to S in the H-case of $U = H_x$, $E_x = H_y = H_z = 0$; S is the boundary of perfectly conducting grating generatrices at the period $0 \leq y \leq 2\pi$, R^2 is the plane of variables y, z ; $g = \{y, z\}$; Φ is a real parameter of the Floquet channel R ; real-value functions $\varepsilon(g) \geq 1$ and $\sigma(g)$ determine the influence of the Floquet channel nonuniformity on the velocity of propagation of perturbation and on its dissipative characteristics; $\overline{\text{int } S}$ is the closure of domains in R filled by metal (i.e., the section of the grating metal generatrices by a plane $x = \text{const}$).

In the specific case of a Floquet channel that is regular on the whole length R ($\text{int } S = \emptyset$; $\varepsilon(g) - 1 = \sigma(g) \equiv 0$), we shall present the solution as an expansion

$$U(g, t) = \sum_n v_n(z, t) \mu_n(y), \quad g \in Q, \quad t > 0, \quad (2)$$

in terms of the system of eigenfunctions $\mu_n(y) = \exp(i\lambda_n y) \cdot (2\pi)^{-1/2}$, $\lambda_n = n + \Phi$, $n \in \{n\} = 0, \pm 1, \dots$ of the homogeneous boundary problem produced by (1) after separation of the lateral coordinate y .

The expansion coefficients $v_n(z, t) = G(\lambda_n) * f_n$ can be obtained as a convolution of functions $G(\lambda_n; z, t) = (-1/2)\chi(t - |z|) J_0[\lambda_n(t^2 - z^2)^{1/2}]$ and $f_n(z, t) = a_n(z, t) - \delta^{(1)}(t) \cdot b_n(z) - \delta(t) \cdot c_n(z)$; here $a_n(z, t)$, $b_n(z)$ and $c_n(z)$ are the Fourier coefficients of $F(g, t)$, $\phi(g)$ and $\psi(g)$ functions, respectively, when the latter functions are series-expanded in terms of the basic system $\{\mu_n(y)\}_n$; $\chi(\dots)$ is Heaviside's function; $\delta^{(m)}(\dots)$ is the generalized derivative of the order of m of the delta-function; $J_m(\dots)$ is the Bessel function.

Expansion (2) gives both the general and the particular (corresponding to the given sources) form of the field of a non-stationary wave propagating in the regular Floquet channel. Its change both in space and in time is completely determined by the system of functions $v(z, t) = \{v_n(z, t)\}_n$, the properties of which justify its role of the universal "evolutionary basis" of non-stationary wave in any finite regular (containing neither sources nor discontinuities) piece of the strip R .

Suppose now that a wave of the type (2) is exciting an open periodic resonator shown in Fig. 1.

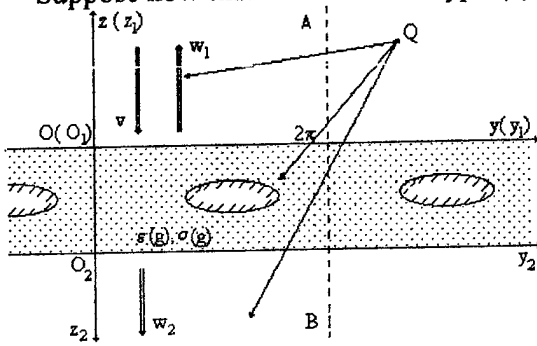


Fig. 1

$$\text{Excitation field } U^i(g, t) = \sum_n v_n(z, t) \mu_n(y)$$

we consider to be non-zero only in the reflection zone A with $z_1 > 0$ (the upper boundary of the discontinuity of the Floquet channel R is located in $z_1 = 0$ plane). We present the secondary field arising both in the reflection zone (A) and in transmission one (B), propagating in the positive directions of z_1 and z_2 , as

$$U_j^s(g, t) = \sum_n w_{nj}(z_j, t) \mu_n(y), \quad z_j \geq 0, j=1,2. \quad (3)$$

Further we introduce, by expressions

$$w'_{nj}(0, t) \equiv \frac{\partial}{\partial z_j} w_{nj}(z_j, t) \Big|_{z_j=0} = \int_0^t \sum_m [R_{nm}^{AA}(t-\tau) \delta_j^1 + T_{nm}^{BA}(t-\tau) \delta_j^2] v_m(0, \tau) d\tau, \quad j=1,2; n, m=0, \pm 1, \dots, \quad (4)$$

the boundary values (on the boundary $z_j = 0$ of the discontinuity of the channel R) of the operator of transformation of the evolutionary basis of a non-stationary wave coming from the upper half space (from the region A):

$$w'_j(0, t) \equiv \{w'_{nj}(0, t)\}_n = [R^{AA} \cdot \delta_j^1 + T^{BA} \cdot \delta_j^2] v(0, \tau); \quad j=1,2. \quad (5)$$

It is obvious that together with the expressions [3]

$$w_{nj}(z_j, t) = - \int_0^t J_0[\lambda_n((t-\tau)^2 - z_j^2)^{1/2}] \chi[(t-\tau) - z_j] w'_{nj}(0, \tau) d\tau, \quad z_j \geq 0, \quad j=1,2, \quad (6)$$

specifying the diagonal operators $E^A(z_1)$ and $E^B(z_2)$:

$$w_j(z_j, t) \equiv \{w_{nj}(z_j, t)\}_n = [E^A(z_1) \delta_j^1 + E^B(z_2) \delta_j^2] w'_j(0, \tau) \quad z_j \geq 0, j=1,2, \quad (7)$$

monitoring the field changes during a "free" run of wave over a finite distance in the regular section of the channel R , the operators R^{AA} and T^{BA} completely characterize all the scattering properties of the grating under its quasiperiodic excitation from the halfspace A.

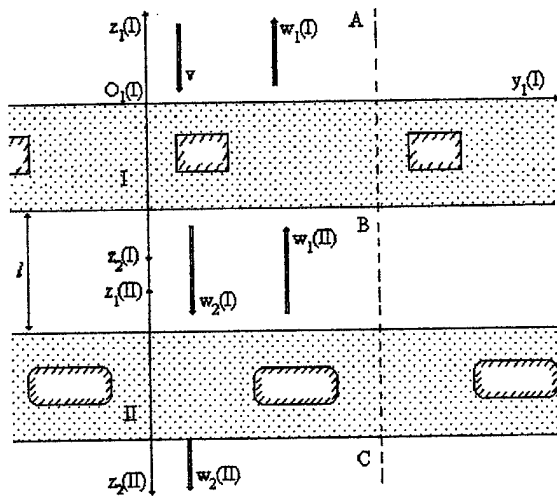


Fig. 2

By determining, as is the case with R^{AA} and T^{BA} , the transformation operators R^{BB} and T^{AB} of the evolutionary basis of the non-stationary wave coming from the halfspace region B, at the boundary $z_2 = 0$, and considering such operator sets to be known for individual elementary gratings, we develop an algorithm of solution of the problem arising in the analysis of the scattering properties of the complex structure containing those gratings. In the model situation shown in Fig.2, the structure contains two 2π -periodic gratings I and II located one above another in parallel planes. The gratings are connected through the Floquet channel B having a finite length ℓ .

Keeping the same notations as accepted before (the obvious changes are caused by presence of two different gratings I and II) and following notations (3) - (7), we obtain (see Fig. 2, $w'_j(I) = \partial / \partial z_j(I) w_j(z_j(I), t)|_{z_j(I)=0}$, and similarly for $w'_j(II)$):

$$\begin{cases} w'_1(I) = R^{AA}(I)[v] + T^{AB}(I)E^B(\ell)[w'_1(II)]; & w'_1(II) = R^{BB}(II)E^B(\ell)[w'_2(I)]; \\ w'_2(I) = R^{BA}(I)[v] + R^{BB}(I)E^B(\ell)[w'_1(II)]; & w'_2(II) = T^{CB}(II)E^B(\ell)[w'_2(I)]. \end{cases} \quad (8)$$

By the method of elimination, system (8) is reduced to the operator equation of the second kind with respect to the unknown vector-function $w'_2(I)$:

$$w'_2(I) = T^{BA}(I)[v] + R^{BB}(I)E^B(\ell)R^{BB}(II)E^B(\ell)[w'_2(I)], \quad (9)$$

and to the transformation formula determining all the components of the field formed by the structure.

The initial "complex" problem has been converted to a form admitting a direct inversion. The operator in the right hand part of (9), because of the finite velocity of propagation of perturbations, influences the unknown vector-functions $w'_2(I)$ having values relating only to the time moments previous to the calculated one. The "complex" grating is reduced to the category of elementary ones after calculation of elements of the boundary operators according to (4) and (5).

The model situations considered above demonstrate practically all the basic features of the proposed method at the stages both of description of the scattering properties of gratings in terms of boundary transformation operators and of construction of algorithms of the analysis of complex periodic structures.

1. V.P. Shestopalov, Yu.K. Sirenko, Dynamic theory of gratings, Kiev: Naukova dumka, 1989.
2. O.A. Ladyzhenskaya, Boundary problems of mathematical physics, Moscow: Nauka, 1973.
3. Yu.K. Sirenko, V.P. Shestopalov, N.P. Yashina, New methods of the dynamic linear theory of open waveguide resonators, J. Comput. Math. and Mathem. Physics, 1997, Vol 37, № 7, pp. 869-877.

Transient Analysis of Transmission Lines with Time-dependent Terminations and General Input

Ahmad Cheldavi: Iran University of science & Technology, Narmak, Tehran, 16844, Iran, Fax: +98-21-7454055 , Tel: +98-21-7808022
E-mail: cheldavi@ece.ut.ac.ir

Abstract

In this paper an exact time-domain solution for wave equation in lossless TEM transmission lines with time-dependent boundary conditions in the input and output terminals will be presented.

First a mathematical closed form time-domain solution for the wave equation in lossless TEM transmissions lines subject to arbitrary terminations will be presented, then this general solution will be specialized for some time dependent resistive terminations.

Foundamentals of transient analysis of transmission lines with random inputs such as white noise also was considered in this paper briefly. in the latter situation the results are in the form of some statistical parameters, such as, correlation function, mean, variance and spectral density of the voltage or current stochastic processes, in the line as a function of time and distance.

1- Introduction

Time dependent loads especially loads with sinusoidal variations are very important in engineering and modelling the actual behaviour of some physical phenomena. moreover when the parameters of the input to the line is not completely known, then frequency domain methods fail to solve such more complicated problem exactly. so we will use the time domain approach to solve such problem.

2- Mathematical Tools

The main problem is shown in fig.(1)

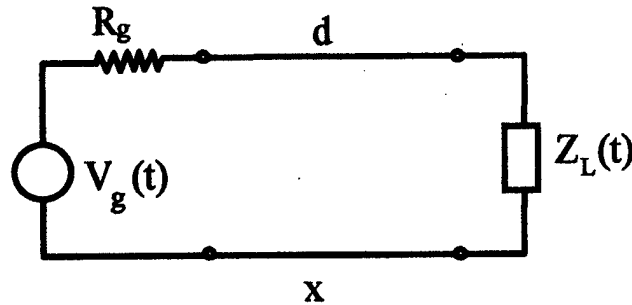


Fig.(1)

Time domain exact solution for the voltage wave propagation in this line, using dallamber solution is, [1]:

$$v(x,t) = M \sum_{m=0}^{\infty} K_g^m V_g(t - x/u - 2md/u) \prod_{k=L}^m K_L[t - x/u - (2k-1)d/u] \\ + M \sum_{m=1}^L K_g^{m-1} V_g(t + x/u - 2md/u) \prod_{k=0}^m K_L[t - x/u - (2k-1)d/u] \quad (1)$$

in which v , K_g and K_L are velocity of the wave and reflection coefficients in the source and load terminals, respectively.

$$K_g = \frac{R_g - R_0}{R_g + R_0}, \quad M = \frac{R_0}{R_g + R_0}, \quad K_L(t) = \frac{Z_L(t) - Z_0}{Z_L(t) + Z_0} \quad (2)$$

3- Statistical Results

If the input to the line is a stationary white noise with mean M_y and correlation function $R_y(\tau)$, the steady state voltage mean and correlation function as a function of time and distance will be (for $Z_L(t) = R_L$):

$$m_v(x,t) = \frac{R_L}{R_L + R_0} m_y \quad (3)$$

$$R_{vv}(x,t) = M^2(1 + K_L^2) R_y(\tau) + K_L[R_y(\tau - 2(x-d)/u) \\ + R_y(\tau + 2(x-d)/u)] \quad (4)$$

4- Sinosoidal Load Termination

Here we present two examples for the sinusoidal load terminations.

Figure (2) shows the voltages in the middle of a 20m length line with $Z_0 = 50$, $R_g = 150$, $V_g(t) = \text{Sin}[(2\pi \times 10^6)t] U(t)$ and $Z_L(t) = 20 + 10 \text{Cos}[(2\pi \times 10^6)t]$.

Figure (3) shows the voltages in the middle of the same line, but with unit step input, and the load is $Z_L(t) = 50 + 50 \text{Cos}[(2\pi \times 10^6)t]$.

5- Reference

A.Cheldavi, H.Oraizi, and M.Kamarei; "Time Domain Analysis of Teransmiton Lines" proc. of. 25th EuMC, Bologna, Italy, Sep. 1995

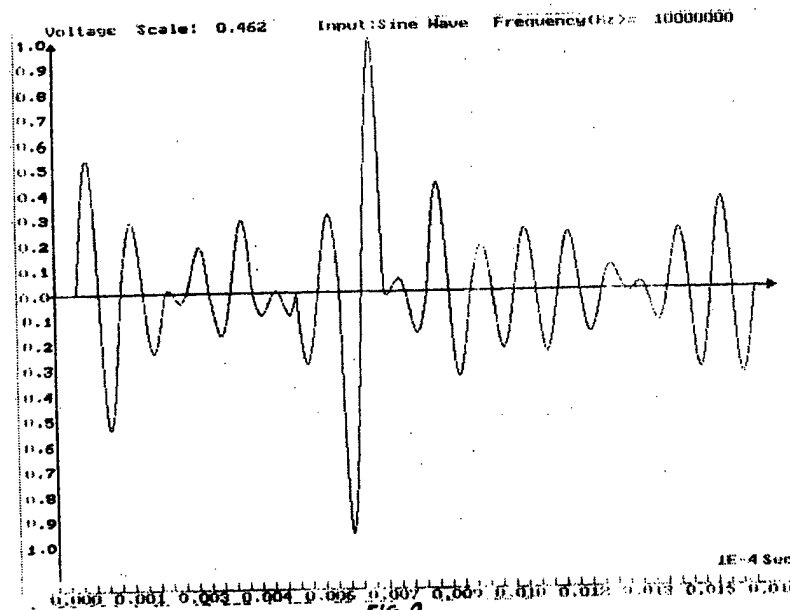


FIG. 2

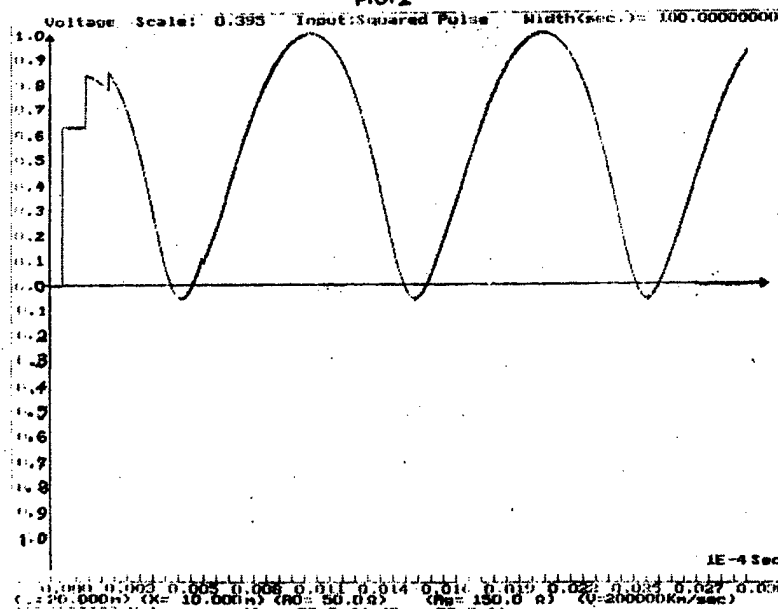


FIG. 3

FDTD METHOD IN PROBLEMS OF PENETRATION OF TRANSIENT FIELDS OF ELECTROSTATIC DISCHARGE INTO A CAVITY

P. Shubitidze, R. Jobava, R. Zaridze, D. Karkashadze, R. Beria, D. Pommerenke,** S. Frei*

Laboratory of Applied Electrodynamics, Tbilisi State University 3 Chavchavadze Ave.,
Tbilisi, 380028, Georgia, Tel & Fax: +995 32 290845, e-mail: lae@resonan.ge;

*Technical University of Berlin, Germany

**Hewlett Packard, Roseville, USA

Abstract - FDTD (Finite Difference Time Domain) method is a well-known method for numerical solution of Electromagnetic Compatibility (EMC) problems. In this paper this method is used to calculate the shielding efficiency (SE) of enclosure with aperture. Transient fields related to indirect Electrostatic Discharge (ESD) are used as incident fields to investigate EMC problem of aperture penetration into cavities.

Metallic shields are commonly used to protect the equipment, sensitive electronic parts of which can be disturbed or even destroyed by transient EM fields. Practical shielding enclosures always contain many apertures such as vents, cable feed-through and seams that allow electromagnetic energy to couple into the structure. This paper presents a numerical study of the coupling of transient fields radiated due to Electrostatic Discharge (ESD) into the metallic enclosure with aperture. Computer simulation of ESD is done using a full-wave Method of Moments in time domain for discharging bodies of revolution located near the ground plane [1-4]. For a discharging structure shaped as spheroid that can be considered as a model of human-hand related ESD, calculated arc currents and fields were compared with experimental data and showed a sufficient for EMC applications accuracy of the developed technique [1-4]. Such realistic fields are used in this paper as incident fields to investigate aperture penetration into cavities. Time domain analysis has been done by using FDTD method.

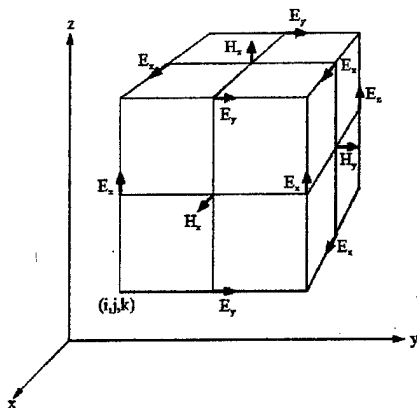


Fig.1. Node structures FDTD cell after Yee [5].

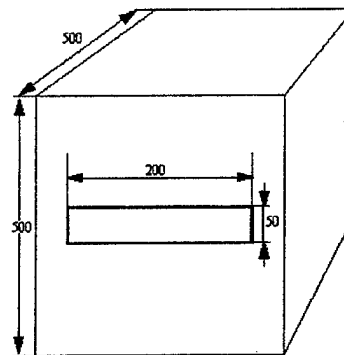


Fig. 2. Configuration of the shielding enclosure.
(All dimensions in mm)

We describe here briefly the FDTD algorithm. It is based on the discretization of the Maxwell equations according to the field component definition illustrated in Fig. 1. For instance, consider the magnetic field components normal to the face of the cubic cell and discrete coordinates $i, j + \frac{1}{2}, k + \frac{1}{2}$ and time $n + \frac{1}{2}$. By using a central difference of the time and space derivatives, it can be updated from its value at the previous time step and from the

electric field components located at the edges of the face at the previous time step, in the following manner:

$$H_x^{n+\frac{1}{2}}(i, j+\frac{1}{2}, k+\frac{1}{2}) = H_x^{n-\frac{1}{2}}(i, j+\frac{1}{2}, k+\frac{1}{2}) - \frac{\Delta t}{\mu_0 \Delta} \left[(E_z^n(i, j+1, k+\frac{1}{2}) - E_z^n(i, j+1, k+\frac{1}{2})) - (E_x^n(i, j+\frac{1}{2}, k+1) - E_x^n(i, j+\frac{1}{2}, k)) \right]$$

where Δ and Δt are the space and time steps, respectively. Similar recursive formula can be established for the remaining field components [5]. To ensure numerical stability, time and space steps have to satisfy the stability criterion (cubic cell): $\frac{\Delta}{\Delta t} \geq \sqrt{3}c$, where c is the light velocity of the medium. The modeled and experimentally measured enclosures are based on cubic metallic box (Fig.2) with reconfigurable front panel. Here we will limit ourselves to some results for the cylinders with rectangular aperture cut in the center of the front panel. The configuration is excited by the plane wave having the same time dependence and magnitude as a transient field of ESD at some distance from the discharging body.

In all calculations below, a metallic spheroid of semi-axes $a=31$ cm and $b=5$ cm is chosen as a discharging object. Spheroid is charged to some voltage denoted as V . Discharge occurs at a distance h from the plane. Fig. 3 shows radiated electric fields for two different cases: a) $V=5$ kV, $h=0.7$ mm; b) $V=10$ kV, $h=1.0$ mm. Observation point is located at the ground plane. The distance to the point of observation from the location of arc is 1m.

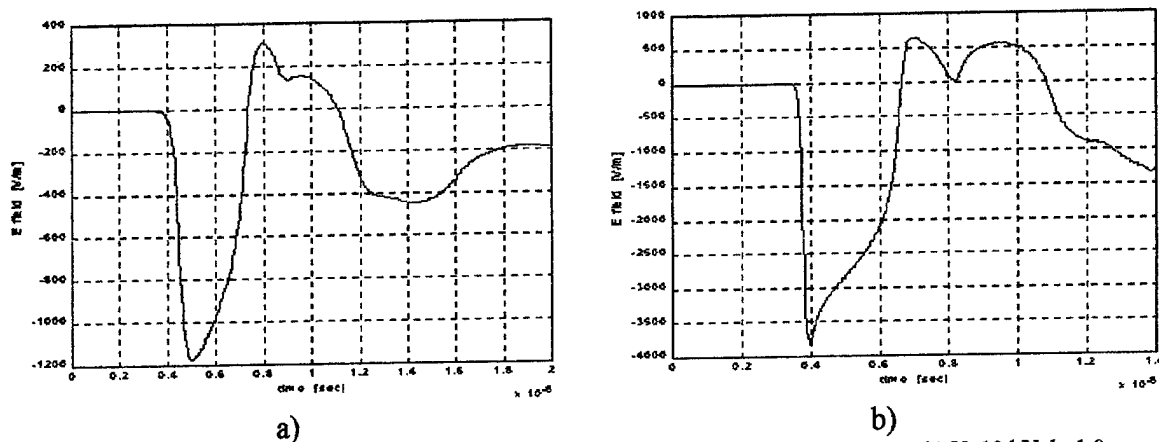


Fig.3. E-field radiated by ESD from spheroid 0.31m and 0.05m semi-axes: a) $V=5$ kV, $h=0.7$ mm; b) $V=10$ kV, $h=1.0$ mm.

We estimate the shielding efficiency of the cavity as a maximum of field inside the cavity normalized to the incident pulse. Characteristic time duration of the ESD fields from the described above geometry dictates the low-frequency scenario of aperture penetration. To investigate the characteristic behavior of ESD fields penetrated into aperture, we calculate aperture penetration of the fields of ESD into infinite perfectly conducting cylinders with rectangular cross sections. The code described above determines the complete electromagnetic field in the space surrounding the cylinder for all time moments of interest. This massive of information can be used to obtain a better insight in the field coupling phenomena. For this purpose we present the field portraits in Fig. 4.

These portraits show the electric field in the space near and inside the cylinder for different moments of time. In Fig. 4, for the moment $ct=2.815$ m the incident pulse approached to the cylinder and the energy began to penetrate via the aperture. The next portrait shows a cylindrical wave inside the cavity with the center located at the aperture. This field propagates

with a small reflection from the walls. Reflection can be detected via curvatures seen after the first peak in the pulse inside the cavity. At $ct=3.75$ one can see the moment when field reaches the right wall of the cylinder. After this, the field begins reflecting from the wall and focusing at some points. As the aperture is quite wide, the incident field is penetrating inside, and all the portraits in Fig. 4 can be explained by considering the pulse propagation inside the cavity. After some time we can expect to see resonant fields inside the cavity.

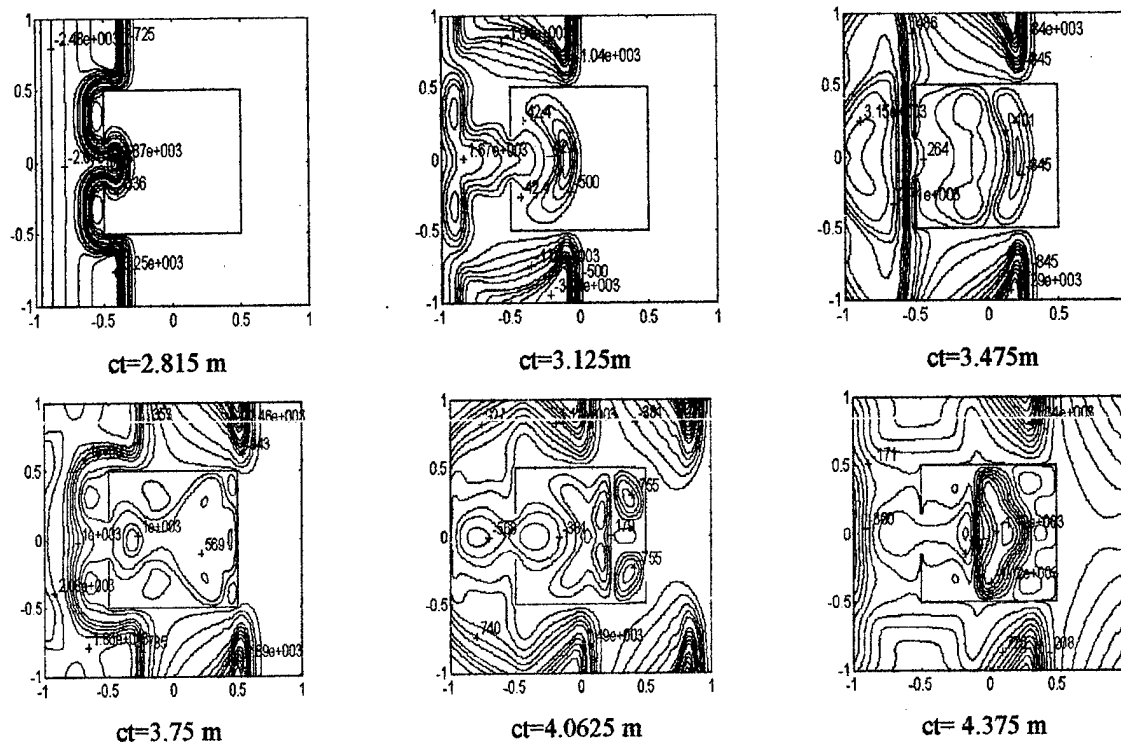


Fig. 4. Time-history of the field inside the cavity. Width of sides of cylinder 1m. Size of rectangular aperture: 0.3m
Incident field is radiated by ESD from 90° (5 kV, 0.7 mm).

These results show that time-domain analysis has its own peculiarities that should be considered carefully from the physical point of view. In the future work our attention will be focused on the investigation of transient field coupling in the cavities having different shapes. Different kind of ESD events (voltages, arc lengths) will be also considered.

We want to thank the Volkswagen Foundation for sponsoring this work.

REFERENCES:

1. R. Zaridze, D.Karkashadze, R.Jobava, D. Pommerenke, M.Aidam. Calculation and Measurement of Transient Fields from Voluminous Object, *EOS/ESD Symp.Proc.*, Phoenix, 1995, pp. 261-266.
2. R.Zaridze, D.Karkashadze, R.Jobava, D. Pommerenke, M.Aidam. "Numerical Calculation and Measurement of Transient Fields from Electrostatic Discharge ", *IEEE Trans. Components, Packaging Manuf. Technology*, Part C: Manufacturing, Vol. 19, No. 3, July 1996, pp 178-183.
3. R.Jobava, D.Karkashadze, R.Zaridze, P.Shubitidze, D.Pommerenke, M.Aidam, "Numerical Calculation of ESD". *Proc. EOS/ESD Symposium*, Orlando, 1996, pp. 203-210.
4. R.Jobava, D.Karkashadze, P.Shubitidze, R.Zaridze, G.Bit-Babic, D.Pommerenke, M.Aidam. "Computer Simulation of ESD", *Proc. EMC Symposium*, Zurich, 1997.
5. K.S. Yee, "Numerical solution of initial value problems involving Maxwell's equations in isotropic media". *IEEE Transactions on Antennas and Propagation*, vol. AP-14, pp.302-307, May 1966.

Arbitrary Signal Radiation of Coaxial Waveguide Aperture

Alexander N. Dumin, Oleg A. Tretyakov

Kharkov State University, Svobody Sq.4., Kharkov, 310077Ukraine,
e-mail: Alexander.N.Dumin@univer.kharkov.ua, otret@edu16.kharkov.ua

Abstract. A transient field radiation of the coaxial waveguide aperture is considered. The approach used is based on the Evolutionary Equations Method in the case of electromagnetic waves propagation in free space. Three-dimensional problem is solved analytically in time domain by means of the Separation of Variables Technique. The results are illustrated by numerical simulation.

Introduction. The application of superwideband signals shows promise for the development of communication systems. In parallel with the classical approach to the problems of transient signal radiation, the analytical methods in time domain attract particular interest because of their clarity from the energy and information standpoint. A technique of this sort is the Modal Basis method, which was intended originally as the procedure of solving the electromagnetic problems in resonators [1] and waveguides [2] filled with nonhomogeneous-layered nonlinear medium.

The essence of the method is a construction of coordinate basis in the cross section plane and an expansion of the transversal field components in terms of the eigen functions of this basis. Unknown expansion coefficients can be evaluated from the set of evolutionary equations that can be recast into three independent partial differential equations, of which two Klein-Gordon equations in longitudinal field components govern independent propagation of the H- and E-waves. The third wave equation describes propagation of the TEM-waves in the waveguides with multiply connected cross-section contour. These equations can be solved in the time domain by the separation of variables method or the Green's function technique, according to which transversal component amplitudes are found by differentiation of the obtained solution with respect to time or longitudinal coordinate.

This approach has been applied to the transient field radiation problems [3]. The self-adjointness of the matrix operators constructed in the plane of cross-section is ensured by the boundary conditions on the perfectly conducting metal in the case of interior problem, whereas the self-adjointness of the same operators in the case of exterior problem is provided by the condition of radiation. The former case is characterized by the discrete spectrum of eigen values while the latter case is marked by the continuous spectrum of eigen values. In response to the change-over from discrete spectrum to the continuous one, the eigenfunctions are modified and the problem solution is an integral of modes over spectral parameter from 0 to ∞ rather than a sum of modes. The problem of unknown evolutionary coefficients evaluation is basically the same except for the transversal wavenumber not being a constant but an integration variable.

The Statement of the Problem. Let a TEM-wave with an arbitrary time dependence propagates in the direction of increasing the longitudinal coordinate z in the semi-infinite coaxial waveguide with the outer radius R and the inner one r . According to [2], electromagnetic field in the interior of the waveguide is presented as

$$\vec{E} = \vec{\rho}^0 \left(\mu_0 / \rho \ln \frac{r}{R} \right) \frac{\partial}{\partial t} I(ct - z); \quad \vec{H} = \vec{\varphi}^0 \left(-1 / \rho \ln \frac{r}{R} \right) \frac{\partial}{\partial z} I(ct - z), \quad (1)$$

where $I(\cdot)$ is an arbitrary function which defines the time dependence.

Suppose that coaxial waveguide has an open end with infinite flange in the cross section at $z = 0$. We use the free-space electromagnetic field expansion in terms of the Modal Basis from [3] in the absence of currents and charge sources:

$$\begin{aligned}\bar{E}(\rho, \varphi, z, t) &= -\sum_{m=0}^{\infty} \int_0^{\infty} d\chi [\nabla \psi_m \times \bar{z}^0] \mu_0 \frac{\partial}{\partial t} h_m + \sum_{n=0}^{\infty} \int_0^{\infty} d\xi \nabla \phi_n \frac{\partial}{\partial z} e_n; \\ \bar{H}(\rho, \varphi, z, t) &= \sum_{m=0}^{\infty} \int_0^{\infty} d\chi \nabla \psi_m \frac{\partial}{\partial z} h_m - \sum_{n=0}^{\infty} \int_0^{\infty} d\xi [\bar{z}^0 \times \nabla \phi_n] \epsilon_0 \frac{\partial}{\partial t} e_n; \\ H_z(\rho, \varphi, z, t) &= \sum_{m=0}^{\infty} \int_0^{\infty} \chi^2 d\chi \psi_m h_m; \quad E_z(\rho, \varphi, z, t) = \sum_{n=0}^{\infty} \int_0^{\infty} \xi^2 d\xi \phi_n e_n,\end{aligned}\quad (2)$$

where the functions $\psi_m(\rho, \varphi; \chi) = J_m(\chi \rho) e^{im\varphi} / \sqrt{\chi}$ and $\phi_n(\rho, \varphi; \xi) = J_n(\xi \rho) e^{in\varphi} / \sqrt{\xi}$ determine the field distribution in the cross section, $J_\nu(\cdot)$ is the Bessel function of order ν , h_m and e_n are the evolutionary coefficients to be found, which must obey the equations

$$\left\{ \frac{1}{c^2} \frac{\partial^2}{\partial t^2} - \frac{\partial^2}{\partial z^2} + \chi^2 \right\} h_m(z, t; \chi) = 0; \quad \left\{ \frac{1}{c^2} \frac{\partial^2}{\partial t^2} - \frac{\partial^2}{\partial z^2} + \xi^2 \right\} e_n(z, t; \xi) = 0.$$

One should match together all the field components at $z = 0$ and make sure that the H-wave radiation is absent, since $h_m(z, t; \chi) \equiv 0$. The boundary and initial conditions on the Klein-Gordon equation solution are of the form:

$$e(z, t; \xi)|_{z=\infty} = 0; \quad \frac{\partial}{\partial z} e(z, t; \xi)|_{z=0} = \left(\mu_0 [J_0(\xi r) - J_0(\xi R)] \frac{\partial}{\partial t} I(ct - z)|_{z=0} \right) / \ln \frac{r}{R} \sqrt{\xi}; \quad (3)$$

$$e(z, t; \xi)|_{t=0} = 0; \quad \frac{\partial}{\partial t} e(z, t; \xi)|_{t=0} = 0,$$

where $e(z, t; \xi) \equiv e_0(z, t; \xi)$ because $e_n(z, t; \xi) \equiv 0$ at $n \neq 0$ by virtue of axial symmetry. We impose the first condition implying that the field amplitude equals to zero at infinity. It will be desirable to specify the function $I(ct - z)$ in the following manner:

$$I(ct - z) = \begin{cases} ct - z, & ct - z \geq 0; \\ 0, & ct - z < 0. \end{cases}$$

Hence, the time-dependence of electric and magnetic fields at the waveguide open end has the step shape given by expressions (1).

If we set up the problem

$$\left\{ \frac{1}{c^2} \frac{\partial^2}{\partial t^2} - \frac{\partial^2}{\partial z^2} + \xi^2 \right\} B(z, t; \xi) = 0$$

for the new function $B(z, t; \xi) = \frac{\partial}{\partial z} e(z, t; \xi)$ with the boundary condition

$B(z, t; \xi)|_{z=0} = C(\xi)H(t)$, where $C(\xi) = (c\mu_0 [J_0(\xi r) - J_0(\xi R)]) / \ln \frac{r}{R} \sqrt{\xi}$, $H(t)$ is Heaviside's function, we can write immediately the solution:

$$B(z, t; \xi) = C(\xi) \left\{ J_0 \left(\xi \sqrt{c^2 t^2 - z^2} \right) + 2 \sum_{m=1}^{\infty} \left(\frac{ct - z}{ct + z} \right)^m J_{2m} \left(\xi \sqrt{c^2 t^2 - z^2} \right) \right\},$$

which was obtained by means of separation of variables method in [4]. With the other

conditions (3) we find the evolutionary coefficient

$$a(z, t; \xi) = (-2C(\xi)/\xi) \sum_{m=0}^{\infty} \left(\frac{ct - z}{ct + z} \right)^{m+\frac{1}{2}} J_{2m+1} \left(\xi \sqrt{c^2 t^2 - z^2} \right). \quad (4)$$

One can draw on formula 2.12.42.2 [5] to find transversal field components of \vec{H} and \vec{E} from (2) by using the first term of the series (4) that yields a leading contribution to the electromagnetic field at great z and t . Precise values of the field strength are obtained from (2) by the numerical integration with respect to ξ .

Numerical Illustrations. The time and angle dependences of the transversal electric field strength are depicted in Figure 1 ($r = 0.5$ m, $R = 1$ m). The time scale is given in the units of (ct) . The distance between the centre of the waveguide open end and the observation points equals to 10 m. Transversal field components are approximately proportional to each other at the chosen observation distances. The dependence of the signal energy in the sector of $0^\circ - 10^\circ$ on the distance is illustrated in Figure 2. The energy in a fixed sector becomes constant starting from some distance, but the longer this distance the more part of the energy concentrated near the axis OZ .

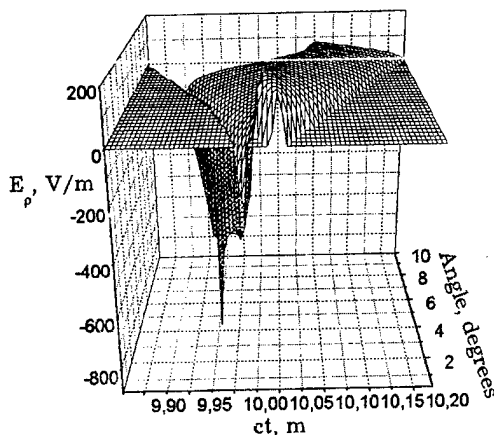


Fig.1. Time and angular dependence of the transversal electric field component.

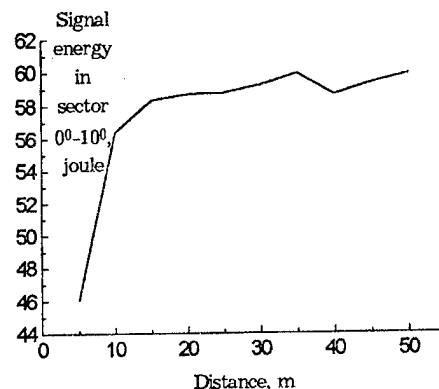


Fig.2. Signal energy in the sector of $0^\circ - 10^\circ$ at different distances.

Conclusions. Transient signal radiation of the coaxial waveguide aperture has certain features of electromagnetic missile. These are: anomalous slowly decreasing amplitudes of field and considerable concentration of the signal energy near the longitudinal axis OZ . A uniform distribution of the field at the aperture is obviously not needed for electromagnetic missile radiation. The main condition for the radiation of such a signal is infinitely fast jump in the time-dependence of a source.

References. [1] O.A. Tretyakov, "Modal Basis Method", Radiotekhnika i elektronika, v.31, N6, pp.1071-1082, 1986 (in Russian).

[2] O.A. Tretyakov, "Waveguide Evolutionary Equations", Radiotekhnika i elektronika, v.34, N5, pp.917-926, 1989 (in Russian).

[3] A.N.Dumin, O.A.Tretyakov, "Radiation of Arbitrary Signals by Plane Disk", Conf. Proc. MMET'96, Lviv, Ukraine, pp.248-251.

[4] S.Nikitskiy, O.Tretyakov, K.Yemelyanov, "An Arbitrary Signal Propagation in Waveguides", Conf. Proc. MMET'96, Lviv, Ukraine, pp.260-263.

[5] A.P. Prudnikov, Yu.A.Brychkov, O.I.Marichev, Integrals and series, Special functions, Moscow, Nauka, 1983.

SOME EXACT SOLUTIONS FOR ELECTROMAGNETIC FIELD IN MEDIA WITH DIFFERENT TYPES OF TRANSIENT CONDUCTIVITY

Irena Yu.Vorgul

*Applied Electrodynamics Chair, Kharkov State University,
4 Svoboda Sq., Kharkov, 310077 Ukraine, e-mail: ira@unicom.kharkov.ua*

Abstract. Electromagnetic field transformation in the media with continuously time-varying conductivity is studied by solving Volterra integral equation for the field. Exact solutions for the fields are obtained for a continuous temporal variation of the medium conductivity from one constant value to another, and for time-splashing conductivity. Their analytical and numerical analysis shows features of wave splitting on the non-abrupt temporal step of conductivity for the former case, and spatial field re-distribution for the latter one.

Investigation of electromagnetic field behaviour in transient media started from the simplest but fundamental case of abrupt temporal change of media parameters [1-2]. It has been shown for different media that the time jump of media parameters leads to electromagnetic wave splitting onto direct and inverse ones [1-3]. Only a few works dealt with continuous temporal changes of environmental parameters, as such the ones by F.A.Harfoush and A.Taflov [4] for harmonic time-dependence and by A.Nerukh [5] for an approximation of continuous change by a sequence of abrupt ones. In these works the problems usually were solved numerically or approximately and only a few types of continuous dependences were considered.

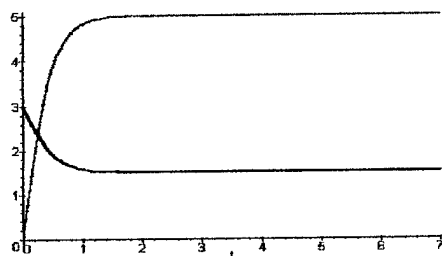
In the presented work we consider electromagnetic field transformation for two cases of the conductivity continuous time dependences. The first is the conductivity changing continuously from one constant value to another, which is actually a more accurate description of the conductivity jump. The second one is a medium with time-splashing conductivity. Such a dependence of conductivity describes many natural and simulated processes having a splash character, especially those which arise due to discharges.

The problems solved exactly display the advantages of a more general analysis, avoiding any doubt about the solution accuracy.

PROBLEMS FORMULATION

The transient media are assumed homogeneous, and the fields are considered to have only a component which is normal to the x axis and independent on the y and z coordinates. That is, one-space-dimensional problem is to be solved.

The conductivity nonstationarity starts at $t = 0$ moment. E_1 is an electrical component of electromagnetic field before the medium change, also called the incident field.



First type of nonstationarity is described by hyperbolic tangent, as Fig.1.shows. It includes cases of the conductivity increasing and decreasing.

Fig.1

The conductivity time splash in the second case is determined as

$$\sigma(t) = \sigma_0 \left\{ A(t+c)e^{-\alpha t} - (t+c) \int_0^t d\tau \frac{e^{-\alpha(t-\tau)}}{\tau+c} \left(1 + \alpha^2 + \frac{2}{(\tau+c)^2} - \frac{2\alpha}{\tau+c} \right) \right\} \quad (1)$$

which can be a splash in the positive values of conductivity (Fig.2(a)) as well as in the negative ones (Fig.2(b)).

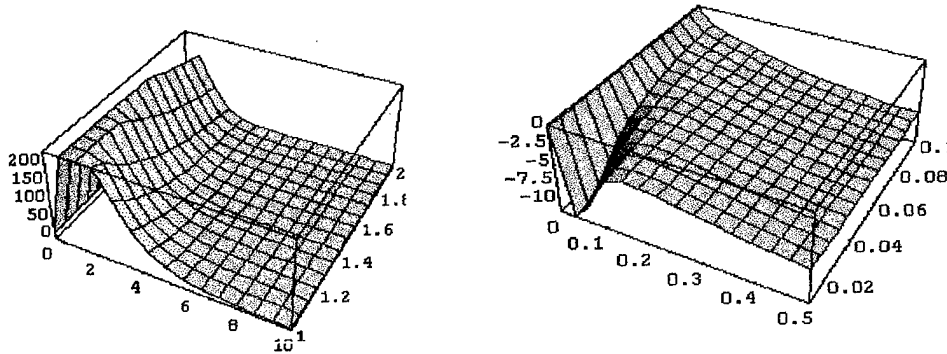


Fig.2. Dependences of conductivity time-splash shape on a and α in (1)

The field E after the nonstationarity starts is to be found, that is we are interested in the transformation of the incident field in the transient media.

No restrictions on the time and space (one-dimensional, as mentioned above) dependence of the incident field were made while obtaining an analytical solution of the problem. Numerical analysis is carried out for the incident field taken as a plane harmonic wave.

Mathematically, the problem is formulated in terms of Volterra integral equation for electric field that has the following form in one-space-dimensional case:

$$E(t, x) = E_1(t, x) - \frac{2\pi}{\epsilon v} \int_{-\infty}^{\infty} dt' \sigma(t') \int_{-\infty}^{\infty} dx' \delta\left(t - t' - \frac{|x - x'|}{v}\right) E(t', x') \quad (2)$$

where δ is Dyra's function, ϵ is a dielectric permittivity, and $v = c/\sqrt{\epsilon}$ is the light velocity in considered media.

PROBLEMS SOLUTIONS AND THEIR ANALYSIS

1) The former problem is solved by reducing the integral equation (2) to a partial differential equation for the field $E(t - x/v, x)$ at the shifted time moments. After some manipulations it is reduced to a first-order partial differential equation which can be solved.

2) The problem for the conductivity splash is solved by resolvent techniques [6]. When the incident field is a plane harmonic wave the following exact solution for the transformed field is obtained:

$$E(t, x) / E_0 = \frac{c}{t+c} (2 - e^{\alpha t}) \cos \frac{\omega}{v} x + \left(\sin \frac{\omega}{v} x + (1/c - \alpha - A c) * \cos \frac{\omega}{v} x \right) * \\ * \frac{1}{t+c} \int_0^t (\tau+c) \exp \left\{ \alpha(t-\tau) - \int_0^{\tau} \varphi(t_1) dt_1 \right\} d\tau, \quad \alpha(t) = \sigma_0 \varphi(t). \quad (3)$$

Its asymptotic and numerical analysis shows that when the splash is large, the incident field amplitude reduces very quickly and before the conductivity starts decreasing it already is equal to zero. In this case the field completely disappears during the conductivity splash and does not appear after the conductivity becomes zero again.

In the opposite case of a small time-splash of conductivity, the field is decreasing before the conductivity reaches its maximum value and increasing after this. When the conductivity has completely disappeared the field takes its initial form.

In the intermediate case, the field was calculated by the exact formula for different values of x . The field time dependence here has a very short splash. Its maximum value is more than 4 times as much as the initial field amplitude. It reduces to the initial value before the conductivity reaches its maximum. These results are for $x = 0$, that is for the points where the initial field had its maximum at the zero time moment. For $x = \pi / 2$ the field time dependence shape seems to have the same form, but the field values here are hundred times less and do not reach the values of initial field at the corresponding moments for constant conductivity. For $x = \pi / 4$, the field splash having the same form as two ones mentioned above, is about one and a half times less than for $x = 0$.

Thus the field under the influence of intermediate time-splash of conductivity is focused in the planes where x is divisible by π that is where the initial field was maximal at the moment the nonstationarity turns on.

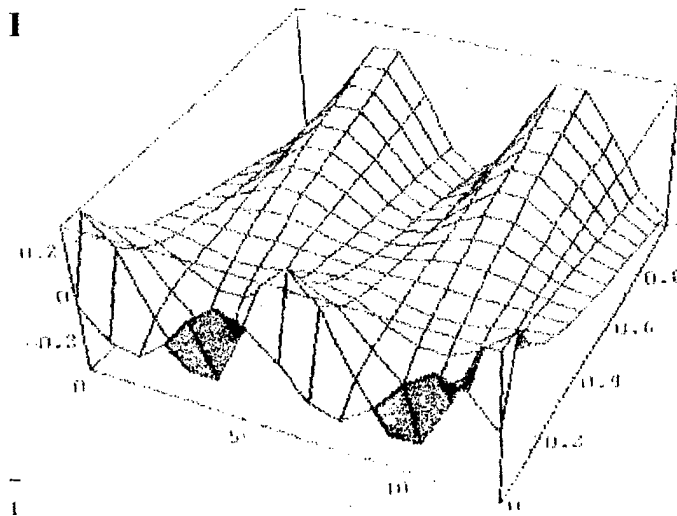


Fig.3.

The opposite situation take place in the case of large conductivity splash (Fig.3). The field is focusing here in the planes where x is divisible by $\pi / 2$, that is where the initial field at zero moment was equal to zero. It can be due that at the planes where the initial field was maximal it had time to disappeared before the conductivity began to reduce.

1. R.L.Fante, *Transmission of electromagnetic waves into time-varying media*, IEEE Trans. Antennas Propagat. 1971. AP-19. p.417-424.
2. L.B.Felsen, G.M.Whitman, IEEE Trans. Antennas Propagat. 1970. AP-18. N2, p.242-253.
3. A.G.Nerukh, I.Yu. Shavorykina, *Transformation of radiation pulse in nonstationary conducting medium*, Radiophysics and Quantum Electronics (Engl.Transl.), Vol.35, 1992, N 3-4, pp.203-209.
4. F.A.Harfoush and A.Taflov. *Scattering of electromagnetic waves by a material half-space with time-varying conductivity*, IEEE Trans. Antennas Propagat., v.39, N 7, 1991, p.898-906.
5. A.G.Nerukh. *Evolutionary Approach in Transient Electrodynamics Problems*. Copyright 1995 by the American Geophysical Union.
6. A.G.Nerukh, N.A.Khizhnyak, *Modern Problems of Transient Macroscopic Electrodynamics*, Test-Radio, Kharkov, Ukraine, 1991. (in Russian)

TRANSIENT ELECTROMAGNETIC FIELD IN A DISSIPATIVE MEDIUM WITH RECTANGULAR PULSE MODULATED PARAMETERS

O. Rybin, A. Nerukh

Kharkov Technical University of Radio Electronics, 14, Lenin av., Kharkov, 310726, Ukraine

A plane electromagnetic wave transformation by a series of repetitive variations of infinite medium parameters is considered. This variation is a modulation of both the permittivity and the conductivity with a rectangular-pulse law. Expressions, which characterise the electric field evolutionary with time, are derived. The time dependences of both the permittivity $\varepsilon(t)$ and the conductivity $\sigma(t)$ of the medium are assumed as:

$$\left. \begin{aligned} \varepsilon(t) &= \varepsilon_0 + (\varepsilon_1 - \varepsilon_0) \sum_{k=1}^N \{ \theta(t - (k-1)T) - \theta(t - \tau_1 - (k-1)T) \}, \\ \sigma(t) &= \sigma_1 \sum_{k=1}^N \{ \theta(t - (k-1)T) - \theta(t - \tau_1 - (k-1)T) \}, \end{aligned} \right\} \quad (1)$$

As it follows from (1), a periodicity of the permittivity and the conductivity variations is t_2 .

During one part of this period, of the duration τ_1 : $\varepsilon(t) = \varepsilon_1$, $\sigma(t) = \sigma_1$, during the other part: $\varepsilon(t) = \varepsilon_0$, $\sigma(t) = 0$, that is at these ones they have the same magnitudes as for $t < 0$.

To solve this problem an evolutionary approach [1] based on the integral equations method is used. To this end, the time half-axis is decomposed to the time intervals where the medium parameters are constant. The expressions for the electric field are

$$\left. \begin{aligned} E_n(t, x) &= F_n(t, x) + \int_{t_{n-1}}^t \int_{-\infty}^{\infty} dx' R_n(t, t', x, x') F_n(t', x'), \\ F_n(t, x) &= E_0(t, x) + \sum_{i=1}^{N-1} \int_{t_{i-1}}^{t_i} \int_{-\infty}^{\infty} dx' K_i(t, t', x, x') E_i(t', x'). \end{aligned} \right\} \quad (2)$$

Here,

$$\begin{aligned} R(t, t', x, x') &= -\frac{1}{2v_1} \left\{ (1-a^2) \frac{\partial^2}{\partial t'^2} + 2\bar{\sigma}_1 \frac{\partial}{\partial t'} \right\} e^{-\bar{\sigma}_1(t-t')} \theta\left(t-t'-\frac{x-x'}{v_0}\right) I_0\left(\sqrt{(t-t')^2 - \frac{(x-x')^2}{v_0^2}}\right) \\ , \quad K(t, t', x, x') &= -\frac{\delta(v_0(t-t') - |x-x'|)}{a^2} \left\{ \bar{\sigma}_1 + \frac{1}{2}(1-a^2) \frac{\partial}{\partial t'} \right\} \quad \text{in the intervals} \\ (i-1)T < t < \tau_1 + (i-1)T, \quad \text{and} \quad R(t, t', x, x') &= 0 = K(t, t', x, x') \quad \text{in the intervals} \\ \tau_1 + (i-1)T < t < iT, \quad i = 1, \dots, N. \quad \text{In these formulas: } a &= \sqrt{\varepsilon_0/\varepsilon_1}, \quad \bar{\sigma}_1 = 2\pi\sigma_1/\varepsilon_1, \\ v_1 &= c/\sqrt{\varepsilon_1}, \quad \text{Re } \sqrt{p^2 - \bar{\sigma}_1^2} > 0. \end{aligned}$$

Let us consider an initial field in the form $E_0(t, x) = e^{i(\omega t - kx)}$, where $k = \omega/v_0$. We introduce the coefficients, which do not depend on the period number

$$d^{\pm} = \frac{a^2}{2iq} \frac{a^2 - 1 - 2s(s \mp iq)}{i(1 \mp q) \pm s} e^{-(\bar{\sigma}_1 \mp i(\Omega \mp \omega))T}, \quad g^{\pm} = \frac{a^2}{2iq} \frac{a^2 - 1 - 2s(s \mp iq)}{i(1 \pm q) \pm s} e^{-(\bar{\sigma}_1 \mp i(\Omega \pm \omega))T},$$

$$s = \bar{\sigma}_1/\omega, \quad q = \sqrt{a^2 - s^2}, \quad t_1 = \omega\tau_1, \quad t_2 = \omega T, \quad f = \left(e^{-(s+i)\tau_1+iT}/2q \right) \left\{ 2q \cos(q\tau_1) + i(1+a^2) \sin(q\tau_1) \right\},$$

$$h = \left(e^{-(s-i)\tau_1-iT}/2q \right) \left\{ 2s - i(1-a^2) \right\} \sin(q\tau_1).$$

Using the mathematical induction method we derive the expressions for an electric field at the arbitrary period:

$$E(t, x) = e^{l(s-iq)t_2} \left(d^+ e^{ilt_2} + g^+ e^{-ilt_2} \right) e^{-\bar{\sigma}_1 t} e^{i(\Omega t - kx)} +$$

$$+ e^{l(s+iq)t_2} \left(d^- e^{ilt_2} + g^- e^{-ilt_2} \right) e^{-\bar{\sigma}_1 t} e^{-i(\Omega t + kx)}, \quad (3)$$

for subintervals $(l-1)T < t < \tau_1 + (l-1)T$ and

$$E(t, x) = A_l e^{i(\omega t - kx)} + B_l e^{-i(\omega t + kx)}, \quad (4)$$

for subintervals $\tau_1 + (l-1)T < t < lT$, $l \geq 2$. Here, $a_l = A_l e^{ilT}$, $b_l = B_l e^{-ilT}$, and a_l, b_l satisfy the recursion relations

$$\begin{pmatrix} a_{k+1} \\ b_{k+1} \end{pmatrix} = \begin{pmatrix} f - h^* \\ -h \quad f^* \end{pmatrix} \begin{pmatrix} a_k \\ b_k \end{pmatrix}. \quad (5)$$

At the first interval ($0 < t < \tau_1$): $a_1 = -f^* e^{-it_2}$, $b_1 = h e^{it_2}$.

For an analysis of behaviour of direct and inverse wave amplitudes at the end of any period one has to consider the relations a_{l+1}/a_l and b_{l+1}/b_l . These relations are determined by the equations:

$$\frac{a_{l+1}}{a_l} = f - \frac{h^*}{C_l}, \quad \frac{b_{l+1}}{b_l} = f^* - h C_l, \quad (6)$$

where $C_l = a_l/b_l$ satisfy the recursion relations

$$C_{l+1} = \frac{-h^* + f C_l}{f^* - h C_l}. \quad (7)$$

The analysis shows that $|C_l| > 1$ as $|C_1| > 1$, that is an absolute value of the direct wave amplitude A_k is greater than the absolute value of the inverse wave amplitude B_k . The analysis also shows that the coefficient C_l can be presented in the form

$$C_l = C_1 + \frac{1}{2hu} X_l, \quad (8)$$

Real variable X_l satisfies the recursion relation

$$X_{l+1} = \frac{4u^2}{4u^2 - X_l}, \quad (9)$$

where $u = \cos(qt_1) \cos(t_2 - t_1) - \frac{a^2 + 1}{2q} \sin(qt_1) \sin(t_2 - t_1)$.

X_I is a function of the period number, for the parameters $\alpha = 1,25$, $s = 0,06$, $t_2 = 16$, is shown in Figs. 1 and 2. These figures illustrate that variation of X_I and the amplitudes of the direct and inverse waves can be periodical (Fig. 1, $t_1 = 7$) as well as monotonous (Fig. 2, $t_1 = 12$).

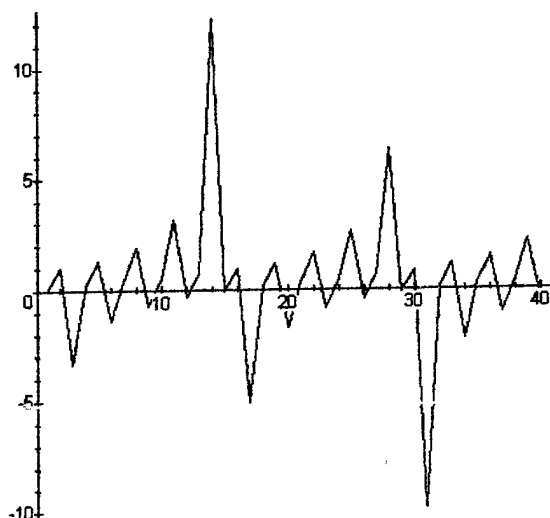


Fig. 1. $\alpha = 1,25$, $s = 0,06$, $t_2 = 16$, $t_1 = 7$

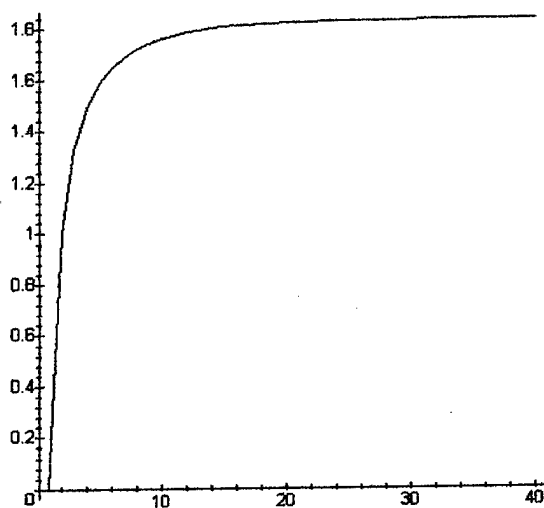


Fig. 2. $\alpha = 1,25$, $s = 0,06$, $t_2 = 16$, $t_1 = 12$

1. A.G. Nerukh, N.A. Khizhnyak, Modern Problems of Nonstationary Macroscopic Electromagnetics, Kharkov, Test-Radio Publ., 1991, (in Russian).

OPTIMUM DESIGN OF RADAR PULSES FOR STEALTH TARGETS (TIME DOMAIN APPROACH)

Ahmad Cheldavi

Iran University of Science and Technology
Narmak, Tehran, Iran, 16844,
fax: 98-21-7454055, e-mail: cheldavi@ece.ut.ac.ir

In this paper, principles of optimum design method of radar nonsinusoidal pulses for stealth targets will be presented. To extract the principles of the method, first we have to obtain a time-domain performance of the special absorber, which is used on the target.

Using the results of this time-domain approach, we can design an optimum pulse figure to maximize the reflected wave energy from the surface of the stealth target. This optimum pulse figure is not necessary unique.

In this paper we use a single-layer model of absorbing material, but this method can be generalized for multiple-layer absorbing materials.

Also we suppose there is only some attenuation during pulse propagation in absorbing material (there is no dispersion). Results of the time-domain analysis of such an absorbing layer over metal backing plate, using the transmission line model in [2] can be found in [1]. Results of [1] can be specialized for single-layer absorbing material; the main problem, which is the transmission line model, was exactly and completely solved in [2].

Then we show, for the same absorbing material structure and the same reflected energy with [3], one can use nonsinusoidal radar pulses with larger time-width (narrow-band pulses). So, it is necessary for time-width of the pulse to be less than propagation delay time in the absorbing material (as it was stated in [3]).

Finally, some optimum nonsinusoidal radar pulses presented for some special applications of stealth targets.

References

- [1] A. Cheldavi, M. Kamarei, Time-Domain Analysis of Capacitive Jaumann Absorber, *Proc. of IEEE MTT*, Denver, Colorado, 1997.
- [2] A. Cheldavi, H. Oraizi, M. Kamarei, Time-Domain Analysis of Transmission Lines, *Proc. of 25th EuMC*, Bologna, Italy, 1995.
- [3] N.J. Mohamed, Nonsinusoidal Radar Signal Design for Stealth Targets, *IEEE Trans. EMC*, vol. 37, no. 2, 1995.

TRAPPING OF AN ELECTROMAGNETIC WAVE BY THE BOUNDARY OF A SUDDENLY CREATED PLASMA HALF-SPACE

M.I. Bakunov and S.N. Zhukov

University of Nizhny Novgorod, 603600, Nizhny Novgorod, Russia

The study of the interaction between electromagnetic waves and bounded plasmas with fast growing density is of considerable interest due to its potential applications in generation of tunable microwave radiation. Fante [1] was the first who discussed some peculiarities of reflection of electromagnetic signals from the plane boundary of time-varying plasma. Later, Kalluri [2] presented complete analysis including both steady-state solution and transient processes in the case of the reflection of a time-harmonic electromagnetic wave by a suddenly created (switched) plasma half-space. Kalluri and Goteti [3] brought the solved problem closer to the practical situation by considering the switched plasma slab. Finally, the effects of a magnetized plasma were examined by Kalluri [4].

In all of the above papers, however, only the degenerate case of normal incidence of electromagnetic wave on the boundary of time-varying plasma was treated. In this paper, we examine the case when the boundary of plasma half-space whose density instantaneously grows in time from one value to another is perpendicular to the plane wave front. The distinguishing feature of this case is the possibility of creation of surface waves guided by the plasma boundary. In other words, the part of the original wave energy may be trapped by the boundary of time-varying plasma via transformation into surface waves.

Initially, when $t < 0$, a plane TM-polarized electromagnetic wave of frequency ω_0 with fields

$$E_y(x,t) = B_z(x,t), \quad B_z(x,t) = B_0 \exp(i\omega_0 t - ih_0 x) \quad (h_0 = \omega_0/c) \quad (1)$$

propagates in unionized medium (gas) with dielectric permittivity $\epsilon \approx 1$ along the x-axis. Then,

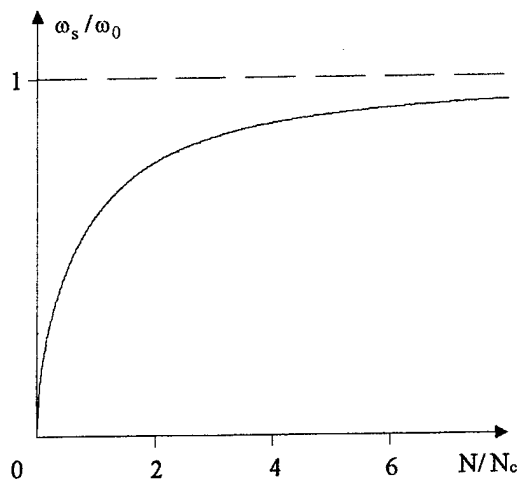


Fig. 1. The frequency conversion coefficient ω_s/ω_0 vs the parameter N/N_c ($N_c = m\omega_0^2/4\pi e^2$ is critical plasma density for the original wave).

propagating along the plasma boundary in the opposite directions are shown to be excited. Their frequencies are given by

$$\omega_{\pm} = \pm \omega_s, \quad \omega_s = \sqrt{\omega_0^2 + \frac{1}{2}\omega_p^2} - \sqrt{\omega_0^4 + \frac{1}{4}\omega_p^4} \quad (2)$$

(see Fig. 1) where $\omega_p = \sqrt{4\pi e^2 N/m}$ is plasma frequency and amplitudes are

$$B_{\pm} = B_0 \frac{(\omega_p^2 - \omega_s^2)(\omega_0 \pm \omega_s)}{2\omega_0 \sqrt{\omega_0^4 + \frac{1}{4}\omega_p^4}} \quad (3)$$

(see Fig. 2). The limit $B_{+}/B_0 \rightarrow 2$ at $N \rightarrow \infty$ seems to be in contradiction with the law of energy conservation. To explain the situation calculations for original wave beam of the form

$$B_z(x, y, 0) = B_0 \frac{\sin(y/a)}{y/a} \exp(-ih_0 x) \quad (4)$$

with $h_0 a \gg 1$ have been done. In this case we arrive at the expression

$$B_{+} = B_0 \frac{(\omega_p^2 - \omega_s^2)(\omega_0 + \omega_s)}{2\omega_0 \sqrt{\omega_0^4 + \frac{1}{4}\omega_p^4}} \gamma \operatorname{arctg} \frac{1}{\gamma} \quad (5)$$

with parameter $\gamma = h_0 a \sqrt{2(1 - \omega_s/\omega_0)}$ and $\omega_0 = ch_0$ (dashed curves at Fig. 2). Thus, B_{+}/B_0 grows only while the region of surface wave localization near the boundary is less than the width of the original beam. For greater N/N_c the amplitude coefficient B_{+}/B_0 decreases.

The free-streaming mode is excited within

the plasma half-space and consists of static magnetic field

$$B_z^{\text{st}}(x, y) = \frac{\omega_p^2}{\omega_0^2 + \omega_p^2} \left[B_z(x, y, 0) - B_0 \exp\left(\frac{y}{c} \sqrt{\omega_0^2 + \omega_p^2} - ih_0 x\right) \right], \quad y < 0, \quad (6)$$

and spatial distribution of dc electric current $j^{\text{st}}(x, y) = (c/4\pi) \operatorname{rot} B^{\text{st}}$.

To investigate the angular distribution of transient outgoing radiation we use the technique proposed in [6]. Spatial density of electromagnetic field energy is integrated over y in the limit $t \rightarrow \infty$ and angular densities of radiated energy in vacuum ($w_{\text{I}}(\theta)$) and in the plasma ($w_{\text{II}}(\theta)$) are obtained (Fig. 3; angle θ is measured from the normal to the boundary both in vacuum and in the plasma, $-\pi/2 < \theta < \pi/2$, $\theta = \pi/2$ coincides with x -direction). In the ideal case of original plane wave it is not possible to estimate energy effectiveness of the wave trapping. Therefore we have analyzed energy relations for the wave beam (4). Energy $W_0 = B_0^2 a / 8$ of the original beam transforms into the surface wave energies

$$W_{\pm} = \frac{cB_{\pm}^2}{16\pi\omega_s} \frac{(1 - \varepsilon_s)(1 + \varepsilon_s^2)}{\varepsilon_s^2 \sqrt{1 - \varepsilon_s}}, \quad (7)$$

where $\varepsilon_s = 1 - \omega_p^2/\omega_s^2$, the radiated energies

$$W_{\text{I,II}} = \int_{-\pi/2}^{\pi/2} w_{\text{I,II}}(\theta) d\theta, \quad (8)$$

and energy of the free-streaming wave

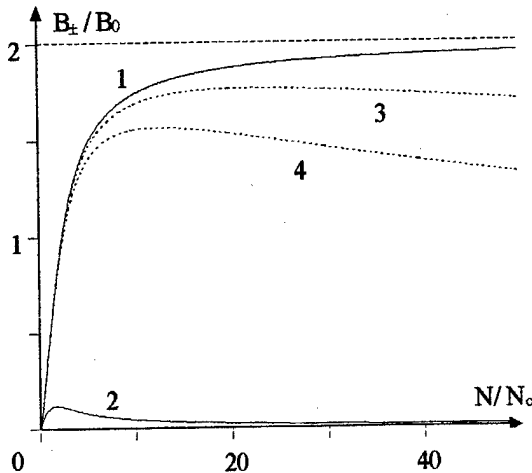


Fig. 2. The amplitude coefficient B_{+}/B_0 (curve 1) and B_{-}/B_0 (curve 2) vs parameter N/N_c for original plane wave. The dashed curves show the coefficient B_{+}/B_0 for the original wave beam with $h_0 a = 10$ (curve 3) and $h_0 a = 5$ (curve 4).

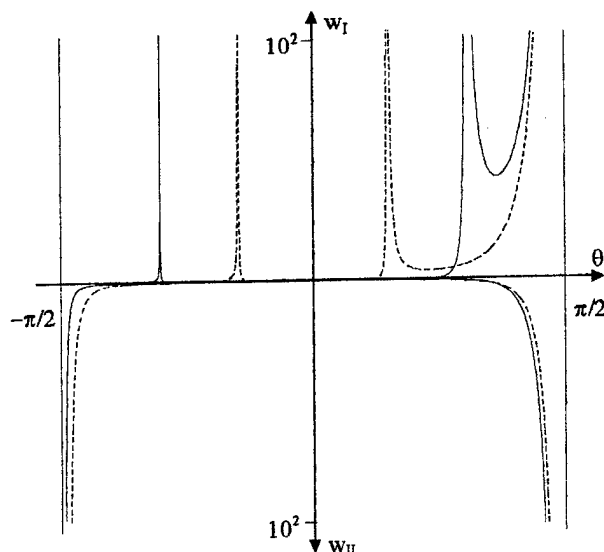


Fig. 3. Angular densities of radiated energy into vacuum $w_I(\theta)$ and plasma $w_{II}(\theta)$ at $N/N_c = 0.5$ (solid curves) and $N/N_c = 4$ (dashed curves). All curves are normalized by $cB_0^2 / 16\pi^2 \omega_0$.

$$W_{st} = \frac{B_0^2 a}{32} \frac{\omega_p^2}{\omega_p^2 + \omega_0^2} \quad (9)$$

Fig. 4 shows the energy distribution in dependence on the created plasma density for the original beam with $h_0 a = 20$. Transformation into the backward surface wave is negligible: $(W_-/W_0)_{\max} \approx 7 \cdot 10^{-4}$ at $N/N_c \approx 1$, whereas more than 40% of the original wave energy may be converted into the forward surface wave. Maximum of the transformation effectiveness is achieved at $N/N_c \sim (h_0 a)^2$ when the scale of the forward surface wave localization in vacuum $(1/h_0)\sqrt{N/N_c}$ coincides in order of magnitude with the width of original beam.

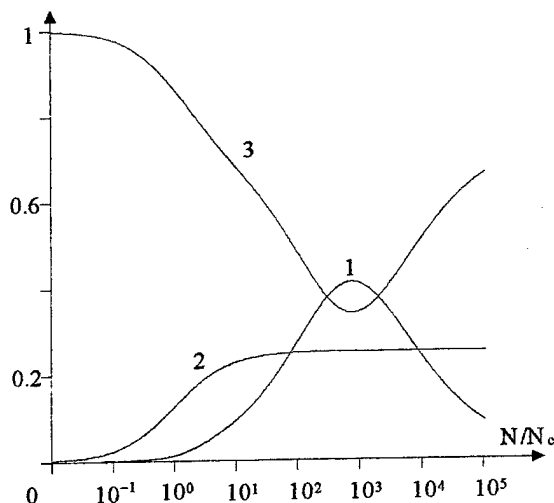


Fig. 4. Energy coefficients W_+/W_0 (1), W_{st}/W_0 (2) and W_-/W_0 (3) vs parameter N/N_c for the original beam with $h_0 a = 20$.

Interestingly, trapping of an electromagnetic wave is accompanied by the concentration of electromagnetic energy near the created plasma boundary, in other words, in a course of transient processes energy is leaking to the created boundary. The most perspective application of the phenomenon of wave trapping is the development of new methods for input of electromagnetic radiation into planar waveguiding structures filled with solid-state (semiconductor) plasma. Nonstationarity of a semiconducting medium can be provided by various mechanisms: carrier injection, photoionization by laser pulse, «switching» of effective mass etc. As the achieved up to now time-scales of nonstationarity lie within picoseconds, these mechanisms can be used for transient input of submillimeter and infrared radiation.

References

1. R.L. Fante, "Transmission of electromagnetic waves into time-varying media," *IEEE Trans. Antennas Propagat.*, vol. AP-19, no.3, pp.417-424, 1971.
2. D.K. Kalluri, "On reflection from a suddenly created plasma half-space: transient solution," *IEEE Trans. Plasma Sci.*, vol.16, no.1, pp.11-16, 1988.
3. D.K. Kalluri and V.R. Goteti, "Frequency shifting of electromagnetic radiation by sudden creation of a plasma slab," *J. Appl. Phys.*, vol.72, no.10, pp.4575-4580, 1992.
4. D.K. Kalluri, "Frequency shifting using magnetoplasma medium: flash ionization," *IEEE Trans. Plasma Sci.*, vol.21, no.1, pp.77-81, 1993.
5. M.I. Bakunov and A.V. Maslov, "Trapping of electromagnetic wave by nonstationary plasma layer," *Phys. Rev. Lett.*, vol.79, no.23, pp.4585-4588, 1997.
6. V.L. Ginzburg and V.N. Tsytovich, *Transition radiation and transition scattering*. Bristol, England; New York, NY: A. Hilger, 1990.

TIME AND FREQUENCY DOMAIN ALGORITHMS OF IMPULSE RESPONSES EVALUATION

V.I.Koshelev, V.T.Sarychev, S.E.Shipilov

High Current Electronics Institute RAS
4, Akademicheskoy ave., 634055 Tomsk, Russia
e-mail: koshelev@hcei.tomsk.su

Development of physics and technology of ultrawideband radiation during last time allowed to radiate into space electromagnetic pulses with a nanosecond duration and power up to 1 GW [1, 2]. So, application of such impulses for radar of both air and underground objects becomes to be promising. When a received signal is a finite set of digital data, a number of problems concerning the determination of properties of sounding objects appears.

In the conditions of full information (input and output signals are known at all temporal axis) the task to find impulse responses (IR) is solved easily on the basis of Fourier transformation. Actually, the coupling between the input signal $X(t)$, output signal $Y(t)$ and IR $h(\tau)$ is determined by the integral relation

$$Y(t) = \int_0^{\infty} h(\tau) X(t-\tau) d\tau \quad (1)$$

In the general case, IR $h(\tau)$ is a linear operator. Making Fourier transformations over the left-handed and right-handed parts of the expression (1), it is easy to obtain

$$h(\omega) = Y(\omega)/X(\omega),$$

where $X(\omega)$, $Y(\omega)$ and $h(\omega)$ are Fourier images of corresponding functions.

A transition from continuous signals to the discretized ones will entail a series of difficulties having a principal character. The main of them are as follows: violation of a causality principle resulting in arising of presignals, appearance of spurious side lobes and zeros in spectral evaluations, finiteness of a frequency band, absence of a sole solution both at the evaluation of radiated and received signal spectra and at the evaluation of impulse responses. By taking into account these factors one can essentially increase the evaluation accuracy of impulse responses.

A complex spectrum (CS) of $X(\omega)$ is determined in the form of a linear model relative to an unknown M-measured vector \mathbf{F} :

$$X(\omega) = \mathbf{F} \cdot \mathbf{f}^*(\omega),$$

where $*$ is the complex conjugation. To this CS corresponds a model N-measured vector

$$\hat{\mathbf{X}} = \frac{1}{2\pi} \int_{-\pi}^{\pi} X(\omega) \mathbf{e}(\omega) d\omega = \mathbf{F} \mathbf{E}$$

Here and later ω is a dimensionless frequency. For substantial signals, the elements of matrix \mathbf{E} are determined according to the expression

$$E_{mn} = \frac{T}{\pi(\tau_m - t_n)} \sin(\pi(\tau_m - t_n)/T).$$

Vector \mathbf{F} is determined by the expression

$$\mathbf{F} = \mathbf{X} \mathbf{E}^{-1},$$

where \mathbf{E}^{-1} is a pseudoreciprocal matrix with respect to \mathbf{E} .

A condition $h(\tau) = 0$ at $\tau < 0$ satisfies the causality principle. Besides, in the paper presented, the cases are considered when the input and output signals satisfy the same condition. Model signals $\hat{X}(t)$, $\hat{Y}(t)$ and IR made on the basis of Fourier transformation by the limited frequency band will not satisfy such condition, i.e. they will have presignals. At least two ways of struggle with prepulses can be suggested:

a) At an invariable frequency band of a signal determined by the frequency of its discretization, the detail of the spectrum describing by increasing the dimension of vector \mathbf{F} is increased. The following expression is suggested to be used as a functional and its minimization allows to evaluate the value of the components of vector \mathbf{F} :

$$\Phi = \frac{1}{T} \int_{-\infty}^0 \left| \hat{X}(t) \right|^2 dt + \left| \hat{\mathbf{X}} - \mathbf{X} \right|^2.$$

b) Expansion of a frequency band up to the interval $(0, \infty)$ is a radical means of suppression the prepulses. In this case the integral Fourier transformation is used for a model function $\hat{X}(t)$ and Fourier coefficients can be found by means of Kotelnikov interpolation or Lagrange interpolation. The latter is more convenient for practical application as it provides more rapid decrease with the frequency rise of absolute values of Fourier coefficient, besides the expressions for them are less unwieldy.

Evaluation of IR is possible in the time domain as well. In this case, convolution integral (1) at interpolation of integrands is transformed into the following vector relation:

$$\mathbf{Y} = \mathbf{H} \cdot \mathbf{D}(\mathbf{X}). \quad (2)$$

The unknown quantity in the expression (2) is the IR vector \mathbf{H} . The dimensions of the vectors and a matrix in (2) are limited by the relations:

$$\dim \mathbf{Y} + \dim \mathbf{H} + \dim \mathbf{X}, \quad \dim \mathbf{D} = \dim \mathbf{Y} \cdot \dim \mathbf{H}.$$

So, solving of the equation (2) is finding of a pseudoreciprocal matrix \mathbf{D}^{-1} . In the given paper, this matrix was found by means of a specially developed procedure of conjugation of rectangular matrixes based on the method of Gram-Schmidt orthogonalization.

In the general case, when impulse response looks like

$$h(\tau) = h_0(\tau) + h_1(\tau) \cdot \frac{d}{d\tau} + \dots \quad (3)$$

the members corresponding to the differentiation operators will appear in the right-handed part of the expression (2):

$$\mathbf{Y} = \mathbf{H}_0 \cdot \mathbf{D}(\mathbf{X}) + \mathbf{H}_1 \cdot \mathbf{D}(\mathbf{X}) + \dots \quad (4)$$

To find the kind of elements of matrixes \mathbf{D}_k , $k > 0$, the interpolation expressions corresponding to a k -derivative should be used. When testing the IR evaluation, the level of influence of the output signal \mathbf{Y} additive noise on the accuracy of IR recovery at the known input signal \mathbf{X} was investigated. The most simple situation was investigated when in the expression (3) one member dominates for IR. In this case the expression (4) comes to the form (2) where either vector \mathbf{X} (if $h_0(\tau)$ is dominating for $h(\tau)$) or the input signal derivative corresponding to the dominating member.

The modeling process consisted of the followings operations. A noise-free vector \mathbf{Y} was calculated by the known initial vectors \mathbf{X} and \mathbf{H} on the basis of (2). Then an white Gaussian noise was added to the signal \mathbf{Y} . Evaluation of vector \mathbf{H} components for the obtained signal was made by three different methods:

- by solving an overdetermined system of linear equations – variant (a);
- on the basis of Fourier transformations when the spectra of the signals \mathbf{X} and \mathbf{Y} were evaluated on the basis of Lagrange interpolation – variant (b);
- on the basis of a traditional finite Fourier transformation – variant (c).

To describe the noise immunity of the IR evaluation algorithm, coefficients μ_h and μ_y , determined by the expressions

$$\mu_h = \log_2 \frac{\langle |\delta \mathbf{H}|^2 \rangle}{|\mathbf{H}|^2}; \quad \mu_y = \log_2 \frac{\langle |\delta \mathbf{Y}|^2 \rangle}{|\mathbf{Y}|^2};$$

were used, where $\langle |\delta \mathbf{H}|^2 \rangle$ and $\langle |\delta \mathbf{Y}|^2 \rangle$ are root-mean-square deviations of vectors \mathbf{H} and \mathbf{Y} . Side by side with the coefficient μ_h , a coefficient

$$\langle \mu_h \rangle = \log_2 \frac{\langle |\mathbf{H} - \bar{\mathbf{H}}|^2 \rangle}{|\mathbf{H}|^2}.$$

was evaluated.

Approbation of the algorithms was made at two model signals $X(t)$: smooth (Fig. 1) and noise-like (Fig. 2). A

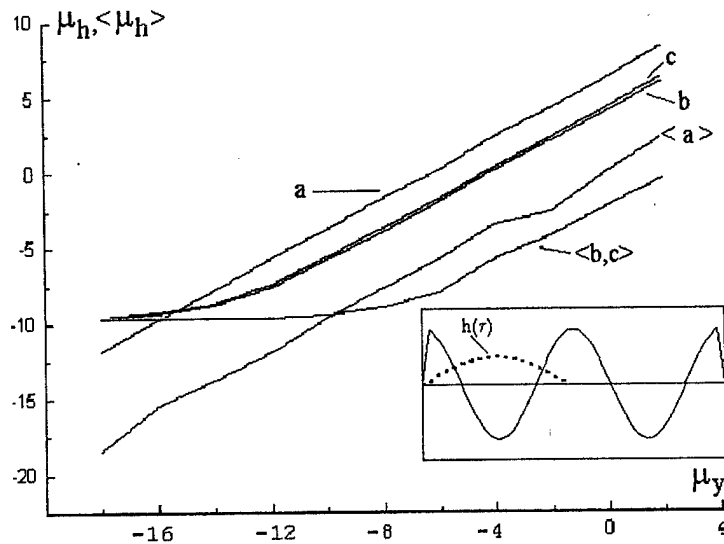


Fig. 1.

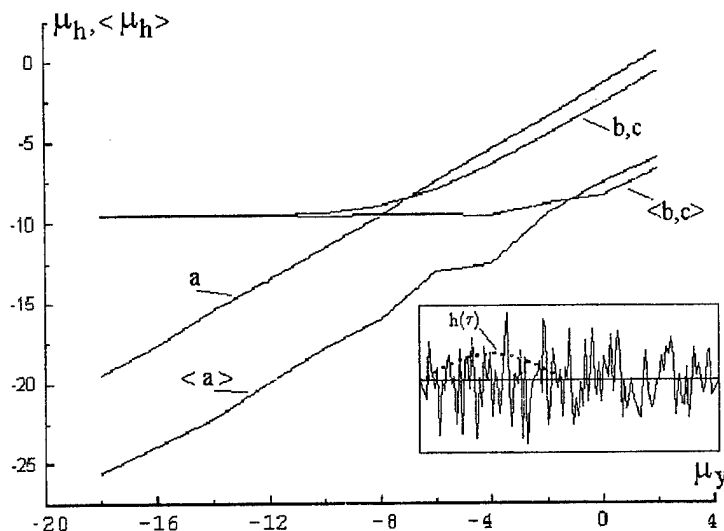


Fig. 2.

model of a IR under recovering is presented in Fig. 1 and Fig. 2 by a dashed line. Fig. 1 and Fig. 2 present the dependencies μ_h and $\langle \mu_h \rangle$ on the coefficient μ_y . Designations of the curves in letters correspond to the algorithm variants by which IR were estimated. Brackets $\langle \rangle$ indicate that the curve corresponds to the averaged coefficient $\langle \mu_h \rangle$ for 64 realizations.

The investigations that have been carried out allowed to make the following conclusions.

- The choice of method of IR evaluation should be made taking into account the output signal noise level. For a weak noise, a preference should be given to solving the system of linear equations in the time domain basis. At a high noise level it is recommended to use spectral methods of IR recovering.
- Averaging of IR evaluations obtained by the time domain algorithm allows to increase their accuracy by the value proportional to the sample volume in the whole investigated range of the output signal noises. Spectral algorithms have saturation by the accuracy of IR evaluations at the sample volume increase.
- The highest noise immunity at the impulse response evaluation have the systems with noise-like signals at the input for which it is

recommended to use a time domain algorithm.

References

1. J.A. Oicles, J.R. Grant, and M.H. Herman, "Realizing the potential of photoconductive switching for HPM applications", *SPIE Proc.* **2557**, pp. 225-236, 1995.
2. V.I. Koshelev, Y.I. Buyanov, B.M. Kovalchuk, Y.A. Andreev, V.P. Belichenko, A.M. Efremov, V.V. Plisko, K.N. Sukhushin, V.A. Vizir, V.B. Zorin, "High-power ultrawideband electromagnetic pulse radiation", *SPIE Proc.* **3158**, pp. 209-219, 1997.

NUMERICAL MODELING OF MEASUREMENTS OF DIELECTRIC MATERIAL CHARACTERISTICS USING NON-SINUSOIDAL SIGNALS

N. N. Kolchigin, S. N. Pivnenko

Chair of Theoretical Radio Physics, Kharkov State University,

Svobody Sq. 4, Kharkov, 310077, Ukraine

Tel: +38-0572-457257, e-mail: Nicolay.N.Kolchigin@univer.kharkov.ua

ABSTRACT

An approximate solution to the problem of reflection of restricted in space transient electromagnetic field from layered lossy dielectric halfspace is described. According to the results obtained an algorithm of determination of dispersion and angular characteristics of dielectric material using the space-time distributions of the reflected field has been derived.

INTRODUCTION

Employment of non-sinusoidal signals for determination of dielectric material characteristics gives one essential advantages as compared to use of continuous time-harmonic signals. These are a high information capacity of each measurement, an opportunity to obtain the dispersion and angular dependencies of the material investigated in short time, a high measurement accuracy in the free space without an anechoic chamber employment due to a possibility to resolve the signals from various scatterers by employing "time window".

SOLUTION TO THE PROBLEM

Pulse method of the measurement of dielectric material characteristics is based on comparison of the pulse signal reflected from the investigated material with the one reflected from perfectly conducting (metal) surface and followed by the obtained data processing usually with the help of the Fourier transform. To interpret correctly the results of experimental measurements the solution of transient electromagnetic waves reflection from stratified dielectric medium have to be used. In the report, an approximate solution of the problem of restricted both in space and time transient field reflection from lossy stratified medium is presented.

The structure under investigation consists of a plane dielectric slab of thickness d , permittivity ϵ'_1 and conductivity σ_1 on a dielectric halfspace of permittivity ϵ'_2 and conductivity σ_2 (Fig. 1). A rectangular aperture antenna uniformly excited with linearly polarized pulsed field is situated at a distance z from the structure. Pulsed wave beam radiated by the antenna is incident upon the structure under an angle α_0 . It is assumed that an observation point is situated in far-field zone which is determined as $r \gg L_{x,y}^2/2cT$ (T is a pulse duration, L_x, L_y are the antenna dimensions, c is speed of light in free space). It is also assumed that the incident and reflected pulses can be well separated in time (for instance, by using "time window"), and only the reflected field will be considered in following analysis.

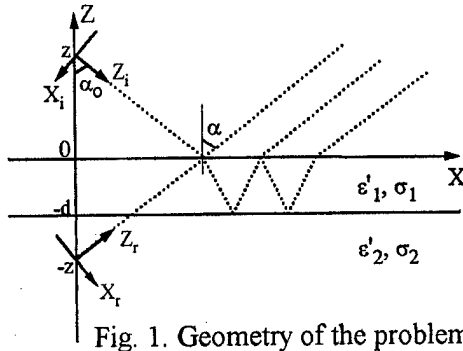


Fig. 1. Geometry of the problem.

Solution of the problem is based on expansion of the incident transient field over time-harmonic plane waves using the integral Fourier transform. Spatial spectrum of the field reflected from the layered dielectric halfspace is found by employing known plane-wave reflection coefficient for the such medium. An integral obtained over wavenumbers is

evaluated in the far zone by the stationary phase method. The field reflected from stratified halfspace can be written as follows [1]:

$$U_r(r, \theta_0, \varphi_0, t) = -\Re e 4 \frac{\pi i}{rc} \cos \theta_0 \int_0^\infty R(\omega, \alpha_0, \theta_0, \varphi_0) U(\omega, \theta_0, \varphi_0) \omega e^{-i\omega\tau} d\omega, \quad (1)$$

where r, θ_0, φ_0 are coordinates of the observation point in a coordinate frame X_r, Y_r, Z_r associated with the reflected field, $R(\omega, \alpha_0, \theta_0, \varphi_0)$ is a reflection coefficient for time-harmonic plane wave of frequency ω which is incident upon the investigated structure under an angle α_0 , $\tau = t - r/c$ is a retarded time, and $U(\omega, \theta_0, \varphi_0)$ is a Fourier counterpart of the incident field.

In a plane of incidence $\varphi_0 = 0$ and $R = R(\omega, \alpha_0 + \theta_0)$. The reflection coefficient R of the investigated structure for linearly polarized time-harmonic plane wave can be written for the cases of s and p polarization in the form, respectively [2]:

$$R_s(\psi) = \frac{\sin(\gamma_1 d)(\gamma_1^2 - \gamma_0 \gamma_2) + i \cos(\gamma_1 d)(\gamma_1 \gamma_2 - \gamma_0 \gamma_1)}{\sin(\gamma_1 d)(-\gamma_1^2 - \gamma_0 \gamma_2) + i \cos(\gamma_1 d)(-\gamma_1 \gamma_2 - \gamma_0 \gamma_1)}; \quad (2)$$

$$R_p(\psi) = \frac{\sin(\gamma_1 d)(\gamma_1^2 - \gamma_0 \gamma_2 \varepsilon_1^2 / \varepsilon_2) + i \cos(\gamma_1 d)(\gamma_1 \gamma_2 \varepsilon_1 / \varepsilon_2 - \gamma_0 \gamma_1 \varepsilon_1)}{\sin(\gamma_1 d)(-\gamma_1^2 - \gamma_0 \gamma_2 \varepsilon_1^2 / \varepsilon_2) + i \cos(\gamma_1 d)(-\gamma_1 \gamma_2 \varepsilon_1 / \varepsilon_2 - \gamma_0 \gamma_1 \varepsilon_1)}; \quad (3)$$

where ψ is an angle of incidence, $\gamma_0 = k_0 \cos \psi$, $\gamma_1 = k_0 \sqrt{\varepsilon_1 - \sin^2 \psi}$, $\gamma_2 = k_0 \sqrt{\varepsilon_2 - \sin^2 \psi}$, $k_0 = \omega/c$ is a wavenumber in free space, $\varepsilon_1 = \varepsilon_1' - i\sigma_1/\varepsilon_0\omega$, $\varepsilon_2 = \varepsilon_2' - i\sigma_2/\varepsilon_0\omega$, $\varepsilon_0 = 8.85 \cdot 10^{-12}$ F/m.

Substituting (2) or (3) into (1) one obtains an expression for the reflected field in the integral form. Solution to the problem could not be derived in an explicit form because of complicate dependence of the reflection coefficients R_s and R_p on frequency. To calculate the integral an algorithm of the Fast Fourier Transform had been used.

NUMERICAL RESULTS

The results of numerical calculation of the reflected field for various observation angles $\alpha = \theta_0 + \alpha_0$ are presented in Fig. 2. In Fig. 2a presented the field reflected from perfectly conducting halfspace for comparison with the case s -polarized field reflected from a dielectric slab (Fig. 2b). The time dependence of the excitation field was chosen to be a first derivative of gaussian function, $L_x = L_y = 0.2\text{m}$, $T = 0.66 \cdot 10^{-9}\text{s}$, $r = 10\text{m}$, $\alpha_0 = 40^\circ$, $d = 0.2\text{m}$, $\varepsilon_2 = 4$, $\varepsilon_3 = 1$, $\sigma_2 = \sigma_3 = 0$. For the chosen ratio between the pulse duration and the aperture dimension ($cT/L_{x,y} = 1$) the radiated pulsed wave beam is found to be strongly diverges.

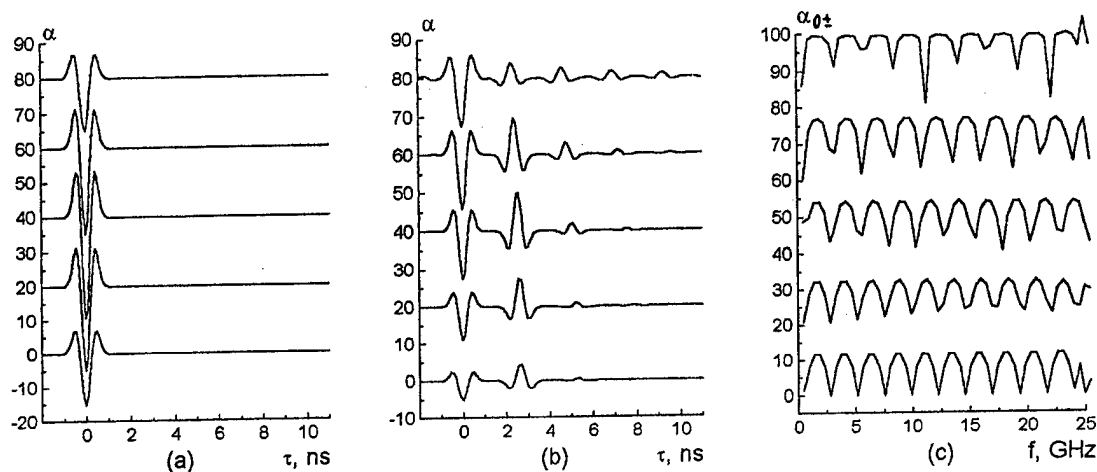


Fig. 2. Time and angular dependencies of the field reflected from metal surface (a) and dielectric slab (b) and angular dependency of the reflection coefficient (c).

This phenomena is illustrated in Fig. 2a in which one can see that for the observation angles $\alpha = 0^\circ$ and 80° magnitude of the pulse is reduced twice as much compared to the main direction $\alpha = 40^\circ$. It can be used for obtaining both frequency and angular dependencies of the reflection coefficient of the investigated material during a single measurement. For this one have to measure the time dependencies of the field reflected from the investigated material for the various observation angles (like those represented in Fig. 2b). Then dividing the frequency spectrum of the measured reflected signal by the frequency spectrum of the signal reflected from metal surface one will obtain the frequency and angular dependencies of the reflection coefficient (Fig. 2c). The method proposed is convenient for the investigation of absorbing materials and covers and for the investigation of the objects with vast varying in time characteristics as well.

CONCLUSION

To determine dielectric material characteristics and to model a measurement process the problem of restricted in space transient electromagnetic field reflection from layered lossy dielectric halfspace has been solved. Numerical calculation of the measurement process allows us to propose some improvements concerning the measurements of dielectric material characteristics.

REFERENCES

- [1] N. N. Kolchigin, S. N. Pivnenko, and V. M. Lomakin, "Influence of Losses in Dielectric Half-Space on Characteristics of Reflected Pulsed 3D Wave Beam," *Radiophysics and Radioastronomy*, vol. 2, no. 3, 1997, pp. 318-322.
- [2] L. M. Brekhovskikh. *Waves in stratified media*. Moscow: Nauka, 1973. (in Russian)

Modeling studies of nonlinear interaction of non-stationary high-power electromagnetic waves with the ionospheric plasma

Konstantin P. Garmash

Department of Space Radio Physics, Kharkiv State University,
4 Svoboda Square, Kharkiv 310077, Ukraine
E-mail: *Konstantin.P.Garmash@univer.kharkov.ua*

The initial set of equations, algorithms for their solution, computer programs, and the results of numerical simulations of nonlinear interaction of non-stationary high-power electromagnetic radiation with plasma in the ionosphere are presented.

The initial set of relations consists of the transfer equation in amplitude of an electromagnetic wave in the approximation of nonlinear non-stationary geometric optics, the set of balance equations in the electron temperature and in the electron number density, as well as in the number density of positive and negative ions. Attachment and recombination processes are taken into account.

The transfer of heat and particles in the transverse direction is neglected. The conditions for the breakdown of the atmosphere by electromagnetic radiation are indicated.

A model of the medium in an altitude range of 50-300 km for daytime and nighttime conditions is presented in a tabular form. The parameters of the medium are assumed to change only with height.

Simulations for a broad band of frequencies (1-1000 MHz) and effective powers (10^3 - 10^9 MW) for both the ordinary and extraordinary components of the electromagnetic wave are performed.

The results of numerical simulations of perturbations in the spatial and temporal parameters of the near-Earth space and in the characteristics of electromagnetic waves are presented.

It is shown that the perturbed parameters of plasma change with time nonmonotonically.

Such a behavior results from the competition of a number of micro-processes in plasma and from the self-effect of the wave in underlying layers. The relative perturbations in the concentrations of particles are determined to reach about one order of magnitude, and those in the electron temperature to reach two orders of magnitude.

The results of modeling efforts are illustrated in Figures 1 and 2.

The author has been supported by Science and Technology Center in Ukraine Grant No. 471.

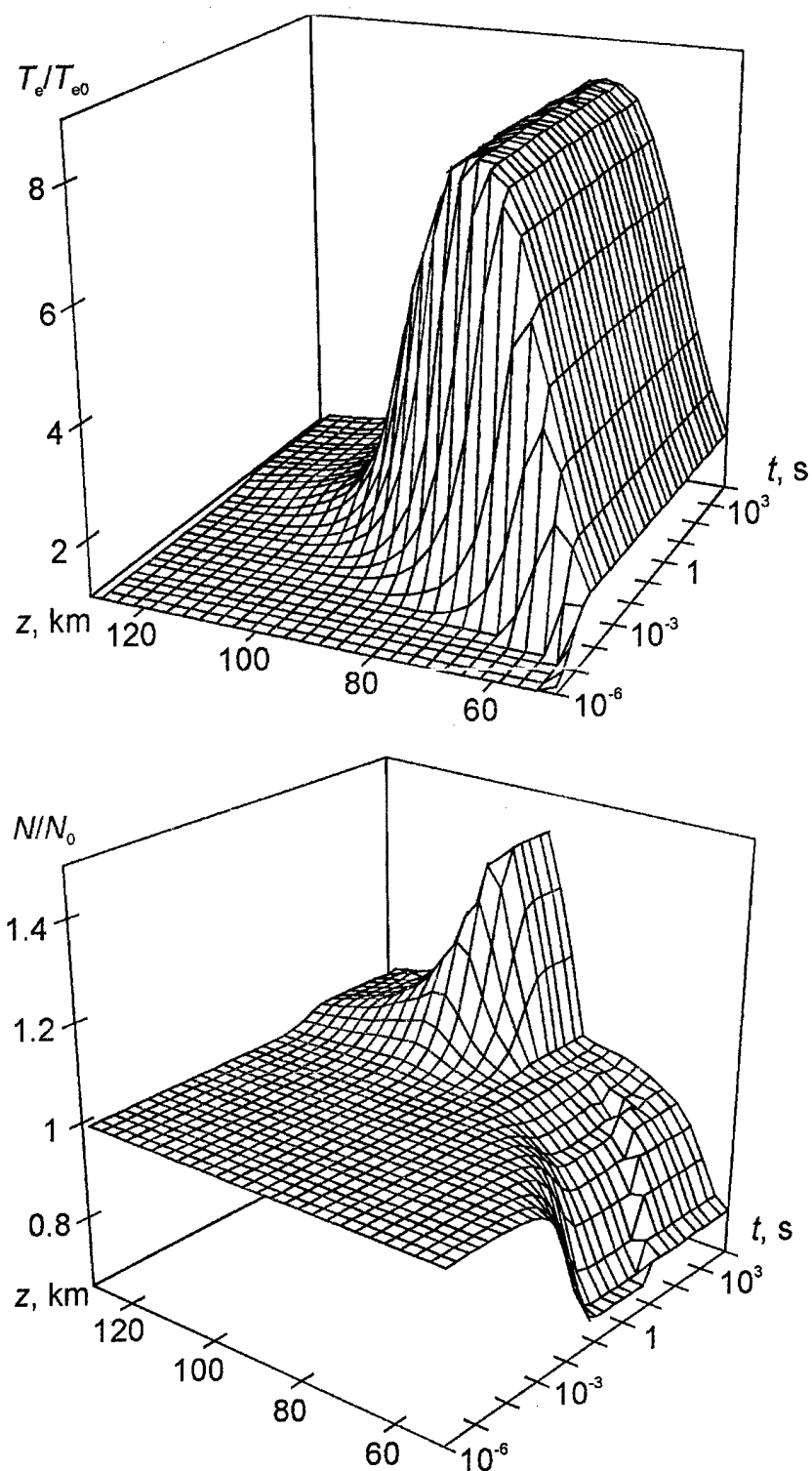


Figure 1. Relative changes in the electron temperature (upper panel) and in the electron number density profiles (lower panel) caused by high-power HF radio waves at a frequency of 10 MHz and effective power of 300 MW. At $t=0$ the plane unmodulated wave arrive at the 50 km altitude.

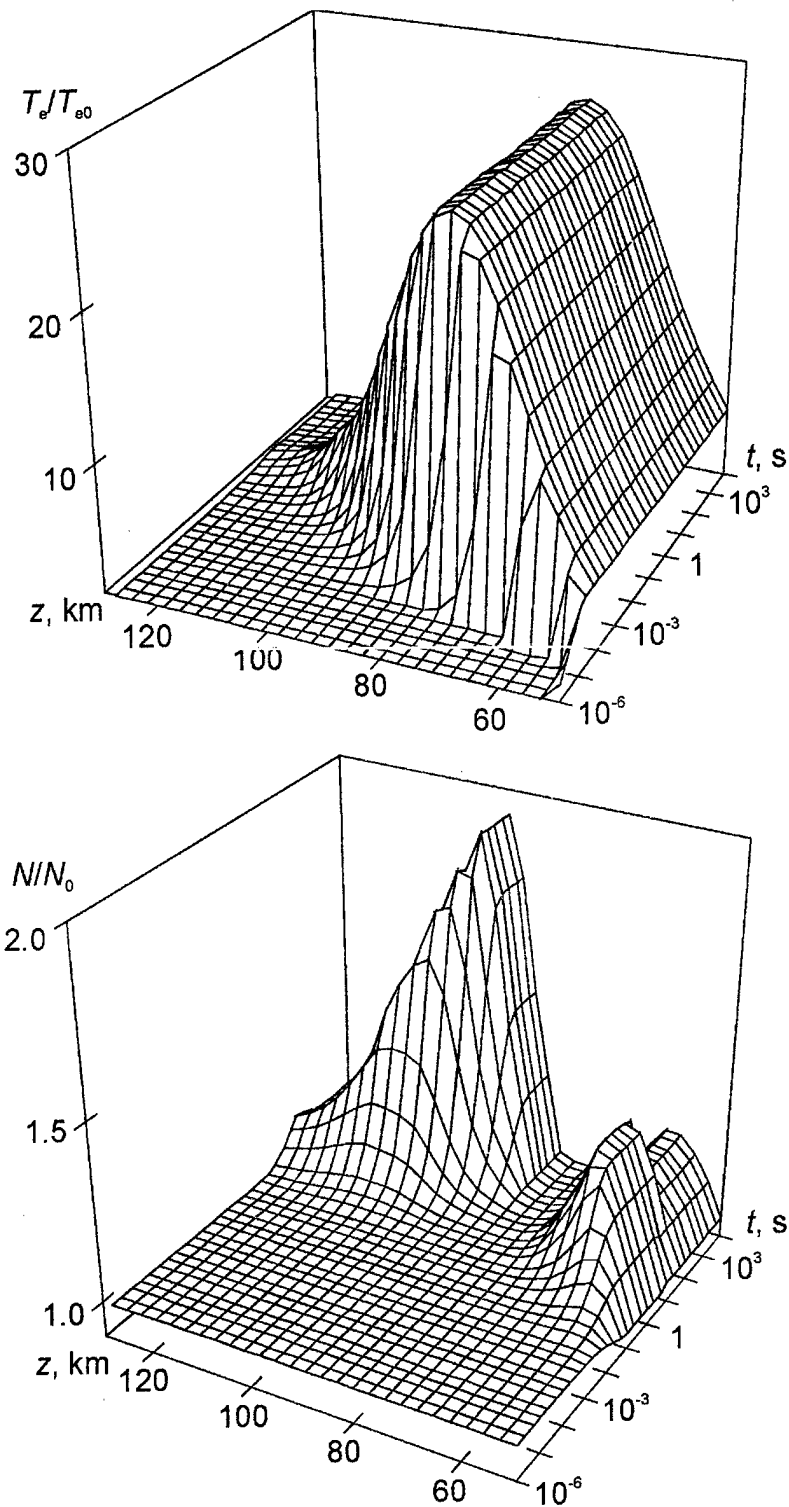


Figure 2. Relative changes in the electron temperature (upper panel) and in the electron number density profiles (lower panel) caused by high-power HF radio waves at a frequency of 10 MHz and effective power of 3 GW. At $t=0$ the plane unmodulated wave arrive at the 50 km altitude.

TRANSIENT WAVES PRODUCED BY A MOVING SOURCE ON A CIRCLE

Victor V. Borisov

Institute of Physics, St. Petersburg University, St. Petersburg, Russia

1. The goal of the present paper is to obtain the solutions of the initial-value problem to the inhomogeneous wave and Maxwell's equations in the space-time domain. We suppose that the point source starts at the fixed moment of time and moves with arbitrary velocity on a circle. General expressions obtained in [1] enable us to give a description of the wavefunctions and components of the vector potential in terms of the transient modes in cylindrical coordinate system. Eventually, we represent the obtained expansions in terms of the Fourier series, whose coefficients are explicit functions of the space-time variables. Due to the property of the delta-function, we manage to sum up the series. We apply the obtained expressions to the description of waves in the particular case of a point source moving with the constant angular velocity and give the relations, which characterize both transient and steady-state waves. We define the space-time domain where the steady-state waves exist.

2. We represent the electromagnetic field vectors \vec{E} and \vec{B} via the scalar and vector potentials Φ and A and use the Lorentz condition:

$$\vec{E} = -\nabla\Phi - \frac{\partial A}{\partial\tau}, \quad \vec{B} = \text{rot}\vec{A}, \quad \frac{\partial\Phi}{\partial\tau} + \text{div}\vec{A} = 0, \quad (1)$$

where $\tau = ct$ is the time variable (c is the velocity of light). Then one can get from Maxwell's equations the scalar wave equation:

$$\frac{\partial^2}{\partial\tau^2}A_i - \nabla^2 A_i = \frac{4\pi}{c}j_i, \quad i = 1, 2, 3, \dots \quad (2)$$

where A_i and j_i are the Cartesian components of the vectors \vec{A} and the current density vector \vec{j} , respectively.

We derive the solutions of equations (2) in cylindrical coordinates ρ, φ, z supposing that $A_1 = A_x$, $A_2 = A_y$, $A_3 = 0$, and the sources on a circle with the radius a are:

$$j_x = -j_\varphi \sin\varphi, \quad j_y = j_\varphi \cos\varphi, \quad j_z = 0, \quad (3)$$

where j_φ is the φ -component of the current density.

3. Suppose now that the point source moves on a circle, then

$$j_\varphi = \frac{1}{2\pi} \frac{\delta(\rho - a)}{\rho} \delta[\varphi - \phi(\tau)] h(z) \quad \tau > 0, \quad j_\varphi = 0 \quad \tau < 0, \quad (4)$$

where $h(z)$ is the Heaviside function, $\delta(\rho - a)$ is the Dirac delta-function, and $\phi(\tau)$ is an arbitrary continuous function. The starting point of the current δ -pulse is $(\rho_0, \phi(0))$. The initial conditions are

$$A_x = A_y = 0, \quad \tau < 0. \quad (5)$$

With the aid of expansions

$$A_i = \sum_m e^{im\varphi} \psi_{im}(\rho, z, \tau), \quad j_i = \sum_m e^{im\varphi} j_{im}(\rho, z, \tau), \quad (6)$$

we obtain from (2) - (5) the following scalar problem:

$$\left[\frac{1}{\rho} \frac{\partial}{\partial \rho} \left(\rho \frac{\partial}{\partial \rho} \right) + \frac{m^2}{\rho^2} + \frac{\partial^2}{\partial z^2} - \frac{\partial^2}{\partial \tau^2} \right] \psi_m = -\frac{4\pi}{c} j_{im}, \quad \psi_m = 0, \tau < 0, \quad (7)$$

where

$$\begin{pmatrix} j_{xm} \\ j_{ym} \end{pmatrix} = \frac{1}{2\pi} \frac{\delta(\rho - a)}{\rho} \delta(z) \begin{pmatrix} -\sin \phi(\tau) \\ \cos \phi(\tau) \end{pmatrix} e^{-im\phi(\tau)} \quad (8)$$

We derive the solutions of the above problem by using a general expression constructed in [1] and find the coefficients of expansion (6) to be

$$\begin{pmatrix} \psi_{xm} \\ \psi_{ym} \end{pmatrix} = \frac{1}{\pi a \rho} \int_T^{\tau - \sqrt{(\rho-a)^2 + z^2}} d\tau' \frac{\cos m\vartheta(\tau')}{\sin \vartheta(\tau')} \begin{pmatrix} -\sin \phi(\tau') \\ \cos \phi(\tau') \end{pmatrix} e^{-im\phi(\tau')} \quad (9)$$

where $T = \max\{0, \tau - \sqrt{(\rho+a)^2 + z^2}\}$, $\cos \vartheta(\tau') = \frac{1}{2a\rho} [\rho^2 + a^2 + z^2 - (\tau - \tau')^2]^{1/2}$,

which is easily transformed into

$$\begin{pmatrix} \psi_{xm} \\ \psi_{ym} \end{pmatrix} = \frac{1}{\pi c} \int_0^{\tilde{T}} d\vartheta \frac{\cos m\vartheta}{s(\vartheta)} \begin{pmatrix} -\sin \phi[\tau - s(\vartheta)] \\ \cos \phi[\tau - s(\vartheta)] \end{pmatrix} e^{-im\phi[\tau - s(\vartheta)]} \quad (10)$$

where $s(\vartheta) = \sqrt{\rho^2 + a^2 + z^2 - 2a\rho \cos \vartheta}$ and $\tilde{T} = \max\{\arccos \frac{1}{2a\rho}(\rho^2 + a^2 + z^2 - \tau^2), \pi\}$.

In the case of the space-time domain given by $\tau - \sqrt{(\rho+a)^2 + z^2} > 0$, we have from (6) and (10):

$$\begin{pmatrix} A_x \\ A_y \end{pmatrix} = \frac{2}{c} \int_{-\pi}^{\pi} d\vartheta \frac{1}{s(\vartheta)} \begin{pmatrix} -\sin \phi[\tau - s(\vartheta)] \\ \cos \phi[\tau - s(\vartheta)] \end{pmatrix} \delta\{\varphi + \vartheta - \phi[\tau - s(\vartheta)]\} \quad (11)$$

To obtain the functions A_x and A_y in the explicit form, we have to solve the equation

$$\varphi + \vartheta - \phi(\tau - \sqrt{\rho^2 + a^2 + z^2 - 2a\rho \cos \vartheta}) = 0 \quad (12)$$

with respect to the variable of integration ϑ .

4. To construct the transient solution in the case $\phi(\tau) = k\tau$ ($k > 0$ is constant), we apply the general expressions (10) and get the coefficients ψ_{xm} and ψ_{ym} in the form:

$$\begin{pmatrix} \psi_{xm} \\ \psi_{ym} \end{pmatrix} = \frac{1}{\pi c} \int_0^{\tilde{T}} d\vartheta \frac{\cos m\vartheta}{s(\vartheta)} \begin{pmatrix} -\sin k[\tau - s(\vartheta)] \\ \cos k[\tau - s(\vartheta)] \end{pmatrix} e^{imk[\tau - s(\vartheta)]}, \quad (13)$$

In the space-time domain $\tau - \sqrt{(\rho + a)^2 + z^2} > 0$, assuming that $r = \sqrt{\rho^2 + z^2} \gg a$ and $\sin \theta = \rho/r$, we have from the above expressions:

$$\begin{pmatrix} \psi_{xm} \\ \psi_{ym} \end{pmatrix} = \frac{1}{2cr} (-i)^m e^{-imk(\tau-r)} \left\{ e^{ik(\tau-r)} J_m[(m+1)ka \sin \theta] + \begin{pmatrix} -i \\ 1 \end{pmatrix} e^{-ik(\tau-r)} J_m[(m-1)ka \sin \theta] \right\} \quad (14)$$

5. Consider now a solution of a scalar wave equation where

$$j = \frac{1}{2\pi} \frac{\delta(\rho - a)}{\rho} \delta[\varphi - \phi(\tau)] h(z) \quad (15)$$

In this case we get the representation of the wavefunction ψ in the form

$$\psi = \sum_m \psi_m(\rho, \varphi, z, \tau) = \frac{1}{\pi c} \int_0^{\bar{T}} d\vartheta \frac{1}{s(\vartheta)} \sum_m \cos m\vartheta e^{im\{\varphi - \phi[\tau - s(\vartheta)]\}}. \quad (16)$$

Assuming that $r \gg a$ and $\phi(\tau) = k\tau$, one can write the terms of the above expansion in the space-time domain $\tau - \sqrt{(\rho + a)^2 + z^2} > 0$ as

$$\psi_m = \frac{1}{cr} e^{-imk(\tau-r) - im\pi/2} J_m(mka \sin \theta) \quad (17)$$

The obtained relations are commonly used for description of the synchrotron radiation (steady-state waves). This result is found by representing the solution of the wave equation in terms of the spherical harmonics. We obtain the explicit expressions for the coefficients ψ_m by using the representation of the solution in terms of the modes in cylindrical coordinate system and describe both transient and steady-state waves.

Acknowledgement. The research described in this publication was made possible in part by the Grant 96-02-17166 from the Russian Foundation for Fundamental Research.

References

- [1] V. V. Borisov, I. I. Simonenko, *J. Phys. A: Math. Gen.*, vol. 27, p. 6243, 1994.

ROTATIONAL MODE OSCILLATIONS IN A CAVITY WITH A TIME-VARYING MEDIUM

Svetlana V.Chumachenko, Oleg A.Tretyakov

Kharkov State University, Chair of Theoretical Radiophysics
Svobody sq., 4, 310077 Kharkov, Ukraine

1.Statement of the problem. The problem of electromagnetic oscillations in a cavity partially filled with a time-varying dielectric is considered (see Fig.1). The state of the field in the dielectric (region II) is determined by the constitutive relation for the polarization vector as $\vec{P}(\vec{E}) = \alpha(t)\vec{E}(\vec{r}, t)$. The coefficient $\alpha(t)$ (or the linear operator of Volterra's kind) determines an electrical susceptibility of the medium in the region II. The problem is solved by the method of modal basis [1-2].

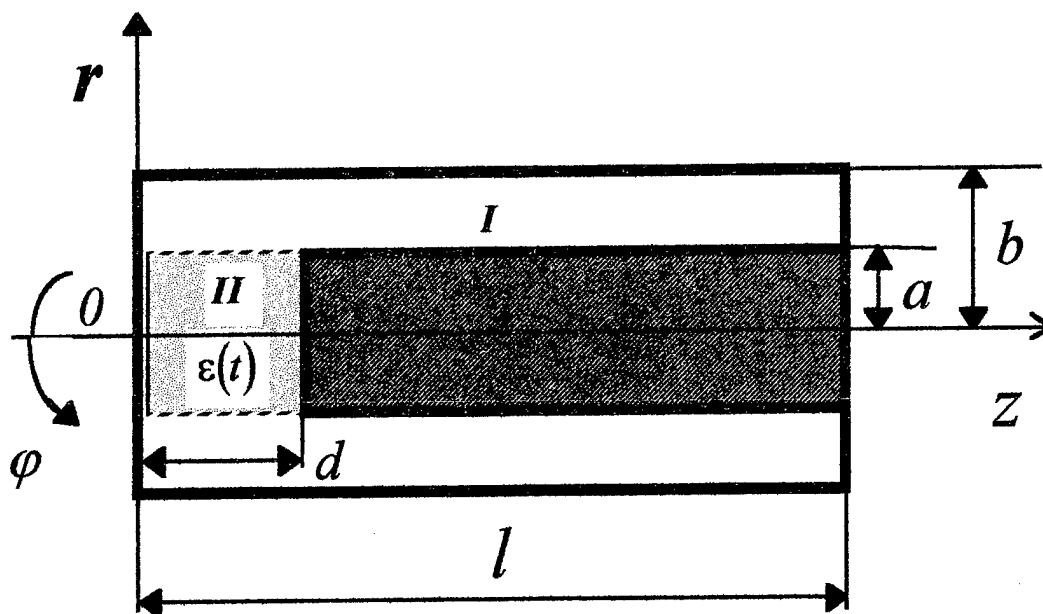


Fig.1. Cavity partially filled with a time-varying dielectric.

Suppose that the intermodal transformations in the dielectric can be neglected. Then every mode will oscillate individually under the influence of the time-varying medium. In this case the electromagnetic field of a rotational mode under consideration can be expressed in the following way:

$$\vec{E}(\vec{r}, t) = e(t)\vec{E}(\vec{r}), \quad \vec{H}(\vec{r}, t) = h(t)\vec{H}(\vec{r}), \quad (1)$$

where the vector functions of co-ordinates are known, and the scalar coefficients depending on time should be sought for. The indices identifying the mode are omitted. The vector-functions of co-ordinates are the basis elements in the space of solutions. In general case they are

determined as a solution of the Dirichlet or Neumann boundary eigenvalue problems for the Laplacian. The scalar time-dependent coefficients satisfy the evolutionary equations, which are obtained after projecting Maxwell's equations on the same basis elements:

$$\begin{cases} \frac{d}{dt}[(1 + \zeta\alpha(t))e(t)] + ickh(t) = 0, \\ \frac{d}{dt}h(t) + ick e(t) = 0, \end{cases} \quad (2)$$

where c is the velocity of light; k is the eigenvalue of the Dirichlet or Neumann boundary eigenvalue problem for the Laplacian; coefficient ζ determines the self-transformation of the mode under consideration due to dielectric in the region II. So, the latter is some function of geometrical parameters of the cavity.

To solve the problem, the eigenvalue k should be found. Solving the evolutionary equations is the main goal of this paper. It will be further obtained in analytical form and analysed in the final part of the paper.

2. Eigenvalue problem for the basis elements. Electromagnetic field of symmetric modes of electric kind can be expressed through the one-component Hertz vector $\vec{\Pi} = \vec{z}_0 \Pi(r, z)$. Potential function of the latter can be written down as follows:

$$\Pi(r, z) = \begin{cases} \Pi_1(r, z) = \sum_{n=0}^{\infty} \varepsilon_n A_n R_n(p_n r) \cos\left(\frac{\pi n}{l} z\right), & a \leq r \leq b, 0 \leq z \leq l, \\ \Pi_2(r, z) = \sum_{m=0}^{\infty} \varepsilon_m B_m J_0(q_m r) \cos\left(\frac{\pi m}{d} z\right), & 0 \leq r \leq a, 0 \leq z \leq d, \end{cases} \quad (3)$$

where

$$R_n(p_n r) = J_0(p_n r) N_0(p_n b) - J_0(p_n b) N_0(p_n r),$$

$$p_n = \sqrt{k^2 - (\pi n/l)^2}, \quad q_m = \sqrt{k^2 - (\pi m/d)^2},$$

ε_j ($j = n, m$) is the Neumann number; J_0, N_0 are the Bessel and Neumann functions; A_n, B_m are the unknown numerical coefficients.

Subjecting the tangential components of electromagnetic field to the boundary conditions at the surface of the cavity, one can obtain a direct formula for the coefficients B_m and a homogeneous matrix equation with respect to the unknown coefficients A_n . A condition of existence of eigenvalue is the vanishing of the determinant that results in the set of independent dispersion equations with respect to the eigenvalues k , namely:

$$\det[\delta_{sn} p_s^2 R_s(p_s a) - \varepsilon_s p_s R'_s(p_s a) L_{sn}] = 0, \quad n = 0, 1, 2, \dots; \quad s = 0, 1, 2, \dots;$$

where k is involved in p_s and q_m , see (3); δ_{sn} is the Kroneker delta;

$$L_{sn} = \sum_{m=0}^{\infty} \varepsilon_m q_m \frac{J_0(q_m a)}{J'_0(q_m a)} K_{ms} K_{mn}, \quad K_{ms} = \frac{1}{2} \left(\frac{\sin \pi(m - s\theta)}{\pi(m - s\theta)} + \frac{\sin \pi(m + s\theta)}{\pi(m + s\theta)} \right).$$

3. Solution of the evolutionary equations. Re-writing the system of evolutionary equations (2) in the matrix form, we can solve it following [3-4]. Further on suppose, for example, that

the coefficient of electric susceptibility is $\alpha(t) = \exp(-\gamma t)$. As a result, we obtain the formulas for the calculation of coefficients $e(t)$ and $h(t)$:

$$e(t) = \frac{\sqrt{C^2 + D^2}}{1 + \zeta \exp(-\gamma t)} \sin(ckt - f_1), \quad h(t) = i\sqrt{C^2 + D^2} \cos(ckt - f_1),$$

where $C = \zeta P - ih^{(0)}$, $D = \zeta Q - e^{(0)}$, $f_1 = \text{arctg} \frac{D}{C}$,

$$P = \frac{e^{(0)}L_2 - ih^{(0)}(L_1 + \zeta L_1^2 - \zeta L_2 L_3)}{1 - \zeta^2 L_1^2 + \zeta^2 L_2 L_3}, \quad Q = \frac{e^{(0)}(L_1 - \zeta L_1^2 + \zeta L_2 L_3) - ih^{(0)}L_3}{1 - \zeta^2 L_1^2 + \zeta^2 L_2 L_3},$$

L_1, L_2, L_3 are functions of t

$$L_1(t) = \frac{2 - (\gamma \sin 2ckt + 2 \cos 2ckt) \exp(-\gamma t)}{\gamma^2 + 4},$$

$$L_2(t) = \frac{\gamma^2 + 2 + [\gamma(\sin 2ckt - \gamma \cos^2 ckt) - 2] \exp(-\gamma t)}{\gamma(\gamma^2 + 4)},$$

$$L_3(t) = \frac{2 - [2 + \gamma(\sin^2 ckt - \gamma \sin 2ckt)] \exp(-\gamma t)}{\gamma(\gamma^2 + 4)}.$$

Notice that the exponent brings the greatest contribution to the functions L_1, L_2, L_3 in some interval of values: $0 \leq t \leq T$, and $\alpha(t) \rightarrow 0$ when $t \rightarrow \infty (t > T)$.

4. Conclusion. Thus in the considered case the time dependences for the unknown field $\vec{E}(\vec{r}, t)$, $\vec{H}(t)$ have been found. They have been obtained in explicit form and are expressed in elementary functions. We suppose that the coefficients for the field $e^{(0)}, h^{(0)}$ are known from the initial conditions.

References.

- [1] O.A. Tretyakov, Modal Basis Method, *Sov. J. Commun. Technol. Electronics*, v.31, N6, 1986.
- [2] O.A. Tretyakov, Essentials of Non-stationary and Nonlinear Electromagnetic Field Theory. Analytical and Numerical Methods in Electromagnetic Wave Theory, M. Hashimoto, M. Idemen, and O.A. Tretyakov (Eds.), Tokyo, Science House, 1993.
- [3] S. Hayashy, Waves in electrical transmission lines, Edited by V. Yu. Lomonosov. Moscow, Nauka, 1960, p.32-50, (Russian transl.).
- [4] E.A. Koddington, N. Levinson, Theory of ordinary differential equations, 1958, p.75 -121, (Russian transl.).

MODELLING TIME-DEPENDENT RADIO WAVE SCATTERING FROM SUB-SURFACE GROUND MEDIUM

Sergiy O. Masalov and Olexander O. Puzanov

Usykov Institute for Radiophysics and Electronics of the National Academy of Sciences of Ukraine
12 Proscura St., Kharkiv, 310085 Ukraine,
e-mail: masalov@ire.kharkov.ua, puzanov@ire.kharkov.ua

Introduction. Lately the interest to non-stationary electromagnetic waves, expanding radar opportunities, is steadily growing. Having a wide low-frequency spectrum, the non-stationary radio waves find a use at sounding absorbing environments, in particular, grounds and rocks, and provide large depth of penetration.

The problem of transient radio-waves scattering on earth structures, discussed here, closely adjoins to a problem of interpretation of results of sounding and is one of the major components of work on the increase of efficiency of a sub-surface radar. Only limited class of similar tasks can be solved analytically [1]. For modeling of non-stationary scattering we use the approach consisting in finding the solution in frequency domain after a normal impedances method [2,3], and its translation in time domain with application of the inverse Fourier transformation. Thus for the given (continuous) law of a humidity change on the depth of a structure on the basis of experimentally received frequency dependences of permittivity and specific conductivity, the appropriate frequency-spatial dependences of these electrical characteristics are formed. In the given work, a mathematical model, features of construction of computing algorithm, basic features of behavior of the transient electromagnetic fields reflected from earth structures are discussed, the examples of the analysis of obtained results through the inverse-conjugate filtration [4] are summarized, and the limits of its applicability are shown.

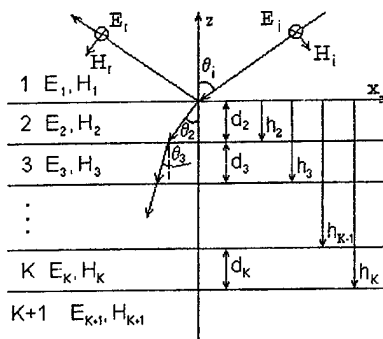


Fig. 1. Geometry of the problem.

2. Method. Suppose that $K-1$ homogeneous dielectric layers of the thicknesses d_k ($k=2 \div K$) are located between the half-spaces 1 ($z > 0$) and $K+1$ ($z < -h_K$) (Fig. 1), thus each of the partial regions is characterized by electrical parameters ϵ_k , μ_k , and σ_k . From the half-space 1, at the angle θ_i , a plane electromagnetic wave is incident on the system of layers. At any dependence on time, and if D_t is a time interval extended enough to capture the whole transient process, and $\varphi(t) = 0$ for $t \notin [0, \Delta t] \subset [0, D_t]$, by use of the direct (F) and inverse (F^{-1}) discrete Fourier transformations in the time domain, the scattered field can be represented as

$$\{u_n(t_n)\} = \text{Re} \left\{ F^{-1} \left\{ \tilde{V}_m(i\omega_m) \right\} F \left[\{ \varphi_n(t_n) \} \right] \{ \exp(-i\omega_m t_0) \} \right\},$$

where $\{\tilde{V}_m(i\omega_m)\}$ are the values of complex amplitudes of necessary components of electric or magnetic fields, or the factors of reflection at the frequencies: $0, \delta f, 2\delta f, \dots, D_f$, found after the normal impedances method [2,3]; t_0 is an entered temporary delay determining a spatial location of the incident pulse front at the moment $t = 0$ relatively to the point with coordinates $[x, z] = [0, 0]$ at given θ_i . It is reasonable to choose

$t_0 = z_0 \sqrt{\epsilon_0 \mu_0} (\cos 2\theta_i) / (\cos \theta_i)$. This sets a location of the incident pulse front, when at the moment $t = 0$ its beginning is observed at the point $[x_0, z_0] = [-z_0 \tan \theta_i, z_0]$, be disposed on the ray of reflection from the upper boundary of the layers.

To find $\{\tilde{V}_m(i\omega_m)\}$, the calculations for the frequencies $0, \delta f, 2\delta f, \dots, \Delta f$ (Δf is a width of a spectrum $\varphi(t)$) are made and then the mirror complex conjugate extension of a definition relatively to the Nyquist' frequency $D_f/2$ under the given below circuit is carried out, equivalent to an introduction of negative frequencies in the continuous Fourier transformation

$$\{\tilde{V}_m(i\omega_m)\} = \begin{cases} \{V_m(i\omega_m)\}, & m = \overline{1, N_{D_f}/2} \\ 0, & m = N_{D_f}/2 + 1 \\ \{V_{N_{D_f}/2+2-m}^*(i\omega_{N_{D_f}/2+2-m})\}, & m = \overline{N_{D_f}/2+2, N_{D_f}} \end{cases}$$

The values of N_{D_t} and N_{D_f} coincide and determine a quantity of discrete temporary readouts of a diffraction field at the moments $0, \delta t, 2\delta t, \dots, D_t$, or a quantity of values $\tilde{V}_m(i\omega_m)$ at the discrete frequencies $0, \delta f, 2\delta f, \dots, D_f$, with $\delta f = 1/D_f$, $D_f = 1/\delta t$. The condition $\Delta f \leq D_f/2$ should be satisfied in the calculations or, that is the same, $\delta t \leq 1/(2\Delta f)$. It is obvious that $\delta t = \Delta t / (N_{\Delta t} - 1)$, whence $N_{\Delta t} \geq 2\Delta t \Delta f + 1$. It is possible to minimize computing expenses by choosing $N_{\Delta t} = 2\Delta t \Delta f + 1$.

3. Transients for single-layered structures. The analysis of the frequency dependences of the absolute value of the reflection factor $|B_1(i\omega)|$ and the results of calculations of diffraction fields with $\theta_i = 0^\circ$ reveal the following features. In the frequency domain, the growth of losses conforms to the reduction of reflection factor $|B_1(i\omega)|$ oscillation (Fig.2), and, in time domain, the reduction of a transient duration. Thus the rise time of each subsequent pulse of a sequence leaving a layer grows, that is connected to a faster attenuation of the high-frequency spectral component. Significant reflection of spectral components of low frequencies (for which $\tan \delta = \sigma / (\epsilon\omega) > 0.2$) from boundaries of the unit of partial regions causes: 1) an increase of the amplitude and a pulse rise time reflected from the upper interface of the structure; 2) a tightening of trailing edges of pulses of a sequence leaving a layer, in the case that $\sigma_2 < \sigma_3$. (If $\sigma_2 > \sigma_3$, the reflections of the low frequencies of a pulse spectrum from boundary of regions 2-3 cannot compensate their decreased level after the passage through the boundary 1-2; in the upper half-space the sequence of two-polar pulses is observed). Thus, the use of single-polarity sounding pulses allows visually to estimate a ratio of the specific conductivities of the border regions; 3) impossibility to use, for underground

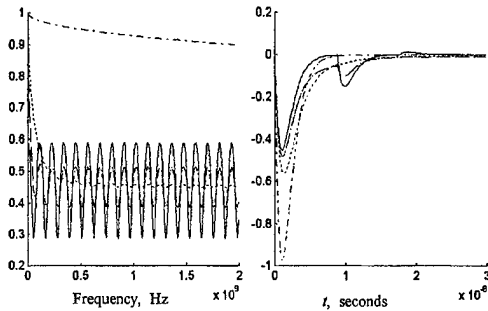


Fig.2. a) Frequency dependences of the absolute value of reflection factor $|B_1(i\omega)|$ for a single-layer structure ($d_2 = 0.5$ m, $\epsilon_1^r = 1$, $\epsilon_2^r = 7$, $\epsilon_3^r = 15$, $\sigma_1 = 0$ Siem/m) at various values of specific conductivities σ_2 and σ_3 : $\sigma_2 = \sigma_3 = 0$ Siem/m (continuous line), $\sigma_2 = \sigma_3 = 1.2 \cdot 10^{-2}$ Siem/m (dotted line), $\sigma_2 = \sigma_3 = 5 \cdot 10^{-2}$ Siem/m (dots), $\sigma_2 = \sigma_3 = 20$ Siem/m (dot-and-dash line); b) time dependence of diffraction fields.

sounding, video pulses of durations $\Delta t \approx \epsilon_2 / \sigma_2$, which spectrum is in the frequency interval $f \in [0, \sigma_2 / \epsilon_2]$, and for which $\tan \delta > 0.2$. This for example, for chestnut loam means a good efficiency of application for the sounding pulses with the low frequency of a spectrum from 47 MHz (for humidity $W=2.5\%$) up to 413 MHz ($W=20\%$); but Δt cannot be too small, as it is not favorable from the power point of view (at an excessively wide spectrum only its insignificant part gets in the oscillating part of $|B_1(i\omega)|$ dependence, which the specific conductivities of environments are minimum). Thus, the efficiency of usage of video pulses for underground sounding is due to the fact that their spectral density is concentrated in the range of the low frequencies, where the oscillating character of $|B_1(i\omega)|$ is most expressed due to smaller values of specific conductivities of environments.

4. Transients at continuous humidity variation along the depth of the structure. Within the framework of the used method, the calculation of the scattering by layers with continuously varied in depth dielectric properties dependent on humidity is reduced to the calculations for an equivalent structure, which replaces the real ones and which is formed by rather thin homogeneous layers. Their thicknesses d_l are determined on the basis of the maximum value of permittivity as a function of frequency in the previous elementary layer. On the other hand, these thicknesses allow to determine spatial coordinates, in conformity with the given law of humidity change $W(h)$, determining in its turn the frequency dependences of permittivity and specific conductivity. Thus, at $\epsilon_{al} = \epsilon_{al}(f, W(h_l))$, $\sigma_l = \sigma_l(f, W(h_l))$, and

$$h_l = \sum_{k=2}^l d_k, \text{ we assume}$$

$$d_l = \frac{c \Delta t}{m \sqrt{\sup(\epsilon_{al-1}(f, l-1))}},$$

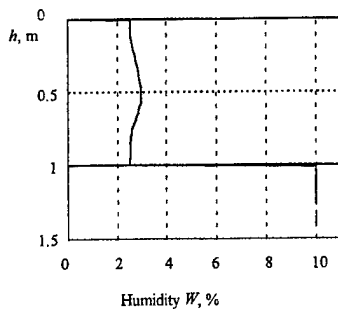


Fig. 4. Law of humidity variation in depth for the structure «gray loam-clay».

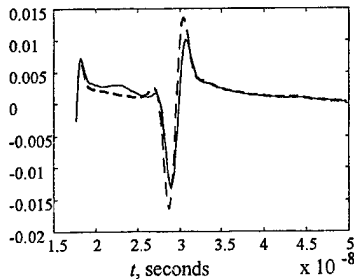


Fig. 5. The pulses reflected from the lower boundary of the layer of gray loam in the case of continuous humidity variation in depth according to Fig. 4 (solid line) and the fixed humidity $W = 2.5\%$ (dotted line).

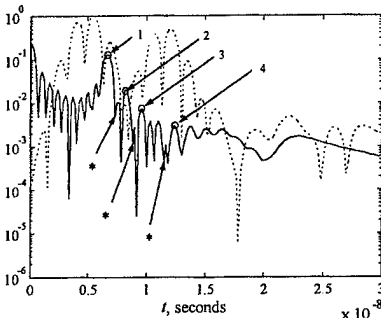


Fig. 8. Dependences on time of the magnitude of diffraction field (dots) and the result of the processing (solid line). The asterisks at arrows denotes characteristic «harbingers» of the reflections, and figures are the numbers of the received responses; the response 1 corresponds to the moment of arrival, at the point of observation, of reflection from the upper boundary of a ground.

References:

- [1]. S.O Masalov, O.O.Puzanov, The diffraction of video-pulses by layered dielectric structures, *Radiofizika i radioastronomiya*, 2, №1, pp. 85-94, 1997 (in Russian).
- [2]. L.M.Brekhovskikh, *Waves in layered media*, Moscow: Akad. Nauk, 1957 (in Russian).
- [3]. K.Demarest, R.Plumb, and Z.Huang, FDTD Modeling of Scatterers in Stratified Media, *IEEE Trans. Antennas and Propagations*, Vol. 43., No 10, pp.1164-1168, 1995.
- [4]. N. Ossumi, K. Ueno. Microwave Holographic Imaging of Underground Objects, *IEEE Trans. on Antennas and Propagation*, Vol. 33, No 2, pp. 152-159, 1985.

This work is in part supported by the STCU fund. Project #366.

where l is a number of the current elementary layer; m is the value showing how much the spatial duration of the pulse exceeds the chosen thickness of a current elementary layer in given environment (for the calculations with the minimum computing expenses and sufficient accuracy, the value $m=100$ is most suitable (minimally acceptable)); f is the frequency.

In the case of frequency-dependent parameters of a layer of gray loam of the thickness of 1 m, laying on the half-space formed by clay, and humidity variation according to Fig.4, the transient process for the time interval between the end of reflection from the loam boundary with air and the end of reflection from the lower boundary is presented in Fig.5. The incident pulse is bidirectional in the considered case, angle of incidence thus is $\theta_i = 10^\circ$, and $z_0 = 1.5$ m. As can be seen, the diffraction field of a video pulse is rather sensitive even to insignificant

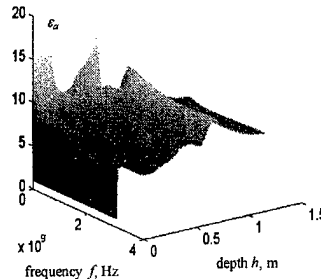


Fig. 6. Frequency-depth dependence of permittivity.

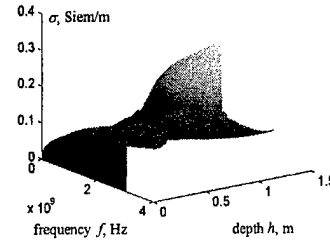


Fig. 7. Frequency-depth dependence of specific conductivity.

fluctuations of the humidity on the depth. The evidence to that is an appreciable decrease of amplitude of reflection from the lower boundary of the layer, some increase of growth times of the field strength, and also an occurrence

of reflections on the moments previous to occurrence of reflections from the lower boundary.

The dependences on depth and frequency of electrical parameters of a typical earth structure «gray loam (0.6 m) - chestnut loam (0.2 m) - clay (0.1 m) - sand », according to the measured law of humidity change in depth, are shown on Fig.6,7. Fig.8 illustrates the behavior of the absolute value of the scattered field in time (dots) for a bidirectional video pulse ($\theta_i = 10^\circ$, $z_0 = 1$ m) and the result of its processing by the method of the inverse-conjugate filtration [4] (solid line). As can be seen, up to the depths of 0.6 m this method allows to allocate rather precisely the moments of formation of reflections from the basic electrical inhomogeneities of the structure. For larger depths, where there is a significant distortion of the form of initial pulse, the used filtration method proves to be inapplicable.

Waveguide Circuits

A Novel Approach to the Computation of Fields inside Waveguides and Cavities by Fourier Series

H. Rahman
Saint Louis University
Department of Electrical Engineering
Saint Louis, MO 63156, USA

Abstract- This paper attempts to present a simple and efficient approach to the analysis of waveguides and cavities using Fourier series. This formulation is broad-based and general that allows field solutions to problems in waveguides and cavities with a considerable computational advantage. Numerical results in the form of current distributions are presented to illustrate the theory.

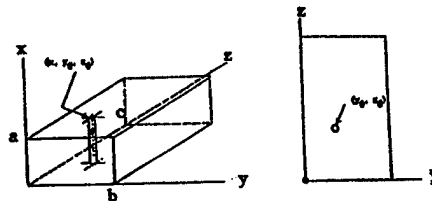
I. INTRODUCTION

The analysis of electromagnetic field problems relevant to waveguides and cavities is associated with the dyadic Green's function which is most appropriately considered as an operator to generate the field from a given source function. Several different but equivalent representations of the dyadic Green's function have been developed by several researchers. The presence of conducting wires within waveguides and cavities was handled by obtaining an integral equation using the Green's dyad, solving it numerically by the method of moments. The dyadic Green's function for a problem of this nature is very difficult to compute numerically. The dilemma of large computation time and the complexity involved in case of dyadic Green's function approach warrants further work [1] in this area.

II. PROBLEM FORMULATION

The geometrical configuration, for the purpose of the problem is shown in Fig. 1. The cavity walls are assumed to be lossless and perfectly conducting. The dimensions of the cavity are represented by a , b , and c in the x , y , and z direction, respectively. Consider a perfectly conducting, round, thin wire of radius r ($r \ll \lambda$) penetrating into the cavity interior through a small hole located at (a, y_0, z_0) . The wire is assumed to be oriented parallel to the x -axis, and is excited by electromagnetic sources exterior to the cavity. Assume further that the media in both the interior and exterior regions are linear, homogeneous, isotropic and lossless, and are characterized by free-space parameters (μ_0, ϵ_0). The time harmonic variation with angular frequency ω and the factor $\exp(j\omega t)$ are understood, and the rationalized MKSC system of units is used throughout. The problem now is to determine the field existing within the cavity, and the currents induced on the wire due to external sources.

Figure 1. (right side)
A rectangular cavity with a single straight wire within it



Since the wire is thin, only the axial component of the wire current need be considered, which can be assumed to have negligible circumferential variation. From the assumed current distribution on the wire, it is evident that the magnetic vector potential, $\underline{A} = \underline{u}_x A_x$, is enough for representing the field inside the cavity, where \underline{u}_x is the unit vector in the direction of x , and A_x is the x -component of \underline{A} .

The magnetic vector potential, \underline{A} , due to a current density \underline{J} in the cavity is a solution of

$$\nabla^2 \underline{A} + k^2 \underline{A} = -\underline{J}, \quad (1)$$

where ∇^2 is the Laplacian operator, k is the wave number, and is given by $k = 2\pi/\lambda$. The current density evidently depends on the assumed axial current, and is expressed as $\underline{J} = \underline{u}_x I(x) \delta(y-y_0) \delta(z-z_0)$, where $\delta(\cdot)$ is a Kronecker delta function. $I(x)$ can be represented by a truncated Fourier cosine series as:

$$I(x) = \sum_{n=0}^M B_n \cos \frac{n\pi x}{a}, \quad (2)$$

where B_n are unknown Fourier coefficients by taking M to be sufficiently large, a good approximation to the specified current on the wire is obtained. We can solve the electric field vector in terms of \underline{A} by

$$\underline{E} = -j\omega\mu_0 \underline{A} + \frac{1}{j\omega\epsilon_0} \nabla(\nabla \cdot \underline{A}). \quad (3)$$

The general expression of the x -component of the electric field, describing all modes existing within the cavity, is

$$E_x = \sum_{m=0}^{\infty} \sum_{n=0}^{\infty} \sum_{p=1}^{\infty} A_{mnp} \cos \frac{m\pi x}{a} \sin \frac{n\pi y}{b} \sin \frac{p\pi z}{c}, \quad (4)$$

where A_{mnp} are the mode amplitudes yet to be determined. Obviously, the field component represented by eq. (4) satisfies the boundary conditions on the walls of the cavity. However, it remains to satisfy the boundary condition on the wire surface.

Equations (1), (3) and (4) can be combined to obtain a relationship between mode amplitudes and Fourier coefficients, and is

$$\begin{aligned} & \sum_{m=0}^{\infty} \sum_{n=1}^{\infty} \sum_{p=1}^{\infty} [k^2 - k_{mnp}^2] A_{mnp} \cos \frac{m\pi x}{a} \sin \frac{n\pi y}{b} \sin \frac{p\pi z}{c} \\ &= \frac{j}{\omega \epsilon_0} \delta(y - y_0) \delta(z - z_0) \sum_{m=0}^{\infty} B_m [k^2 - (\frac{v\pi}{a})^2] \cos \frac{v\pi x}{a}, \end{aligned} \quad (5)$$

where

$$K_{mnp}^2 = (\frac{m\pi}{a})^2 + (\frac{n\pi}{b})^2 + (\frac{p\pi}{c})^2 \quad (6)$$

We must assume that the series given by Eq.(4) converges uniformly over the fundamental ranges, dictated by the cavity dimensions, $0 \leq x \leq a$, $0 \leq y \leq b$, $0 \leq z \leq c$. Now multiplying both sides of Eq. (5) by the product $\cos(m'\pi x/a) \sin(n'\pi y/b) \sin(p'\pi z/c)$ and carrying out integrations term by term over the fundamental intervals by forming suitable inner products, one ends up with solution to A_{mnp} in terms of the unknown Fourier coefficients as

$$A_{mnp} = \frac{4jB_m [k^2 - (m\pi/a)^2]}{bc\omega\epsilon_0 [k^2 - K_{mnp}^2]} \sin \frac{n\pi y_0}{b} \sin \frac{p\pi z_0}{c}. \quad (7)$$

Note that the indices m', n', p' have been changed back to m, n, p respectively to avoid notational complexity, and orthogonality properties have been utilized to obtain Eq. (7). Substitution of Eq. (4) into Eq. (7) results in

$$E_x = \sum_{m=0}^{\infty} \sum_{n=1}^{\infty} \sum_{p=1}^{\infty} \frac{4jB_m [k^2 - (m\pi/a)^2] \sin \frac{n\pi y_0}{b} \sin \frac{p\pi z_0}{c}}{bc\omega\epsilon_0 [k^2 - K_{mnp}^2]} \cos \frac{m\pi x}{a} \sin \frac{n\pi y}{b} \sin \frac{p\pi z}{c}. \quad (8)$$

It is sufficient to enforce only the condition that the axial component of the electric field vanish on the wire surface. In case of a thin wire, the boundary condition is applied to a single generatrix along the wire surface, whereas, in case of a thick wire, although the current is still assumed to reside on the wire axis, the boundary conditions are applied on four generatrices spaced equally around the wire surface. The boundary condition appropriate for this problem is

$$E_x - z(x)I(x) = -E_x^{inc}, \quad (9)$$

where $z(x)$ is defined as the impedance function of position, and E_x^{inc} is the impressed field.

Define a testing function of the following form:

$$W_u = \cos \frac{u\pi x}{a} \delta(y - y_0 - r) \delta(z - z_0), \quad (10)$$

where r is the radius of the thin wire under consideration. Substituting E_x and I_z from Eq. (2) respectively into Eq. (9), multiplying both sides of the resulting equation scalarly by W_u and finally performing integrations within the limits of the cavity dimensions, we have

$$\sum_{v=0}^M Z_{uv}^q B_v + \sum_{v=0}^M Z_{uv}^I B_v = V_u, u = 0, 1, 2, \dots, M, \quad (11)$$

$$Z_{uv}^q = \sum_{n=1}^{\infty} \sum_{p=1}^{\infty} \frac{4[k^2 - (v\pi/a)^2] \sin \frac{n\pi y_0}{b} \sin \frac{n\pi(y_0+r)}{b} \sin^2 \frac{p\pi z_0}{c}}{jbc\omega\epsilon_0 [k^2 - k_{mnp}^2]} \int_0^a \cos \frac{u\pi x}{a} \cos \frac{v\pi x}{a} dx, \quad (12)$$

$$Z_{uv}^I = \int_0^a z(x) \cos \frac{u\pi x}{a} \cos \frac{v\pi x}{a} dx, \text{ and} \quad (13)$$

$$V_u = \int_0^a E_x^{inc} \cos \frac{u\pi x}{a} dx. \quad (14)$$

Equation (11) can be expressed in matrix form, and is

$$[Z_{uv}][B_v] = [V_u], \quad (15)$$

where

$$[Z_{uv}] = [Z_{uv}^a] + [Z_{uv}^l]. \quad (16)$$

Note that $[Z_{uv}]$ is an $(M+1) \times (M+1)$ matrix, since $u = 0, 1, 2, \dots, M$ and $v = 0, 1, 2, \dots, M$. If the matrix $[Z_{uv}]$ is non-singular, its inverse exists. The unknown Fourier coefficients B_v are then given by

$$[B_v] = [Z_{uv}]^{-1} [V_u]. \quad (17)$$

Substitution of B 's in Eq. (7) determines A_{wmp} , which, in turn determine the field E_x inside the cavity. Also, by substituting B 's in Eq. (2) we obtain the current distribution on the wire inside the cavity. Once the current distribution on the wire is known, other information pertaining to the wire-cavity problem are easily determined.

III. NUMERICAL RESULTS

Selected numerical results are presented to illustrate the approach to the solution of field problems relevant to an electromagnetic cavity. Results are computed for a cavity with dimensions $3 \times 4 \times 5$, with the wire of radius .0001, being located at $(x, 1.5, 2.0)$. $E_x^{\text{inc}} = \delta(x-3)$ and $z(x) = Z_0 \delta(x)$ are chosen, when Z_0 is the lump impedance at $x=0$. The infinite Fourier series has been truncated to arbitrary M term to approximate the current distribution on the wire. An extensive numerical testing demonstrates that M (F_c on graph) of the order of only 10 provides satisfactory results as shown in Fig. 2. It reveals that the current distribution remains practically the same as the number of Fourier coefficients increases beyond 10, demonstrating the convergence of the solution. In formulating the problem, the modes corresponding to x variation have been dispensed with by using the Fourier technique which essentially employs the properties of orthogonality. Impedance elements, composed of doubly infinite sum is reduced to a simply infinite sum by employing a closed form solution. The resulting sum pertaining to y variation is truncated, and numerically tested as shown in Fig. 3. A faster convergence can be obtained for a thicker wire when the boundary condition is enforced on four generatrices.

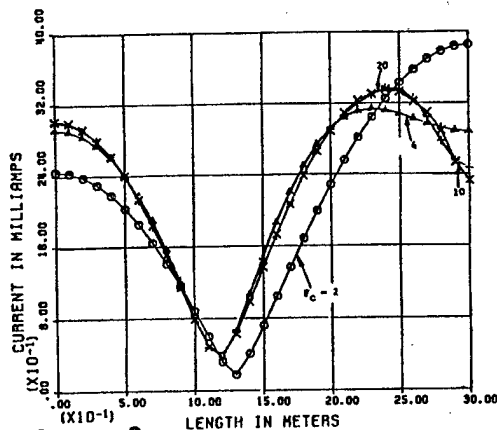


Figure 2. Current magnitude on a single, straight thin-wire for different numbers of Fourier coefficient F_c , computed with $f = 60$ MHz, $n = 1000$ and $Z_0 = 50$ ohms.

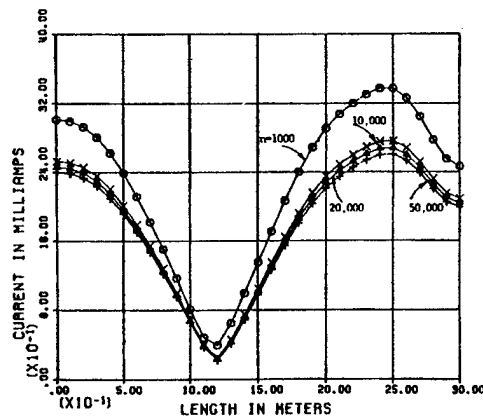


Figure 3. Current magnitude on a single, straight thin-wire for various mode indices n , computed with $F_c = 10$, $f = 60$ MHz, $Z_0 = 50$ ohms and $D/2 = .0001$.

IV. CONCLUSION

The example of determining fields and currents induced on conducting wires, developed in section III, introduces the concept of Fourier series method which can be easily extended to various electromagnetic field problems relevant to waveguides and cavities. Waveguide problems provide comparatively easier solutions since the field existing in waveguide is associated with a doubly infinite sum. This method bypasses the dyadic Green's function approach thereby leading to a solution which is computationally easier to handle. This method provides a solution which is economical and computationally stable. This formulation is broad-based and general that allows field solutions to problems in waveguides and cavities with a considerable computational advantage.

References

- [1] Rahman H., and J. Perini, "Current on a wire parallel to two walls of a rectangular cavity" *Journal of Electromagnetic Waves and Applications*, Vol. 2, No. 3/4, 195-317, 1988.

MICROWAVE CAVITY WITH NONLINEAR LOAD

Diana V. Semenikhina

Taganrog State University of Radio Engineering, Taganrog, Russia, airpu@tsure.ru

Abstract A rigorous solution and numerical results for the problem of excitation of a resonator with nonlinear load are presented. Numerical results are obtained for the excitation by a primary source, whose first or third harmonic in frequency is close to resonance at the fundamental mode H_{101} . It was discovered that the amplitude of the third harmonic of field exceeds the amplitude of the field at fundamental frequency by 20...40 dB.

1. INTRODUCTION

In a series of the previous publications [1,2], solutions of exterior and interior nonlinear problems of electromagnetic wave excitation and scattering were discussed. Numerical results and experimental studies have revealed the phenomenon of nonlinear excitation and scattering for the bodies with natural nonlinear contacts or with nonlinear loads such as microwave diodes. In the case of exterior problems they can be considered as a weak effect. They need to be taken into account in a number of special cases. If these effects would be used in antenna design, it is necessary to develop the measures for amplification of higher harmonic fields excited due to nonlinear loads.

Solution of internal nonlinear boundary problems enables one to investigate electromagnetic wave excitation by nonlinear loads of internal regions for example, in waveguides and resonators. Analysis of the problem about a waveguide excitation is caused by the fact that nonlinear effects even due to natural contacts have an essential influence on the waveguide workability [3]. The problem about a nonlinear load excitation in a microwave resonator is one of important problems for a practical application in the microwave device engineering. First, whereas the resonator is a frequency-selective system and can serve as an amplifier of the fields of higher harmonics excited on the nonlinear load if their frequencies are resonant. Second, nonlinearly loaded resonators are already applied in microwave devices but approximate methods of their analysis are used.

In the present paper, a rigorous solution and numerical results for the problem of excitation of a resonator with nonlinear load are offered.

2. NONLINEAR BOUNDARY VALUE PROBLEM

We consider a cavity resonator formed by a section of rectangular air-filled waveguide loaded with a distributed nonlinear load in the form of cross-shaped narrow non-uniform nonlinear contact with the cubic V-I characteristic located at $z = z_k$. In the internal region of the resonator primary source distributions $\vec{j}^{e(m)pr}$ are set (Fig. 1 a), where index 2 refers to currents at the wall $x=a$, and index 4 to the one $x=0$. In these equations, an auxiliary magnetic source at each observation point has the same direction as the magnetic current on the site. The problem is solved by the method of integral equations with the use of the Lorentz lemma and nonlinear boundary conditions (NBC), which are derived from the following mathematical model of nonlinear contact (Fig. 1 b).

Assume that the contact is narrow along z ($\Delta z \ll \lambda_n$), where λ_n is the n -th harmonic wavelength. Then the electric current flows across the contact along z , and magnetic one flows along x and y on the wide and narrow walls of the resonator, respectively (Fig. 1). Decompose the contact into elementary cells whose sizes are $\Delta \ll \lambda_n$.

Within the limits of a cell the currents can be considered constant and parameters of the contact do not vary. We consider parameters of cubic V-I characteristic connecting the current i and voltage U are given at each cell. Then local NBC at each cell can be obtained as follows [4]:

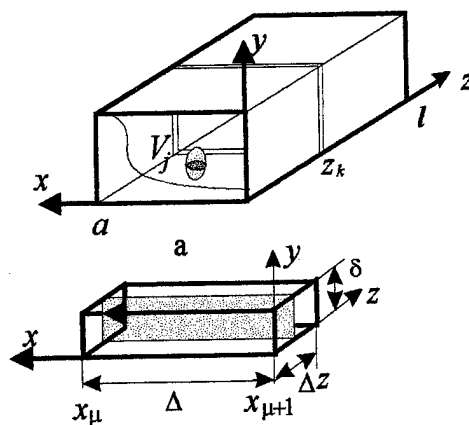


Fig. 1

$$J_{1/3n,z}^3(x_\mu)\Delta x = -A_{1/3n}(x_\mu)\Delta z J_{1/3n,x}^m(x_\mu) + \\ + B_{1/3n}(x_\mu)\Delta z^2 \sum_{s=-\infty}^{\infty} J_{1/3s,x}^m(x_\mu) J_{1/3n-s,x}^m(x_\mu) - \\ - C_{1/3n}(x_\mu)\Delta z^3 \sum_{q=-\infty}^{\infty} J_{1/3n-q,x}^m(x_\mu) \times \\ \times \sum_{s=-\infty}^{\infty} J_{1/3q-s,x}^m(x_\mu) J_{1/3s,x}^m(x_\mu),$$

where the indices 1 and 3 relate to the currents on the top and bottom walls, respectively; and A_n, B_n, C_n coefficients defined by the nonlinear load parameters.

Further the Lorentz lemma is applied, and the auxiliary field is chosen as a field in a resonator without nonlinear loads satisfying the boundary conditions $E_\tau = 0$ at the resonator walls.

The system of nonlinear integral equations is solved by the method of moments with piece-constant basis functions and Dirac weighting functions. The observation point is consecutively placed on each site and NBC are applied. As a result, a system of nonlinear algebraic equations (NAES) for the harmonic amplitudes of magnetic surface currents in nonlinear cells is obtained:

$$-A_{1n}(x_\mu)\Delta z J_{1n,x}^m(x_\mu) + B_{1n}(x_\mu)\Delta z^2 \sum_{s=-\infty}^{\infty} J_{1s,x}^m(x_\mu) J_{1n-s,x}^m(x_\mu) - C_{1n}(x_\mu)\Delta z^3 \times$$

$$\sum_{q=-\infty}^{\infty} J_{1n-q,x}^m(x_\mu) \sum_{s=-\infty}^{\infty} J_{1q-s,x}^m(x_\mu) J_{1s,x}^m(x_\mu) = \int_{V_j} \bar{j}_n^{m,cm} \bar{H}_n^m dV +$$

$$+ \Delta z \sum_{\mu=1}^N [J_{1n,x}^m(x_\mu) \int_{x_\mu-\Delta x/2}^{x_\mu+\Delta x/2} H_{n,x}^{m,x} dx + J_{3n,x}^m(x_\mu) \int_{x_\mu-\Delta x/2}^{x_\mu+\Delta x/2} H_{n,x}^{m,x} dx] +$$

$$\Delta z \sum_{\mu=1}^N [J_{2n,y}^m(y_\mu) \int_{y_\mu-\Delta y/2}^{y_\mu+\Delta y/2} H_{n,y}^{m,x} dy + J_{4n,y}^m(y_\mu) \int_{y_\mu-\Delta y/2}^{y_\mu+\Delta y/2} H_{n,y}^{m,x} dy],$$

where index 2 relates to the currents at the wall $x=a$, and index 4 at the one $x=0$. In these equations, auxiliary magnetic source at each observation point has the same direction as a magnetic current in the cell.

3. NUMERICAL RESULTS AND CONCLUSIONS

The total field in the resonator can be found either with the aid of Lorentz lemma or as a superposition of primary source field and the ones of the secondary sources in the form of piece-constant magnetic currents on the nonlinear contact at all harmonic frequencies whose amplitudes are determined by NAES. In the calculations the second way has been chosen. The computational experiment was carried out for a resonator 23 x 10 x 10 mm with a nonlinear

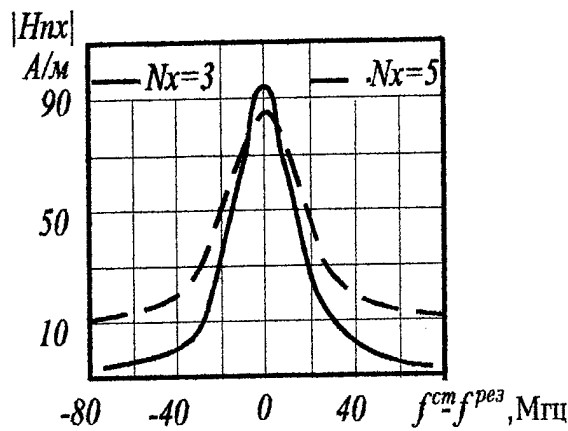


Fig.2

contact (of the width 10^{-2} mm) excited by a primary magnetic source in the middle of the forward wall.

The resonance characteristics for the field of the third harmonic excited by the nonlinear contact located only at a top wall are shown in Fig. 2. It was obtained that the amplitude of the field third harmonic exceeded the amplitude of the field at fundamental frequency by 20...40 dB. The resonant characteristics for the third field harmonic have the width of the order of 1 %. The difference of the first harmonic from the third

one at the resonant frequency depends on the primary source amplitude and off the resonance it is effected also by the source frequency (Fig. 3). Generally, the difference between the first harmonic and the third one off the resonance remains at the same level as in the waveguide with a similar nonlinear contact and exceeds the first harmonic by 40 ...50 dB. Results of numerical experiments conducted at the frequencies of the first harmonic close to resonance are interesting also. From Fig. 4, in which the field harmonic amplitude dependences on the primary source amplitude are shown, it is visible a sharp increase of not only the first but also the third field harmonic due to a resonance. The field of the third harmonic becomes comparable with the fundamental frequency field (difference is around 10 ...15 dB). Thus, even near a fundamental mode resonance not taking into account the field of the third harmonic leads to a grave error.

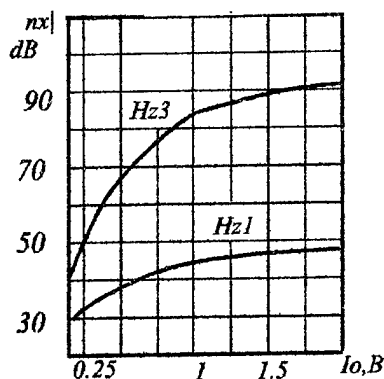


Fig.3

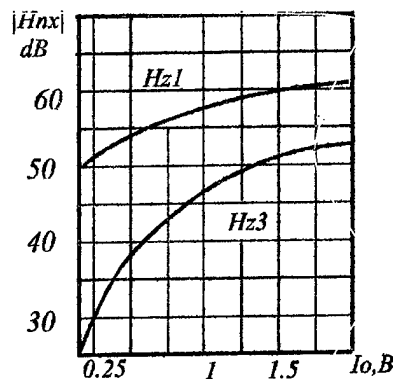


Fig.4

REFERENCES

- [1] B.M.Petrov, D.V.Semenikhina, A.I.Panichev, A New Analysis Method of Nonlinear Problem, *Proc. 1993 Int. Symp. on Nonlinear Theory and its Application*, Hawaii, 1993.
- [2] D.V.Semenikhina, Investigation of Electrodynamical Nonlinear Effects in Microstrip and Waveguide Transmission Lines, *Proc. 1995 Intern. Symp. on Nonlinear Theory and its Application*, Las Vegas, 1995.
- [3] B.S.Jakunin, O.N.Barilovoch, Influence of products of nonlinearity to RRL parameters, *Electric communication*, 1975.- no7. pp. 34-36.
- [4] B.M.Petrov, Nonlinear boundary condition, *Radio Electronics and Communications Systems*, v.35, N3, pp.30-37. 1992.

The Method of Analysis of the Diffraction on Step Discontinuities

Igor V. Petrusenko

Dniepropetrovsk State University,
Naukovy lane, 13, Dniepropetrovsk-50, Ukraine, 320625,
e-mail: petrus@rff.dsu.dp.ua

Abstract.

The new technique of the inversion of a principal part of the integral equation with weighted singularities in the kernel was applied to problem of wave diffraction on a step discontinuities in waveguide. The properties of resulting matrix operator were investigated.

Introduction.

The mathematical models for modern CAD systems have a number of specific properties concerning to an accuracy, speed of numerical convergence and stability of evaluations. Frequently it is meaningful to apply approximate methods to modelling of such electrodynamics key problems, which have analytical solution poorly approaching for computing. The raise of effectiveness of such approximate methods has a large impotence for development of a CAD systems software.

The field calculation within a region of space bounded by a surface of geometrically complicated shape may be obtained by means of dividing the whole region of the field determination into a number of simple partial subregions. The equations of the applied electrodynamics methods which use the idea of a region decomposition and boundary conditions of the fourth kind would be noted on the base of the Green's identities formalism. At such form the presence of singularities in a kernel of the resulting integral equation exposes easily. It is connected with the moving and fixed singularities of the Green function of a simple partial region, which suppose a clear physical interpretation. The methods of a complete or partial inversion of the principal part of resulting integral operator lead to effective mathematical models.

As it was shown in [1], the method of partial overlapping regions [2] is an equivalent regularisation of the convolution-type equations of a mode-matching technique. In the given paper the regularisation technique is advanced for deriving more effective mathematical models, than the method of partial overlapping regions produces.

Theory.

In [3] the technique of the inversion of a principal part of the electrodynamics singular integral operators was developed and substantiated. An integral equation to solve for one of electromagnetic field vectors is formulated for each of partial region using the integral theorems of the diffraction theory. The field continuity on a common part of the partial regions leads to the integral equation with complicated kernel. According to this method the initial equation of the first kind is rearranged to the equivalent form

$$\int_{\Omega} \left\{ \left[K_1(\bar{r}|\bar{r}') + \chi M(\bar{r}|\bar{r}') \right] + \chi \left[K_2(\bar{r}|\bar{r}') - M(\bar{r}|\bar{r}') \right] \right\} U(\bar{r}') d\bar{r}' = f(\bar{r}), \bar{r} \in \Omega, \quad (*)$$

where $K_i(\bar{r}|\bar{r}')$, $i=1,2$, are the Green functions or their derivatives, $M(\bar{r}|\bar{r}')$ is a special constructing regularisation kernel. In (*) the first sum in the square brackets is the simply invertable part of compound kernel and second part is a continuous function. As it can be shown the method of partial overlapping regions is the special case of the new technique.

To demonstrate further development of this approach it is necessary to consider not abstract but the specific problem. As such problem conveniently to choose problem of wave's diffraction on a step in the parallel - plate waveguide, which would be solved by many other methods.

We shall consider the case of a diffraction dominant mode of a wide waveguide. The relation of the field continuity on the line $x \in [0, b]$ with reference to boundary condition at the step looks like

$$U_1(x, z) = U_{inc}(x, z) + \begin{cases} \int_0^b \left[U_2(x', z') \frac{\partial G_1}{\partial z'} \right]_{z'=0} dx', & (LM) \\ - \int_0^b \left[G_1 \frac{\partial U_2(x', z')}{\partial z'} \right]_{z'=0} dx', & (LE) \end{cases} \quad \begin{matrix} x \in [0, a]; \\ 0 \leq z < \infty. \end{matrix}$$

The Green function $G_1(x, z|x', z')$ of the wide waveguide can be expressed in terms of Green function $G_1^{(v)}(x, z|x', z')$ of closed area $[0, a] \times [0, c]$ with reference to mirror reflections in metal walls. It yields the integral equation

$$\left. \frac{\partial U_2}{\partial z} \right|_{z=0} = \left. \frac{\partial U_{inc}}{\partial z} \right|_{z=0} + \left\{ \frac{\partial}{\partial z} \int_0^b \left[U_2(x', z') \frac{\partial G_1^{(v)}}{\partial z'} \right]_{z'=0} dx' \right\}_{z=0} - \left. \frac{\partial R}{\partial z} \right|_{z=0}; \quad (LM)$$

$$U_2(x, 0) = U_{inc}(x, 0) - \int_0^b \left[G_1^{(v)}(x, 0|x', 0) \frac{\partial U_2}{\partial z'} \right]_{z'=0} dx' + R(x, 0), \quad (LE)$$

where

$$R(x, z) = \sum_{m=1}^{\infty} \left[\tilde{U}(x, 2cm + z) \mp \tilde{U}(x, 2cm - z) \right],$$

$$\tilde{U}_1(x, z) = U_1(x, z) - U_{inc}(x, z).$$

Using Galerkin's method and representation of Green function $G_1^{(v)}(x, z|x', z')$ in the form of Fourier-series expansion in the closed area $[0, b] \times [0, c]$ as it was made in [3]

$$G_1^{(v)}(x, 0|x', 0) = \sum_{n=0}^{\infty} \psi_n^{(2)}(x) \psi_n^{(2)}(x') \frac{cth \gamma_n c}{\gamma_n} + \\ + \sum_{n=0}^{\infty} \sum_{m=0}^{\infty} \psi_n^{(2)}(x) \psi_m^{(2)}(x') \tilde{V}_{nm}; \quad \gamma_n = \sqrt{\left(\frac{n\pi}{b}\right)^2 - \tilde{k}^2}; \quad (LE)$$

we finally obtain the infinite matrix equation

$$(I + D_2)B + D_1A = f.$$

Here B and A are the vectors of unknown coefficients for the second and first semi-infinite waveguide respectively.

Theorem. The matrix operators $D_1, D_2 : l_p \rightarrow l_p, 1 \leq p \leq \infty$, defined by the elements

$$d_{mn}^{(1)} = O \left(\sin(n\pi\theta) \frac{\sqrt{mn} \exp(-nt)}{m^2 - n^2\theta^2} \right), \quad t, \theta > 0;$$

$$d_{mn}^{(2)} = O \left(\sum_{p=1}^{\infty} \frac{\sqrt{mn}}{p^2 + m^2\tau^2} \cdot \frac{p}{p^2 + n^2\tau^2} \right), \quad \tau > 0,$$

are compact.

For a case of LM-wave diffraction the form of final matrix equation is the similar as the one given above.

Conclusion.

It is shown for the key problem of waves diffraction on the step discontinuity in the parallel-plate waveguide that proposed regularisation technique converts the initial integral equation into the infinite matrix equation, which permits efficient solving by a computer.

- [1] Petrusenko I.V. et al., "Method of partial overlapping regions for the analysis of diffraction problems", IEE Proc. - Microw. Antennas Prop., 1994, vol. 141, N 3, pp. 196 - 198.
- [2] Prokhoda I.G., Chumachenko V.P., "The method of partial overlapping regions to investigation of the complicated form waveguide-resonator systems", Izv. Vuzov. Radiophysics, 1973, v.16, N 10, pp. 1578-1581.
- [3] Petrusenko I.V., "New technique for solving of electrodynamics singular integral equations", Proc. of MMET'96, 10 - 13 Sept., 1996, Lviv, pp. 125 - 127.

DIFFRACTION BY A THICK DIAPHRAGM IN PARALLEL-PLATE WAVEGUIDE

Olga Gavrilko

Department of Mathematical Physics and Computational Mathematics,
Kharkov State University, Svobody sq., 4, Kharkov, Ukraine, 310077
Tel. +380-(572)37-17-50, E-mail olga@kvn.kharkov.ua

In this paper we discuss the problem of an electromagnetic wave diffraction by a thick inhomogeneous diaphragm in the parallel-plate waveguide. Our approach is based on the analytical method of Boundary Singular Integral Equations (SIE) [1]. Similar problems are frequently encountered in the computer-aided design of waveguide circuits. They are normally reduced to the matrix equations by the mode-matching approach. To obtain a stable and accurate algorithm, analytical semi-inversion has been used in [2,3]. Unlike this, we develop discrete mathematical model and numerical algorithm by using the technique of [5].

1. Introduction

We consider diffraction of the principal electromagnetic E-polarized mode (dependence on time is $e^{-i\omega t}$) by a thick inhomogeneous diaphragm in the parallel-plate waveguide.

The geometry of the problem is shown in Figure 1.

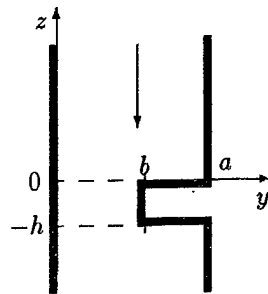


Fig.1. Thick diaphragm in a parallel-plate waveguide. Vertical boundaries of the waveguide and diaphragm are perfectly conducting. Horizontal surfaces of the diaphragm are impedance.

The total electric field vector is $\vec{E} = (E_x, 0, 0)$. Let us denote $E_x = u(y, z)$. Maxwell's equations that describe the model can be reduced to the Helmholtz equation $\Delta u + k^2 u = 0$ with the following conditions on the vertical boundaries:

$$u(0, z) = 0, \quad z \in R; \quad u(a, z) = 0, \quad z > 0, \quad z < -h; \quad u(b, z) = 0, \quad -h < z < 0; \quad (1)$$

and "impedance" condition on the horizontal surfaces of the diaphragm:

$$\frac{\partial u}{\partial z}(y, 0) + \zeta u(y, 0) = 0, \quad \frac{\partial u}{\partial z}(y, -h) - \zeta u(y, -h) = 0, \quad (b < y < a, \quad \zeta = \zeta_1 + i\zeta_2, \quad \zeta_1 \times \zeta_2 \neq 0). \quad (2)$$

We request also, for the total field, satisfying the radiation condition and the edge condition at the right two-sided edges.

Decompose the total field $u(y, z)$ as

$$u(y, z) = \begin{cases} u_0(y, z) + u^+(y, z), & z > 0, \quad 0 \leq y \leq a \\ \bar{u}(y, z), & -h < z < 0, \quad 0 \leq y \leq b \\ u^-(y, z), & z < 0, \quad 0 \leq y \leq b \end{cases} \quad (3)$$

where

$$u_0(y, z) = \left(e^{i\sqrt{k^2 - (\frac{\pi}{a})^2}z} + \frac{-i\sqrt{k^2 - (\frac{\pi}{a})^2} - \zeta}{-i\sqrt{k^2 - (\frac{\pi}{a})^2} + \zeta} e^{-i\sqrt{k^2 - (\frac{\pi}{a})^2}z} \right) \sin \frac{\pi y}{a}, \quad (ka > \pi)$$

is the sum of the incident and reflected fields in the case of diaphragm completely blocking the waveguide ($b = 0$), and the functions $u^+(y, z)$, $\bar{u}(y, z)$, $u^-(y, z)$ are the diffracted fields in the domains $\{z > 0, 0 < y < a\}$, $\{-h < z < 0, 0 < y < b\}$, $\{z < -h, 0 < y < a\}$, respectively. Note, that

$$u_0(0, z) = u_0(a, z) = 0, \quad z > 0; \quad \frac{\partial u_0}{\partial z}(y, 0) + \zeta u_0(y, 0) = 0, \quad y \in (0, a). \quad (4)$$

Conditions (1) tell us the following modal expansions for $u^\pm(y, z)$ and $\bar{u}(y, z)$

$$u^+(y, z) = \sum_{n=1}^{\infty} A_n e^{-\gamma_n z} \sin \frac{\pi n}{a} y, \quad 0 \leq y \leq a, \quad z > 0 \quad (5)$$

$$u^-(y, z) = \sum_{n=1}^{\infty} B_n e^{\gamma_n(z+h)} \sin \frac{\pi n}{b} y, \quad 0 \leq y \leq a, \quad z < -h \quad (6)$$

$$\bar{u}(y, z) = \sum_{n=1}^{\infty} \left[D_n e^{-\bar{\gamma}_n(z+h)} + C_n e^{\bar{\gamma}_n z} \right] \sin \frac{\pi n}{b} y, \quad 0 \leq y \leq b, \quad -h < z < 0 \quad (7)$$

where $\gamma_n = \sqrt{\left(\frac{\pi n}{a}\right)^2 - k^2}$, $\bar{\gamma}_n = \sqrt{\left(\frac{\pi n}{b}\right)^2 - k^2}$. Taking into account the radiation condition, we choose $\operatorname{Re} \gamma_n \geq 0$, $\operatorname{Im} \gamma_n \leq 0$, $\operatorname{Re} \bar{\gamma}_n \geq 0$, $\operatorname{Im} \bar{\gamma}_n \leq 0$.

2. Singular Integral Equations.

Following the main idea of the Boundary SIE Method [1], we introduce new functions $F^{\pm}(y)$, $y \in (0, a)$ as follows:

$$F^+(y) = \left(\frac{\partial u^+}{\partial z} + \zeta u^+ \right) \Big|_{(y,0)} = \sum_{n=1}^{\infty} A_n (\zeta - \gamma_n) \sin \frac{\pi n}{a} y, \quad (8)$$

$$F^-(y) = - \left(\frac{\partial u^-}{\partial z} - \zeta u^- \right) \Big|_{(y,-h)} = \sum_{n=1}^{\infty} B_n (\zeta - \bar{\gamma}_n) \sin \frac{\pi n}{a} y. \quad (9)$$

The important characteristics of the functions $F^{\pm}(y)$ are:

1. $F^{\pm}(y) = 0$, $y \in (b, a)$;
2. Taking into account the continuity of electromagnetic field and the statement (4), we get another representation for the functions $F^{\pm}(y)$, namely:

$$F^+(y) = \sum_{n=1}^{\infty} [D_n (\zeta - \bar{\gamma}_n) e^{-\bar{\gamma}_n h} + C_n (\zeta + \bar{\gamma}_n)] \sin \frac{\pi n}{b} y, \quad y \in (0, b); \quad (10)$$

$$F^-(y) = \sum_{n=1}^{\infty} [D_n (\zeta + \bar{\gamma}_n) + C_n (\zeta - \bar{\gamma}_n) e^{-\bar{\gamma}_n h}] \sin \frac{\pi n}{b} y, \quad y \in (0, b); \quad (11)$$

3. Considering the behavior of the field at the edges we request the functions $F^{\pm}(y)$ to have the form as

$$F(y) = \frac{v^{\pm}(y)}{b\sqrt{1-y^2}}, \quad v^{\pm}(y) = w^{\pm}(y)\sqrt{1-y^2},$$

where $v^{\pm}(y)$ belong to the class of the Holder functions $C^{r,\alpha}(0, b)$, $0 < \alpha < 1$.

4. Representations of the coefficients A_n , B_n , C_n and D_n , ($n \in N$) by means of $F^{\pm}(\xi)$ ($|\xi| < b$) functions are as follows:

$$A_n = \frac{1}{a(\zeta - \gamma_n)} \int_{-b}^b F^+(\xi) \sin \frac{\pi n}{a} \xi d\xi, \quad D_n = \frac{1}{b(Y_n^2 - X_n^2)} \int_{-b}^b [F^+(\xi) Y_n - F^-(\xi) X_n] \sin \frac{\pi n}{b} \xi d\xi \quad (12)$$

$$B_n = \frac{1}{a(\zeta - \gamma_n)} \int_{-b}^b F^-(\xi) \sin \frac{\pi n}{a} \xi d\xi, \quad C_n = \frac{1}{b(Y_n^2 - X_n^2)} \int_{-b}^b [F^-(\xi) Y_n + F^+(\xi) X_n] \sin \frac{\pi n}{b} \xi d\xi \quad (13)$$

where $X_n = \bar{\gamma}_n + \zeta$, $Y_n = (\zeta - \bar{\gamma}_n) e^{-\bar{\gamma}_n h}$.

On using the Fourier representations (5)-(7) and continuity property of electromagnetic field at $z = 0$, we come up with equations:

$$\sum_{n=1}^{\infty} \frac{\pi n}{a} A_n \cos \frac{\pi n}{a} y - \sum_{n=1}^{\infty} \frac{\pi n}{b} [D_n e^{-\bar{\gamma}_n h} + C_n] \cos \frac{\pi n}{b} y = -u_0'(y), \quad y \in (0, b); \quad (14)$$

$$\sum_{n=1}^{\infty} A_n \sin \frac{\pi n}{a} y_0 - \sum_{n=1}^{\infty} [D_n e^{-\bar{\gamma}_n h} + C_n] \sin \frac{\pi n}{b} y = -u_0(y_0), \quad y_0 \in (0, b) \quad (15)$$

A similar pair of equations is derived from from continuity conditions at $z = -h$.

Let us consider the Hilbert operator with cotangent kernel: $(H_c G)(x) = \frac{1}{2c} \int_{-c}^c \cot \frac{\pi}{2c} (y - x) G(y) dy$.

Applying operators H_a and H_b to functions $F^+(\xi)$ and the property 1 of F^{\pm} functions, we get the following statements:

$$(H_a F)(y) = \sum_{n=1}^{\infty} A_n (\zeta - \gamma_n) \cos \frac{\pi n}{a} y = \frac{1}{2a} \int_{-b}^b \cot \frac{\pi}{2a} (\xi - y) F^+(\xi) d\xi$$

$$(H_b F^+)(y) = \sum_{n=1}^{\infty} (C_n X_n + D_n Y_n) \cos \frac{\pi n}{b} y = \frac{1}{2b} \int_{-b}^b \cot \frac{\pi}{2b} (\xi - y) F^+(\xi) d\xi.$$

Taking into account integral representations (12)-(13) of coefficients A_n , B_n , C_n , D_n , we rewrite (14) and (15) in equivalent forms:

$$\begin{aligned} \int_{-b}^b \left[\frac{1}{2a} \cot \frac{\pi}{2a}(\xi - y) + \frac{1}{2b} \cot \frac{\pi}{2b}(\xi - y) F^+(\xi) \right] d\xi - \frac{1}{a} \int_{-b}^b K_a(\xi, y) F^+(\xi) d\xi \\ - \frac{1}{b} \int_{-b}^b [K_1(\xi, y) F^+(\xi) + K_2(\xi, y) F^-(\xi)] d\xi = u_0'(y, 0), \\ \int_{-b}^b [Q_1(\xi, y_0) + Q_2(\xi, y_0)] F^+(\xi) d\xi + \int_{-b}^b Q_3(\xi, y_0) F^-(\xi) d\xi = -u_0(y_0, 0), \end{aligned}$$

where $K_a(\xi, y)$, $K_1(\xi, y)$, $K_2(\xi, y)$, $Q_3(\xi, y)$ are some smooth functions. Functions $Q_1(\xi, y)$ and $Q_3(\xi, y)$ have the logarithmic singularities, which can be isolated.

Thus, we have reduced the original diffraction problem to the set of SIE with additional conditions.

3. Discrete Mathematical Model

For the creation of discrete mathematical model we use the technique of Discrete Singularities Method [5]. Interpolation Gaussian quadratures are applied both to the singular integrals, and to the regular ones. The integrals with logarithmic singularities are discretized by the formula from [6]. Based on the suggested mathematical model a numerical experiment was worked out. We calculated $|A_n|$, $|B_n|$, $|C_n|$ and $|D_n|$ coefficients under the different values of a , b , ζ and h parameters. An example of numerical experiment is shown in Figure 2.

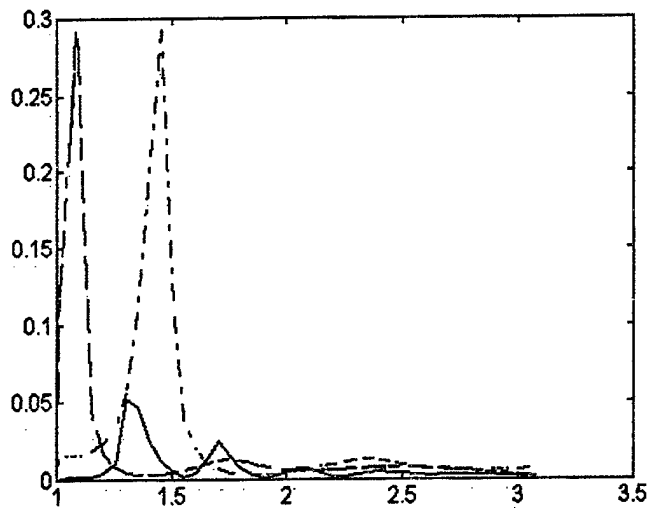


Fig.2. The dependence of $|B_1|$ on the wavenumber k with the following values of parameters:

$$a = \pi, b = \frac{\pi}{2}, h = 1, \zeta = -\frac{ik}{Z_s}$$

1. $Z_s = 2.4784 \cdot 10^{-3} + i1.4648 \cdot 10^{-2}$ is the impedance of niobium at $T = 8.83K$ [7];

2. $Z_s = 8.23657 \cdot 10^{-3} + i2.64552 \cdot 10^{-2}$ is the impedance of a smooth niobium layer on a dielectric layer at $T = 8.83K$ [7];

3. $Z_s = 1.10491 \cdot 10^{-2} + i3.54889 \cdot 10^{-2}$ is the impedance of a rough niobium layer on a dielectric layer at $T = 8.83K$ [7];

REFERENCES

1. Y. V. Gandel, T. C. Polyanskaya, System of Singular Equations of Certain Mixed Boundary-Value Problems of Mathematical Physics, *J. Soviet Mathematics*, 1990, vol. 48, no 2, pp. 144-152
2. A. A. Kirilenko, S. A. Masalov, V. P. Shestopalov, Wave Scattery from Inductive Diaphragms of Finite Thickness in Rectangular Waveguides, *Radiotekhnika*, KGU Press, no4, pp. 61-68, 1967 (in Russian).
3. V. P. Lyapin, M. B. Manuilov, G. P. Sinyavsky, Quasi-analitical Method for Analysis of Multisection Waveguide Structures with Step Discontinuities, *Radio Science*, vol. 31, no 6, pp. 1761-1772, 1996.
4. Y. V. Gandel, M. B. Krasnyanskyy, Mathematical Model for the Calculation of Step-like Inhomogeneity in the Plane Waveguide, *Boundary Problems for Differential Equations*, Kiev, IM NAS Press, no 1 (17), 1998.
5. I. K. Lifanov, *Singular Integral Equations and Discrete Vortices*, Utrecht: VSP, 1996.
6. Z. T. Nazarchuk, *Singular Integral Equations in Diffraction Theory*, Lviv, PMI NAS Press, 1994.
7. V. F. Kravchenko, A. B. Kazarov, V. I. Pustovoit, Influence of Rough Surface of Superconductive Wedge on its Electromagnetic Characteristics, *Russian Physics Doklady*, vol. 353, no 5, pp. 61-615, 1997 (in Russian).

Architecture of Dielectric Bandpass Filters with Symmetric Characteristics

Alexander Trubin

National Technical University - KPI, 2110, Peremogy Prospect, 37, Kiev, 252056 Ukraine

Abstract

The problem of electromagnetic wave scattering from a system of coupled Dielectric Resonators (DR) placed in a cut off waveguide section has been examined. It has been established a common form of characteristic equation for the coupled oscillations, that realizes frequency-symmetrical S matrix parameters. A new structure of the coupling between DRs is indicated as well. Analytical expressions of the power transmission coefficients and experimental investigations of 4 and 5 cylindrical DRs in a microstrip line is given.

Introduction

The scattering characteristics of the DR system in metallic cavity depend on their mutual location, non resonant transmission and, for example, in microstrip structures, on the presence of parasitic modes, etc. We consider here the problem of determination of DR structure that realizes frequency-symmetrical scattering parameters: $|T(\Delta\omega)| = |T(-\Delta\omega)|$, where $\Delta\omega = \omega - \omega_0$, ω_0 is the center frequency.

Common form of Characteristic Equation of Symmetric DR Filter

We shall try to answer the question: what conditions will lead to the S matrix frequency symmetry of the DR filter scattering parameters? To this end we consider the characteristic equation which determines eigenvalues of the coupling operator K [1]:

$$\lambda^N + \alpha_1 \lambda^{N-1} + \alpha_2 \lambda^{N-2} + \dots + \alpha_{N-1} \lambda + \alpha_N = 0 \quad (1)$$

where $\alpha_s = \alpha_s(\tilde{k}, k_{12}, k_{13}, \dots)$ are the complex functions of the coupling coefficients;

$\lambda_s = 2(\Delta\omega_s + i\omega_s'') / \omega_0$; $\Delta\omega_s = \omega_s - \omega_0$; $\omega_s + i\omega_s''$ is the coupled oscillation frequency of the N DR

system ($s = 1, 2, \dots, N$). Solutions λ_1, λ_2 of (1) will be called anticonjugate if $\lambda_2 = -\lambda_1^*$, where "*" is the complex conjugation symbol. (1) has a pair of anticonjugate solutions only if the coefficients α_{2s} are real, and α_{2s+1} are imaginary:

$$\alpha_{2s}^* = \alpha_{2s}; \quad \alpha_{2s+1}^* = -\alpha_{2s+1}. \quad (2)$$

We have established that if all the solutions of (1) except the imaginary ones are anticonjugate, the filter S params are frequency symmetric. In reality, eigenoscillations of the DR system that form a pair of anticonjugate solutions have identical Q factors, but their resonant frequency detunings differ by sign. The sum of the oscillations form the frequency symmetrical scattering parameters.

Architecture of DRs with Symmetric Scattering Parameters

At first we shall examine four DRs symmetrical geometry. We shall denote a single DR of such a system by a point, the coupling between DRs through the cut off field by a straight line, and the coupling through a propagating wave by an oscillating line (Fig. 1, b-d). In arbitrary case obtained from [1], the power transmission coefficient of the four DRs symmetric filter is given by

$$T = \frac{b_1^1}{2\sqrt{d^+}} \cdot \frac{k}{Q_1} - \frac{b_1^2}{2\sqrt{d^+}} \cdot \frac{k}{Q_2} - \frac{b_1^3}{2\sqrt{d^-}} \cdot \frac{k}{Q_3} + \frac{b_1^4}{2\sqrt{d^-}} \cdot \frac{k}{Q_4} \quad (3)$$

where $k = \tilde{k} \cdot Q^D$ is the coupling coefficient between the input or output DR and line;

$$Q_s = Jm\lambda_s \cdot Q^D + \omega / \omega_s - 2iQ^D(1 - \omega / \omega_s); \quad Q^D = 1 / \text{tg}\delta; \quad b_1^{1,2} = \lambda_{1,2} - k_{23}; \quad b_1^{3,4} = \lambda_{3,4} + k_{23};$$

$$\lambda_{1,2} = \frac{i}{2} \cdot \tilde{k} + \frac{1}{2} (k_{14} + k_{23}) \mp \sqrt{d^+}; \quad \lambda_{3,4} = \frac{i}{2} \cdot \tilde{k} - \frac{1}{2} (k_{14} + k_{23}) \mp \sqrt{d^-};$$

$$d^{\pm} = \left[\frac{i}{2} \tilde{k} \pm \frac{1}{2} (k_{14} - k_{23}) \right]^2 + (k_{12} \pm k_{13})^2. \quad (4)$$

In Fig. 1, a it is shown the measured (by dots) and computed from (3), (4) (by a solid curve) insertion loss $\pm 20 \lg |T|$ of the filter composed from the cylindrical DRs and a microstrip-line. This curve is readily seen to be non - frequency - symmetric. From (2) or (4) the symmetry will take place under the conditions: $k_{14} = k_{23} = 0$ (Fig. 1, b), or $k_{13} = k_{24} = 0$ and $k_{23}^2 = k_{14}^2 = 4k_{12}^2 - \tilde{k}^2$ (c), or $k_{12} = k_{34} = 0$ and $k_{23}^2 = k_{14}^2 = 4k_{13}^2 - \tilde{k}^2$ (d).

The coupled oscillations of DR structures are determined from the obtained simple conditions (2) before the solution of the corresponding scattering problem. For example, even eigenoscillations of the five DRs system are found from the symmetry conditions: $k_{15} = k_{24} = 0$ and either $k_{13} = k_{35} = 0$ (Fig. 1, e); or $k_{23} = k_{34} = 0$ (Fig. 1, f); or $k_{12} = -k_{14}$; $k_{45} = -k_{25}$ (Fig. 1, g). The systems shown in Fig. 1, e, g have 5 types and that in Fig. 1, f has 4 nontrivial types of the coupled oscillations. The power transmission coefficient of the filter shown in Fig. 1, e, for example, has the form

$$T = -\frac{\lambda_1}{i\tilde{k}} \cdot \frac{(\lambda_2 - i\tilde{k})(\lambda_3 - i\tilde{k})}{(\lambda_1 - \lambda_2)(\lambda_1 - \lambda_3)} \cdot \frac{k}{Q_1} + \frac{\lambda_2}{i\tilde{k}} \cdot \frac{(\lambda_1 - i\tilde{k})(\lambda_3 - i\tilde{k})}{(\lambda_1 - \lambda_2)(\lambda_2 - \lambda_3)} \cdot \frac{k}{Q_2} -$$

$$-\frac{\lambda_3}{i\tilde{k}} \cdot \frac{(\lambda_1 - i\tilde{k})(\lambda_2 - i\tilde{k})}{(\lambda_1 - \lambda_3)(\lambda_2 - \lambda_3)} \cdot \frac{k}{Q_3} - \frac{\lambda_4}{(\lambda_5 - \lambda_4)} \cdot \frac{k}{Q_4} + \frac{\lambda_5}{(\lambda_5 - \lambda_4)} \cdot \frac{k}{Q_5} \quad (5)$$

where

$$\lambda_1 = (\tilde{k} / 3 + s_1 + s_2)i;$$

$$\lambda_{2,3} = \left[\tilde{k} / 3 - \frac{1}{2} (s_1 + s_2) \right] i \mp \frac{\sqrt{3}}{2} (s_1 - s_2); \quad (6)$$

$$\lambda_{4,5} = i / 2\tilde{k} \mp \left[(k_{12} - k_{14})^2 - (\tilde{k} / 2)^2 \right]^{1/2}$$

$$\text{and } s_{1,2} = \left[r \pm (q^3 + r^2)^{1/2} \right]^{1/3}; \quad r = \tilde{k} / 3 \left[(\tilde{k} / 3)^2 - 1 / 2 (k_{12} + k_{14})^2 + 2k_{23}^2 \right];$$

$$q = 1 / 3 (k_{12} + k_{14})^2 + 2 / 3 k_{23}^2 - (\tilde{k} / 3)^2; \quad (q^3 + r^2 > 0).$$

In Fig. 1, h shows the measured and computed from (5), (6) insertion loss of the five DR frequency symmetric filter.

Conclusion

A common form of the coefficients of the characteristic equation providing frequency - symmetric scattering parameters has been found. New structure of the coupling and analytical expressions of the power transmission coefficients of the four and five DR symmetric filters was established and verified. Measured characteristics of these filters are in acceptable agreement with theoretical calculations.

References

- [1] A. A. Trubin, "Scattering of Electromagnetic Waves on a System of Coupling High - Q Dielectric Resonators", Proc. Int. Conf. Mathematical Methods in Electromagnetic Theory, Lviv, pp. 350 - 353, 1996.

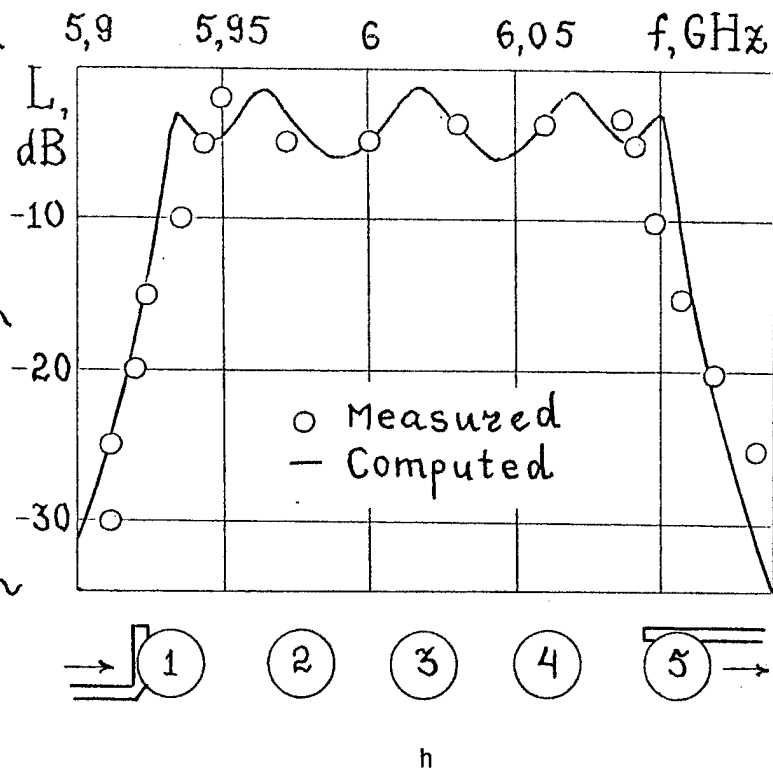
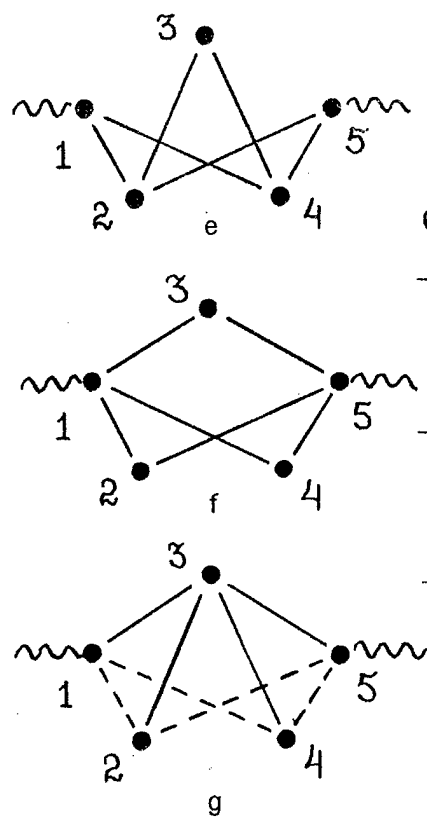
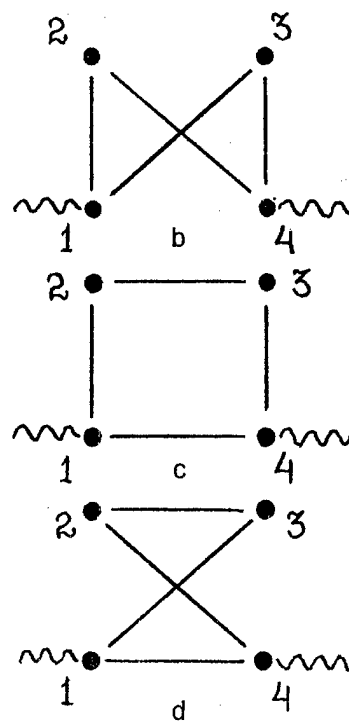
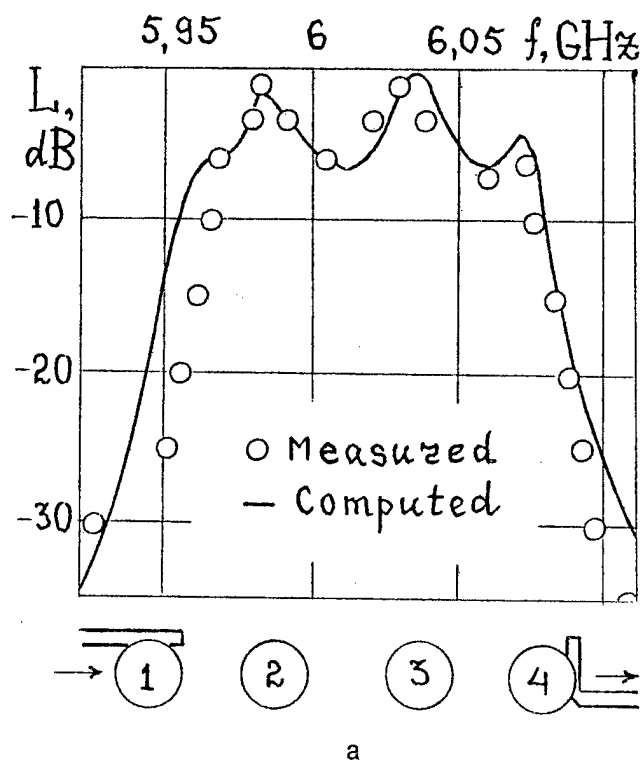


Fig. 1

NUMERICAL SIMULATION OF SOME PLANAR MICROWAVE GYROTROPIC STRUCTURES

S. A. Ivanov & P. I. Dankov
Faculty of Physics, Sofia University, Sofia, Bulgaria.

Introduction

The numerical simulation of different gyrotropic structures plays an increasing role in modern microwave practice. In comparison with the usual analytical/experimental methods known for a number of years it can propose a considerable saving of time and efforts combining with some new possibilities for improvement of the analysis before realization of the structures. Below this new alternative is demonstrated for the case of stripline circulator operating in S-band and below ferromagnetic resonance. The consideration is done with a planar model analysis [1] which offer a reasonable compromise between time consumption and accuracy.

Theoretical Background

The main steps of the planar model analysis includes: i) Replacing of the coupling stripline width W and disk resonator radius R with its planar equivalents of the same height h and characterized with effective dimensions W_e and R_e respectively; ii) Assuming a magnetic wall approximation for the investigated planar models the analysis is done in closed-form, and as a result of that, the convenient expressions for the main junction parameters - Input impedance Z_{in} , Isolation IS , Return Loss RL etc. are obtained; iii) Through a computer simulation an extensive information for behaviour of the above mentioned junctions parameters is easy obtained in advance before experiments.

The described procedure was demonstrated in [1] for an S-band stripline circulator. Because the junction input impedance deviates considerably from standard value $Z_0 = 50$ ohms, the matching of the investigated nonreciprocal structure seems to be one of the important circulator problems. In [1] this task was solved with one- and double-step quarter wave transformers. This way however, leads to a considerable increasing of the junction dimensions. The inherently matched stripline Y-junction described in [2] can be considered as an alternative of the classical stripline circulator because its dimensions are determined on ferrite disk diameter mainly. So, the Y-junction construction is appropriate for the case when a narrow band devices are of interest. If some wider operation bandwidth is necessary and the circulator dimensions should be as small as possible a new decision for circulator design should be proposed.

The investigated structure consists of two perpendicularly magnetized ferrite disks with diameter D_f and height h . The radius R of the disk conductor is assumed to be smaller than ferrite radius $D_f/2$. The stripline conductors thickness t is supposed to be thin enough, i.e. $t/h \ll 1$. At these conditions the planar equivalents of resonator and coupling lines can be introduced as it is point out with a dashed lines on Fig. 1. The expressions for calculation of the junction input impedance Z_{in} and circulator isolation IS are as in [1], but with the corrections for the characteristic impedance formula of the ferrite stripline Z_{cf} [2] determining the load impedance Z_L . The matching of the nonreciprocal junction shown in Fig.1 is done through a two short ferrite striplines.

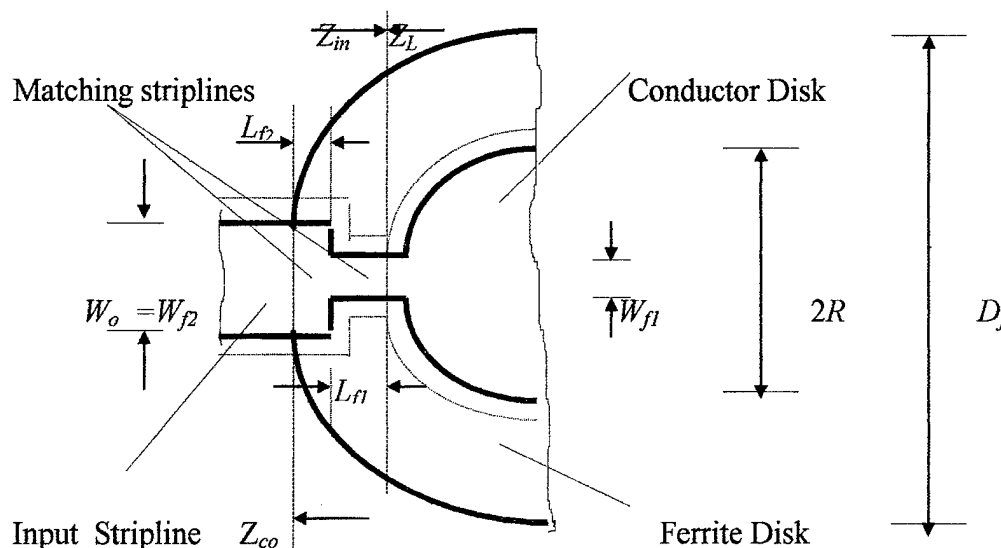


Fig.1

The width W_{f1} , W_{f2} and the length L_{f1} , L_{f2} of the coupling matching lines, as well as the radius of conductor R and magnetizing field H_i should be determined for proper circulator operation. This aim is done through a numerical simulation of the described nonreciprocal junction. During optimization procedure the principle of frequency compensation was used elsewhere. For this purpose the dimensions of the coupling matching lines were varied until the condition $R_{in} + jX_{in} \Leftrightarrow R_L - jX_L$ was satisfied.

Numerical results

The numerical calculations are done for S-band junction with ferrite disk dimensions: $D_f = 22$ mm and $h = 2$ mm. The ferrite parameters: saturation magnetization $M_s = 700$ G and permittivity $\epsilon_f = 14.5$ are taken as for substituted I-Al garnet - a material typically used. The input stripline of 50Ω is designed for a conductors of width $W_o = 5.6$ mm and thickness $t = 0.1$ mm. The simulation procedure is realized through a FORTRAN program SLC2TF which operates in dialogue regime and can calculate the junction characteristics when the dimensions of the coupling striplines are varied. The practical realization of this procedure is convenient to be done for different width W_{f1} and constant values of the lengths L_{f1} , L_{f2} and W_{f2} . As a result of simulation a number of configurations for matching striplines dimensions were proposed. It was found out that the operational bandwidth is increased when the coupling angle $\psi = \arcsin(W_{f1}/2R)$ decreases. This tendency is explained with the weaker frequency dependence of the junction input impedance at smaller coupling angles. For example the matching structure characterized with dimensions $L_{f1} = 3.5$ mm, $L_{f2} = 1.5$ mm, $W_{f2} = 5.6$ mm and coupling width values $W_{f1} = 2.5, 2.0, 1.5$ and 1 mm provides the values for the bandwidth (characterized at level IS > 20 dB) 110, 170, 210 and 260 MHz respectively. In all cases the mechanism of the above mentioned frequency compensation has took place. For the last case that is illustrated in Table 1, where all necessary calculation data are summarized. As can be seen the proposed configuration of the coupling ferrite striplines ensure matching of the junction with radius $R = 6$ mm in the frequency range 2.34-2.60 GHz.. With a small degradation the bandwidth

can be slightly shifted (± 50 MHz) up and down through a deviation of the magnetizing field H_i in the range 90 - 150 Oe.

Table 1

$R = 6$ mm, $W_{f1} = 1.0$ mm, $L_{f1} = 3.5$ mm, $W_{f2} = 5.6$ mm, $L_{f2} = 1.5$ mm, $H_i = 120$ Oe

f , GHz	k/μ	IS , dB	R_L , Ω	X_L , Ω	R_{in} , Ω	X_{in} , Ω	0 dB	IS	-20 dB
2.320	0.97	-16.65	14.3	-10.9	12.7	8.4	*****		
2.340	0.95	-20.60	14.2	-10.7	13.0	9.2	*****		
2.360	0.94	-22.32	14.1	-10.5	13.1	9.2	*****	*	
2.380	0.93	-24.45	13.9	-10.3	13.1	9.3	*****	***	
2.400	0.92	-27.24	13.8	-10.1	13.2	9.3	*****	***	
2.420	0.91	-31.26	13.7	- 9.9	13.3	9.4	*****	*****	
2.440	0.90	-33.36	13.5	- 9.7	13.1	9.5	*****	*****	
2.460	0.89	-41.03	13.4	- 9.5	13.2	9.5	*****	*****	
2.480	0.88	-37.15	13.3	- 9.3	13.3	9.5	*****	*****	
2.500	0.87	-31.11	13.2	- 9.0	13.4	9.6	*****	*****	
2.520	0.86	-27.46	13.0	- 8.8	13.5	9.6	*****	***	
2.540	0.86	-24.92	12.9	- 8.6	13.6	9.6	*****	**	
2.560	0.85	-23.00	12.8	- 8.4	13.8	9.6	*****	*	
2.580	0.84	-21.46	12.7	- 8.2	13.9	9.6	*****		
2.600	0.83	-20.11	12.6	- 8.0	14.0	9.6	*****		
2.620	0.82	-19.03	12.5	- 7.8	14.1	9.6	*****		

It is interesting to point out that the presented data are comparable with the results obtained for the case when a quarter-wave transformer is used [1]. This statement is proved with a program SLC1TD which calculates the parameters of circulator matched with dielectric ring. For the junction with radius $R = 10$ mm and coupling width $W = 6.5$ mm the optimum transformer parameters are: $W_d = 3$ mm, $L_d = 7$ mm and $\epsilon_d = 15$. At these conditions the circulator will operate with $H_i = 70$ Oe in the bandwidth 2.40-2.65 GHz, which practically coincides with that in Table 1. The construction of circulator matched with dielectric ring however, has several disadvantages. It is more expensive, less technological in production and has greater dimensions.

Conclusion

The proposed procedure for numerical simulation of nonreciprocal ferrite junction can produced a number of new design and decisions for below resonance stripline circulators. The principle of the frequency compensation between the junction input and loading impedances can be successfully used for broadening of the frequency range as well as for optimization of the matching procedure. In this way a considerable time and efforts can be saved during practical realization of different microwave gyrotropic devices.

Acknowledgement: This work was done with the help of Contract TH 606/96 of the National Science Foundation.

References

1. S. A. Ivanov, Application of the planar model to the analysis and design of the Y-junction strip line circulator, *IEEE Trans. Microwave Theory Tech.*, 43, 1995, 1551-1560.
2. S.A. Ivanov, Inherently matched Y-junction stripline circulator, *IEEE Trans. Microwave Theory Tech.*, 5, 1997, pp. 648-652.

SOLUTION OF THE PROBLEM OF EXCITATION OF RECTANGULAR WAVEGUIDE SECTION WITH LONGITUDINALLY-INHOMOGENEOUS MEDIUM

Yu. M. Penkin

Kharkov State University RFF

4, Svoboda sq., Kharkov, 310077, Ukraine

Tel.(0572) 45-75-48, Fax (0572) 47-18-16, E-mail: Yu.M.Penkin @ univ. kharkov. ua

Dielectric elements and structures of different geometry, placed inside rectangular waveguide sections, are widely used in microwave techniques such as control, limiting and stabilizing devices. Dielectric «inserts» with flat boundaries filling the whole rectangular section of waveguides belong to one of the simple types of such inhomogeneities. Such inserts can serve as functional elements of phase shifters and filters, dielectric windows, layers of absorbing coatings, etc. In electromagnetic analysis of most of them it is necessary to consider the problem of excitation of three-layer dielectric structure placed inside a waveguide section. Orientation of boundaries between the layers (across the axis of the waveguide) determines such a filling as longitudinally-inhomogeneous. Thus a solution of the problem of excitation of rectangular waveguide section with three-layer longitudinally-inhomogeneous filling is of great practical interest.

It is known that exact analytical investigation of the fields in a plane-irregular in longitudinal direction structure can be done in a convenient way by the method of cross-sections [1] that is based on the field expansion in each cross-section of a regular waveguide in terms of the eigenwaves of a certain standard waveguide with parameters coinciding in this cross-section with parameters of irregular waveguide. This very method, as a matter of fact, is used when considering the sharp irregularities of the step type of the open waveguide cross-section or, in other words, a junction of two open waveguides [1]. Obtained matrix equations have infinite order. Their analytical solution can be found only approximately using any small parameter characterizing the perturbation (smoothness of transition, value of material parameter jump at the junction, etc.). Numerical investigation of the fields in considered waveguide dielectric structures can be efficiently realized by using the methods of integral equations [2], singular integral equations [3] or partial domains [4].

Nevertheless, the problem of excitation of electromagnetic waves in the domains with coordinate boundaries can be solved conveniently with the aid of the Green's tensor function for the Hertz vector potentials. Thus, in [5] they are built for homogeneously filled rectangular waveguides and resonators as well as for other domains, whose boundaries partly or fully coincide with coordinate surfaces of an orthogonal cylindrical coordinate system (including rectangular one). Here, solutions of the vector equations for the Green's functions were built in the form of the series expansion of three (one longitudinal and two cross-sectional) vector functions in terms of the scalar eigenfunctions. It turns out that by a similar method, not using more complicated apparatus of the Green's field functions, one can solve the problem of excitation of the considered dielectric structure for longitudinal (oriented along the axis of the waveguide) given currents. The present paper is devoted to building the Green's functions of magnetic and electric types for the sections of rectangular waveguides with three-layer longitudinally-inhomogeneous filling excited by such currents.

Consider three types of waveguides sections: infinite waveguide (Fig. 1, a), semi-infinite waveguide (Fig. 1, b) and rectangular resonator (Fig. 1, c). Let us introduce a coordinate system, whose axis Z is directed along the axis of rectangular waveguide and the axes x and y along the contour of its cross-section, that is along the wider and narrower walls having dimensions a and b , respectively. In the Figure, longitudinal sections are presented with indication of coordinate boundaries of dielectric layers and face walls (all the walls of waveguide structures are considered as perfectly conducting).

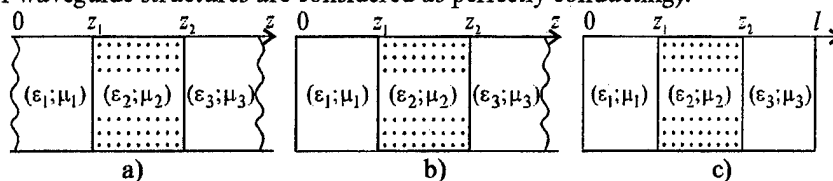


Figure 1.

The expressions of [5] corresponding to the case of longitudinal given currents, for the Green's tensor functions of rectangular waveguide are used as the key ones:

$$G^e = \sum_{m,n=0}^{\infty} \frac{(2 - \delta_{0m})(2 - \delta_{0n})}{ab} \sin \frac{m\pi x}{a} \sin \frac{m\pi x'}{a} \sin \frac{n\pi y}{b} \sin \frac{n\pi y'}{b} h_{mn}^e(z, z'); \quad (1)$$

$$G^M = \sum_{m,n=0}^{\infty} \frac{(2-\delta_{0m})(2-\delta_{0n})}{ab} \cos \frac{m\pi x}{a} \cos \frac{m\pi x'}{a} \cos \frac{n\pi y}{b} \cos \frac{n\pi y'}{b} h_{mn}^M(z, z');$$

where δ_{0m}, δ_{0n} are the Kronecker symbols; (x', y', z') are the coordinates of the source point, and (x, y, z) are the coordinates of the point of observation; functions $G^e, h_{mn}^e(z, z')$ are the functions of electric and $G^M, h_{mn}^M(z, z')$ of magnetic type, respectively.

Universality of expressions (1) lies in the fact, that they contain dependences on the longitudinal coordinate z in implicit form defined by functional coefficients $h_{mn}^{e(M)}(z, z') = h^{e(M)}$. They should be found from the Helmholtz inhomogeneous equations by the method of variation of arbitrary constants in the layer, where the given currents are located, and from the homogeneous equations in the rest layers of the dielectric structure. Such an approach is justified because for a waveguide with transversal layers of dielectric excited by the longitudinal currents the structure of waveguide modes remains invariant, and this gives an opportunity to build a full system of independent transverse and longitudinal vector eigenfunctions similarly to [5].

Unknown coefficients in the representations of the functions $h_s^{e(M)}$ (s is the number of the dielectric layer) can be found from the sets of equations obtained from the boundary conditions for $h_s^{e(M)}$ on the surfaces of dielectric layers. They are formulated in accordance with the behaviour of normal and tangential components of unknown vector fields:

$$h_s^{e(M)} = h_{s+1}^{e(M)}, \quad a_s^{e(M)} \cdot \frac{\partial h_s^{e(M)}}{\partial z} = a_{s+1}^{e(M)} \cdot \frac{\partial h_{s+1}^{e(M)}}{\partial z}, \quad (2)$$

where $a_s^e = 1/\epsilon_s$ for the functions h_s^e , and $a_s^M = 1/\mu_s$ for the functions h_s^M (ϵ_s and μ_s are the relative dielectric and magnetic constants of the medium in the layer with the number s , respectively). While deriving electric Green's function on the face wall structures, functions h_s^e must satisfy a homogeneous Neumann boundary condition, and in the case of magnetic Green's function h_s^M must satisfy a homogeneous Dirichle boundary condition. For semi-infinite front layers, the functions $h_s^{e(M)}$ must satisfy a condition of radiation at infinity.

The obtained expressions for the functions $h_{mn}^{e(M)}(z, z')$ can be reduced to the following form, in the case of the given sources located in the layer with parameters $\epsilon_1; \mu_1$:

$$h_{mn}^{e(M)}(z, z') = \begin{cases} F^{e(M)}(z, z'), & z < z'; \\ F^{e(M)}(z, z') - \frac{4\pi}{\gamma_1} \sin \gamma_1(z - z'), & z' < z < z_1; \\ \Phi^{e(M)}(z') \cdot \Phi_1^{e(M)}(z), & z_1 < z < z_2; \\ \Phi^{e(M)}(z') \cdot \Phi_2^{e(M)}(z), & z > z_2, \end{cases} \quad (3)$$

where:

1) in the case of infinite waveguide (Fig. 1, a):

$$\begin{aligned} \Phi_1^{e(M)}(z) &= -4\pi \left[\cos \gamma_2(z_2 - z) + \frac{i\gamma_3 a_3^{e(M)}}{\gamma_2 a_2^{e(M)}} \sin \gamma_2(z_2 - z) \right]; \quad \Phi_2^{e(M)}(z) = -4\pi e^{-i\gamma_3(z - z_2)}; \\ \Phi_1^{e(M)} &= \gamma_2 \frac{a_2^{e(M)}}{a_1^{e(M)}} \sin \gamma_2(z_2 - z_1) - i\gamma_3 \frac{a_3^{e(M)}}{a_1^{e(M)}} \cos \gamma_2(z_2 - z_1); \quad \Phi_2^{e(M)} = -\frac{\gamma_1}{4\pi} \Phi_1^{e(M)}(z_1); \end{aligned} \quad (4)$$

$$\Phi^{e(M)}(z') = e^{-i\gamma_1(z_1 - z')} / [\Phi_1^{e(M)} - i\Phi_2^{e(M)}];$$

$$F^{e(M)}(z, z') = \frac{2\pi}{i\gamma_1} \left(e^{i\gamma_1(z - z')} - e^{-i\gamma_1(z_1 - z)} \cdot \Phi^{e(M)}(z') \cdot [\Phi_1^{e(M)} + i \cdot \Phi_2^{e(M)}] \right)$$

2) in the case of semi-infinite waveguide (Fig. 1, b):

$$\begin{aligned}
\Phi^e(z') &= \cos \gamma_1 z' / (\Phi_1^e \cdot \cos \gamma_1 z_1 + \Phi_2^e \sin \gamma_1 z_1); \quad \Phi^M(z') = \sin \gamma_1 z' / (\Phi_1^M \sin \gamma_1 z_1 - \Phi_2^M \cos \gamma_1 z_1); \\
F^e(z, z') &= -\frac{4\pi}{\gamma_1} \cos \gamma_1 z \cdot (\sin \gamma_1 z' - \operatorname{tg} \gamma_1 z_1 \cdot \cos \gamma_1 z' + \Phi^e(z') \Phi_2^e / \cos \gamma_1 z_1) \\
F^M(z, z') &= \frac{4\pi}{\gamma_1} \sin \gamma_1 z \cdot (\cos \gamma_1 z' + \operatorname{tg} \gamma_1 z_1 \cdot \sin \gamma_1 z' - \Phi^M(z') \Phi_1^M / \cos \gamma_1 z_1)
\end{aligned} \quad (5)$$

Functions $\Phi_1^{e(M)}(z)$ and $\Phi_2^{e(M)}(z)$, as well as auxiliary coefficients $\Phi_1^{e(M)}$ and $\Phi_2^{e(M)}$, are analogous to the case of infinite waveguide (4);

3) in the case of rectangular resonator (Fig. 1, c):

$$\begin{aligned}
\Phi_1^e(z) &= 4\pi \left[\cos \gamma_2(z_2 - z) \cdot \cos \gamma_3(z_2 - l) + \frac{\gamma_3 \epsilon_2}{\gamma_2 \epsilon_3} \sin \gamma_2(z_2 - z) \sin \gamma_3(z_2 - l) \right]; \\
\Phi_1^M(z) &= -4\pi \left[\cos \gamma_2(z_2 - z) \cdot \sin \gamma_3(z_2 - l) - \frac{\gamma_3 \mu_2}{\gamma_2 \mu_3} \sin \gamma_2(z_2 - z) \cos \gamma_3(z_2 - l) \right]; \\
\Phi_2^e(z) &= 4\pi \cos \gamma_3(z - l); \quad \Phi_2^M(z) = -4\pi \sin \gamma_3(z - l); \\
\Phi_1^e &= \gamma_3 \frac{\epsilon_1}{\epsilon_3} \cos \gamma_2(z_2 - z_1) \cdot \sin \gamma_3(z_2 - l) - \gamma_2 \frac{\epsilon_1}{\epsilon_2} \sin \gamma_2(z_2 - z_1) \cos \gamma_3(z_2 - l); \\
\Phi_1^M &= \gamma_3 \frac{\mu_1}{\mu_3} \cos \gamma_2(z_2 - z_1) \cdot \cos \gamma_3(z_2 - l) + \gamma_2 \frac{\mu_1}{\mu_2} \cos \gamma_2(z_2 - z_1) \sin \gamma_3(z_2 - l).
\end{aligned} \quad (6)$$

Expressions for the auxiliary coefficients $\Phi_2^{e(M)}$ are analogous to the case of infinite waveguide (4), and those for the functions $\Phi^{e(M)}(z')$ and $F^{e(M)}(z, z')$ are analogous to the case of semi-infinite waveguide (5).

By the same method the functions $h_{mn}^{e(M)}(z, z')$ can be obtained for the given sources located in the other layers of the dielectric structure. In (4)-(7), $\gamma_s^2 = k_s^2 - (m\pi/a)^2 - (n\pi/b)^2$, where $k_s = \omega \sqrt{\epsilon_s \mu_s}$ is the wave number and ω is the frequency. The constructed Green's functions give an opportunity to determine the longitudinal components of electric $\Pi_z^e(x, y, z)$ and magnetic $\Pi_z^M(x, y, z)$ Hertz vectors in every region of the considered waveguide-dielectric structures in the form of a volume integral:

$$\Pi_z^{e(M)}(x, y, z) = \frac{1}{4\pi i \omega \epsilon_s(\mu_s)} \int_V j_z^{e(M)}(x', y', z') G^{e(M)} dV, \quad (7)$$

where V is the volume of the s -th layer, in which the given longitudinal electrical $j_z^e(x', y', z')$ or magnetic $j_z^M(x', y', z')$ currents are located, $(\epsilon_s; \mu_s)$ are the parameters of dielectric layer, in which $\Pi_z^{e(M)}$ is to be found. The form of expression for $G^{e(M)}$ is defined by (1) and by the concrete form of the functions $h_{mn}^{e(M)}(z, z')$. Based on the known coefficients, the sought electromagnetic fields are determined with the aid of $\Pi_z^{e(M)}$.

Thus the constructed Green's functions of the sections of rectangular waveguides with three-layer longitudinally-inhomogeneous filling, in the case of excitation by longitudinal given currents, enable one to widen the possibilities of mathematical simulation of various electromagnetic problems, including problems of diffraction on inhomogeneities inside considered waveguide-dielectric structures.

References

1. V.V. Shevchenko, Smooth Transitions in Open Waveguides, Moscow: Nauka, 1969 (in Russian).
2. R. Mittra (Ed.), Computer Techniques for Electromagnetics, University of Illinois, Urbana, Illinois: International series of monographs in electrical engineering, vol. 7, 1973.
3. L. Lewin, Theory of Waveguides. Techniques for the solution of waveguide problems, London, Butterworth and Co (Publishers) Ltd., 1975.
4. V.V. Nikolsky, Variational Elements for the Inner Problems of Electromagnetics, Moscow: Nauka, 1967 (in Russian).
5. B.A. Panchenko, Green's Tensor Functions of the Maxwell Equations for Cylindrical Domains, Radiotekhnika, N15, 1970, pp. 82-91 (in Russian).

Millimeter Wave Evanescent Mode Power Combiner-Gunn Oscillator in Suspended Stripline Configuration

A. K. Poddar, J. K. Bansal and K. N. Pandey

Armament Research & Development Establishment, Pune-21

Defence Research and Development Organisation, India

E-mail : <general@drarde.ren.nic.in> or <sankar@iucaa.ernet.in>, Fax: + 91 (0) 212 335102

Abstract

In the search for low cost high power semiconductor diode oscillator device, a new millimeter wave evanescent mode power combiner with Gunn diode oscillator at 35 GHz employing combination of suspended stripline and evanescent mode resonator is developed. With a 35 GHz diode rated at 100 mW, stable power output of more than 180 mW is achieved over a tuning range of about 3.5 GHz. The oscillator is simple in fabrication, cost effective and is amenable for integration with other planar circuits.

Introduction

Gunn diode is one of the most important solid state millimeter-wave source. It exhibits low noise and a wide operating frequency range and capable of generating power 100 mW or greater. Although enhanced power output can be easily obtained from IMPATT devices, these are usually not suitable because of higher noise. Therefore employing more than one diode in series shows promise as a method for increasing the output power of these devices as millimeter-wave oscillator. Most of the application of Gunn diode oscillator at Ka-band are based on its compact size, light weight and stability. Some of the applications are in missile-guidance and tracking, traffic control radar, satellite communication, helmet mounted trans-receiver system for soldiers, pattern recognition, weather prediction etc.

Millimeter wave oscillators in MIC form offer advantages in terms of small size and ease of integration with other planar circuits. Since an oscillator forms an essential part of a millimeter receiver front end, its development leading to simplicity of fabrication and lower circuit losses while retaining the advantages of MIC fabrication is of considerable importance. Bulk of published literature on Gunn diode oscillators are in waveguide and microstrip configurations [1,2]. Recent paper [3] has proven feasibility of utilizing Gunn diode oscillator

employing evanescent mode guide as a resonator in suspended stripline configuration. Most millimeter wave Gunn diode oscillators reported in MIC form employ microstrip medium with Varactor tuning [4]. For application not requiring electronic tuning, microstrip oscillator employing evanescent mode resonator offers an attractive cost-effective solution. In the circuit reported [4], Gunn diode is mounted inside a section of evanescent mode waveguide and resonance is achieved by tuning out the capacitive reactance of the diode with the inductive reactance of the evanescent guide section. The output is taken through a microstrip electromagnetically coupled to the evanescent mode guide. It is well known that in millimeter wave band, the microstrip tends to be excessively lossy. A low loss planar transmission line which overcomes this problem is the suspended stripline. In the present paper, the low loss feature of the suspended stripline and the inductive property of the evanescent mode guide are utilized to realize a simple, small size, low cost, Ka-band power Combiner, with broad-band performance.

Evanescent Mode Resonators

Microwave oscillations in an evanescent mode wave guide (EMWG) were first observed in high power TWTs. The occurrence of pass bands below cut-off often was given an explanation for the conditions, and the fact that this phenomenon can have useful applications was later demonstrated in the field of passive microwave components. Components for microwave integrated circuits with EMWG resonators which is having very high value of quality factor was reported [5], and the properties of evanescent mode resonator as now are well understood. In this technique, inductance is realized by a short section of rectangular wave guide below cut off. It is well known that a rectangular waveguide operating at a frequency far below its dominant mode cut-off frequency behaves like a pure inductance, and therefore stores magnetic energy. Resonance conditions are established by introduction of a device that stores

electrical energy, such as active devices that are capacitive in nature.

An EMWG (evanescent mode wave guide), of length L , impedance Z_0 and propagation constant γ can be represented by a π section, shown in Figures 1 and 2. In present power combiner circuit shorted end π -section EMWG is used. The main feature of the equivalent circuit is that the individual elements closely approach genuine lumped elements. The relationship between reactance and frequency normally associated with a distributed network is absent. Broad-band operation should therefore be a characteristic of active device (Gunn-diode) used with evanescent mode resonators over a large frequency range. The lumped element nature is considered a problem of matching the impedance of an active device over a large frequency range. If distributed elements are used for matching purposes, the operating bandwidth is degraded due to the parasitic pass bands associated with these elements. Normally, these pass-bands are related harmonically to the operating frequency. However, with evanescent mode resonators, as long as frequency of operation does not exceed the cut-off frequency of the waveguide, additional pass bands do not exist. At higher frequency, parasitic pass band are possible, but these do not fall at harmonics of the working frequency.

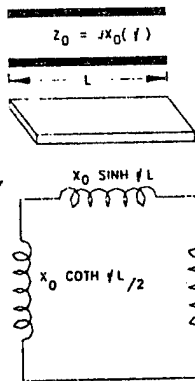


Figure 1

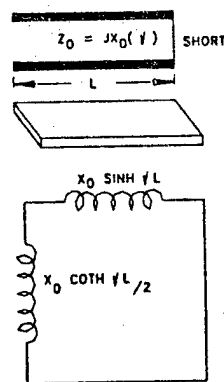


Figure 2

Fig.1 Length of the EMWG and equivalent circuit (π -section)Fig.2 Length of the shorted end EMWG and equivalent circuit (π -section)

Oscillator Configuration

As illustrated in Figure 3, the oscillator employs a suspended stripline terminated in an evanescent mode guide section. The evanescent mode guide is formed by simply extending the suspended stripline channel (without the substrate) with reduced dimensions. The dual Gunn-diode is shunt mounted in series configuration at the end of the suspended stripline so that the evanescent guide section presents an inductive

load to the Gunn-diode. A dielectric screw is inserted from the opposite side of the substrate so that the diode makes firm contact with the strip conductor. Unlike in [4], where biasing the diode requires bonding a wire to the anode, in this configuration DC bias is easily provided through a low pass filter printed as part of the suspended stripline circuit. The evanescent mode section located immediately next to the diode presents an inductive load to the Gunn diode. Additional tuning screw is provided in the vicinity of the diode to facilitate the tuning. The output can be taken either through a K-type coaxial connector connected to the suspended stripline or through a Ka-band rectangular waveguide via a suspended stripline probe transition. The latter arrangement is shown in Fig.3.

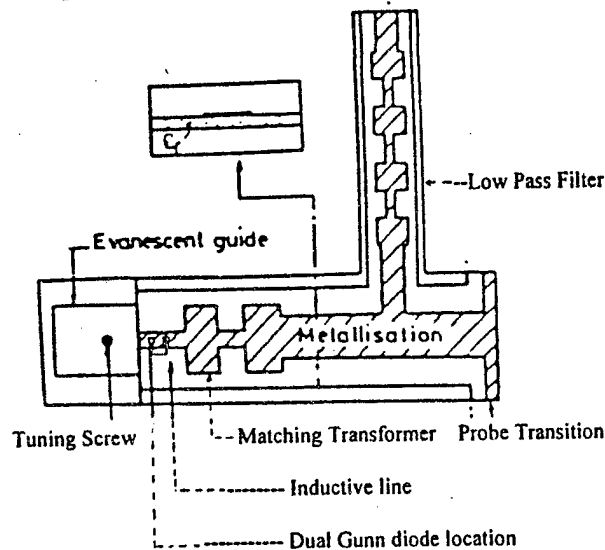


Fig.3 Layout of EMWG power combiner in suspended stripline configuration.

Equivalent Circuit and Design

Figure 4 shows the equivalent circuit of the oscillator. The circuit elements L_1 , C_1 and C_2 constitute a π -equivalent circuit representation for the encapsulation of the diode. The diode is supported in the channel by means of a brass-metallic post. This post is represented by a T-network composed of the capacitance C_0 in series and a shunt reactance consisting of the series combination of an inductance L_s and a capacitance C_g . The capacitance due to tuning screw is represented as C_m . L is due to an inductive line printed as a part of the matching network. The capacitive reactance due to C_0 accounts for the phase variation of the field across the post in the direction of propagation, due to its finite diameter.

The oscillator is designed at 35 GHz by considering the following main aspects: (i) accurate modeling of the resonant-region taking into account the equivalent circuit of the dual-Gunn diode, admittance

due to the mount and the load presented by the evanescent mode waveguide (ii) computation of the overall impedance of the above network and establishing resonance condition (iii) arrangement for dc biasing the diode through a low pass filter and bias-suppressor (iv) the transition from suspended stripline to Ka-band output waveguide.

The equivalent dual device impedance Y_d (where Y_{d1} and Y_{d2} corresponding to MDT-diode1 & diode2) is a strong function of the frequency and DC bias current and a weak function of the RF current and temperature. The equivalent circuit admittance Y_c is a function of only the frequency. The criteria for circuit-controlled steady-state oscillation are given by, $\text{Im}(Y_d + Y_c) = 0$ and $\text{Re}(Y_d) \geq \text{Re}(Y_c)$, where $Y_c = G_c + jB_c$, is the load admittance transferred to the equivalent dual diode plane.

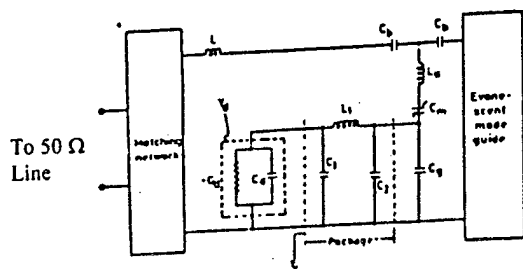


Fig.4 Equivalent circuit of power-combiner EMWG Gunn oscillator.

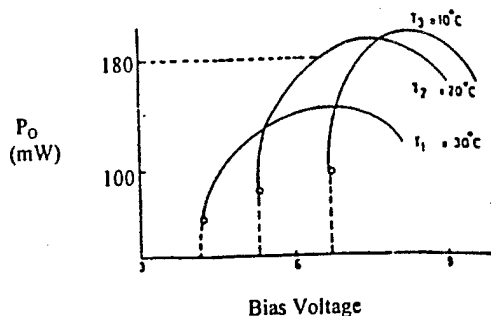


Fig. 5 Combiner power output as a function of bias voltage.

Experimental Results

The evanescent mode Power-Combiner Gunn oscillator as configured in Figure 5 is fabricated using two MDT diode (MG 1018-16) rated at 100 mW. Each diode and its resonant condition was tested individually and optimised maximum power at desired frequency. Two diodes were then stacked in a common EMWG and tested as a single resonant assembly. The operating current for the dual diode oscillator was 1.09 Amp. Biasing the diodes from separate power supplies or single power supply did not make significant difference in the results. Different spacing between diodes were tested, but

only small change in frequency and power was observed. The output is taken from a Ka-band waveguide via a suspended stripline probe transition. Figure 5 shows a graph of the measured output power versus the bias voltage. The oscillator offers more than 180 mW of power output at 20°C. With a variable short provided at one end of the output Ka-band waveguide the oscillator could be tuned over a frequency range of about 3.5 GHz around 35 GHz. For oscillator requiring coaxial output, this tuning is provided by the tuning screw in the evanescent guide.

Conclusion

A new configuration of a suspended stripline Ka-band power Combiner with two Gunn diode employing evanescent guide as part of the resonant circuit is reported. Further more the evanescent mode combining concept may be extended to two to more diodes in suspended stripline configuration. The oscillator permits nearly 100 % combining efficiency, in addition to offering advantages in terms of low cost, ease of biasing, easy tunability over a bandwidth of about 3.5 GHz, small circuit losses and ease of integration with other planar components.

Acknowledgment

The authors would like to express our gratitude to Prof. B. Bhat and Prof. S. K. Koul at CARE, IIT-Delhi for providing valuable guidance and suggestion. We would like to thank to Dr. S. K. Salwan, Director-ARDE for giving encouragement and permission to publish this paper.

References

1. D. Rubin, Varactor-tuned millimeter wave MIC oscillator, IEEE Trans. Microwave Theory and Tech., Vol. MTT-24, pp. 866-867, Nov. 1976.
2. R. Tahim, G.M Hayashibara and K. Chang, High performance millimeter-wave suspended stripline Varactor-tuned Gunn VCO, Electronics Lett., Vol.22, No.20, pp.1057-1059, Sept.- 1986.
3. A. K. Poddar, S. K. Koul, and B. Bhat, Millimeter wave evanescent mode Gunn oscillator in suspended stripline configuration, IR&MM Wave, 22nd international conference, pp. July 20-25 1997.
4. S. Bharj MM-Wave evanescent mode oscillator, Microwave Journal, Vol.28 pp. 313-317, May 1985
5. K. Schunemann, R. Knochel and G. Begemann, Components for microwave integrated circuits with evanescent mode resonators, IEEE Trans., Microwave Theory and Technique Vol. MTT-25, no. 12, PP. 1026-1031, Dec. 1977.

NUMERICAL ALGORITHM FOR THE DESIGN OF PLANE JUNCTION OF TWO WAVEGUIDES WITH ARBITRARY STEPPED BOUNDARIES OF CROSS-SECTIONS

Anatoly A. Kirilenko

Institute of Radiophysics and Electronics of the National Academy of Sciences of Ukraine
12 Akad. Proskura St., Kharkov, 310085 Ukraine

The usage of waveguides with nonstandard cross-sections or pieces of such waveguides as fragments of complicated diaphragms or frequency-selective surfaces is now a common practice in microwave engineering. Therefore the general key-building blocks that are oriented on arbitrary waveguide geometry, as well as the specialized key blocks for the fixed geometries are needed when developing the software for exact design of microwave devices. We shall discuss here the computation of the S-matrixes of a plane junction between two different waveguides with arbitrary stepped boundaries of cross-sections. H- and Π -waveguides [1], T- and cross-shape waveguides, L-waveguides and waveguides having cross-section similar to the Jerusalem cross [2] are particular cases of such waveguides. In the absence of an exact specialized algorithm, the approach briefly outlined below can be used as a tentative tool of simulation of plane junction of two waveguides with nonstandard smooth cross-sectional boundaries approximated by the stepped contours [3]. The latter approach is useful, for example, for a rapid preliminary estimation of "what if?" ideas in the microwave design, before running more exact specialized algorithms.

Let us describe the waveguide cross-sections S_0 and S_1 as two sets of rectangular domains where two sides of each of the latter are metallized (see Fig. 1). Similar division is common for the majority of conventional methods of such waveguide modal basis calculation based on the mode-matching technique or on the surface integral equation for the fields on the domain boundaries. The used here form of the field expansions is oriented on the transverse resonance method, where the above-mentioned domains can be treated as pieces of plane waveguides. Such an approach is the most convenient one within the frames of large modeling packages, where a set of various plane waveguide key-building blocks enables one to form rapidly the dispersion equations for the most complicated cross-sections.

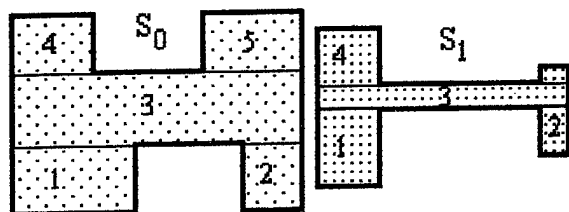


Fig. 1. Cross-sections of two connected waveguides and their division into partial domains

Arbitrary cross-section of considered type can be completely characterized with the aid of geometry matrix $G_m[0 \leq j \leq J_m, 0 \leq k \leq 3]$, where j is the number of domain, J_m is the total number of domains, m is the number of waveguide. The elements of the i -th line describe

sequentially the abscissa of the left lower edge of the partial domain, the width of the corresponding waveguide, the ordinate of the left lower edge of the domain, and the length of the plane waveguide section. The single restriction imposed on the G_m -matrices is as follows: the cross-section of the l -st waveguide must be placed completely within the cross-section of

the 0-th waveguide, as it is supposed to use the mode-matching method to find a required S-matrix. In the opposite case it is possible to implement a "zero-length virtual rectangular waveguide" having the cross-section bounded by the "extreme" fragments of initial boundaries. After that the problem is reduced to two standard ones and to the assembling the final geometry by the S-matrix technique.

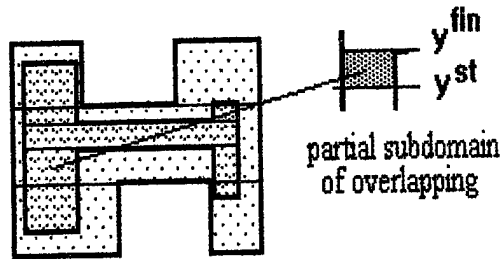


Fig.2 Overlapping of cross-sections and partial subdomain of overlapping of the 3-rd domain of the 0-th WG with the 1-st domain of the 1-st WG

the 1-st waveguide and fixing their overlapping. Such an operation produces a matrix $CR[0 \leq i \leq I, 0 \leq k \leq 3]$ that characterizes the set of overlapping sub-domains. Here i is the ordered number of sub-domain, $I < J_0 J_1$ is the total number of sub-domains. The elements of the i -th line define sequentially the numbers of corresponding overlapping domains of S_0 and S_1 , y^{st} and y^{fin} are the ordinates of the lower and upper boundaries of the i -th overlapping sub-domain, respectively. The problem of calculation of the matrix of coupling integral consists in summing up the partial integrals over the set of overlapping sub-domains according to the CR -matrix. Thus, for the " p "-th mode of the 0-th waveguide and the " s "-th mode of the 1-st waveguide we have the following coupling integral, where $s^{(v,k)}$ denotes the k -th domain of cross-section S_v .

$$\iint_{S_1} \begin{pmatrix} \rightarrow^{(0)} \\ e_p \end{pmatrix} \begin{pmatrix} \rightarrow^{(1)} \\ e_s \end{pmatrix} dS = \sum_{k=0}^{J_0-1} \sum_{j=0}^{J_1-1} \iint_{S^{(0,k)} \cap S^{(1,j)}} \begin{pmatrix} \rightarrow^{(0)} \\ e_p \end{pmatrix} \begin{pmatrix} \rightarrow^{(1)} \\ e_s \end{pmatrix} dS = \sum_{k=0}^{J_0-1} \sum_{j=0}^{J_1-1} \iint_{S^{(0,k)} \cap S^{(1,j)}} \Pi_{ps}^{uv} dS$$

Suppose now that the mode bases of both waveguides have been found and ordered by a set of transversal wave numbers- $\chi_s^{(v)}$, where $v=0,1$ and $s=0,1,2,\dots$ are the number of the waveguide and of the mode in this waveguide, respectively, and by corresponding set of vectors of the Fourier-amplitudes: $a_{sm}^{(v,j)}$, $b_{sm}^{(v,j)}$ of the expansions of the Hertz vector within each j -th domain. Here we emphasize the standard character of sub-domain geometries (see Fig.2-metallized side walls and open or shortened upper and lower walls) and standard presentation of eigenmode fields. It becomes clear that this is a proper way to develop a generalized algorithm for the analysis of junction between two waveguides with stepped boundaries, based on a standard procedure of calculation of partial coupling integrals for arbitrary sub-domains.

The latter have the form of the double sums and up to the constant determined by the chosen normalization of the eigenmodes, we have, for example, for the TE -waves in both waveguides:

$$\begin{aligned}
\Pi_{ps}^{HH} = & \sum_{n=0}^N i\omega_{pn}^{(k)} a_{pn}^{(k)} \sum_{m=0}^M i\omega_{sm}^{(j)} (a_{sm}^{(j)} e_{nm}^{aa} - b_{sm}^{(j)} e_{nm}^{ab})_{cc_{nm}} - \\
& - \sum_{n=0}^N i\omega_{pn}^{(k)} b_{pn}^{(k)} \sum_{m=0}^M i\omega_{sm}^{(j)} (a_{sm}^{(j)} e_{nm}^{ba} - b_{sm}^{(j)} e_{nm}^{bb})_{cc_{nm}} + \\
& + \sum_{n=1}^N \beta_n^{(k)} a_{pn}^{(k)} \sum_{m=1}^M \beta_m^{(j)} (a_{sm}^{(j)} e_{nm}^{aa} + b_{sm}^{(j)} e_{nm}^{ab})_{ss_{nm}} + \\
& + \sum_{n=1}^N \beta_n^{(k)} b_{pn}^{(k)} \sum_{m=1}^M \beta_m^{(j)} (a_{sm}^{(j)} e_{nm}^{ba} + b_{sm}^{(j)} e_{nm}^{bb})_{ss_{nm}}
\end{aligned}$$

where, for example,

$$\begin{aligned}
\beta_n^{(k)} &= \frac{n\pi}{a^{(k)}}, \quad ss_{nm} = \int_{x^{(j)}}^{x^{(j)}+a^{(j)}} \sin(\beta_n^{(k)}(x-x^{(k)})) \sin(\beta_m^{(j)}(x-x^{(j)})) dx, \\
\omega_{pn}^{(k)} &= \sqrt{\chi_p^{(k)2} - \beta_n^{(k)2}}, \quad e_{nm}^{aa} = \int_{y^{(j)}}^{y^{(j)}} \exp(i\omega_{pn}(y-y^{(k)}) + i\omega_{sm}(y-y^{(j)})) dy
\end{aligned}$$

Such an algorithm was first realized in a general form by V. I. Tkachenko, as a C++ code, and has been tested for the plane junctions of rectangular, ridged and double-ridged waveguides. After developing a generalized algorithm of the search for the eigenmode bases of generalized waveguides with piecewise boundaries specified by their G -matrixes, we shall obtain an extremely powerful and versatile tool for high-precision microwave CAE.

REFERENCES

1. J. Bornemann, F. Arndt, Modal S-matrix design of metal finned waveguide components and its application to transformers and filters, *IEEE Trans. MTT*, vol. 40, no 7, 1992.
2. J. A. Arndt, F. A. Pelow, Resonant-grid quasioptical diplexers, *Bell System Techn. J.*, vol. 54, no 2, 1975.
3. A. A. Kirilenko, M. V. Orlov, Approximating decomposition for the analysis of smooth inhomogeneities, *J. Commun. Techn. Electronics (Engl. Transl.)*, vol. 41, pp. 1028-1032, 1991.

NUMERICAL INVESTIGATION OF MULTIPLE RECTANGULAR APERTURE IRISES IN RECTANGULAR WAVEGUIDE

L. P. Mos'pan, A. A. Kirilenko, V. I. Tkachenko

Institute of Radiophysics and Electronics of the National Academy of Sciences of Ukraine
12, Acad. Proskury St., Kharkov, 310085, Ukraine

It is known that rectangular irises are conventional elements of microwave waveguide circuits. However application area of them is limited essentially by their low quality factor. Using multiple aperture irises makes it possible to design circuits with non-conventional features. For example, a design of easy manufactured bandpass filters based on multiple irises with four equal apertures was reported in [1]. Frequency response of multiple rectangular irises with different apertures was firstly studied in [2]. It appears that such irises have a bandstop feature but this attractive result has been obtained on the basis of approximate model. So, development of proper rigorous model is of particular interest. The purpose of this paper is to

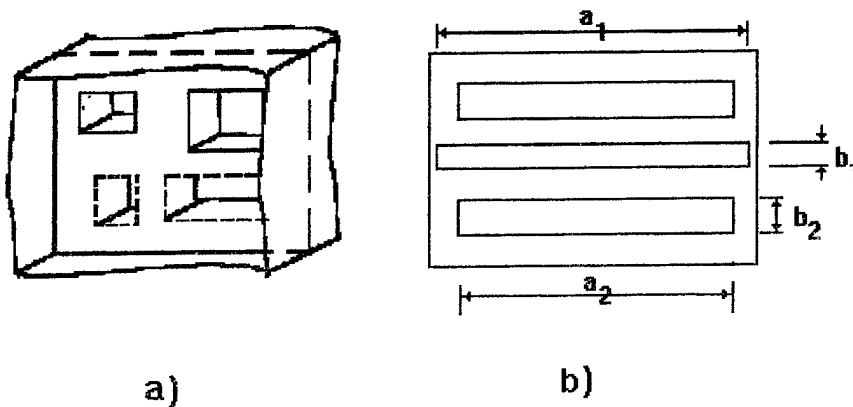


Fig. 1 Multiple rectangular aperture iris

develop rigorous numerical models of multiple rectangular irises with different apertures and to study their frequency response.

The structure under consideration is shown in Fig. 1a. It represents itself a multiple iris placed in a rectangular waveguide. Iris cross-section contains arbitrary number of different rectangular apertures. Exact numerical model of the structure has been developed by solving a adequate discontinuity problem, that is N-furcated double plane discontinuity. Solution of this problem was obtained by the mode-matching technique. S-matrix of multiple aperture iris was obtained from the S-matrix of discontinuity with the aid of the generalized scattering matrix technique. To examine the validity of developed model, irises with single, two and three apertures were studied numerically. Obtained numerical results were compared with numerical and experimental data cited in [1,2,3], and a good agreement between them was observed. Besides, the phenomenon of the relative convergence of obtained solution and the problem of choosing the optimal number of modes inside iris apertures were also studied to provide accurate results.

As it was reported in [4], frequency response of a multiple iris with at least two different apertures has two resonances corresponding to the total transmission and one resonance corresponding to the total rejection. In order to reveal a mechanism of forming the latter resonance, numerical studies were carried out for the iris, whose cross-section is presented in Fig. 1b. The iris cross-section contains three rectangular apertures located one

under another. Upper and bottom apertures have equal dimensions. The third aperture of different dimensions is located symmetrically between them. Numerical studies were carried out for a number of three-aperture irises placed in rectangular $22.86 \times 10.16 \text{ mm}^2$ waveguide within the single-mode frequency range. Scattering parameters of the irises were calculated accounting for 100 to 120 H-modes and a proper number of E-modes in the circuit. A required number of E-modes was taken in such a manner that maximum transversal wave numbers of the H-mode and E-mode were equal. The number of H- and E-modes inside iris apertures were taken respectively to their cross section dimensions.

An effect of changing the dimensions of iris apertures on the iris frequency response has been numerically studied for the irises with different dimensions of their apertures. As a first example, the iris with central aperture of 16.86 by 1.52 mm^2 is considered. The height of the upper and bottom apertures is 2.52 mm , whereas the width of them is changed from 7 mm to 22 mm . Frequency responses versus $K=a/\lambda$ for of this iris are presented in Fig. 2 for some values of a_2 . All the above mentioned resonances are observed on the plots for the iris with apertures, wide dimensions of which are close to each other. While changing a_2 in such a manner that a_2 and a_1 are close, the character of frequency response itself is not changed whereas the resonant frequencies of total rejection resonance and one of the total transmission resonance are shifted. The band of rejection resonance is changed essentially. Resonant frequency of the second total transmission resonance remains the same. As the second example, the iris with central aperture of $22.86 \times 1.52 \text{ mm}^2$ is considered. The width of the upper and bottom apertures $a_2 = 19 \text{ mm}$ whereas the height of the upper and bottom apertures b_2 is changed. Frequency responses of the iris are presented in Fig. 3 for different values of b_2 . It reveals that the effect of changing the height of upper and bottom apertures on the iris frequency response is essentially less than the one of changing the wide dimension of them

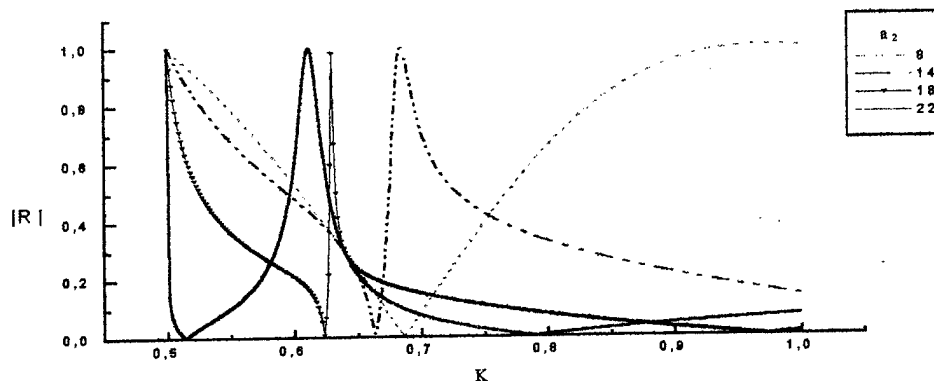


Fig. 2 Frequency response of three aperture iris for different values of bottom and upper apertures width a_2 although it leads to similar results. Changing the dimensions of the central aperture shows a similar effect on the iris frequency response as changing the dimensions of upper and bottom apertures. Similar results were obtained for a five-aperture iris, cross section of which contained two pairs of equal apertures, located symmetrically with respect to the central aperture.

According to obtained data, the lower resonant frequency corresponding to the total transmission resonance is determined mainly by the dimensions of the aperture having the greater width; the upper resonant frequency corresponding to the total transmission resonance is defined mainly by the dimensions of the aperture having the smaller width. Rejection resonance is formed by "combining" the frequency responses of the iris apertures. By choosing

appropriate dimensions of the iris apertures (i.e. by playing with electromagnetic interaction of iris apertures), it is always possible to achieve high quality of rejection resonance (see Fig.4), which has the same nature as conventional rejection resonance known before. Rejection resonance at a desired frequency with a required quality factor can be obtained easily by choosing proper dimensions of the iris apertures. So, it is obvious that the rejection filters based on the multiple rectangular aperture irises can be designed, and such filters are easy in manufacturing because of their simple geometry.

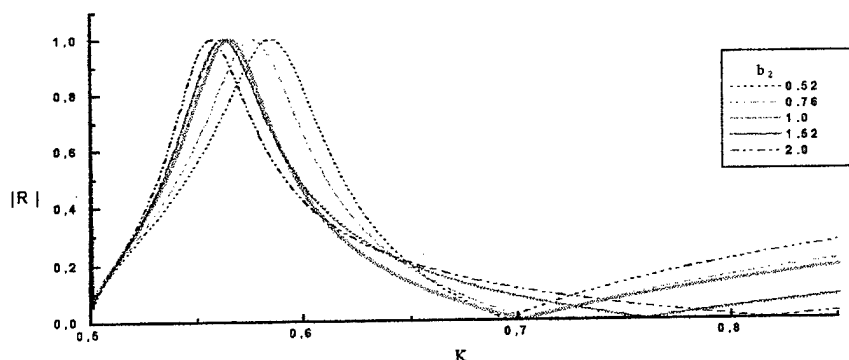


Fig. 3 Frequency response of three aperture iris for different values of bottom and upper apertures height b_2

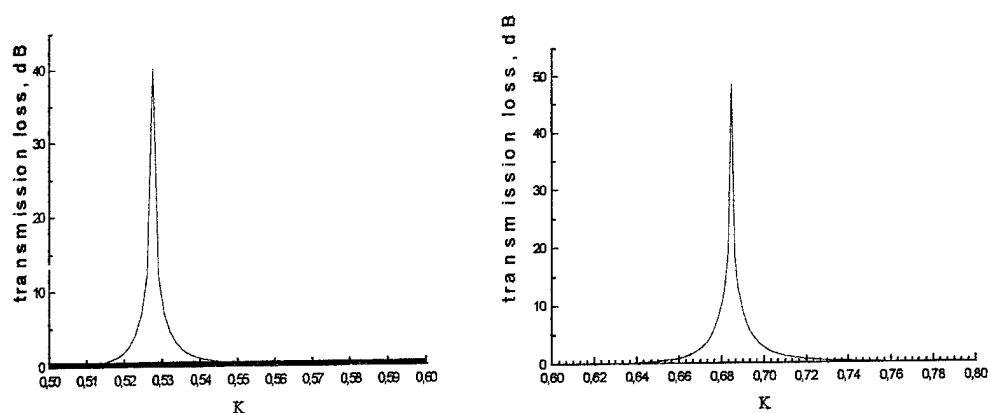


Fig. 4 Transmission loss for two different three aperture irises

References

1. W. Hauth, R. Keller, U. Papziner, R. Ihmels, T. Sieverding, F. Arndt, Rigorous CAD of multiport coupled rectangular waveguide components, *Proc. European Microwave Conf.*, 1993, pp. 611-614.
2. N. G. Paterson, I. Anderson, Bandstop iris for rectangular waveguide, *Electronics Lett.*, 1976, vol. 12, No 22, pp. 592-594.
3. V.G. Alybin, N. M. Gordyuhina, et al., Double resonance waveguide iris, *Radiotekhnika i Elektronika*, 1981, No 8, pp. 1605-1613.
4. A. A. Kirilenko, L. P. Mos'pan, Double aperture irises in a rectangular waveguide, *Radiofizika i Elektronika*, IRE NAS Press, 1997, No 2 (in Russian).

MAGNETIC FIELD FINDING IN THE SOURCE-REGION OF LONGITUDINAL SLOT IN A WAVEGUIDE FILLED WITH LAYERED DIELECTRIC

Ludmila P. Yatsuk

Kharkov State University, Svobody Sq.4., Kharkov, 310077 Ukraine,
e-mail: Ludmila.P.Yatsuk@univer.kharkov.ua

Abstract. The problem of finding the scattering matrix coefficients of longitudinal slot in a waveguide filled with a layered dielectric is under consideration. The difficulties of representation of the field excited by a longitudinal magnetic current in the source region are discussed. The new way of this representation is proposed, ensuring convergence of the excitation solution.

Introduction. There are different ways of an excitation problem solution for an arbitrary magnetic current in a waveguide. The solving of this problem is necessary for obtaining the scattering matrix elements of slot inhomogeneity. The field is to be found in the region where a slot is located. In the case of a longitudinal slot the problem can be easily solved for an empty waveguide but not for the waveguide filled with a layered dielectric. The main reason of it consists of the impossibility to construct the Green's function for a vector potential when the medium in a waveguide is layered. The Green's function for a field and the eigenwaves method are followed with the solution which is not admissible for calculations. The essence of this problem and one of the ways of overcoming it are discussed in this paper.

The main part. Let us consider a waveguide filled with three-layered dielectric in parallel to the narrow walls of the waveguide. The permittivities of layers are $\epsilon_1, \epsilon_2, \epsilon_3$. The longitudinal slot of length L and width d is cut in the broad wall of the waveguide over one of the layers. The electric field \vec{e}_s can be found from the magnetic field continuity condition on the slot surface. If we use the Galerkin method with \vec{e}_n ($n=1, 2, 3, \dots$) as a basis set for finding \vec{e}_s , it is necessary to find the field under the slot excited by the magnetic current \vec{J}^m equivalent to \vec{e}_n .

In the case of an empty waveguide this field can be found with the aid of magnetic vector potential for which the Green's function is constructed using the set of the independent vector eigen functions of the waveguide cross section

$$[\nabla\psi^m, \vec{z}^0], \nabla\chi^m, \vec{z}^0\chi^m, \quad (1)$$

where

$$\psi^m = \sin \frac{m\pi x}{a} \sin \frac{n\pi y}{b}, \quad (2)$$

$$\chi^m = \cos \frac{m\pi x}{a} \cos \frac{n\pi y}{b}, \quad (3)$$

$m, n = 0, 1, 2, \dots$; a, b are the dimensions of the broad and narrow waveguide wall, respectively.

It was shown in [1] that the independence of the functions (1) is due to the fact that they originate from the full set of vector eigen functions \vec{L}, \vec{M} and \vec{N} introduced by Hansen [2]. The set (1) is available because the boundary conditions for \vec{L} and \vec{M} are the same. The

transverse eigen values for the eigen vectors are the same as well. All this enables one to unite all these functions under a common operation of summation and obtain the convergent series for the required field. This is valid for an infinite waveguide with a homogeneously filling.

Another situation is taking place in the case of layered filling of a waveguide. The boundary conditions for the functions \vec{L} , \vec{M} and \vec{N} on the boundaries of adjacent layers of dielectric are different. Their eigen values are to be calculated from different dispersion equations. So, the set (1) of independent transverse and longitudinal functions cannot be constructed. It does not give an opportunity of traditional Green's function construction for the vector potential. As a consequence, the Green's function for a field or the eigen waves method (EWM) [3] is to be used in order to obtain the required field in the source region.

There are two ways of Green's function construction depending on a choice of longitudinal direction: along the waveguide axis or normally to it (or to the boundaries of the adjacent layers). The first way was used in [4 - 6], the second in [7, 6]. When the source is a magnetic current, neither the first way-Green's function nor the eigen waves method yields a solution suitable for calculations. The structure of the solution obtained with EWM [3] is as follows:

$$\vec{H}(\vec{e}_s) = \sum_s C_s(z) \vec{H}_s + \sum_s C_{-s}(z) \vec{H}_{-s} - \vec{z}^0 \frac{J_z^m}{i\omega\mu_a} \quad (4)$$

Here $\vec{H}_{\pm s}$ are the vector-functions representing magnetic field of the mode indicated with index s , $C_{\pm s}(z)$ are the amplitude coefficients depending on the coordinate z within the source region, \vec{z}^0 is the unit vector along the z -axis, ω is the frequency, μ_a is the absolute magnetic permeability, J_z^m is the projection of the vector of volume magnetic current density on the z -axis.

Volume density J_z^m is connected with the surface density J_{zs}^m by the relation:

$$J_z^m = J_{zs}^m \delta(y), \quad (5)$$

where $\delta(y)$ is the Dirac delta-function.

It means that the third term in (4) is divergent, so are the first two sums. The same situation occurs when the first way-Green's functions for the field are used. Using the second way-Green's functions is equivalent to solving the non-homogeneous Maxwell equations from the very beginning with the aid of the Fourier integral. It requires an integration in the complex plane using the residue theory and results in very complicated expressions for the required field.

The most compact expressions could be obtained if the third term in (4) is laid out in series and united somehow with the first two terms. But the problem in the proper choice of basis functions to be used in the expansion. In [1], it was shown that the additional term in (4) is exclusively due to the compulsory presence of potential functions in the expressions describing the field inside the source region. This leads to conclusion that this term in (4) is to be expanded using only the potential basis.

The potential eigen functions \vec{L} are as follows:

$$\vec{L} = \nabla \varphi, \quad (6)$$

where φ satisfies the equation

$$\Delta \varphi_j + k^2 \varepsilon_j \varphi_j = 0, \quad (7)$$

with j denoting the number of the dielectric layer, and boundary conditions

$$\frac{\partial \varphi_j}{\partial n} = 0 \quad (8)$$

$$\mu_j \frac{\partial \varphi_j}{\partial n} = \mu_{j+1} \frac{\partial \varphi_{j+1}}{\partial n_{j+1}} \text{ and } \varphi_j = \varphi_{j+1} \quad (9)$$

at the perfect metal, and at the boundaries of adjacent layers, respectively.

Equations (8) and (9) lead to the dispersion equations for determining the eigen values of the function φ . The solution of (7) gives the infinite set of orthogonal functions, which were used for the expansion of the extra term in (4). All three functions \vec{L} , \vec{M} and \vec{N} have the same eigen values $\frac{n\pi}{b}$ along the narrow wall in the cross section. So three series in (4) can be united under the sign of sum over the index n . The terms of this series are three sums over the eigen values, obtained from three dispersion equations for \vec{L} , \vec{M} and \vec{N} functions, or potential functions and LM - and LE -waves. It was numerically shown that these terms converge to zero not worse than $1/n^2$. It means, that the series obtained is convergent.

Conclusions. On the ground of investigations of this paper it is clear that the excitation problem for a waveguide with layered dielectric excited with a magnetic current could be solved by using two method. One can either apply the Green's function technique to the normal direction to the boundaries of adjacent layers, or modify EWM expanding the extra term in terms of the potential vector eigen functions.

References.

- [1] R.E. Collin, On the incompleteness of E- and H-modes in waveguides, *Canadian Journal of Phys.*, 1973, V.51, pp. 1135 - 1140.
- [2] P.M. Morse, H. Feshbach, *Methods of Theoretical Physics*, Moscow, In. Lit., 1958 (in Russian).
- [3] L.A. Wainstein, *Electromagnetic waves*, Moscow, Sov. Radio, 1957.
- [4] H. Jin, D.Eng, W. Lin, Dyadic Greens functions for a rectangular waveguide with an E-plane dielectric slab, *IEE Proc.*, 1990, pt. V. 137, N 4, pp.231-234.
- [5] J. Jubert and D.A. McNamara, Dyadic Green's function of the electric type for inhomogeneously loaded rectangular waveguides, *IEE Proc.*, 1989. pt. H. V 136. N 6, pp. 469-474.
- [6] B.A. Panchenko, E.I. Nefedov, *Microstrip Antennas*, Moscow, Rdio i Svyaz', 1986 (in Russian).
- [7] L.B. Felsen, N. Marcuvitz, *Radiation and Scattering of Waves*, Moscow: Mir, 1978, (English Translation)

WAVEGUIDE SECTION OF SEQUENTIALLY INCLUDED IDENTICAL ELEMENTS

V.B. Kazanskiy, V.V. Podlozny, V.V. Khardikov

Chair of Theoretical Radiophysics, Kharkov State University, 310077, Kharkov, Ukraine

ABSTRACT

This paper presents a solution of the problem of symmetric wave diffraction on a set of identical periodical elements in circular waveguide. Each period includes elementary inhomogeneities such as ring, radial diaphragm or resistive film, and adjusting magnetodielectric spacers. Period can be equivalently characterized as a four-pole. Analytical formulas for the scattering coefficients are obtained by using the matrix polynomial theory. In these formulas, the indices of Mauguin polynomials depend on the number of identical elements in the waveguide.

GEOMETRY AND METHOD OF SOLUTION

The analyzed section of a circular waveguide consists of N identical elements with «period» L . The waveguide has radius a . Each of identical elements contains two magnetodielectric spacers. The spacers have different widths b_j ($b_1 + b_2 = L$) and are specified by permittivity ϵ_j and permeability μ_j . There is a thin resistive film (RF) or a nondissipative anisotropic conductive film (D) of equivalent conductivity Y_u between them. We suppose these elementary inhomogeneities do not transform the incident field. That is why we can describe the basis element (period) by a transfer matrix of an equivalent four-pole $T(t_{jk})$. The filling material in the input and in output waveguides is characterized by the permittivities ϵ_0, ϵ_T and permeabilities μ_0, μ_T , respectively (Fig. 1).

Either $E_{0n} - (s = e)$ or $H_{0n} - (s = h)$ mode diffraction problem is considered with the $\exp(-i\omega t)$ time dependence. The amplitudes of the modes in the right direction of propagation are

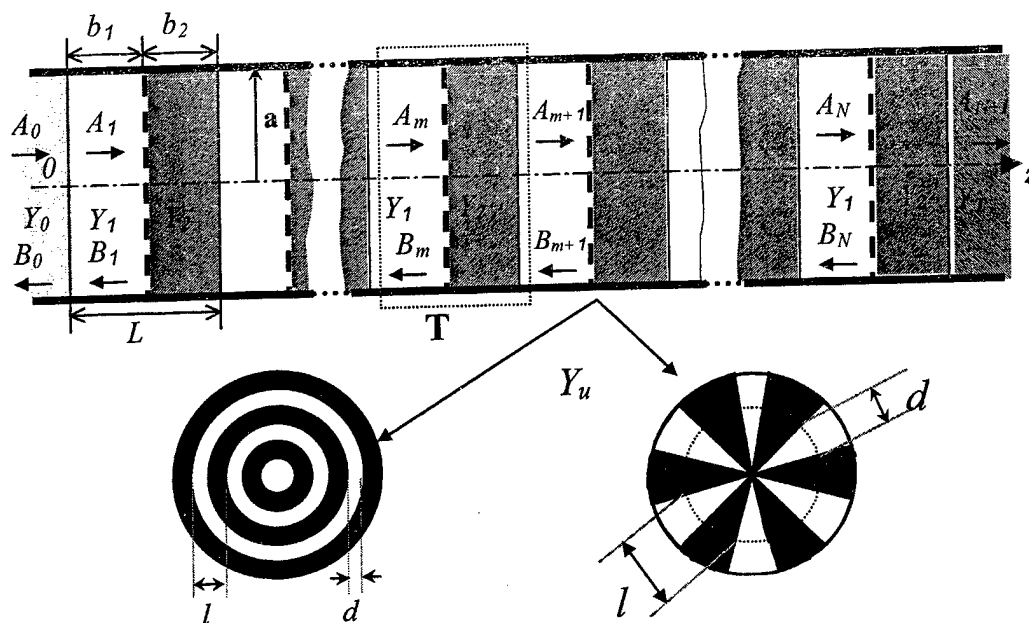


Fig. 1. Waveguide inhomogeneities

denoted as A_m and in the opposite direction as B_m . The amplitudes of propagating waves on the shadow border (between the N th and $(N+1)$ -th media) are related in such a way that: $A_N = a_0 A_{N+1}$, $B_N = b_0 A_{N+1}$. The coefficients a_0 and b_0 depend on the filling material of the output waveguide ($z \leq NL$). For example, if $\varepsilon_T = \varepsilon_1$, $\mu_T = \mu_1$, then $a_0 = t_{11}$, $b_0 = t_{12}$. The relation between the amplitudes at the m -plane ($z = mL^+$, $m = 1, 2, \dots, N-1$) and the amplitudes at the borders of the section ($z = 0$) is:

$$\begin{pmatrix} A_0 \\ B_0 \end{pmatrix} = \frac{1}{2\sqrt{Y_0 Y_1}} \begin{vmatrix} Y_0 + Y_1 & \pm(Y_0 - Y_1) \\ \pm(Y_0 - Y_1) & Y_0 + Y_1 \end{vmatrix} \begin{pmatrix} A_1 \\ B_1 \end{pmatrix}, \quad \begin{pmatrix} A_{N-m} \\ B_{N-m} \end{pmatrix} = \mathbf{T}^m \begin{pmatrix} a_0 A_{N+1} \\ b_0 A_{N+1} \end{pmatrix} \quad (1)$$

The upper sign in (1) corresponds to the H_{0n} -mode and the lower sign corresponds to the E_{0n} -mode with the wave admittances: $Y_j^h = \sqrt{\varepsilon_j / \mu_j} \left[1 - (v_{0n} / ka \sqrt{\varepsilon_j \mu_j})^2 \right]^{1/2}$ and $Y_j^e = \sqrt{\varepsilon_j / \mu_j} \left[1 - (\mu_{0n} / ka \sqrt{\varepsilon_j \mu_j})^2 \right]^{1/2}$, respectively, where μ_{0n} and v_{0n} are the zeroes of the Bessel functions of zero and first order.

Since the determinant $|\mathbf{T}| = 1$, the roots of the characteristic equation $\xi + \xi^{-1} - X = 0$, where $X = t_{11} + t_{22}$, satisfy the condition: $\xi_1 = \xi_2^{-1}$. This feature and the matrix polynomial theory [1] enable us to obtain:

$$\mathbf{T}^m = \begin{vmatrix} t_{11}P_m - P_{m-1} & t_{12}P_m \\ t_{21}P_m & t_{22}P_m - P_{m-1} \end{vmatrix}, \quad (2)$$

where $P_m(X) = (\xi^m - \xi^{-m}) / (\xi - \xi^{-1})$ are the Mauguin polynomials [2]. These polynomials satisfy the recurrence formulas: $P_0 = 0$, $P_1 = 1$, $P_2 = X$, $P_m = XP_{m-1} - P_{m-2}$.

To obtain the reflection coefficient, $R = B_0 / A_0$, and transmission coefficient $T = A_{N+1} / A_0$, the transfer matrix of the basis element must be determined.

TRANSFER MATRIX OF A BASIS ELEMENT

The corresponding periods l of a ring and radial diaphragms are significantly smaller than the wavelength λ ($\alpha \approx kl/\pi \ll 1$). Such a feature of the diaphragms allows considering them as nondissipative anisotropic conducting films. Two-side equivalent boundary conditions (EBC) are valid for them. In the local coordinate system (\vec{s} is the parallel unit vector along the strip direction, $\vec{\tau}$ is the normal unit vector to the strip direction, \vec{z}_0 is the normal vector to the diaphragm plane), EBC take the form [3]:

$$\begin{aligned} iY_p^+ E_s &= (\vec{s}, [\vec{z}_0, \vec{H}_1 - \vec{H}_2]) + i \frac{M}{k} \frac{\partial}{\partial s} (\varepsilon_1 E_{z1} - \varepsilon_2 E_{z2}), \\ (\vec{\tau}, [\vec{z}_0, \vec{H}_1 - \vec{H}_2]) &= iY_p^- \left[E_\tau + i \frac{M}{k} \frac{\partial}{\partial s} (\mu_2 H_{z2}) \right], \end{aligned} \quad (3)$$

where $M = (\mu_1 + \mu_2) / (\varepsilon_1 + \varepsilon_2)$, $Y_p = \alpha \varepsilon_1 \varepsilon_2 \ln 0.5(1-u)$, $Y_p^+ = -(\mu_1 + \mu_2) / (\alpha \ln 0.5(1+u))$, $u = \cos(\pi d/l)$ is the filling parameter. For a resistive film (Y_σ) we use resistive boundary conditions [4]: $\vec{E}_{t1} = \vec{E}_{t2}$; $[\vec{z}_0, (\vec{H}_1 - \vec{H}_2)] = Y_\sigma \vec{E}_{t1}$.

Besides of these, a basis element includes the boundaries between half-infinite waveguides with the admittances Y_1^s , Y_2^s and regular sections with the propagation constants: $h_j^{(h)} = \sqrt{k^2 \varepsilon_j \mu_j - \mu_{0n}^2 (v_{0n}^2)} / a^2$, $j = 1, 2$. Application of these expressions yields a transfer matrix \mathbf{T} for E_{0n} - and H_{0n} - modes with the following elements:

$$\begin{aligned} t_{11} &= \frac{1}{4Y_1Y_2} \left\{ (Y_1 + Y_2)(Y_1 + Y_2 + Y_u^s) e_1^- e_2^- + (Y_2 - Y_1)(Y_1 - Y_2 + Y_u^s) e_1^- e_2^+ \right\}, \\ t_{12} &= \pm \frac{1}{4Y_1Y_2} \left\{ (Y_2 - Y_1)(Y_1 + Y_2 + Y_u^s) e_1^- e_2^- + (Y_1 + Y_2)(Y_1 - Y_2 + Y_u^s) e_1^- e_2^+ \right\}, \\ t_{21} &= \pm \frac{1}{4Y_1Y_2} \left\{ (Y_1 + Y_2)(Y_1 - Y_2 - Y_u^s) e_1^+ e_2^- + (Y_2 - Y_1)(Y_1 + Y_2 - Y_u^s) e_1^+ e_2^+ \right\}, \\ t_{22} &= \frac{1}{4Y_1Y_2} \left\{ (Y_2 - Y_1)(Y_1 - Y_2 - Y_u^s) e_1^+ e_2^- + (Y_1 + Y_2)(Y_1 + Y_2 - Y_u^s) e_1^+ e_2^+ \right\}, \end{aligned} \quad (4)$$

where $e_j^\pm = \exp(\pm ih_j b_j)$. In (4), the upper sign corresponds to the H_{0n} -modes and the lower sign to the E_{0n} -modes. The type of the excitation mode determines the values of wave admittances and propagation constants. In view of this reason we must choose also the wave admittances Y_j and the propagation constants h_j ($j=1, 2$). The admittance Y_j^s characterizes an equivalent conductivity of the localized discontinuity. For a resistive film: $Y_u^e = Y_u^h = Y_\sigma$. In the case of the ring diaphragm: $Y_u^h = iY_p^+$, $Y_u^e = iY_p^-$, and of the radial diaphragm: $Y_u^h = iY_p^-(1 + f^h)$, $Y_u^e = iY_p^+/(1 + f^e)$, where $f^{h(e)} = \mu_{0n}^2 \{v_{0n}^2\} M / (ka)^2$.

If the admittance of the illuminated layer (Y_0) is the same as the admittance of the input waveguide (Y_T), the formulas for the reflection ($R=B_1/A_1$) and transmission coefficients ($T=A_{N+1}/A_1$) are quite simple:

$$T = [a_0(t_{11}P_{N-1} - P_{N-2}) + b_0t_{12}P_{N-1}]^{-1} \quad R = [a_0t_{21}P_{N-1} + b_0(t_{22}P_{N-1} - P_{N-2})] \times T \quad (5)$$

Presented solution enables one to investigate (by choosing a_0 and b_0) both reflecting structures ($Y_T \rightarrow \infty$), and transparent structures.

CONCLUSION

Presented method is universal to any types of periodic waveguide structures, composition of their basis elements, or open or closed nature of transmission lines.

REFERENCES

- [1] F. R. Gantmaher, *Matrix Theory*, Moscow: Nauka Publ., 1967 (in Russian).
- [2] H. Levine, *Unidirectional Wave Motions*, -Amsterdam, 1978.
- [3] V. B. Kazanskiy, "Electrodynamic model of the multifunction control system", *Turkish J. of Physics*, no. 11, pp.1467-1471, 1995.
- [4] Y. I. Veselov, S. B. Rajevskiy, *Layered Metal-Dielectric Waveguides*, Moscow: Radio I Svyaz Publ., 1988 (in Russian).

CALCULATION OF FULL-WAVE S-MATRICES OF MONOAXIALLY UNIFORM (2D) ELEMENTS IN RECTANGULAR WAVEGUIDES

Tatyana Vasilyeva, Anatoly Kirilenko, Leonid Rud', Vladimir Tkachenko

Institute of Radiophysics and Electronics of the National Academy of Sciences of Ukraine
12 Acad. Proskura St., Kharkov, 310085 Ukraine

Discontinuities that are uniform along one of the transversal axes form a wide class of conventional elements of rectangular waveguides: H - and E -plane bends and steps, H - and E -plane tees and cross-junctions, different bifurcations, and so on. On the other hand, their mathematical models in the S -matrix form are often used in the calculation of more complicated discontinuities, in particular 3D ones. There is one more reason to consider such a class of elements in the calculation of full-wave S -matrices as a special group, but not as a particular case of corresponding 3D structures. The matter is that the 3D boundary-value problems for such structures may be reduced to a set of 2D ones. The investigation of the latter has a long history and there are sophisticated methods of such problems solving that heavily take into account geometrical peculiarities and are much more efficient than general methods usually used for the analysis of 3D discontinuities. It is a well known fact that in the case of 2D structures the residue-calculus method is the most efficient one for the waveguide steps, method of inversion of difference part of matrix operators is the for H -plane angled bends, standard mode-matching procedures are the best for 90° waveguide crosses, moment methods that take into account field singularities is well tailored for waveguide bifurcations, steps and other discontinuities, etc.

In view of these reasons, in the development of modeling softwares based on the S -matrix technique, it makes sense to work out a special tool that produces full-wave S -matrices of the structures of interest by using well-known algorithms for a solution of corresponding scalar problems. Let us define as $\{TM^\alpha\}$ and $\{TE^\alpha\}$, a rectangular waveguide basis in terms of the modes of magnetic (TM) or electric (TE) type, the field of which is normal to the axis $O\alpha$ ($\alpha = x, y, z$), so that the total field can be expressed in terms of the corresponding $E(H)_\alpha$ -component. In the case of N -port, the structure of which is uniform along the Oy axis, modal basis of $\{TM^y\}$, $\{TE^y\}$ type is related with $\{TM^z\}$, $\{TE^z\}$ one by the following equations:

$$\begin{aligned}\{TM^y\} &= \left(-i \frac{N_{nm}}{k_{ny}^2 \chi^2} \frac{n\pi}{b} \right) \{TM^z\} + \left(-i \frac{k_0 \varepsilon}{W_0} \frac{N_{nm}}{k_{ny}^2 \chi^2} \frac{m\pi}{a} \right) \{TE^z\}, \\ \{TE^y\} &= \left(\mp i k_0 W_0 \mu \frac{N_{nm}}{k_{ny}^2 \chi^2} \frac{m\pi}{a} \right) \{TM^z\} + \left(\pm i \frac{N_{nm}}{k_{ny}^2 \chi^2} \frac{n\pi}{b} \right) \{TE^z\},\end{aligned}$$

where ζ is the propagation constant of a considered mode, $k_0 = \omega \sqrt{\varepsilon_0 \mu_0}$, $W_0 = \sqrt{\mu_0 / \varepsilon_0}$, $\chi = \sqrt{(m\pi/a)^2 + (n\pi/b)^2}$, $k_{ny} = \sqrt{k_0^2 \varepsilon \mu - (n\pi/b)^2}$, N_{mn} is the norm of $TM^z(TE^z)_{mn}$ mode defined relatively to the transversal electric field.

Denote the elements of the scattering matrix of considered 3D device as $S_{qp}^{ji} = S_{(m_j, n_j), (m_i, n_i)}^{ji}$ where $i, j=1, 2, \dots, N$ is a port number. We define the index n^{\max} as a maximum value of n along all n , and $m_{n_i}^{\max}$ as maximum value of m for a fixed n in the i -th port. To find S -matrix of N -port in a standard $\{TM^z\}$ and $\{TE^z\}$ modal basis, it is sufficient to calculate the following set of S -matrices for corresponding 2D discontinuities (scalar boundary-value problems):

$$\begin{aligned} Se_n^{ji} \left[1: m_{n_j}^{\max}, 1: m_{n_i}^{\max} \right] & \text{ with } n=0, 1, \dots, n^{\max} \text{ (} TM_{mn}^y \text{ -modes, Dirichlet problem),} \\ Sh_n^{ji} \left[0: m_{n_j}^{\max}, 0: m_{n_i}^{\max} \right] & \text{ with } n=1, 2, \dots, n^{\max} \text{ (} TE_{mn}^y \text{ -modes, } i, j=1, 2, \dots, N, \text{ Neumann problem).} \end{aligned}$$

When solving the corresponding scalar boundary-value problems, the wave number k must be replaced by k_{ny} for each n . So, the time-consuming problem of full-wave S -matrix calculation is reduced to the solving of $2n^{\max} + 1$ simpler scalar problems. Having the set of matrices Se_n and Sh_n , one can find the resulting S -matrix in the $\{TM^z\}$ and $\{TE^z\}$ modal basis by the following algorithm. Firstly, if $n_j \neq n_i$ for the given spatial uniformity of our N -port, we have that

$$S(TE^z \leftarrow TE^z) = S(TM^z \leftarrow TE^z) = S(TE^z \leftarrow TM^z) = S(TM^z \leftarrow TM^z) \equiv 0.$$

Secondly,

$$\begin{aligned} S(TE^z \leftarrow TE^z)_{(m_j, n), (m_i, n)}^{ji} &= \left(-i \frac{k_0 \varepsilon}{W_0} \frac{N_{m_j, n}^{(j)}}{k_{ny}^2 \chi_{m_j, n}^{(j)2}} \frac{m_j \pi}{a_j} \right) Se_n^{ji}(m_j, m_i) \left(i \frac{1}{N_{m_i, n}^{(i)}} k_0 W_0 \mu \frac{m_i \pi}{a_i} \right) \\ &+ \left(\pm i \frac{N_{m_j, n}^{(j)}}{k_{ny}^2 \chi_{m_j, n}^{(j)2}} \frac{n \pi}{b} \zeta_{m_j, n}^{(j)} \right) Sh_n^{ji}(m_j, m_i) \left(\mp i \frac{1}{N_{m_i, n}^{(i)}} \frac{n \pi}{b} \zeta_{m_i, n}^{(i)} \right), \\ S(TM^z \leftarrow TE^z)_{(m_j, n), (m_i, n)}^{ji} &= \left(-i \frac{N_{m_j, n}^{(j)}}{k_{ny}^2 \chi_{m_j, n}^{(j)2}} \frac{n \pi}{b} \zeta_{m_j, n}^{(j)} \right) Se_n^{ji}(m_j, m_i) \left(i \frac{1}{N_{m_i, n}^{(i)}} k_0 W_0 \mu \frac{m_i \pi}{a_i} \right) \\ &+ \left(\mp i k_0 W_0 \mu \frac{N_{m_j, n}^{(j)}}{k_{ny}^2 \chi_{m_j, n}^{(j)2}} \frac{m_j \pi}{a_j} \right) Sh_n^{ji}(m_j, m_i) \left(\mp i \frac{1}{N_{m_i, n}^{(i)}} \frac{n \pi}{b} \zeta_{m_i, n}^{(i)} \right). \end{aligned}$$

Similar expressions are valid for $S(TE^z \leftarrow TM^z)_{(m_j, n), (m_i, n)}^{ji}$ and $S(TM^z \leftarrow TM^z)_{(m_j, n), (m_i, n)}^{ji}$ scattering matrix coefficients.

With the aid of above described common scheme, algorithms for calculation of full wave S matrices for the rectangular waveguide discontinuities such as tee, symmetrical and nonsymmetrical one-side step, and bifurcation were worked out. Let us demonstrate the

efficiency of the proposed "scalarization" approach in the problems of a double-side step and a resonant diaphragm in rectangular waveguide that are shown in Fig. 1.

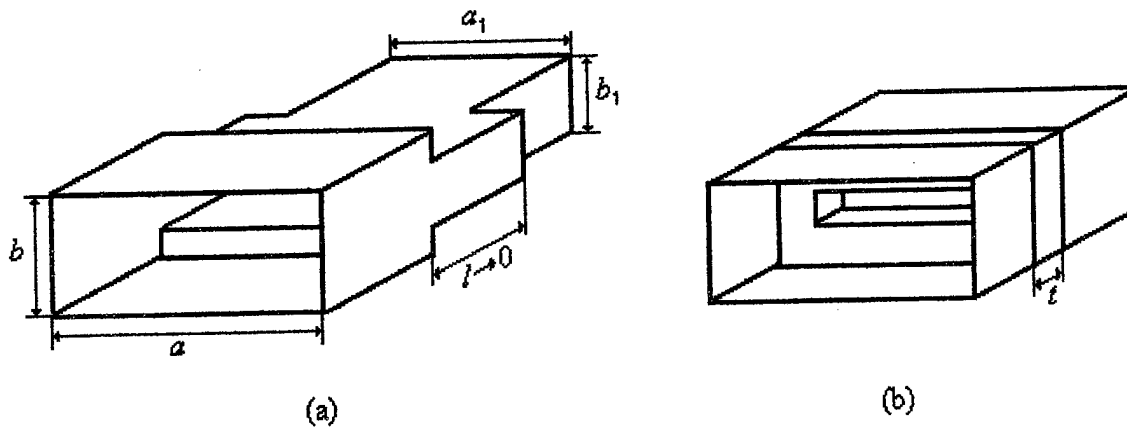


Fig. 1. Structures analyzed by the "scalarization" approach

The first structure (see Fig. 1a) is considered as a sequence of the E - and H -plane one-side steps with the length of coupling waveguide $l=0$ (virtual waveguide). Calculation of the full-wave S -matrix for each 2D step was performed by the "scalarization" approach (mode-matching technique was used for calculating the set of 2D scalar steps), and then the generalized S -matrix technique was applied for 3D step. The last technique was applied also to analyze the resonant diaphragm as a junction of two double-side steps at the distance of t (see Fig. 1b). For verification of obtained numerical data, the same 3D structures were calculated by the well known mode-matching technique. The results of comparison are presented below in the Table for the case of $a \times b = 23 \times 10$ mm, $a_1 \times b_1 = 15 \times 0.5$ mm, $t = 1$ mm. When using the proposed algorithm, the data are obtained by taking into account $N_1 = 30$ modes in the larger waveguides and $N_2 = 10$ in the smaller ones. As for the mode-matching technique, these values were chosen according to Mittra's rule and they were equal to $N_1 = 613$, $N_2 = 20$. One can see that both results are in close agreement even at frequencies near the resonant ones. However, direct using the mode-matching method to analyze the considered 3D structures requires CPU time that is tens times greater than the new approach.

	double-side step				resonant diaphragm			
	"scalarization" approach		mode-matching technique		"scalarization" approach		mode-matching technique	
f , GHz	$ S_{11}^{(11)} $	$\arg S_{11}^{(11)}$	$ S_{11}^{(11)} $	$\arg S_{11}^{(11)}$	$ S_{11}^{(11)} $	$\arg S_{11}^{(11)}$	$ S_{11}^{(11)} $	$\arg S_{11}^{(11)}$
8.0	1.0000	-176.34	1.0000	-176.33	0.9655	-164.64	0.9645	-164.42
8.5	1.0000	-175.07	1.0000	-176.06	0.9270	-157.67	0.9247	-157.32
9.0	1.0000	-173.19	1.0000	-173.17	0.8389	-146.68	0.8330	-146.06
9.5	1.0000	-169.36	1.0000	-169.31	0.6172	-127.73	0.6022	-126.64
10.0	0.0921	-135.10	0.0837	-139.13	0.1377	-97.49	0.1130	-96.07
10.5	0.8004	179.89	0.8002	179.86	0.3947	113.70	0.4109	114.72
11.0	0.8457	179.77	0.8455	179.76	0.6858	133.79	0.6924	134.32
11.5	0.8654	179.71	0.8653	179.71	0.8162	145.24	0.8190	145.51
12.0	0.8768	179.67	0.8766	179.67	0.8797	152.18	0.8810	152.33

ELECTROMAGNETIC ANALYSIS OF THE E-PLANE WAVEGUIDE STEP

V.A. Karlov

Dept. of Radiophysics, Dniepropetrovsk University, 13 Naukovy St., Dniepropetrovsk 320625
UKRAINE Tel: 28 0562 467995, Fax 7 0562 465523 E-mail: garry@rff.dsu.dp.ua

Abstract: Using the method of overlapping regions, an electromagnetic model of the rectangular resonance cavity in the E-plane is developed. Based on the theory of transmission lines, scattering matrixes of the single ports (of the steps in the E-plane) for the cavities of various lengths are calculated. The theoretical results thus obtained agree well with experimental data and can aid the design of a standards of the reflection and transmission coefficients.

INTRODUCTION

Parameter determination of the measurement standards of the reflection and transmission coefficients by numerical methods is a perspective tendency in the microwave metrology. The reflection coefficient of an E-plane waveguide step has a smooth frequency dependence. Such discontinuities are used as reference loads.

ELECTROMAGNETIC MODEL OF THE WAVEGUIDE CAVITY

In the present paper electromagnetic calculation of a scattering matrix of rectangular resonance cavity in the E-plane is made by means of the method of overlapping regions [1]. The configuration of the resonance cavity is shown in Fig. 1.

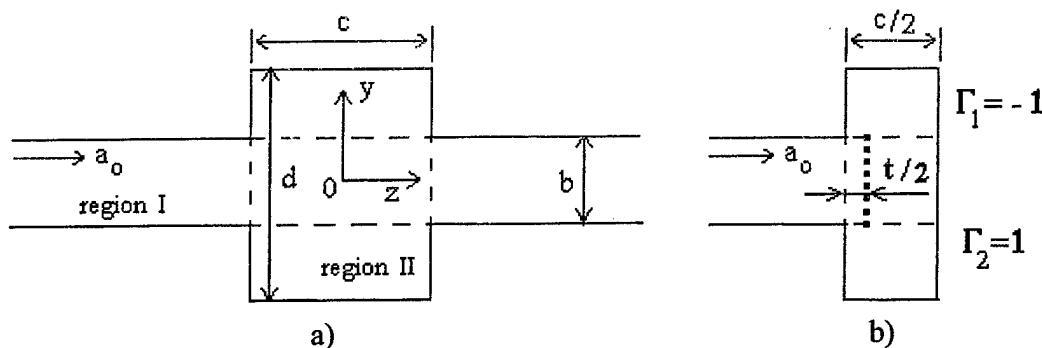


Fig. 1. (a) Rectangular resonance cavity in the E-plane. (b) The eigenports of the cavity.

The protruding arm, region I, is a rectangular waveguide (of dimensions a and b , a being the broader dimension) which supports the dominant H_{10} mode only. In junction the modal fields must be H -type only (i.e. having no electric field component E_x) and their dependence from x takes the form $\sin \pi/a(x + a/2)$. Regions I and II are the overlapping regions with boundaries:

$$\text{region I:} \quad -\frac{a}{2} \leq x \leq \frac{a}{2}, \quad -\frac{b}{2} \leq y \leq \frac{b}{2}, \quad -\infty < z < \infty;$$

$$\text{region II:} \quad -\frac{a}{2} \leq x \leq \frac{a}{2}, \quad -\frac{d}{2} \leq y \leq \frac{d}{2}, \quad -\frac{c}{2} < z < \frac{c}{2}.$$

The system of integral equations for the regions I and II allowing to find the H_x -magnetically field component of the LE_{1n} -mode can be written as

$$H_1(y, z) = \int_{-d/2}^{d/2} G_1(y, z, y', z') \left(\frac{\partial H_2(y', z')}{\partial y'} \Big|_{y'=\frac{b}{2}} - \frac{\partial H_2(y', z')}{\partial y'} \Big|_{y'=-\frac{b}{2}} \right) dz' + a_0(y, z); \quad (1)$$

$$H_2(y, z) = \int_{-b/2}^{b/2} G_2(y, z, y', z') \left(\frac{\partial H_1(y', z')}{\partial z'} \Big|_{z'=\frac{c}{2}} - \frac{\partial H_1(y', z')}{\partial z'} \Big|_{z'=-\frac{c}{2}} \right) dy',$$

where G_q - is a Greens function, $a_0(y, z) = \exp(-\gamma_0 z)$ - is an incident field produced by the magnetic current j_x .

The system of integral equations (1) is reduced by the method of eigenfunctions to the simultaneous linear algebraic equations in the unknown scattering matrix elements S_{ij} of the rectangular resonance cavity (Fig. 1,a).

LOCALIZATION OF THE E - STEP

Scattering matrixes of the single ports (of the steps in the E-plane) for the cavities of various lengths c have been calculated using the theory of transmission lines. The method of E-step localization is based on using the two eigenvalue of the cavity, conditions of the antisymmetry, and unitary E-step matrix. A correction of a reference plane of the eigenports (Fig. 1,b) for finding the parameters of steps was made. The amendments (the distance $t/2$ on Fig 1,b) to reference planes that provide independence of the modulus of the reflection coefficient of steps, when computing the parameters of cavities of various lengths, were found.

NUMERICAL RESULTS AND DISCUSSIONS

Fig. 2 depicts the dependence of the modulus (a) and phase (b) of the reflection coefficient of the E-plane for the various amendments t of the length cavity c . The dependencies are got when the cross-section waveguide is $a \times b = 28.5 \times 6.3 \text{ mm}$, the cross-section cavity is $a \times d = 28.5 \times 12.6 \text{ mm}$, the excitation frequency $F=8 \text{ GGz}$, the number of the taken into account higher-order modes $N=15$. Figure 2,a shows that $|S_{11}| = \text{const} = 0.305$ when $t=1.78822 \text{ mm}$ and the nonuniformity of the modulus and phase reflection coefficient for $c=26.5 \text{ mm}$ is small. Fig. 3 depicts the frequency dependence of the modulus of the reflection coefficient of the E-plane (a) and the amendments t (b). The capacitive component of the input reactance of the E-plane steps have been determined with the aid of the calculated amendments to reference planes of the cavity. The calculated parameters of the E-step capacitive component are in a good agreement with the data known from manuals [2].

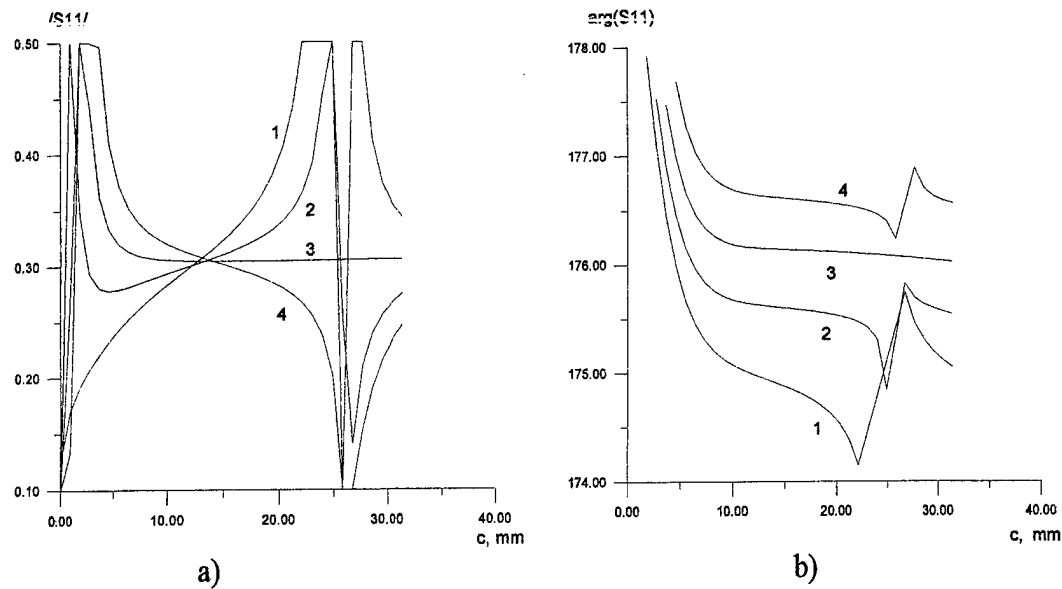


Fig. 2. An reflection coefficient of the E-step as a function of the cavity size c . $F=8\text{GGz}$, $d/b=2$, $N=15$; 1 - $t=0$, 2 - $t=1\text{ mm}$, 3 - $t=1.78822\text{ mm}$, 4 - $t=2.5\text{ mm}$

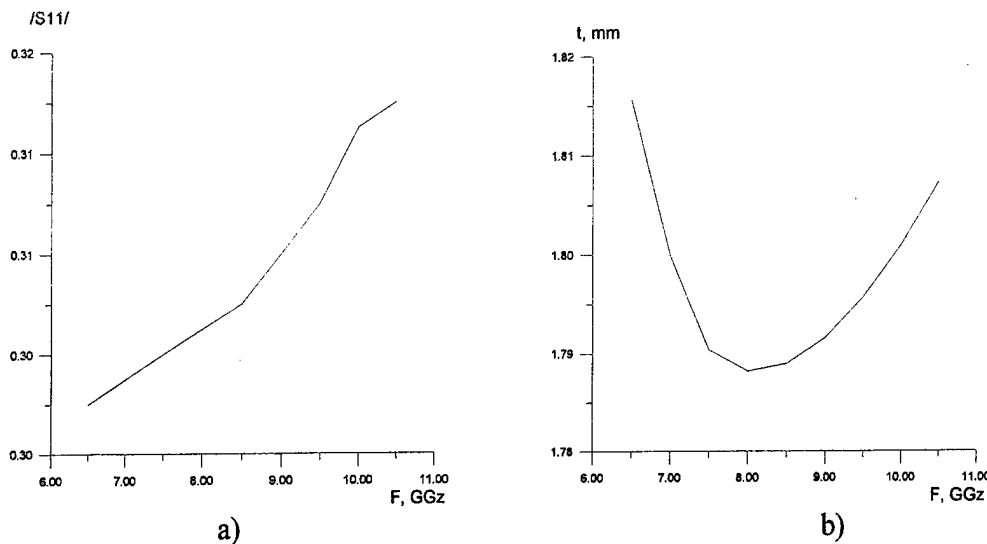


Fig. 3. The frequency dependence of the modulus of the reflection coefficient of the E-plane (a) and the amendments t (b).

The obtained results can be used in the metrology of microwave range in the process of designing a standards of the reflection and transmission coefficients.

REFERENCES

- [1] Petrusenko I.V., Yakovlev A.B., Gnilenko A.B., 1994, "Method of partial overlapping regions for the analysis of diffraction problems", *IEE Proc.- Microw. Antennas Propag.*, 141, 196-198.
- [2] Marcuvitz N., 1951, *"Waveguide Handbook"* Vol 10, MIT Radiation Lab. Series, Chap. 5, McGraw-Hill, New York.

OBJECT-ORIENTED APPROACH TO THE DEVELOPMENT OF SPECIALIZED AND GENERAL SOFTWARE FOR MICROWAVE CAE & CAD

Vladimir Tkachenko

Institute of Radiophysics and Electronics of the National Academy of Sciences of Ukraine
12 Acad. Proskura St., Kharkov, 310085 Ukraine

The problems of a computer-oriented research of microwave devices have become an independent field of applied microwave CAE over the last 20 years. Under the pressure of growing requirements for the generality of the design process, they have evolved from algorithmization of particular problem solutions to creation of multifunctional packages belonging to the maker of microwave devices. There are two design directions that have formed on this way. They represent two inner conflicting sides of the design process, namely generality and adequacy. The first direction represents an attempt to embrace a wide range of design problems using simple and, as a rule, very fast but not always rigorous algorithms. The cited above range of problems is wide that implies both availability of design techniques and variety of electromagnetic objects. The second direction is characterized by the usage of rigorous and exact models of electromagnetic level and it develops in the form of problem-oriented packages whose functional specification is strongly tied to highly specialized description algorithms of a certain electromagnetic structure. As a result, the topology of the structures of interest is predetermined and in the design process it can be modified only by the principles determined beforehand (the design algorithm imposes the manipulation of the design object form).

This work is dedicated to creation of the problem-oriented electromagnetic design systems by using special C++ classes. The main purpose was the development of a tool that would allow to hide behind the shield of finished program codes those stages of programming that are inevitable and often present difficulties in realization, the ones that emerge in problems of wave scattering design processes. Let us illustrate it by the following example. It is difficult to picture a program package for the band pass filter synthesis without certain stages. They are building a circuit theory prototype, solving the boundary-value problems for the key elements, the synthesis functions and recomposition of the parts of the filter, as well as optimization of filter parameters taking into account the interaction of fringing fields, etc.

The spectrum of problems that occur at each of the stages is so inhomogeneous and wide (for instance, from the secondary problems of correct memory allocation to the principal ones, such as relative convergence problem) that it turns the problem of interest into a privilege of only high-skilled professionals. In addition, taking into account that the manufacturing of a more-or-less complete program product is human-time-consuming, we can easily understand why the designers are so eager to get a maximum unification of the finished parts of program codes aimed at solving standard problems. This desire was the main incentive for realization of our project. The use of the SES-technology opportunities [1] and the mechanism of heritage in the classes of the object-oriented C++ language provides a basis for solving the problem of interest. General structure of the problem-oriented system can be represented as an aggregate of descriptors (S -matrices), a device recomposition scheme and special techniques. A program support was realized for the first two concepts in the SES-technology, that provides, from the one hand, the maximum generality of research and from the other, an automatic adjustment of the calculation process to the minimum time consumption (including buffering and many-dimensional interpolation of S -matrices). By adding to this tool a number of unified techniques for controlling the sequence of calculations, we can create generators of applications of certain directions. A combined usage of the SES-technology and specialized synthesis methods of devices with specified characteristics is shown below by the example of the frequency filter generator. It is of importance that the cited sets of classes realize such a design skeleton, where practically every single function can be replaced, from altering the synthesis strategy in general to changing the concept of making decisions at any significant point of design. Fig. 1 outlines a schematic diagram of an N -section in-line type filter.

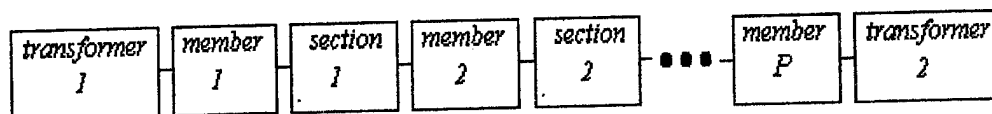


Fig. 1

Let us name as a member of the filter a microwave two-port of arbitrary type that realizes one of the three characteristics, such as: a) required reflection coefficient at a fixed frequency, b) required quality, c) options a) and b) simultaneously. In particular, the variant c) realizes such characteristics as specified values of K -inventors or specified values of the coupling coefficient between two resonant cavities. Let us explain the implementation of the variant c) in the filter members, using the example of a filter with additional, non-consequent couplings. Let us assume that for a dual mode filter it is necessary to synthesize an input element that presents a rectangular diaphragm in the junction of rectangular and circular waveguides. Traditionally a specified input quality is demanded of this diaphragm. However the number of parameters of such a diaphragm (dimensions, shift and the tilt angle relative to the input rectangular waveguide) enables us to demand also the specified coupling between the waves of the vertical and horizontal polarizations. If this problem can be solved then for a two-section filter we can do away with three diaphragms instead of using five of them.

The concept of transformer refers to a microwave two-port whose function consists in transmission between the input waveguide and the filter itself. Such a situation occurs, for instance, in the case of designing filters on the reduced cross-sections of rectangular or ridged waveguides. Fig. 2 shows the class hierarchy intended for the program realization of the filter member notion. The solid lines denote a direct heritage in the derived class of the basic class properties. The dotted lines show that in the upper-level class the objects belonging to the low-level class are made. The names of classes comprised in bold type frames denote their belonging to the library of SES-technology classes. Let us consider this diagram in more detail.

Class *Parameter* represents a set of techniques for saving, archiving on a disk and connection with dialog windows in an interface variant of those structure parameters that do not change in the process of synthesis.

Class *Data* performs the same functions for parameters under synthesis.

Class *Response* is a container for saving and archiving the frequency characteristics of the filter members (return loss, insertion loss, total insertion loss, argument and some others). The objects of this class are beneficial while performing a comparative analysis of electromagnetic characteristics of different scatterers.

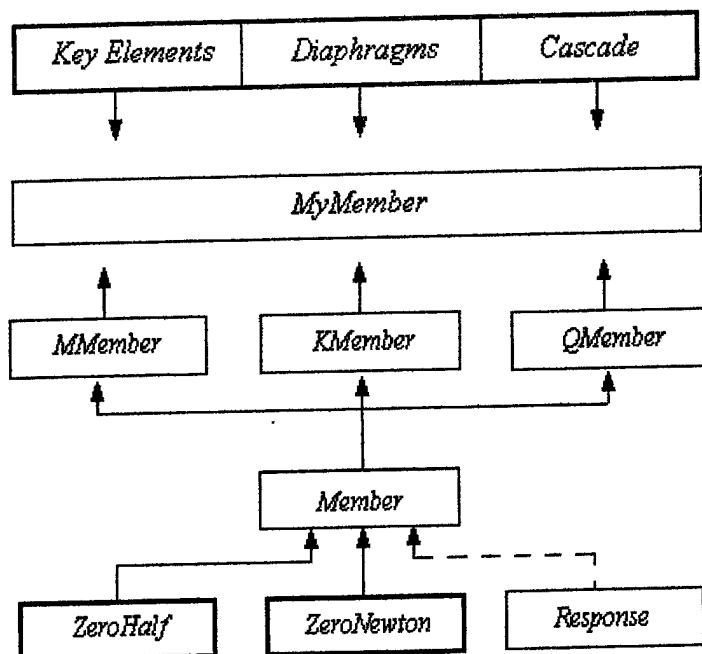


Fig. 2.

Two classes *ZeroHalf* and *ZeroNewton* realize the methods of zero searching for the functions of one or more variables and provide a basis for the geometrical parameter synthesis of filter members. The derived classes such as *Mmember*, *Kmember*, *Qmember* and *Fmember* realize the synthesis functions of the scatterer geometrical parameters in accordance with the given coupling coefficients, *K*-invertors, or *q*-factors, respectively. *Fmember* class realizes the functions in accordance with the variant c). The total number of filter members equals $P=N+1$ for a dual mode filter (DMF), band pass filter (BPF), low pass filter (LPF), band stop filter (BSF), and $P=N$ for a resonant window filter (RWF). While creating its own class for a filter member, one should indicate one of the four abstract upper-level classes as the basic class, and then in the constructor of this class he is supposed to create a dynamic object using the library set of the SES-technology descriptors. It is necessary to realize only one function that brings the pointers back to the synthesized scatterer parameters. In accordance with the object-oriented program strategy, the functions of the basic class may be substituted for its own ones. Fig. 3 illustrates the class heritage for creation of a system of designing the filters and the corresponding prototypes. The main functions of these classes are listed below.

The prototype synthesis is realized according to the traditional circuit theory schemes proposed by Cohn [2], Rhodes [3], Levy [4], Wanselow [5], and some other authors.

The prototype optimization: in the practice of microwave filter design, additional requirements may occur that can not be accounted on the circuit theory level. This can be formulated, for instance, in the form of required suppression level at the fixed frequencies within the stopband. Since in prototype classes the functions of frequency response calculations are realized, the application of optimization algorithms (the objective functions are realized here in different variants) enables one to obtain the best initial data for the synthesis. One more field

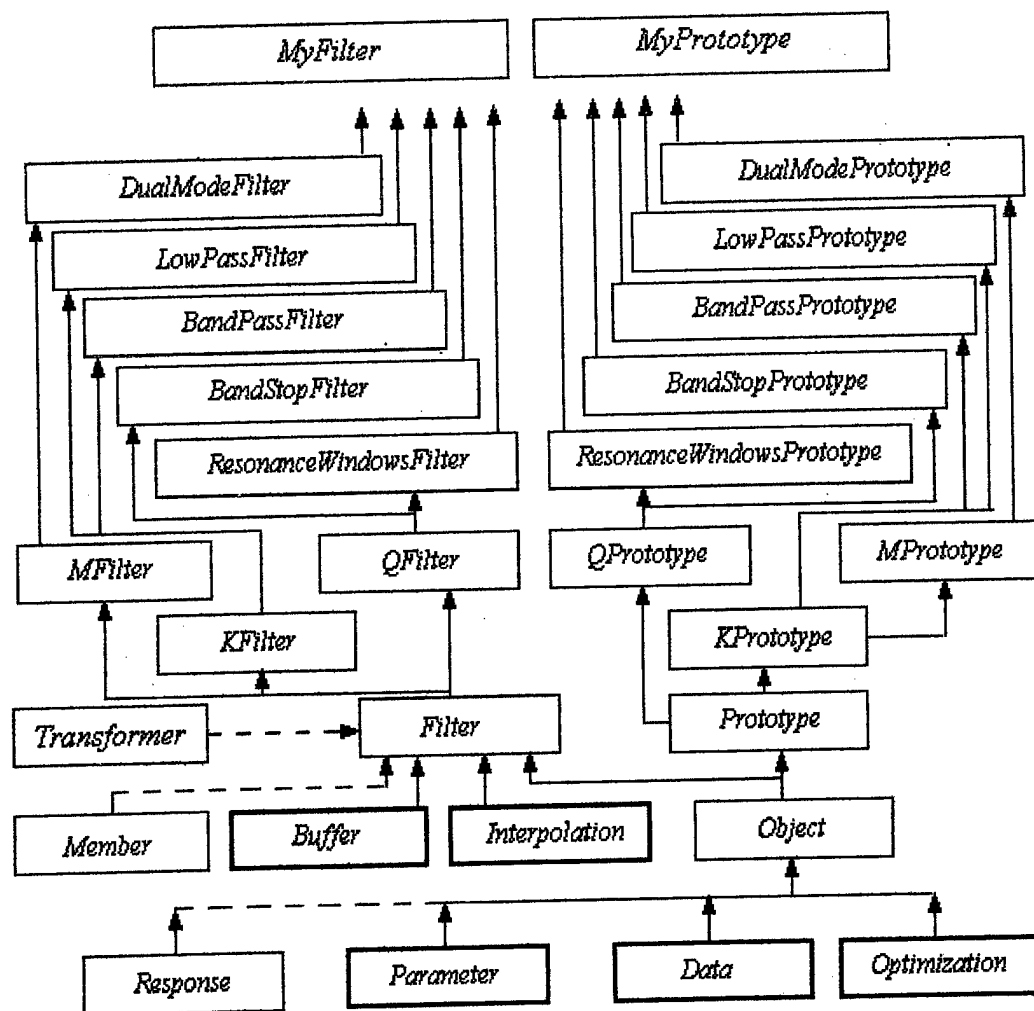


Fig. 3

is the creation of one prototype using a prototype of some different kind. For instance, we may synthesize K -invertors for a band pass prototype, transform them into coupling coefficients and use the latter as an initial approximation while searching for parameters of non-consequent prototype in accordance with the resulting frequency response.

Filter synthesis. It is initialized by an object of prototype class and is realized in three stages. First the filter members are synthesized then the section lengths are reconstructed for the case of a single-mode interaction of the filter members. This stage is individual for each of the five types of filters. The refinement of section lengths is provided for BPF in a multimode regime, as in the case of narrow band filters the fringing field interaction leads to a significant shift of the pass band. Our experience of designing different filters suggests that after the synthesis stage, the characteristics of an electromagnetic model can differ significantly from those required. This can be best appreciated for DMF, when the obtained configuration can not serve as an initial approximation for the following optimization. Therefore at the last stage the iterative refinement of filter parameters is carried out. Two schemes are realized here. First, we calculate the frequency response of the filter in the multimode regime, reconstruct a new specification for the filter synthesis, synthesize an intermediate prototype and start the synthesis process over again. Second, we calculate the frequency response of the filter in a multimode regime, reconstruct intermediate prototype by using the optimization method, correct the initial prototype with the aid of an intermediate one, and repeat the synthesis process over again.

Filter optimization is initialized by the object of the prototype class. Several standard objective functions are realized, including, for instance, the function aimed at the minimization of the mismatch functional between the frequency responses of the electromagnetic and circuit theory models. If it is necessary, then each of them can be replaced by its own objective function. The filter optimization is based on repeated solving the direct problem at a non-predicted parameter state of filter members at specified frequency points. If therewith the optimization parameters do not change the geometry of key scatterers (for instance, in the E -plane strip diaphragm filter), then we can apply the *Buffer* class functions. The latter ensure a preliminary calculation and saving of the S -matrices of key elements (this, as a rule, presents a very time-consuming problem). From this point on the *Filter* class functions provide a very quick reconstruction of the filter frequency response. Class *Interpolation* ensures one more possibility for a radical acceleration of the calculation process. Its functions reconstruct the filter frequency response on the basis of approximation models of key scatterers (the many-dimensional polynomial interpolation of S -matrices is used).

The author greatly appreciates a valuable discussion on the subject of this communication with Profs. A. A. Kirilenko and L. A. Rud'.

References

- [1] A. A. Kirilenko, V. I. Tkachenko, "System of electromagnetic simulation of microwave and millimeter-wave devices", *Izvestiya Vuzov Radioelektronika*, vol. 39, No 9, pp. 17-28, 1997 (in Russian).
- [2] G. L. Matthaei, L. Young, E. M. T. Jones, *Microwave Filters, Impedance Matching Networks and Coupling Structures*, New York: McGrawHill, 1964.
- [3] J. D. Rhodes, *Theory of Electrical Filters*, New York: Wiley, 1976.
- [4] R. Levy, "Tapered corrugated waveguide lowpass filters", *IEEE Trans. Microwave Theory Techniques*, vol. 13, No 5, pp. 514-539, 1965.
- [5] R. Wanselow, "Prototype characteristics for a class of dual-mode filters", *IEEE Trans. Microwave Theory Techniques*, vol. 23, No 8, pp. 708-711, 1975.

MODELING THE BEAM EXCITATION OF PLANAR WAVEGUIDE WITH RECTANGULAR IRREGULARITIES

G.I. Zaginaylov, V.D. Dushkin, V. Korostyshevski, P.V. Turbin

Dept. of Technical Physics, Kharkov State University, Svobody Sq. 4, Kharkov, Ukraine

The problem of the beam interaction with irregular waveguide is of considerable interest for high-power microwave electronics. Since the waveguides used there have a diameter much greater than the operational wavelength, and the shape of irregularities is close to rectangular one, a plane model of a waveguide with the piecewise constant cross-section is quite reasonable. Due to the strong dependence of the output power and the operational frequency on the mode conversion effects caused by irregularities [1], it is very desirable to have an accurate and flexible mathematical model for their analysis.

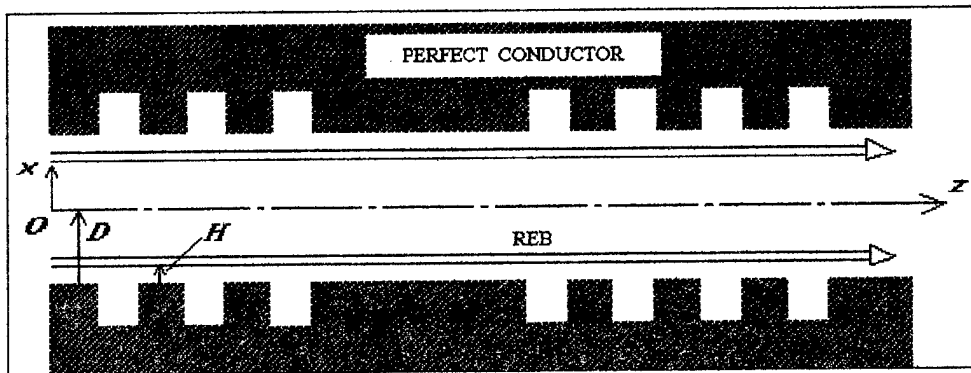


Figure 1:

Consider a symmetric plane waveguide with m non-identical grooves of rectangular shape (see Fig. 1) driven by the relativistic electron beam, for which we shall use the simplest model: thin, magnetized, modulated current of given amplitude: $\vec{I} = (0, 0, I_z)$, $I_z(x, z, t) = I_0 g(x) \exp(ikz/\beta - i\omega t)$ where $k = \omega/c$, $\beta = V/c$, $d/dx[\ln g(x)] \gg k/2\pi$, ω is the modulation frequency, V is the beam velocity, c is the velocity of light. The beam drives in the waveguide the fields of TM polarization (E_x, H_y, E_z). Finding them can be easily reduced to the following boundary-value problem (taking into account the symmetry of the problem with respect to the z -axis):

$$\left(\frac{\partial^2}{\partial x^2} + \frac{\partial^2}{\partial z^2} + k^2 \right) \Psi(x, z) = \frac{4\pi}{c} \frac{\partial I_z}{\partial x}, \quad x, z \in \Omega \quad (1)$$

$$\frac{\partial \Psi}{\partial n} \Big|_S = 0, \quad \Psi|_{x=0} = 0, \quad (2)$$

$$\Omega = \bigcup_{q=1}^m \{D < x < D + h_q, a_q < z < b_q\} \cup \{0 \leq x \leq D, -\infty < z < \infty\},$$

S is the boundary of the waveguide, $\Psi \equiv H_y$, $E_x = (1/ik)(\partial \Psi / \partial z)$, $E_z = -(1/ik)(\partial \Psi / \partial x + (4\pi/c)I_z)$, a_q, b_q are the coordinates of the walls of the q th groove, h_q is its depth.

We seek the solution of the value-boundary problem (1), (2) satisfying the radiation condition at $z \rightarrow \pm\infty$ and Meixner's condition near geometric singularities in the form

$$\Psi = \begin{cases} \Psi^+ + \Psi_0, & 0 \leq x \leq D, \quad z \in \mathbb{R} \\ \Psi_q^-, & D < x < D + h_q, \quad z \in \mathbb{L}_q \end{cases}, \quad (3)$$

where $\mathbb{R} = (-\infty, \infty)$, $\mathbb{L}_q = (a_q, b_q)$, $q = 1, \dots, m$, Ψ_0 is the partial solution of equation (1) with the boundary conditions $(\partial\Psi_0/\partial x)|_{x=D} = 0$, $\Psi_0|_{x=0} = 0$ that can be easily found in the explicit analytical form. We seek the function $\Psi^+(x, z)$ in terms of Fourier integral, and $\Psi_q^-(x, z)$ in terms of Fourier series. Furthermore, demanding the continuity of the total field $\Psi(x, z)$ and its x -derivative at the intervals $z \in \mathbb{L}_q$, $x = D$, and using the technique developed in [2-4] we derive the following basic equation on a set of intervals

$$\int_{\mathbb{L}} G(z - \zeta) F(\zeta) d\zeta + \int_{\mathbb{L}_q} [\Psi_q(z - \zeta) + \Psi_q(z + \zeta - 2a_q)] F(\zeta) d\zeta = \exp(ikz/\beta), \quad z \in \mathbb{L}_q, \quad q = 1, \dots, m, \quad (4)$$

$$\Psi_q(x) = \frac{1}{h_q} \sum_{n=0}^{\infty} \frac{\epsilon_n \operatorname{ch}[\gamma_n^q(d_q - |x|)]}{\gamma_n^q \operatorname{sh} \gamma_n^q d_q}, \quad G(x) = \frac{1}{2\pi} \int_{-\infty}^{\infty} \frac{\operatorname{th}(\lambda(\xi)D)}{\lambda(\xi)} \exp(i\xi x) d\xi,$$

$$\lambda(\xi) = \sqrt{\xi^2 - k^2}, \quad \operatorname{Re} \lambda \xi \geq 0, \quad \operatorname{Im} \lambda \xi \leq 0, \quad \gamma_n^q = \lambda(\pi n/h_q), \quad \mathbb{L} = \bigcup_{q=1}^m \mathbb{L}_q,$$

$$\epsilon_n = \begin{cases} 1/2, & n = 0 \\ 1, & n > 0 \end{cases}, \quad F(z) = \frac{\partial \Psi^+}{\partial x} \Big|_{x=D}.$$

In the limit of $D \rightarrow \infty$, the kernel of (4) coincides with that obtained in [2-4]. However, for the fixed D , the integrand in $G(x)$ can have a finite number of simple pole singularities on the contour of integration, and, consequently, the integral for $G(x)$ does not exist in common sense. A proper representation for it can be obtained by introducing a weak absorption in whole space: $k = k' + ik''$, $0 < k'' \ll k'$. This causes the shifts of the singularities from the integration contour into the complex plane of ξ . Then, deforming the contour of integration into the upper or lower half-plane of the complex variable ξ , we get a convenient analytical representation for $G(x)$:

$$G(x) = \frac{\operatorname{sign}(x)}{D} \sum_{n=0}^{\infty} \frac{e^{i\xi_n |x|}}{\xi_n}, \quad (5)$$

where $\xi_n = \sqrt{k^2 - \pi^2(n + 1/2)^2/D^2}$, $\operatorname{Re}(\xi_n) \geq 0$, $\operatorname{Im}(\xi_n) \geq 0$. After this it is convenient to carry out a numerical analysis of (4) by the method of discrete singularities [2-4]. Alternative approaches such as the direct moment method or the Riemann-Hilbert Problem technique, which are now used in computational electromagnetics appear to be less efficient in the considered case.

References

- [1] V.I. Koshelev et al., Proc. Int. Conf. BEAMS'96, Prague, Czech. Republic (1996).
- [2] Yu.V. Gandel, V.D. Dushkin, G.I. Zaginaylov, *Electromagnetic Waves & Electronic Systems*, v. 1, N 1, p. 38-48 (1996).
- [3] G.I. Zaginaylov, Yu.V. Gandel, P.V. Turbin, *Microwave and Opt. Tech. Lett.*, v. 16, N 1, p.250-54 (1997).
- [4] Yu.V. Gandel, G.I. Zaginaylov, *Doklady Akad. Nauk Rossii*, v. 359, N 4, (1998).

SOME FERRITE CONTROL COMPONENTS IN A SECTION OF CUT-OFF WAVEGUIDE

F.M. Repa

**Radiotechnical Department
National Technical University of Ukraine "KPI"
Ul. Politekhnicheskaya, 12, 252056, Kiev, Ukraine
Tel.(fax): 380-(044)-2418416**

A comparison analysis of electromagnetic structure – a constant cross-section of finite length cut-off waveguide (SCW) and stepped to reduce/increase of cross-section of cut-off waveguide in SCW (SRC) is expounded.

An algorithm of design of the mentioned structures has been built. In the present paper, the results of a solution of the problem of coupling of rectangular waveguides through such structures are presented.

By the mode matching technique applied for eigenfields at the waveguide junction boundary, the integral equation set has been converted into a matrix equation. Here we used a Galerkin variational method, whose solution determines the values of the tangential electric field in the openings. The convergence of the obtained solution to the exact one has been proved.

Using such a design approach, the structures tunable by magnetic field: ferrite and ferrite-waveguide resonators in SCW and SRC are considered.

A method is presented for calculating the elements of the scattering matrix, the absorption coefficients, the width of the passband, and the resonant frequency of a system consisting of ferrite and ferrite-waveguide resonators. Analytic relationships are derived and graphical dependences are obtained, which provide an engineering computation to be performed for various designs of ferrite films.

The utilization of compound ferrite dielectric plates for the linearization of the field frequency characteristic is shown.

METHOD OF MEASURING ELECTROMAGNETIC CHARACTERISTICS OF MATERIALS

Viktor I. Naidenko, Sergey P. Kapustyansky, Alexander P. Prokopenko

National Technical University of Ukraine "Kyiv Polytechnic Institute"
37, prospect Peremogy, Kyiv-56, 252056, Ukraine

Measuring electromagnetic characteristics of various media is a starting point in the development of many microwave technologies and instruments. This problem has been attracting a permanent attention [1]. One of the most simple and promising methods is the method of a partially filled waveguide with a shortened end [2].

In a waveguide having a shortened end, a homogeneous along certain direction sample is placed. Then the wave propagation along such a partially filled waveguide is measured. Provided that the detector used for measuring the field is a quadratic one, we can derive the equation:

$$|E|^2 = U(z) = A(\operatorname{ch} 2\gamma z - \cos 2\beta z) \quad (1)$$

where A is the amplitude of the measured value, $\beta = 2\pi/\lambda_w$ is the propagation constant of the waveguide mode, γ is the mode attenuation constant.

Recovering the sample material characteristics, such as ϵ' and ϵ'' , or ϵ' and $\operatorname{tg}\delta$, is to be done based on the solution of the inverse electromagnetic problem [2].

A method of determining γ from the measured distribution of (1) is known [2]. It is normally considered that determining β does not present any problem. To find γ , one has to determine the first point in the distribution (1), in which $|E|^2$ equals to the value of $|E|^2$ in the first minimum. Further, by using the expansion of the function $\operatorname{ch} x$ in terms of the Taylor series and keeping only the first two terms, one finds the formula for γ [2]. As experience shows, the accuracy of measuring ϵ' and ϵ'' is far from desired, and sharply decreases with increasing γ . So, the goal of the presented work is to provide a mathematical background to determination of β and γ , and hence ϵ' and ϵ'' .

1. Usage of Further Minima and Refining the Method

If γ is small, then the first minimum is very shallow. Therefore the point of the minimum $|E|^2$, is located very near to the shortened end. The field distribution near the shortened end is not accessible for measuring as it is severely disturbed by the probe. This inaccessible distance is not less than the depth of the probe insertion. The latter depth must be sufficient to have the detected signal higher than the level of noise and clutter.

It is possible to remove these shortcomings of the method by using the second, third, etc., minima of (1). One can show that if n is the number of the minimum, then

$$\gamma = 2 \sin(2\pi\xi_n) / (\lambda_w \sqrt{n^2 - 4\xi_n^2}), \quad (2)$$

where $\xi_n = z_n/\lambda_w$, z_n is the distance from the shortened end to the first point where the value of the function (1) equals to that in the n -th minimum. If $n=1$ we obtain the result derived in [2].

One can make the range of validity of this method wider by taking into account the third term in the Taylor expansion. Then we arrive at

$$\gamma = \lambda_w^{-1} \sqrt{6(\sqrt{1 + 4 \sin^2 2\pi\xi_n (n^2 + 4\xi_n^2)} / (3(n^2 - 4\xi_n^2)) - 1) / (n^2 + 4\xi_n^2)}. \quad (3)$$

2. Smoothing Algorithm

If γ is small, it is reasonable to integrate (1) with respect to z . Then we have

$$U_I(z) = \int_0^z U(z) dz = A \left[\frac{1}{2\gamma} sh 2\gamma z - \frac{1}{2\beta} \sin 2\beta z \right]. \quad (4)$$

Comparing (4) with (1), we can see that if γ is small, then the first term is now $\beta\gamma$ times greater than the second term. Besides, the curve has been smoothened.

At the points of minima of the original curve ($z=n\lambda_w/2$), the second term is zero. Therefore

$$U_I(n\lambda_w/2)/U_I(q\lambda_w/2) = sh(n\gamma\lambda_w)/sh(q\gamma\lambda_w). \quad (5)$$

For $n=2$ and $q=1$, $n=3$ and $q=2$, etc., one can derive a closed-form expression for γ .

Integrate (4) with respect to z . Then we have

$$U_{II}(z) = \int_0^z U_I(z) dz = \frac{A}{2} \left[\frac{1}{\gamma^2} sh^2 \gamma z - \frac{1}{\beta^2} \sin^2 \beta z \right] \quad (6)$$

Comparing (6) with (1), we can see that if γ is small, then the first term is now $\beta^2\gamma^2$ times greater than the second one. Besides, the curve has been smoothened once again.

At the points of minima of the original curve ($z=n\lambda_w/2$), the second term is zero. Therefore

$$\sqrt{U_{II}(n\lambda_w/2)/U_{II}(q\lambda_w/2)} = sh(n\gamma\lambda_w)/sh(q\gamma\lambda_w). \quad (7)$$

For the mentioned values of n and q one can derive a closed-form expression for γ .

Combining (1) and (6) we obtain:

$$2A(1 + \gamma^2/\beta^2) \sin^2 \beta z = U - 4\gamma^2 U_{II}. \quad (8)$$

At the points $z=0.25\lambda_w(2n-1)$, $n=1,2,\dots$ $\beta^2 = 2A\gamma^2/(U - 4\gamma^2 U_{II} - 2A)$

Combining (1), (4) and (6) we arrive at the following expression for the amplitude:

$$A = 2\gamma^2 (U U_{II} - U_I^2) / (U sh^2 \gamma z - 2U_I sh 2\gamma z + 4U_{II} \gamma^2 ch^2 \gamma z). \quad (9)$$

So, the first part of the problem: determining β and γ by the results of measurements, has been solved.

The second part: reconstruction of ε' and ε'' by the obtained β and γ , requires a solution of the eigenvalue electromagnetic problem about the modes of a partially filled rectangular waveguide. The solution of this problem is obtained by the mode matching method.

3. Solution of the Eigenvalue Problem

As the symmetry plane of the structure, $x=0$, is the "electric wall", for the principle mode and $y=0$ is the "magnetic wall", we can consider only a quarter of the structure cross section (Fig. 1). It is divided into two partial regions: I ($0 \leq x \leq d_1$) and II ($d_1 \leq x \leq a$). In turn, region I consists of two subregions I.1 and I.2: the first is filled with a dielectric having relative dielectric permittivity $\varepsilon_{1.1}$ ($0 \leq y \leq l$), the second with $\varepsilon_{1.2}$ ($l \leq y \leq b$). The field in a waveguide, partially filled with dielectric, is hybrid, therefore the solution in each partial region is presented as a sum of LE and LM modes. In each region, components of electromagnetic field are denoted through the y -components of the potentials. As the given area is inhomogeneous in the y -direction, expressions for magnetic and electric potentials in the first region are complicate:

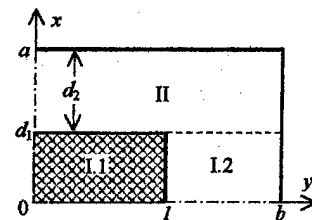


Fig. 1

$$A_y = \sum_{n=1}^{\infty} \tilde{A}_{n1} \sin(\tilde{\gamma}_{n1} x) \psi_{n1}^e(y), \quad F_y = \sum_{n=1}^{\infty} B_{n1} \cos(\gamma_{n1} x) \psi_{n1}^h(y), \quad (10)$$

where

$$\psi_{n1}^h(y) = \begin{cases} \frac{\cos \chi_{1n1} y}{\cos \chi_{1n1} l}, \\ \frac{\sin \chi_{2n1} (b-y)}{\sin \chi_{2n1} (b-l)}, \end{cases} \quad \psi_{n1}^e(y) = \begin{cases} \frac{\sin \tilde{\chi}_{1n1} y}{\sin \tilde{\chi}_{1n1} l}, \\ \frac{\cos \tilde{\chi}_{2n1} (b-y)}{\cos \tilde{\chi}_{2n1} (b-l)}, \end{cases}$$

$$\chi_{1n1}^2 + \gamma_{n1}^2 + \Gamma^2 = k^2 \epsilon_{1.1}, \quad \chi_{2n1}^2 + \gamma_{n1}^2 + \Gamma^2 = k^2 \epsilon_{1.2}, \quad \tilde{\chi}_{1n1}^2 + \tilde{\gamma}_{n1}^2 + \Gamma^2 = k^2 \epsilon_{1.1}, \quad \tilde{\chi}_{2n1}^2 + \tilde{\gamma}_{n2}^2 + \Gamma^2 = k^2 \epsilon_{1.2},$$

Γ is the longitudinal constant of the propagation. Dependence on time and coordinate z in the form of $\exp[j(\omega t - \Gamma z)]$ is omitted.

The constants χ_{1n1} , χ_{2n1} , $\tilde{\chi}_{1n1}$, $\tilde{\chi}_{2n1}$ are derived from (10) and from the equations:

$$\frac{\tilde{\chi}_{1n1}}{\epsilon_{1.1}} \operatorname{ctg} \tilde{\chi}_{1n1} l = \frac{\tilde{\chi}_{2n1}}{\epsilon_{1.2}} \operatorname{tg} \tilde{\chi}_{2n1} (b-l), \quad \chi_{1n1} \operatorname{tg} \chi_{1n1} l = \chi_{2n1} \operatorname{ctg} \chi_{2n1} (b-l)$$

For the second partial region:

$$A_y = \sum_{n2=0}^{\infty} \tilde{A}_{n2} \sin \tilde{\gamma}_{n2} (d_2 - x) \sin \tilde{p}_{n2} (y), \quad F_y = \sum_{n2=0}^{\infty} B_{n2} \cos \gamma_{n2} (d_2 - x) \cos p_{n2} (y), \quad (11)$$

where $p_{n2} = \frac{\pi}{b} (n_2 + 1/2)$, $p_{n2}^2 + \gamma_{n2}^2 + \Gamma^2 = k^2 \epsilon_2$, $\tilde{p}_{n2} = p_{n2}$.

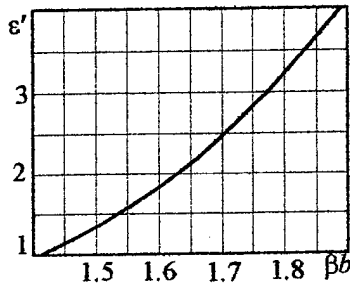


Fig. 2

Continuity of the tangential components of electric and magnetic fields at the boundary of the partial regions leads to a set of functional equations. Galerkin's method then is used to transform it into the matrix equation for \tilde{A}_{n1} , B_{n1} , \tilde{A}_{n2} , B_{n1} . The wavenumbers of modes in the dielectric waveguide are obtained by solving the equation obtained by demanding the determinant to be zero.

The results of computations have shown that the very accurate

results for both the dispersion and the expansion amplitudes can be obtained by taking into account 20 terms (10 for LE modes and 10 for LM modes) in each region. The calculated dependence of ϵ' on βb for $l/b=0.364$ and $d_1/a=0.289$ is shown in Fig. 2.

4. Experimental Results

The numerical integration was carried out by Simpson's method. The measured dependence (1), integrals (4) and (6), amplitude A and the right-hand part (8) are shown in Fig.3.

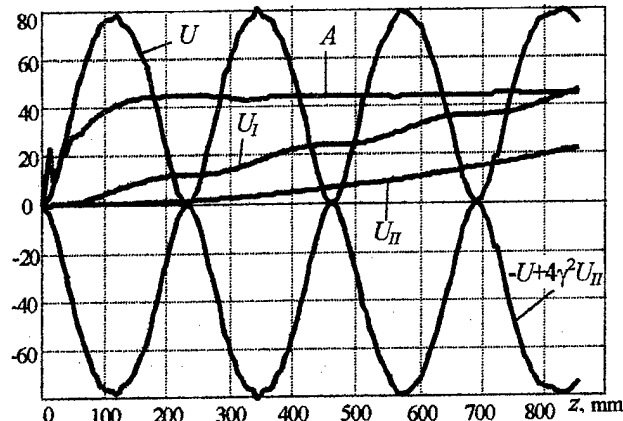


Fig. 3

References

1. M.D.Deshpande, C.J.Reddy, P.I.Tiemsin and R.Cravey, A new approach to estimate complex permittivity of dielectric materials at microwave frequencies using waveguide measurements, *IEEE Trans. on MTT*, v. MTT-45, No. 3, pp. 359-365, 1997.
2. A.A.Brandt, Investigations of the dielectrics in microwave band, Moscow, 1963, (in Russian).

RESONANT SYSTEM OF SELECTION AND ABSORPTION OF WAVEGUIDE MODE

O. V. Bondarenko, V. B. Kazanskiy

Chair of Theoretical Radiophysics, Kharkov State University, 310077, Kharkov, Ukraine

ABSTRACT:

Nonsymmetric inhomogeneous lateral expansion of a plate-parallel waveguide containing dielectric layers, a resistive film, and a grating of metallic strips is studied. A propagation constant is found from two-sided equivalent boundary conditions, and scattering coefficients are obtained from the solution of diffraction problem with the method of moments.

DISPERSION EQUATION SCATTERING COEFFICIENTS

A lateral expansion of a plate-parallel waveguide with the length L contains dielectric layers with widths b_j , permittivities ϵ_j , and permeabilities μ_j ($j=1,2,3$). There is a grating of closely spaced conducting strips with period l and gap width d at the boundary $y=0$ ($0 \leq z \leq L$),

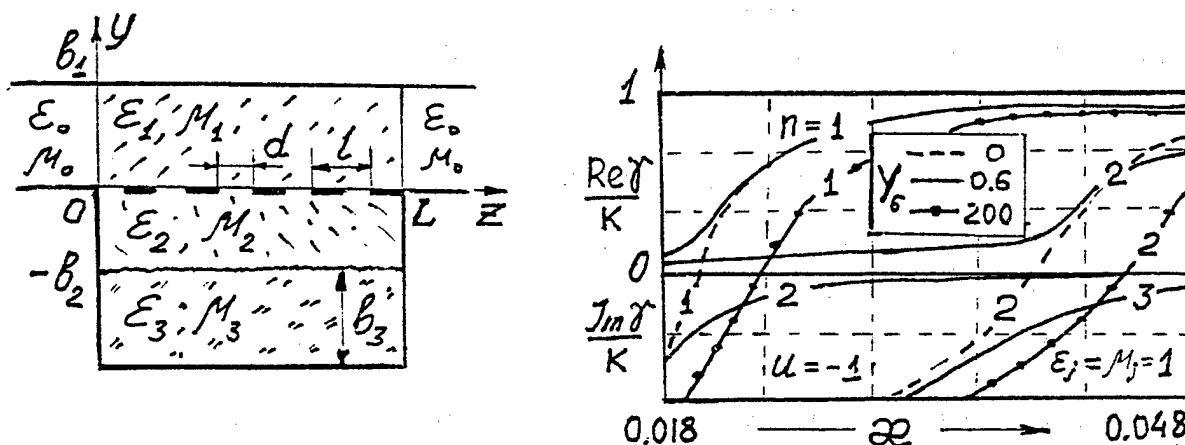


Fig. 1. Geometry. Dispersion dependences, $b_1/l=20$; $b_2/l=b_3/l=3$

$\pi/l \ll 1$ and a resistive film (RF) at $y = -b_2$. The whole structure is homogeneous along the ox axis (Fig.1). E_p - or H_p - mode with the propagation constant $\gamma_0(p) = \sqrt{k^2 \epsilon_0 \mu_0 - (\pi p/b_1)^2}$ is incident from the region $z < 0$. The scattered field is found in the class of longitudinal waves characterized by electrical ($s=e$) or magnetic ($s=h$) vector potential [1]: $\vec{E}^e = -\text{rot} \vec{y}_0 \Pi^e$, $\vec{H}^h = \text{rot} \vec{y}_0 \Pi^h$.

Expansion of the field in terms of orthonormalized eigenfunctions $\Phi_{\nu j}^s(y)$ in the resonator can be presented in the form:

$$\Pi_j^s = \sum_{\nu=0}^{\infty} [C_{\nu}^s \exp(i\gamma(\nu)z) + D_{\nu}^s \exp(-i\gamma(\nu)z)] \Phi_{\nu j}^s(y) \quad (1)$$

The propagation constant $\gamma(\nu) = \sqrt{k^2 \varepsilon_j \mu_j - k_{y_j}^2(\nu)}$ is found from the problem of propagation of waves. Its solution together with the two-side equivalent boundary conditions at the grating and RF [2,3] results in a dispersion equation relatively to $\gamma(\nu)$:

$$Y_g^s = \bar{Y}_1^s \operatorname{ctg}(k_{y1} b_1) + \frac{\bar{Y}_3^s \operatorname{ctg}(k_{y3} b_3) - iY_\sigma - \bar{Y}_2^s \operatorname{tg}(k_{y2} b_2)}{\bar{Y}_2^s + (\bar{Y}_3^s \operatorname{ctg}(k_{y3} b_3) - iY_\sigma) \operatorname{tg}(k_{y2} b_2)} \bar{Y}_2^s, \quad (2)$$

where $Y_g^h = (\mu_1 + \mu_2)/(\alpha \ln(1+u)/2)$, $Y_g^e = -\alpha(\varepsilon_1 + \varepsilon_2) \ln(1-u)/2$, $u = \cos(\pi d/l)$, $\bar{Y}_j^h = k_{y_j}/k\mu_j$, $\bar{Y}_j^e = k\varepsilon_j/k_{y_j}$. Using the method of moments for the solution of diffraction problems, we get two independent systems of equations

$$\begin{Bmatrix} X_n^s \\ Z_n^s \end{Bmatrix} - \sum_{m=\begin{Bmatrix} 0,e \\ 1,h \end{Bmatrix}}^{\infty} \begin{Bmatrix} X_m^s \operatorname{cth}\left(\frac{i\gamma_0(m)L}{2}\right) \\ Z_m^s \operatorname{th}\left(\frac{i\gamma_0(m)L}{2}\right) \end{Bmatrix} \sum_{\nu=0}^{\infty} \frac{Y_{1\nu}^s L_{m\nu}^s L_{n\nu}^s}{\sqrt{Y_{0m}^s Y_{0n}^s}} = 2\delta_p^n \begin{Bmatrix} \mp 1 \\ \pm 1 \end{Bmatrix}, \quad (3)$$

where $\begin{Bmatrix} L_{m\nu}^e \\ L_{m\nu}^h \end{Bmatrix} = \begin{Bmatrix} k_{y1}(\nu)/N_\nu^e \\ \pi m/N_\nu^h b_1 \end{Bmatrix} \frac{\sqrt{2/b_1} \sin(k_{y1}(\nu) b_1)}{(\pi m/b_1)^2 - (k_{y1}(\nu))^2}$, $Y_{j\nu}^e = k\varepsilon_j/\gamma(\nu)$, $Y_{j\nu}^h = \gamma(\nu)/k\mu_j$,

$[N_\nu^s]^2 = \int_{-(b_2+b_3)}^{b_1} [\Phi_\nu^s(y)]^2 dy$ is the normalization factor, the upper sign refers to E_p -modes and lower sign - to H_p -modes. Transformation coefficients of the exciting p -wave into n -wave in the reflected (R_{np}) and transmission (T_{np}) fields can be obtained from the following formulas:

$$R_{np}^s = \mp \delta_p^n + (Z_n^s - X_n^s)/2; \quad T_{np}^s = \exp(-i\gamma_0(n)L) (Z_n^s + X_n^s)/2$$

Similar sets of the algebraic equations can be derived when solving the problems of diffraction of waves at homogeneous lateral waveguide expansion. (See, for example, [4] and bibliography there). A characteristic property of the presented solution is that the propagation constant $\gamma(\nu)$ of the relevant infinite waveguide depends on its substructure, grating parameter, and a resistive film (8).

ANALYSIS OF SOLUTION

If the structure is excited by H_p -modes, the scattered field consists only of superposition of guided modes ($n \geq 1$). Under the excitation by E_p -modes quasi *TEM*-mode ($n=0$) exists as well.

If we consider the frequency interval $\alpha \ll 1$, average values of ε_j , μ_j and filling parameter - $0.9 \leq u \leq 0.9$, equivalent conductivities satisfy inequalities $|Y_p^h| \gg 1$, $|Y_p^e| \ll 1$. For this reason the grating does not practically influence the phase and amplitude-frequency characteristics of E_p -modes, but changes substantially the critical frequencies (α_c) of H_p -modes. Even in the absence of the dissipative losses in filling media ($\operatorname{Im} \varepsilon_j = \operatorname{Im} \mu_j = 0$), the propagation constant in the expansion containing a resistive film has complex value. When its conductivity is small ($Y_\sigma \ll 1$), the imaginary part of it is in the low frequency range: $\alpha < \alpha_c$, and the real part is in the high frequency range: $\alpha > \alpha_c$, and in good agreement with corresponding values at $Y_\sigma = 0$. However, in the case under consideration, in low-frequency interval $\operatorname{Re} \gamma$ has small

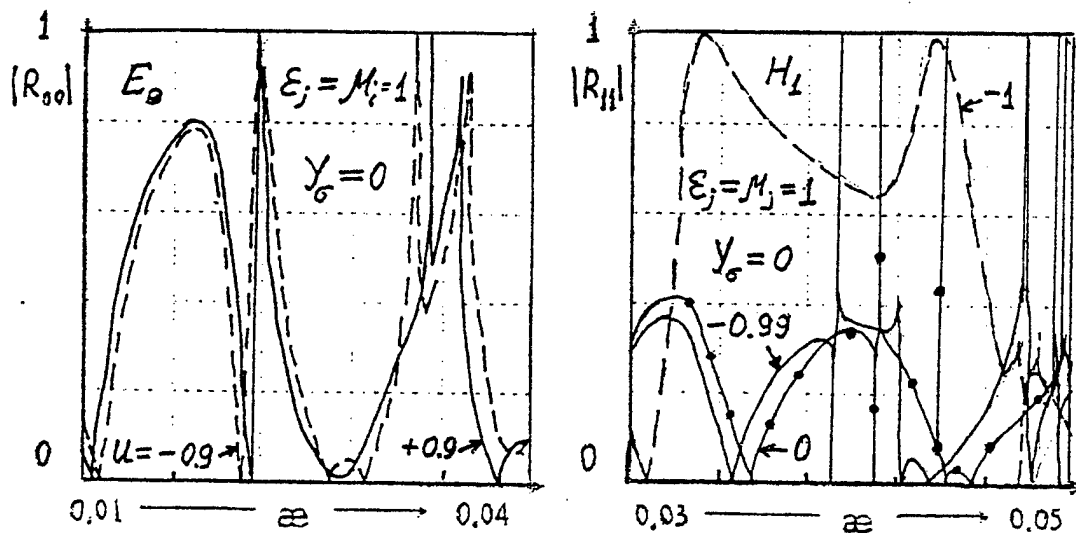


Fig. 2 Frequency dependences of $|R|$, $b_1/l=20$; $b_2/l=b_3/l=5$; $L/l=4$.

value not equal to zero. That is why the gradient of the dispersion dependence is much less at the critical frequency ($\omega = \omega_c$), than when RC is absent. Dispersion dependence of three layered structure ($b_1+b_2+b_3$) wide with high conductivity of RC ($Y_0 \gg 1$) presents the properties of two-layered structure (b_1+b_2) wide, since RC acts like a conducting surface.

Scattering coefficients of E_p -modes for a homogeneous expansion do not practically depend on the grating filling parameter. Characteristic feature of the frequency dependence of $|R_{00}|$ (Fig. 3a) reflects the conditions of arising of new propagating modes and resonant regimes ($n \geq 1$). Since the coupling between the resonator and the feeding waveguide for the E_p -modes is strong, then the level of their mutual transformations is high, and the resonances at trapped-mode oscillations have a low Q-factor. For H_p -modes, a resonant coupling is weak. Inserting a grating with a small filling parameter ($u \sim -0.99$) changes abruptly the resonance frequencies and increases strongly the Q-factors of the trapped-mode resonances (up to 10^4).

A resistive film does not practically change the resonance frequencies, but influences critically on the Q-factors of resonances as well as the level of the mutual transformations of the waves.

CONCLUSION

Considered model of a control device is a structural generalization of the known quasi-open waveguide systems. Presence of the local dissipative and polarization-sensitive elements in the resonant region opens away to new applications of these structures and substantially enlarges their functional opportunities.

REFERENCES

- [1] Y. V. Yegorov, *Partly Filled Layered Waveguides*, Moscow: Sov. Radio, 1967 (in Russian).
- [2] V. B. Kazanskij, "Electrodynamic Model of the Multifunctional Control System," *Turkish Journal of Physics*, vol. 19, no. 11, pp. 1467-1471, 1995.
- [3] N. Y. Bliznyuk, O. V. Bondarenko, V. B. Kazanskij, "Electromagnetic modeling of a resonant commutator," *Microwave and Optical Technology Letters*, vol. 12, no. 1, pp. 44-48, 1997.
- [4] V. P. Shestopalov, A. A. Kirilenko, L. A. Ryd, *Resonant Scattering of Waves*, vol. 2. Waveguide Discontinuities, Kiev: Naykova Dymka, 1986 (in Russian).

Electromagnetic Signal Processing

Circuit Modeling for Super-High Speed Processing Spatially Modulated Field Signals

G.A. Kouzaev, A.S. Tcherkasov

Moscow State Institute of Electronics and Mathematics (Technical University)

3/12 B. Tryokhsvyatitsky per., 109028 Moscow

Tel. 916-8882, e-mail: lmis@miem-as.ins.ru, root@onti.miem.msk.su

Abstract. This article examines the physical basis of the superfast SIC components for Processing Spatially Modulated Electromagnetic Field Signals. The analysis of the main physical effects which are capable to influence on SIC components speed. The possibility of fulfillment of subpicosecond analog and digital operations for spatially modulated signals with the help of passive microstrip micron-sized components is conducted. The outcomes of subpicosecond switch simulation are discussed. The integration concept for such elements in SIC, constructed on principles of digital pseudo-holography is offered.

Introduction. The denseness magnification of integration of SIC elements together with growth of their work action causes the growth of signals space complexity conditioned by electromagnetic interconnections. In [1] the special discrete characteristic of spatially modulated field - the topological scheme - was offered to use for the purposes of digital information input. The earlier developed theory (topological approach for boundary problems of an electrodynamics) has allowed to make a conclusion about a possibility of fulfillment for some logic operations with the help of passive (strip) components. The first device simulation outcomes which permits to switch it with subpicosecond speed in different stratum of the three-dimensional signal circuit depending on space topology, are considered in [2].

Physical analysis and theoretical results. The present article purpose is to research three main problems in this area: influence of solid-state effects in conductors and dielectrics on signals processing processes, creation of perspective subpicosecond element basis for digital processing of the spatially-modulated signals and problems of new elements integration in perspective SIC.

The essential influence upon perspective elements performances have the physical effects in solid-states and diffractive phenomena on strip transmission line discontinuities in subpicosecond modes area of signals processing. By the outcomes, indicated in Table 1, of the analysis of various physical effects, on the basis of micron strip engineering the creation of unquantum circuit components with subpicosecond speed is possible.

The digital components for processing spatially - modulate signals are constructed on the base of the usage of field topology for input, transfer and information processing. A typical signal of a similar kind can be a sequence of impulses even (logic 1) and odd (logic 0) modes in connected strip lines (Fig. 1, a, b). The number of logic operations above such signals manages to be realized without use of semiconducting elements with significant time delay. On Fig. 2, a, b the switch permitting to switch logic signals (impulses of even and odd modes of micron-sized coupled strip transmission lines) into different layers of the three-dimensional circuit is represented. In the equivalent scheme the final sizes of resistors and their parasitic reactivity was taken into account. The duration of transients for signal switching of a signal did not exceed several picosecond shares, and the delay it made was no more than 0,03 ps. The settlement energy costs to fulfill that operation have appeared on the order smaller, than for transistor analogs.

Application of the new super-high speed circuits. The article discusses the new VLSI concept, taking into account the tendency to create three-dimensional circuits with superdense elements accommodation. The evaluations specify, that owing to electromagnetic interinfluences space frequency of signals fields in electronic IC may be compared to a bit density in the optical three-dimensional holograms. It is offered to design the perspective specialized electronic IC on the basis of simulation of the holographic effects in picosecond impulses frequency band with the usage of a similarity method. The principle of a field topological modulation will allow to use digital methods to realize holographic principles of construction for the new circuits. Thus, the number of processing signal operations is offered to be executed at the expense of superfast effects such as a diffraction of waves on strip components, and other necessary operations, for example, management of interconnections structure, switching of compared images frames, amplification and signals generation to realize with the help of semiconducting components. The given IC architecture and the principles of its work will allow to unite functional advantages of the electronic and optical circuits during spatially - modulated signals processing. This report will discuss the circuitry solutions from this area.

Conclusion. Method and circuitry of superfast (subpicosecond logic processing of spatially (topologically) modulated signals by the passive strip components were considered. The evaluations of physical effects influencing on time processes of picosecond signals processing were indicated. The conclusion about a basic possibility of creation of strip circuits with subpicosecond speed was made. The outcomes about theoretical modeling of the topologically modulated signals switch were discussed. The new concept of superdense IC, constructed on the basis of holographic effects physical analog-digital modeling for the topologically modulated signals was developed.

Table 1. Time scales of main physical effects in IC elements

No	Physical effect	Time or frequency evaluation of an effect
1.	Limited mode velocity in microstrip transmission lines. Time delay of signal in a microstrip transmission line on the substrate with dielectric permittivity ϵ :	$\sim 33.3 \sqrt{\epsilon}$, fs/ μ m
2.	Inertia of interaction of electromagnetic field with free charge in the region of low values of photon energy.	Defined by efficient or free mass of charges
3.	Maxwell relaxation time of charges in conductors:	$\sim 0.001 - 0.01$ fs
4.	Collective effects in the electronic plasma. Period of plasma frequency in the conductors:	$\sim 0,067 - 0,2$ fs
5.	Relaxation phenomenas in dielectric. Time constant of electronic polarization: Time constant of atomic polarization	$\sim 1 - 10$ fs $\sim 10 - 10000$ fs
6.	Minimal time of transition an electron from one energy level on the another in atom	$\sim 1 - 10$ fs
7.	Typical theoretical time of electron relaxation in quantum nanoelements:	100-1000 fs
8.	Electron-phonone interaction. Resonant frequency in conductors:	~ 10 THz
9.	Transient-time effects on discontinuities of strip transmission lines of micron sizes. Time constant of transient process on discontinuities (Idealized Oliner model for discontinuities):	~ 10 fs
10.	Excitation of higher modes on discontinuities of microstrip transmission lines in VLSI. Cut-off frequency of the first higher mode:	$\sim 10 - 100$ THz
11.	Excitation of surface waves in micron microstrip transmission lines. Critical coupling frequency of the strip and surface modes:	10-100 THz

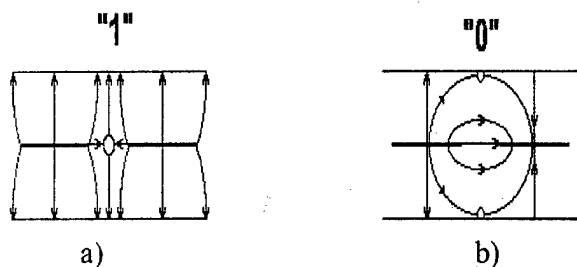


Fig. 1.

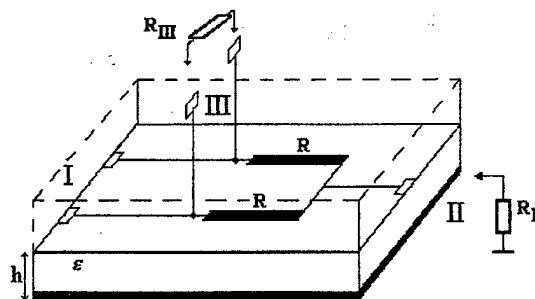
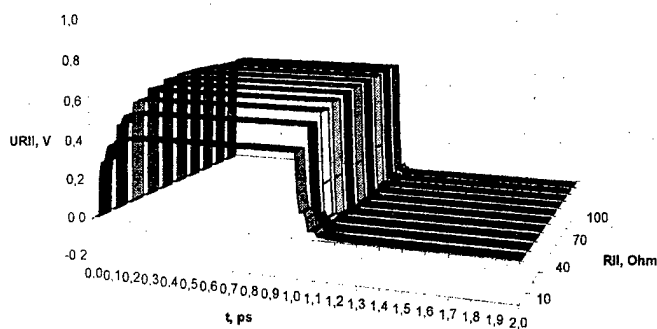
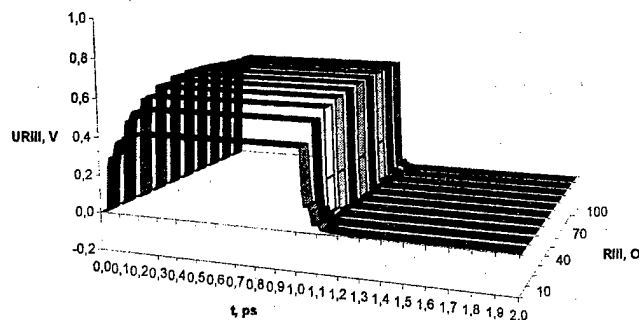


Fig. 2.



a)



b)

Fig. 3.

Transient characteristics of the switch for topologically modulated signals.

a) Output signal on the port II (logical 1 on the input I)

b) Output signal on the port III (logical 0 on the input I)

$R=18 \text{ Ohm}$, $\epsilon=3.5$, $h=3 \text{ mm}$, $Z_e=84.32$, $Z_o=47.85$.

The work is sponsored in part with the Russian Foundation for Basic Research.

References.

- [1] G.A. Kouzaev. Topological Pulse Modulation of Electromagnetic Field and Super High-Speed Logical Circuits in Microwave Range. // Proc. of the Int. URSI Symp. on Electromagnetic Theory. St. Petersburg, Russia. May 23-26. 1995.
- [2] G.A. Kuzaev, V.I. Gvozdev. Topological Pulse Modulation of Field and New Microwave Circuits Design for Superspeed Operating Computers. // Proc. of Symp. on Signals, Systems and Electronics. San Francisco. Oct. 25-27. 1995.

MODEL OF SIGNALS FOR DIGITAL ANTENNA ARRAY WITH MUTUAL COUPLING ON THE BASIS OF FACE-SPLITTING MATRICES PRODUCT

V. I. Slyusar, V. L. Buryachok

Scientific Center of Problems of Protection from High-Precision Weapon

Kiev Institute of Ground Forces

Kiev, Andruschenko Street, 4, e-mail: swadim@777.com.ua

When considering the multicoordinate digital antenna arrays (DAA) with mutual coupling of channels there arises a problem of compact matrix record of the responses of reception channels. For the solution of the given problem it is proposed to operate with a special type of the product of matrices, named as "face-splitting" ($a \boxtimes b = [a_{ij} \cdot B_i]$) and "transposed face-splitting" product (TFSP) ($a \blacksquare b = [a_{ij} \cdot B_j]$), respectively, [1].

With the aid of TFSP it is possible to obtain the variant of analytical model of two-coordinate DAA with mutual coupling:

$$U = (F \otimes W)(Q \blacksquare V) \cdot A, \quad (1)$$

where U is a block-vector of voltages of the responses of DAA channels, Q , V is the $R \times M$ matrix of the directivity characteristics of primary channels in azimuth and elevation angle planes,

$$Q = \begin{bmatrix} Q_1(x_1) & Q_1(x_2) & \cdots & Q_1(x_M) \\ Q_2(x_1) & Q_2(x_2) & \cdots & Q_2(x_M) \\ \vdots & \vdots & \ddots & \vdots \\ Q_R(x_1) & Q_R(x_2) & \cdots & Q_R(x_M) \end{bmatrix}, \quad V = \begin{bmatrix} V_1(y_1) & V_1(y_2) & \cdots & V_1(y_M) \\ V_2(y_1) & V_2(y_2) & \cdots & V_2(y_M) \\ \vdots & \vdots & \ddots & \vdots \\ V_R(y_1) & V_R(y_2) & \cdots & V_R(y_M) \end{bmatrix};$$

$$Q \blacksquare V = \begin{bmatrix} \begin{bmatrix} Q_1(x_1) \\ \vdots \\ Q_R(x_1) \end{bmatrix} \begin{bmatrix} V_1(y_1) \\ \vdots \\ V_R(y_1) \end{bmatrix} & \begin{bmatrix} Q_1(x_2) \\ \vdots \\ Q_R(x_2) \end{bmatrix} \begin{bmatrix} V_1(y_2) \\ \vdots \\ V_R(y_2) \end{bmatrix} & \cdots & \begin{bmatrix} Q_1(x_M) \\ \vdots \\ Q_R(x_M) \end{bmatrix} \begin{bmatrix} V_1(y_M) \\ \vdots \\ V_R(y_M) \end{bmatrix} \\ \begin{bmatrix} Q_2(x_1) \\ \vdots \\ Q_R(x_1) \end{bmatrix} \begin{bmatrix} V_1(y_1) \\ \vdots \\ V_R(y_1) \end{bmatrix} & \begin{bmatrix} Q_2(x_2) \\ \vdots \\ Q_R(x_2) \end{bmatrix} \begin{bmatrix} V_1(y_2) \\ \vdots \\ V_R(y_2) \end{bmatrix} & \cdots & \begin{bmatrix} Q_2(x_M) \\ \vdots \\ Q_R(x_M) \end{bmatrix} \begin{bmatrix} V_1(y_M) \\ \vdots \\ V_R(y_M) \end{bmatrix} \\ \vdots & \vdots & \ddots & \vdots \\ \begin{bmatrix} Q_R(x_1) \\ \vdots \\ Q_R(x_1) \end{bmatrix} \begin{bmatrix} V_1(y_1) \\ \vdots \\ V_R(y_1) \end{bmatrix} & \begin{bmatrix} Q_R(x_2) \\ \vdots \\ Q_R(x_2) \end{bmatrix} \begin{bmatrix} V_1(y_2) \\ \vdots \\ V_R(y_2) \end{bmatrix} & \cdots & \begin{bmatrix} Q_R(x_M) \\ \vdots \\ Q_R(x_M) \end{bmatrix} \begin{bmatrix} V_1(y_M) \\ \vdots \\ V_R(y_M) \end{bmatrix} \end{bmatrix};$$

F , W is the $R \times R$ matrix of mutual coupling,

$$F = \begin{bmatrix} 1 & F_{12} & \cdots & F_{1R} \\ F_{21} & 1 & \cdots & F_{2R} \\ \vdots & \vdots & \ddots & \vdots \\ F_{R1} & F_{R2} & \cdots & 1 \end{bmatrix}, \quad W = \begin{bmatrix} 1 & W_{12} & \cdots & W_{1R} \\ W_{21} & 1 & \cdots & W_{2R} \\ \vdots & \vdots & \ddots & \vdots \\ W_{R1} & W_{R2} & \cdots & 1 \end{bmatrix}, \quad |F_{nm}| < 1, |W_{nm}| < 1;$$

$A = [\hat{a}_1 \ \hat{a}_2 \ \cdots \ \hat{a}_M]^T$ is the vector of complex amplitudes of signals of M sources.

With the aid of identities [2]:

$$(F \otimes W)(Q \otimes V) = (F \cdot Q) \otimes (W \cdot V),$$

one can obtain that

$$U = P \cdot A, \text{ where } P = (F \cdot Q) \otimes (W \cdot V) \quad (2)$$

By using the method of maximum likelihood, an estimation of parameters of M sources of signals of two-coordinate DAA it is possible to be carried out, by a minimization of a functional not differing in form from that used in one-coordinate case. Indeed, it is possible to write down:

$$L = \{U - P \cdot A\}^* \{U - P \cdot A\} = \min$$

The measuring procedure in the two-coordinate variant is reduced to the minimization of expression:

$$L = \text{tr}[G \cdot R], \text{ where } G = P \cdot (P^* \cdot P)^{-1} \cdot P^*, \quad R = U \cdot U^*.$$

With the account of (2), on the basis of matrix Neudecker derivative [3] an information fisher's block-matrix describing the accuracy of joint estimation of angular coordinates is obtained [4]:

$$I = \frac{1}{\sigma^2} \cdot \begin{bmatrix} P^T \cdot P & \vdots & (A^* \otimes P^T) \cdot \frac{\partial P}{\partial Y} \\ \cdots & \vdots & \cdots \\ \left(\frac{\partial P}{\partial Y}\right)^T \cdot (A \otimes P) & \vdots & \left(\frac{\partial P}{\partial Y}\right)^T \cdot (A A^* \otimes 1_{RR}) \cdot \frac{\partial P}{\partial Y} \end{bmatrix},$$

where $\frac{\partial P}{\partial Y}$ is the Neudecker derivative of the matrix P by the vector Y formed by unknown estimations of angular coordinates of M sources; 1_{RR} is the identity matrix of dimension $R \times R$; \otimes is the symbol of Kronecker-products of matrices.

References

1. V. I. Slyusar, New Operations of Matrices Products for Applications of Radars, in *Proc. Direct and Inverse Problems of Electromagnetic and Acoustic Wave Theory (DIPED-97)*, Lviv, 1997, P. 73-74 (in Russian).
2. V. I. Slyusar, The Family of the Face-Splitting Matrices Product and its Characteristics, *Kibernetika i sistemny analiz*, 1998, to be published (in Russian).
3. T. Kollo, Matrix Derivative for Multidimensional Statistics, Tartu University Press, 1991. pp. 24 - 29.
4. V. I. Slyusar, Accuracy of Linear Digital Antenna Array at Joint Estimation of Range and Angular Coordinate of M Sources, in *Proc. ICATT-97*, Kyiv, 1997, pp. 110 - 111.

UNIFIED STRUCTURE AND APPROACH FOR PERFORMING FAST TRANSFORMATIONS AND NONLINEAR OPERATIONS

K.Egiazarian, D.Gevorkian, S.Atourian, J.Astola, T.Saramaki,
Signal Processing Laboratory, Tampere University of Technology,
P.O.Box 553, FIN-33101, Tampere, Finland,
tel. +358 3 3652923, fax +358 3 3653857, e-mails karen, gevday, sam, jta, ts@cs.tut.fi
V.Lukin

Dept. 507, Kharkov Aviation Institute, 17 Chkalova St., 310070, Kharkov, Ukraine,
tel. +38 0572 442352, fax +38 0572 441186, e-mail lukin@xai.kharkov.ua

Abstract. A unified structure for performing fast discrete orthogonal transformations like Fourier, Walsh, Haar, Cosine and Sine ones and nonlinear operations like scanning window data sorting for order statistic and L-filters is proposed and described. It permits to implement a wide class of techniques used in signal and image processing applications.

Keywords: unified structure, fast transformations, nonlinear operations.

1. Introduction

Different discrete orthogonal transformations like Fourier, Walsh, Haar, Cosine and Sine ones as well as nonlinear operations, for example, scanning window data sorting are widely used for analysis of microwave device performance (antenna array pattern synthesis, control and investigation of noise influence [1]), digital signal and image processing - linear and nonlinear filtering and enhancement [2,3]. This deals with several aspects. First, many linear filtering techniques can be more easily realized in the spectral domain [2]. Second, a lot of discrete orthogonal transforms have fast algorithms and they are characterized by very similar flow graphs [4]. Third, the data sorting operations used for many nonlinear filters - median, order statistic, L-filters, etc. - also have fast algorithms with flow graphs similar to those ones used for transformations. These obstacles run us into idea that a unified structure able to execute all these operations with switching only the mode of elementary node performance can be designed.

2. Discrete Orthogonal Transform Families. Unified Representation

A general class of linear orthogonal transform is the class the transform matrices, which can be presented in the following form:

$$H_n = P^{(o)} H^{(i)} = P^{(o)} \left[\bigoplus_{i=1}^q \bigoplus_{s=0}^{N/r_i-1} V^{(i,s)} P^{(i)} \right] \quad (1)$$

where $N = r_n r_{n-1} \dots r_1$ is the order of the transform; $r_i \in \{r_1, \dots, r_n\}$ for $i = n+1, \dots, q$; $V^{(i,s)}$ are $(r_i \times r_i)$ matrices called spectral kernels and the symbol \oplus denotes the direct sum of matrices [5]. Varying the number q , permutation matrices $P^{(i)}$, $i=1, \dots, q$ and spectral kernels $V^{(i,s)}$, which play the role of parameters in the unified representation (1), a large class G of orthogonal transforms can be formed. The common property of the transforms from G is possessing fast transform algorithms. It should be noted that different representations of the form 1) may exist for the same matrix, or equivalently, different sets of parameters may correspond to the same transform. The representation (1) is more convenient from the parallel implementation standpoint because it separates arithmetical operations (corresponding to direct sums) and data exchange operations (corresponding to permutation matrices) each from the other. One important property of orthogonal transforms from G is

that $H_{EN} \in G \Leftrightarrow H_{EN}^{-1} \in G$, i.e. both inverse and direct transforms belong to the same class. This family includes such classical transforms as discrete Fourier, Walsh, Walsh-Hadamard (DFT, DWT, DWHT, respectively) ones as well as Haar, Cosine and Sine transforms.

Among many useful properties of the unified parametric approach based on (1) let us mention the following:

1. Representation (1) gives a unified approach to fast transform algorithms, thus, not a fixed transform but certain families of them can be implemented using unified, parametrically controlled (or programmable) fast sequential and parallel algorithms and architectures. This means the universality (or multifunctionality) and the flexibility of software and hardware tools designed according to this approach.
2. The structure permits to consider the problem of searching the best (according to some features) transform while fixing some other features. Besides, hybrid transforms can be synthesized within the same framework.

The unified structure of fast transform algorithms is presented in Fig.1 in a generalized form. The nodes of the flow graph (bold dots in Fig.1) are divided into $q+1$ levels, the i -th level representing the vector $z_i = [\delta_i^{(1)}, \dots, \delta_i^{(N-1)}]$, $i=0, \dots, q$. There are edges only between nodes of adjacent levels. The sets of edges nodes correspond to permutation matrices $P^{(q)}, P^{(q-1)}, \dots, P^{(0)}$. So the outputs of blocks $P^{(q-1)}$ (See Fig.1) represent the vector $Z_i' = P^{(q-1)} \times Z_i$. The blocks $V^{(i,s)}$, $i=0, \dots, q-1$; $s=0, \dots, N/r_i-1$, represent executions of the basic operations which are simple discrete linear transforms with non-identity matrices $V^{(i,s)}$ of smaller (compared to N) size r_i . Therefore, computations of the i -th stage consists of: a) permutations of the components of Z_i according to $P^{(q-1)}$; b) dividing the resulting vector Z_i' into N/r_{q-1} subvectors $Z_{i,s}$ and c) implementation of the set of basic operations. So, two types of operations are performed in a fast algorithm. The first is called *radix- r butterfly* and the second is the permutation (or reordering) operation. It is worth saying that some preliminary operations, in particular data weighting [1] can be performed before transformation fulfilling.

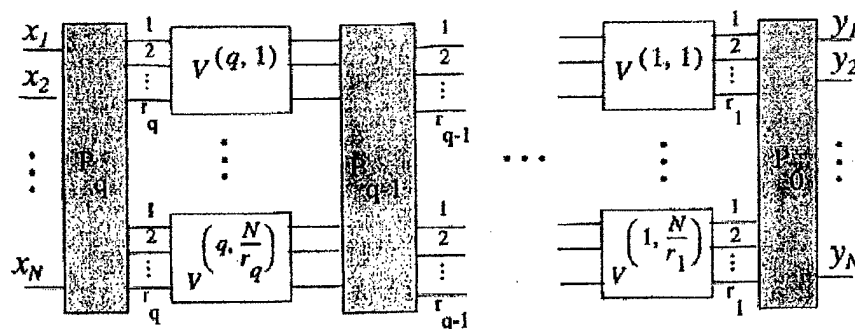


Fig.1. Generalized scheme of the unified structure

3. Nonlinear Operations and Unified Structure.

Let us consider now an enlarged model of the flow-graph in Fig.1 allowing also some nonlinear transformations including complete sorting of input data. Formally, fast algorithm of the transform $y=F(x)$ where x is a vector of N input samples and $F(\bullet)$ is some operator (linear or nonlinear) executed by the flowgraph consists of q stages. So when basic operations of (1) are nonlinear then the output of the flowgraph is a bank of N different stack filters. Such filters have been called FFT-ordered L-filters [6].

In the simplest case of $r=2$ the basic operations are

$$\begin{cases} V(1) = \alpha_{1,1}U(1) + \alpha_{1,2}U(2) \\ V(2) = \alpha_{2,1}U(1) + \alpha_{2,2}U(2) \end{cases} \quad (2)$$

for the linear case which is called "butterfly" and for the nonlinear case "compare and swap" operation

$$\begin{cases} V(1) = \rho(U(1), U(2)) \\ V(2) = \rho^*(U(1), U(2)) \end{cases} \quad (3)$$

where ρ is min or max operator and ρ^* is max or min operator, respectively.

It is known that L-filters involve many known ones as subclasses: median, α -trimmed, min/max filters, for many weighted order statistic ones the L-filter with very close properties can be found. Moreover, sigma and K-nearest neighbor filter can be interpreted as L-filters with temporarily or spatially varying parameters. This makes possible to apply the proposed unified structure for implementation of different adaptive filtering procedures both with generally converging adaptation [7] and local one [8]. It is expedient from the standpoint that among L-filters almost always exists one being optimal for suppression of noise with observed probability density function.

Conclusions

The unified structure and approach for performing a wide set of different fast transformations and nonlinear operations (filtering) is proposed. It is useful for many practical applications of microwave device synthesis and analysis, digital signal and image processing. The main advantage consists in the fact that the efficiencies of different transformations compared to each other and that one optimal for solving the task at hand can be selected or updated in adaptive manner.

References

1. V.V.Lukin, T.Saramaki, I.P.Anukhin, "Array Step-like Apodization Function Synthesis, Parameter Optimization and Implementation Aspects", Proceedings of MMET '96, pp. 65-68, Lviv, Ukraine, Sept. 1996.
2. W.K. Pratt, Digital Image Processing, 2-nd ed., Wiley, 1991.
3. J.T. Astola, P. Kuosmanen, "Fundamentals of Nonlinear Digital Filtering", CRC Press, NY, USA, 1997, 276 p.
4. A.V. Oppenheim, R.W. Schaffer, Discrete-Time Signal Processing, Englewood Cliffs, NJ: Prentice Hall, 1989.
5. C.C. Aggarwal, N. Jain, P. Gupta, "An efficient selection algorithm on the pyramid", Information Processing Letters, Vol. 53, pp. 37-47, 1995.
6. K.O. Egiazarian, J.T. Astola, S.M. Atorian, D.Z. Gevorgian, "Nonlinear filters based on ordering by FFT structure", Proceedings of IS&T/SPIE Symp. on Electronic Imaging: Science and Technology, V.2662, pp. 106-117, San Jose, CA, USA, Feb.1996.
7. K. Egiazarian, J.Astola, S. Atourian, D. Gevorgian, "Adaptive LMS FFT-ordered L-Filteres", Proceedings of IS&T/SPIE Symp. on Electronic Imaging: Science and Technology, V. 3026, pp.34-45, San Jose, CA, USA, Feb.1997.
8. Lukin V.V., Ponomarenko N.N., Astola J.T., Saarinen K.P., "Algorithms of image nonlinear adaptive filtering using fragment recognition by expert system", Proceedings of IS&T/SPIE Symp. on Electronic Imaging: Science and Technology, V. 2662, pp. 179-190, San Jose, CA, USA, Feb.1996.

**Analysis of the Ishimaru parabolic equation:
the Laguerre invariance of the output time impulses shape**

A.A. Galuza, A.S. Mazmanishvili

Kharkov State Polytechnical University
Frunze st. 21, Kharkov, 310002, Ukraine
e-mail: mazmani@kpi.kharkov.ua

In a linear approximation, a monochromatic impulse $I_{out}(t)$ passed through diffusing medium can be given by

$$I_{out}(t) = \int G(t-t') I_{in}(t') dt', \quad (1)$$

where $I_{in}(t')$ is the initial impulse and $G(t)$ is Green function.

According to

$$G(t) = \frac{1}{2\pi i} \int \Gamma(\eta) \exp(-\eta t) d\eta, \quad (2)$$

where $\Gamma(\eta)$ is the coherence function related to $G(t)$ by the Fourier transformation, the problem of determining Green function $G(t)$ is equal to that of determining $\Gamma(\eta)$.

Ishimaru [1] studied the coherence function and the time behavior of an impulse radiated by plane the $z = 0$ and detected at the distance $z = L$ at the point $\mathbf{r} = \mathbf{0}$. He did not include the dissipative attenuation into his approximation. This paper is an attempt to extend the Ishimaru's model by taking this effect into consideration. To do it, let us study an extension of the Ishimaru equation taking account of the dissipative properties of the medium

$$\left(\frac{\partial}{\partial z} + \frac{\nu}{2} \frac{\partial}{\partial \mathbf{r}} \mathbf{r} + a_\eta(z) \frac{\partial^2}{\partial \mathbf{r}^2} + b(z) \mathbf{r}^2 \right) \Gamma(z, \mathbf{r}; \eta) = 0 \quad (3)$$

with the initial condition $\Gamma(0, \mathbf{r}; \eta) = 1$. In this equation, $a_\eta = \eta/2ck^2$; $b = \rho(z)\sigma_p k^2/4\alpha_p$, where ν is the attenuation coefficient, k is the wave number of EM radiation, c is the velocity of light, $\rho(z)$ is the concentration of the scatterers; σ_p is the scattering cross-section; α_p is the angular coefficient of scattering which is approximately equal to the ration of the scatterers diameter D to the EM wave length λ [1,2].

Within the random paths model, an output impulse can be represented as a superposition of subimpulses which arrive at the detection point along different paths due to the scattering. In this case, the EM impulses propagation can be considered a diffusion stochastic process. This is the Ornstein-Uhlenbeck dissipative stochastic process which is the solution to the Langevin equation $\partial \mathbf{r}(z)/dz = \nu \mathbf{r}(z) + u(z)$, where ν is the attenuation and $u(z)$ is the generating process. Here $u(z)$ is "white noise" [3].

The solution to equation (3) can be written as a path integral over every path starting at the points $\{\mathbf{r}_0\}$ of the plane $z = 0$ and finishing at the detection point of $(z = L, \mathbf{r}_L = \mathbf{0})$

$$\Gamma(z, \mathbf{r}, \eta) = \int d^2 \mathbf{r}_0 \langle z = 0, \mathbf{r}_0 | \exp \left(- \int_0^L |\mathbf{r}(z)|^2 dz \right) | z = L, \mathbf{0} \rangle. \quad (4)$$

The correlator $K_\eta(z, z')$ of the process $\mathbf{r}(z)$ is the following:

$$K_{\eta}(z, z') = g(z)\eta \exp(-\nu|z - z'|), \quad g(z) = \frac{\rho(z)\sigma_p}{8\nu c \alpha_p} \quad (5)$$

The required function $\Gamma(z, \mathbf{r}, \eta)$ has the form of

$$\Gamma(z, \mathbf{r}; \eta) = \exp(-\nu L) \prod_{k=1}^{\infty} (1 - \eta/\xi_k)^{-1}, \quad (6)$$

where $\{\xi_k\}$ is the set of the eigenvalues corresponding to the set of the solutions $\{f_k(z)\}$ of the integral equation

$$f(z) = \int_0^L K_{\eta}(z, z') f(z') dz'. \quad (7)$$

Solving the eigenvalue problem results in the following equation:

$$\Gamma(z = L, 0; \eta) = \frac{2\nu(r_0 + r_L)}{(r_0 + \nu)(r_L + \nu) \exp(R_{0,L}) - (r_0 - \nu)(r_L - \nu) \exp(-R_{0,L})}, \quad (8)$$

where

$$r_0 = \sqrt{\nu^2 + 2\eta\nu g(0)}, \quad r_L = \sqrt{\nu^2 + 2\eta\nu g(L)}, \quad R_{0,L} = \int_0^L \sqrt{\nu^2 + 2\eta\nu g(z)} dz \quad (8a)$$

Equations (2) and (8) are the general solution of the problem. Let us underline some regularities of the found Green function $G(t)$:

- a) all roots of (8) are simple;
- b) $G(0) \equiv 0$;
- c) function $G(t)$ is exponentially damped as $t \rightarrow \infty$;
- d) function $G(t)$ has the only maximum and two inflection points.

The above reveals the Laguerre property of the output time impulses. Quantitatively, those regularities can be expressed via low-order statistical moments of function $G(t)$.

Zero moment equals to

$$\langle 1 \rangle_L = \exp(-\nu L). \quad (9)$$

The higher moments we obtain considering $G(t)$ a distribution density. Time reference point being $t = T_1 = L/c$, the impulse center (its first moment) is as follows:

$$\langle t \rangle_L = \left(\int_0^{\infty} G(t) dt \right)^{-1} \int_0^{\infty} t G(t) dt = \int_0^L g(z) dz. \quad (10)$$

The impulse width $\sigma_L = \left(\langle t^2 \rangle_L - \langle t \rangle_L^2 \right)^{1/2}$ is defined by its standard deviation. With (8), we obtain the following dependence of its mean-square width:

$$\sigma_L^2 = -\frac{g(0)g(L)}{2\nu^2} (1 - \exp(-2\nu L)) + \frac{1}{\nu} \int_0^L g^2(z) dz. \quad (11)$$

If the initial impulse is σ_{in} wide, then the output impulse mean-square width is $\sigma_{out} = (\sigma_{in}^2 + \sigma_L^2)^{1/2}$.

We have carried out numerical experiments with (2) and (8) to check the found behavior of $I_{out}(t)$. In the experiments, there were two types of the density dependence $\rho(z)$ in (5). The first dependence $\rho_1(z) = const$ and the other $\rho_2(z)$ was chosen of Gaussian kind. The results of the experiments are given in figures 1 and 2. In the figures, the curves are represented in arbitrary units with the calculation parameters being picked out to show qualitative results.

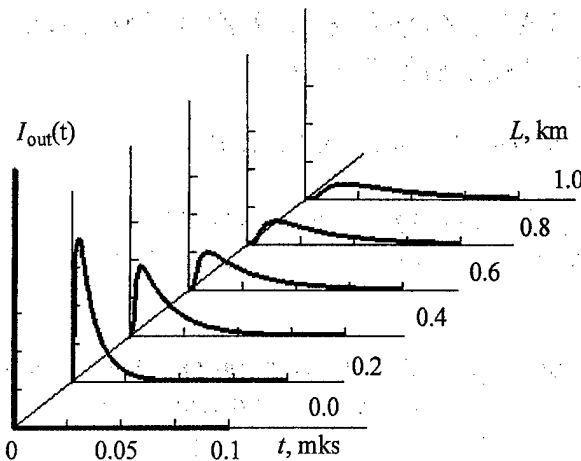


Figure 1. Output time impulse evolution for uniform density distribution.

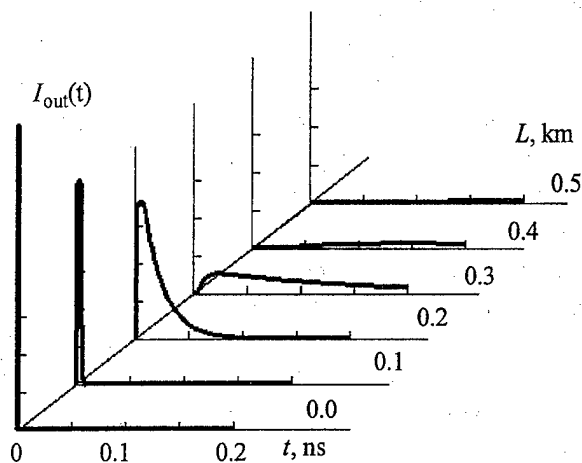


Figure 2. Output time impulse evolution for Gaussian-type density distribution.

and standard deviation. All the impulse time dependences obtained in the conducted numerical experiments behave similar to Laguerre-type curves.

Thus, we have shown that the approach utilized in Ishimaru's model to describe a time EM impulse shape behavior in homogeneous nondissipative scattering medium can be extended to inhomogeneous dissipative media. The model extension is based on Ornstein-Uhlenbeck dissipative stochastic process application. We have also found the explicit expression for the problem Green function. The time-dependent term of the found Green function is of Laguerre type for all the considered conditions.

Figure 1 shows the evolution of the output impulse for ρ_1 with the following parameters: $\nu = 10^{-3} m^{-1}$, $\sigma_p = 3 \cdot 10^{-10} m^2$; $\alpha_p = 3 \cdot 10^{-2}$; $\rho_1 = 10^4 m^{-3}$. As one can see, $I_{out}(t)$ steadily stretches as L increases.

Figure 2 shows the results obtained for Gaussian-type density distribution ρ_2 with the center at $L = 0.375$ km and the standard deviation of 0.1 km. All the calculation parameters are the same as in fig. 1 but $\nu = 10^{-6} m^{-1}$. In the figure, one can see that the impulse shape tracks the chosen density ρ_2 parameters values.

In particular, before the impulse runs into the scatterers, it keeps δ -like shape. The impulse noticeable stretching begins after it enters the central zone of the density distribution.

Also, both figures show that the stretching is accompanied by the impulse energy decrease.

In addition we have accomplished numerical experiments for different values of the parameters which influence the impulse shape, namely, the density distribution center location

1. Ishimaru A. *Theory and Application of Wave Propagation and Scattering in Random Media*. Proc. IEEE, **65**, 1030-1061 (1977).
2. Flatte S. M. *Wave Propagation Through Random Media: Contributions from Ocean Acoustics*. Proc. IEEE, **71**, 1267-1294 (1983).
3. Rytov S. N. *Introduction to statistical radiophysics* (in Russian). - Nauka, Moscow 1966.

SUCCESSIVE APPROACH AND NON-TRADITIONAL REGULARIZATION TO SPECTRAL PARAMETER ESTIMATION BY LEAST SQUARE METHOD

M. V. Andreev, V. F. Borulko, and O. O. Drobakhin

*Department of Radiophysics, Dnipropetrovsk State University
13 Nauchny pereulok, Dnipropetrovsk, 320050, Ukraine*

Abstract: Particularities of stable least square spectral parameter estimation technique with successive growing model order and adaptive regularization are considered. Advantages of novel approach are displayed by results of numerical simulation of complex reflection coefficient spectral analysis for the case of phase distortion due to signal propagation in waveguide.

INTRODUCTION

Spectral parameter estimation (SPE) methods are very powerful in various applications. The least square method (LSM) of SPE is more general and accurate but it consumes more computer resource. SPE methods can be used for layered structures, microwave component parameter measurements [1-3]. Peculiarity of this approach is spectral analysis of frequency domain data. Exponential model is supposed to be relevant. Successive algorithm of LSM has allowed us to take into account multiple reflections in the data and estimate an order of exponential model. This approach provides non-traditional regularization in the case of phase distortions and non-adequacy of model in the form of sum of exponentials. For example, the problems mentioned arise in experimental data processing by method [3] if the experimental data are obtained using waveguide with frequency dispersion and therefore phase distortion in the exponential model. All these facts induce splitting spectral components but the proposed non-traditional regularization overcomes this situation.

BASIC CONCEPTION

The method is based on searching the best values (minimum) of cost function (CF) ρ formed as square norm of difference between experimental \vec{R}_E and model \vec{R}_M discrete data

$$\rho = \|\vec{R}_E - \vec{R}_M\|_2^2 = \frac{1}{N} \sum_{n=1}^N \left| R_E(\omega_n) - \sum_{m=1}^M r_m \cdot \exp(-j\omega_n t_m) \right|^2, \quad (1)$$

where N is number of frequency points of observation (measurement); ω_n are frequencies of measurement; M is order of exponential model; r_m and t_m are parameters of exponential model. For arbitrary fixed t_m , minimizing ρ is equivalent to searching optimal projector P to space L_M spanned by vectors $\vec{e}_m = [\exp(-j\omega_n t_m)]_{n=1..N}$. Using $N \times M$ matrix F_M with columns \vec{e}_m , we obtain optimal projector as $P = FF^+$, where F^+ is Moore-Penrose inverse matrix. Using Hermitian and idempotent properties of P , cost function can be transformed to

$$\rho = \|\vec{R}_E\|^2 - (\vec{R}_E, P\vec{R}_E). \quad (2)$$

Minimization of CF (2) is equivalent to maximization of CF $\delta = (\bar{R}_E, P\bar{R}_E) = (\bar{R}_E, \bar{R}_M)$, where model is equal $\bar{R}_M = F\bar{r}$ (\bar{r} is vector of amplitudes), and this cost function is equal to

$$\delta = \frac{1}{N} \cdot \sum_{n=1}^N R_E^*(\omega_n) \cdot R_M(\omega_n). \quad (3)$$

Expression for cost function (3) is given by

$$\delta(t_1, t_2, \dots, t_M) = \sum_{k,m=1}^M (-1)^{k+m} \cdot G_k \cdot G_m^* \cdot \frac{\det H_{km}}{\det H}, \quad (4)$$

where $H = F^H F$ is Gram matrix in basis \bar{e}_m , H_{km} is matrix H without row k and column m , G_k is Fourier transform (FT) of \bar{R}_E in point t_k . For the most simple case $M=1$ cost function is $\delta(t_1) = |G_1|^2$. Thus, the maximum of cost function (3) coincides with maximum of Fourier transform modulus.

Successive algorithm is based on block structure of matrix H_M (Gram matrix of M -th model order). For the M -th model order CF may be calculated recurrently using parameters estimated for the $(M-1)$ -th order one according to

$$\rho_M = \rho_{M-1} - |\Delta G_M|^2 / d_M, \quad (5)$$

where $\Delta G_M = G_M - \bar{h}_{M-1}^H H_{M-1}^{-1} \bar{g}_{M-1}$ is time difference signal in point t_M ; $d_M = 1 - \bar{h}_{M-1}^H \cdot H_{M-1}^{-1} \cdot \bar{h}_{M-1}$; $G_M = (\bar{e}_M, \bar{R}_E)$ is value of FT in point t_M ; $\bar{h}_{M-1} = [(\bar{e}_M, \bar{e}_k)]_{k=1..M-1}$; \bar{g}_{M-1} is vector with samples of time signal for t_1, t_2, \dots, t_{M-1} . Complex amplitude of the M -th component is equal to $r_M = \Delta G_M / d_M$. The process of model order increasing must be interrupted, taking into account assumed noise level, ρ_{M-1} and ρ_M . The procedure discussed above permits the model order to be determined. This problem is very important for components situated closely.

In the last case it is necessary to use a regularization to avoid computing problem. The traditional Tikhonov's regularization in form $\rho^\alpha = \|\bar{R}_E - F\bar{r}\|_2^2 + \alpha \|\bar{r}\|_2^2$ with regularization parameter α induces following expressions in proposed algorithm

$$d_M^\alpha = d_M + \alpha \quad (\text{for } M=1: d_1^\alpha = 1 + \alpha, H_1^{-1\alpha} = 1/(1 + \alpha)). \quad (6)$$

This regularization reduces standard deviation of the estimates. But it requires to determine optimal value of the regularization parameter α . The novel algorithm provides a non-traditional regularization by introduction of regularization parameter

$$\alpha = \left| \rho_{M-1} - |\Delta G_M|^2 / d_M \right| \text{ in } d_M \text{ according to}$$

$$d_M^\alpha = d_M + \alpha / d_M \quad (\text{for } M=1: d_1^\alpha = 1 + \alpha, H_1^{-1\alpha} = 1/(1 + \alpha)). \quad (7)$$

The regularization protects from splitting estimated parameters, what happens inevitably under conditions of Tikhonov's regularization.

For the novel algorithm the model order is being increased successively. This mean protects from estimation of additional noise spectral components. This regularization protects partially from splitting of true components. If components are situated very closely, the amplitude r_m of one of them will become approximately equal zero.

If two spectral peaks after FT are overlapping and forming single common peak, the following technique is used. After FT and estimation of single peak parameters the model data with estimated parameters are subtracted from frequency-domain signal. Parameters of two maximum peaks of residue are used as initial guesses of optimization procedure. If amplitudes of latter peaks are lower than noise level the decision of presence of only single peak are taken.

NUMERICAL SIMULATION RESULTS

Testing the method was carried out for data those are corresponded to measurements of complex reflection coefficient of metal plates, located in distance 31 sm from reference plane (in frequency band $21 \div 41$ GHz, $N=101$). This distance consists of rectangular waveguide with cross-section 7.2×3.4 mm and length 25 sm and 6 sm in free space. LSM method with $M=2$ without regularization gives merge of estimated locations ($t_1=t_2$) and significant growth of estimated amplitudes ($r_1=38.6$; $r_2=37.6$). In this situation the traditional Tikhonov's regularization caused splitting estimated peaks ($r_1=0.5$; $r_2=0.5$). The novel regularization has given physically reasonable estimates of peaks amplitudes ($r_1=1.0$; $r_2=0.0$).

Numerical research of the best value of regularization parameter in form (6) was carried out for case $t_1=0.20$, $t_2=0.25$, $f_1=-1$, $f_N=1$, $N=101$ and unit amplitudes in presence of noise with standard deviation $\sigma=10^{-3}$. In absence of regularization ($\alpha=0$) mean square error (MSE), defined as a sum of displacement and standard deviation, was $6.1 \cdot 10^{-3}$ (for generalized pencil-of-function method (GPOFM) [4] it was $7.9 \cdot 10^{-3}$). Optimal value $\alpha=10^{-5}$ has reduced MSE in almost 50 times. It was $1.7 \cdot 10^{-4}$, thus the displacement of the estimates has decreased on 2 order, that shows necessity of use of a regularization in LSM to receive significant advantage above GPOFM. The mentioned researches were carried out for different levels of noise in the data. For $\sigma=8 \cdot 10^{-3}$ without regularization ($\alpha=0$) MSE was $6.0 \cdot 10^{-2}$, for found optimal value $\alpha=1.5 \cdot 10^{-4}$ it was $1.4 \cdot 10^{-3}$. For $\sigma=1 \cdot 10^{-4}$ without regularization ($\alpha=0$) MSE was $6.0 \cdot 10^{-4}$, for found optimal value $\alpha=5 \cdot 10^{-6}$ it was $2.1 \cdot 10^{-5}$.

REFERENCES

- [1] H.Vanhamme, "High resolution frequency-domain reflectometry", *IEEE Trans. Instrumentation and Measurement*, Vol. IM-39, No. 2, Apr.1990, pp.369-375.
- [2] E.A.Robinson, "Spectral Approach to Geophysical Inversion by Lorentz, Fourier, and Radon Transforms", *Proc. IEEE*, Vol. 70, No. 9, Sept. 1982, pp. 1039-1054.
- [3] M.V.Andreev, V.F.Borulko, O.O.Drobakhin, "One-dimensional Inverse Problem Solution for Multilayered Dielectric Structures Using Least-Square Spectral Estimation Method", *Proc. of the 1995 URSI Int. Symp. on Electromagnetic Theory*, St.Petersburg, Russia, May 23-26, 1995, pp. 148-151.
- [4] Y.Hua, T.K.Sarkar, "Generalized Pencil-of-Function Method for Extracting Poles of an EM System from Its Transient Response", *IEEE Trans. Antennas and Propag*, Vol. AP-37, No. 2, Feb. 1989, p. 229-233.

ANALYSIS OF MUELLER MATRIX ELEMENTS MEASUREMENT ERROR INFLUENCE ON ITS PHYSICAL REALISABILITY.

Konstantin E. Yushtin, Sergey N. Savenkov,

Radiophysics dept., Kiev Taras Shevchenko Univ., Vladimirska 64, Kiev, 252017, Ukraine

e-mail : sns@boy.rpd.univ.kiev.ua.

Abstract

The one of the main aspect of the Mueller matrix measurement is the aspect of physical realisability of the Mueller matrix. Condition for the physical realisability of Mueller matrices is the transformation Poincare sphere of the probing radiation to the Poincare sphere of output radiation. In practice, it means, that polarization degree of output radiation must be in range from 0 to 1 for any polarization state of probing radiation. But there can be the situation, when experimentally measured Mueller matrix may give us polarization degree of output radiation more than 1, so, unrealizable Stokes vector. Such Mueller matrix is called physically unrealizable. But, in practice, the availability of measurement error may cause situation, when experimental (properly measured) Mueller matrix of real object is physically unrealizable. Thus, conditions of physical realisability, taking into account Mueller matrix elements measurement error, are obtained.

Introduction

Methods, based on studying of changes of polarization state of electromagnetic radiation after reflection, scattering or transition through the object, are called polarization methods. Last time, polarization methods played very important role in the studying and analysis of different anisotropy objects. The explanation of this is in the great increasing of information, taken about the investigating object.

The electromagnetic radiation can be presented by the Stokes vector S in the following form [1]:

$$S = (I, Q, U, V)^T \quad (1)$$

This presentation contains information about polarization state of electromagnetic radiation, including depolarization. Polarization degree of electromagnetic radiation can be calculated by next formulae [1]:

$$P = \frac{\sqrt{Q^2 + U^2 + V^2}}{I} \quad (2)$$

where Q, U, V, I - are the component of output Stokes vector.

For any possible electromagnetic radiation, polarization degree must be in range 0..1. If this condition doesn't fulfilled, then the Stokes vector is physically unrealizable. All physically realizable polarization state may be geometrically presented using equation of the sphere:

$$x^2 + y^2 + z^2 \leq R^2 \quad (3)$$

and point, defined by there component (Q, U, V) of the Stokes vector must be in the sphere with radius I - it is condition for the physical realisability of the Stokes vector [2]. This sphere is called Poincare sphere of polarization state of the radiation [1].

The linear interaction of probing radiation with the investigated object (interaction without change of radiation frequency), can be fully expressed by Mueller matrix 4x4 of real elements, which transforms Stokes vector of polarization state of probing radiation into output Stokes vector of output electromagnetic radiation. In case of linear interaction, Mueller matrix contains all possible information of anisotropy properties of the object [1].

Mueller matrix formalism was suggested in 1948, but, for today, the question of physically unrealizable Mueller matrix does not solved completely. There was some attempts to analyze experimentally obtained Mueller matrices, but there pays no attention to measurement error influence [2,3,4]. If, for any reason, there is one state of probing radiation, for polarization degree of output electromagnetic radiation is more than 1, then this Mueller matrix is physically unreliable [1-4].

As example, let us consider the ideal polarizator - polarization degree of output radiation is 1 for all polarization states of probing radiation. In case of measurement error presence, it is the typical situation when

after model probing of experimental Mueller matrix by fully polarized radiation we can obtain output polarization degree more than 1, so, this Mueller matrix must be physically unreliable.

This is only one evidence of imperfection of definition physical unreliability. So, the goal of this work is to present inequation, defining physically realizable objects and taking into account measurement error. Another task, which is solved in this work, is the estimation of the measurement error, with which experimentally obtained Mueller matrix is physically realizable.

For all these purposes we have given correspondent analytical expressions

Theory

The one of the most exploited methods is the methods of the model probing. In this method, we analyze Mueller matrix by the virtual (mathematical) probing by radiation with any possible polarization states. This method may give us anisotropic characteristic of the object. The question of physical realisability of made measurements is also the question of correctness of the measurement method. For today, measurement error presence make it impossible to make conclusion about its physical reality. At present time, the simplest way is to say, that if there is a polarization state of probing radiation, for which output Stokes vector is physically unrealizable, then, this Mueller matrix is physically unreliable [1-4]

So, let us consider arbitrary Mueller matrix :

$$M = \begin{bmatrix} M_{11} & M_{12} & M_{13} & M_{14} \\ M_{21} & M_{22} & M_{23} & M_{24} \\ M_{31} & M_{32} & M_{33} & M_{34} \\ M_{41} & M_{42} & M_{43} & M_{44} \end{bmatrix} \quad (4)$$

We shall analyze output polarization degree, so we will use model probing by fully polarized radiation. It is known, that the Stokes vector of fully polarized electromagnetic radiation can expressed in the following form :

$$S = \begin{bmatrix} 1 \\ \cos(2 \cdot \theta) \cdot \cos(2 \cdot \varepsilon) \\ \sin(2 \cdot \theta) \cdot \cos(2 \cdot \varepsilon) \\ \sin(2 \cdot \varepsilon) \end{bmatrix} \quad (5)$$

where θ is azimuth of ellipse polarization, ε is the ellipticity of polarization state.

It is obvious, that for some polarization state of probing radiation the measurement error influence may provide the polarization degree more than 1. And now the task is to calculate divergence of polarization degree, caused by the measurement error.

We have found expressions for maximum output polarization degree independent of input polarization state. Considering it as the function of 16 variables, we have expanded it into Taylor series by measurement error and taken linear estimation. It is quite physically substantiated, because quadratic error dependence is neglectively less [5].

Let the measurement error of Mueller matrix element be δ , then we can write conditions for the physical realisability of the object in the following way:

$$\begin{aligned} \sum_{k=2}^4 (M_{k,1} + M_{k,4})^2 - (M_{11} + M_{14})^2 &\leq \sum_{k=1}^4 |M_{k,1} + M_{k,4}| \cdot \delta \\ \sum_{k=2}^4 (M_{k,1} - M_{k,4})^2 - (M_{11} - M_{14})^2 &\leq \sum_{k=1}^4 |M_{k,1} - M_{k,4}| \cdot \delta \\ \sum_{k=2}^4 (M_{k,1} + M_{k,3})^2 - (M_{11} + M_{13})^2 &\leq \sum_{k=1}^4 |M_{k,1} + M_{k,3}| \cdot \delta \\ \sum_{k=2}^4 (M_{k,1} - M_{k,3})^2 - (M_{11} - M_{13})^2 &\leq \sum_{k=1}^4 |M_{k,1} - M_{k,3}| \cdot \delta \end{aligned} \quad (7)$$

$$\begin{aligned}
\sum_{k=2}^4 (M_{k,1} + M_{k,2})^2 - (M_{11} + M_{12})^2 &\leq \sum_{k=1}^4 |M_{k,1} + M_{k,2}| \cdot \delta \\
\sum_{k=2}^4 (M_{k,1} - M_{k,2})^2 - (M_{11} - M_{12})^2 &\leq \sum_{k=1}^4 |M_{k,1} - M_{k,2}| \cdot \delta \\
\sum_{k=2}^4 M_{k,2} \cdot M_{k,3} - M_{12} \cdot M_{13} &\leq \sum_{k=1}^4 (|M_{k,2}| + |M_{k,3}|) \cdot \delta \\
\sum_{k=2}^4 M_{k,2} \cdot M_{k,4} - M_{12} \cdot M_{14} &\leq \sum_{k=1}^4 (|M_{k,2}| + |M_{k,4}|) \cdot \delta \\
M_{12}^2 + M_{13}^2 + M_{14}^2 - M_{11}^2 &\leq \sum_{k=1}^4 |M_{1,k}| \cdot \delta
\end{aligned}$$

We can test the execution of inequalities (7) and make conclusion about its physical realisability, basing on the standard device measurement error. So, if Mueller matrix of the object satisfies this conditions then we have all reason to claim that it is physically realizable.

From other hand, we can also find the least measurement error δ , for which conditions (7) are fulfilled, so, we can make estimation of Mueller matrix measurement error, basing on experimentally measured Mueller matrix.

Conclusions

For example, let's consider one simple example - experimentally measured Mueller matrix of the empty space:

$$\begin{bmatrix}
1 & -0.0104 & -0.0234 & -0.0057 \\
0.0035 & 1.0123 & 0.0161 & 0.0015 \\
-0.0030 & -0.0096 & 0.9879 & -0.0049 \\
-0.0049 & -0.0037 & -0.0128 & 0.9995
\end{bmatrix} \quad (8)$$

It is evident, that this matrix is physically unrealizable by [1-4], but we have made proper measurement (!) [5-6]. At the same time, the conditions (7) are fulfilled for standard device measurement error $\delta = 0.03$. And this is typical error for our Mueller polarimeter, and this Mueller matrix is physically realizable with measurement error $\delta \geq 0.015$.

So, we have presented inequations, characterizing physically realizable Mueller matrices, measured with measurement error δ .

We can also estimate 9 measurement errors to fulfil each inequation from (7). The maximal of these measurement errors will be taken as a least measurement error, with which this Mueller matrix can be physically realizable.

References

1. M.Born, E.Wolf, "Principles of optics", Oxford, 1968, 719 p.
2. R.Simon "Nondepolarizing systems and degree of polarization", Optics Communications, 77 (1990), 5-6, p.349-354.
3. M.Sanjay Kumar and R.Simon "Characterization of Mueller matrices in polarizaion optics", Optics Communications, 88(1992),4-6, p.464-470.
4. R.Barakat "Condition for the physical realizability of polarization matrices characterizing passive systems", Journal of modern optics, 34, 1535-1544 (1987).
5. S.N.Savenkov, K.E.Yushtin, B.M.Kolisnychenko, Y.A.Skoblya "The influence of dynamic Mueller-polarimeter parameters upon the error of the measured results", SPIE Proc. 32, Vol. 3199, paper № 32.
6. Kolisnichenko B.N., Savenkov S.N., Marienko V.V. Real time polarization laserous diagnostic system. SPIE Vol. 2329-21.-1994.

TWO-STAGE APPROACH TO IMAGE COMPRESSION USING WAVELET AND PIECEWISE-LINEAR TRANSFORMS

Dorota Biela-Wiraszka

Kielce University of Technology, Department of Electronics and Telecommunication
Aleja Tysi¹clecia PP 7, 25-314 Kielce, Poland
e-mail: ketdb@eden.tu.kielce.pl

1. Introduction

In contemporary world the information presented in the form of image becomes more and more popular. Systems like Windows or WWW use this way of presentation for most applications. In the other hand, transmitting and storing huge files containing image data require enormous memory size and broadband communication. Thus, seeking new methods of image compression is still well appreciated. In the paper a new approach to image compression, using Wavelet and Piecewise-Linear Transforms is presented.

2. The Transformations

2.1. One-Dimensional Case

For a discrete signal $x(n)$, $n = 0, 1, 2, \dots, N-1$ any discrete transform, mapping the signal from the original domain to the transform domain can be given in the form of the generalised Fourier series [1,8,13,17]:

$$x(n) = \sum_{i=0}^{N-1} c_i \cdot \varphi_i(n) \quad n = 0, 1, 2, \dots, N-1 \quad (1)$$

where:

- c_i - coefficients of the expansion (spectrum);
- $\varphi_i(n)$ - set of the basis functions, constituting the transformation kernel.

The expansion coefficients are defined by the following:

$$c_i = \frac{1}{q_i} \sum_{n=0}^{N-1} x(n) \cdot \varphi_i(n) \quad n = 0, 1, 2, \dots, N-1 \quad (2)$$

where q_i - normalising coefficients, depending on the type of transformation.

The above equations define a pair of transformations: forward (2) and inverse (1). In order to obtain the required type of transformation, appropriate basis functions must be used in (1) and (2). Specific cases of the Wavelet and PWL Transforms are presented below.

a) The Wavelet Transform

The Discrete Wavelet Transform is defined according to (1) and (2), when the basis functions $\varphi_i(n)$ are chosen to be the discrete basis wavelets [3,4,7,10,15]:

$$h_{i,k}(n) = a_0^{-\frac{i}{2}} \cdot h(a_0^{-i} \cdot n - k) \quad (3)$$

where: i - scale coefficient, k - translation coefficient.

The discrete basis functions are scaled and translated versions of the basic wavelet, given by the following equation:

$$h_i(n) = \frac{1}{\sqrt{i}} h\left(\frac{n}{i}\right) \quad (4)$$

The shape of the basic wavelet can be chosen dependently on the application. Among many proposed functions particularly the Daubechies wavelets are well appreciated, because of their fractal character and compact support. [3,4,15]

The normalising coefficient in (2) is constant and independent on the analysed signal.

b) The PWL Transform

The PWL (Periodic Walsh Piecewise-Linear) Transform is defined according to (1) and (2) with the basis functions chosen as the discrete PWL functions [5,6,12,13,14]:

$$\varphi_i(n) = PWL_i(n) \quad (5)$$

where $PWL_i(n)$ - set of discrete PWL functions defined as the result of integrating the Walsh functions and supplementing the obtained set of functions with the constant function $PWL_0(n) = 1$. [13,14]

The normalising coefficients in (2) are given by (6):

$$q_i = -\frac{1}{2^{k+1}} \quad (6)$$

where k - index of PWL group, $k = 1, 2, \dots, \log_2 N$.

2.2. Two-Dimensional Case

Expansion of the above transformations into two-dimensional case is derived straight from the one-dimensional case. The transforms described above are applied to rows and columns of the analysed two-dimensional signal, i.e. the image. Detailed description can be found in [13].

3. The compression algorithm

For effective compression performance an image of a given class is first modelled by the compression algorithm to generate some intermediate representation of image depending on the chosen method of compression. The attention has been concentrated on the step of modelling, where the two-stage transformation is used to generate the intermediate representation of the image.

First, the original image is wavelet transformed to obtain a pre-intermediate representation, consisting of four subimages (see Fig.1b), being the result of spatial low-pass and high-pass filtering. At this stage the zonal sampling is performed and only the low-pass filtered subimage is kept.

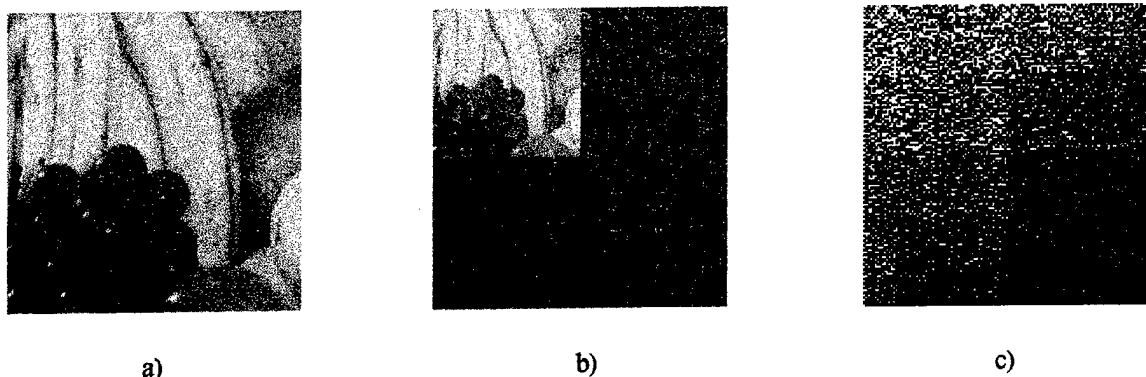


Fig.1. Examples of a) original image, b) Wavelet Transform of the original, c) PWL Transform of the selected zone

Second, the pre-compressed image is PWL transformed, what produces the PWL spectrum of the former representation (see Fig.1c). Then the threshold compression is performed and the final intermediate representation of the image is obtained.

Reconstruction of the original image requires similar two-stage decompression process. First, the Inverse PWL Transform is calculated, and then the intermediate reconstruction is transformed by the Inverse Wavelet Transform.

4. Results of experiments

The above compression algorithm has been applied to a set of typical test images. The distortion of the reconstructed image is measured in terms of classical criteria: mean square error (MSE) and Peak Signal-To-Noise-Ratio (PSNR), defined by (6) and (7), respectively.

$$MSE(I, \tilde{I}) = \frac{1}{M \cdot N} \sum_{i=0}^{M-1} \sum_{j=0}^{N-1} (I(i, j) - \tilde{I}(i, j))^2 \quad (6)$$

$$PSNR(I, \tilde{I}) = 10 \log_{10} \frac{255^2}{MSE(I, \tilde{I})} \text{ [dB]} \quad (7)$$

where:

I, \tilde{I} - original and reconstructed image, respectively;

M, N - number of rows and columns in the original and reconstructed image.

Some results of application of the two-stage compression are presented in Fig.2.

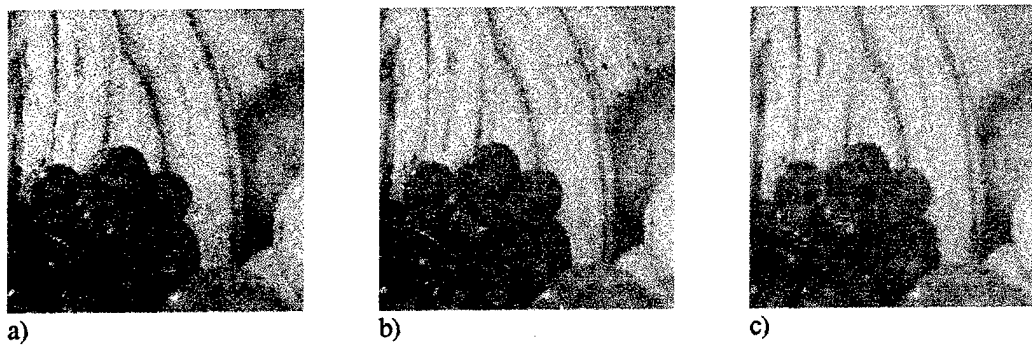


Fig.2. Two-stage compression versus various threshold values p : a) $p = 0.01$, b) $p = 0.1$, c) $p = 1$.

On the base of subjective visual evaluation we can state that the results obtained for $p = 0.01$ and $p = 0.1$ are acceptable. Significant distortion can be noticed for $p = 1$.

The comparison of compression results for different types of images is depicted in Fig.3.

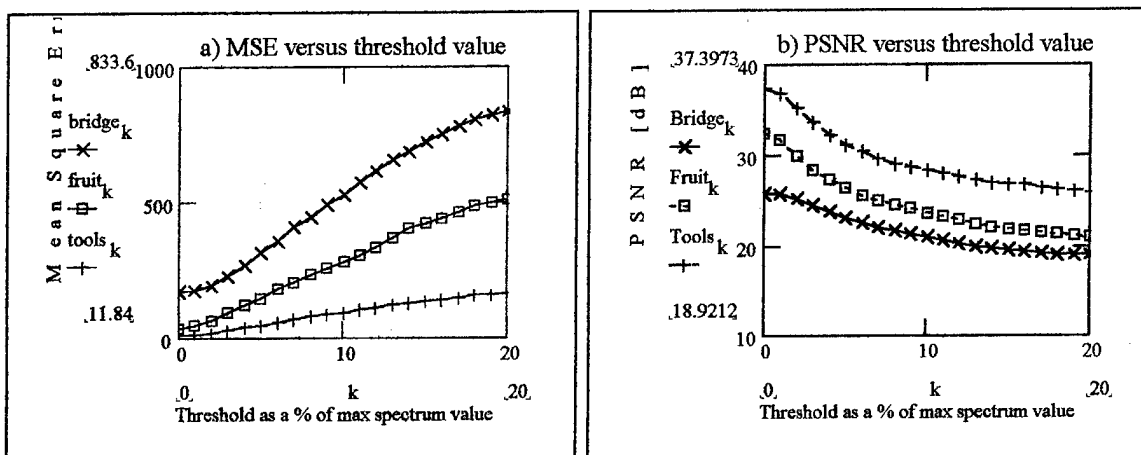


Fig.3. a) MSE versus threshold value, b) PSNR versus threshold value

We can state that both coefficients, as MSE and PSNR strongly depend on the type of image. They get better values for images containing few details (example: *Tools*) than for images with many details (example:

Bridge). In general, both MSE and PSNR are acceptable for threshold values not exceeding about 5% maximum value of the spectrum coefficients.

4. Conclusions

The proposed approach to image compression applies two types of transformations, which combine different methods of compression. During the first stage the Wavelet Transform produces a special representation of the image, containing in particular a subimage being a result of spatial low-pass filtering. Thanks to the zonal compression scheme only this subimage is forwarded to further processing. At the second stage the PWL Transform gives the PWL spectrum, which is then compressed by the threshold compression scheme. Considering the computational and visual results we can state that the proposed scheme is effective, but strongly dependent on the type of processed image. Thus looking for a relation defining types of images predestined for such a two-stage compression remains the subject of further research.

References:

1. Ahmed N., Rao K., "Orthogonal Transforms for Digital Signal Processing", Springer-Verlag, N.Y. 1975.
2. Biela-Wiraszka D., Chodorek R., "Zastosowanie dwuwymiarowych przekształceń odcinkowo-liniowych w kompresji obrazów", Proc. of "Współpraca badawcza Politechniki Świętokrzyskiej z krajowymi i zagranicznymi ośrodkami naukowymi i przemysłowymi", Kielce 1995.
3. Chui C. K., "An Introduction to Wavelets", Academic Press, New York 1992.
4. Daubechies I., "Ten Lectures on Wavelets", SIAM, Philadelphia, Pennsylvania 1992.
5. Dziech A., Biela-Wiraszka D., "Problemy kompresji danych a jakość aproksymacji obrazów z zastosowaniem dwuwymiarowych przekształceń odcinkowo-liniowych", Proc. of KST, Bydgoszcz 1995.
6. Dziech A., Pardyka I., Biela-Wiraszka D., Chodorek R., "Zagadnienia kompresji i aproksymacji obrazów z zastosowaniem dwuwymiarowych przekształceń odcinkowo-stałych i odcinkowo-liniowych", Proc. of "Przetwarzanie Sygnałów'93", Poznań 1993.
7. Dziech W., Biela-Wiraszka D., "Problemy kompresji sygnałów z zastosowaniem transformaty falkowej", Proc. of KST, Bydgoszcz 1997.
8. Elliot D. F., Rao K. R., "Fast Transforms - Algorithms, Analyses, Applications", Academic Press, New York 1982.
9. Haar A., "Zur Theorie der orthogonalen Funktionen-Systeme", Math. Ann., 69, 1910.
10. Mallat S. G., "A Theory for Multiresolution Signal Decomposition: The Wavelet Representation", IEEE Trans. on Pattern Analysis and Machine Intelligence, Vol. 11, No 7, July 1989.
11. Pardyka I., Biela-Wiraszka D., Ślusarczyk P., Baran R., "Problemy kompresji obrazów z wykorzystaniem dwuwymiarowego przekształcenia odcinkowo-liniowego HPL", Proc. of KST, Bydgoszcz 1997.
12. Pardyka I., Chodorek R., Biela D., "Problemy aproksymacji obrazów z zastosowaniem dwuwymiarowych przekształceń PWL", Proc. of KST, Bydgoszcz 1992.
13. Pardyka I., Biela-Wiraszka D., Ślusarczyk P., Baran R., "Image Compression Using Piecewise-Linear Transforms", Proc. of XX KKTOiUE, Kołobrzeg 1997.
14. Pardyka I., Smolewski I., "Piecewise-Linear Transforms", Final Report of the Individual Fellowship within EEC, Wuppertal 1993.
15. Rioul O., Vetterli M., "Wavelets and Signal Processing", IEEE SP Magazine, October 1991.
16. Rosenfeld A., Kak A. C., "Digital Picture Processing", Academic Press, New York, San Francisco, London 1976.
17. Skarbek W., "Metody prezentacji obrazów cyfrowych", Akademicka Oficyna Wydawnicza PLJ, Warszawa 1993.

REGULARIZATION OF DATA PROCESSING IN SIX-PORT REFLECTOMETRY

O.O.Drobakhin

*Radiophysics Dept., Dniepropetrovsk State University,
13 Nauchny pereulok, Dniepropetrovsk, 320050 Ukraine*

Abstract: Six-port data processing on base of holographic technique with three reference signals and corresponding means of generalized residual formalizes regularization are discussed.

INTRODUCTION

Now traditional way of complex reflection and transmission coefficient determination is use of vector analyzer in form of six-port reflectometer or four-port reflectometer with different successive loads that are utilized as source of reference signals. The four-port reflectometer is an ordinary phase-meter with two summers, traditional realization of which is use of magic T. Usually simultaneous solution of three quadratic equations is searched. For non-linear problems, it is difficult to realize traditional ways of regularization. But both reflectometers realize holographic approach with three reference signals [1], thus special system of linear equation can be formed. This fact opens perspectives of the use of Tikhonov's regularization.

In differ from the traditional approaches, six-port analyzer on base of E-plane cross-junction of standard rectangular waveguides has been developed [2]. This device divides the input power in four approximately equal parts. Simultaneously it serves for summation of a signal under test with three reference signals obtained by dividing the input signal.

Peculiarity of use of the cross-junction is an opportunity to evaluate scattering matrix elements with use of rigorous electrodynamic methods. The cross-junction has rather smooth frequency characteristics in whole work band of rectangular waveguide.

HOLOGRAPHIC METHODS WITH THREE REFERENCE SIGNALS

E-plane cross-junction of standard rectangular waveguides is used as the basic element of six-port analyzer [2]. The cross-junction is described with scattering matrix S_{ij} . Using clockwise numbering of ports we assume that input port is port 1 then port 4 is port for attachment of standards and loads under test. The system transforms into ill-posed system by the use of port 3 to attach load. From symmetry of the device, $S_{21} = S_{41} = S_{14} = S_{12} = S_{34} = S_{32}$ follows. Matched power meters are connected to ports 1,2,3. Directional detectors are used as matched power meters, which measure voltages $U_{1,2,3}$ proportional to corresponding powers $P_{1,2,3}$ in ports 1,2,3. Additionally directional detector for input power P_0 measurement is connected to port 1. Multiple reflections between device under test and transducer was taken into account by new variable A_4 , which is bilinear transform of reflection coefficient $A_4 = \Gamma S_{41} / (1 - \Gamma S_{44}) = A'_4 + jA''_4$.

According to the technique [1] of processing in the holography with three reference signals the following system of two linear equations have to be solved

$$Ba = q, \quad a = \begin{bmatrix} A'_4 \\ A''_4 \end{bmatrix}, \quad q = \begin{bmatrix} q_{mn} / 2 \\ q_{kl} / 2 \end{bmatrix}, \quad (1)$$

where B is matrix with elements $B_{11} = \text{Re}(S_{m1}^* S_{m4}) |S_{n4}|^2 - \text{Re}(S_{n1}^* S_{n4}) |S_{m4}|^2$, $B_{12} = \text{Im}(S_{m1}^* S_{m4}) |S_{n4}|^2 - \text{Im}(S_{n1}^* S_{n4}) |S_{m4}|^2$, $B_{21} = \text{Re}(S_{k1}^* S_{k4}) |S_{l4}|^2 - \text{Re}(S_{l1}^* S_{l4}) |S_{k4}|^2$, $B_{22} = \text{Im}(S_{k1}^* S_{k4}) |S_{l4}|^2 - \text{Im}(S_{l1}^* S_{l4}) |S_{k4}|^2$.

Values q_{mn} , which determine elements of the vector \mathbf{q} , equals to

$$q_{mn} = (p_m - p_{0m}) |S_{n4}|^2 - (p_n - p_{0n}) |S_{m4}|^2 \quad (2)$$

with $p_0 = |S_{11}|^2$ and $p_i = |S_{Li1}|^2 U_{c0} U_i / (U_{ci} U_0)$, where S_{Li1} is equal to $S_{11} + S_{i4} S_{11} \Gamma_c / (1 - S_{11} \Gamma_c)$. Γ_c is a calibrating standard reflection coefficient, U_{c0} and U_0 are the voltages of input power under calibration and measurement correspondingly, U_{ci} and U_i are voltages being measured in cross-junction ports under calibration and measurement correspondingly. In differ from the scheme of processing [1] for our case it is necessary to multiply the first term in (2) on $|S_{n4}|^2$, and the second term in (2) on $|S_{m4}|^2$.

REGULARIZATION PROCEDURE

Holographic processing [1] replaces three quadratic equations to linear algebraic system. Thus, the standard Tikhonov's regularization [5] for linear system can be used

$$(B^T B + \alpha I) \mathbf{a} = B^T \mathbf{q}. \quad (3)$$

Numerical experiment has shown, that the solution of (3) with $\alpha = 0$ coincides with the solution obtained according to the method of radical center with accurate to calculation error. Principle of generalized discrepancy demands to estimate norm of difference of rigorous operator and its approximation. That is rather difficult. According the generalized discrepancy principle of regularization parameter depends on solution norm. We practically determined regularization parameter from best value for standard load with reflection coefficient that was approximately equal to reflection coefficient of load under test.

Principle of generalized residual formalizes regularization parameter α searching as the root of equation

$$\|B\mathbf{a}^\alpha - \mathbf{q}\|^2 = (\delta + h \|\mathbf{a}^\alpha\|)^2 + \mu^2, \quad (4)$$

where δ is measure of error in \mathbf{q} , $h = \|B - B_r\|$, and B_r is rigorous operator, $\mu = \inf \|B\mathbf{a} - \mathbf{q}\|$ is measure of inconsistency. Values δ , h , μ can be determined by calibration procedure with three standard loads. It is very important that according to (5) α depends on value of A_4 , thus α is function of load reflection coefficient.

Unfortunately A_4 substantially depends from value of Γ . Variation of the phase of Γ from 0° to 360° with step 20° have showed that $|A_4|$ has changed in ~ 2.5 times for $|\Gamma|=1$, in 1.5 times for $|\Gamma|=0.5$ and only in ~ 1.2 and 1.09 times for $|\Gamma|$ equal to 0.2 and 0.1 correspondingly. Thus, choosing α for standard loads with rather small RC allows us to determine optimal value, for large values of $|\Gamma|$ the approach is failure. This fact explains that α optimal for $|\Gamma| \approx 0.2$ have given accurate result for $|\Gamma| \approx 0.1$ and vice versa. But utilization of α optimal for metallic plate has not been successful for sliding short circuit piston.

CONCLUSIONS

The traditional variants of six-port reflectometer has direct links Γ and solution of linear algebraic system therefore The proposed approach is more perspective in this case.

REFERENCES

- [1] Bates, R.H.T., M.J.McDonnel. "Image Restoration and Reconstruction," Clarendon Press, Oxford, 1986.
- [2] Drobakhin, O.O., V.F.Borulko, and V.A.Karlov, " Millimeter Apparatus for Transmission Line and Dielectric Material Measurements by Multifrequency Methods," CPDM-96 Conference Digest, Germany, Braunschweig, pp. 598-599.

ON THE ONE-TO-ONE CORRESPONDENCE OF MUELLER AND JONES MATRIX FORMALISMS UNDER NATURAL CONDITIONS.

Sergey N. Savenkov, Konstantin E. Yushtin, Borys M. Kolisnychenko, Yuri A. Skoblya
Radiophysics dept., Kiev Taras Shevchenko Univ., Vladimirska 64, Kiev, 252017, Ukraine
e-mail : sns@boy.rpd.univ.kiev.ua

Abstract

It is known, there is a reciprocal correspondence between deterministic Mueller matrices and matrices of the Jones for nondepolarizing objects. However, in practice, it is mostly failed to define a matrix of the Jones corresponding an experimental Mueller matrix of deterministic object. The reason of such situation is a presence of experimental errors of Mueller matrix measurements. In the paper the method of finding of a deterministic Mueller matrix closest to initial experimental matrix is offered and for which the correspondent Jones matrix can be found. The measurement error influence on a possibility of transformation of the measured Mueller matrix to a Jones one for consequent detail analysis is investigated. The correspondent analytical expressions of transfer of experimental Mueller matrix in a Jones matrix are presented.

Introduction

Recently polarization methods of studying different complex object attract many attention. This is chiefly concerned with the fact, that polarization methods are giving all possible information in the case of linear EM radiation/object interaction.

It is known, that single monochromatic electromagnetic radiation can be completely represented by the Maxwell vector (also known as Jones vector) in the following form :

$$E = (E_x, E_y)^T \quad (1.1)$$

where E_x and E_y are the electric vector components of the monochromatic electromagnetic radiation.

It is known, that electromagnetic radiation can be also presented by fourcomponent Stokes vector in the following form, where all components have the units of intensity :

$$S = (I, Q, U, V)^T \quad (1.2)$$

Presentation by Stokes vector is much useful and complete, because it is contained information about depolarization, absent in case of presentation by Jones vector.

In case of scattering radiation depolarization absence, the linear interaction of probing radiation with studied object (the interaction without change of electromagnetic radiation frequency), can be fully described by using Jones matrix [1]. This matrix is 2x2 of complex elements. In case of existing scattering radiation depolarization, Jones matrix formalism cannot be used. Such linear interaction of probing radiation with studied object can be fully described by using of Mueller matrix (the most common case), 4x4 matrix with real elements.

In practice, Mueller matrix is measured the most often, because , at first, it contains information of depolarization, at second, it shows connection between two Stokes vectors - input and output, components of which has the dimensions of intensity, which can be easily measured by using single photodetector.

For the first time Mueller matrix formalism was suggested in 1948. So, the history of Mueller matrix measurement methods is quite long, but, at present time, the number of works, in which results of Mueller matrix measurement of real objects and analysis of information contained in it, are quite limited [2-6].

Any investigated object, which can be characterized by its Jones matrix is called deterministic object, and its Mueller matrix belongs to deterministic class of Mueller matrix.

It is well known[2], that Mueller matrix may be easily recalculated to correspondent Jones matrix in case of satisfying next conditions :

$$\begin{aligned} (M_{11} + M_{21})^2 - (M_{12} + M_{22})^2 &= (M_{13} + M_{23})^2 + (M_{14} + M_{24})^2 \\ (M_{11} + M_{12})^2 - (M_{21} + M_{22})^2 &= (M_{31} + M_{32})^2 + (M_{41} + M_{42})^2 \\ (M_{11} + M_{22})^2 - (M_{21} + M_{12})^2 &= (M_{33} + M_{44})^2 + (M_{43} + M_{34})^2 \end{aligned} \quad (1.3)$$

But, in practice, the existence of measurement error make it impossible to satisfy equations (1.3) and, accordingly, it is impossible to recalculate directly experimentally obtained Mueller matrix of the deterministic

object into Jones one. That's why, the main goal of this work is to elaborate the method of deterministic part extraction from the experimentally measured Mueller matrix of deterministic object.

Theory

The awkward transition formulas from the Jones matrix like :

$$J = \begin{bmatrix} x_1 + i \cdot x_2 & x_3 + i \cdot x_4 \\ x_5 + i \cdot x_6 & x_7 + i \cdot x_8 \end{bmatrix} \quad (2.1)$$

into correspondent Mueller matrix K are well known [1,2].

Experimentally measured Mueller matrix in mostly cases have the 16 independent real elements, which cannot be concerned each other by strictly equations, that's why it must be written in the following way :

$$M_0 = \begin{bmatrix} M_{11} & M_{12} & M_{13} & M_{14} \\ M_{21} & M_{22} & M_{23} & M_{24} \\ M_{31} & M_{32} & M_{33} & M_{34} \\ M_{41} & M_{42} & M_{43} & M_{44} \end{bmatrix} \quad (2.2)$$

If we strictly know the fact, that investigated object belongs to deterministic class, then we have physical ground to seek the nearest Mueller matrix, belonging to deterministic class. Then, we can recalculate last to the Jones matrix. The closest Mueller matrix will be determined by the norm of difference between experimentally measured and deterministic matrix :

$$\sigma = \|K - M_0\| = \sum_{i,j} (M_{ij} - K_{ij})^2 \quad (2.3)$$

This parameter σ is the function of 8 parameters, then condition for the minimum is the next :

$$d\sigma = 0 \quad (2.4)$$

or the same in term of derivatives:

$$\frac{\partial \sigma}{\partial x_k} = 0, \quad k = \overline{1,8} \quad (2.5)$$

Simplifying of (2.5), we will take the next set of equations :

$$\begin{aligned} & (M_{11} + M_{12} + M_{21} + M_{22}) \cdot x_1 + (M_{13} + M_{23}) \cdot x_3 - (M_{14} + M_{24}) \cdot x_4 + (M_{31} + M_{32}) \cdot x_5 + \\ & + (M_{41} + M_{42}) \cdot x_6 + (M_{33} + M_{44}) \cdot x_7 + (M_{43} - M_{34}) \cdot x_8 = 4 \cdot \|x\| \cdot x_1 \\ & (M_{11} + M_{12} + M_{21} + M_{22}) \cdot x_2 + (M_{14} + M_{24}) \cdot x_3 + (M_{13} + M_{23}) \cdot x_4 - (M_{41} + M_{42}) \cdot x_5 + \\ & + (M_{31} + M_{32}) \cdot x_6 - (M_{43} - M_{34}) \cdot x_7 + (M_{33} + M_{44}) \cdot x_8 = 4 \cdot \|x\| \cdot x_2 \\ & (M_{13} + M_{23}) \cdot x_1 + (M_{14} + M_{24}) \cdot x_2 + (M_{11} - M_{12} + M_{21} - M_{22}) \cdot x_3 + (M_{33} - M_{44}) \cdot x_5 + \\ & + (M_{34} + M_{43}) \cdot x_6 + (M_{31} - M_{32}) \cdot x_7 + (M_{41} + M_{42}) \cdot x_8 = 4 \cdot \|x\| \cdot x_3 \\ & -(M_{14} + M_{24}) \cdot x_1 + (M_{13} + M_{23}) \cdot x_2 + (M_{11} - M_{12} + M_{21} - M_{22}) \cdot x_4 - (M_{34} + M_{43}) \cdot x_5 + \\ & + (M_{33} - M_{44}) \cdot x_6 - (M_{41} + M_{42}) \cdot x_7 + (M_{31} - M_{32}) \cdot x_8 = 4 \cdot \|x\| \cdot x_4 \\ & (M_{31} + M_{32}) \cdot x_1 - (M_{41} + M_{42}) \cdot x_2 + (M_{33} - M_{44}) \cdot x_3 - (M_{34} + M_{43}) \cdot x_4 + \\ & + (M_{11} + M_{12} - M_{21} - M_{22}) \cdot x_5 + (M_{13} - M_{23}) \cdot x_7 + (M_{24} - M_{14}) \cdot x_8 = 4 \cdot \|x\| \cdot x_5 \\ & (M_{41} + M_{42}) \cdot x_1 + (M_{31} + M_{32}) \cdot x_2 + (M_{34} + M_{43}) \cdot x_3 + (M_{33} - M_{44}) \cdot x_4 + \\ & + (M_{11} + M_{12} - M_{21} - M_{22}) \cdot x_6 + (M_{14} - M_{24}) \cdot x_7 + (M_{13} - M_{23}) \cdot x_8 = 4 \cdot \|x\| \cdot x_6 \\ & (M_{33} + M_{44}) \cdot x_1 + (M_{34} - M_{43}) \cdot x_2 + (M_{31} - M_{32}) \cdot x_3 + (M_{42} - M_{41}) \cdot x_4 + \\ & + (M_{13} - M_{23}) \cdot x_5 + (M_{14} - M_{24}) \cdot x_6 + (M_{11} - M_{12} - M_{21} + M_{22}) \cdot x_7 = 4 \cdot \|x\| \cdot x_7 \\ & (M_{43} - M_{34}) \cdot x_1 + (M_{33} + M_{44}) \cdot x_2 + (M_{41} - M_{42}) \cdot x_3 + (M_{31} - M_{32}) \cdot x_4 + \\ & + (M_{24} - M_{14}) \cdot x_5 + (M_{13} - M_{23}) \cdot x_6 + (M_{11} - M_{12} - M_{21} + M_{22}) \cdot x_8 = 4 \cdot \|x\| \cdot x_8 \end{aligned} \quad (2.6)$$

where $\|x\| = x_1^2 + x_2^2 + x_3^2 + x_4^2 + x_5^2 + x_6^2 + x_7^2 + x_8^2$.

This set (2.6) can be rewritten in the following form :

$$Ax = \|x\| \cdot x \quad (2.7)$$

The analysis of this set shows, that this set has 8 solves, except trivial (zero Jones matrix). As the main matrix A is symmetrical, that's why there are only four independent solves. The steps in solving this set must be next :

- determination of eigenvectors and eigenvalues of matrix A.
- the selection of closest to $4 \cdot M_{11}$ eigenvalue.
- to normalize selected eigenvector equal on selected eigenvalue for taking $x_1..x_8$, i.e, recalculated Jones matrix.

Experimental examples.

We presents examples of well known deterministic objects analysis:

Object	Empty Space	Ideal linear polarizator
Experi- mental Mueller matrix	$\begin{bmatrix} 1 & -0.0104 & -0.0234 & -0.0057 \\ 0.0035 & 1.0123 & 0.0161 & 0.0015 \\ -0.0030 & -0.0096 & 0.9879 & -0.0049 \\ -0.0049 & -0.0037 & -0.0128 & 0.9995 \end{bmatrix}$	$\begin{bmatrix} 1 & 0.774 & 0.632 & -0.001 \\ 0.778 & 0.61 & 0.50 & -0.001 \\ 0.593 & 0.468 & 0.382 & -0.004 \\ 0.003 & 0.002 & 0.002 & 0 \end{bmatrix}$
Theoreti- cal Mueller matrix	$\begin{bmatrix} 1 & 0 & 0 & 0 \\ 0 & 1 & 0 & 0 \\ 0 & 0 & 1 & 0 \\ 0 & 0 & 0 & 1 \end{bmatrix}$	$\begin{bmatrix} 1 & \cos(2 \cdot \theta) & \sin(2 \cdot \theta) & 0 \\ \cos(2 \cdot \theta) & \cos^2(2 \cdot \theta) & \cos(2 \cdot \theta) \cdot \sin(2 \cdot \theta) & 0 \\ \sin(2 \cdot \theta) & \cos(2 \cdot \theta) \cdot \sin(2 \cdot \theta) & \sin^2(2 \cdot \theta) & 0 \\ 0 & 0 & 0 & 0 \end{bmatrix}$
Theoreti- cal Jones matrix	$\begin{bmatrix} 1 & 0 \\ 0 & 1 \end{bmatrix}$	$\begin{bmatrix} \cos^2(2 \cdot \theta) & \cos(2 \cdot \theta) \cdot \sin(2 \cdot \theta) \\ \cos(2 \cdot \theta) \cdot \sin(2 \cdot \theta) & \sin^2(2 \cdot \theta) \end{bmatrix}$
Recalcu- lated Jones matrix	$\begin{bmatrix} 0.706 + i \cdot 0.001 & i \cdot 0.001 \\ -0.009 - i \cdot 0.003 & 0.708 - i \cdot 0.001 \end{bmatrix}$	$\begin{bmatrix} 0.889 - i \cdot 0.001 & 0.317 + i \cdot 0.001 \\ 0.301 + i \cdot 0.001 & 0.107 + i \cdot 0.001 \end{bmatrix}$

As you can see, this method decreases the measurement error influence and extracts deterministic part enough well.

Conclusions

We have developed new method of recalculation experimentally obtained Mueller matrix of deterministic object into correspondent Jones matrix. This gives us the possibility to decrease measurement error influence.

References

- 1.M.Born, E.Wolf "Principles of optics",Oxford,1966.
- 2.R.M.A.Azzam, N.M.Bashara "Ellipsometry and polarized light", N.Holland publ.,Comp., 1977.
- 3.C.S.Brown, A.E.Bak "Unified formalism for polarization optics with application to polarimetry on a twisted optical fiber", Opt. Engin., **34**,1625-1635 (1995).
- 4.R.Simon "Nondepolarizing systems and degree of polarization", Optics Communications, **77** (1990), 5-6, p.349-354.
- 5.M.Sanjay Kumar and R.Simon "Characterization of Mueller matrices in polarizaion optics", Optics Communications, **88**(1992),4-6, p.464-470.
- 6.S.N.Savenkov, V.V.Marienko "Classification and recognition method of objects? based on their anisotropy properties", SPIE vol.2490-13-1995.

On Some Characteristics of Electromagnetic Environment

Vladimir B. Trigubovich

Belarusian State University of Informatics and Radio Electronics
Department of Radio Systems
6, P. Brovka str., 220027 Minsk, Belarus
E-mail: info@cit.org.by

Abstract. This paper discusses an approach to estimation of statistical characteristics of arising of intermodulation interferences. Statistical model of electromagnetic environment that enables us to solve this problem is proposed. Special attention is paid to determination of electromagnetic environment model in time and power. Illustrative numerical results are given. An algorithm based on the direct Monte-Carlo simulation is used.

One of the important problems of electromagnetic compatibility (EMC) is forming a model of radio interfering influence on receiver. In this paper, we discuss some points in determination of model of electromagnetic (EM) environment. Special attention will be paid to studying the conditions in EM environment that lead to intermodulation (IM) interferences.

As the interfering influence on receiver is massive and random, it must be registered by means of the methods of probability theory and mathematical statistics. Therefore the statistical theory of EMC [1] offers a statistical model of EM environment.

Consider a model of EMI as an n -dimensional system of random points. In this model we suppose that interfering signals are characterized by the set of random signal parameters X_i ($i \in [1, \dots, n]$), and hence can be estimated by means of the n -dimensional probability density function (PDF), $\omega(X_1, X_2, \dots, X_n)$.

In the case of statistical independence of EMI parameters:

$$\omega(X_1, X_2, \dots, X_n) = \prod_{i=1}^n \omega(X_i), \quad X_i \in DX_i,$$

where DX_i are the ranges of radio interference (RI) parameters X_i , $\omega(X_i)$ are one-dimensional PDFs of RI parameters.

In order to have intermodulation interferences arrived it is necessary to satisfy certain conditions:

- 1) coincidence of RIs in time domain;
- 2) fulfilling the frequency conditions of IM;
- 3) sum of RI's power forming IM interference must exceed the threshold level of intermodulation P_{im}

$$\sum_i P_i \geq P_{im}. \quad (1)$$

So we are especially interested in the PDFs of RI in time t , frequency f , power P .

Suppose that EMI is formed, in general, by N different RI sources. A first approximation to characterize the performance of these sources in time domain is a stochastic process without after-effect [2] known as Poisson process. Time interval τ between two occurrences of interfering signals has PDF given by

$$\omega_j(\tau) = \lambda_j \exp(-\lambda_j \tau)$$

where λ_j is the intensity of the Poisson law, $\lambda_j = N_j' / T_0$, where N_j' is the number of occurrences in observation period T_0 , $j=1, \dots, N$. As for PDF of RI duration $\omega(T)$, it can be improved separately.

By using the methods presented in [3] we can estimate the coincidence probability of 2, 3, ..., k RIs and the mean duration of pulses of coincidence process, that is a measure of after-effect in the integral process $\omega(\tau)$.

As for PDF of radio interferences in the frequency domain, $\omega(f)$, we suppose RI sources to be uniformly distributed, so that

$$\omega(f) = 1/Df,$$

and RI spectrum width is

$$\Delta f = k/T, \quad k \geq 1,$$

where T is the RI duration.

To determine an opportunity to satisfy the condition (1), PDF of RI power $\omega(P)$ is to be considered. Different approaches to $\omega(P)$ determining are available. In [1], for example, a class of hyperbolic distribution functions is proposed. RI power has PDF as

$$\omega(P) = \beta P^{-m}, \quad P_0 \leq P \leq P_{\max},$$

where β is a normalization factor, m is the distribution parameter, $m > 0$, P_0 is the receiver threshold level. The amplitude range $D = P_{\max}/P_0$ of interfering power and the ratio $\text{Dim} = P_{\text{im}}/P_0$ are important parameters of EM environment as well.

In order to estimate an opportunity to satisfy the condition (1), we define the probability P that the power of a single RI exceeds the threshold level of intermodulation, P_{im} . This probability is determined as

$$P = \int_{P_{\text{im}}}^{P_{\max}} \beta P^{-m} dP.$$

Some numerical results are shown in Figs. 1 and 2. Dependences of probability P were investigated for the following set of EM environment parameters D : $D=1E6$, $D=1E7$, $D=1E8$, $D=1E9$, $D=1E10$, $D=1E11$, $D=1E12$

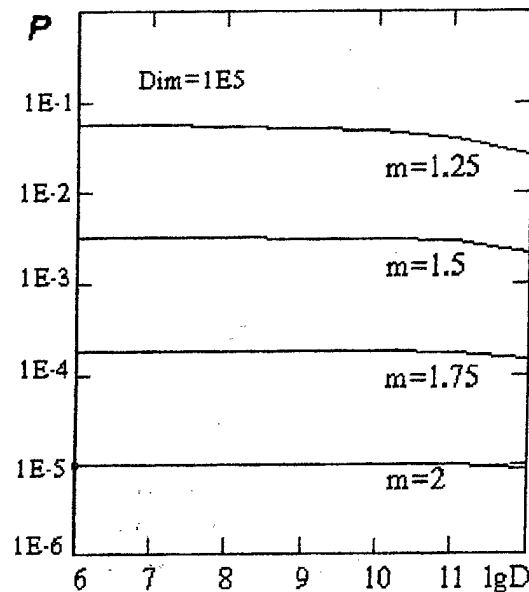


Fig. 1.

In Fig. 1 we show the probability P of exceeding the single interference threshold level P_{im} versus D , with PDF $\omega(P)$ parameter $m=1.25, 1.5, 1.75, 2$.

As can be concluded, P is a decreasing function of m . This can be explained by the increasement of the mean of RI power in accordance with decreasement of m . This dependence was obtained when Dim was equal to $1E5$.

Dependences of the probability P on EM environment parameters Dim and D are shown in Fig. 2. EM environment parameter m is equal to 1.5. Dependences of P on EM parameter Dim do not need any special comments.

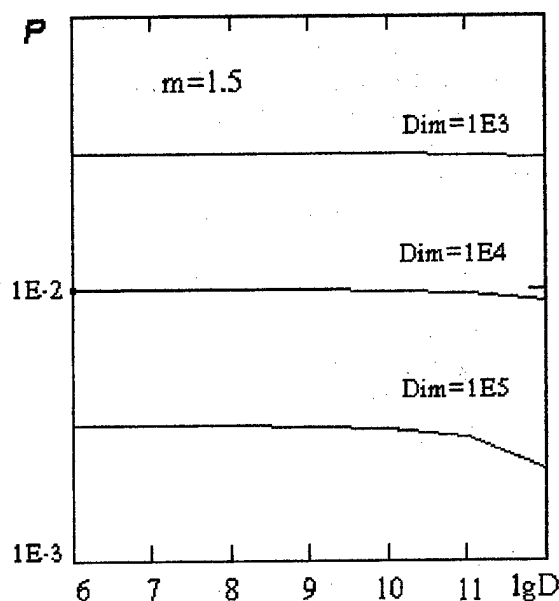


Fig. 2

In this work, the dependence of the probability P for the different EM environment parameters: m, D, Dim has been investigated.

It is known that probability of arising of IM interference formed by more than 5 RI signals is negligibly small. In this research, by using the Monte-Carlo method, it was shown that under conditions of increasing the number of interfering signals from 1 to 5, the probability P increases proportionally.

The method proposed in this paper enables us to set the concrete values of RI parameters λ, D, Dim and the number of RI sources to estimate the probability weights of IM interferences formed by 1, 2, ..., k interfering signals.

References.

1. A. F. Aporovich, *Statistical Theory of Electromagnetic Compatibility of Radio Systems*, Minsk: Nauka Publ., 1984 (in Russian).
2. B. V. Gnedenko, *Theory of Probability*, Moscow: Mir Publ., 1973 (in Russian).
3. N. M. Sediakin, *Elements of the Theory of Random Impulse Processes*, Moscow: Sov. Radio Publ., 1965 (in Russian).

ON SUBSURFACE RADAR DATA PROCESSING*

Kovalenko V.O.

Institute of Radio-Physics and Electronics National Academy of Sciences of Ukraine
Ak. Proskura street, 12, 310034, Kharkiv, Ukraine.

INTRODUCTION

Development of the videopulse subsurface scanning systems is task of the modern radio-physics and is investigated by many authors. The videopulse (ultrawideband) scanning systems usually produce data that are hard to interpret. This implies a necessity of developing the efficient data processing algorithms. Very efficient ones can be obtained on the basis of the synthetic aperture method (SAM). The SAM was initially created for the Side Looking Radars in remote sensing data processing but can also be applied to the subsurface scanning data [1]. The SAM algorithm can be divided on two stages: the inverse-matched filtering of the reflected by the medium signal and the spatial convolution of the set of returned signals. The first stage, where the time derivative of the signal illuminated is used as reference function, is aimed to the sharpening the echo-returns and thus to increasing the vertical resolution. The second stage is aimed to the convolution of the hyperbola-like reflection of buried objects and thus to increasing the horizontal resolution.

However the natural media which are to be investigated have a considerable value of conductivity, so they change the shape of the signals propagating through them. This is the reason why the efficiency of the classical SAM algorithm application to such media is rather limited. Another problem connected with the SAM algorithm application is the quick growth of the computational time needed to provide a spatial convolution of the massive set of the echo-returns. In this paper we represent two methods which enable one:

1. to consider the scanning signal shape distortion in media using the a-priori information about the medium under investigation;
2. to shorten the computation time about 3 times during the convolution of the echo-returns set.

PROBLEM STATEMENT

The results of the ultrawideband subsurface radar system work usually are implemented as a set of the echo-returns $\{v(x_r, t)\}_{r=1}^M, t \in [0; \Theta]$ (Θ is the total recording time) which characterize the subsurface structure in the rectangular area which is defined by the length of the scanning route and Θ . They are implemented as a matrix $N \times M$, where N is the quantity of the time samples in each realization and M is the quantity of the realizations on the route. The classical SAM supposes that connection between the signals received at the point $(x_R, 0)$ and transmitted at the point $(x_R + L, 0) = (x_T, 0)$ is established as follows:

$$v(x_R, t) = \frac{1}{2\pi V} \int_{\Gamma} \frac{z(L_T + L_R)}{(L_T L_R)^2} p(x, z) e^{-\alpha(L_T + L_R)} u'(t - \frac{L_T + L_R}{V}) dx, \quad (1)$$

where V is the velocity in the medium, Γ is the object contour, $p(x, z)$ is the complex reflectance amplitude, x_r is the point at the route, $L_T = \sqrt{(x - x_T)^2 + z^2}$, $L_R = \sqrt{(x - x_R)^2 + z^2}$ are the distances between the antennas and the contour point, α is the attenuation constant. The relation (1) corresponds to the Fresnel-Kirchhoff diffraction theory.

The data processing using SAM is reduced to the applying to the $v(x_r, t)$ an inverse-matched filter with the transfer function:

$$H_1(f) = \frac{V_1^*(f)}{1 - \eta + \eta |V_1(f)|^2} \cdot \sum_{i=1}^I c_i \cos 2\pi f t_i \quad (2)$$

where f is the frequency, $0 < \eta < 1$, $\{c_i\}_1^I, \{t_i\}_1^I$ are the sets of the predefined parameters, $*$ means the complex conjugation, and $V_1(f)$ is the spectrum of the time derivative of the radiated signal. Then the spatial convolution of the echo-returns set is provided by:

$$b(x, z) = \int_A w(x_r, \frac{L_T + L_R}{V}) \cdot \frac{z \cdot (L_T + L_R)}{(L_T L_R)^2} e^{-\alpha(L_T + L_R)} dx_r \quad (3)$$

Here A is the implementation of the route, $w(x, t)$ is the output of the filter defined by (2), $b(x, z)$ is the so-called imaging function [2], i.e. a result of the data processing.

INVERSE-MATCHING FILTER MODIFICATION

The first problem considered is the scanning pulse shape distortion in conducting media (see Fig. 1). The Fresnel-Kirchhoff diffraction model, represented by (1), does not take it into account, and thus filter (2) does not work properly. The shape of the radiated pulse can be estimated by using preliminary information about the medium under investigation. One can consider the conducting medium as a filter with the transfer function that can be obtained as follows [3]:

$$G(d, \omega) = |\Gamma(\omega)| \exp\{-d\alpha(\omega) - i(\varphi_\Gamma(\omega) - d\beta(\omega))\}, \quad (4)$$

$$\Gamma(\omega) = |\Gamma(\omega)| e^{i\varphi_\Gamma(\omega)}, \quad \Gamma(\omega) = \frac{2 \frac{\omega}{c}}{\frac{\omega}{c} + \beta(\omega) + i\alpha(\omega)},$$

$$\alpha(\omega) = \frac{\omega}{c} \sqrt{\varepsilon_1(\omega) \sinh\left(\frac{1}{2} a \sinh \frac{\sigma_1(\omega)}{\omega \varepsilon_0 \varepsilon_1(\omega)}\right)}, \quad \beta(\omega) = \frac{\omega}{c} \sqrt{\varepsilon_1(\omega) \cosh\left(\frac{1}{2} a \sinh \frac{\sigma_1(\omega)}{\omega \varepsilon_0 \varepsilon_1(\omega)}\right)} \quad (5)$$

Here $G(d, \omega)$ is the transfer function at the depth d , $\omega = 2\pi f$, f is the frequency, ε_0 is the free space permittivity, ε_1 is the related permittivity of the medium, conductivity, σ_1 is the medium conductivity, c is the free space velocity.

The shape of electromagnetic pulse in loam estimated accordingly to (5) is presented at the Fig.1. The filter (2) uses $u'(t)$ as the reference function and this can result in unpredictable errors at the output. On the other hand the approximation of $G(d, \omega)$ demands to use only the values of ε_1 and σ_1 which both can be estimated beforehand. It is suggested to use following function instead of $u'(t)$, as the reference one in (2), in order to obtain more information from the depth d :

$$V_d(t) = F^{-1} \left[G(d, \omega) F \left[\frac{d}{dt} F^{-1} [(F[u(t)]) G(d, \omega)] \right] \right] \quad (6)$$

Here $F[\dots]$ means Fourier transform and $u(t)$ is the scanning signal. Fig. 2 represents the real echo-profile (a), and results of its procession by using (2) with $u'(t)$ and $V_d(t)$, $d = 2$ (c, d) respectively.

It can be seen from (2) that modified that modified filter more accurately represents the data from the range of depths of 1.8 to 2.2 m.

MODIFICATION OF THE CONVOLUTION PROCEDURE

Replacing the integrals in (3) with finite sums, one obtains:

$$B_{xz} = \sum_{r=1}^M w_{r\tau} z \frac{L_T + L_R}{(L_T L_R)^2} e^{\alpha(L_T + L_R)}, \quad (7)$$

where B_{xz} is the sampled imaging function, $w_{r\tau}$ is the sampled output of the filter (2), M is the quantity of the realizations in the route $\tau = \left[\frac{L_T + L_R}{2} \right]$, and $[\dots]$ means the integer part. Further,

$$L_T = \sqrt{(x-r)^2 dx^2 + z^2 dz^2}, \quad L_R = \sqrt{(x-r-\lambda)^2 dx^2 + z^2 dz^2}, \quad \text{where } dx = \frac{L}{M}, \quad L \text{ is the length of the route,}$$

$dz = \frac{\theta}{N}$, $\lambda = \frac{T-R}{dx}$. If λ is integer (this means the following: every point of radiation becomes later the one of reception so this requirement can be satisfied physically), then the following equalities hold:

$$L_R = L_T(x, z, r + \lambda), \quad (8)$$

$$L_T(x+1, z, r) = \sqrt{(x-(r-1))^2 dx^2 + z^2 dz^2} = L_T(x, z, r-1), \quad (9)$$

So one does not need to recount the quantities of L_R on each step and $L_T(x+1, r, z)$ is counted $\frac{2N}{N+\lambda}$ times less ($\frac{N}{\lambda} \cong 10$ in our usual experiments).

Furthermore, taking into account the fact that $1 \leq \tau \leq N$ and monotonous character of its variation, (7) can be replaced with:

$$B_{xz} = \sum_{r=x}^{\tau \leq N} w_{r\tau} z \frac{L_T + L_R}{(L_T L_R)^2} e^{\alpha(L_T + L_R)} + \sum_{r'=x}^{\tau \leq N} w_{r'\tau} z \frac{L_T + L_R}{(L_T L_R)^2} e^{\alpha(L_T + L_R)}, \quad (10)$$

where $r' = x - r$. This leads to decreasing of the computations because of the "tails" cutting.

Modified in such a manner algorithm is working approximately three times more rapidly than classical one and gives the same results.

CONCLUSION

Natural and numeric experiments results show that sophisticated algorithms for subsurface radar system data processing can be developed on the basis of the synthetic aperture algorithm. Nevertheless some modifications of this algorithm have to be done in order to achieve reasonable results in the real media data processing. In this paper the algorithms aimed at the correction of the inverse-matched filter and computation time shortening are presented.

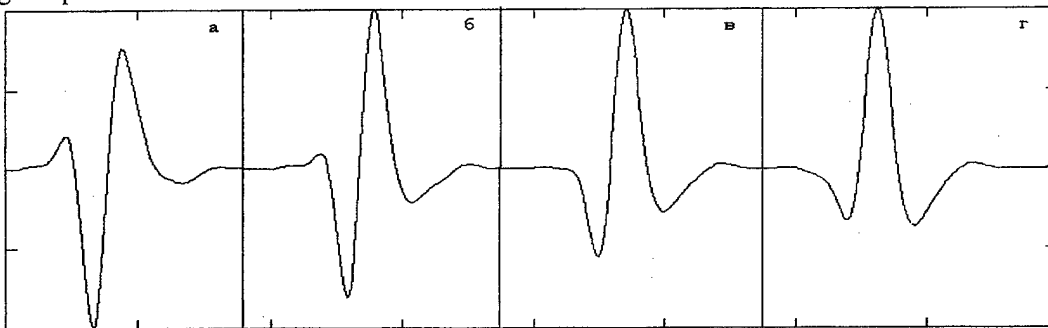


Fig.1 Radiated pulse and its shape at the depths of 1, 2, 5 meters in the loam ($\epsilon_r = 7$, $\sigma = 1.2 \cdot 10^{-2}$)

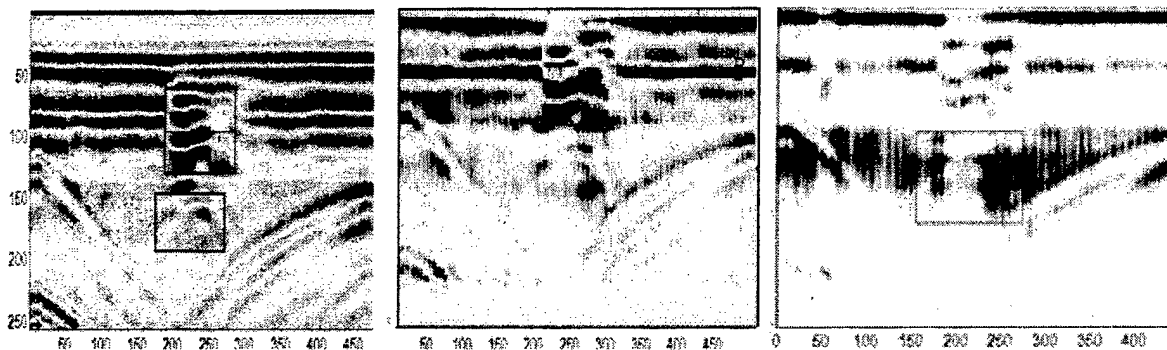


Fig. 2 Real echo-profile and results of its filtering by the classical and modified inverse-matched filters.

REFERENCES

1. N.Osumi, K.Ueno, Microwave Holographic Imaging Method With Improved Resolution, IEEE Trans. Antennas Propag., pp.1018-1026, no 10, 1984
2. N.Osumi, K.Ueno Microwave Holographic Imaging of Subsurface Objects, IEEE Trans. Antennas Propag., pp.152-159, no 2, 1985
3. R.King, M.Smith, Antennas In Matter, Moscow: MIR, 1984 (Russian translation).

* This work is partially supported by the STCU foundation. Project #366

PRINCIPLE OF FOURIER HOLOGRAPHIC PROCESSING IN MULTIFREQUENCY MICROWAVE MEASUREMENTS

O.O.Drobakhin

*Radiophysics Dept., Dniepropetrovsk State University,
13 Nauchny pereulok, Dniepropetrovsk, 320050 Ukraine*

Abstract: Technique of impulse structure characteristic calculation on base of scalar multifrequency measurements using holographic approach with two reference signals is proposed. Conditions of the technique realization are presented. Method of combination of modulus of autocorrelation function spectrum and phase of spectrum of cross-correlation function with reference signal is discussed. Application of the approach for antenna pattern extraction from multifrequency data measured under conditions of reflecting environment is illustrated.

INTRODUCTION

Time signal synthesis method on base of multifrequency measurements of complex reflection coefficient (RC) is powerful mean to localize discontinuities in microwave components and layered dielectric structures via spectral analysis of experimental data [1,2]. If multifrequency amplitude scalar measurements is rather simple, phase measurements is a problem. Use of vector analyzer such as six-port is traditional way of complex reflection and transmission coefficient measurements. If the purpose to obtain time-domain signal, an ordinary scalar reflectometer can be applied. It has additional reference reflection (comparison reflectometer). Transformation of time-domain signal after time-gating to frequency domain gives complex RC as function of frequency. Similar to filtering, time-gating distorts boundaries of frequency band. Time-gating is a linear operation thus it can not separate completely informative and spurious parts of time-domain signals. This fact induces additional components of error.

It was shown [3] that if distance between reference discontinuity and a structure under test (SUT) was provided more value than SUT electric thickness, one could obtain a part of result of transformation into time domain coinciding with time-domain signal calculated by Fourier transform of complex RC. Reference reflection can appear as before or after reflections of SUT. This idea was applied to measure reflection characteristics of dielectric structures in free space using reflection from waveguide open end as the reference signal. Requirement to increase the distance between antenna and SUT demands to use a horn instead the open end of waveguide. The latter has gain 6-7 dB, horn's gain is approximately 20-25 dB. But the horn has two discontinuities. Both of them play role of reference reflections.

BASIC STRATEGY

Let us analyze amplitude reflectivity $A(\omega)$ in presence two reference reflections r_1 and r_2 with time delay t_1 and t_2 from SUT with complex RC $R(\omega)$. Then $A(\omega)$ is given by

$$\begin{aligned}
 A(\omega) = k|r_1 \exp(+j\omega t_1) + r_2 \exp(+j\omega t_2) + R(\omega)|^2 = k\{|r_1|^2 + |r_2|^2 + |R(\omega)|^2 + r_1^* R(\omega) \exp(-j\omega t_1) + \\
 + r_1 R^*(\omega) \exp(j\omega t_1) + r_2^* R(\omega) \exp(-j\omega t_2) + r_2 R^*(\omega) \exp(j\omega t_2) + r_1^* r_2 \exp[j\omega(t_2 - t_1)] + \\
 + r_1 r_2^* \exp[-j\omega(t_2 - t_1)]\}.
 \end{aligned}
 \tag{1}$$

For horn, experiments show that the autocorrelation function $r_A(t) = F^{-1}\{|R(\omega)|^2\}(F^{-1}\{ \} - \text{the inverse Fourier transform})$ is more powerful than cross-correlation functions $r_R'(t) = F^{-1}\{r_1^* R(\omega) \exp(-j\omega t_1)\}$ and $r_R''(t) = F^{-1}\{r_2^* R(\omega) \exp(-j\omega t_2)\}$ if reflection of metal plate is measured. For SUT's with RC 0.2-0.3, these functions are comparable. For SUT's with RC approximately equals 0.05, cross-correlation functions are dominated. Similar to open end preliminary processing in form $1 - A / (k_2 |r_0|^2)$ with $|r_0|^2 = |r_1 \exp[j\omega(t_2 - t_1)] + r_2|^2$ is impossible due to small values in $|r_0|^2$. Autocorrelation function of horn $k|r_0|^2$ is subtracted from experimental data $A(\omega)$ which are square of modulus of sum of horn reflection (reference signal) and SUT reflection.

After subtraction $k|r_0|$ from $A(\omega)$ we have

$$A'(\omega) = k\{|R(\omega)|^2 + r_1^* R(\omega) \exp(-j\omega t_1) + r_1 R^*(\omega) \exp(j\omega t_1) + r_2^* R(\omega) \exp(-j\omega t_2) + r_2 R^*(\omega) \exp(j\omega t_2)\}. \quad (2)$$

Cross-correlation functions $r_R'(t)$ and $r_R''(t)$ are not overlapping if t_1, t_2 and $|t_1 - t_2|$ are greater than time of propagation in SUT. For SUT time-domain signal extraction, any cross-correlation function $r_R'(t)$ or $r_R''(t)$ can be used. If only cross-correlation $r_R'(t)$ is used, situation can be simplified. The conditions for time intervals must be realized only for reference discontinuity r_1 , the first in the horn. Thus the length of horn must be longer than SUT electrical thickness. The latter requirement can be relaxed if impulse function of SUT has tendency to decrease. Effect of cross-function overlapping is negligibly small in this case.

Measurements are multifrequency ones. Butterworth form time-gating the result of inverse Fourier transform for extracting the cross-function and direct Fourier transform allows us to reconstruct frequency complex RC. Normalization is reached by dividing the frequency data by ones for metallic plate.

Analysis of (2) shows that combination of time-gating and inverse Fourier transform can extract $k|R(\omega)|^2$. After square rooting modulus of RC is obtained. Phase information is taken from the inverse Fourier transforms of the cross-correlation function. This approach is appropriate if frequency property of reference reflection is not optimal thus the error of modulus reconstructed from cross-correlation function is rather large. Another appropriate situation is one then autocorrelation is greater than any cross-correlation functions but under real conditions all spurious reflections form their proper autocorrelation functions. Spectra of all these functions have identical support thus informative autocorrelation function is corrupted. Practical significance of this approach lies in situation then additional signals are absent or rather small.

THE PRINCIPLE OF FOURIER IN ANTENNA PATTERN DETERMINATION

The principle of Fourier holography can be used to extract signal of direct way in antenna pattern (AP) measurement by multifrequency methods under conditions of reflecting environment. According to [4] we assume that the direct signal can be represented as $F(\omega) = A \exp(-j\omega T_1)$, signals caused by antenna range reflections as

$$F(\omega) = \sum A_i \exp(-j\omega T_i)$$

with time delay T_i . The reference signal has similar form with time delay T_0 . Then, the signal registered is square of sum of reference, direct and multipath signals. Measurement of amplitude of transmission coefficient is simpler than one of complex data at many frequencies. Squares of modulus of AP taken without the reference signal (this component after transformation to the time domain corresponds to autocorrelation function of AP) and the reference signal modulus against frequency can be measured separately. Subtracting two latter components from basic data one can obtain amplitude of direct signal by means of parametric spectral analysis, for instance the Prony's method. Repeating this set of operations for all discrete angles and dividing by the maximum value of direct signal amplitude one estimates AP after elimination of environmental effect influence. Normalization by the square of reference signal amplitude eliminates influence of generator characteristic and improves estimation accuracy.

CONCLUSIONS

Application of Fourier holography principle for complex characteristic reconstruction under situation then two reference signals are present can be realized for scalar multifrequency measurements if time of propagation in structure under test is less than time intervals between reference signals and between structure and each of reference signals. Forming complex reflection coefficient as function of frequency by the combination of the modulus of autocorrelation function spectrum and the phase of spectrum of the cross-correlation function is appropriate if spurious reflections are negligibly small. Analogous approach can be utilized for signal of direct way extraction from multifrequency data measured under conditions of antenna range with environmental reflections.

REFERENCES

- [1] H.Vanhamme, "High resolution frequency-domain reflectometry," *IEEE Trans. Instrumentation and Measurement*, vol. 39, no.2, Apr. 1990, pp. 369-375.
- [2] M.V.Andreev, V.F.Borulko, and O.O.Drobakhin, "One-dimensional Inverse Problem Solution for Multilayered Structures Using Least-Square Spectral Estimation Method", Proc.of the 1995 URSI Int.Symp. on Electromagnetic Theory, St.Petersburg, Russia, May 23-26, 1995, pp.148-151.
- [3] O.O.Drobakhin, V.F.Borulko, and V.A.Karlov, " Millimeter Apparatus for Transmission Line and Dielectric Material Measurements by Multifrequency Methods," CPEM-96 Conference Digest, Germany, Braunschweig, pp.598-599.
- [4] Chaloupka, H., M.Galka, and A.Schlendermann, "Determination of Antenna Radiation Pattern from Frequency-Domain Measurements in Reflecting Environment", *Electronics Letters*, vol. 15, no.17, Aug. 1979, pp.512-513.

Estimating the parameters of spectra in problems of remote radio sounding of near-Earth plasmas

Stanislav G. Leus and Sergey N. Pokhil'ko

Department of Space Radio Physics, Kharkiv State University,
4 Svoboda Square, Kharkiv 310077, Ukraine
E-mail: *Leonid.F.Chernogor@univer.kharkov.ua*

The accuracy and resolution of remote sensing instruments employing radio-wave techniques can be increased by applying the methods of estimation of the model parameters. On the basis of a priori information on the structure of signals, effective computing algorithms for the construction of models of investigated process are used. A data model is assumed to consist of a limited number of plane waves (oscillations) embedded in noise, and the signal-to-noise ratio $q > 1$.

Methods of spectral estimation based on Levinson's, Berg's, Cholesky's and least squares algorithms with a solution of the system of the linear equations by Gauss's method are used in the simulations.

Applying different methods of an autoregressive parameter estimation, computer simulations are conducted at various values of q and for a number of waves (oscillations).

The effects of the order of autoregressive models on the results of evaluation are investigated, as well as the effects of the length of the time series.

The accuracy and stability of the spectral component estimator most of all depends on the magnitude of q . Frequently it is enough to limit its magnitude by $q = 5-10$.

The least effective for computing is Gauss's algorithm which allows to obtain the most stable and unbiased estimates. The application of the algorithms to nonlinear fitting does not result in an essential improving of the estimates obtained. The results of experimental investigations of the ionospheric plasma at various altitudes obtained from the HF Doppler sounding technique, partial reflection technique, etc. are presented.

The radar equation for remote radio sounding of distributed targets with ultra-wideband radio signals

Leonid F. Chernogor and Oleg V. Lazorenko

Department of Space Radio Physics, Kharkiv State University,

4 Svoboda Square, Kharkiv 310077, Ukraine

E-mail: *Leonid.F.Chernogor@univer.kharkov.ua*

Ultra-wideband (UWB) radio signals are signals the bandwidth of which is of the order of magnitude of or equal to the average value of the frequency.

Recently such signals have been widely employed for sounding natural resources, monitoring in glaciology, hydrology, etc., as well as in air navigation radar. We have studied the possibility of using UWB signals for remote radio wave sounding of the atmosphere, the ionosphere, the magnetosphere, and the near-Earth environment. For this purpose in particular, the radar equation is derived for remote sensing instruments employing radio wave techniques; it takes into account the features of distributed targets and relates the signal-to-noise ratio at the input of the receiving system to the parameters of the facility and the medium. The mathematical models of UWB signals are suggested.

The computer simulations of the dependence of the signal-to-noise ratio q on the wideband index and on the mean frequency of UWB signals, as well as on the parameters of the facility and media, are performed. The applicability of these results to the radio sounding of near-Earth space with the mesosphere-stratosphere-troposphere (MST) radar, incoherent scatter

radar and partial reflection facilities is discussed. In case of narrow-band signals,

$$q = \frac{P_s}{P_n} = \frac{PGS_a\sigma}{(4\pi)^2 R^4 P_n}$$

where P is the power of sounding signals, G is the gain of the transmitting antenna, S_a is the effective aperture of the receiving antenna, σ is the volume scattering cross section of a beam-filling target, R is the range.

The equation for UWB signals remains the same, but P , S_a , σ , P_n , and also R for distributed targets become functions of f . In this case,

$$P_s = \frac{1}{(4\pi)^2} \int_{f_{\min}}^{f_{\max}} p(f) G(f) S_a(f) \frac{\sigma(f)}{R^4(f)} df, \quad p(f) = \frac{2}{\tau} |\tilde{S}(f)|^2,$$

$$P_n = kT_n(f_0) \int_{f_{\min}}^{f_{\max}} F(f) df$$

where f_{\min} , f_{\max} , f_0 are the minimum, maximum and mean frequencies in the signal spectrum, respectively, k is Boltzman's constant, $T_n(f_0)$ is the noise temperature at the mean frequency in the signal spectrum, $F(f)$ is the dimensionless noise (interference) distribution as a function of frequency, τ and $\tilde{S}(f)$ are a pulse length and a complex signal power distribution as a function of frequency, respectively.

L. F. Chernogor has been supported by Science and Technology Center in Ukraine Grant No. 471.

RESULTS OF THE DYNAMIC RADAR TARGET CHARACTERISTICS CALCULATIONS IN THE DECAMETRIC WAVE BAND

V.A.Kovalchuk

Kharkov Military University, Svoboda sq. 6, Kharkov, 310043, Ukraine

The problem of target scattering analysis is very important for radar. It becomes complicated considerably in over-the-horizon radar, where a number of additional factors caused by ionosphere influence, earth surface, etc. appear. The total sum of these factors can change the radar characteristics of the target (RCT) such as the elements of polarization scattering matrix. The RCT determination is realized either by experiments or by physical and mathematical simulation. Experiments and physical simulation requires considerable material and temporal expenses and can be carried out, as a rule, in the presence of a number of limiting conditions. Mathematical simulation of RCT has no such disadvantage. But the main goal: reliability of obtained results, must be achieved in this case. It puts strict requirements on the choice of mathematical model.

Presented mathematical model is worked out for decametric wave band and enables one to evaluate the dynamic RCT moving over an arbitrary earth surface. The model basis is a four-beam signal propagation scheme. According to this scheme the electromagnetic field at the observation point is determined as the sum of radio wave fields scattered by the target to the observation point both directly and after reflections from the earth surface (in various combinations).

Model bloc-diagram is presented in Fig.1. Target type, its motion characteristics, the incident electromagnetic wave parameters and the type of underlying earth surface are referred to the model input data.

The static RCT are determined in the first bloc. For this purpose a problem of radio wave reflection from unmoving target of complex shape located in free space is solved. In the over-the-horizon radar the typical target dimensions are comparable with the radar signal wavelength. In this case the problem of radio wave scattering can be solved approximately if a continuous target surface is replaced by a net wire approximating the target shape. After that the set of integral equations is reduced to a set of linear integral equations in accordance to the methods described in [1]. There were worked out three models representing target characteristic types: strategic bomber, fighter and cruise missile.

The model of earth surface is presented in the second bloc. The earth surface is defined by the form of correlation function, correlation interval, variance of irregularity heights, electrical parameters, level of sub-surface water, presence of vegetation, bushes, woods, reservoirs, etc. We assume that these data are a priori well known in statistical sense.

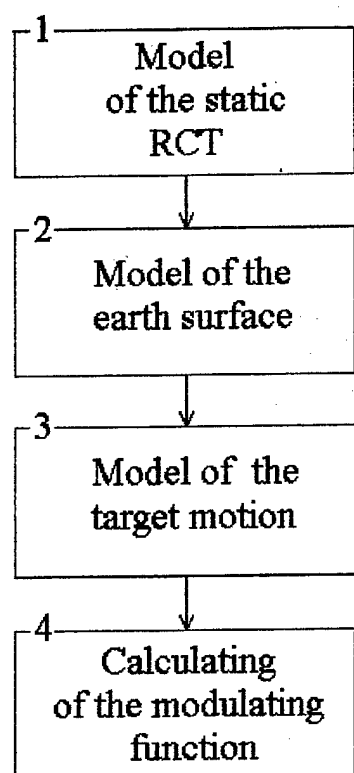


Fig. 1

The target motion model is represented in the third bloc. Each new target position is defined as $x_1 = x_0 + V/f$, where x_0 is the previous target position, V is the target motion velocity, f is the frequency of the radar pulse repetitions.

In the fourth bloc all specular points at the earth surface, with taking into account the possible shadows that one surface irregularity throws at another, and also the total electromagnetic field at the observation point are determined. The sequence of pulses scattered by the target is called the modulating function. The obtained modulating function was analyzed in the frequency and time domains: distribution laws of reflected signal parameter were determined, frequency spectra of modulating function and its correlation function were calculated, the Doppler frequency spectrum width of the scattered signal and correlation interval of the

modulating function were evaluated. The results were averaged for ten realiza-

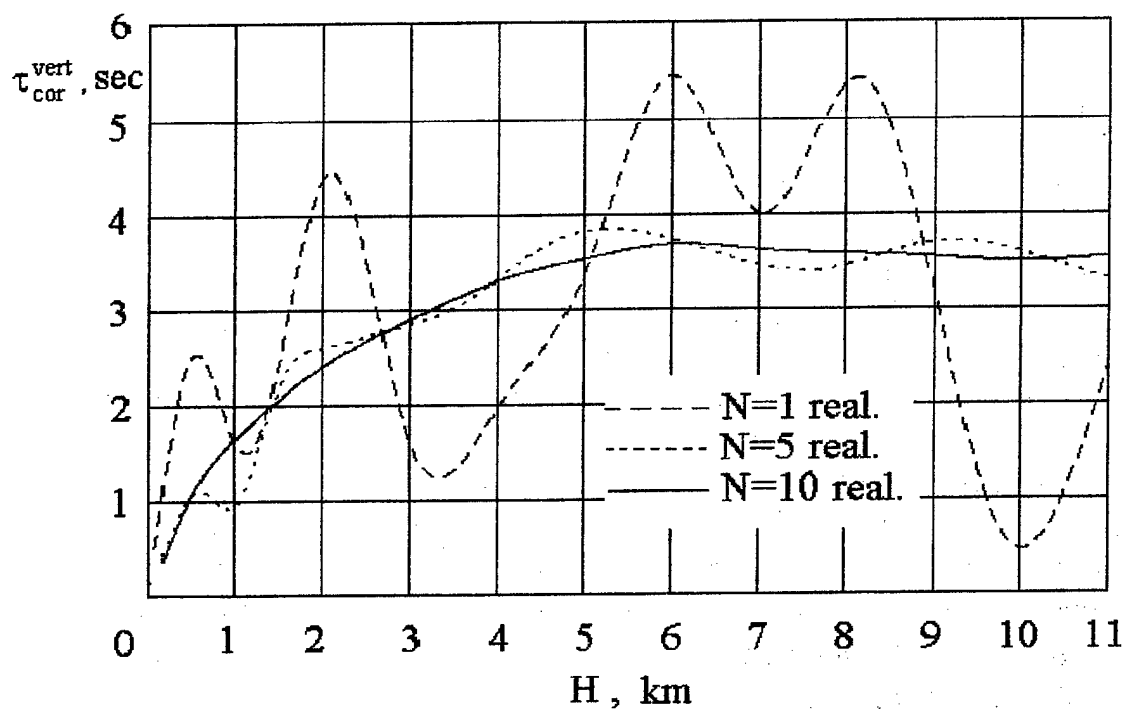


Fig. 2

tions of the ground surface.

The typical modeling results are presented in Fig.2 and Fig.3. In Fig.2, a correlation interval τ_{cor} of modulating function for the vertically polarized signal is shown. In this case the target is a fighter flying with the speed of 300 meters

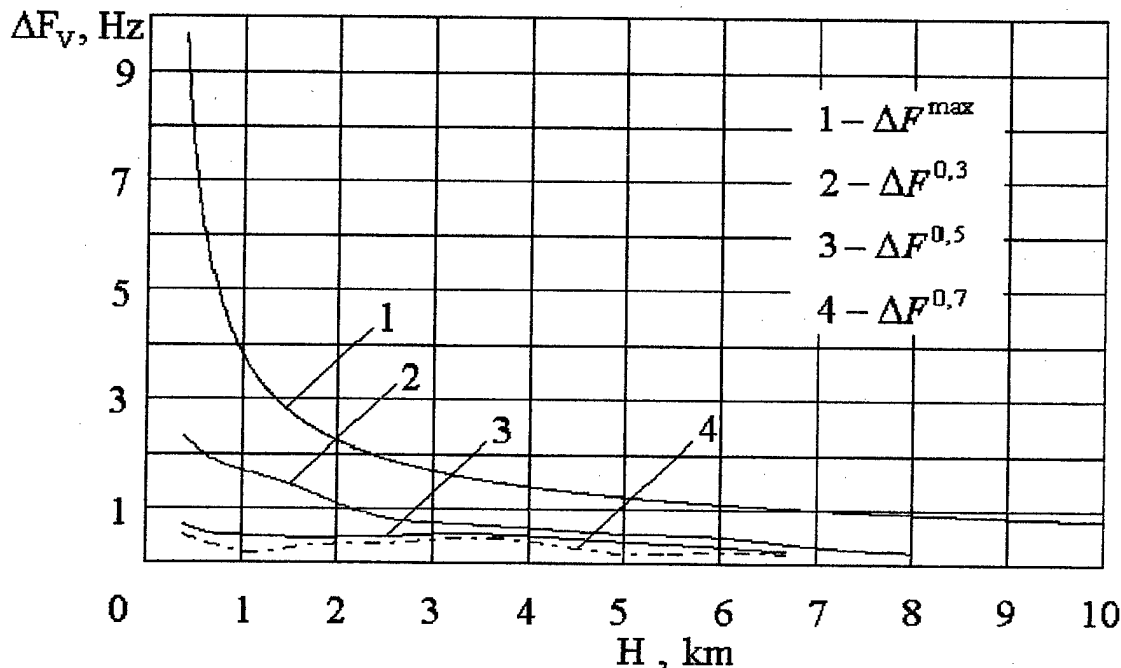


Fig. 3

per second above the earth surface with parameters: surface correlation function of a Gauss type, correlation radius is 2000 m, dispersion of roughness heights is 100m^2 , soil type is a black earth. The results were averaged for N samples of the earth surface. The Doppler frequency spectrum width at the different levels of the scattered vertically polarized signals and the estimate of the maximum Doppler frequency spectrum width are shown in Fig.3.

Analogous theoretical results obtained for all target types.

The analysis of simulation results enables us to state the following. Statistical characteristics of signals scattered by aerodynamic target depend on its flight height. We can distinguish three height ranges at which the difference from statistical characteristics is observed most distinctly. The laws of reflected signal parameter distributions, correlation intervals of modulating function of various target types differ from each other. These differences form a basis of target recognition algorithms.

REFERENCES.

1. Computational Methods in Electromagnetics. Ed. By R.Mitra, M.: Mir, 1977.-485 p.

DETECTING QUADRATIC-TYPE NONLINEARITIES OF RANDOM PROCESSES IN THE PRESENCE OF ADDITIVE NOISE

Vladimir G. Galushko

Institute of Radio Astronomy, National Academy of Sciences of Ukraine
4, Chervonopraporna Str., 310002, Kharkov, Ukraine

The problem of detecting nonlinear effects often arises in investigations of different physical, engineering and other systems. These can be, for example, nonlinear distortions in radio devices, coupling of waves in nonlinear media, or nonlinear mechanisms of their generation. A powerful tool for solving this problem is the use of cumulants or their associated Fourier transforms, known as polyspectra [1,2]. However, the estimation of cumulants (or polyspectra) of real processes (especially for fairly long realizations) requires considerable computation resources, in particular, RAM. The present paper illustrates the potentials of the so called " $1\frac{1}{2}$ D - spectra", $\Gamma(\omega)$, for solving the problem of detecting weak quadratic-type nonlinearities of random processes in the presence of additive noise [2]. This technique is a particular case of the bispectral analysis being, however, much easier in use.

The response, $u_0(t)$, of a quadratic-type nonlinear system to an input process, $u_s(t)$, can be represented as

$$u_0(t) = u_s(t) + k \cdot u_s^2(t),$$

with k being the nonlinearity factor. Because of the noise, the input of an analyzer oriented toward detection of this type of nonlinearity and estimation of k is

$$u(t) = u_0(t) + n(t), \quad (1)$$

where $n(t)$ is the random noise. As can be shown, for a random stationary process $y(t)$ the " $1\frac{1}{2}$ D - spectrum" is

$$\Gamma_y(\omega) = \int_{-\infty}^{+\infty} d\omega' B_y(\omega, \omega') = \frac{1}{2\pi} \int_{-\infty}^{+\infty} d\tau C_y(\tau, \tau) e^{-i\omega\tau},$$

where $B_y(\omega, \omega')$ and $C_y(\tau, \tau)$ are the bispectrum and third-order cumulant of $y(t)$, respectively. Since $C_y(\tau, \tau) = \langle y(t) \cdot y^2(t+\tau) \rangle$ (the angular brackets denote the expectation procedure), $\Gamma_y(\omega)$ can be regarded as a cross-spectrum of $y(t)$ and $y^2(t)$. Hence, the functional diagram of the algorithm can be represented as it is shown in Fig. 1. If $u_s(t)$ and $n(t)$ are mutually independent stationary zero-mean Gaussian processes and k is sufficiently small, then $\Gamma(\omega)$ can be written as

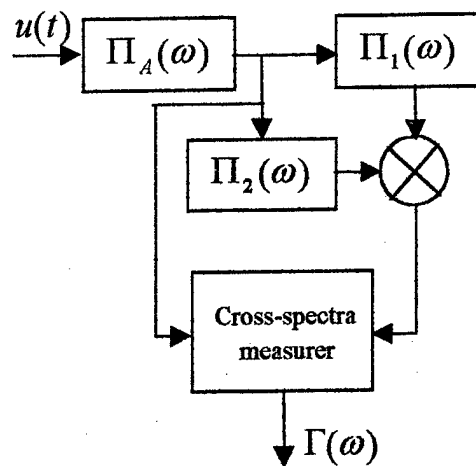


Fig. 1 Functional diagram of the algorithm for calculating $\Gamma(\omega)$: $\Pi_A(\omega)$, $\Pi_1(\omega)$ and $\Pi_2(\omega)$ are responses of the analyzer input device and filters, respectively

$$\Gamma(\omega) = 2k \int_{-\infty}^{+\infty} d\xi |\Pi_1(\omega/2 + \xi)| |\Pi_2(\omega/2 - \xi)| \cdot Q(\omega, \xi) e^{i\Phi(\omega, \xi)} \quad (2)$$

Here $|\cdot|$ denotes the absolute values of the complex functions;

$$\Phi(\omega, \xi) = \varphi_A(\omega/2 + \xi) + \varphi_A(\omega/2 - \xi) - \varphi_A(\omega) + \varphi_1(\omega/2 + \xi) + \varphi_2(\omega/2 - \xi);$$

$$Q(\omega, \xi) = |\Pi_A(\omega)| |\Pi_A(\omega/2 + \xi)| |\Pi_A(\omega/2 - \xi)| [< |S_s(\omega)|^2 > < |S_s(\omega/2 + \xi)|^2 > + \\ + < |S_s(\omega)|^2 > < |S_s(\omega/2 - \xi)|^2 > + < |S_s(\omega/2 + \xi)|^2 > < |S_s(\omega/2 - \xi)|^2 >];$$

$< |S_s(\omega)|^2 >$ is the power spectrum of $u_s(t)$; and $\varphi_A(\omega)$, $\varphi_1(\omega)$ and $\varphi_2(\omega)$ are phase responses of the analyzer and the filters, respectively. In Eq. 2 we have omitted the terms which contribute at $\omega = 0$ and assumed $|\Pi_A(0)| = 0$. In practical situations expectations are replaced by sample averages and, hence, the following estimate can be suggested:

$$\hat{\Gamma}(\omega) = \frac{1}{N} \left(\frac{T}{2\pi} \right)^2 \sum_{i=1}^N \int_{-\infty}^{+\infty} d\omega' \hat{S}_i(\omega) \hat{S}_i(\omega') \hat{S}_i^*(\omega + \omega'), \quad (3)$$

where $\hat{S}_i(\omega) = \frac{1}{T} \int_0^T dt u_i(t) e^{-i\omega t}$, and $N = T_o / T$ is the number of T -length realizations of the $u(t)$ process within the total observation time T_o . As can be shown, Eq. (3) yields unbiased and consistent estimates of $\Gamma(\omega)$ with variances σ_{Re}^2 and σ_{Im}^2 of real and imaginary parts of $\hat{\Gamma}(\omega)$, respectively (for a sufficiently small k)

$$\sigma_{Re}^2 = \sigma_{Im}^2 = \frac{1}{4N} \left[\int_{-\infty}^{+\infty} d\xi |\Pi_{1r}|^2 D(\omega, \xi) + \right. \\ \left. + \frac{4\pi}{T} |\Pi_A(\omega)|^4 |\Pi_A(2\omega)|^2 \Pi_{2r}(\omega) < |S_u(\omega)|^2 >^2 < |S_u(2\omega)|^2 > \right]$$

Here

$$D(\omega, \xi) = |\Pi_A(\omega)|^2 |\Pi_A(\omega/2 - \xi)|^2 |\Pi_A(\omega/2 + \xi)|^2 < |S_u(\omega)|^2 > \times \\ \times < |S_u(\omega/2 - \xi)|^2 > < |S_u(\omega/2 + \xi)|^2 >; \\ \Pi_{1r}(\omega, \xi) = \Pi_1(\omega/2 - \xi) \Pi_2(\omega/2 + \xi) + \Pi_1(\omega/2 + \xi) \Pi_2(\omega/2 - \xi); \text{ and} \\ \Pi_{2r}(\omega) = \Pi_1(\omega) \Pi_2^*(2\omega) \Pi_1(2\omega) \Pi_2^*(\omega) + |\Pi_1(2\omega)|^2 |\Pi_2(\omega)|^2 + \\ + |\Pi_1(\omega)|^2 |\Pi_2(2\omega)|^2 + \Pi_1^*(2\omega) \Pi_2(\omega) \Pi_1^*(\omega) \Pi_2(2\omega).$$

Since T_o is always finite, σ_{Re}^2 and σ_{Im}^2 are actually non-zero values and, hence, $\Gamma(\omega)$ is usually estimated with some error. To reduce the error, several procedures can be applied, e.g., frequency averaging or the use of a duly selected approximation for $\Gamma(\omega)$.

The phase response, $\varphi_A(\omega)$, in Eq. (2) is not always known with a required accuracy. This difficulty can be overcome by the use of sufficiently narrow band filters. The most suitable are rectangular filters (e.g., synthesized numerically). If the filter bandwidth is significantly smaller than $\Pi_A(\omega)$, then we obtain

$$|\Gamma(\omega)| = 2k \int_{-\infty}^{+\infty} d\xi |\Pi_1(\omega/2 + \xi)| |\Pi_2(\omega/2 - \xi)| \cdot Q(\omega, \xi). \quad (4)$$

To estimate k from Eq. (4) one needs a knowledge of $\langle |S_s(\omega)|^2 \rangle$, while in the most of practical cases this information is absent. However, there is a possibility to resolve this problem. Let us assume the spectral density of noise to be a constant value within the frequency band of the analyzer, i.e. $\langle |S_n(\omega)|^2 \rangle = I^2 = \text{const}$, while $\langle |S_s(\omega)|^2 \rangle$ depends on frequency. Since for a sufficiently small k

$$\langle |S_s(\omega)|^2 \rangle \approx \langle |S_u(\omega)|^2 \rangle - I^2,$$

and we can write, in accordance with Eq. (4):

$$|\hat{\Gamma}(\omega)| = k[A(\omega)I^4 - 2B(\omega)I^2 + C(\omega)]. \quad (5)$$

Here

$$A(\omega) = 6 \int_{-\infty}^{+\infty} d\xi |\Pi_1(\omega/2 + \xi)| |\Pi_2(\omega/2 - \xi)| |\Pi_A(\omega, \xi)|;$$

$$B(\omega) = 2 \int_{-\infty}^{+\infty} d\xi |\Pi_1(\omega/2 + \xi)| |\Pi_2(\omega/2 - \xi)| |\Pi_A(\omega, \xi)| \times$$

$$\left\{ \langle |S_u(\omega)|^2 \rangle + \langle |S_u(\omega/2 + \xi)|^2 \rangle + \langle |S_u(\omega/2 - \xi)|^2 \rangle; \right\}$$

$$C(\omega) = 2 \int_{-\infty}^{+\infty} d\xi |\Pi_1(\omega/2 + \xi)| |\Pi_2(\omega/2 - \xi)| Q_u(\omega, \xi); \text{ and}$$

$$|\Pi_A(\omega, \xi)| = |\Pi_A(\omega)| |\Pi_A(\omega/2 + \xi)| |\Pi_A(\omega/2 - \xi)|.$$

The function $Q_u(\omega, \xi)$ can be obtained from $Q(\omega, \xi)$ (see Eq.(2)) by replacing $\langle |S_s(\omega)|^2 \rangle$ with $\langle |S_u(\omega)|^2 \rangle$. If $|\hat{\Gamma}(\omega)|$ is measured at two frequencies, ω_1 and ω_2 , then we have a set of two equations with respect to I^2 and k .

The proposed algorithm was tested by means of a numerical simulation. Standard software was applied to generate statistically independent random Gaussian processes $u_s(t)$ and $n(t)$ with specified parameters. At the first stage the real and imaginary terms of $\Gamma(\omega)$ were estimated from Eq. (3) at two frequencies. The inaccuracy pertaining to the estimates was reduced by using an approximation function matched to the expected $\Gamma(\omega)$ in the best way for the given shape of $\langle |S_u(\omega)|^2 \rangle$ and $I^2 = \text{const}$ and filter responses. Then the modulus of $\Gamma(\omega)$ was calculated at both frequencies. Finally, by solving a set of two equations like Eq. (5), the nonlinearity factor k was found. The relative errors in determining k did not exceed 10% for $N = 1000$. Hence, the algorithm proved to be quite acceptable for practical applications.

References

- [1] J. M. Mendel, Tutorial on higher-order statistics (spectra) in signal processing and system theory: theoretical results and some applications, Proc. IEEE, 79 (1991), p.p. 278 – 304.
- [2] A. W. Wernik, Methods of Data Analysis for Resolving Nonlinear Phenomena. In: H. Kohl, Ruster, and K. Schlegel (Eds.), Modern Ionospheric Science, European Geophys. Society, Berlin, 1996, p.p. 322 – 345.

General-purpose computer-controlled polarization state transformer for modern automatic Mueller-polarimeter

Sergey N. Savenkov, Roman I. Gorelkov

Radiophysics depart., Kiev Taras Shevchenko Univ., Vladimirska 64, Kiev, 252017, Ukraine

e-mail : sns@boy.rpd.univ.kiev.ua

Abstract

Recently considerable attention is still attracted to creation and development of various schemes of Mueller-polarimeters. However, there are some disadvantages in existing models. In present paper the general-purpose electronically controlled transformer of polarization using electrooptical effect is suggested to utilize it as a main part of modern Mueller-polarimeter. Application of this transformer is shown to give some significant advantages, such as:

- any polarization state of probing radiation can be realized (generally, the whole Poincare sphere);
- high speed of measurements (up to 5-10 microsec. per single measurement);
- possibility of full automatization of Mueller-polarimeter and measurement process;
- multi-frequency (spectral) measurements (frequency range is limited with other parts of Mueller-polarimeter, in particular, on photodetector);
- functional elasticity (the possibility of work in main polarimetry measurement regimes: four-polarization method, dual rotating-compensator method; measurement of studied object response to any polarization state of probing radiation; Jones matrix measurement etc.).

Introduction

At present time there is a variety of methods to investigate linear interaction of electromagnetic radiation and studied object. It is known the interaction can be fully characterized by Mueller matrix [1], which describes the transformation of polarization state of probing radiation into output radiation, received by photodetector.

Any polarization state of quasimonochromatic radiation (non-, partly- or fully-polarized) can be presented by 4-dimension Stokes vector, having such form: $S = \{I; Q; U; V\}$, where components of Stokes vector give us all information about predominant types of polarization [1]. As we said above, Mueller matrix describes the transformation of polarization state of radiation through interaction, and mathematically it is the matrix operator of linear transformation from Stokes vector of probing radiation to Stokes vector of output radiation:

$$S_{out} = [M]S_{in} \quad (1)$$

So, the measurement of Mueller matrix of studied objects is of great interest because of its great informativity. Usually, the basic scheme of Mueller-polarimeter consists of three blocks: polarization state generator PSG (forming probing radiation), studied object and polarization state analyzer PSA (analyzing polarization state of radiation after its interaction with object). The principle of measuring Mueller matrix is based on irradiation of object by different states of polarization (at least four) and calculating Mueller matrix by analyzing output radiation. Differences between some schemes of Mueller-polarimeters are in particular execution of PSG and PSA and conforming calculations. Analyzing some particular schemes of Mueller-polarimeters [2-6], some their disadvantages were found: 1) low level of automatization and comparatively long time of measuring, which don't permit us to study some objects with fluctuating characteristics; 2) high level of Mueller matrix elements measurements error; 3) some schemes contain excessive quantity of optical elements, which makes some difficulties, connected with automatization and calibration of the device; 4) measurements are carrying out only on one wavelength of probing radiation, that's why there's no any information about disperse properties of studied objects; 5) narrow range of applications (low level of functional elasticity), making some difficulties when use of Mueller-polarimeter for other measurements (measuring Jones matrix, analysis of polarization state of studied radiation, etc.). To decrease these disadvantages improved polarization state generator using electrooptical effect is suggested in this paper.

Mueller-polarimeter scheme.

We suggest to use in polarization state transformer of probing channel to make it multipurpose electrically controlled elements with linear phase and amplitude (ideal) anisotropy. Full functional scheme of Mueller-polarimeter is shown on Fig.1 below.

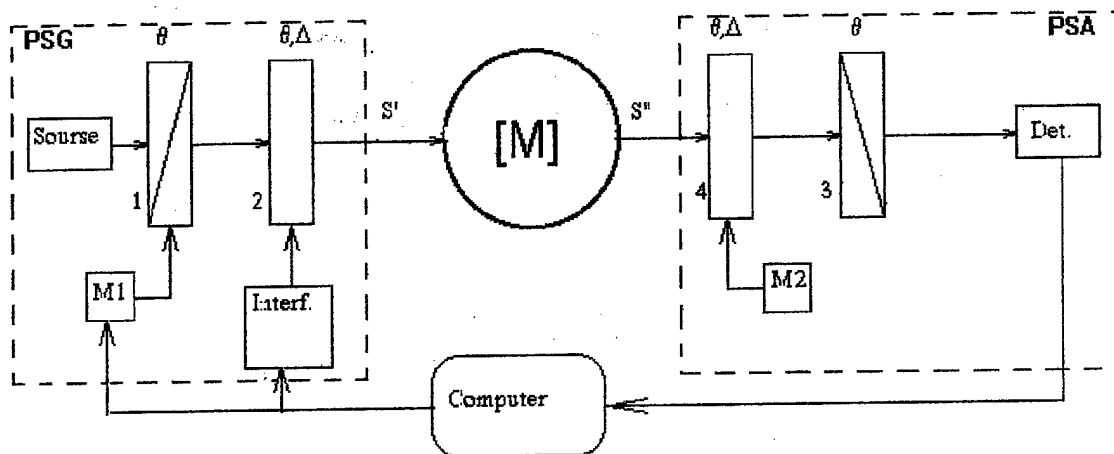


Fig.1.

Now, consider additional advantages of this Mueller-polarimeter:

- 1) it is fully automatic and have high speed of measurements;
- 2) it have complete functional elasticity (without major changes it gives us opportunity to conduct analysis of polarization state of studied light, measurements of Jones matrices, investigation of studied object response to given polarization state etc.).
- 3) it can operate in comparatively wide frequency band.

Particularly, this frequency band caused by working band of utilized photodetector. We conducted the measurements on 2 wavelengths, generated by helium-neon laser LG-126: 0.63um and 1.15um, which are in working band of utilized photodetector (PEM-62). So, the Mueller-polarimeter can measure dispersion characteristics, containing additional information on studied object. By the way, in this case switching from one wavelength to another is comparatively easy operation which could be done program-simulated.

4) it contains very limited number (the quantity of elements is minimally necessary for Mueller-polarimeter) of optical elements and that is why it is comparatively easy in calibration and alignment.

5) The measurement error must be at least twice lower than measurement error of Mueller-polarimeter [5] because polarization state generator supplies any needed polarization state (in details, look below) and that's why Mueller-polarimeter can operate under absolute minimal COND [8].

Mathematical support of PSG.

Optical scheme of PSG (polarization state generator) is shown on Fig.1 above. To make radiation with needed polarization state we can operate by azimuth of polarizer θ_1 , azimuth of retardation plate θ_2 and its retardance Δ_2 . So, we have 3 degrees of freedom, that is enough to maintain 2 degrees of freedom of polarized radiation (azimuth θ and ellipticity angle ε). That's why we'll show below that we can maintain any needed polarization state using retardation plate with $\Delta = \pi / 2$. With the help of computer, we can automatically keep stable this value of retardation after switching to another wavelength. As a source of radiation we must use any monochromatic source of depolarized (but collimated) or circularly-polarized light (we use He-Ne laser with retardation plate $\lambda / 4$).

Making some matrix calculations to find Stokes vector of radiation on the output of PSG (under condition that $\Delta_2 = \pi / 2$), we have:

$$S_{in} = \frac{1}{2} \begin{bmatrix} 1 \\ \cos(2\theta_1) - \sin(2\theta_2) \sin(2\theta_2 - 2\theta_1) \\ \sin(2\theta_1) + \cos(2\theta_2) \sin(2\theta_2 - 2\theta_1) \\ \sin(2\theta_2 - 2\theta_1) \end{bmatrix} \quad (2)$$

We must maintain polarization state with any needed parameters θ and ε , so according Stokes vector is shown:

$$S_{in} = \frac{1}{2} \begin{bmatrix} 1 \\ \cos(2\varepsilon) \cos(2\theta) \\ \cos(2\varepsilon) \cos(2\theta) \\ \sin(2\varepsilon) \end{bmatrix} \quad (3)$$

Therefore, after calculations from (2) and (3) we have the needed values for θ_1 and θ_2 :

$$\begin{cases} \theta_1 = \theta - \varepsilon \\ \theta_2 = \theta \end{cases} \quad (4) \quad \text{or} \quad \begin{cases} \theta_1 = -\frac{1}{2} \arcsin s_1 + \frac{1}{2} \arcsin \left(\frac{s_2}{\sqrt{1-(s_3)^2}} \right) \\ \theta_2 = \frac{1}{2} \arcsin \left(\frac{s_2}{\sqrt{1-(s_3)^2}} \right) \end{cases} \quad (5) \quad \text{when Stokes}$$

vector of the needed radiation is given in form: $S_{in} = [1; s_1; s_2; s_3]$. We can see that formulas (4) or (5) can maintain any polarization state because they give us correspondence between parameters of the needed radiation and azimuths θ_1, θ_2 of polarization devices. So, given PSG is multipurpose.

Adaptation to work at any working wavelength.

The calculations below are to make correction in work of analyzing channel (see Fig.1) when Mueller-polarimeter provide dynamic measurement regime at some wavelength. Based on characteristic matrix of PSA (Fig.1) we have expression for intensity, received by photodetector:

$$I = 0.25 \{ S_{out}^0 + (\cos^2(2\theta_4) + \sin^2(2\theta_4) \cos \Delta_4) S_{out}^1 + (\cos(2\theta_4) \sin(2\theta_4) (1 - \cos \Delta_4)) S_{out}^2 - \sin(2\theta_4) \sin \Delta_4 S_{out}^3 \} \quad (6)$$

where $S_{out} = \{S_{out}^0; S_{out}^1; S_{out}^2; S_{out}^3\}$ is Stokes vector of analyzed radiation, θ_4 and Δ_4 - parameters of retardation plate in analyzing channel (Fig.1). From (6) we can take information about corrections, needed after switching to another wavelength. For example, in dynamic scheme of Mueller-polarimeter [5,6], where $\theta_4 = \omega t$, we have expressions for Fourier-components of intensity:

$$\begin{aligned} 1) & \text{constant component: } I_0 = 0.25 \{ S_{out}^0 + [1 - (1 - \cos \Delta_4) 0.5] S_{out}^1 \\ 2) & \text{with } \sin(2\omega t): I_1 = -0.25 \sin \Delta_4 S_{out}^3 \\ 3) & \text{with } \cos(2\omega t): I_2 = 0.125 (1 - \cos \Delta_4) S_{out}^1 \\ 4) & \text{with } \sin(4\omega t): I_3 = 0.125 (1 - \cos \Delta_4) S_{out}^2 \end{aligned} \quad (7)$$

So, probing channel needs no any apparatus changes when switching to another working wavelength (see above), expressions (7) allow us to take into account needed corrections utilizing the dependence of Δ_4 on wavelength.

References:

1. Gerrard H.G. "Modern description of polarized light: matrix methods" // Optics and Laser Technology - 1982 - vol.14, N6, pp.309-319.
2. Hauge P.S. "Mueller matrix ellipsometry with imperfect compensators" // Journal of Optical Society of America - 1978 - vol.68, N11.
3. Kostova E.M., Ivanchev N.P., Kostov M.K. "Polarimeter with Electrogyratory Modulators" // Bulgarian Journal of Physics - 1986 - N13.
4. Шутов А.М. "Оптические схемы устройств измерения параметров поляризованного излучения" // "ОМП" - 1985 - N11.
5. Марьенко В.В., Савенков С.Н. "Активная Стокс-поляриметрия в условиях частично поляризованной фоновой засветки" // "Оптика атмосферы и океана" - 1993 - т.6, N11.
6. Марьенко В.В., Колисниченко Б.Н., Савенков С.Н. "Автоматизированная система для исследования поляризационной структуры оптического поля, рассеянного природными объектами" // "Оптика атмосферы и океана" - 1993 - т.6, N11.
7. Savenkov S.N., Yushtin K.E., Kolisnychenko B.M., Skoblya Yu.A., "Influence of dynamic Mueller-polarimeter parameters upon the error of the measured results" // SPIE Proc. - vol.3199, N32.

AUTHORS INDEX

A

Afanasyev N.T., 883
 Afinogenov A.Yu., 505
 Alekseev G.V., 142
 Aleksiejunas R., 565
 Alexandrov Y.N., 649
 Alexandrova A.A., 649
 Andreev M.V., 432
 Andriychuk M.I., 127
 Anohina O.D., 589, 591
 Anokhin V., 160
 Apelt'cin V.F., 495
 Artemiev V.V., 553
 Astola J., 426
 Atourian S., 426
 Azarenkov N.A., 658, 691

B

Bagatskaya O.V., 886
 Bakumenko A., 520
 Bakunov M.I., 340
 Balik H.H., 580, 606
 Bansal J.K., 384, 550
 Bartolic J., 171
 Bartuli E.R., 841
 Beley V.S., 288
 Beria R., 327
 Biela-Wiraszka D., 438
 Bit-Babik G., 124
 Blank A.Y., 860
 Blinova N.K., 586
 Bliznyuk N.Y., 739
 Bogdanov F., 544
 Bondarenko O.V., 415
 Bonnet-BenDhia A.-S., 792
 Boriskina A.V., 525
 Boriskina S.V., 810
 Borisov V.V., 318, 352
 Borulko V.F., 432, 676, 700
 Borzenkov I.A., 523
 Brand Y., 615
 Branspiz Yu.A., 240, 258, 609
 Brjuzgalov G.A., 819
 Brovenko A.V., 775
Brundell J.B., 29, 304
 Bugaev A.S., 844
 Bulgakov A.A., 556
 Buryachok V.L., 424
 Buyanov Yu.I., 312

C

Caspar C., 911
Chakrabarti A., 79
 Cheldavi A., 324, 339
 Chernogor L.F., 154, 457
 Chertov P., 198
 Chesnokov S.S., 927
Chew W., 92
 Chikichev I.S., 813
 Chu Q., 644
 Chudinovich I.Yu., 603
 Chumachenko S.V., 355
 Chumachenko V.P., 514, 766, 798
 Churmakov D.Y., 905
 Chursin V., 249
 Churyumov A.N., 889
 Cutzach P.-M., 528

D

Damata W., 559
 Dankov P.I., 378
 Davidovich M., 757
 Denisenko I.B., 658, 691
 Dikmen F., 745
 Dolzhikov V.V., 246
 Donchenko V.A., 292
 Donetsk I., 531
 Doroshenko V.A., 754
Dowden R., 29, 304
 Drobakhin O.O., 432, 442, 453
 Drogobitsky R., 804
 Dubrovka F.F., 547
 Dumanli M., 514
 Dumin A.M., 330
 Dushkin V.D., 409
 Dyachenko Yu., 234

E

Egiazarian K., 426
 Egorova N.P., 583
 Ehrhardt A., 911
 Eminov S.I., 553, 730, 748
Engheta N., 43
 Epp V.Ya., 167
Ergin A., 92

F

Fatafutdinov V.V., 880
 Filipov Ju.E., 673
 Filonenko A.B., 589, 591
 Fisanov V.V., 682

Foisel H.-M., 911

Frei S., 327

G

Gaidai Yu., 908

Gaikovich K.P., 23, 151, 255, 622, 874

Galchenko N., 562

Galishnikova T.N., 189

Galushko V.G., 462

Galuza A.A., 429

Gapon A.V., 691

Garanina L.V., 860

Gardiol F.E., 615

Garmash K.P., 154, 349

Gavrilov S.P., 164

Gavrilyako O.V., 372

Gayvoronskaja S.A., 222

Georgiev G.N., 685

Georgieva-Gross M.N., 685

Gevorkian D., 426

Gevorkyan E.A., 853

Gilman M., 869

Girka I.O., 225, 652, 710

Girka V.O., 697

Gis O.M., 133

Glushkov E., 784

Glushkova N., 784

Gokov A.M., 271

Gorelko R.I., 465

Gorelyshev S.A., 315

Gorobets N.N., 556, 568

Goshin G.G., 664

Grechko L.G., 860

Gura K.N., 930

Gusakov A.V., 822

Guseva E.V., 612

Gushchin V.V., 266

Guzev M.A., 877

H

Hashimov A.B., 502

Hayakawa M., 29, 277, 296

Hobara Y., 296

I

Ichikawa K., 807

Ikiz T., 517

Ilinski A.S., 189

Ivanilov V.E., 700

Ivanov S.A., 378, 600

Ivaska V., 252, 565

J

Jablonski T., 61**Jandhyala V.**, 92

Jatsenko N., 574

Jatsenko Y., 574

Jobava R., 327

Jonkus V., 252

K

Kalaida V.T., 292

Kaloshin V.A., 157

Kapilevich B.Y., 832

Kapustin U.U., 618

Kapustyanskii S.P., 412

Karacuha E., 514, 733, 745

Karaman M., 629

Karchevskii E.M., 787

Karkashadze D., 544

Karlova V.A., 402

Kascheev S.B., 288

Kasyanov A.O., 212

Katayama K., 807

Kazakova N.A., 274

Kazanskiy V.B., 396, 415

Kechribaris C., 163

Khardikov V.V., 396

Khizhnyak A.N., 520, 742

Khizhnyak N.A., 206, 574, 649, 819

Khoroshun V.V., 772, 828

Khrutchinsky A.A., 905

Kirilenko A.A., 387, 390, 399

Kobayashi K., 727, 763

Kochergov R.N., 641

Kokodiy N.G., 237

Kolchigin N.N., 346

Kolesnik A.G., 274

Kolev N.Z., 499

Kolisnychenko B.M., 444

Komarov S.A., 597, 736

Kondratenko D.A., 835

Kontar E.P., 688

Korol M.A., 303

Koshelev V.I., 312, 343

Koshikawa S., 727, 763

Kouzaev G.A., 421

Koval A.A., 880

Kovalchuk V.A., 459

Kovalenko V.O., 450

Kovalevsky A.A., 240

Kovalevsky M.Yu., 722
 Kovostyshevski V., 409
 Kovtun P.K., 652
 Kramarenko K.Yu., 206
 Krapyvny A.V., 798
 Kravchenko V.F., 228
 Kravetz R., 908
 Kravtsov Y.A., 889
 Kudintseva I.G., 295
 Kulizhsky A.V., 883
 Kuryliak D., 763
 Kuzmichova E.V., 920

L

Lakhtakia A., 822
 Lapshin V.I., 688, 697, 710
 Lazebny B.V., 288
 Lazorenko O.V., 457, 621
Lenoir M., 35
 Lerer A.M., 531, 829
 Leus S.G., 456
 Liang C., 644
 Lipachev E.K., 174
 Litovchenko K.C., 889
 Litvinenko D.L., 180
 Litvinenko G.V., 285
Litvinenko L.N., 42
 Lugina N.E., 664
 Lukin V., 426
 Lyalinov M.A., 517
 Lyaschenko V.A., 556
 Lysak V.V., 914
Lyshevsky S.E., 88
 Lytova A.Yu., 603

M

Makarov A.I., 850
 Makarov N.M., 872, 891
 Maksimenko A.S., 789
 Maksimenko S.A., 822
 Malyushkin A.V., 716
 Marakasov D.A., 682
Marciniak M., 106, 923
 Markov V.I., 589, 591
 Martynenko S.I., 271, 298
 Marushchenko N.B., 225
 Masalov S.A., 358
 Mashutin A.I., 736
 Matsushima A., 751
 Mazmanishvili A.S., 279, 429
 Meglinsky I.V., 927
 Mel'nik V.N., 688

Metskhvarishvili D., 544
Michielssen E., 92
 Mikhnev V.A., 115
 Milstein K.A., 917
 Mitrofanova T.G., 167
 Mityagina M.I., 889
 Mizernik B.N., 706
 Mohan A., 894
 Molchanov O.A., 277
 Moroz A.V., 872
 Mosig Ju.R., 615
 Mos'pan L.P., 390
 Motrich V.V., 860
 Muzychenko A.V., 315
 Myand S.V., 298

N

Naidenko V.I., 412, 612
 Nazarchuk Z., 195, 763, 804
 Nechesa A.V., 589, 591
 Nerukh A.G., 148, 309, 336
 Neto A.D.D., 559
 Nevzlin B., 234
 Nickolaenko A.P., 294, 295, 296, 303
 Nikita K.S., 163
 Nikitin K.V., 632
 Nikolaev N.E., 145
Nosich A.I., 104, 739, 810
Nyquist D.P., 55

O

Obukhovets V.A., 136, 212
 Odarenko E., 249
 Ogata M., 727
 Ogourtsov S., 832
 Okuno Y., 751
 Onufrienko V., 219
 Osharin A.M., 534
 Ovcharenko E.V., 292
 Ovsyannikov O., 195, 804
 Ozturk I., 629

P

Padney K.N., 384, 550
 Palenskis V., 252
 Palto A.A., 115
 Panasyuk A.S., 142
 Panchenko A.Yu., 847
 Pankratov L., 260
 Panov D.V., 142
 Papkovich V.G., 673
 Pastushenko A.V., 609
 Pavlenko I.V., 225

Paznukhov V.E., 288
 Penkin Y.M., 381
 Perov A.O., 321
 Petrusenko I., 369
 Piankov V.P., 766
 Piven S.V., 212
 Pivnenko S.N., 346
 Pleshchinskaya I.E., 781
 Pleshchinskii N.B., 781, 801
 Plisko V.V., 312
 Poddar A.K., 384, 550
 Podlevskyi B., 121
 Podlozny V.V., 209, 396
 Pogoryelov E.A., 917
 Pogrebnyak V.A., 719
 Pogrebnyak V.V., 844
 Pokhil'ko S.N., 456
 Poljarus A.V., 880
 Pommerenke D., 327
 Popenko N.A., 543
 Popov G.V., 877
 Poyedinchuk A.Y., 775
 Prijmenko S.D., 819
 Prokopenko A.P., 412, 612
 Prosvirnin S., 186, 301
 Puzanov A.O., 358
 Puzirkov S.Yu., 697
 Pyatak N.I., 706

R

Rabinowicz L.M., 294, 295
 Radchenko V.V., 769
 Radtsig Yu.Yu., 553
 Rahman H., 363
 Ramdani K., 792
 Reizenkind Ya.A., 829
 Repa F.M., 411, 930
 Reshnyak O.O., 133
 Reznik A.N., 255
 Rodger C.J., 282, 304
 Rogozhkin E.V., 279
 Rokhman A.G., 288
 Rozhkov A.A., 722
 Rozumenko V.T., 154, 271
 Rud' L., 399
 Ryazantseva N.V., 192
 Rybin O., 336

S

Sadov S.Y., 201
 Samokhin A.B., 618

Samokhvalov M., 902
 Saramaki T., 426
 Sarychev V.T., 343
 Saveljev V.V., 571
 Savenko P., 121, 139, 160
 Savenkov S.N., 435, 444, 465
 Scherbatko I., 309
 Selin V.I., 243, 577
 Semenikhina D.V., 366
 Senyk T., 195
 Serbest A.H., 517
 Serebryannikov A.E., 825
 Sergeev V.I., 222
 Sestroretskii B.V., 600
Shanker B., 92
 Shcherbina V.A., 265, 625
 Shepilko Ye.V., 511
 Shevchenko V.V., 145
Shifrin K., 69
 Shinkevich B.M., 274
 Shipilov S.E., 343
 Shirnen A.A., 183
 Shmat'ko A., 249
 Shubitidze P., 327, 544
 Shubova R.S., 298
 Shulga S.N., 716, 886
 Shvedchikova I., 635
 Shvelidze R.R., 540
 Shvets A.V., 277, 303
 Silva P.H.F., 559
 Singh N., 894
 Sinko V.G., 142
 Sipus Z., 171
 Skipetrov S.E., 927
 Skobelev S.P., 632
 Skoblya Yu.A., 444
 Skrivervik A.K., 615
 Sledkov V.A., 829
 Slepyan G.Ya., 789, 822
 Slyusar V.I., 424
 Smith P.D., 760
Smith P.D., 73
Song J., 92
 Sorokin S.N., 130, 571
 Spitsyn V.G., 866
 Spivak A., 635
 Stepanyuk V.N., 164
 Strebel B., 911
 Sukharevsky I.V., 537

Sukharevsky O.I., 315, 508
Sukhinin S.V., 98, 835
 Sukhoivanov I.A., 899
 Suriadny A.S., 279
 Svezhentsev A.Ye., 795
 Syvozalizov N.A., 828
 Szczesny W., 923

T

Tanaka K., 807
 Tanaka M., 807
 Tanyer S.G., 629
 Tarapov S.I., 231
 Tarasov Yu.V., 891
 Tavzarashvili K., 124
 Tcherkasov A.S., 421
 Tchernyava M.B., 151
 Terent'ev Yu., 204
 Tereshchenko V.M., 547
 Thomson N.R., 282
 Timchenko A.I., 863
 Tinin M.V., 883
 Tishetskiy Yu.O., 658
 Tkach M., 121
 Tkachenko V.I., 390, 399, 405
 Tokarsky P.L., 246
 Topolyuk Yu.P., 133
 Tretyakov O.A., 330
 Trigubovich V., 447
 Trubin A., 375
 Tsvetkovskaya S., 531
 Tsymbal A.M., 271
 Tuchin V.V., 927
 Tuchkin Y.A., 733, 745
 Tumakov D.N., 801
 Turbin P.V., 409
 Turk A., 733
 Tyrmov O.F., 271
 Tyzhnenko A.G., 638

U

Usin V.A., 589, 591
 Uzunoglu N.K., 164

V

Vartanyan S., 562
 Vashinsky S.E., 537
 Vasilyeva T., 186, 399
 Velichko L.G., 177
 Veliev E.I., 727
 Venetsky A.S., 157
 Verbitskii I.L., 214

Vertiy A.A., 164
 Vinogradova E.D., 760
 Vinogradov S.S., 742
 Vinogradov V.V., 285
 Voinivskiy I.V., 164
 Voinova L.J., 748
 Voitovich N.N., 133
 Vorgul I.Yu., 148, 333
 Vorobiov S.N., 180
 Vytovtov K., 667

W

Wait J.R., 282

Y

Yachin V.V., 192
 Yamamoto N., 277
Yampolski Y.M., 42, 288
Yashina N.P., 50
 Yatsuk L.P., 393, 586
 Yatzuk K.P., 540
 Yelisseyeva N.P., 568
 Yevtushenko O.M., 822
 Yuan W., 644
 Yukhanov Yu.V., 118, 130
 Yumov I.B., 838
 Yushtin K.E., 435, 444

Z

Zabolotskiy A.M., 231
 Zaets W., 908
 Zaginaylov G.I., 265, 409
 Zagirnyak M.V., 258
 Zalevsky G.S., 508
 Zaridze R., 124, 327
 Zasovenko V.G., 798
 Zatcepin P.M., 597, 736
 Zentner R., 171
 Zhevakin S.A., 857
 Zhilin A.V., 622
 Zhironkina A.V., 586
 Zhuchenko S.A., 265
 Zhukov S.N., 340
 Ziemelis J., 198
 Zinenko I.L., 766
 Zinenko T.L., 751